Origin, controlling factors, and statistical modelling of methylmercury concentrations in tunas at a global scale

Anaïs Medieu

DOCTORAT SCIENCES BRETAGNE DE LA MER LOIRE ET DU LITTORAL

UBO
Université de Bretagne Occidentale

THESE DE DOCTORAT DE

L'UNIVERSITE
DE BRETAGNE OCCIDENTALE

ECOLE DOCTORALE N° 598
Sciences de la Mer et du littoral
Spécialité : « Ecologie marine »

Par
Anaïs MEDIEU

Origin, controlling factors, and statistical modelling of methylmercury concentrations in tunas at a global scale

Thèse présentée et soutenue à Plouzané, le 10 mai 2022
Unité de recherche : Laboratoire des Sciences de l'Environnement Marin, LEMAR, UMR 6539

Rapporteurs avant soutenance :

Paco BUSTAMANTE
Professeur, Université de La Rochelle

Carl LAMBORG
Professeur, University of California

Composition du Jury :

Paco BUSTAMANTE : rapporteur
Professeur, Université de La Rochelle

Carl LAMBORD : rapporteur
Professeur, University of California

Géraldine SARTHOU : présidente de jury
Directrice de Recherche, CNRS

Krishna DAS : examinatrice
Maître de conférence, Université de Liège

Frédéric MENARD : examinateur
Directeur de Recherche, IRD

Anne LORRAIN : directrice de thèse
Directrice de Recherche, IRD

David POINT : co-encadrant
Chargé de Recherche, IRD

Invité(s):

Olivier GAUTHIER : co-encadrant
Maître de conférence, UBO

“Why do I stand up here? Anybody?
I stand upon my desk to remind myself that we must constantly look at things in a different way”

John Keating - Dead Poets Society

Remerciements / Acknowledgements

Comme un long voyage, cette thèse a été une aventure intense et enrichissante, nourrie de nombreuses et belles rencontres et du soutien de mes proches.

Pour commencer je souhaite adresser un immense merci à mes encadrants principaux, Anne Lorrain et David Point. Que de chemin parcouru à vos côtés en trois ans et demi ! Un grand merci pour votre confiance, votre patience, votre investissement et votre passion communicative pour la recherche qui m'ont permis de m'approprier pleinement ce sujet et d'apprendre tant de choses. J'ai pris beaucoup de plaisir à réfléchir et travailler avec vous et je me réjouis de pouvoir continuer à le faire durant les prochains mois. Merci aussi à Olivier Gauthier d'avoir accepté de co-encadrer cette thèse, et d'avoir répondu présent lorsque j'en avais besoin.

Impossible de tous les citer mais je remercie bien évidemment l'ensemble des propriétaires d'échantillons de thons, et à travers eux les équipes d'échantillonnage en mer, au port et à l'usine, sans qui ce travail n'aurait pu être réalisé. Merci pour leur confiance et leur participation à ce beau projet collaboratif. Je pense en particulier à Leanne Fuller et Shane Griffiths, qui m'ont accueilli chaleureusement à l'IATTC et ont été d'une grande disponibilité. Un très grand merci aussi à Valérie Allain pour ses conseils toujours avisés, ainsi qu'à Heidi Pethybridge pour sa disponibilité et son aide précieuse quand je pouvais me sentir un peu seule avec mes modèles. Je n'oublie pas non plus l'équipe de PIRATA, en particulier Jérémie Habasque, Bernard Bourlès et l'ensemble des échantillonneurs, et espère un jour pouvoir faire partie de l'aventure.

> *It is not possible to cite them all but I would like to thank all the tuna sample owners, and the sampling teams at sea, during landing and at the factory, without whom this work would not have been possible. Thank you for your interest and participation in this beautiful collaborative project. I am thinking in particular of Leanne Fuller and Shane Griffiths, for their warm welcome and their help during my mission in IATTC. A big thank you also to Valérie Allain for her valuable advice, and to Heidi Pethybridge for her availability and her precious help when I could feel a little bit alone with my models. I don't forget the PIRATA team, in particular Jérémie Habasque, Bernard Bourlès and all the sampling team, and I hope one day to have the opportunity to be part of the adventure.*

Je remercie beaucoup les équipes du GET et du MIO pour m'avoir initiée aux subtilités du cycle du mercure (pas facile !), en particulier Jeroen Sonke, Lars-Eric Heimburger, Hélène Angot, et Laure Laffont. Je suis aussi reconnnaissante à Anders Bignert et David Streets qui ont tous deux répondu présents lorsque je les ai sollicités en toute fin de thèse. Un très grand merci également à Pearse Buchanan pour sa contribution active à ce travail, sa disponibilité, sa patience et ses petits cours de rattrapage en biogéochimie marine, le tout à distance. Ce travail a aussi bénéficié des conseils avisés d'Alessandro Tagliabue, Laurent Bopp, Christophe Menkes et Christopher Somes.

> *I am very grateful to the GET and MIO teams for introducing me to the subtleties of the mercury cycle (not easy!), in particular Jeroen Sonke, Lars-Eric Heimburger, Hélène Angot, and Laure Laffont. I also thank Anders Bignert and David Streets for their interest and their contribution in this project when I contacted them at the very end of my thesis. A huge thank you to Pearse Buchanan for his active contribution to this work, his availability, his patience and his little courses on marine biogeochemistry, all from distance. Thanks also to Alessandro Tagliabue, Laurent Bopp, Christophe Menkes and Christopher Somes for their advice.*

Je suis également très reconnaissante envers David Gillikin et Anouk Verheyden de l'Union College, et Andrew Revill du CSIRO pour les analyses d'isotopes stables, et pour avoir fait leur maximum pour

rattraper le retard pris suite à la pandémie. Au LEMAR, je remercie beaucoup Jean-Marie Munaron, Hervé Le Delliou et Fanny Sardenne pour m'avoir formée et éclairée dans les différentes manips de labo. J'ai aussi une pensée pour Jérémy Collin et Thilbaut Le Bars du service informatique pour leur aide technique sur Styx.

Many thanks to David Gillikin and Anouk Verheyden from Union College, and to Andrew Revill from CSIRO for stable isotope analyses. They did their best to make sure I was not too penalised by the closure of their respective laboratories during the pandemy.

Je remercie aussi chacun des membres du jury d'avoir accepté d'évaluer ce travail, ainsi que Véronique Loizeau et Tiphaine Chouvelon pour leur intérêt porté à mes travaux, leurs précieurs conseils et leurs encouragements durant les comités de thèse.

I would like to thank all the members of the jury for having accepted to evaluate this work, as well as Véronique Loizeau and Tiphaine Chouvelon for their interest in this work, their precious advice and their encouraging words during the thesis committees.

Parce que cette thèse est l'aboutissement de plusieurs rencontres et d'opportunités professionnelles, j'aimerais aussi remercier ici l'ensemble des personnes qui m'ont fait confiance en m'ouvrant les portes de l'écologie marine quand j'étudiais encore l'agronomie et les milieux forestiers. Je pense tout d'abord à Richard Pillans, Russ Babock et aux équipes de Gladstone et Ningaloo pour leur générosité, et pour m'avoir permis de vivre cette première expérience incroyable de terrain sur les écoystèmes corraliens.

Because this thesis is the result of several professional experiences and opportunities, I would also like to thank all the people who trusted me and gave me the access to marine ecology while I was styding agronomy and forestry. First, I am thinking of Richard Pillans, Russ Babock and the Gladstone's and Ningaloo's teams for their generosity and for having allowed me living this first incredible field experience on coral ecosystems.

Bien sûr je pense aussi à Sandrine Vaz grâce à qui j'ai pu poursuivre l'aventure marine et avec qui j'ai pris beaucoup de plaisir à découvrir les enjeux liés à la pêcherie chalutière dans le Golfe du Lion. Je pense également à l'Observatoire Thonier, en particulier Pascal Bach, qui m'a donné l'opportunité d'embarquer pendant deux mois sur un senneur dans l'Océan Indien, puis de continuer dans le fabuleux monde de la pêche aux thons depuis les quais des Seychelles. De cette expérience dans l'Océan Indien, je souhaite aussi remercier l'ensemble des équipages français SAPMER et CFTO pour leur accueil à bord et leur partage de connaissances et d'expériences. Merci aussi à Emmanuel Chassot et Patrice Dewals qui, chacun a sa façon, m'a transmis le virus de cette pêcherie, contribuant ainsi indirectement à cette thèse. Manu, qui a continué à répondre présent durant ces trois dernières années quand j'avais une question « pêche aux thons ». Je n'oublie pas les équipes de la Seychelles Fishing Authority pour leur accueil, et ai une pensée toute particulière pour l'ami Abdul. Enfin de cette expérience je remercie énormément Nathalie Bodin, qui au-delà de sa participation active à cette thèse, m'a fait confiance et a partagé avec beaucoup de générosité sa passion pour l'écologie trophique, sans quoi je n'aurais pas eu l'opportunité de faire cette thèse.

Je remercie très fort tous les copains/collègues de l'IUEM sans qui le quotidien aurait été bien triste et la fin de thèse douloureuse. Un immense merci à la grande Odeline – mi superwoman, mi ange gardien - pour bien des raisons, entre autre les petits mots des dernières semaines qui ont été d'un grand

réconfort. Un grand merci aussi à Lulu, binôme de thèse, à Pierrot, force tranquille du bâtiment D, et à l'enthousiaste Sandrine. Je pense aussi à la triplette Fanny, Romina et Mariana pour les pauses thés ou mousseux, à Raul, Mathilde, Zahirah, Gwendoline, Thomas, Claudie, Evelyne, mais aussi à Christophe pour ses conseils et encouragements depuis l'autre rive. Un grand merci également à la folle équipe d'impro de l'IUEM pour les grands moments de rigolade du lundi midi. Parmi les copains de labo, j'ai enfin une grosse pensée pour la joyeuse équipe du GET pour son accueil chaleureux et festif à chacune de mes missions : Christelle, Marina, Paty, Chuxian et Bea.

Un énorme merci à tous les copains d'avant Brest qui ont suivi ça de loin mais toujours avec intérêt : les amies de SupAgro, la mini-meute GMN, les copains des Seychelles, la familia de corazón argentina, et les Dudu.

Je remercie aussi infiniment ma famille auprès de qui il est toujours bon se ressourcer. Mon père d'abord pour m'avoir entre autre transmis son goût d'apprendre et son intérêt pour l'information. Et bien sûr ma sœur et ma mère pour m'avoir toujours soutenue et encouragée dans chacun de mes projets, faisant à chaque fois leur maximum pour qu'ils puissent se réaliser. A vous deux je vous dois tant, et ce bien au-delà de cette thèse.

Mes derniers remerciements sont pour Pablito. Tu as été un roc dans cette folle aventure, en étant toujours disponible pour moi, en m'encourageant, notamment dans les moments de doutes. Nos discussions m'ont aussi aidée à développer mon sens critique et ont ainsi largement contribué à ma réflexion sur ce travail. Merci pour ta patience, ton amour, tes rires. Merci pour tout.

Table of content

List of tables and figures

Thesis outline

Published peer-review articles during the thesis (5)

Barbosa, R.V., Point, D., **Médieu, A.**, Allain, V., Gillikin, D.P., Couturier, L.I.E., Munaron, J.-M., Roupsard, F., Lorrain, A., under review. Tuna mercury concentrations in blood and muscle mirror seawater methylmercury in the Western and Central Pacific Ocean. Marine Pollution Bulletin, 180, 113801. https://doi.org/10.1016/j.marpolbul.2022.113801

Médieu, A., Point, D., Itai, T., Angot, H., Buchanan, P.J., Allain, V., Fuller, L., Griffiths, S., Gillikin, D.P., Sonke, J.E., Heimbürger-Boavida, L.-E., Desgranges, M.-M., Menkes, C.E., Madigan, D.J., Brosset, P., Gauthier, O., Tagliabue, A., Bopp, L., Verheyden, A., Lorrain, A., 2022. Evidence that Pacific tuna mercury levels are driven by marine methylmercury production and anthropogenic inputs. PNAS 119, 8. https://doi.org/10.1073/pnas.2113032119

Renedo, M., Point, D., Sonke, J.E., Lorrain, A., Demarcq, H., Graco, M., Grados, D., Gutiérrez, D., **Médieu, A.**, Munaron, J.M., Pietri, A., Colas, F., Tremblay, Y., Roy, A., Bertrand, A., Bertrand, S.L., 2021. ENSO Climate Forcing of the Marine Mercury Cycle in the Peruvian Upwelling Zone Does Not Affect Methylmercury Levels of Marine Avian Top Predators. Environ. Sci. Technol. 55, 15754–15765. https://doi.org/10.1021/acs.est.1c03861

Médieu, A., Sardenne, F., Lorrain, A., Bodin, N., Pazart, C., Le Delliou, H., Point, D., 2021b. Lipid-free tuna muscle samples are suitable for total mercury analysis. Marine Environmental Research 169, 105385. https://doi.org/10.1016/j.marenvres.2021.105385

Médieu, A., Point, D., Receveur, A., Gauthier, O., Allain, V., Pethybridge, H., Menkes, C.E., Gillikin, D.P., Revill, A.T., Somes, C.J., Collin, J., Lorrain, A., 2021a. Stable mercury concentrations of tropical tuna in the south western Pacific ocean: An 18-year monitoring study. Chemosphere 263, 128024. https://doi.org/10.1016/j.chemosphere.2020.128024

Articles under review or in preparation (2)

Médieu, A., Point, D., Buchanan, P.B., Pethybridge, H., Allain, V., Bodin, N., Angot, H., Fuller, L., Ferriss, B.E., Munoz, L., Lucena-Frédou, F., Adams, D.H., Logan, J.M., Gillikin, D.P., Sonke, J.E., Heimburger-Boavida, L.-E., Revill, A.T., Ménard, F., Galván-Magaña, F., Itai, T., Jinadasa, B.K.K.K., Pizzochero, A.C., Torres, J.P.M., Luna-Acosta, A., Madigan, D.J., Renedo, M., Verheyden, A., Munaron, J.M., Tagliabue, A., Bopp, L., Laffont, L., Gauthier, O., Lorrain, A., in prep. Tropical tunas mirror patters of mercury bioavailability and pollution in the global ocean.

Médieu, A., Point, D., Sonke, J.E., Buchanan, P.B., Bodin, N., Adams, D.H., Streets, D.G., Bignert, A., Ménard, F., Choy, C.A., Allain, V., Itai, T., Ferriss, B.E., Bourlès, B., Laffont, L., Gauthier, O., Lorrain, A., in prep. Long-term trends of tuna mercury concentrations for the global ocean.

Published peer-review articles not directly related to the thesis (2)

Artetxe-Arrate, I., Fraile, I., Farley, J., Darnaude, A.M., Clear, N., Rodríguez-Ezpeleta, N., Dettman, D.L., Pécheyran, C., Krug, I., **Médieu, A.**, Ahusan, M., Proctor, C., Priatna, A., Lestari, P., Davies, C., Marsac, F., Murua, H., 2021. Otolith chemical fingerprints of skipjack tuna (Katsuwonus pelamis) in the Indian Ocean: First insights into stock structure delineation. PLOS ONE 16, e0249327. https://doi.org/10.1371/journal.pone.0249327

Sardenne, F., Bodin, N., **Médieu, A.**, Antha, M., Arrisol, R., Le Grand, F., Bideau, A., Munaron, J.-M., Le Loc'h, F., Chassot, E., 2020. Benefit-risk associated with the consumption of fish bycatch from tropical tuna fisheries. Environmental Pollution 267, 115614. https://doi.org/10.1016/j.envpol.2020.115614

Oral presentations at international conferences (2)

Médieu, A., Point, D., Itai, T., Angot, H., Buchanan, P.B., Allain, V., Fuller, L., Griffiths, S., Gillikin, D.P., Sonke, J.E., Heimburger-Boavida, L.-E., Desgranges, M.-M., Menkes, C.E., Madigan, D.J., Brosset, P., Gauthier, O., Tagliabue, A., Bopp, L., Verheyden, A., Lorrain, A., 2021a. Pacific tuna mercury levels driven by marine methylmercury production and anthropogenic emissions. Presented at the Goldschmidt conference, virtual.

Médieu, A., Point, D., Bodin, N., Receveur, A., Houssard, P., Allain, V., Logan, J.M., Pethybridge, H., Ferriss, B.E., Itai, T., Ménard, F., Gauthier, O., Lorrain, A., 2019a. Is there enough data to perform robust spatial and temporal analyses of mercury levels in commercial tuna at a global scale? Presented at the IMBeR Future Ocean2, Brest, France.

Posters presented at international conferences (2)

Médieu, A., Receveur, A., Point, D., Gauthier, O., Allain, V., Menkes, C.E., Lorrain, A., 2020. Stable mercury levels and trophic position in three tropical tuna species in the South-West Pacific Ocean over the past 18 years. Presented at the Ocean Sciences Meeting 2020, San Diego, CA, USA.

Médieu, A., Receveur, A., Point, D., Gauthier, O., Allain, V., Menkes, C.E., Lorrain, A., 2019b. No temporal trend of mercury levels in tropical tuna species of the southwestern Pacific Ocean. Presented at the 14th International Conference on Mercury as a Global Pollutant, Krakow, Poland.

Popularization activities (3)

Intervention with secondary school students within the French national program "Les Cordées de la Réussite", which aims at fighting against self-censorship and encouraging students' academic ambitions, Collège Paul-Henri Cahingt, Londinières (France), 2022.

Science popularization article in the Pacific Community Fisheries Newsletter #166, 2022. *Tuna help to map mercury concentrations in the ocean*. French version in SI Appendix H; English version on line: https://coastfish.spc.int/en/publications/bulletins/fisheries-newsletter/530

Talk to secondary teachers at the Sea and Education Summer School, Plouzané (France), 2021. *Is it sustainable and healthy to eat tunas?*

Teaching experience (2)

Master degree, academic year 2020-2021, Université Bretagne Occidentale:
Sciences and Society (30 hours).

Bachelor degree, academic year 2019-2020, Université Bretagne Occidentale:
Biostatistics (40 hours, tutorial and practical work),
Animal biology (18 hours, practical work).

Student supervision (3)

Clément Le Goc, IUT Brest-Morlaix, 2 mois, 2022. *Analyse de deux métalloïdes dans des matrices biologiques différentes, le sélenium (Se) dans les poissons tropicaux et l'arsenic (As) dans les sargasses holopélagiques*.

Antoine Le Gohalen, Master student, 6 months, 2021. *Selenium concentrations and selenium-mercury balance in commerical fish species at the global scale.*

Chloé Pazart, Master student, 2 months, 2019, *Effects of lipid extraction on total mercury concentrations in tunas.*

Mobility

MARBEC (Sète, France): one trip (8 days) in December 2018.

Géosciences Environnement Toulouse (GET, Toulouse, France): 10 trips (109 days in total) from 2018 to 2021.

Inter-American Tropical Tuna Commission (La Jolla, California, USA): one trip (20 days), February 2020.

Collaborations (47)

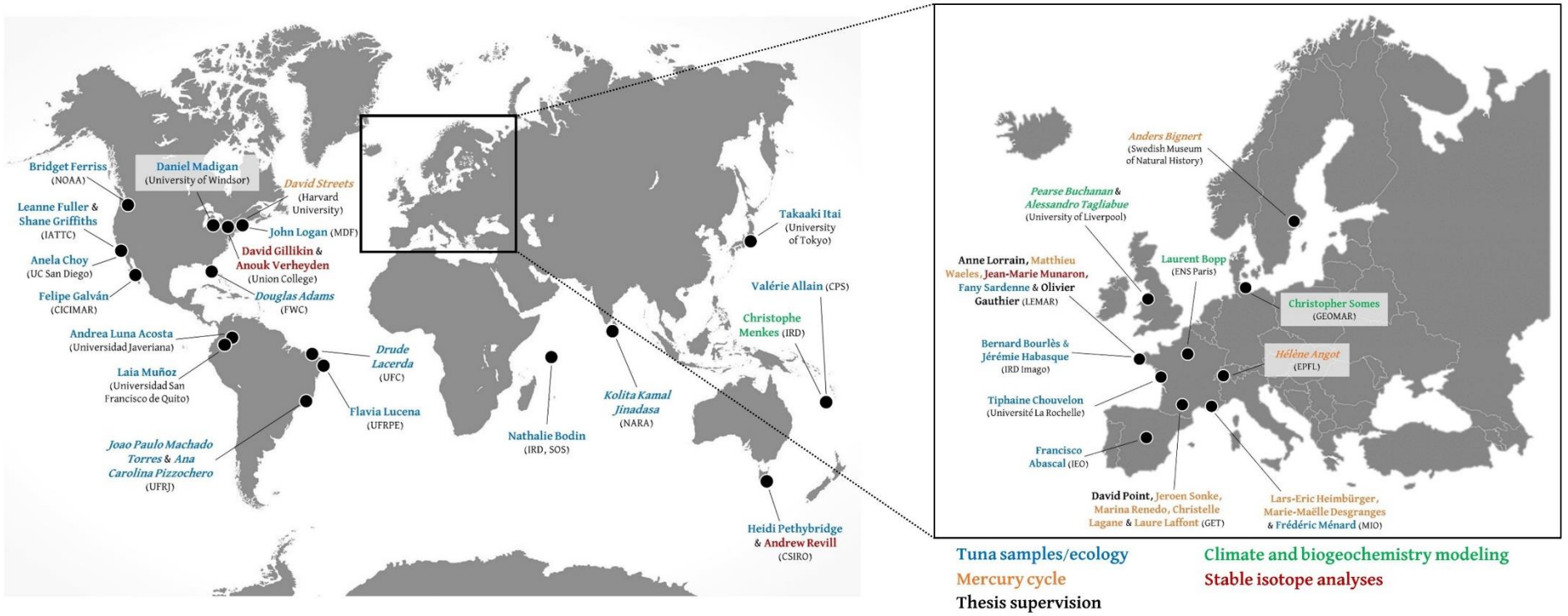

Figure 1. Collaborations involved in this thesis. Italic text shows the ones developed during this thesis.

General introduction

Mercury, a global contaminant of major concern for human health and ecosystems

Mercury (Hg, atomic number of 80, and atomic mass of 200.59 $g.mol^{-1}$) is a unique element that exists in liquid form at room conditions of temperature and pressure. It can be found under three different chemical forms: elemental gaseous Hg (Hg^0), divalent inorganic form (Hg^{2+}) and organic forms, the most toxic ones, hereafter defined as methylmercury (MeHg), which include monomethylmercury (CH_3Hg) and dimethylmercury ($(CH_3)_2Hg$). All of these forms are linked together by chemical and biological reactions, like methylation/demethylation, and oxidation/reduction.

Because of its different chemical forms and its unique physicochemical properties, Hg naturally occurs in all environmental compartments. In the atmosphere, Hg is mainly present as Hg^0 favouring its mobility over long distances before being transferred into the ocean. The atmosphere is considered as the most important pathway for the worldwide dispersion and transport of Hg, and oceanic concentrations are heavily influenced by the large ocean-atmosphere Hg exchanges (Fitzgerald et al., 1998; Mason and Sheu, 2002). Quantifying the global sources, speciation, fate, transport, and transformations of Hg in all environmental compartments is therefore necessary to understand the importance of emissions from natural and anthropogenic sources in contributing to MeHg production in aquatic systems, and to its bioaccumulation through marine food webs.

The entry into force in August 2017 of the United Nations Environmental Program Minamata Convention on Mercury (ratified by 137 countries in February 2022) is a milestone in international efforts to control Hg inputs into the environment and to protect human health from its harmful effects (www.mercuryconvention.org). Governments and policy makers must therefore balance economic, environmental, and health interest. Monitoring of biotic and abiotic Hg concentrations and trends has consequently be identified as a priority to evaluate the effectiveness of the Convention in meeting its goals.

Global mercury cycle

Mercury sources to the environment

Mercury is emitted naturally to the atmosphere, mainly as gaseous elemental Hg^0, by geothermal activity, and volcanism as primary release. Mercury emissions also include re-emissions of previously deposited Hg over land and water bodies (Figure 1) (Mason and Pirrone, 2009).

Mercury is also released to the atmosphere from a large number of man-made sources, which considerably modified the global Hg cycle (Figure 1). These anthropogenic inputs include fossil fuel power plants, artisanal small-scale gold mining, non-ferrous metals manufacturing, cement production, and waste disposal. Humans started using Hg to extract gold, silver, copper, and other

materials about 4,000 years ago, exploiting its high electrical conductivity and ability to form amalgam with other metals. Yet, about 95 % of all-time anthropogenic releases have been estimated to occur during the five last centuries, with releases greatly influenced by events that occurred worldwide and in specific regions of the world (Figure 2A) (Streets et al., 2019a). In the past, releases have been largest in North America and Europe, and mainly related to Hg extraction and use in the production of gold and silver (Figure 2B). However, anthropogenic releases in these two regions have declined since the 1970s, following emission reduction measures. Conversely, anthropogenic Hg releases associated with the energy sector in Asia have sharply increased in the recent decades, making this region the first contributor of Hg worldwide (Figure 2A). In Africa and Middle East, almost all Hg is relatively recent (i.e., emitted since 1850), and because of continued use of Hg in artisanal and small-scale gold mining, these two regions remain major contributors.

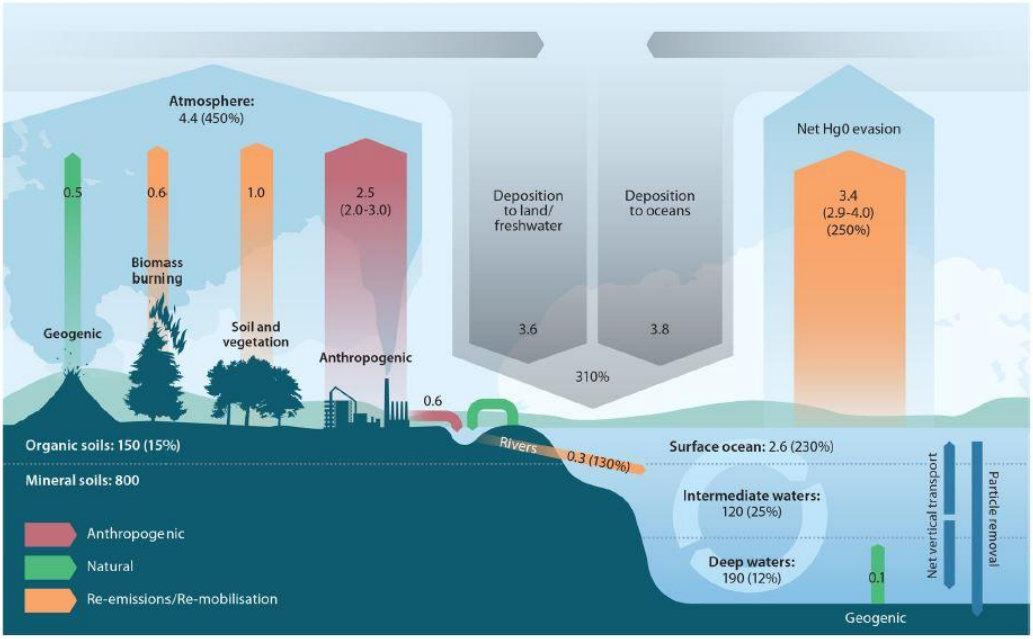

Figure 2. Updated global mercury budget illustrating the anthropogenic impact on the mercury cycle since the pre-anthropogenic period (i.e., prior to 1450 AD), from Outridge et al. (2018). Ranges are given in brackets after the best estimate values; percentages in brackets represent the estimated increase in mass (kt) or flux ($kt.y^{-1}$) due to human activities since the pre-anthropogenic period.

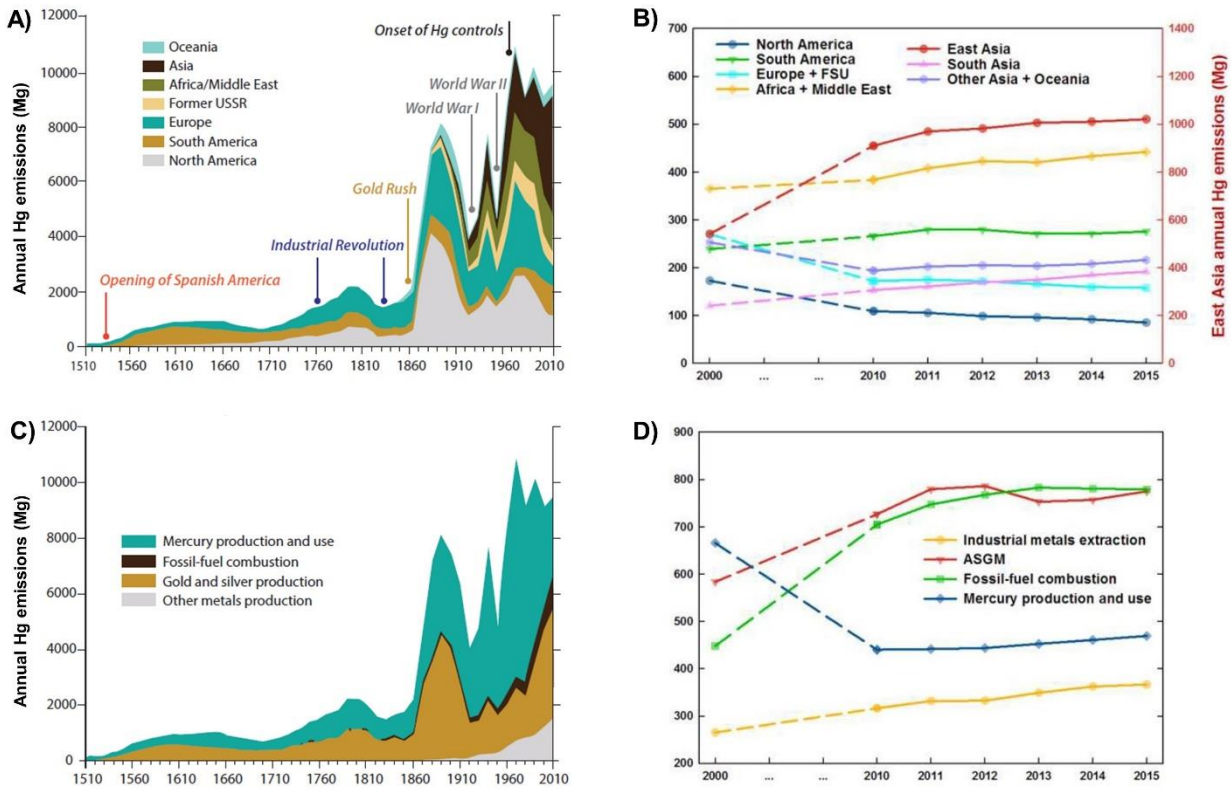

Figure 3. Temporal trends of annual anthropogenic mercury (Hg) releases to the environment, adapted from Streets et al. (2019a, 2019b) by the Pacific Community. **A)** and **B)** show the trends by region, during the period 1510-2010, and 2010-2015, respectively. **C)** and **D)** show the trends by source types, during the period 1510-2010, and 2010-2015, respectively.

Global mercury budget

Once emitted to the atmosphere, Hg from natural and anthropogenic sources are merged together, transported and recycled among the main environmental compartments (i.e., air, soil, and waters) on timescales of years to decades, until it is eventually removed from the surface system through burial in coastal and deep ocean sediments, lake sediments, and subsurface soils over centuries (Amos et al., 2013; Fitzgerald and Lamborg, 2014). Historical anthropogenic Hg therefore continues to cycle throughout biogeochemical compartments for a long time after its first release to air, representing what is called a “legacy” of Hg enrichment in the environment. Understanding how legacy Hg contributes to the current Hg cycle is crucial to predict ecosystem responses to reductions in anthropogenic emissions, such as those targeted by the Minamata Convention. Given its scale and biogeochemical complexity, and the lack of detailed Hg records, the Hg cycle is best described with budgets derived from global-scale models and literature compilations. Information on historical Hg accumulation can also be drawn from multiple natural archives, including aquatic sediment, peat, ice cores, and biological tissues (e.g., fish scale, bird feathers and eggs) (Engstrom et al., 2014; Martínez-Cortizas et al., 1999; Schuster et al., 2002; Tzadik et al., 2017; Xu et al., 2011).

In the latest revised global budget (Outridge et al., 2018), human activities, including legacy Hg, are estimated to have increase current atmospheric Hg concentrations by about 450 % above natural levels (i.e., prevailing before 1450 AD). Present-day anthropogenic emissions to air are

estimated at 2,500 ± 500 $Mg.y^{-1}$ (Figure 1), while natural sources (i.e., primary emissions + re-emissions) are estimated at 5.2 $Mg.y^{-1}$ (Pirrone et al., 2010). Mercury concentrations in surface marine waters are suspected to have tripled compared to the pre-anthropogenic conditions (Lamborg et al., 2014), showing some lag with atmospheric changes given the longer residence time of Hg in surface waters (Amos et al., 2013). In deeper marine waters, the budget shows increases of only 12–25 % resulting from the slow rate of penetration of anthropogenic Hg into the large deep-water reservoir (Amos et al., 2013).

In line with the spatial distribution of anthropogenic Hg emissions, observations and model outputs show higher atmospheric Hg^0 concentrations in the northern hemisphere compared to the southern hemisphere (Figure 3) (Horowitz et al., 2017; Sprovieri et al., 2016). Sediment and peat records of anthropogenic Hg deposition also suggest a larger anthropogenic Hg enrichment (by a factor of 4) in the northern hemisphere (C. Li et al., 2020). Complementary data of Hg species in seawater and marine biota are needed to investigate if similar latitudinal enrichment patterns ultimately occur in marine reservoirs.

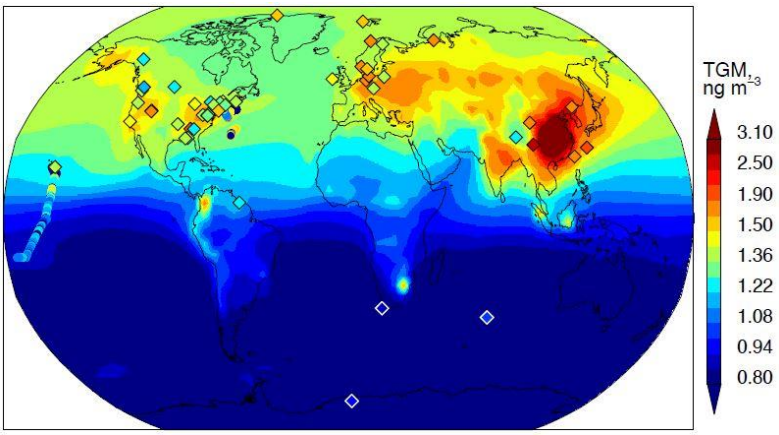

Figure 4. Global distribution of total gaseous mercury (TGM) concentrations in surface air, from Horowitz et al. (2017). GEOS-Chem global model values (background) are annual means for 2009-2011, and observations (symbols) are for 2007-2013.

Marine mercury cycle

First measurements of Hg in the open-ocean were mostly limited to the upper water column (< 1000 m) and by high detection limits of methylated Hg species (Mason et al., 1998; Mason and Fitzgerald, 1990). In the past two decades, further development of clean sampling protocols, and lower detection limits, coupled to the establishment of global-scale oceanographic survey programs (i.e., CLIVAR and GEOTRACES) have improved our understanding of the biogeochemical cycle of Hg in the global ocean. To date, more than 200 high-resolution and full depth profiles of Hg speciation are available, covering the Arctic, Atlantic, Pacific, and Southern Oceans (Figure 4) (Bowman et al., 2020b).

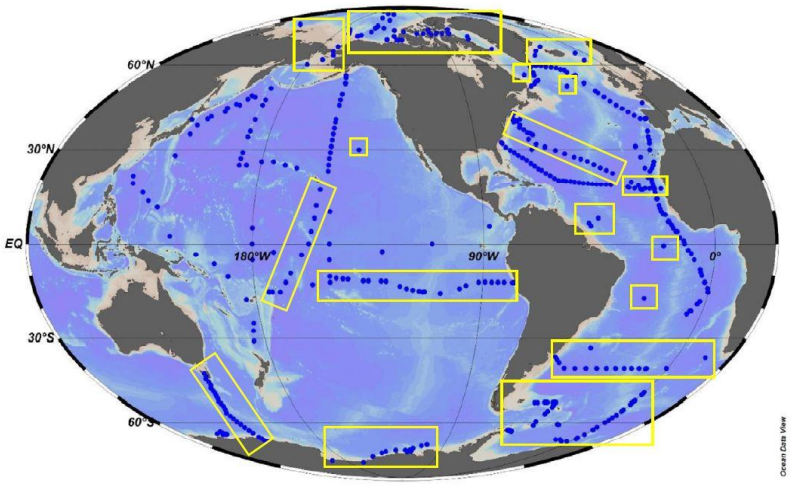

Figure 5. Ocean transects where published mercury data is available, from Bowman et al. (2020). Yellow boxes indicate stations where full depth mercury speciation is available.

Mercury sources and sinks in the ocean

Sources of Hg to the open ocean commonly include inputs from direct atmospheric deposition, ocean margins (i.e., rivers and estuarine), groundwater, benthic sediments, and hydrothermal vents. Direct atmospheric dry and wet deposition of Hg^{2+} is largely recognized by measurements and models to be the primary source of Hg, with global inputs to the ocean ranging from 14 to 29 $Mmol.y^{-1}$ over the past decades (Figure 1) (Mason et al., 2012). Nevertheless, a recent study using the stable isotope composition of total Hg in seawater and marine biota indicated that global atmospheric Hg^0 uptake by the ocean is equally important as Hg^{2+} total deposition (Jiskra et al., 2021). Mercury contribution from other sources to the open ocean are much smaller on a global basis. Rivers can deliver significant amounts of Hg to coastal oceans, possibly at similar levels than atmospheric deposition (Amos et al., 2014; Sunderland and Mason, 2007; Zhang et al., 2015). Because of their large amount of precipitations, low latitudes coastal regions (30°N – 30°S) are estimated to receive the largest river discharges, and high flow events, which are becoming more common with climate change, are expected to be responsible for larger Hg export to coastal oceans in the coming decades (Liu et al., 2021). At the global scale, only 6 % of river Hg is estimated to reach the open ocean (Figure 1) (Zhang et al., 2014), and riverine inputs are therefore often considered negligible in global Hg models. Submarine groundwater discharge and input from deep-sea hydrothermal vents are estimated to deliver even less Hg to the global open ocean (Lamborg et al., 2006; Mason et al., 2012).

Re-emission to the atmosphere is the major sink for ocean Hg (Figure 1), and on a global basis, it concerns most (~ 70 %) of Hg deposited in marine ecosystems (Mason et al., 2012). Hg^{2+} can be photo-chemically and microbially reduced to Hg^0, often resulting in oversaturation of surface waters and evasion of Hg^0 to the atmosphere. The large air-sea exchange of Hg^0 depends on a complex interplay of parameters, including aqueous Hg^{2+} reduction and oxidation Hg^0 rates, and wind physics (e.g., speed, current) (Zhang et al., 2019). Today, there is still a need to better constrain these parameters in global Hg models if we want to correctly predict how Hg levels in the ocean will respond to changes in Hg emissions to air, and to climate change (Outridge et al., 2018). Vertical export of Hg bound to particles or organic ligands and removal to sediment is a long-term sink for Hg in ocean (Figure 1) (Amos et al., 2013; Lamborg et al., 2016). Mechanisms behind particulate scavenging and

burial remain poorly understood but likely include sorption to various non-living phases of particles and cell surfaces, and uptake into living organisms. Methylmercury accumulation through marine food webs is another sink for Hg in oceans. Mercury removal through fisheries is another sink for Hg in oceans, although it is often considered modest compared to other global ocean loss estimates. It is suspected to have increased over time, as a result of increasing fishing pressure, especially on upper-trophic-level organisms, and was estimated over 13 metric tonnes in 2014 (Lavoie et al., 2018).

Mercury speciation and distribution in the water column

Mercury speciation in seawater includes different chemical forms: Hg^{2+} and monomethyl-Hg, as well as Hg^0 and dimethyl-Hg, both dissolved gaseous species. Each of these species reflect an equilibrium governed by a combination of biotic and abiotic mechanisms involving methylation/demethylation, and oxidation/reduction (Figure 5) (Fitzgerald et al., 2007) coupled with transfer process among the main marine reservoirs., yet a full understanding of all these reactions is still lacking.

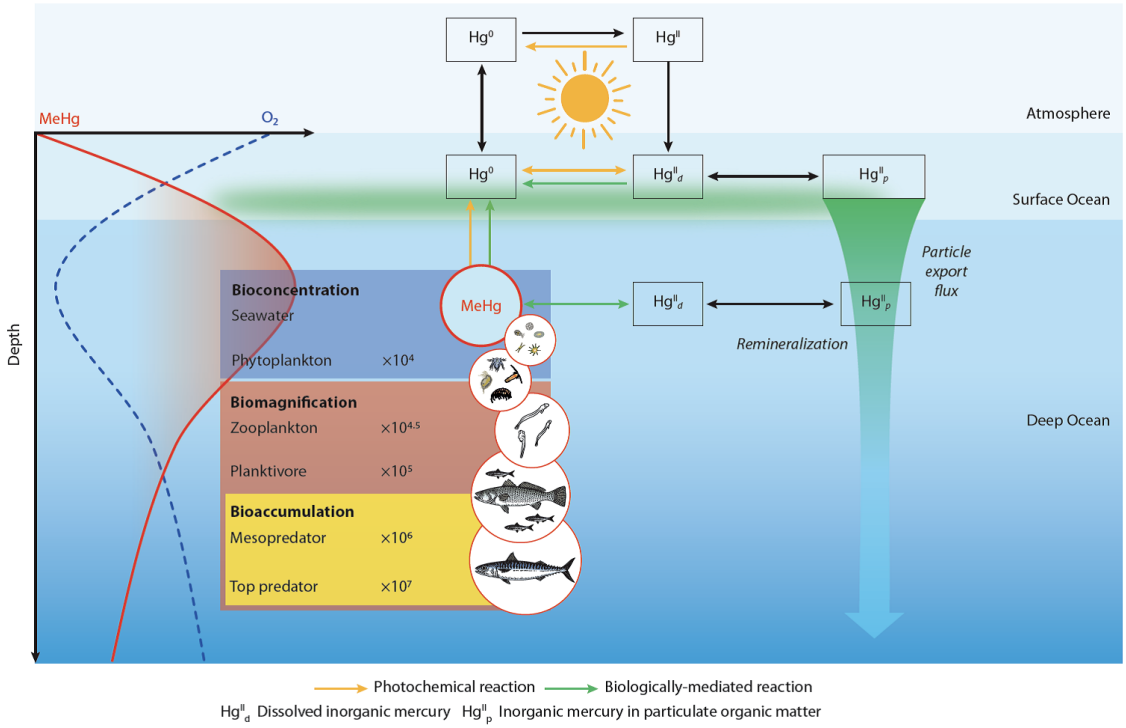

Figure 6. Simplified schematic of marine mercury cycle, from AMAP and UN Environment (2019)

Total Hg concentrations in seawater has both scavenged- and nutrient-type vertical distribution, mainly controlled by external sources of Hg to the surface ocean and scavenging by biomass and inorganic particles. In the Atlantic and Pacific Oceans, total Hg concentrations in the thermocline waters (150 – 1000 m) exceed those of the upper water column (< 150 m) (Bowman et al., 2016, 2015; Hammerschmidt and Bowman, 2012), exhibiting opposite patterns than those in the Arctic and Southern Oceans (Agather et al., 2019; Cossa et al., 2011). Total Hg concentrations generally peak at ~ 1 pM in the upper 1000 m of the global ocean, with lowest values (< 1 pM) measured in the central and eastern Pacific, and the Labrador Sea (Bowman et al., 2020b). Anthropogenic Hg emissions

are thought to have tripled the levels of total Hg in the thermocline waters (100 – 1,000 m) of the global ocean relative to deeper older waters (Lamborg et al., 2014), yet still unclear is how those anthropogenic Hg inputs are converted into MeHg in oceans.

Since the first open ocean measurements in the late 1980s, MeHg concentrations have been thought to be low in surface waters, maxima in the intermediate layers, especially in low-oxygen regions, and low to relatively constant in deeper waters (> 1000 m). This general vertical distribution was consistent with *in situ* formation of MeHg in relation to the decomposition of organic matter. Yet, vertical Hg profiles across the global ocean now reveal three important depth regions for MeHg (Figure 6): i) surface ocean (0 – 2 m), ii) subsurface chlorophyll maximum (< 150 m), and iii) thermocline waters depleted in oxygen (150 – 1000 m) (Bowman et al., 2020b). In surface waters, although (photo-)degradation and gas evasion remove monomethyl-Hg and dimethyl-Hg, respectively, MeHg concentrations represent 3 – 34 % of total Hg in the global ocean. Peaks of MeHg in subsurface chlorophyll maximum (i.e., in the oxygenated euphotic zone where optimal light and nutrient conditions fuel phytoplankton growth) were first measured in the Mediterranean Sea where they were strongly related to phytoplankton dynamics (Heimbürger et al., 2010), and were found more recently in vertical profiles from the Atlantic and Pacific Oceans (Bowman et al., 2015, 2016). Though less common than maxima in thermocline waters, these MeHg peaks likely result from i) either *in situ* Hg^{2+} methylation or the import of MeHg from sinking particulate matter, and ii) loss of methylated Hg in surface and deep waters, through net demethylation and/or export (see next section on Hg methylation and demethylation). Peaks of MeHg in oxygen thermocline waters are supposed to result from heterotrophic microorganisms respiring sinking organic matter (Bowman et al., 2015; Cossa et al., 2011; Hammerschmidt and Bowman, 2012; Sunderland et al., 2009). In the global ocean, MeHg represent 4 – 19 % of total Hg in subsurface waters (< 150 m), and 3 – 41% in thermocline waters (Bowman et al., 2020b), but with spatial heterogeneity among ocean basins. In the Atlantic Ocean in particular, the northern hemisphere shows higher proportion of MeHg than in the southern hemisphere, in both subsurface and thermocline waters (Bowman et al., 2015; Bratkič et al., 2016). Conversely, the Pacific Ocean is characterized by less spatial variability, with MeHg representing ~ 20% of total Hg in subsurface and thermocline waters, except in the upwelling stations (Bowman et al., 2016; Hammerschmidt and Bowman, 2012; Munson et al., 2015; Sunderland et al., 2009). Coastal and equatorial upwelling regions in the Pacific indeed exhibit higher proportions of MeHg compared to adjacent stations, with MeHg peaks found in the oxycline (< 100 m), where decreasing oxygen concentrations are driven by intense heterotrophic microbial respiration (Figure 6). However, in the Mauritanian upwelling region in the north Atlantic Ocean, such MeHg patterns are not observed (Bowman et al., 2015).

Elemental gaseous Hg^0 has a nutrient-type profile in the ocean, resulting from its evasion to the atmosphere from surface waters, its production in subsurface waters (by (photo)chemical Hg^{2+} reduction and monomethyl-Hg degradation), and its accumulation at depth (Lee and Fisher, 2019; Monperrus et al., 2007).

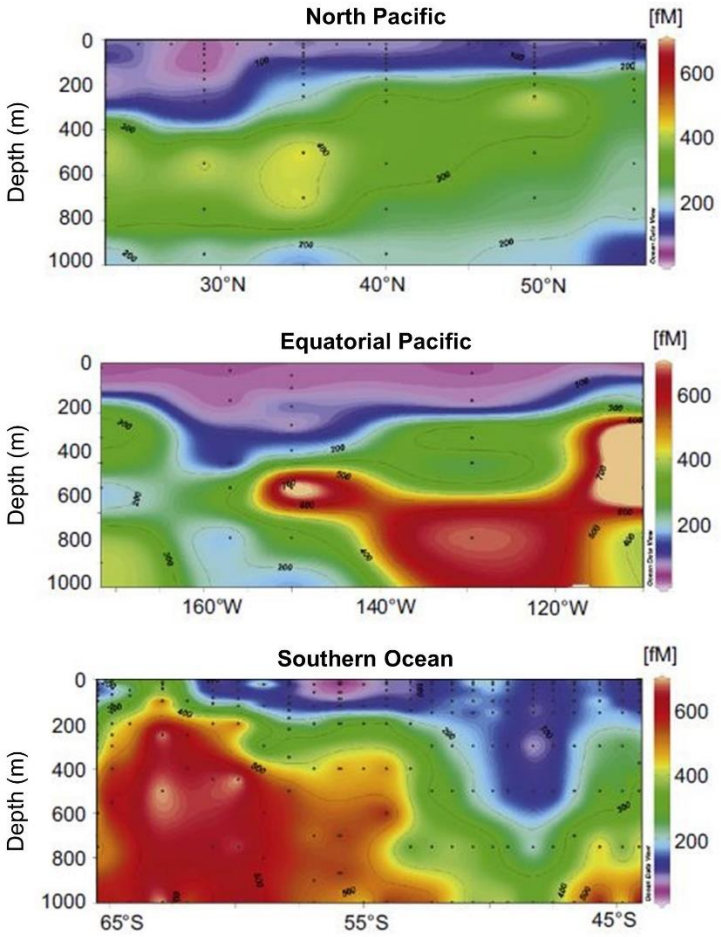

Figure 7. Vertical profiles of methylmercury (monomethyl-mercury and dimethyl-mercury) concentrations in various ocean basins, from Mason et al. (2012). Data used to produce these profiles: equatorial Pacific (Mason and Fitzgerald, 1993), north Pacific (Sunderland et al., 2009), and southern Ocean (Cossa et al., 2011).

The comparison of Hg concentrations, vertical profiles, and basin-wide distribution from various oceanic datasets relies on the assumption that different collection and analytical methods accurately quantify each chemical form of Hg. Inter-calibration exercises performed within the international GEOTRACES program (geotraces.org) showed improvements in the accuracy of total Hg measurements at low concentrations in seawater. Yet, because of low ambient MeHg concentrations in the ocean, and a variety of analytical methods, inter-comparison of open-ocean MeHg is still complicated. Moreover, a continued effort within the international community on obtaining accurate Hg profiles on a large spatial scale and at a high resolution remains needed for modelling Hg in the global ocean. Measurements in the Indian Ocean in particular are still lacking, while important for better understanding Hg distribution and speciation in oligotrophic conditions. Development of temporal datasets is also crucial to examine the seasonality of Hg methylation, and to predict responses of seawater MeHg concentrations to both changes in anthropogenic Hg releases to the environment, and climate change.

Mercury methylation and demethylation in oceans

Mercury methylation and demethylation are key reactions regulating the Hg cycle in marine environment as they determine the fate and net production of MeHg in the water column and constrain its bioavailability in marine food webs.

Mercury methylation, i.e., production of monomethyl-Hg and dimethyl-Hg from Hg^{2+}, occurs simultaneously in seawater through biological activities and abiotic pathways. Biotic methylation is commonly recognized as the main source of monomethyl-Hg in oceans, and was first attributed to the activity of sulfate-reducing bacteria in anoxic sediments (Compeau and Bartha, 1985). More recently, iron-reducing bacteria and methanogens have also been identified as Hg methylators in anoxic environments (Fleming et al., 2006; Hamelin et al., 2011). Monomethyl-Hg in offshore marine fish was then first hypothesized to originate via physical advection and bioavection mechanisms from benthic sediments (Chen et al., 2008). The biotic methylation involves cellular uptake of Hg^{2+} by active transport, methylation of Hg^{2+} in the cytosol, and export from the cell (Schaefer et al., 2011), and the methylation process itself is supposed to occur through an enzymatic pathway, mainly controlled by the *hgcAB* gene cluster (Parks et al., 2013). This gene cluster was found in the genome of diverse organisms, primarily in sulfato- and iron-reducing bacteria, and methanogenic archae (Gilmour et al., 2013; Parks et al., 2013), as well as in metagenomes from seawater, marine sediments, soils, and animal microbiota (Podar et al., 2015). More recently, Villar et al. (2020) found high abundance and expression of the *hgcAB* genes across all ocean basins, mainly associated to the microaerophilic bacteria *Nitrospina* (Figure 7), highlighting metagenomic and metatranscriptomic evidence that the genetic potential for microbial methylmercury production is widespread in oxic seawater. This agrees with geochemical hints pointing to *in situ* Hg^{2+} methylation in the open water column in oxygenated surface waters (Heimbürger et al., 2010; Monperrus et al., 2007). This biotic methylation pathway is likely to be related to the remineralisation of sinking particulate organic matter (Figure 5), which is supposed to provide inorganic Hg as the substratum while stimulating the activity of bacteria (Cossa et al., 2009; Hammerschmidt and Bowman, 2012; Heimbürger et al., 2010; Sunderland et al., 2009). Further studies remain needed to test the contribution of *Nitrospina* to Hg methylation and to determine the physiochemical parameters controlling their methylation activity levels. Other avenues of research also need to be explored to better understand biotic methylation: i) possible *hgcAB* methylation occurring in low-oxygen microenvironments, like sinking particles and aggregates (Bianchi et al., 2018; Ortiz et al., 2015), and ii) other methylation pathways that do not involve *hgcAB*. Abiotic methylation, first reported in the 1990s, has long been considered as a minor mechanism compared to biotic methylation, being restricted to particular environmental conditions (Celo et al., 2006). However, the use of enriched Hg isotopes ($^{202}Hg^{2+}$) has demonstrated these abiotic mechanisms in the Pacific and Arctic Oceans, likely involving Hg^{2+} methylation by dead bacterial cells, or extracellular methylation (Lehnherr et al., 2011; Munson et al., 2018).

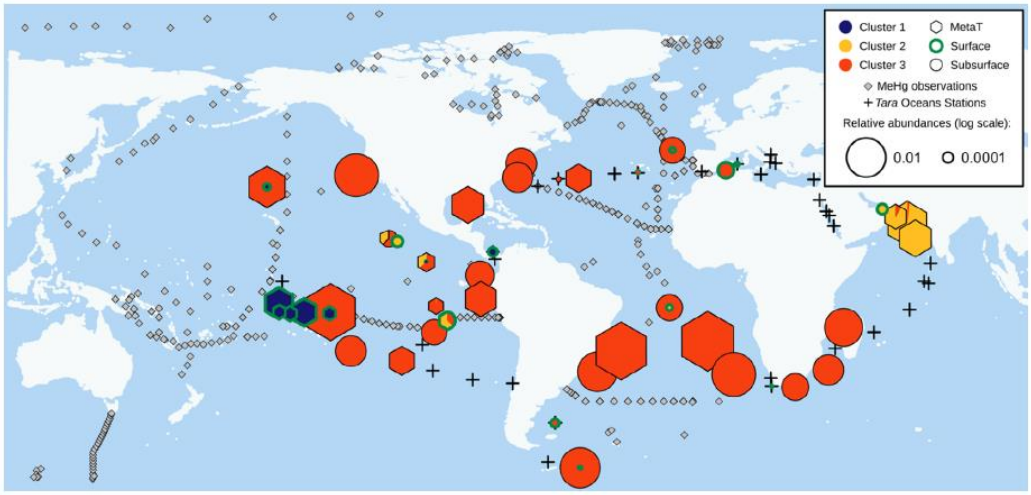

Figure 8. Biogeography of *hgcAB* genes in the global ocean (coloured symbols), from Villar et al. *(*2020*)*. Circles show stations were *hgcAB* genes were found in metagenomes only, hexagons indicate stations where *hgcAB* transcripts were also found in metatranscriptomes, and black crosses represent stations without detected *hgcAB* genes. Symbol size is proportional to the cumulated *hgcAB* homologue genes abundances. The pie charts indicate the cluster attribution of marine bacteria: cluster 1 (blue) = *Desulfobacterales*, *Clostridiales* and *Desulfovibrionales;* cluster 2 (yellow) = *Syntrophobacterales* and *Chloroflexi*; and cluster 3 (red) = *Nitrospina*.

Similarly, demethylation, i.e., dimethyl-Hg degradation into monomethyl-Hg, and subsequently Hg^{2+}, can be induced by biotic and abiotic mechanisms, and remains overall poorly understood, so as the stability of MeHg in the oceanic water column. Photoinduced MeHg demethylation (i.e., degradation by sunlight) is the main abiotic mechanism in aquatic environments. While relatively rapid in freshwater lakes, it is much slower in marine waters, likely due to stable MeHg-chloride complexes, the dominant form of MeHg in seawater (compared to more degradable sulfur-containing ligands of MeHg in freshwater) (Zhang and Hsu-Kim, 2010). Biotic MeHg degradation includes two types of reactions: reductive demethylation and oxidative demethylation. Reductive demethylation of monomethyl-Hg is carried out by bacteria possessing the *mer* operon. Monomethyl-Hg is first demethylated by an enzyme (organomercurial lyase, *merB*) into Hg^{2+}, which is in turn degraded into Hg^0 inside the bacterial cell by another enzyme (mercuric reductase enzyme, *merA*), and finally excreted from the cell (Boyd and Barkay, 2012). Expression of *merA* is supposed to occur in high Hg concentrations (> 50 pM) conditions (Morel et al., 1998), yet *mer* genes have been recently identified in the Arctic at Hg concentrations < 1 pM (Bowman et al., 2020a). Oxidative demethylation, although poorly understood, is suspected to occur under certain conditions, as a by-product of sulfate-reducing bacteria metabolism, with MeHg being degraded into Hg^{2+}, CO_2, and a small amount of CH_4 (Barkay et al., 2003).

To date, the mechanisms of methylation and demethylation in marine environments remain largely poorly understood, although some recent advances have been possible, especially with the use of enriched Hg isotopes. Also important yet poorly documented are the climate-induced changes of MeHg formation, especially the impacts of changes in ocean circulation, productivity, and growth of oxygen minimum zones (Mason et al., 2012). Understanding the net balance between these two mechanisms is fundamental to predict the amount of bioavailable MeHg at the base of marine food webs, and by extension in upper trophic levels.

Bioconcentration, bioaccumulation and biomagnification of methylmercury in marine trophic webs

Depending on its chemical form, Hg in seawater can enter marine food webs (i.e., bioconcentration), accumulate in organisms' tissues over time (i.e., bioaccumulation), and build up through trophic levels, resulting in high Hg concentrations in marine top predators (i.e., biomagnification).

Mercury incorporation in marine food webs

Microorganisms like bacteria, phytoplankton and protozoan are the primary entrance access of Hg in marine food webs. Mercury incorporation at the base of marine food webs differs among the chemical species present in seawater. While Hg^0 and dimethyl-Hg are not reactive and diffuse inside and outside microorganisms (Morel et al., 1998), MeHg and Hg^{2+} enter marine food webs by passive uptake (i.e., diffusion) of uncharged and lipophilic chloride complexes (e.g., $HgCl_2$, CH_3HgCl, and organic complexes) across the cell of phytoplankton (Kim et al., 2014; Lee and Fisher, 2016; Mason et al., 1996). There is also evidence for active uptake or facilitated mechanisms via the binding to cell surface ligands and internalization (Pickhardt and Fisher, 2007; Schaefer et al., 2014), which could explain MeHg uptake into algae at low ambient water Hg concentrations (Gosnell et al., 2021). Mercury concentrations in phytoplankton can be 100 000 times higher than in ambient water, which represents the largest Hg increase in marine food webs (Schartup et al., 2018). Laboratory studies with multiple marine phytoplankton species demonstrated that cell surface area to volume ratios provide a good proxy for MeHg uptake (Figure 8A), resulting in differential uptake of MeHg and inorganic Hg among algae species (Gosnell et al., 2021; Kim et al., 2014; Lee and Fisher, 2016). Conversely, high concentrations of dissolved organic matter may inhibit phytoplankton MeHg uptake by forming large complexes with MeHg in seawater that reduce transport across the cell membrane (Figure 8B) (Luengen et al., 2012; Schartup et al., 2015). Given these relationships, differences of ecosystem functioning are likely to impact microorganisms MeHg uptake. In less productive ecosystems, where smaller phytoplankton with greater surface area to volume ratio are more abundant, nutrient uptake may be more efficient, which is supposed to enhance MeHg uptake (Lee and Fisher, 2016). Conversely, higher nutrient status can lead to a greater abundance of larger cells, reducing nutrient uptake and potentially also MeHg uptake (Hein et al., 1995). With climate change and anthropogenic activities, terrestrial discharges of both nutrients and dissolved organic matter are increasing, inducing shifts in nutrient status and productivity in coastal marine ecosystems. Modelling approaches suggest that these shifts could lead to a decline in phytoplankton MeHg concentrations (Driscoll et al., 2012; Schartup et al., 2018), yet this change may be dampened following trophic transfer to zooplankton due to the competing influences of growth dilution and increased dietary ingestion as zooplankton body sized increases (Schartup et al., 2015).

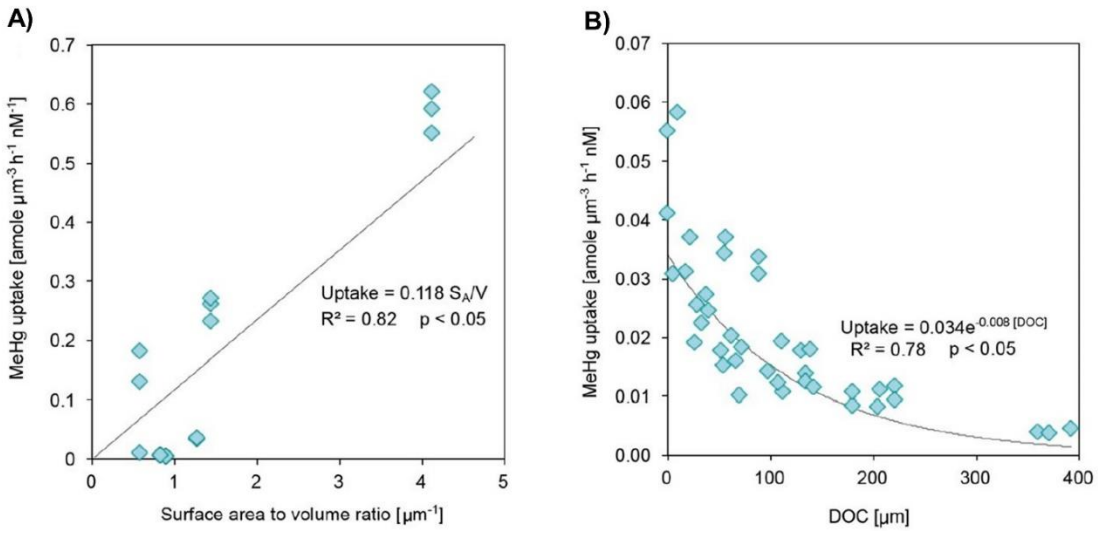

Figure 9. Factors affecting methylmercury (MeHg) uptake by phytoplankton, from Schartup et al. (2018). Relationships between phytoplankton MeHg uptake rate and **A)** cell surface area to volume ratios (based on experimental data reported by Lee and Fisher (2016)), and **B)** dissolved organic carbon (DOC) concentrations (based on data from Luengen et al. (2012)), respectively.

Bioaccumulation and biomagnification of methylmercury

Once entered the base of marine food webs, Hg biomagnifies along trophic levels, with phytoplankton dietary intake by zooplankton being the dominant pathway compared to smaller direct uptake from seawater (10 – 20 %) (Lee and Fisher, 2017). While both MeHg and inorganic Hg accumulate in primary producers, only MeHg biomagnifies in upper trophic levels, mainly because of differential affinity to thiol groups (i.e., sulfhydryl groups, -SH). In phytoplankton cells, inorganic Hg is principally sequestered by thiol groups in the membrane, while MeHg, being less reactive, accumulates in cell cytoplasm. During phytoplankton grazing, the cell membrane is less assimilated than the inner components (Le Faucheur et al., 2014; Morel et al., 1998), resulting in efficient assimilation of MeHg in zooplankton (Mason et al., 1996). Lower variability of MeHg concentrations were found in zooplankton than in phytoplankton, likely due to the competing processes between growth dilution of Hg, and consumption of greater quantities of MeHg enriched prey at larger sizes (Schartup et al., 2018). At each trophic level, MeHg is efficiently biomagnified mainly through dietary intake, leading to higher MeHg concentrations and higher ratio of MeHg to total Hg concentrations in a consumer relative to its prey.

At the individual scale, MeHg also accumulates through time, as it is more efficiently assimilated than excreted, leading to higher MeHg concentrations in older/larger marine organisms. Although the distribution kinetics of Hg (i.e., rates of transfer between tissues) may vary among marine fish species, experimental studies and pharmacokinetic models developed on *Cyprinodon variegatus* and *Gadus morhus* give first insights on internal Hg distribution (Amlund et al., 2007; Leaner and Mason, 2004). Once ingested, MeHg was taken up into the intestinal tissue within hours, followed by a slow release to blood and the other organs, the bloodstream being considered as the conduit linking of MeHg exchange between the different organs (Figure 9). Exchange between blood and the viscera organs was then relatively slow, with maximum MeHg uptake in the gill and liver occurring at 1.5 day following dietary exposure. Finally, with a substantial lag time, the majority of MeHg was transported

to the rest of the body (i.e., muscle tissues) where MeHg bioaccumulated in the protein fraction of the muscle, mostly by forming complexes with the amino acid cysteine.

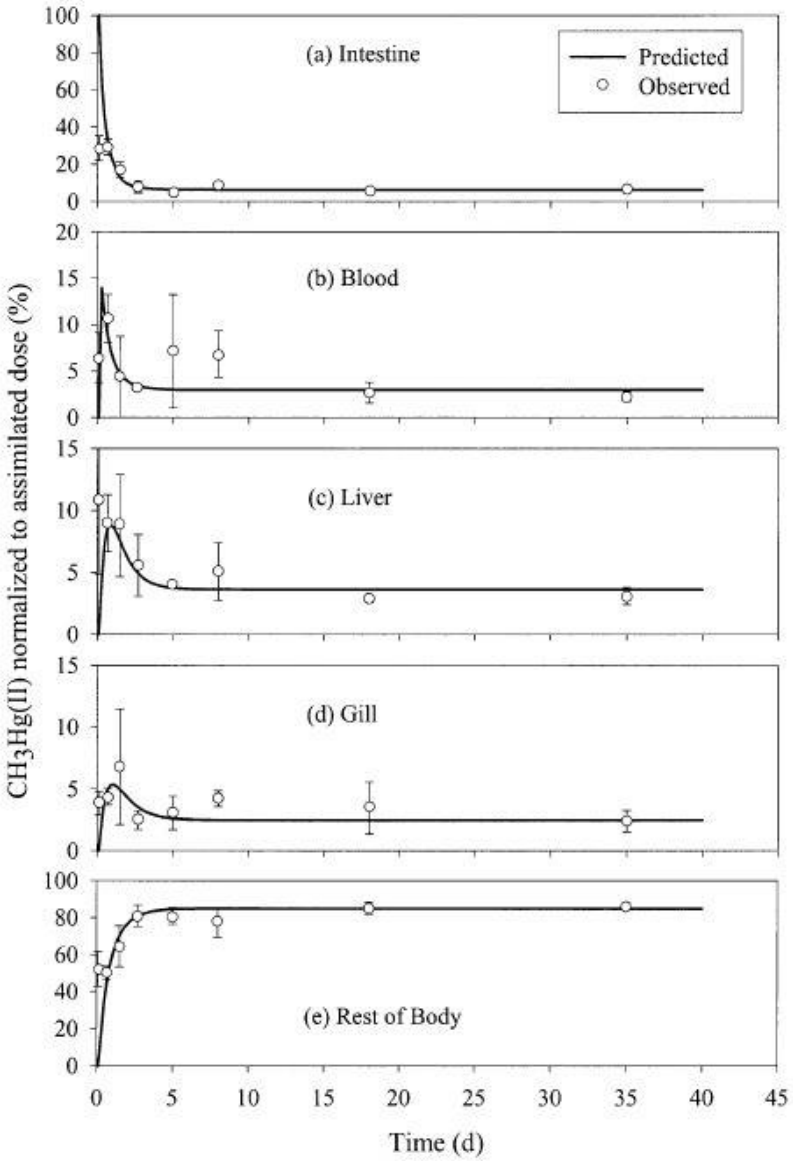

Figure 10. Distribution kinetics of methylmercury in the different organs of *Cyprinodon variegatus* after a single dose of methylmercury-spiked flake food, from Leaner et Mason (2004).

Most of the experimental studies on Hg accumulation explored only dietary aspects as they are considered the main pathway for Hg accumulation in organisms. Yet, a waterborne MeHg uptake through gills has been suggested as a potential complementary source of MeHg for different marine species (Boddington et al., 1979; Cossa et al., 1994; Hall et al., 1997). In particular, Wang et al. (2011) showed that fish MeHg direct uptake was controlled by swimming speed and respiration rates. This additional MeHg uptake could modify our understanding of the real exposure and kinetic distribution of MeHg in marine species, especially in fast swimming fishes like tunas, that display physiological adaptations of their oxygen transport system to support high metabolic performance.

Mercury and human health

Most humans are exposed to low levels of Hg, which are not likely to cause adverse health effects. Nevertheless, because it can induce severe toxic effects, including cardiovascular, reproductive, and developmental toxicity, neurotoxicity and immunotoxicity (Genchi et al., 2017), Hg is one of the top ten chemicals or groups of chemicals of major public health concern according to World Health Organization. The toxicity degree of Hg mainly relies on the assimilated chemical form, the dose, frequency and route of exposure, and the age or developmental stage of the person exposed (Bernhoft, 2012).

Routes of exposure, toxicokinetics and health effects of inorganic and organic mercury

Humans are exposed to MeHg mainly through their diet, primarily from fish and other marine species as MeHg biomagnifies in marine food webs. Rice consumption has been recognized recently as another important MeHg exposure pathway to humans, not only in Asia (Abeysinghe et al., 2017), but also in the rest of the world, likely because rice-based products have been increasingly popular in recent years globally (Liu et al., 2019). Other significant routes of exposure include inhalation during occupational activities, i.e., activities where Hg compounds are produced, used or incorporated in processes (e.g., chlor-alkali plants, Hg mines, Hg based small-scale gold and silver mining) (Clarkson et al., 2003). Finally, humans can also be exposed to Hg^0 and inorganic Hg by inhalation and dermal contact due to the wild-spread use of Hg-containing products in our daily life, including dental amalgam, thermometer, and skin-lightening creams and soaps (Clarkson et al., 2003; WHO and UNEP Chemicals, 2008).

The toxicokinetics (i.e., absorption, distribution, metabolism, and excretion) and health effects of Hg are highly dependent on the chemical form to which the person has been exposed (Figure 10). In its metallic form (i.e., liquid), Hg^0 is not significantly absorbed or transformed by the human digestive system, and is almost completely excreted by the organism. Conversely, inhalated Hg^0 vapours are actively absorbed by the lungs and transported throughout the body, including the brain, the targeted organ of Hg^0, as Hg^0 crosses easily the blood-brain and placenta barriers. In most tissues, Hg^0 is rapidly oxidised to Hg^{2+} and largely excreted from the body; yet with massive acute exposure to Hg vapour, bronchitis or respiratory failure can develop. Chronic exposure to significant doses of Hg^0 vapour usually produces neurological dysfunction, with nonspecific symptoms like weakness or fatigue at low levels, and mercurial tremor or erethism (e.g., behavioural or personal changes, loss of memory, insomnia) at high levels. These symptoms may regress with cessation of exposure, but persistent neurological symptoms are common (Bernhoft, 2012; Langford and Ferner, 1999). Inorganic Hg, either ingested or transformed, have low lipophilicity and therefore does not cross the blood-brain barrier efficiently, and rather accumulates in the kidney. Acute poisoning with Hg salts can lead to gastrointestinal and renal damage, and in extreme cases to death. Chronic poisoning with Hg salts is rare, usually also involving concomitant occupational exposure to Hg^0 vapour (Bernhoft, 2012; Langford and Ferner, 1999). Methylmercury, once ingested, is rapidly and extensively absorbed through the gastrointestinal tract, before being distributed throughout the body, and passing the blood-brain and placenta barriers, thanks to its great affinity to thiol groups like cysteine, as explained before in fish tissues. The binding between Hg and thiol groups can also cause disruption of key enzymatic processes and subsequent cell dysfunction, which may disrupt neurological processes

(Bjørklund et al., 2017). Methylmercury mainly affects the nervous system, especially during its developmental stage, and MeHg prenatal exposure to foetuses is responsible for impaired neurological development, which may lead to neurobehavioral deficits in children, including slowed processing of visual information, decreased IQ, diminished comprehension and perceptual reasoning, and impaired memory (Bernhoft, 2011; Langford and Ferner, 1999; WHO and UNEP Chemicals, 2008). Adult exposure to high MeHg concentrations can also have negative effects on brain function, with symptoms including attention span, fine-motor function, and verbal memory, and can lead as well to blood pressures alterations and abnormal cardiac function (Landrigan et al., 2020).

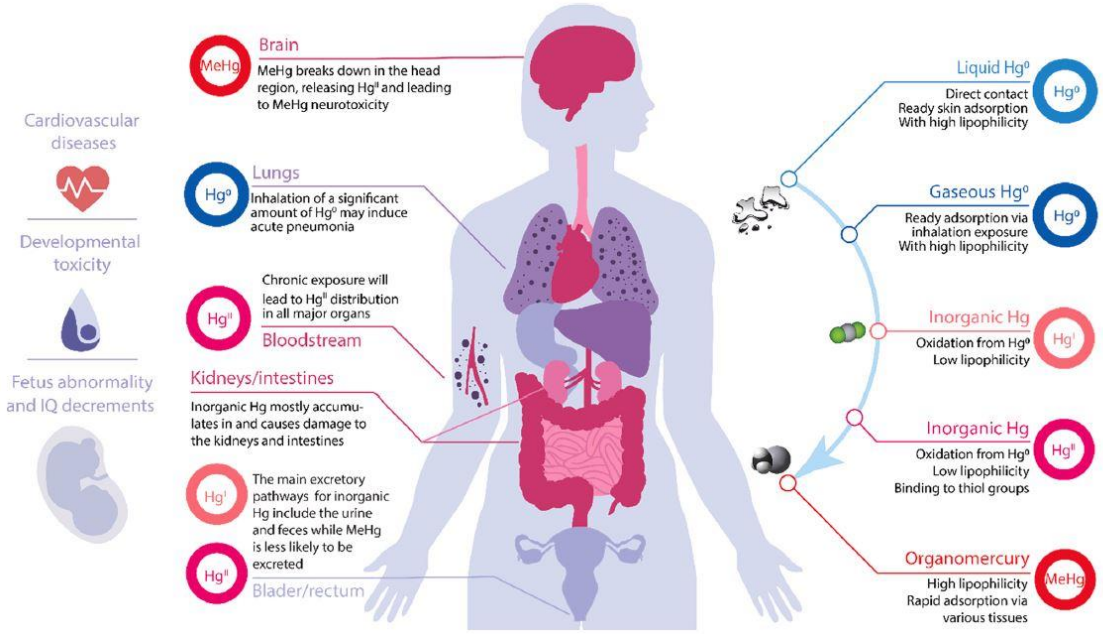

Figure 11. Schematic representation of mercury bioavailability and its toxic effects for human health, from Li et al. (2021)

Susceptible populations, and efforts to reduce human exposure

Given the main exposure sources, the toxicokinetics properties and the health effects of the different Hg chemical forms, two groups of persons are generally more sensitive to Hg exposure. The first group include foetuses, newborn, young children, and teenagers as developing organs (e.g., fetal nervous system) are the most sensitive to Hg toxic effects. In the United Stated for instance, between 317,000 and 637,000 babies are estimated to be born each year with losses of cognitive functions after prenatal exposures to MeHg, as a result of fish consumption with high levels of MeHg by their mothers during pregnancy (Trasande et al., 2005). The second group corresponds to people who are regularly exposed (i.e., chronic exposure) to high Hg levels, like populations relying on subsidence fishing or people occupationally exposed to high levels of Hg, including communities working and living in artisanal and small-scale gold mining areas where Hg levels in miners are on average nearly three times higher of that of the general population (UN Environment, 2019).

Since the Minamata event that resulted in the poisoning of thousands of fish consumers in the 1950s, and the identification of MeHg neurological toxic effects, more than 30 birth cohort studies have been conducted worldwide to better quantify the harmful effects, especially on the developing

brain, associated to Hg exposure in susceptible populations (Figure 11A). These birth cohorts confirm that groups consuming large amounts of seafood (e.g., Seychelles, Spain), freshwater fish (e.g., Brazil), and/or marine mammals (e.g., Faroe Islands, Inuit communities of the Arctic) have the highest Hg exposures. But they highlight as well that cohorts in which a MeHg-associated adverse health effect outcome was observed are not restricted to these highly exposed groups. In the Faroe islands for instance, where the diet is rich in fish and include high-Hg pilot whale meat, 7-year-old-children with higher prenatal Hg exposure had low scores for attention, language skills or memory (Figure 11B) (Grandjean et al., 1997; Weihe et al., 1996). Follow-up of these children to age 22 years indicated that these deficits persist and appear to be permanent (Debes et al., 2016). Conversely, a similar study in Seychelles Islands found no convincing evidence for an association between prenatal exposure and child development in the fish-eating population (Figure 11C) (Davidson et al., 2010). This highlights that much remains to be learned about the physiological responses associated to human Hg exposure, about interactions between Hg and other chemicals and environmental factors including climate change, and about the role of genetic differences among populations in mediating exposure levels.

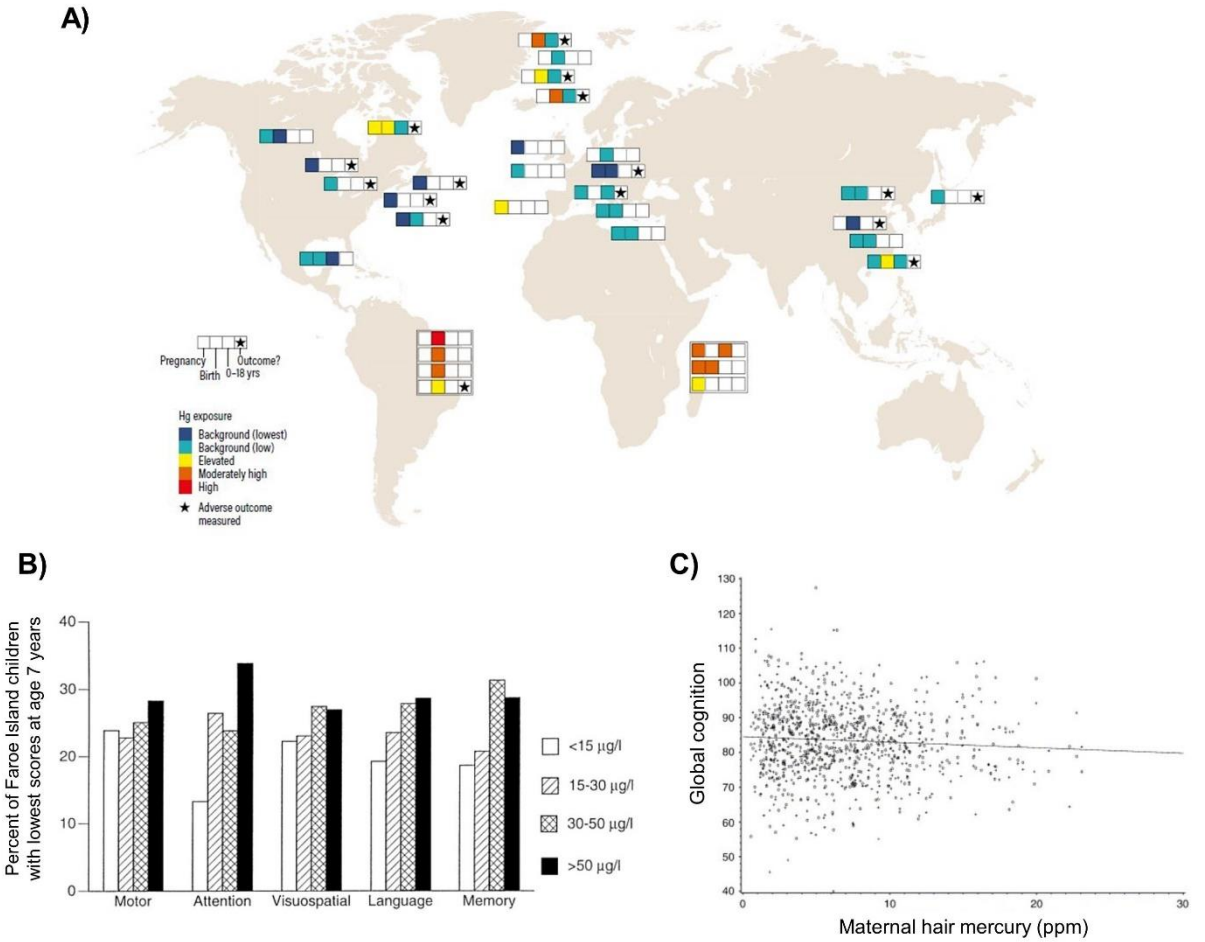

Figure 12. Mercury (Hg) exposure levels and cognition effects. **A)** Location of Hg birth cohort studies showing Hg exposure levels and detection of mercury-associated adverse outcomes, from UN Environment (2019). **B)** Percent of Faroe Island 7-year-old children with lowest scores in relation to their prenatal mercury exposure, from Grandjean et al. (1997). **C)** Global cognition of Seychelles children at 66 months and 107 months in relation to their prenatal total mercury exposure, from Davidson et al. (2006).

In terms of efforts to reduce human exposure, the major highlights of the Minamata Convention include a ban on new Hg mines, the phase-out of existing ones, the phase out and phase down of Hg use in a number of products and processes, as well as control measures on emissions to air and on releases to land and water, and the regulation of the informal sector of artisanal and small-scale gold mining. The Convention also addresses interim storage of Hg and its disposal once it becomes waste, sites contaminated by Hg as well as health issues. In parallel, human exposure to Hg is estimated by the measurement of Hg in human tissues, mostly hair, urine, blood, and umbilical cord blood, through national human biomonitoring programs (UN Environment, 2019). Regarding human exposure associated to fish consumption in particular, food safety guidelines have been defined to reduce risks: Hg concentrations should not exceed 1 $mg.kg^{-1}$ wet weight (ww) in large predatory fishes like tunas, and 0.5 $mg.kg^{-1}$ in other fishes (Codex Alimentarius, 1991). Tolerable daily or weekly intakes (i.e., intakes of Hg estimated to be safe) are also defined for different people categories (e.g., young children, pregnant women, and adults) and different seafood products to take into account the differences of Hg toxicity associated to the dose and frequency of Hg consumed, and the age or developmental stage of the person exposed. Moreover, benefit-risk assessments for different people categories are increasingly used to assess the nutritional value of fishes while considering their Hg content (Sardenne et al., 2020; Wang et al., 2019). Although they are the primary exposure to MeHg, seafood products are indeed also critical to food and nutrition security as they represent an important source of proteins, essential fatty acids, vitamins and minerals, especially for coastal communities (Bell et al., 2015).

Tunas, bio-indicators of mercury contamination in oceans?

Knowing the adverse effects of Hg for both human health and the environment, Hg concentrations have been measured for decades in different biotic and abiotic environmental reservoirs. Most of these monitoring studies are generally restricted to limited temporal and/or spatial scales, and therefore do not allow exploring all the poorly understood mechanisms driving the formation, bioavailability and accumulation of MeHg in the marine environment. Moreover, quantifying Hg concentrations and speciation in seawater remains overall challenging, costly and time-consuming, given the low Hg levels in these reservoirs, and the relatively complex analytical protocols.

To overcome these technical issues and cope with the objectives of the Minamata Convention at protecting human health and the environment from anthropogenic Hg releases, monitoring Hg programs increasingly rely on bio-indicator species, i.e., on organisms that are able to reflect Hg exposure in a given ecosystem, integrating local and global Hg sources over different spatial and temporal scales. In the Arctic for instance, marine mammals and seabirds are commonly used as bio-indicator species of Hg contamination (Masbou et al., 2015a; Point et al., 2011; Renedo, 2018). In the temperate and tropical marine environments, tunas are suspected to be good bio-indicators of Hg contamination in pelagic food webs because of their dietary MeHg accumulation, resulting in relatively high Hg concentrations in their tissues (Chouvelon et al., 2017; Choy et al., 2009; Lee et al., 2016; Nicklisch et al., 2017). Moreover, tunas are highly exploited species, monitored by regional fishery management organizations through several sampling programs, and therefore represent a possible gold mine of biological samples for robust temporal and/or spatial Hg studies.

The term “tuna” includes 15 species of ocean fish, all belonging to the Scombridae family and the *Thunnini* tribe. Among them, seven are of major commercial importance (Figure 12), ranking in terms of global tuna catches as follows: skipjack (*Katsuwonus pelamis*, 57 %), yellowfin (*Thunnus albacares*, 29 %), bigeye (*T. obesus*, 8 %), albacore (*T. alalunga*, 5 %), and bluefin (Atlantic, Pacific, and Southern bluefin combined, 1 %) (ISSF, 2021). Skipjack, yellowfin, bigeye and albacore share common particular biological and ecological characteristics. In particular, i) they are worldwide distributed and not restricted to a particular ocean basin like bluefin tunas, and ii) they display more restricted movement pattern compared to bluefin that are able to undergo transoceanic migrations. Therefore, in this thesis, we have decided to focus on the three tropical species (i.e., bigeye, yellowfin, and skipjack) and albacore exclusively, and unless specified, the term “tuna” will hereafter refer to these four species only.

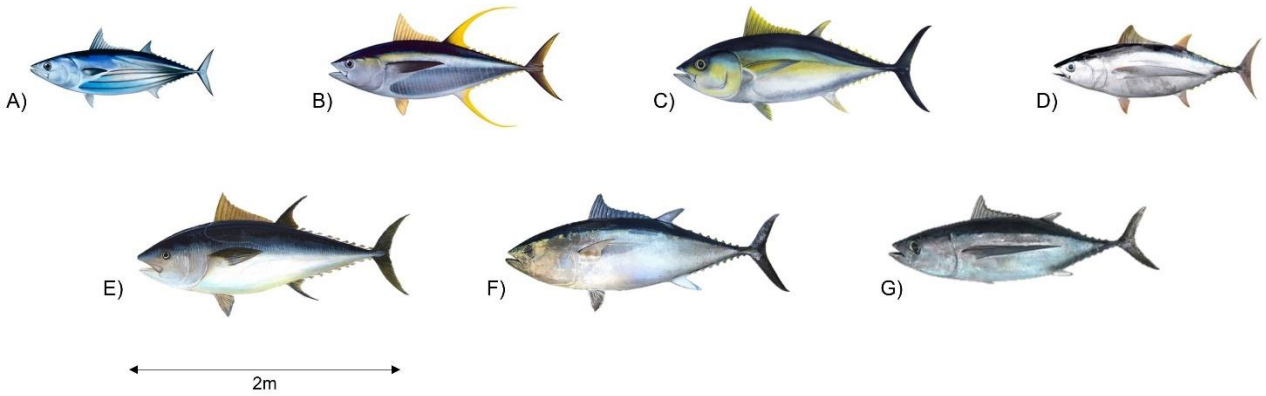

Figure 13. Pictures of the seven tuna species of commercial importance: **A)** skipjack (*K. pelamis*), **B)** yellowfin (*T. albacares*), **C)** bigeye (*T. obesus*), **D)** albacore (*T. alalunga*), **E)** Atlantic bluefin (*T. thynnus*), **F)** Pacific bluefin (*T. orientalis*), and **G)** Southern bluefin (*T. maccoyii*).

Worldwide exploitation and consumption of tunas

Tunas are among the most exploited and consumed seafood worldwide, with skipjack ranking as the third most exploited marine fish worldwide after Alaska pollock (*Gadus chalcogrammus*) and Peruvian anchovy (*Engraulis ringens*) (FAO, 2018). Since the 1950s, global tuna catches have rapidly and steadily increased until the early 2000s, and although they appeared to have stabilized since then, annual catches have kept increasing in recent years, reaching 5.3 million tonnes in 2019 (Figure 13) (ISSF, 2021). The western Pacific Ocean supports the largest tuna fisheries (which represents ~ 52 % of the global tuna catches), followed by the Indian Ocean (21%), the eastern Pacific Ocean (13 %), and the Atlantic Ocean (11 %) (Figure 14) (ISSF, 2021). Tuna exploitation relies on a variety of gears, with surface gears (e.g., purse seine) targeting mainly surface species like skipjack and juveniles of both yellowfin and bigeye, while deeper gears (e.g., longline) allow the catch of adult yellowfin, bigeye and albacore (Figure 14).

In addition to being a major component of the global fishing industry, the seven commercial tuna species are also amongst the world's most valuable fish, with a global commercial value of around US$ 33 billion, i.e., about 24 % of the value of the global seafood industry (Macfadyen, 2016). This benefits to a globalised international industry, but also supports the livelihoods and employment of local communities and fishermen who depend on them (FAO, 2018). Tuna production is driven by two main markets: i) the traditional canned tuna dominated by light meat species like skipjack and yellowfin, being the most consumed form and representing the cheapest protein animal, and ii) sashimi/sushi products, where red meat species like bluefin and bigeye tunas are preferred (FAO, 2018).

In terms of food and nutrition security, they provide a major source of proteins, essential fatty acids, vitamins, and minerals (Di Bella et al., 2015; Sirot et al., 2012). In Pacific Island countries and territories, they have been consequently identified as key food resources for good nutrition to complement declining coastal resources in a context of high levels of diabetes and obesity (Bell et al., 2015; Di Bella et al., 2015).

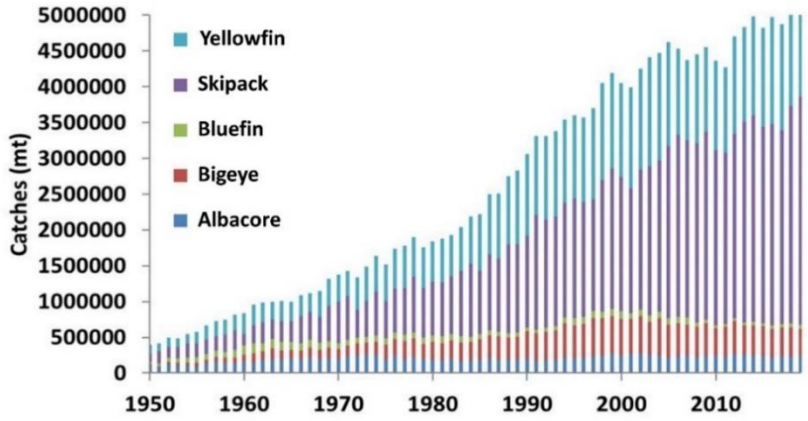

Figure 14. Temporal evolution (1950-2019) of the global tuna catches (tonnes) per commercial species, from ISSF (2021).

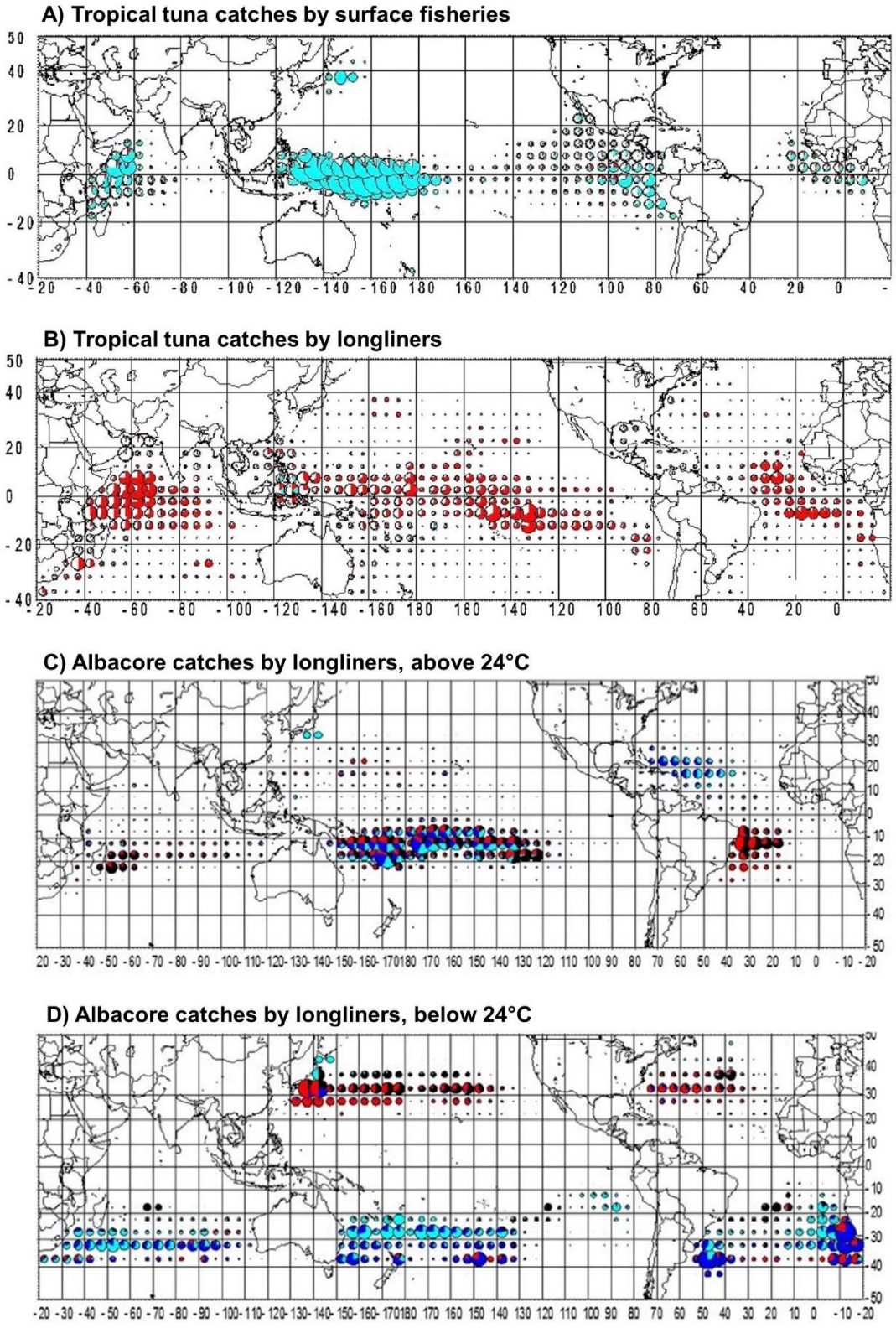

Figure 15. Average distribution of annual tuna catches by industrial fisheries. **A)** and **B)** show tropical tuna catches by surface industrial fisheries (2001 - 2010), and longliners (1997 - 2006), respectively, from Fonteneau and Hallier (2015). Colours refer to tuna species: light blue = skipjack, white = yellowfin, and red = bigeye. **C)** and **D)** show albacore catches by longliners (1960 - 2012), above and below 24°C, respectively, from Nikolic et al. (2017) (N.B. Colours refer to the period of the year). The size of circles is proportional to the tonnage captured.

Tuna biology and ecology across the global ocean

Anatomical, physiological and metabolic characteristics of tunas

Tunas display anatomical and physiological features and adaptations that allow them to optimize the search and capture of prey in the pelagic realm, and to meet their high metabolic demands.

The vast majority of tuna species, including our four study species, are unique among the bony fishes as they possess a counter-current heat exchanger system of retia mirabilia (i.e., a vein-arterial vascular system for heat conservation in muscles, viscera and brain), allowing them to maintain their body temperature above that of surrounding waters (Collette et al., 2001). This regional endothermy along with a fusiform and elongate body shape, complementary metabolisms in red and white muscle, and frequency modulated cardiac output, support a continuous and relatively fast swimming, and reduce thermal barriers to habitat exploration (Graham and Dickson, 2004). Regional endothermy also allows for more intense metabolic activities than in ectotherms as several biological functions are temperature dependent (e.g., energy production, optic nerve efficiency, or digestive enzymes activities) (Carey et al., 1984; Dickson, 1996). Yellowfin and skipjack possess both central and lateral heat exchangers, although lateral retia mirabilia are relatively small. Conversely, bigeye have no central heat exchanger, but a well-developed lateral one, and an additional retia which aims at increasing the temperature of the viscera, brain and eyes. These physiological particularities allow bigeye to explore deeper and cooler waters (Carey et al., 1971; Graham, 1975).

Tunas also display both physical and physiological modifications of the oxygen transport system in order to support their high metabolic performance (Bushnell and Jones, 1994). Their large gill surface area (approximately seven to nine times larger than that of rainbow trout) combined to a thin blood-water barrier, and a small water to branchial capillarity diffusion distance, enable over 50 % O_2 extraction efficiencies (compared to 25 – 33 % in other fishes) (Brill and Bushnell, 2001). Moreover, their large heart, elevated hematocrit (i.e., the proportion of red blood cells in blood), and particular blood affinity to O_2, support high blood O_2 carrying capacities, exceeding those of other fishes (Graham and Dickson, 2004). Species differences in the haemoglobin affinity to O_2 correlate with differences of habitat and behaviour. For instance, the higher O_2 affinity of bigeye, compared to yellowfin and skipjack, along with a large Bohr effect (i.e., release of O_2 from haemoglobin proteins as a result of their affinity to CO_2) improves its resistance to hypoxia and is another reason why this species can experiment deeper dives (Lowe et al., 2000).

Biogeography, horizontal movements, and vertical habitat utilization

Differences of geographic distribution areas and vertical habitats among tuna species mainly rely on species-specific abilities and tolerances to environment characteristics, in particular to oxygen and temperature.

Tropical tunas and albacore are widely distributed over the Pacific, Atlantic, and Indian Oceans, roughly between 50°N and 50°S. Skipjack is mainly found in tropical waters, while yellowfin and bigeye commonly inhabit both subtropical and tropical waters. Albacore is found in temperate and tropical

waters, and display more restricted geographic limits than tropical tunas: in the Indian Ocean for instance, its distribution ranges from 5°N to 40°S, with adults mainly occurring between 5°N and 25°S (ISSF, 2021). Albacore and skipjack are known to also inhabit the Mediterranean waters (Arrizabalaga et al., 2004; Saber et al., 2020), while yellowfin and bigeye are rarely found in this sea (Bielsa et al., 2021; Tsagarakis et al., 2021).

Although classified as highly migratory species, tropical tunas have been shown to display relatively restrictive movements and site fidelity (Anderson et al., 2019; Fonteneau and Hallier, 2015; Richardson et al., 2018; Schaefer et al., 2015; Sibert and Hampton, 2003), compared to other species like Atlantic bluefin tuna that undergo large trans-Atlantic migrations (Block et al., 2005). Similar nitrogen stable isotope patterns between tunas and particulate organic matter also suggest relative residency of tunas at the sub-regional scale (Graham et al., 2010; Houssard et al., 2017). Migration patterns of albacore remain overall less understood because tagging studies are relatively limited for this species compared to tropical tunas (Nikolic et al., 2017). In the Pacific and Atlantic Oceans, the migration of albacore between hemispheres is considered negligible (Arrizabalaga et al., 2004; Lewis, 1990), but some particular migration patterns have been reported within each hemisphere of the Pacific Ocean. In the north Pacific, westward movements of juveniles albacore have been reported (Ichinokawa et al., 2008), while in the western central Pacific, latitudinal migration patterns related to albacore life history are suspected (Farley et al., 2013). In the South African region, albacore populations from the southeast Atlantic and southwest Indian Oceans have been recently hypothesized to be demographic independent (Nikolic et al., 2020).

Regarding vertical distribution, tropical tunas generally prefer relatively warm and stratified waters (Arrizabalaga et al., 2015; Druon et al., 2017; Reygondeau et al., 2012). Skipjack, yellowfin and juvenile bigeye occupy the epipelagic layer, preferentially inhabiting the surface mixed layer above the thermocline (50 – 200 m), and waters with sea surface temperature from 18 to 31°C (Barkley et al., 1978; Pecoraro et al., 2017). Skipjack and yellowfin generally limit their forays to depths where water temperatures are no more than 8°C below surface layer temperatures, and ambient oxygen levels are above 3.5 mL $O_2.L^{-1}$ (Brill et al., 2005). By contrast, adult bigeye are known to occupy depths below the thermocline and to display daily vertical movement patterns presumably to exploit more effectively prey organisms (Fuller et al., 2015; Song et al., 2009). At their maximum depths, bigeye frequently experience prolonged exposure to ambient temperatures around ~ 5°C (that are up to 20°C colder than surface layer temperatures), and oxygen concentrations less than 1.5 mL $O_2.L^{-1}$ (Brill et al., 2005). During the night, bigeye remain near the surface, mostly within the mixed layer where temperatures are uniformly warm; at dawn, they dive below the thermocline, targeting prey organisms of the vertically-migrating deep-scattering layer, and remain throughout the day foraging at depth above the oxygen minimum zone (Schaefer et al., 2009). Despite temperatures preferences restricting tropical tuna vertical distribution, electronic tagging has shown that these species are able to perform deep dives: as deep as 600 m for skipjack (eastern equatorial Pacific, Schaefer and Fuller, 2007), 1,000 m for yellowfin (western Indian, Dagorn et al., 2006), and 1,900 m for bigeye (eastern equatorial Pacific, Schaefer and Fuller, 2010). For albacore, vertical behavior was shown to differ substantially between tropical and temperature latitudes. At tropical latitudes, albacore exhibit a distinct diel vertical pattern occupying shallower warmer waters above the mixed layer depth at night, and deeper cooler waters below the mixed layer depth during the day. By contrast, there was little evidence of a vertical diel pattern for albacore at temperate latitudes, with fish limited to shallower waters almost all of the time (Williams et al., 2015).

Because they depend primarily on species-specific tolerance to temperature and oxygen conditions, these general vertical patterns can vary in space and time with local/regional environmental conditions. In the Pacific Ocean in particular, the depth distribution of bigeye has been shown to display a longitudinal pattern, mainly explained by the thermocline depth and the water column stratification, resulting in tuna depth becoming progressively shallower from west to east (Figure 15) (Abascal et al., 2018). Knowing the effects of El Niño Southern Oscillation on sea surface temperature and the water column stratification in the Pacific Ocean, this longitudinal depth distribution of bigeye could be impacted by strong El Niño/La Niña events (Figure 15). In addition to this natural variability, the deployment of thousands of fish aggregation devices (i.e., man-made floating objects released at sea to attract tunas) by purse seiners is likely to modify the behavior and vertical movement patterns of tropical tunas, with juveniles suspected to occupy shallower habitats when associated to these floating objects (Leroy et al., 2013; Phillips et al., 2017).

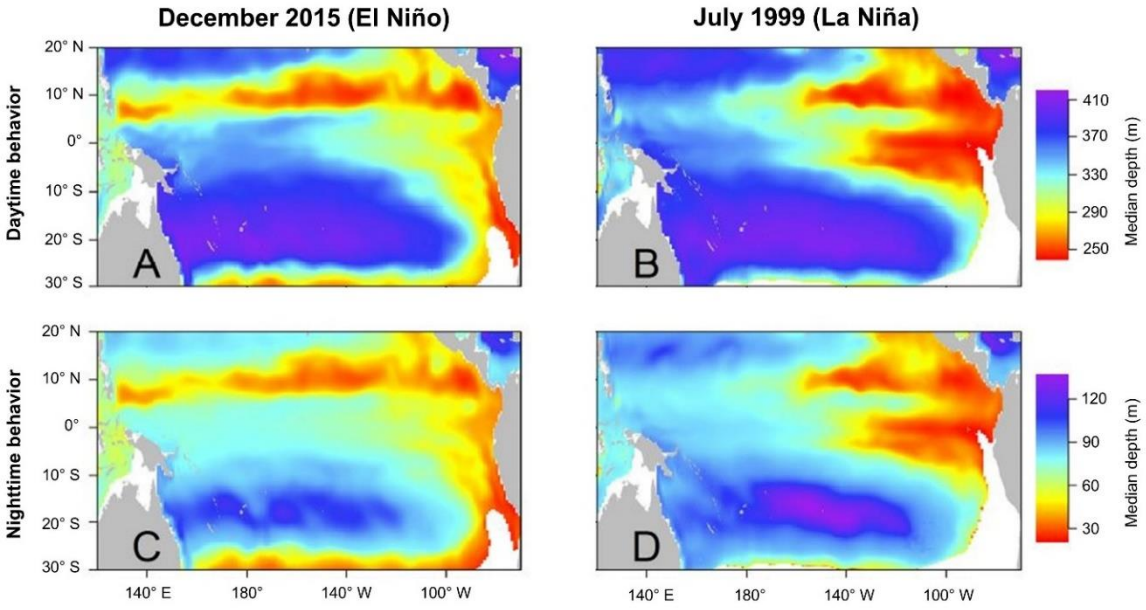

Figure 16. Predicted daytime (**A** and **B**) and nighttime (**C** and **D**) depths of bigeye tuna, under strong El Niño (**A** and **C**), and La Niña (**B** and **D**) conditions, from Abascal et al. (2018).

Trophic ecology

Diet composition, trophic position, and feeding pathways of tropical tunas and albacore have been studied for decades (Graham et al., 2007; Houssard et al., 2017; Lorrain et al., 2020; Ménard et al., 2007; Olson et al., 2014; Pethybridge et al., 2018a; Sardenne et al., 2019b, 2016; Young et al., 2010b), using mainly stomach content analysis, and nitrogen and carbon stable isotopes. Tunas are considered opportunistic predators as they display a generalized foraging strategy characterized by high prey diversity and overall low abundance of all prey types in the diet, which allow them to support elevated energy requirements, and high metabolic activities (Olson et al., 2016). The diets of skipjack, yellowfin, bigeye, and albacore in each of the three oceans consists mainly of a wide range of mid-trophic micronekton species (nearly 300 prey taxa), i.e., fishes, crustaceans, cephalopods, and

gelatinous organisms in the 2-20 cm size range (Figure 16) (Duffy et al., 2017). Tunas feed mainly during daytime, and display general reduced nighttime feeding (Olson et al., 2016).

Figure 17. Diversity of mid-trophic micronekton preys in the region of New Caledonia (southwestern Pacific Ocean) © Elodie Vourey/CPS.

Although tunas are all generalist opportunistic predators, some interspecific diet differences have been identified in the three oceans, mainly related to changes in feeding depth, prey size composition, and feeding time of day. Therefore, the most important prey generally range from epipelagic scombrid for both surface skipjack and yellowfin, to mesopelagic paralepidid fishes for bigeye, and vertically-migrating euphausiid crustaceans for albacore (Duffy et al., 2017). As a result, even if tunas generally share similar functional trophic roles, deeper-foraging species (i.e., bigeye and albacore) have been identified to display a higher trophic position globally, compared to surface species (i.e., skipjack and yellowfin) (Pethybridge et al., 2018a).

In addition to interspecific differences, diet varied spatially at both global and regional scales. In highly productive coastal waters of the eastern Pacific where upwelling occurs, a low prey diversity was evident, while in the central and western Pacific Ocean, characterized by low productivity, a high diversity of micronekton prey was detected (Duffy et al., 2017). These spatial changes of diet are in accordance with the global variability of tuna trophic positions, which were recently found to decline in areas with reduced oxygen at depth, in both the eastern Pacific and northern Atlantic Oceans (Pethybridge et al., 2018a). Regional studies show contrasting results regarding ontogenetic shifts in feeding behaviors and trophic status. Some studies have observed ontogenetic shifts in tuna prey species composition and size distribution, with tunas of all sizes consuming small prey and larger individuals consuming increasingly broad range of prey sizes (Graham et al., 2007; Young et al., 2010b), while others found little impact of individual fish length fish size on tuna trophic position (Houssard et al., 2017; Ménard et al., 2007). At the global scale, individual fish length appeared to be of weaker importance to explain spatial variability of both diet and trophic positions in tunas (Duffy et al., 2017; Pethybridge et al., 2018a).

Temporal diet shifts have been also observed for different species in various ocean basins. In the western Indian Ocean, the main prey of both yellowfin and skipjack shifted from small pelagic anchovy *Engraulis japonicus* in the 1980s to the stomatopod *Natosquilla investigatoris* in the 2000s (Bashmakov et al., 1991; Potier et al., 2002; Roger et al., 1994). Similarly, likely resulting from a reduction in primary production combined to a vertical expansion of the oxygen minimum zone in the central and eastern tropical Pacific, yellowfin diet patterns had changed from primarily larger epipelagic fishes in the 1990s to a diverse array of smaller mesopelagic species and a crustacean in the 2000s (Olson et al., 2014). Despite these temporal changes in diet in some particular ocean basins, trophic position of tropical tunas and albacore remained overall stable over the last decades, suggesting that broad-scaled ecosystem functions (e.g., food chain length) have not changed (Pethybridge et al., 2018a).

General life history traits

Compared to other species, tunas all exhibit rapid growth and achieve large body sizes. Although the methods for estimating growth parameters do not always converge, a comparison of their growth functions (i.e., the change of length as a function of age) reveals that tunas have evolved different growth strategies (Table 1) (Murua et al., 2017). They attain asymptotic sizes (i.e., the mean length tunas would reach if they were to grow for an infinitely long period, L_∞) from 60 cm fork length (FL) for skipjack, to 300 cm FL for bigeye, and reach L_∞ at different rates (*K*) ranging from 0.95 y^{-1} (skipjack) to values < 0.1 y^{-1} (bigeye). Skipjack, followed by yellowfin, is considered the fastest growing tuna species. Tropical tunas from both the Pacific and Atlantic Oceans, and albacore from the three oceans, are thought to display simple von Bertalanffy growth models, while tropical tunas from the Indian Ocean are likely to exhibit more complex two-stanza models (i.e., a significant change in growth rate between juveniles and adults) (Eveson et al., 2015; Murua et al., 2017). Associated to different growth patterns, tunas also display different strategies of reproduction, with skipjack being mature at shorter lengths than other species (Table 1).

Table 1. Non exhaustive list of life history traits of bigeye, yellowfin, skipjack and albacore tunas in the Atlantic, Indian, and Pacific Oceans. Available growth parameters per tuna species and ocean were obtained in Murua et al. (2017), while reproduction parameters were obtained in Juan-Jordá et al. (2016). L_∞ = asymptotic length, K = growth rate coefficient, L_{50} and a_{50} = length and age at which 50 % of the population reaches maturity, respectively.

Species	Ocean	Maximum observed length (cm)	Maximum observed age (y)	Range of L_∞ (cm)	Range of *K* (y^{-1})	Growth model	Range of L_{50} (cm)	a_{50} (y)
Bigeye	Atlantic	206	12	210 – 300	< 0.20	Von Bertalanffy	110 – 120	not available
	Indian	200	15	151 – 160	0.06 – 0.45	two-stanza	86 – 120	1.9
	Pacific	198	16	156 – 215	0.20 – 0.47	Von Bertalanffy	87 – 135	2.2
Yellowfin	Atlantic	191	6.5	175 – 196	0.27 – 0.57	Von Bertalanffy	108	not available
	Indian	178	9	125 – 197	0.21 – 0.83	two-stanza	75 – 120	not available
	Pacific	167	not available	148 – 200	0.25 – 0.81	Von Bertalanffy	69 – 112	2.4
Skipjack	Atlantic	96	6	80 – 112	0.15 – 2.96	Von Bertalanffy	42 – 52	2
	Indian	82	not available	60 – 95	0.23 – 0.98	two-stanza	37 – 47	1.5
	Pacific	75	not available	75 – 107	0.30 – 1.25	Von Bertalanffy	38 – 48	not available
Albacore	Atlantic	120	13	105 – 148	0.13 – 0.32	Von Bertalanffy	not available	not available
	Indian	120	7	113 – 164	0.11 – 0.19	Von Bertalanffy	not available	not available
	Pacific	128	15	97 – 145	0.13 – 0.34	Von Bertalanffy	71 - 90	4.5

Mercury levels in tunas in the global ocean: current knowledge

Variability of mercury concentrations among tuna species and ocean areas

Located at the top of marine pelagic food webs, tunas display high MeHg concentrations, sometimes exceeding food safety guidelines (1 $mg.kg^{-1}$ fresh tissue, i.e., ~3.3 $mg.kg^{-1}$ dry weight), with MeHg being the major chemical form (generally > 90 %) of total Hg in tuna muscle (SI Appendix A). A literature review of total Hg concentrations in white muscle of tropical tunas and albacore clearly shows that these concentrations are highly variable among individuals, species and ocean areas (Figure 17; SI Appendix A), suggesting that human exposure to MeHg strongly depends on tuna species and tuna catch location.

Fish length has been shown to be of primarily importance to explain intra-specific variability of Hg concentrations in all tuna species from several ocean areas, illustrating the natural bioaccumulative properties of MeHg in organisms (Figure 18 A) (Besada, 2006; Cai et al., 2007; Chen et al., 2014, 2011; Houssard et al., 2019; Kojadinovic et al., 2007; Peterson et al., 1973; Rivers et al., 1972; Sompongchaiyakul et al., 2008; Teffer et al., 2014). In addition to fish length, variability of MeHg concentrations among species and ocean areas is likely governed by a complex interplay between physiological (i.e., growth, metabolism and assimilation/excretion efficiencies), ecological (i.e., foraging depth and food web structures), biogeochemical (i.e., baseline *in situ* MeHg production and bioavailability), and physical (i.e., thermocline depth, and sea surface temperature) processes. In the Andaman Sea, lower Hg concentrations in yellowfin than in bigeye of same size have been hypothesized to result from different growth rates, with higher growth rates in yellowfin likely resulting to higher Hg dilution and consequently lower Hg concentrations (Menasveta and Siriyong, 1977). Differences of feeding ecology may also explain interspecific differences, with species with lower trophic position like skipjack and yellowfin, expected to exhibit lower Hg concentrations than bigeye. Several studies have found positive linear relationships between Hg concentrations and nitrogen stable isotope ratio, often used as a proxy of tuna trophic position (see chapter 5), illustrating this Hg biomagnification along the pelagic food webs (Bodin et al., 2017; Cai et al., 2007; Senn et al., 2010; Teffer et al., 2014). Nevertheless, a recent spatial study from the western central Pacific Ocean suggested that tuna trophic position was of minor importance to explain variable Hg concentrations in tunas (Houssard et al., 2019). Conversely, foraging depth was identified as the main driver to explain the spatial variability of length-standardized Hg concentrations in tunas (Figure 18 B) (Houssard et al., 2019), with higher Hg concentrations found in species (e.g., bigeye) and individuals that are able to undergo deeper dives, likely facilitating the access to mesopelagic preys with enhanced Hg concentrations, as already suggested for pelagic fishes from the northern central Pacific (Hawaii, Choy et al., 2009). Differences of Hg sources, and/or differential methylation production within the water column may also impact Hg accumulation in tunas, although these processes have not been clearly investigated yet, mainly because of the difficulty to disentangle all the processes at play.

To date, the vast majority of Hg monitoring studies in tunas (> 45) are localized studies, with only one global study available, highlighting significant variability of Hg concentrations in yellowfin among ocean basins, yet without adequately addressing the causes of these variations (Nicklisch et al., 2017).

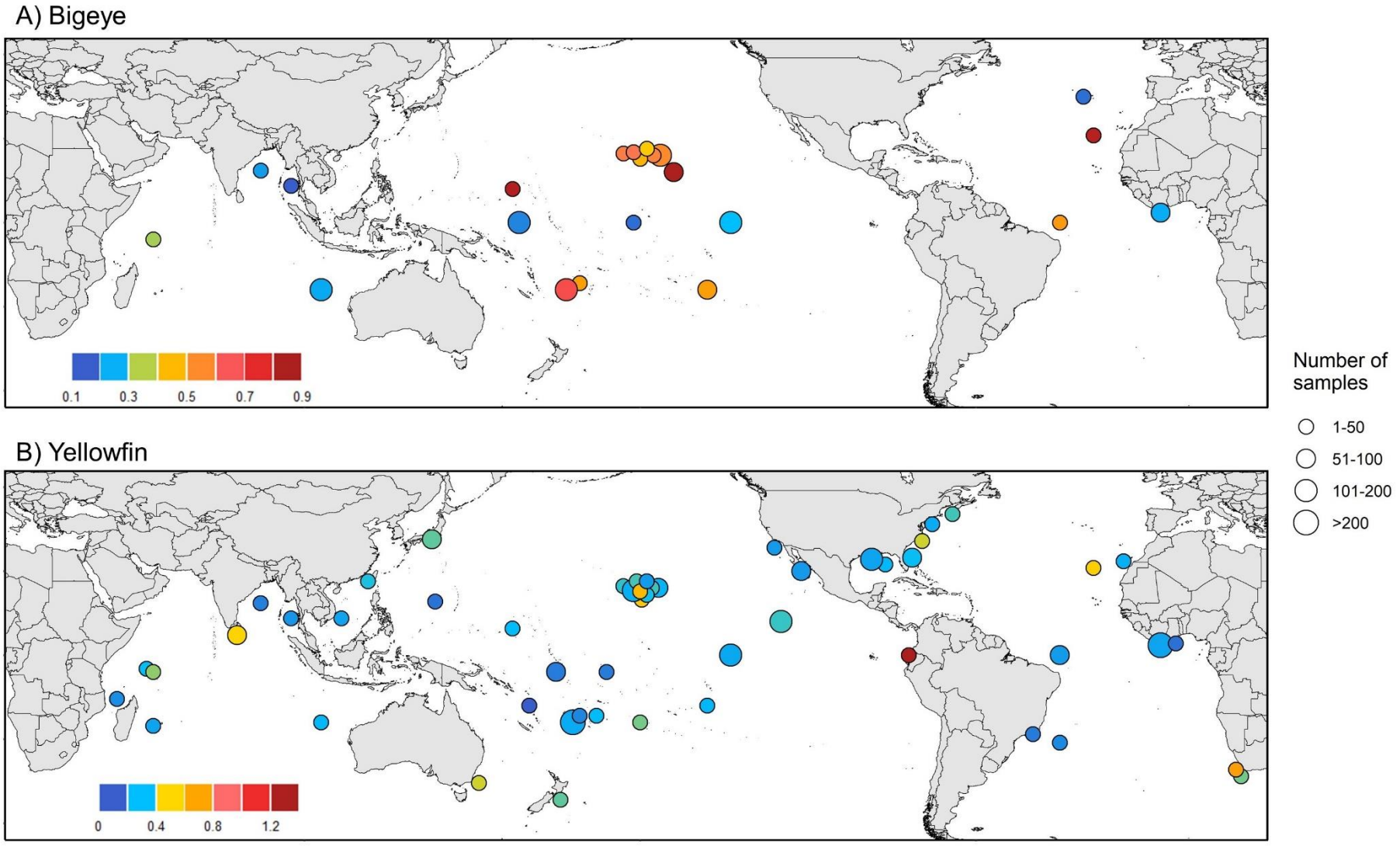
A) Bigeye
0.1
0.3
0.5
0.7
0.9
B) Yellowfin
0
0.4
0.8
1.2
Number of samples
1-50
51-100
101-200
>200

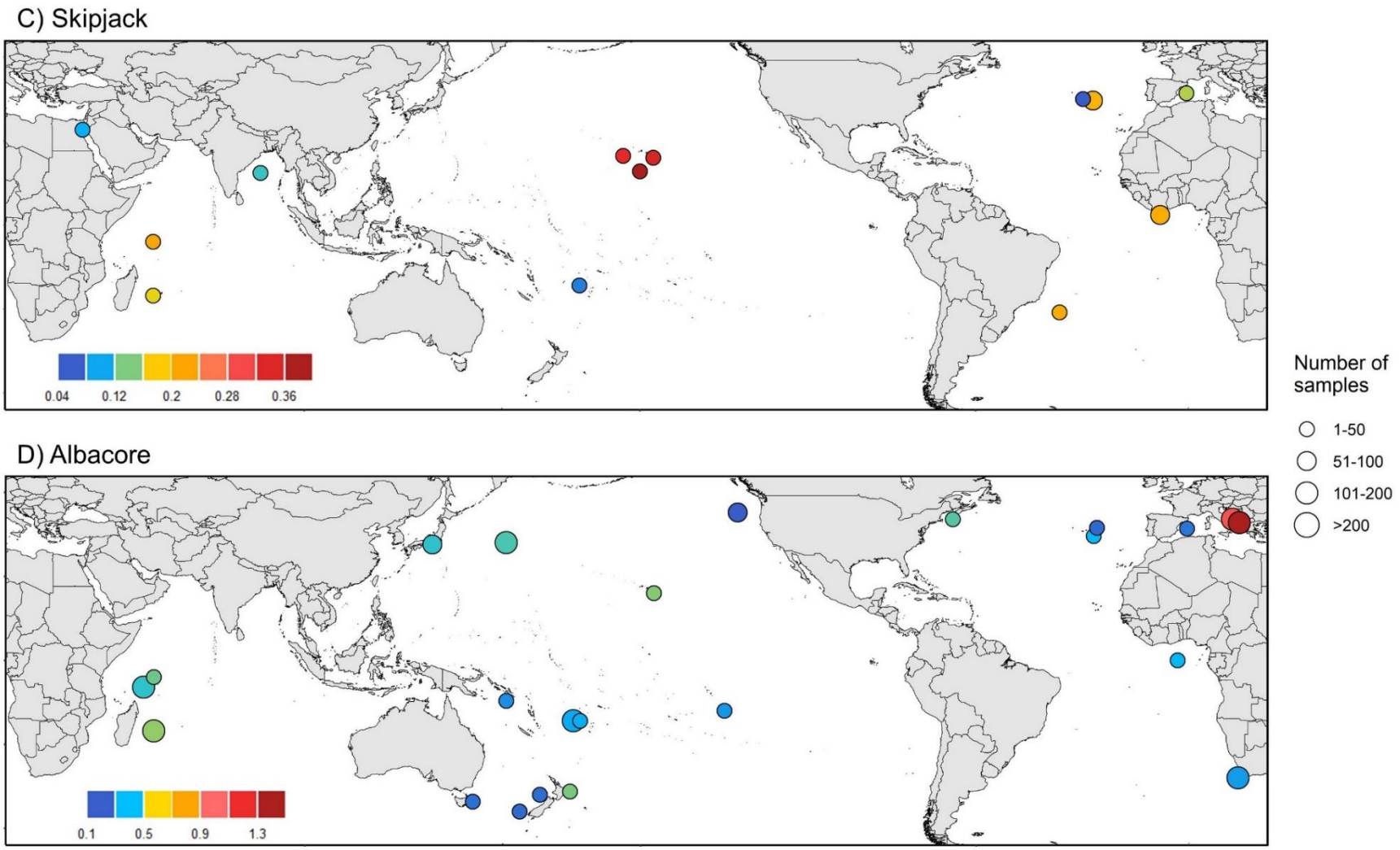

Figure 18. Literature review of mercury concentrations in tropical tunas. Spatial variability of Hg concentrations (mg.kg^{-1}, wet weight) in white muscle tissue of **A)** bigeye, **B)** yellowfin, **C)** skipjack, and **D)** albacore tunas at the global scale. The size of circles is proportional to the number of samples, and the colour of circles refers to total mercury concentrations measured in tuna muscle. References and detailed information used to produce these maps are reported in SI Appendix A, Table S1 of the manuscript.

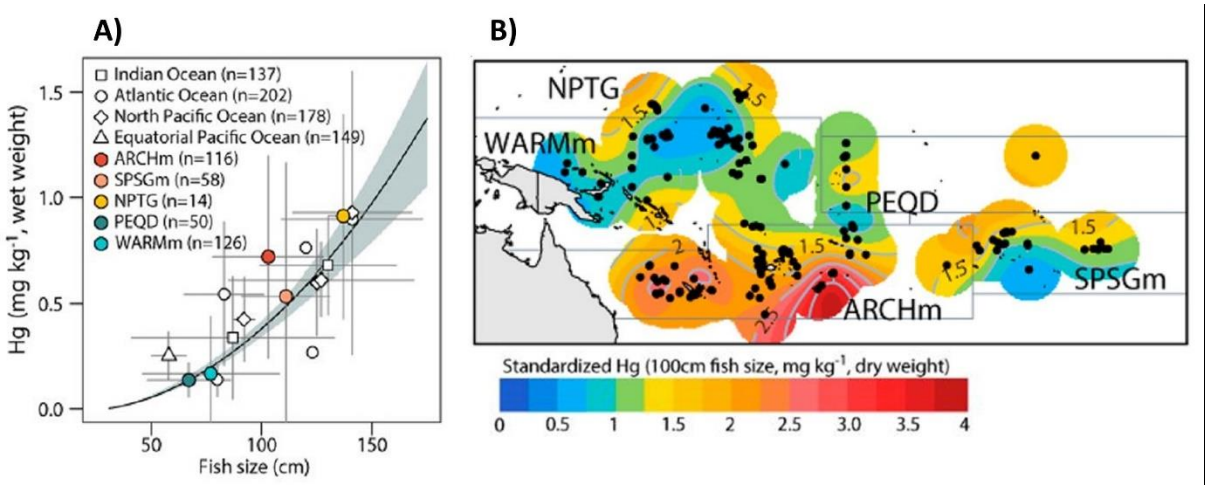

Figure 19. Drivers of mercury (Hg) accumulation in tunas. **A)** Literature review illustrating the positive relationship between Hg concentrations and fish length in bigeye tuna, from Houssard et al. (2019). The black line shows the fitted Hg bioaccumulative curve adjusted on data from the western and central Pacific Ocean, and the shaded area shows 95% of confidence interval. **B)** Smoothed contour map of length-standardized mercury concentrations (mg.kg^{-1}, dw) in bigeye, from Houssard et al. (2019). Modified Longhurst biogeochemical provinces as defined in Houssard et al. (2017): ARCHm: Archipelago deep basins modified, SPSGm: South Pacific Subtropical Gyre modified, NPTG: North Pacific Tropical Gyre, PEQD: Pacific Equatorial Divergence, and WARMm: Warm pool modified.

Uptake, distribution, excretion and accumulation of methylmercury in tunas

Methylmercury enters in fish via two different pathways: waterborne dissolved Hg uptake via respiration and dietary Hg uptake through consumption of contaminated prey. As in many fishes, the relative importance of these two pathways remain overall poorly understood in tunas (Post et al., 1996). Dietary uptake is generally considered as the dominant pathway (Ferriss and Essington, 2014a), yet given their anatomical, physiological and metabolic adaptations (e.g., continuous and fast swimming, large gill surface area, and small water to branchial capillarity diffusion distance), waterborne uptake could be of higher importance in tunas, compared to other fishes.

By forming complexes with proteins (Harris, 2003), MeHg is readily distributed to all tissues via the bloodstream before being partially eliminated, transformed, and stored in various tissues. To date, there are very few data on Hg organotropism in tunas, showing contrasting results. For instance, higher Hg concentrations were found in muscle than in liver for different tuna species (Licata et al., 2005; Torres et al., 2016), while the opposite pattern was also reported in same species (Kojadinovic et al., 2007; Storelli et al., 2005). These variable Hg ratios between muscle and liver may be associated to differential metabolic activities and physiological needs at a given period among individuals, but also to variable environmental conditions. For instance, freshwater fishes in localities lightly contaminated were found to accumulate more Hg in muscle than in liver, while freshwater fishes from heavily contaminated areas exhibited the opposite pattern (Havelková et al., 2008). Conversely, physiological requirements associated to reproduction are unlikely to influence much Hg bioaccumulation in tunas as no significant differences of Hg concentrations between males and females have been reported for several tuna species from distinct ocean basins (Chanto-García et al., 2021; Chen et al., 2014; Kojadinovic et al., 2007; Ordiano-Flores et al., 2011).

Different Hg ratios among tissues could also be related to internal detoxification processes. Muscle is often considered as the final storage of MeHg in fish, reflecting a relatively long-time Hg exposure (Kwon et al., 2016; Oliveira Ribeiro et al., 1999), while liver, a metabolically active organ, has been showed to be involved in MeHg detoxification in many marine mammals, but also in some bird and fish species (Gajdosechova et al., 2016; Ikemoto et al., 2004; Manceau et al., 2021a). Briefly, this detoxification pathway relies on the formation of non-toxic insoluble tiemmanite (HgSe) granules after the mobilization and demethylation of MeHg by selenium (Se). In yellowfin and skipjack from the western Indian Ocean, the correlation between Hg and Se in liver was found to increase with Hg impregnation, with molar concentrations of Se much higher than those of Hg, suggesting possible conditions for Se mediated Hg detoxification in liver of these two tropical tunas (Kojadinovic et al., 2007). Another possible site for MeHg biotransformation is the digestive tract, which not only serves as the first barrier for the ingested MeHg, but also may participate in the transformation processes, as found in marine and freshwater fishes (Li et al., 2019; Wang et al., 2017). Pan-Hou et Imura (1981) detected a significant decrease of extractable MeHg in pure cultures of bacteria isolated from yellowfin digestive tract, suggesting the capacity of intestinal microbiota in Hg demethylation. Yet, these results have to be considered with caution as they were obtained under in vitro experiment conditions, therefore the microbiota that exhibits Hg transformation abilities may not represent an effective demethylator in tuna gut. To date, there is no evidence of internal MeHg detoxification processes in tunas, and overall, further investigation are needed to better quantify inorganic and organic Hg burdens among tissues and organs, and to ultimately understand the internal distribution dynamics, and the resulting toxicological effects of Hg in tunas.

Temporal trends of tuna mercury concentrations and uncertain responses to variable anthropogenic mercury releases and climate and ecosystem changes

Anticipating changes in human exposure depends on our ability to capture and predict spatial and temporal Hg trends in aquatic food webs. In particular, understanding to what extent MeHg concentrations in aquatic biota will track changes in anthropogenic Hg releases is of major importance when evaluating the effectiveness of the Minamata Convention. Only three temporal studies of Hg concentrations in tunas are available to date, showing distinct results regarding Hg long-term trends. In the central north Pacific Ocean (Hawaii), stable Hg concentrations were found in yellowfin between the 1970s and the 1990s (Kraepiel et al., 2003). In the same region, Drevnick et al. (2015; 2017) later suggested that Hg concentrations increased between 1970s and 2008 in both yellowfin (+ 5.5 ± 1.6 % per year during 1998 and 2008) and bigeye (+ 3.9 ± 2.1 % per year during 2002 and 2008) (Figure 19A). These later two studies, although relying on five sampling years only, hypothesized that the temporal Hg increase of tuna Hg levels resulted from increasing anthropogenic Hg loadings, mainly delivered along the coast of the northwestern Pacific Ocean, a region characterized by elevated Hg emissions to the atmosphere (Streets et al., 2019a). Conversely, in the North Atlantic, Lee et al. (2016) revealed a decline of Hg concentrations in Atlantic bluefin tuna of about 2.4 % between 2004 and 2012 (Figure 19B), likely mirroring the reduction of anthropogenic emissions and deposition in North America. Although they display opposing long-term Hg trends, these results suggest a link between anthropogenic Hg fluctuations and Hg in tunas at local and regional scales. In a recent review of Hg time series in different aquatic biota, Wang et al. (2019) found in most cases that Hg temporal trends in biota did not mirror concurrent Hg trends in atmospheric deposition and concentrations. Authors

hypothesized that the impact of changing atmospheric inputs on biotic Hg is masked by two main factors: i) the aquatic environment contains large quantities of legacy Hg that remain available for bioaccumulation, and ii) biotic Hg trends are affected by changes occurring in multi-causal, local and regional processes (e.g., climate and trophic ecology) that control the speciation, bioavailability and bioaccumulation of both current and legacy emitted Hg.

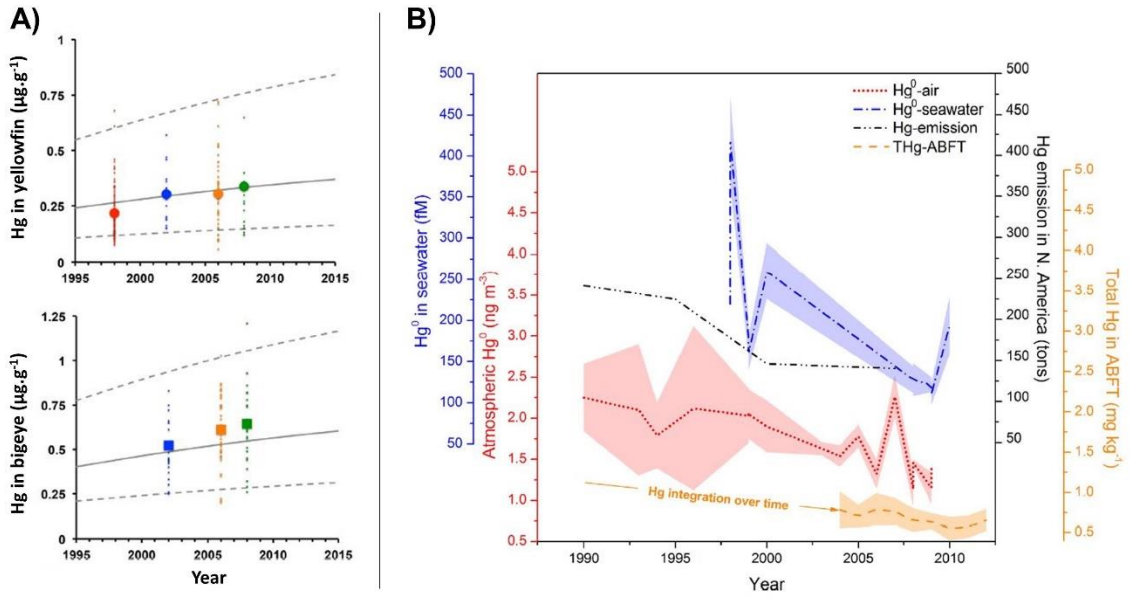

Figure 20. Literature review of long-term trends of mercury (Hg) concentrations in tunas. **A)** Increasing total Hg concentrations in yellowfin (top) and bigeye (bottom) from the northern central Pacific Ocean (Hawaii) between 1998 and 2008, from Drevnick and Brooks (2017). **B)** Declining total Hg concentrations in Atlantic bluefin tuna (ABFT, orange) between 2004 and 2012, in relation to reduced anthropogenic Hg emissions from North America (black), and atmospheric elemental mercury (Hg^0) concentrations (red), and Hg^0 in seawater (blue) in the North Atlantic Ocean, from Lee et al. (2016).

Indeed, also important when considering changes of Hg cycle in marine food webs, are the confounding effects of ecological- and/or climate-induced changes. Recent model predictions showed that increasing Hg concentrations in Atlantic bluefin and Atlantic cod (*Gadus morhua*) were related to increasing seawater temperatures and dietary shifts initiated by overfishing, respectively (Schartup et al., 2019). Experimental studies on estuarine and freshwater fishes also predicted enhanced MeHg bioaccumulation with warmer temperatures (Dijkstra et al., 2013; Maulvault et al., 2016). Among the potential climate-induced changes of the global Hg biogeochemical cycle, Krabbenhoft & Sunderland (2013) hypothesized as well modified atmospheric rates and patterns of deposition as a result of weaker global circulation and elevated temperatures. Similarly, increased precipitations intensity and incidence of extreme storm events may lead to enhanced Hg inputs to aquatic systems through direct deposition, runoff, and evasion (Krabbenhoft and Sunderland, 2013; Liu et al., 2021). In marine ecosystems in particular, changes in ocean circulation, productivity and growth of oxygen minimum zones are expected to alter patterns and rates of MeHg production in seawater (Mason et al., 2012). Moreover, widespread nutrient enrichment of coastal ecosystems is likely to modify MeHg formation in many ecosystems (Mason et al., 2012). Overall, further multidisciplinary investigation is needed to better understand the responses of MeHg bioaccumulation in marine food webs to variable

anthropogenic Hg inputs, and the forcing induced by climate changes at the ecosystem level. Understanding the changes of Hg biogeochemical cycle induced by multiple synergistic and antagonistic drivers is indeed crucial for anticipating future human and wildlife exposures and risks. Tropical tunas, and to a lesser extent, albacore tuna, as emblematic and widely distributed and exploited marine top predators, could represent good Hg bio-indicator species to investigate these major questions. Yet global spatial and temporal studies of Hg concentrations in these species remain needed to guarantee that they are capable to reflect Hg exposure in pelagic ecosystems, integrating local and global Hg sources over different spatial and temporal scales.

General context, positioning, objectives and structure of the thesis

Scientific background

This thesis is rooted at the national level in the framework of the ANR MERTOX project (unravelling the origin of methylMERcury TOXin in marine ecosystems, 2017 - 2021), which aims at tackling two unanswered questions of i) where MeHg accumulated in marine pelagic fish originates from, and ii) what fundamental processes govern marine MeHg formation. In particular, it is part of the work package 1 (Figure 20), which attempts to explore the potential for using the advanced isotopic techniques for measuring heavy (Hg) and light (carbon) MeHg isotopes, combined to ecological tracers and the isotopic baseline carbon signature, to capture the origin, fate, and ecodynamics of MeHg in marine pelagic fish. The MERTOX project provides a multi-disciplinary and collaborative framework to address the questions about the origin of Hg in pelagic fish as it brings together specialists in the marine Hg cycle (MIO, Marseille), and in the atmosphere (GET, Toulouse), researchers with strong experience in tuna ecology (LEMAR, Brest), and stable isotopic analyses of MeHg applied to food webs (GET, Toulouse), as well as specialists in climate and isotope modelling at the global scale (LMD, Paris).

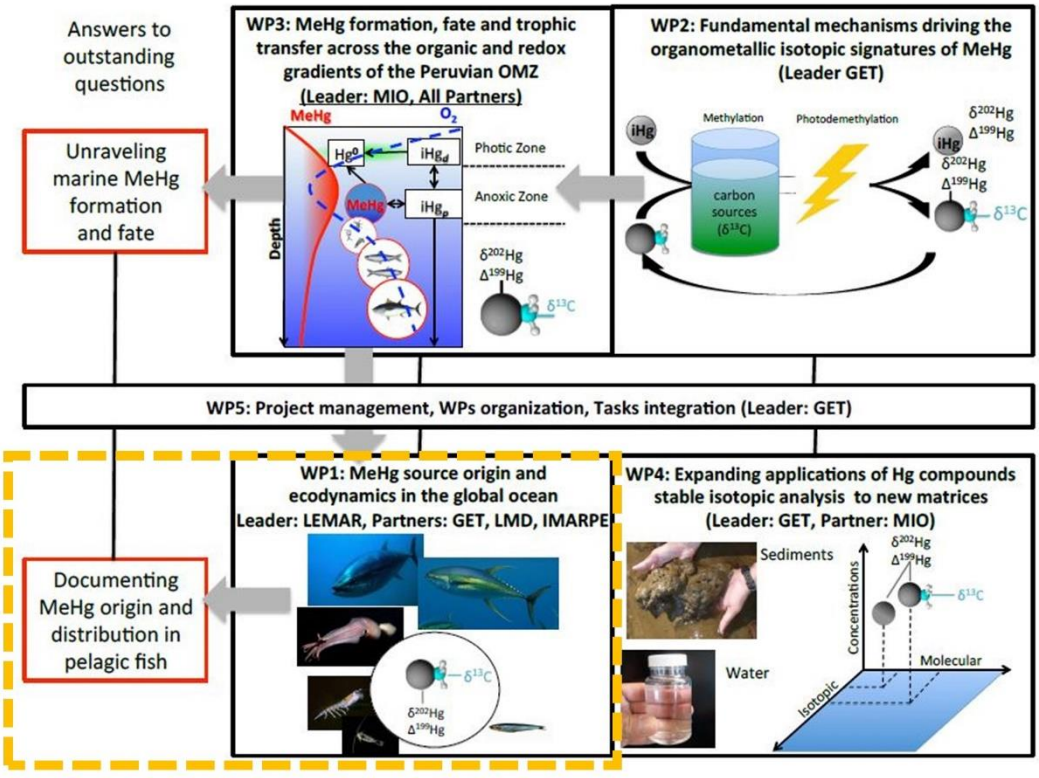

Figure 21. Conceptual framework of the MERTOX project organisation and workflow, from ANR MERTOX, David Point. The dashed orange line represents the specific work package (WP1) in which is specifically rooted this thesis.

At the international level, this thesis is under the umbrella of the IMBER CLIOTOP program (Climate Impact on Top Predators) and particularly in the working group on top predators and their trophic ecology that has been in place since 2009. This international program brings together some 20 members, 9 countries and 16 research institutions working on the sharing of samples and biomarker data on top predators and their valuation. Thus, more than 5,000 tuna samples collected in the global ocean from 2000 to 2015 were analyzed in carbon ($\delta^{13}C$) and nitrogen ($\delta^{15}N$) stable isotopes, providing key insights on broad-scale patterns of trophic structure, movements, and trophodynamics of tunas in relation to environmental conditions. In particular, tuna $\delta^{13}C$ values were shown to decline between 2000 and 2015 in all oceans, likely resulting from shifts in phytoplankton species composition and physiology (Lorrain et al., 2020). Conversely, tuna $\delta^{15}N$ ratios remained stable over the same period, suggesting that broad-scaled ecosystem functions like food chain length have not changed (Pethybridge et al., 2018a). At the spatial scale, tuna trophic positions were variable and declined in areas with reduced oxygen at depth (i.e., eastern Pacific and northern Atlantic Oceans). This suggests that habitat compressions resulting from the expansion of minimum oxygen areas and ocean warming may impact the trophic structure of marine food webs and the corresponding foraging habitat of marine top predators (Pethybridge et al., 2018a). Tuna $\delta^{13}C$ values also displayed high spatial variability, with values decreasing with increasing latitudes in relation to sea surface temperature (Logan et al., 2020). In addition to a strong expertise in tuna ecology, this collaborative program provides a gold mine of already collected and preserved tuna samples with corresponding individual metadata (e.g., fish length, fishing date and position, $\delta^{13}C$ and $\delta^{15}N$ values) (Bodin et al., 2020), available for Hg analyses to characterize spatial and/or temporal Hg trends in tunas at the global scale.

Finally, this study comes after the Pacific Fund VACOPA project (spatial VAriations of COntaminants levels in PAcific ocean trophic webs) and Patrick Houssard's thesis (2014 – 2017) on trophic ecology and Hg bioaccumulation in tunas in the south- and central- western Pacific Ocean. In this region, higher tuna trophic position was found in the southern latitudes compared to the equator, likely resulting from a deeper thermocline depth which increase tuna vertical habitat and access to mesopelagic prey of higher trophic position (Houssard et al., 2017). Total Hg concentrations in same specimens also displayed spatial variability, which was mainly explained by fish size and thermocline depth, while tuna trophic position and primary production were of weaker importance (Houssard et al., 2019). In addition to providing thousands of already analysed Hg data in tunas, this first high-resolution spatial study also constitutes a first milestone to understand Hg bioaccumulation in tunas in relation to environmental factors and trophic dynamics at the regional scale.

Questions, objectives and structure of the thesis

As specified in the general introduction, fundamental questions on where, how, and when MeHg is formed in the global ocean remain unanswered. Current societal challenges are to understand how climate change, and/or the implementation of reduction Hg emissions measures, will impact MeHg production in oceans, and its distribution along the pelagic food chain. Regarding tunas, while relatively high Hg concentrations have been reported in different tuna species, broad-scale spatial and temporal studies remain needed to better characterize the processes driving Hg accumulation in these marine top predators. In this context, we defined several questions for this thesis:

- How and why do vary Hg concentrations among tuna species?
- How do vary tuna Hg concentrations at both regional and global scales?
- Can we reveal temporal trends of tuna Hg concentrations at regional and global scales?
- Do tuna Hg levels reflect natural biogeochemical processes leading to more or less MeHg concentrations at the base of marine food webs?
- To what extent tuna Hg concentrations are influenced by ecological processes?
- Do tuna Hg concentrations reflect anthropogenic Hg emissions?
- How climate change is susceptible to influence tuna Hg concentrations?
- Are tunas good indicator species for Hg bio-monitoring in the oceans in the context of the Minamata Convention?

This thesis therefore aims to tackle the yet-answered question of what controls the origin and fate of MeHg in tunas at the global scale. The specific objectives are to: **i) build an extended database of Hg concentrations in different tuna species in the global ocean**, **ii) investigate the spatial and temporal variability of tuna Hg concentrations at regional and global scale**, **and iii) identify the main processes governing Hg concentrations in tunas**.

The rest of the manuscript follows the classical structure: materials and methods, results and general discussion (Figure 21). The results section is divided into 4 chapters, as follows:

The two first chapters investigate the temporal patterns of tuna Hg concentrations at sub-regional and global scales. Chapter 1 first analyses a unique long-term, continuous and large Hg dataset in the three tropical tunas (i.e., bigeye, yellowfin, and skipjack) from the southwestern Pacific Ocean between 2001 and 2018. We use combined tuna ecological, and marine physical and biogeochemical variables to explore the main drivers of temporal variability in tuna Hg levels. Chapter 2 compiles Hg data from the existing literature, alongside newly acquired tropical tuna Hg concentrations to explore Hg temporal variability in six contrasted regions of the global ocean from 1970 to 2020. We explore and discuss the extent of considering inter-annual differences of tuna Hg levels governing long-term trends, and highlight different temporal responses of tuna Hg content to changes in anthropogenic Hg emissions, depending on the ocean region.

The two last result chapters provides global maps of Hg concentrations in tropical tunas at high-spatial resolution and identify the main factors governing this spatial variability. Chapter 3 first explores the geographical patterns of skipjack Hg concentrations in the Pacific Ocean. With the combined use of tuna ecological data, marine physical and biogeochemical variables, and estimates of atmospheric Hg concentrations, we also explore the relative contribution of tuna foraging ecology, marine biogeochemistry, and anthropogenic Hg emissions, to observed tuna Hg concentrations. Chapter 4 performs similar spatial study but at the global ocean, and including the three tropical tunas.

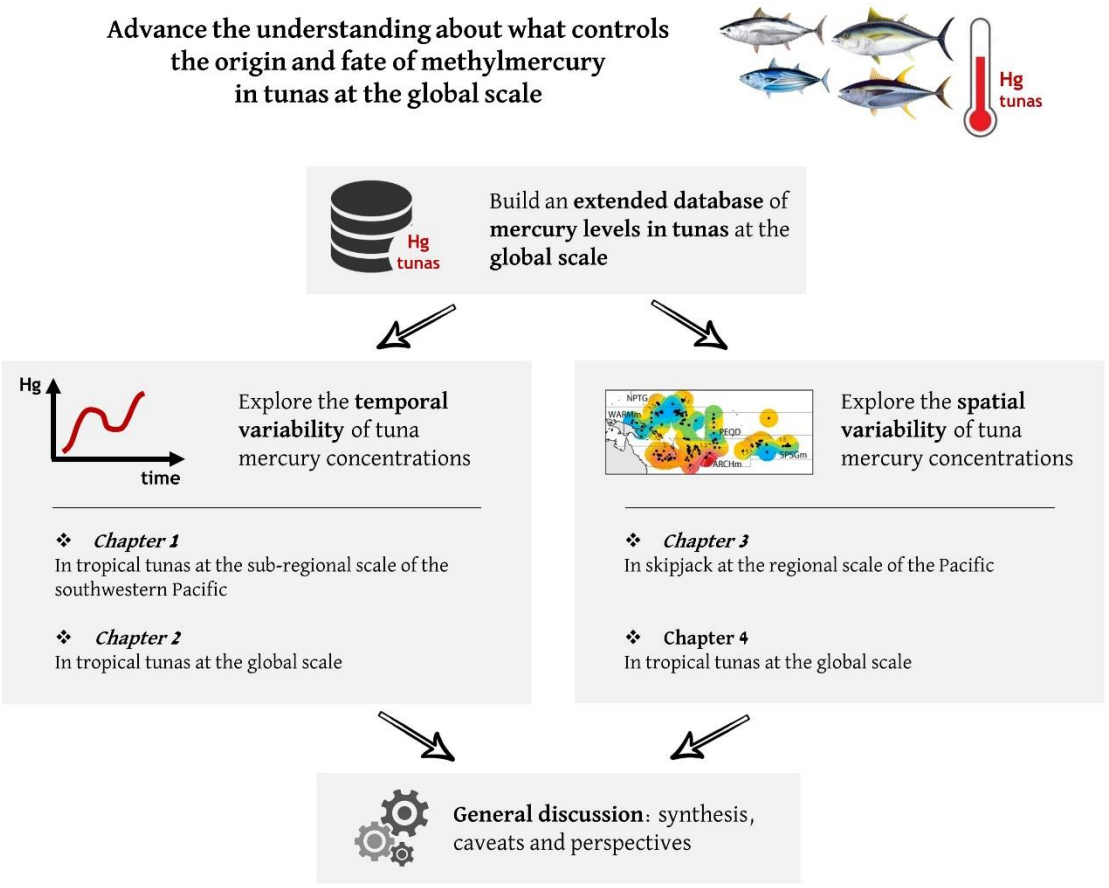

Figure 22. Conceptual framework of the thesis structure.

Chapters 1 - 4 have been prepared for publication so there will be some overlap between the general introduction and methodology, and the respective introduction and methodologies.

A global and multidisciplinary approach combining biochemical tracers in tunas to biogeochemical, oceanic and atmospheric model outputs

Biochemical tracers and ecosystem models used in trophic ecology and marine mercury biogeochemistry

In addition to total Hg concentrations, we used a combination of biochemical tracers measured in tuna samples, as well as ecosystem models outputs, to investigate the potential effects of trophic ecology, ocean biogeochemistry, and anthropogenic Hg emissions on Hg bioaccumulation in tunas. This chapter introduces these biochemical tracers and ecosystems models, and presents their broad applications, advantages and limitations in trophic ecology and Hg biogeochemistry.

Carbon and nitrogen stable isotope ratios: tracers of ecological and biogeochemical processes

Isotopic compositions are commonly used as ecological and biogeochemical tracers to examine trophic dynamics in food webs (Pethybridge et al., 2018b), investigate movement patterns of animals (Graham et al., 2010; McMahon et al., 2013a) and track Hg sources and dynamics (Blum et al., 2013; Point et al., 2011).

Isotopes of a given chemical element are atoms whose nucleus have the same number of protons (i.e., same atomic number) but a different number of neutrons, resulting in different mass numbers (i.e., sum of neutrons and protons). Each isotope of a given element is then characterized by its mass number. This slight difference of mass number is responsible of slight physico-chemical differences between two isotopes of a single element and leads to isotopic fractionation, i.e., an enrichment of one isotope relative to another between two substances or two coexisting phases of the same substance in a natural system. The vast majority of isotopes, including carbon and nitrogen, show mass-dependent fractionation (MDF), which involves an enrichment of products in lighter isotopes whereas heavier isotopes will remain in the reactant during a given process. Some isotopes, (Hg, sulphur and oxygen) also display mass-independent fractionation (MIF), i.e., they are involved in photochemical processes where the amount of isotope separation is not proportional to the mass difference of the isotopes.

The abundance of stable isotopes vary naturally between the biosphere reservoirs and between trophic levels. The isotopic composition of an element (X) within a sample corresponds to the abundance ratio of heavy (Y) to light (Z) isotopes (typically rare to abundant), relative to the same ratio in international standards. It is reported on a delta scale (δ), representing sample deviations from an internationally certified standard, and is expressed as parts per thousand (‰):

$$\delta^{Y}X = \left(\frac{\frac{^{Y}X}{^{Z}X}sample}{\frac{^{Y}X}{^{Z}X}standard} - 1 \right) \times 1{,}000$$

Nitrogen and carbon stable isotopes

As monomethyl-Hg is known to biomagnify along trophic webs mainly via dietary exposure, it has become essential to characterize the trophic ecology of tunas to better understand their monomethyl-Hg exposure and concentrations. A variety of tools is currently used to examine the diet composition of a predator and in general the trophic interactions in marine food webs. Among them, stomach content analysis, which includes the analysis of scats and spews, has been widely used since the 1950s (Hynes, 1950) and remains the best method to provide quantifiable information of directly ingested prey at specific taxonomic levels. Yet stomach content analysis is known to be a highly involved tool, as it requires large sampling programs, taxonomic expertise, and the ability to determine soft-bodied prey and integrate feeding beyond short-term scales. Electronic tagging is another commonly-used tool in trophic ecology studies by characterizing the vertical habitat of a pelagic predator; yet it is very expensive and cannot be deployed on early-life history stages of marine animals (Graham et al., 2007). Stable isotope ratios of nitrogen (^{15}N:^{14}N, $\delta^{15}N$) and carbon (^{13}C:^{12}C, $\delta^{13}C$) are by far the most commonly used isotopes in trophic ecology studies, followed by hydrogen (^{2}H:^{1}H, $\delta^{2}H$), oxygen (^{18}O:^{16}O, $\delta^{18}O$) and sulphur (^{34}S:^{32}S, $\delta^{34}S$) isotope ratios (McMahon et al., 2013b).

The use of $\delta^{15}N$ and $\delta^{13}C$ relies on the fact that lighter isotopes are preferentially used and excreted during the metabolic reactions compared to heavier isotopes (i.e., MDF), resulting in predictable fractionation shift in $\delta^{15}N$ values, and to a lesser extent $\delta^{13}C$ values, between trophic levels (Fry, 2006). These changes in isotopic ratios between a consumer's tissue and its prey, defined as tissue to diet trophic discrimination factors, differ among trophic levels, species, tissues and the quality of the ingested nutrients, and result from a complex interplay of processes, including variable fractionation during metabolic transformations in consumer's tissues. For ^{15}N in particular, a meta-analysis showed large differences of trophic discrimination factors according to the main biochemical form of nitrogen excretion (e.g., urea, uric acid, and ammonia), with differences generally preserved among trophic positions (i.e., carnivores, herbivores, and mixed) and taxon (i.e., vertebrates *versus* invertebrates) (Figure 22) (Vanderklift and Ponsard, 2003). Isotopic routing, i.e., differential allocation of isotopically distinct dietary constituents (e.g., proteins, lipids and carbohydrates) to different tissue constituents (Schwarcz, 1991), can lead as well to differences between tissues and diet (Martinez del Rio et al., 2009). Tissue to diet trophic discrimination factors are difficult to obtain, mainly because of the challenges of maintaining species in captivity, and is commonly set at 2.4 ‰ for nitrogen in tropical tuna muscle tissues, following Olson et al. (2010) and Lorrain et al. (2015), and derived from Vanderklift and Ponsard (2003).

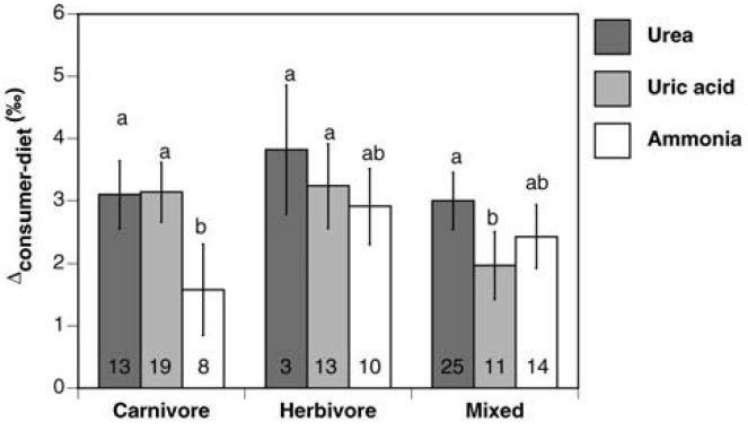

Figure 23. ^{15}N trophic discrimination factors ($\Delta_{consumer-diet}$, mean ± 95% confidence intervals) among organisms classified according to their primary form of excretion (i.e., urea, uric acid, and ammonia) and their diet (i.e., carnivore, herbivore, and mixed), from Vanderklift and Ponsard (2003). Numbers within the bars indicate the sample size. Groups sharing the same letter (a, b) are not significantly different.

Both $\delta^{15}N$ and $\delta^{13}C$ ratios are also affected by biogeochemical processes occurring at the base of the food web. In marine ecosystems, primary producers, including phytoplankton, bacteria and marine snow, can rely on atmospheric N_2 for nitrogen fixation, or inorganic deep-water nitrate (i.e., NO_3^-, NO_2^-, NH_4^+) for nitrate-based production, both of which are distinguished by a unique nitrogen isotopic signature (from -2 to 0 ‰, and from 4 to 6 ‰, respectively) (Wada and Hattori, 1990). This variability of the dominant nitrogen species assimilated, combined to the variable demand for the nitrogenous nutrients by primary producers, and the nitrogen biogeochemical cycling, result in large spatial and temporal patterns of the baseline isotopic composition (Lorrain et al., 2015b). Accounting for the $\delta^{15}N$ values of primary producers in an ecosystem is therefore crucial to estimate the trophic position of a consumer. Few detailed maps of measured $\delta^{15}N$ baseline values (i.e., isoscapes) are available in oceanic waters, with the most comprehensive provided by McMahon et al. (2013b) (Figure 23 A). On the other hand, $\delta^{13}C$ values in a consumer provide a reliable measure of the foraging location and the associated carbon sources because of the low trophic fractionation of ^{13}C, and therefore largely reflect spatial differences of $\delta^{13}C$ values in primary producers (Fry, 2006). This spatial variability of baseline $\delta^{13}C$ values (Figure 23 B) is influenced by the fractionation processes caused by equilibration of CO_2 between the atmosphere and surface dissolved inorganic carbon pools during photosynthesis, and is mainly driven by the availability of dissolved inorganic carbon and ocean temperatures (McMahon et al., 2013b).

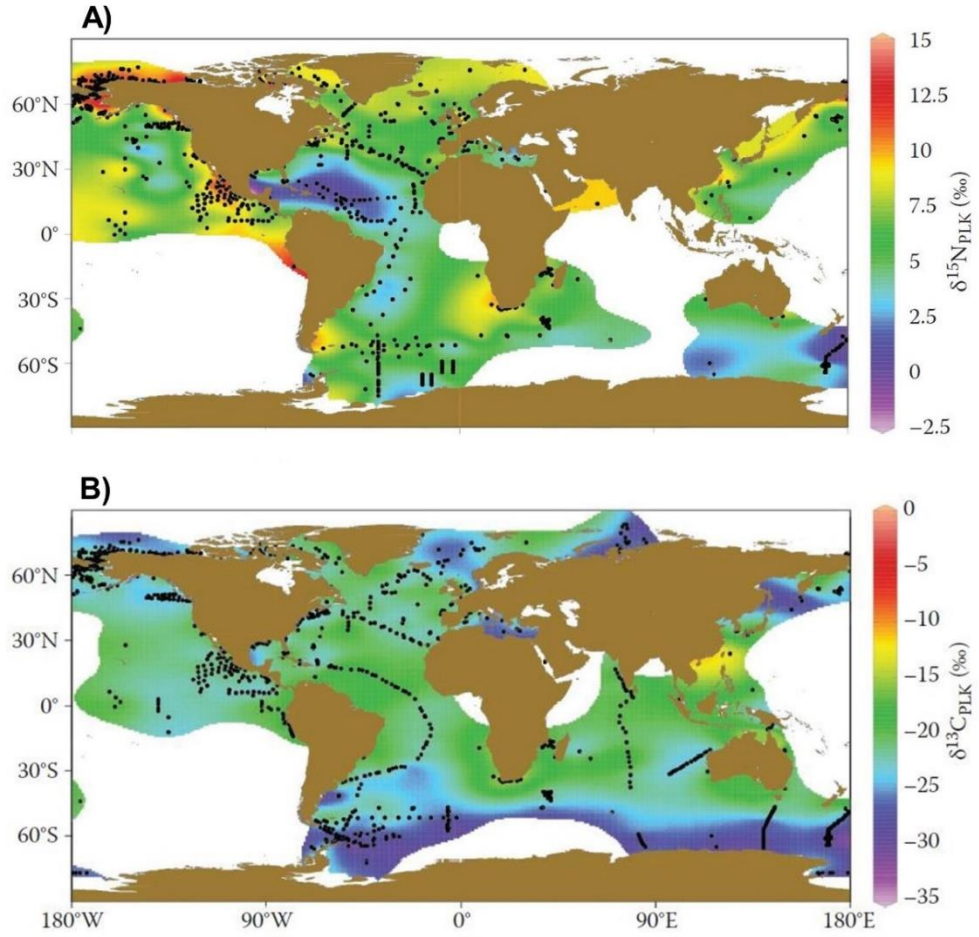

Figure 24. Horizontal isoscapes of plankton **A)** nitrogen stable isotope ($\delta^{15}N_{PLK}$) values, and **B)** carbon stable isotope ($\delta^{13}C_{PLK}$) values, in the surface waters (top 200m) of the world's ocean, from McMahon et al., (2013b). The black dots represent the sample locations.

In addition to trophic position estimates and carbon sources, $\delta^{15}N$ and $\delta^{13}C$ values can provide information on diet shifts, and potential movement patterns, when tissue turnover rates are known (Graham et al., 2010; Phillips and Eldridge, 2006). Isotopic turnover is defined as the time it takes for a given consumer tissue to reflect the isotopic composition of food resources. It depends on metabolic processes within animal tissues, mass, and growth, all of which vary with ontogeny, and across taxa and tissue types (Buchheister and Latour, 2010; de la Higuera et al., 1999; Madigan et al., 2012). In particulate organic matter, turnover rates are estimated at a few weeks (Dore et al., 2002), while in white muscle tissue of bluefin tuna, they have been estimated at 6 and 9 months, for ^{15}N and ^{13}C, respectively (Madigan et al., 2012). Integrating these differential turnover rates between the baseline and the upper-trophic-levels is therefore also crucial when exploring spatial and temporal trophic patterns of a consumer.

Compound-specific stable isotopes analysis and trophic position estimates

Thanks to advances in mass spectrometry, it is now possible to obtain precise and accurate stable isotope measurements from individual biological compounds, including amino acids or fatty

acids. Compound-specific stable isotope analysis (CSIA) offers new perspectives to estimate trophic position of an organism and track nutrient flow along marine food webs as it helps avoiding many of the confounding variables that make challenging the interpretation of bulk tissue stable isotope values. Trophic dynamic studies using amino acid CSIA rely on differential isotopic fractionation of individual amino acid during trophic transfer. Some amino acids (e.g., phenylalanine and glycine) are said "source" (Sr-AA) when they show little-to-no fractionation between diet and consumer and then reflect the $\delta^{15}N$ signature at the base of the food web. On the other hand, other amino-acids (e.g., glutamic acid and leucine) are said "trophic" (Tr-AA) as they are being enriched in ^{15}N at each trophic level (Popp et al., 2007) (Figure 24 A). Therefore, amino acid CSIA techniques represent advantages for trophic ecology studies as they allow to better quantify the variability in food web baseline values, food chain length and transfer efficiencies, and thus to derive more accurate estimates of trophic positions (Choy et al., 2015; Lorrain et al., 2015b). The general equation to estimate a consumer's trophic level (TP_{CSIA}) using amino acid CSIA is as follows:

$$TP_{CSIA} = \frac{\delta^{15}N_{Tr-AA} - \delta^{15}N_{Sr-AA} + \beta_{Tr-Sr}}{TDF_{Tr/Sr}} + 1$$

where $\delta^{15}N_{Sr-AA}$ and $\delta^{15}N_{Tr-AA}$ are the $\delta^{15}N$ values of the consumer source and trophic amino acids respectively, β_{Tr-Sr} represents the difference in $\delta^{15}N$ values between Tr-AA and Sr-AA in primary producers and $TDF_{Tr/Sr}$ is the trophic discrimination factor, i.e., the ^{15}N enrichment between Tr-AA and Sr-AA ($\Delta^{15}N_{Tr\text{-}AA}$ - $\Delta^{15}N_{Sr\text{-}AA}$) per trophic level (Chikaraishi et al., 2009) (Figure 24 B).

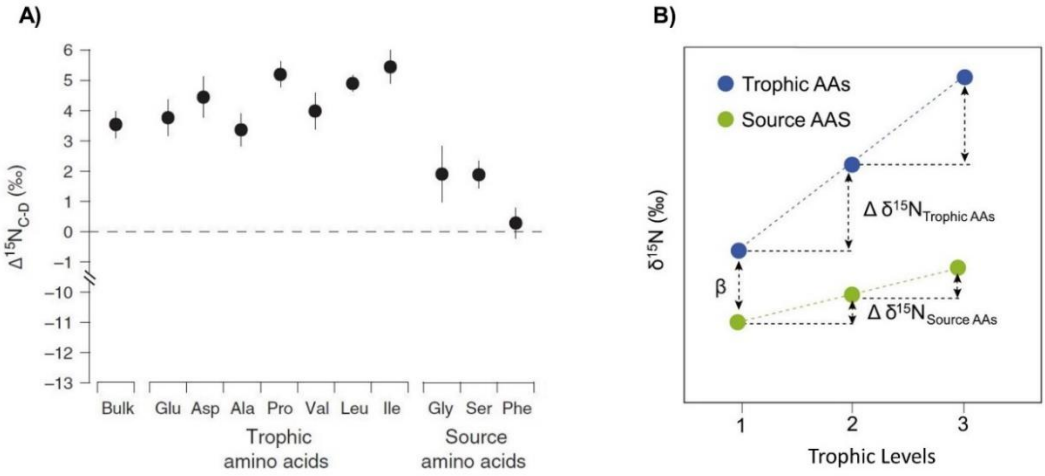

Figure 25. Trophic fractionation of source and trophic amino acids. **A)** Bulk tissue and individual amino acid stable nitrogen isotope trophic fractionation ($\Delta^{15}N_{C\text{-}D}$, mean ± standard deviation) between a consumer (feather of gentoo penguins, *Pygoscelis papua*) and its diet (muscle of Atlantic herring, *Clupea harengus*), adapted from McMahon et al., (2015). **B)** Schematic relationship between $\delta^{15}N$ values of both source and trophic amino acids (AAs) and trophic levels, from Won et al., (2018). β indicates the offset between the $\delta^{15}N$ values in trophic amino acid and source amino acid in a primary producer.

While CSIA analysis was sold as the magic tool to separate baseline and trophic effects, and therefore estimate a consumer's trophic position, recent studies have pointed out some limitations. Growing evidence suggests high variability of $TDF_{Tr\text{-}Sr}$ within and among taxa, likely mechanically related to variation in animal biochemistry and physiology, especially to diet quality and mode of nitrogen excretion (Figure 25 A) (McMahon and McCarthy, 2016). Similarly, β_{Tr-Sr} values are highly

variable among taxa and tissues, with degree of vascularization providing the greatest source of variability (vascular autotroph = -6.6 ± 3.4 ‰; non-vascular autotroph = 3.3 ± 1.8 ‰) (Figure 25 B & C) (Ramirez et al., 2021). Trophic position estimates using amino acid CSIA are highly sensitive to changes in both $TDF_{Tr\text{-}Sr}$ and $\beta_{\mathrm{Tr-Sr}}$ values, yet the relative influence of $\beta_{\mathrm{Tr-Sr}}$ values tend to dissipate at higher trophic levels (Ramirez et al., 2021). In addition to the variability of $TDF_{Tr\text{-}Sr}$ and $\beta_{\mathrm{Tr-Sr}}$ values, a major limitation of amino acid CSIA techniques is that they are costly because of the time-consuming analytical work required.

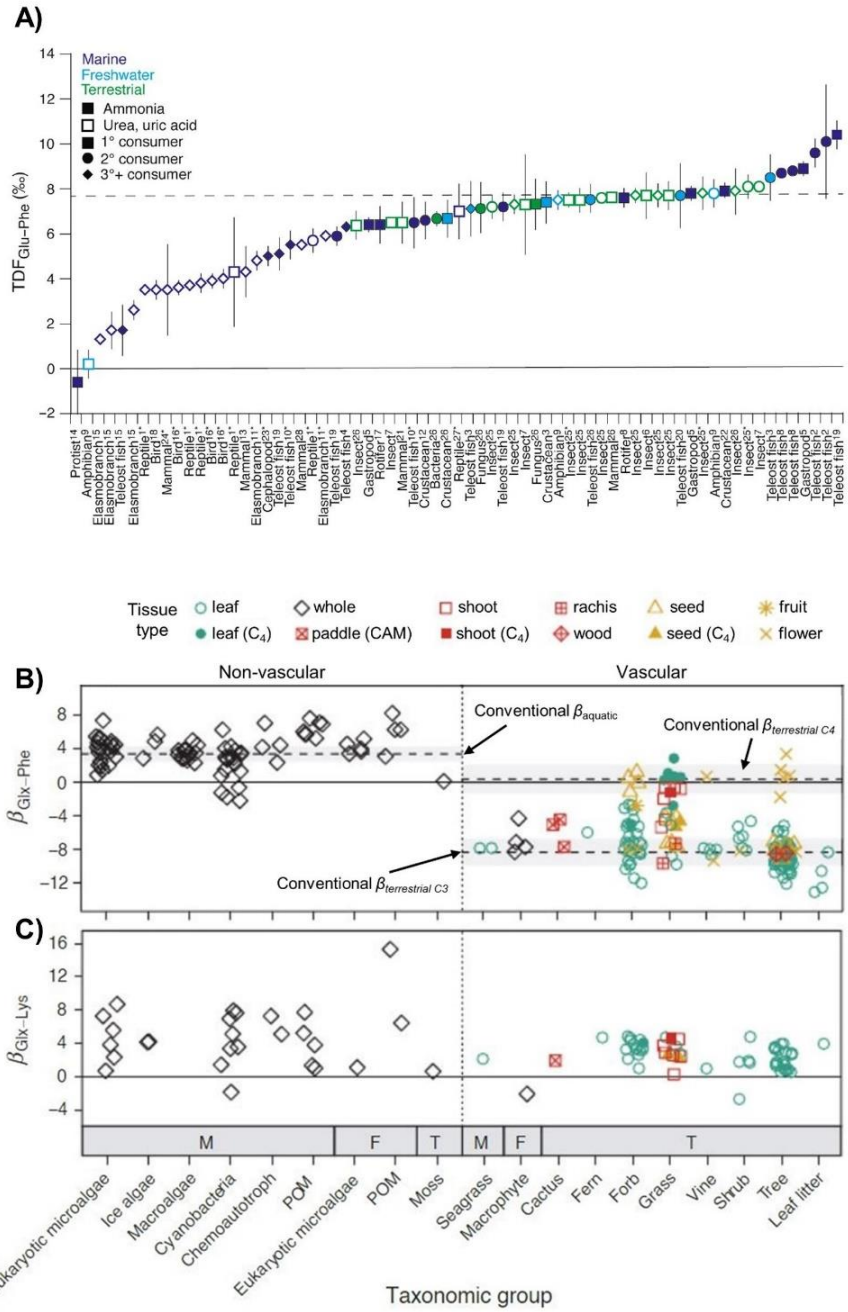

Figure 26. Variability of trophic discrimination factors and β_{Tr-Sr} among taxa. **A)** Mean (± standard deviation) of published trophic discrimination factors ($TDF_{Glu\text{-}Phe}$) for a wide range of consumer-diet pairings, from McMahon and McCarthy (2016). Dark blue, cyan, and green symbols represent marine, freshwater, and terrestrial consumers, respectively; filled and open symbols represent ammonia- and urea/uric acid-producing consumers, respectively; and square, circle, and diamond symbols represent primary, secondary, and tertiary

(and higher) consumers, respectively. **B)** and **C)** show the variability of published $\beta_{Glx\text{-}Phe}$, and $\beta_{Glx\text{-}Lys}$ values, respectively, in different taxonomic groups, habitat types (i.e., M = marine, F = freshwater, T = terrestrial), tissue type, and mode of photosynthesis, from Ramirez et al. (2021). Dashed lines and shaded ribbons denote the conventionally applied β values (mean ± standard deviation) for aquatic (3.4 ± 0.9 ‰, Chikaraishi et al., 2009), terrestrial C_3 (-8.4 ± 1. 6‰, Chikaraishi et al., 2010), and terrestrial C_4 (0.4 ± 1.7 ‰, Chikaraishi et al., 2010) primary producers.

The use of global model estimates to explore physical, biogeochemical and atmospheric controls on mercury concentrations in tunas

In addition to analytical advances, the recent development of global physical and biogeochemical models now allows better quantifying the variability of ocean (thermo-)dynamics and baseline processes, and tracking nutrient flow along marine food webs. Combined together, ocean and biogeochemical models provide a robust view of the baseline bottom-up biogeochemical controls on upper trophic levels (e.g., effects of changes in phytoplankton iron uptake on upper trophic biomass, Tagliabue et al., 2020). In tuna ecology, these ocean and biogeochemical models highlighted the importance of sub-surface environmental variables, in particular oxygen minimum zone intensity, primary production, and nutrient supply, to explain spatial variability of tuna trophic positions (Pethybridge et al., 2018a).

Physical and biogeochemical models also represent an alternative to missing marine MeHg models to investigate the mechanisms governing both formation and bioavailability of MeHg at the base of marine food webs. Global marine Hg chemistry and transport models are being developed (Archer and Blum, 2018; Semeniuk and Dastoor, 2017; Zhang et al., 2019), yet they remain overall limited by the lack of oceanic Hg data, and the lack of knowledge on marine biogeochemical processes governing methylation and demethylation reactions in the ocean.

Conversely, thanks to long-term and continuous Hg monitoring at several sites of the world (Slemr et al., 2015; Zhang et al., 2016), atmospheric Hg models have been shown to predict reasonable spatial patterns of gaseous elemental Hg in near-surface air (Travnikov et al., 2017). These models therefore represente a good alternative to missing high resolution worldwide-observed Hg data in the atmosphere, and allowing the prediction of global Hg fluxes and concentrations in the atmosphere and the surface boundary layer.

Materials and methods

In this thesis, we focused on Hg concentrations in tuna white muscle samples only, as it is the commonly used tissue in studies investigating both trophic ecology and Hg bioaccumulation, but also the final storage for MeHg in fish. Moreover, although considered to reflect long-time exposure to Hg (muscle Hg turnover in captive bluefin tuna ~ 2.8 years, Kwon et al., 2016), a recent collaborative study, comparing total Hg concentrations in blood and white muscle in tunas from the western Pacific Ocean, highlighted the pertinence of these two tissues for large-scale Hg monitoring studies (Barbosa et al., 2022).

About 5,800 tuna samples with total Hg concentrations were compiled from published and unpublished regional studies and assembled into our global database (Figures 26 & 27). This corresponds to records of 1,422 bigeye, 2,467 yellowfin, 1,003 skipjack, and 900 albacore tunas. The majority of these tuna muscle samples (n ~ 3,400) were already available as part of the CLIOTOP international collaborative project (Bodin et al., 2020), with about 1,000 Hg concentrations analyses already performed in the central and western Pacific Ocean (Houssard et al., 2019). Mercury data from the literature were also integrated in the global database (*n* ~ 1,500), as long as individuals' fish length and sampling date and coordinates (i.e., longitude and latitude) were available, as these metadata are needed to explore both spatial and temporal trends of Hg accumulation in tunas. New samples were also collected specifically for this study (*n* = 292). This chapter presents the methodologies relative to i) the samples collection, ii) the analytical methods for total Hg concentrations and ecological tracers, and iii) the extraction of models outputs. Figure 28 shows the number of biochemical analyses performed during this thesis, versus the number of data already collected when integrated into the global database. Figure 29 summarizes all the biochemical tracers and model outputs, and their specific use in this study.

Tuna sampling

Tuna samples collection

Tuna samples were collected onboard commercial, recreational and scientific fishing boats by multiple research programs (Figure 26). Metadata, i.e., date, position and gear type, were provided for each sample, and sampling spanned from 1997 to 2020. Fork length (FL) was measured and ranged from 29 to 185 cm (98 ± 38, mean ± sd), 30 to 180 cm (96 ± 33), 25 to 90 cm (56 ± 13), 20 to 120 cm (86 ± 25) for bigeye, yellowfin, skipjack, and albacore respectively. For each fish, a white muscle sample tissue was collected and stored frozen prior to analyses.

Figure 27. Pictures of tuna sampling. **A)** purse seiner operating in the Indian Ocean, **B)** tuna sampling onboard a purse seiner during the landing at Victoria Port (Seychelles) ©T. Vergoz, **C)** landing of tunas ©CPS, **D)** piece of tuna muscle, and **E)** longliner operating in the southwestern Pacific waters ©CPS.

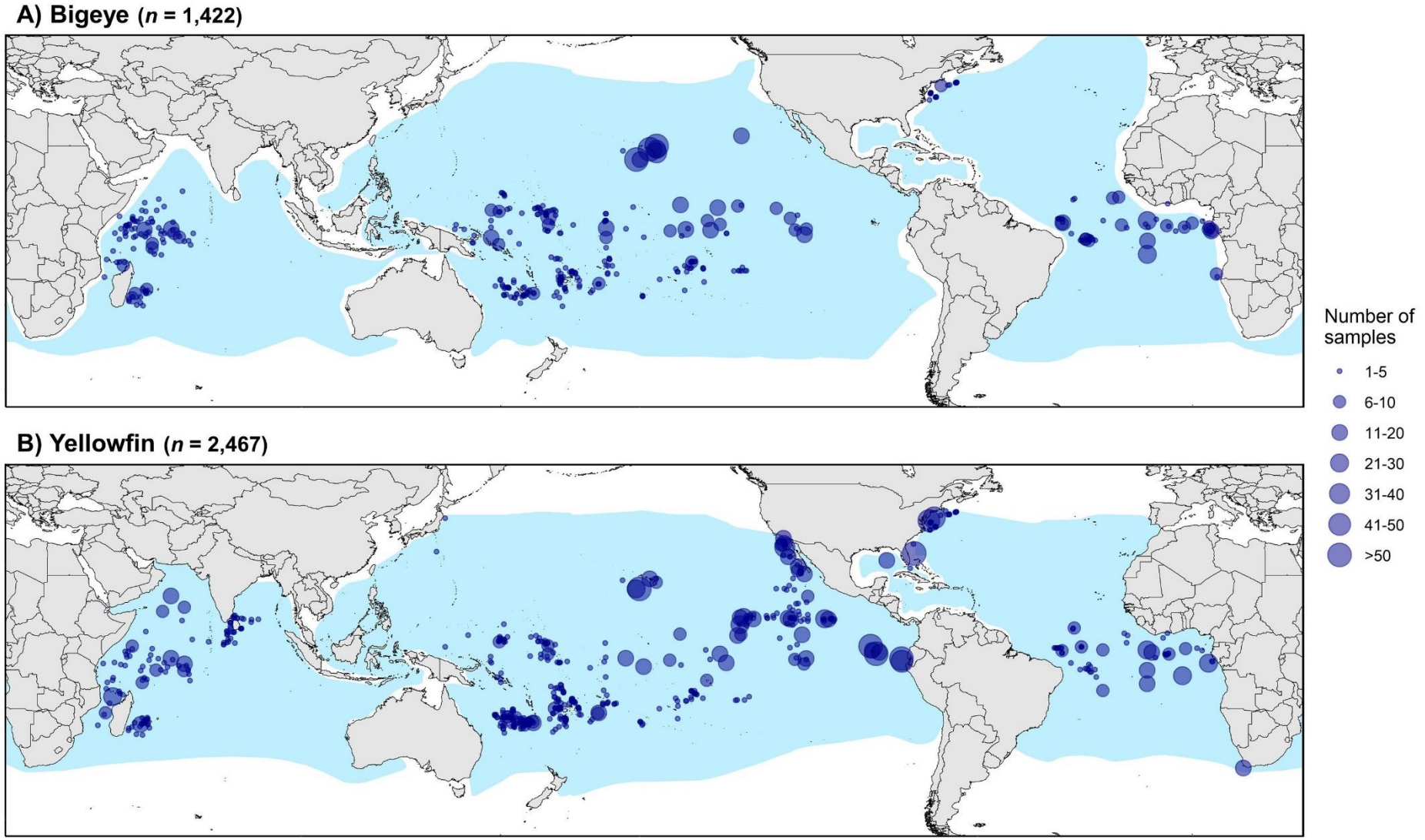
A) Bigeye (n = 1,422)
B) Yellowfin (n = 2,467)
Number of samples
1-5
6-10
11-20
21-30
31-40
41-50
>50

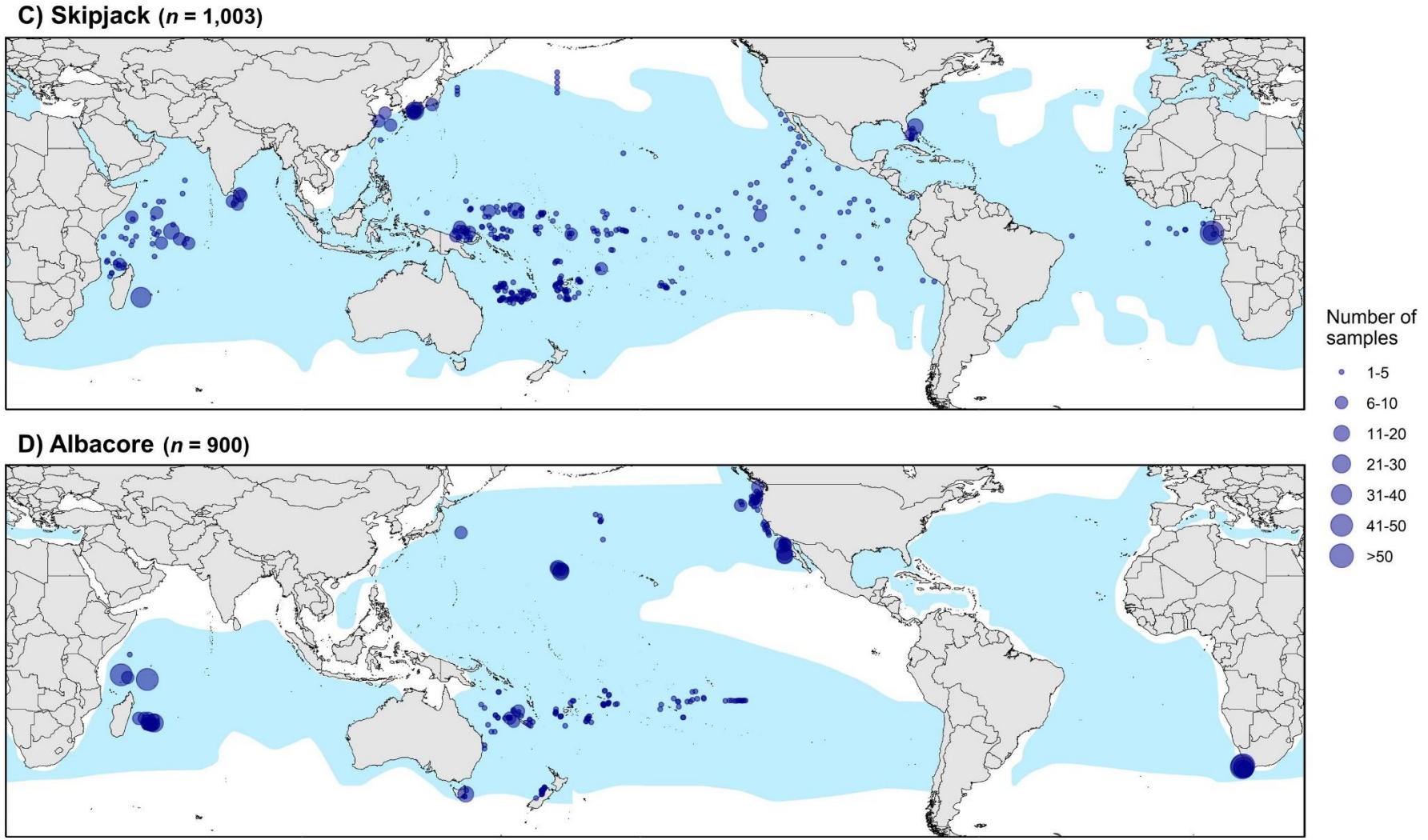

Figure 28. Sample provenance with mercury concentrations (dark blue circles) and the potential habitat distribution (light blue) of **A)** bigeye, **B)** yellowfin, **C)** skipjack, and **D)** albacore tunas. The size of circles is proportional to the number of individuals collected. The distributions of potential habitat distribution were obtained from the IUCN Red List Spatial Data of tunas (IUCN, 2017).

Age estimation

Given that Hg bioaccumulates with fish age and length, and that tuna growth is suspected to vary among species and ocean basins (Murua et al., 2017), we estimated fish age to explore the effect of differential growth patterns on tuna Hg bioaccumulation. We used growth parameters from the respective last tuna stock assessments when data were available (Dortel et al., 2015; Eveson et al., 2015; Farley et al., 2020; Hallier et al., 2005; ICCAT, 2014, 2019; Vincent et al., 2019), or from recently published studies (Griffiths et al., 2019) (SI Appendix B, Table S1). As recommended in the stock assessments of albacore and tropical tunas, we used two growth curves in the Pacific Ocean (i.e., eastern and western), and one single curve in the Indian Ocean. In the Atlantic, while one growth curve was used for bigeye and yellowfin, two separated curves were fitted for eastern and western Atlantic skipjack.

Analytical methods

Total mercury concentrations analyses

Among the total number of tuna samples, 1,458 (~ 25 % of the global database) were analysed for total Hg concentrations during this thesis (Figure 28). Total Hg concentrations were measured on powdered and homogenized white muscle samples in different laboratories, with laboratory-specific reference standards, and following two different analytical methods (SI Appendix B, Table S2). For the majority of the samples (n = 3767, ~ 65 %), total Hg concentrations were obtained by thermal decomposition, gold amalgamation and atomic absorption spectrometry (DMA-80, Milestone, Italy). Newly-analysed samples during this thesis were analysed with this method at GET (Toulouse, France) (SI Appendix B, Table S2). The rest of the dataset (n = 2025, 35 %) were measured by acid digestion followed by cold vapor atomic fluorescence spectroscopy. Blank and biological standard reference materials were routinely used in each analytical batch to check Hg measurement accuracy and traceability. Most of the samples were analysed freeze-dried; and in case of fresh frozen samples, we converted Hg concentrations considering 70 % of moisture in white muscle of tropical tunas (Bodin et al., 2017; Houssard et al., 2019; Kojadinovic et al., 2006), so that all total Hg concentrations are expressed on a dry weight (dw) basis. Total Hg concentrations reflect MeHg concentrations as most of total Hg (> 90%) is in its methylated form in tunas (Houssard et al., 2019; Senn et al., 2010; Storelli et al., 2002; Voegborlo et al., 2006).

While the majority of total Hg concentrations were obtained on bulk powder samples, some were measured on lipid-free powders (n < 12 %), as recommended for $\delta^{13}C$ analyses to avoid bias related to lipid content (see next paragraph). The effect of lipid extraction on total Hg concentrations has been investigated during this thesis, and the resulting study, published in Marine Environmental Pollution as a short communication, is presented on SI Appendix C (Médieu et al., 2021b). We found that lipid extraction with dichloromethane, a neutral solvent commonly used in trophic ecology studies, has no effect on total Hg concentrations, likely resulting from i) the affinity of MeHg to proteins in tuna muscle, ii) the low lipid content in tropical tuna muscle tissues, and iii) the non-polar nature of dichloromethane. These results allowed us to use equivalently bulk samples and lipid-free samples to document in parallel tuna Hg concentrations at a global scale.

Bulk muscle carbon and nitrogen stable isotopes

To explore the potential effects of changes in trophic position, habitat, and feeding pathway, we combined bulk muscle $\delta^{13}C$ and $\delta^{15}N$ values to total Hg concentrations when possible. A total of 4,262 $\delta^{13}C$ and $\delta^{15}N$ values were therefore added in our global database, corresponding to 1,082 bigeye, 1,721 yellowfin, 730 skipjack, and 729 albacore tunas. Among these 4,262 records, 3,204 were already available and combined from published or unpublished studies, while 1,041 were determined during this thesis when enough material was left (Figure 28).

Lipid extraction methods

In the central Atlantic and western Indian Oceans, most of the available $\delta^{13}C$ and $\delta^{15}N$ records were obtained on lipid-free muscle powders (*n* = 705), in order to take into account the influence of lipids on $\delta^{13}C$ values (DeNiro and Epstein, 1977). Lipids were removed, either manually or automatically (i.e., high temperature and pressure), as detailed below and recommended for routine analysis of lipids/fatty acids and/or prior $\delta^{13}C$ and $\delta^{15}N$ analyses (Bodin et al., 2009; Ménard et al., 2007). Two neutral solvents were used, dichloromethane or cyclohexane, as they have been shown to have negligible effects on the $\delta^{15}N$ values across tissues and tropical tuna species (Sardenne et al., 2015). For homogeneity, during this thesis we extracted lipids on all samples collected in central Atlantic and western Indian Oceans prior to $\delta^{13}C$ and $\delta^{15}N$ analyses (*n* = 264) at LEMAR (Plouzané, France) (Figure 28). We used the automated extraction with dichloromethane, as in Bodin et al., (2009), to reduce handling steps and to ensure increased reproducibility.

Manual extraction: Following the method of Ménard et al. (2007), 100 ± 4 mg of powdered and dried muscle sample were mixed with 10 mL of solvent for 1 h using a rotary shaker. The mixture of the powder and the solvent was then separated by centrifugation at 2500 rpm for 10 min at 10°C. The lipid-free powders were then stored in a dry-room until $\delta^{13}C$ and $\delta^{15}N$ analyses.

Automated extraction: 150 ± 10 mg of homogenized dried samples were extracted with 20 mL of solvent at 100°C under 1400 psi for 10 min using an ASE 350 Accelerated Solvent Extractor (Dionex, Voisins de Bretonneux, France), following the method of Bodin et al. (2009). The lipid-free powders were stored in a dry-room until $\delta^{13}C$ and $\delta^{15}N$ analyses.

Isotope ratio mass spectrometry

Carbon and nitrogen stable isotopes were measured on homogenized freeze-dried samples (either bulk or lipid-free) packed in tin cups and analysed with an elemental analyser (i.e., on-line C-N analyser or Costech elemental analyser) coupled to an isotope ratio mass spectrometer (SI Appendix B, Table S2). Results were reported in the δ unit notation and expressed as parts per thousand (‰) relative to international standards (atmospheric N_2 for nitrogen and Vienna Pee Dee belemnite (VPDB) for carbon). Depending on the laboratory, a combination of certified and/or in-house reference materials were used to determine that uncertainty was below 0.2 ‰. Tuna $\delta^{13}C$ values were corrected for lipids, either with chemical extraction (*n* = 948, 22 %), or using a mass balance equation for samples with elevated lipid content (C:N > 3.5, *n* = 764, 18 %), with parameters derived from Atlantic bluefin tuna muscle (Logan et al., 2008). The vast majority of samples analysed in this thesis were analysed in D. Gillikin's lab at Union College (New York, USA).

Amino acid compound-specific nitrogen stable isotopes

A total of 149 tuna samples with amino acid compound specific $\delta^{15}N$ values were compiled in the global database, corresponding to 24 published data (Houssard et al., 2017; Lorrain et al., 2015b), and 125 newly-analysed amino acid compound-specific $\delta^{15}N$ data on selected tuna samples during this thesis at the CSIRO (Tasmania, Australia) (Figure 28). Freeze-dried samples were prepared by acid hydrolysis followed by esterification and trifluoroacetylation as per Dale et al. (2011). The $\delta^{15}N$ isotope values of individual amino acids were determined with a Trace GC gas chromatograph interfaced with a Delta V Plus isotope ratio mass spectrometer (IRMS) through a GC-C combustion furnace (980°C), reduction furnace (650°C) and liquid N_2 cold trap. The samples (0.5 µL) were injected splitless onto a forte BPX5 capillary column (30 m × 0.32 mm × 1.0 µm film thickness) at an injector temperature of 180°C with a constant helium flow rate of 1.5 $mL.min^{-1}$. The column was initially held at 50°C for 2 min and then increased to 120°C at a rate of 10°C.min^{-1}. Once at 120°C, the temperature was increased at a rate of 4°C.min^{-1} to 195°C and then at 5°C.min^{-1} to 235°C where it was held for 5 min. The temperature was then further increased to 300°C at 15°C.min^{-1} and held for 8 min. All samples were analysed at least in triplicate. The $\delta^{15}N$ values were normalised as follows: each sample analysis consisted of three separate IRMS analyses bracketed by a suite of amino acids with known $\delta^{15}N$ values. The slope and intercept of known versus measured values were then used to correct the measured values for the sample set.

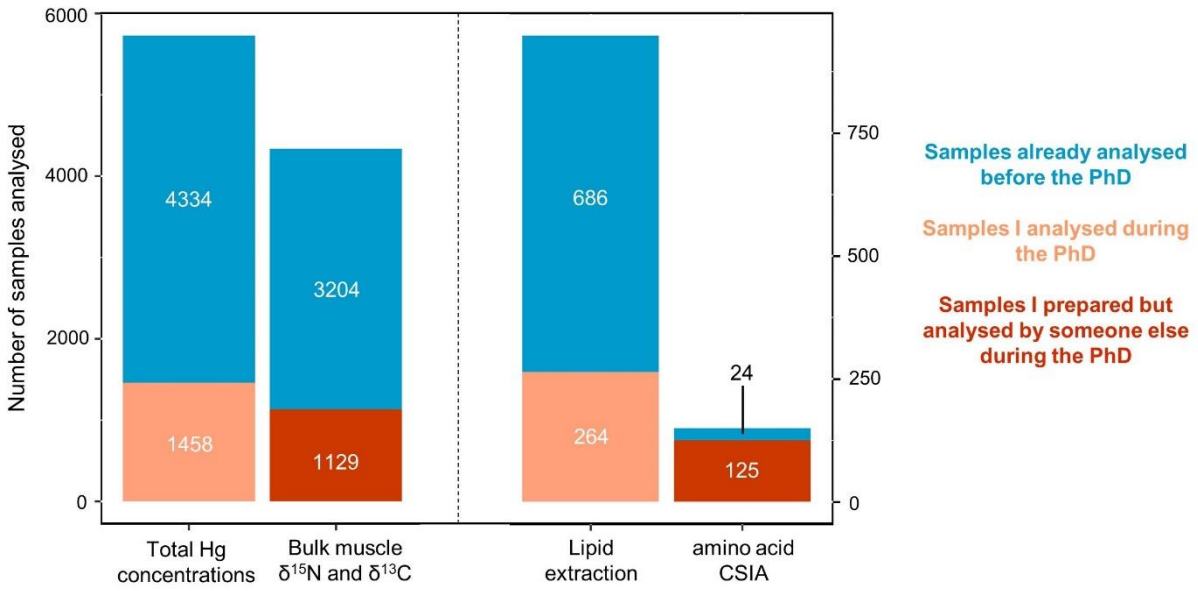

Figure 29. Summary of analytical analyses. Number of samples analysed for total mercury (Hg) concentrations, bulk muscle nitrogen ($\delta^{15}N$) and carbon ($\delta^{13}C$) stable isotopes, and amino acid compound-specific stable isotopes (CSIA). The number of lipid extractions performed prior to $\delta^{15}N$ and δ^{13} analyses is also presented. Colours indicate if analyses were performed before or during the thesis, and in the latter case, if I did the analyses or just prepared the samples before someone else did the analyses.

Extraction of ecosystem and environmental model outputs

Biogeochemical and physical oceanic model outputs: tracers of marine Hg cycle and tuna ecology

Ocean physical and biogeochemical model outputs were obtained with two methodologies during this thesis. In Chapter 1, we extracted surface variables: monthly mean sea surface temperature (SST in °C) from the National Oceanic and Atmospheric Administration (NOAA, https://www.ncdc.noaa.gov/oisst (Reynolds et al., 2002); and monthly chlorophyll-a observations (Chl-a, mg.m_3) from a continuous dataset of merged L4 Ocean Colour products provided by GlobColour (http://globcolour.info). Monthly means of net primary production (NPP, mg $C.m^{-2}.day^{-1}$) were derived from a vertically generalized production model (VGPM, http://www.science.oregonstate.edu/ocean.productivity/custom.php; Behrenfeld and Falkowski, 1997). Variables at depth or sub-surface included the mixed layer depth (MLD) and depths of the 12°C and 20°C isotherms (D_{iso12} and D_{iso20}, m), all obtained from the monthly global ARMOR3D L4 dataset (Guinehut et al., 2012).

For Chapters 2-4, thanks to the expertise of climate modeling scientists involved in the MERTOX project, we used the isotope-enabled version of the Pelagic Interactions Scheme for Carbon and Ecosystem Studies (PISCES) biogeochemical model, attached to the Nucleus for European Modelling of the Ocean (NEMO) general ocean circulation model (Aumont et al., 2015). The ocean engine of NEMO is a primitive equation model adapted to regional and global ocean circulation problems. It is intended to be a flexible tool for studying the ocean and its interactions with the others components of the earth climate system over a wide range of space and time scales (Gurvan et al., 2019). The ecosystem component of PISCES includes two phytoplankton types (nanophytoplankton and diatoms), two zooplankton types (microzooplankton and mesozooplankton) and an implicit nitrogen fixer group. Ocean model resolution is nominally 2° but approaches 0.5° near the equator and poles, while vertical resolution varies between 10 and 500 m thickness over 31 levels between the surface and abyssal ocean. Ocean variables extracted with NEMO-PISCES included sea surface temperature (at 5 m depth), total chlorophyll averaged over the upper 100 m, net primary production, depths of the 20°C, 18°C, and 12°C isotherms, oxygen concentration at 375 m, depth of net heterotrophy (defined as the depth at which autotrophy is overcome by heterotrophy). We also extracted the rate of organic carbon exported through 100 m, and at the depth of net heterotrophy.

For the two methodologies, all ocean variables were extracted from grid cells nearest to the date and location of tuna samples. Given the long Hg isotopic turnover during bioaccumulation in tuna white muscle (~ 700 days; Kwon et al., 2016), we assumed that Hg values of a given individual captures at a single date and place are not exclusively explained by the environmental conditions at this date but also prior conditions over previous months. As ^{15}N turnover in tuna white muscle is approximately 6 months (Madigan et al., 2012), averages of ocean variables were extracted over six months prior to the actual sampling dates, as already done in previous studies on tropical tuna species (Houssard et al., 2019; Pethybridge et al., 2018a).

Carbon and nitrogen stable isotope model estimates: tracers of lower trophic levels processes

During this thesis, we derived estimated baseline $\delta^{15}N$ and $\delta^{13}C$ data using two different models. Following previous work in the CLIOTOP framework (Logan et al., 2020; Pethybridge et al., 2018a), we first used the Model of Ocean Biogeochemistry and Isotopes (MOBI, Somes et al., 2017) (Chapter 1). This model includes a three-dimensional (3D, 1.8° x 3.6 ° horizontal, 19 vertical levels) ocean circulation model forced with fixed monthly climatological winds (Weaver et al., 2001), which does not account for inter-annual variability. The biogeochemical component is a 2N2PZD (2 Nutrients, 2 Phytoplankton, 1 Zooplankton, and 1 Detritus) ecosystem model (Somes and Oschlies, 2015). The processes in the model that fractionate the nitrogen isotopes (i.e., preferentially incorporate ^{14}N into the product) are phytoplankton NO_3 assimilation (6 ‰), zooplankton excretion (4 ‰), N_2 fixation (1 ‰), water column denitrification (20 ‰) and benthic denitrification (6 ‰), in which the respective fractionation factor yields the $\delta^{15}N$ difference between substrate and product (Somes et al., 2010). The baseline $\delta^{15}N$ values reproduce the major features in a global seafloor $\delta^{15}N$ database (Tesdal et al., 2013).

For Chapters 2-4, we derived estimated baseline $\delta^{15}N$ and $\delta^{13}C$ data with PISCES biogeochemical model. Sources of carbon included rivers (-28 ‰ for dissolved organic carbon and 0 ‰ for dissolved inorganic carbon) and atmospheric CO_2 (-6.6 ‰ under preindustrial conditions). Sources of nitrogen included rivers (2 ‰), atmospheric deposition (-4 ‰) and nitrogen fixation by diazotrophs (-1 ‰). Extracted variables included $\delta^{15}N$ of nitrate ($\delta^{15}N_{NO3}$) and particulate organic matter ($\delta^{15}N_{POM}$) averaged over the upper 100 m, $\delta^{13}C$ of dissolved inorganic carbon ($\delta^{13}C_{DIC}$) and particulate organic matter ($\delta^{13}C_{POM}$) averaged over the upper 100 m, and vertically integrated net primary production.

Like ocean physical and biogeochemical variables, baseline stable isotope signature were extracted at each tuna samples location, and averaged over a six-month period preceding individual capture date to account for Hg and nitrogen turnover in tuna white muscle.

GEOS-Chem mercury model outputs: tracers of atmospheric mercury

The global chemical transport model GEOS-Chem (www.geos-chem.org), version v11-02 was used to simulate total gross Hg deposition fluxes to ecosystems, and atmospheric Hg^0 concentrations in the atmosphere. GEOS-Chem is a global model of atmospheric chemistry driven by meteorological inputs from the Goddard Earth Observing System (GEOS) of the NASA Global Modeling and Assimilation Office (MERRA-2). The model couples a 3D atmosphere (Holmes et al., 2010), a 2D surface-slab ocean (Soerensen et al., 2010), and a 2D terrestrial reservoir (Selin et al., 2008) at different horizontal resolutions (i.e., 6° x 7.5°, and 2° x 2.5°). GEOS-Chem allows projecting present-day and future total (wet + dry) gross Hg deposition fluxes to ecosystems, and elemental Hg^0 concentrations in the atmosphere. The gaseous elemental Hg^0 surface fluxes include anthropogenic sources, biomass burning, and geogenic activities, as well as bidirectional fluxes in atmosphere-terrestrial and atmosphere-ocean exchanges (Song et al., 2015). For further details, a comprehensive description of the model is available in Angot et al. (2018) and Travnikov et al. (2017). The simulation was performed using an anthropogenic emissions inventory developed for the year 2015 in the context of the latest Global Mercury Assessment (UN Environment, 2019). In order to account for inter-annual variability,

the simulation was performed with meteorological data for the years 2013-2015 following a one-year spin-up. Annually-averaged Hg^0 concentrations and total deposition fluxes were extracted from grids where tuna samples were collected. In order to account for the spatial migration of tunas, Hg^0 concentrations and deposition fluxes were averaged over adjacent grid boxes. Adjacent grid boxes with a fraction of ocean < 50 % were not taken into account in the average calculation. Model outputs were evaluated against available globally-distributed observations.

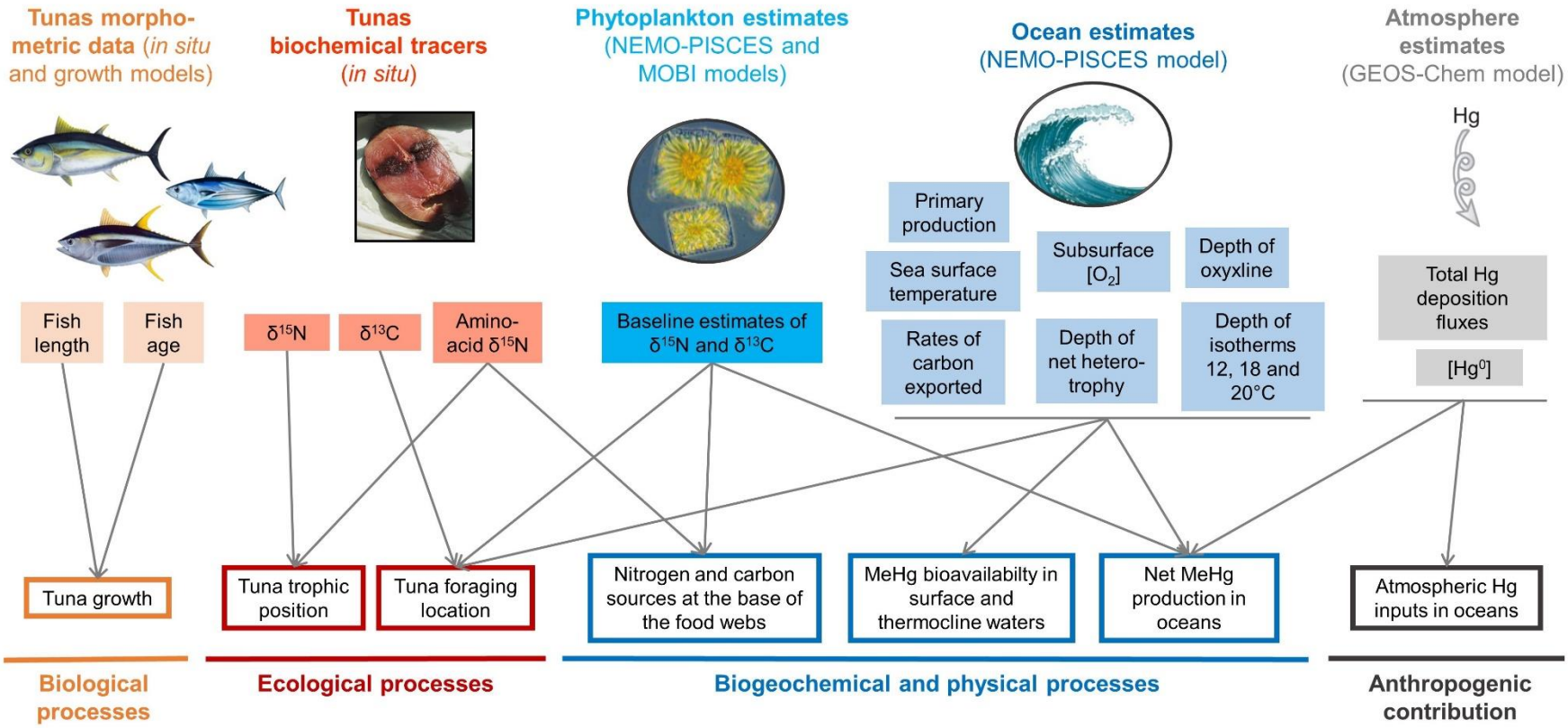

Figure 30. A combination of tuna morphometric data, biochemical tracers and model outputs used to explore the main drivers of mercury (Hg) concentrations in tunas. Fish length was measured for each individual, and used to estimate tuna's age using species- and ocean- specific growth models. Bulk muscle nitrogen ($\delta^{15}N$) and carbon ($\delta^{13}C$) stable isotopes were measured in tuna samples, as well as compound specific amino acid stable isotope composition. The NEMO-PISCES and MOBI models were used to estimate for each individual baseline carbon and nitrogen stable isotope signature. The NEMO-PISCES model was also used to estimate a combination of ocean variables including surface (sea surface temperature, SST; net primary production, NPP; and rates of carbon exported over 100 m) and sub-surface or deep (mixed layer depth, MLD; rates of carbon exported at the depth of net heterotrophy; subsurface $[O_2]$; depth of oxycline; depth of net heterotrophy; and depths of isotherms 12, 18, and 20°C) variables. Similarly, for each tuna samples, the GEOS-Chem Hg model was used to estimate elemental Hg concentrations ($[Hg^0]$) in the atmosphere, and gross Hg deposition fluxes.

Results

Chapter 1. Stable mercury concentrations of tropical tunas in the south western Pacific Ocean: An 18-year monitoring study

Anaïs Médieu[1], David Point[2], Aurore Receveur[3], Olivier Gauthier[1], Valérie Allain[3], Heidi Pethybridge[4], Christophe E. Menkes[5], David P. Gillikin[6], Andrew T. Revill[4], Christopher Somes[7], Jeremy Collin[1], Anne Lorrain[1]

[1]Univ Brest, CNRS, IRD, Ifremer, LEMAR, F-29280 Plouzané, France
[2]Observatoire Midi-Pyrénées, GET, UMR CNRS 5563/IRD 234, Université Paul Sabatier Toulouse 3, Toulouse, France
[3]Pacific Community, Oceanic Fisheries Programme, Nouméa, New Caledonia
[4]CSIRO Oceans and Atmosphere, Hobart, Tasmania, Australia
[5]ENTROPIE (UMR 9220), IRD, Univ. de la Réunion, CNRS, Nouméa, New Caledonia
[6]Department of Geology, Union College, 807 Union St., Schenectady, NY, 12308, USA
[7]GEOMAR Helmholtz Centre for Ocean Research Kiel, Düsternbrooker Weg 20, 24105 Kiel, Germany

Manuscript published in Chemosphere (https://doi.org/10.1016/j.chemosphere.2020.128024)

Abstract

Global anthropogenic mercury (Hg) emissions to the atmosphere since industrialization are widely considered to be responsible for a significant increase in surface ocean Hg concentrations. Still unclear is how those inputs are converted into toxic methylmercury (MeHg) then transferred and biomagnified in oceanic food webs. We used a unique long-term and continuous dataset to explore the temporal Hg trend and variability of three tropical tuna species (yellowfin, bigeye, and skipjack) from the southwestern Pacific Ocean between 2001 and 2018 (n = 590). Temporal trends of muscle nitrogen ($\delta^{15}N$) and carbon ($\delta^{13}C$) stable isotope ratios, amino acid (AA) $\delta^{15}N$ values and oceanographic variables were also investigated to examine the potential influence of trophic, biogeochemical and physical processes on the temporal variability of tuna Hg concentrations. For the three species, we detected significant inter-annual variability but no significant long-term trend for Hg concentrations. Inter-annual variability was related to the variability in tuna sampled lengths among years and to tuna muscle $\delta^{15}N$ and $\delta^{13}C$ values. Complementary AA- and model-estimated phytoplankton $\delta^{15}N$ values suggested the influence of baseline processes with enhanced tuna Hg concentrations observed when dinitrogen fixers prevail, possibly fuelling baseline Hg methylation and/or MeHg bioavailability at the base of the food web. Our results show that MeHg trends in top predators do not necessary capture the increasing Hg concentrations in surface waters suspected at the global oceanic scale due to the complex and variable processes governing Hg deposition, methylation, bioavailability and biomagnification. This illustrates the need for long-term standardized monitoring programs of marine biota worldwide.

Introduction

Mercury (Hg) is a widely distributed trace element of particular concern to human and ecosystem health. Its toxicological effects are strongly dependent on the physical properties of its different chemical forms (Hintelmann, 2010). Gaseous elemental Hg is emitted to the atmosphere through natural (volcanism and erosion) and anthropogenic (fossil fuel combustion and artisanal gold mining) processes (Pirrone et al., 2010). In open ocean regions, the dominant source of inorganic Hg (iHg) is atmospheric deposition with other inputs coming from ocean margins, groundwater, benthic sediments and hydrothermal vents (Selin et al., 2007). Only a fraction of iHg is naturally converted into methylmercury (MeHg), the organometallic form of Hg characterized by strong neurotoxicity, persistence and unique biomagnification properties in food webs. Over the past 150 years of the industrial era, anthropogenic Hg use and emissions have considerably modified the natural global Hg cycle (Selin et al., 2008). Models suggest that anthropogenic activities have increased atmospheric Hg concentrations and have tripled the iHg content in the global ocean surface waters (Lamborg et al., 2014), but with suspected sub-regional differences. In particular in the North Pacific Ocean, surface water Hg concentrations have been reported to be higher in the eastern North Pacific than in the western North Pacific (Sunderland et al., 2009). Most global models utilize ocean Hg data collected in oceanic regions from the northern hemisphere, but questions have risen about how well these models describe potential hemispherical ocean patterns with lower Hg concentrations reported in the southern atmosphere (Horowitz et al., 2017).

Humans are exposed to MeHg primarily by the consumption of marine fish, especially of top predators such as tuna (Mergler et al., 2007; Sunderland, 2007) as MeHg biomagnifies naturally in marine food webs (Cai et al., 2007; Ordiano-Flores et al., 2012, 2011). Mercury concentrations in tuna are known to vary geographically between ocean basins and species (Chouvelon et al., 2017; Houssard et al., 2019; Kojadinovic et al., 2006; Nicklisch et al., 2017), sometimes exceeding food safety guidelines (1 $mg.kg^{-1}$ fresh

tissue) (WHO and UNEP Chemicals, 2008). Mercury concentrations in organisms are governed by a complex interplay between physiological (age/length, metabolism and assimilation efficiencies), ecological (foraging depth and food web structures), biogeochemical (baseline *in situ* MeHg production and bioavailability) and physical (thermocline depth and sea surface temperature) processes (Cai et al., 2007; Chouvelon et al., 2017; Choy et al., 2009; Teffer et al., 2014). Recently, a spatial study from the western Pacific Ocean suggested that fish length and deeper thermoclines (used as a proxy of tuna foraging habitat) were the two main drivers enhancing Hg concentrations in tuna, with tuna trophic position (TP) and oceanic primary production being of less importance but still influencing tuna Hg concentrations (Houssard et al., 2019).

Despite their relatively high MeHg concentrations, tuna species are among the most popular fish species consumed worldwide (FAO, 2018). In the central and western Pacific Ocean, tuna fisheries accounted in 2017 for about 80 % of the total Pacific Ocean catches and 54 % of the global tuna catch (Williams and Reid, 2018). For Pacific Island countries and territories, the large tuna resources deliver great economic benefits through the sale of fishing access to distant water fishing nations and employment in fish processing (Bell et al., 2011; Gillett, 2009). In terms of food and nutrition security, tuna also represent a major source of proteins, essential fatty acids, vitamins and minerals (Di Bella et al., 2015; Sirot et al., 2012). These species have been consequently identified as key food resources for good nutrition to complement declining coastal resources in a context of high levels of diabetes and obesity in this region, while taking into account their Hg content (Di Bella et al., 2015).

Anticipating changes in human Hg exposure depends on our ability to capture and predict spatial and temporal Hg trends in marine food webs. Only two temporal studies of tuna Hg content are available to date, showing distinct results regarding Hg longterm trends. In the northern central Pacific Ocean (Hawaii), Drevnick et al. (2015) suggested that Hg concentrations in yellowfin tuna (*Thunnus albacares*) increased by at least 3.8 % per year between 1971 and 2008, despite considering only three sampling years. Conversely, in the North Atlantic Ocean, Lee et al. (2016) revealed a decadal decline of Hg concentrations in Atlantic bluefin tuna *(T. thynnus*) of about 2.4 % between 2004 and 2012, suggesting potential benefits of the reduction of anthropogenic emission in North America. Unfortunately, no complementary trophic ecology data were available in those two studies to discuss if confounding ecological factors might contribute to the contrasted temporal trends of Hg content documented worldwide.

Stable isotope ratios of nitrogen ($\delta^{15}N$) and carbon ($\delta^{13}C$) are widely used to examine trophic ecology of marine organisms (Fry, 2006). In particular, $\delta^{13}C$ values provide information on basal organic carbon sources while $\delta^{15}N$ values are used to estimate the TP of a consumer as they increase predictably between prey and consumers. Therefore, $\delta^{15}N$ values are commonly used to explore Hg biomagnification along trophic webs (Atwell et al., 1998; Cai et al., 2007; Teffer et al., 2014). In addition to diet (i.e., trophic effects), variability of basal stable isotopic composition (i.e., baseline effects) also affects consumer $\delta^{15}N$ values (Lorrain et al., 2015b). Thus, $\delta^{15}N$ values also represent a potential proxy to infer baseline biological processes fuelling Hg methylation and/or net basal MeHg bioavailability. To account for complex primary production dynamics influencing the isotopic baseline, and produce accurate measures of a consumer's TP, amino acid compound-specific $\delta^{15}N$ analyses (AA-CSIA) are also used (Bradley et al., 2015; Lorrain et al., 2015b). Within a consumer, the $\delta^{15}N$ values of source amino acids (Sr-AA; e.g., phenylalanine and glycine) track the $\delta^{15}N$ values at the base of the food web, while trophic AA (Tr-AA; e.g., glutamic acid), being enriched in ^{15}N with each trophic level, provide information about a consumer's TP (Popp et al., 2007). Overall, the combination of muscle stable isotope ratios and AA-CSIA is a powerful tool to investigate both Hg methylation and biomagnification along food webs.

The specific objectives of our study were to i) investigate longterm trends of Hg concentrations in tuna from the New Caledonia-Fiji sub-region in the southwestern Pacific Ocean, and to ii) identify the main drivers of inter-annual variability of tuna Hg concentrations among physiological, ecological, biogeochemical and physical parameters. We analysed a unique long-term, continuous and large Hg dataset (*n* = 590) in three commercial tropical tuna species (yellowfin, *Thunnus albacares*; bigeye, *T. obesus*; and skipjack, *Katsuwonus pelamis*) from 2001 to 2018. Complementary muscle $\delta^{15}N$ and $\delta^{13}C$ values, AA-CSIA and model estimated phytoplankton $\delta^{15}N$ values were also used to explore the possible influence of biogeochemical and ecological factors on Hg content in tuna (i.e., changes in nutrient sources, primary productivity and tuna TP reflecting pathways of energy transfer). Finally, a suite of oceanographic variables (sea surface temperature, chlorophyll-a, net primary production, mixed layer depth, depths of isotherms 20°C and 12°C and oceanic El Niño index) were also included as potential explanatory factors of inter-annual variability in tuna Hg concentrations.

Materials and Methods

Study area

Within the large oceanic region of the southwestern Pacific Ocean, the New Caledonia-Fiji sub-region is characterized by similar marine systems in terms of ocean dynamics, phytoplankton, zooplankton, and micronekton (Le Borgne et al., 2011). Oceanographic parameters are known to be driven by wind regimes, in particular southeast oriented trade winds and northwest oriented winds, associated with the monsoon season. During austral summers (from December to May), the trade winds become prevalent while the north-west oriented winds are more important during austral winters (from May to December) (Cravatte et al., 2015; Lorrain et al., 2015a). Compared to other regions in the Pacific Ocean where primary production mainly relies on NO_3^- (with particulate organic matter (POM) $\delta^{15}N$ values ~ 4 ‰), our study area is known to be a hotspot of N_2 fixation (POM $\delta^{15}N$ values ~ 1‰), with diazotrophy showing some spatial and large seasonal variability (Bonnet et al., 2017; Garcia et al., 2007; Shiozaki et al., 2014). In the sub-region of New Caledonia-Fiji, a significant and unique effort of collecting and archiving tuna samples has been conducted since 2001 within the Pacific Marine Specimen Bank (https://www.spc.int/ofp/PacificSpecimenBank). Previous analyses of specimens from this tissue bank showed homogeneous Hg values in the New Caledonia and Fiji region (Houssard et al., 2019), which justifies the consideration of this sub-region to address temporal trends. Furthermore, Houssard et al. (2017) showed that tuna were relatively resident at this sub-regional scale as demonstrated by the similar isotope patterns between particulate organic matter and tuna in New Caledonia and Fiji.

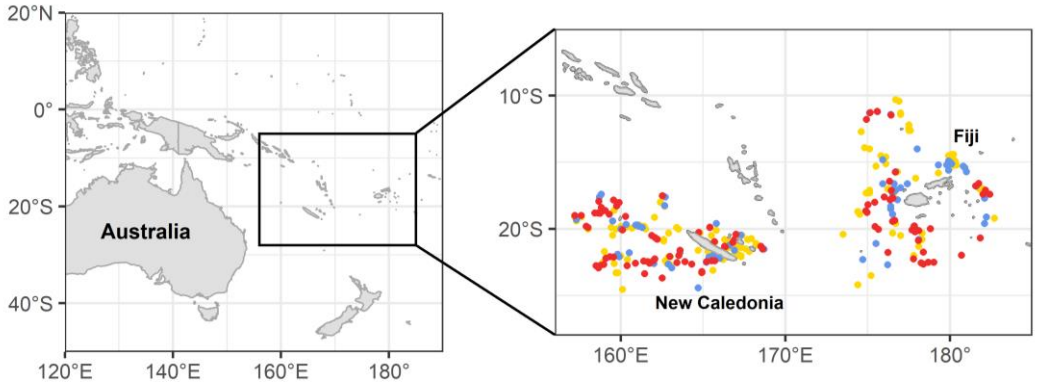

Figure 31. Sampling location of bigeye (blue), yellowfin (yellow), and skipjack (red) caught around New Caledonia and Fiji.

Sample and data collection

Tuna sampling: Tuna samples were taken from the Pacific Marine Specimen Bank, corresponding to 326 yellowfin, 116 bigeye and 148 skipjack tuna, spanning the 2001-2018 time period (n_{total} = 590) (SI Appendix D, Table S1). Sampling was performed onboard commercial fishing boats (longline) by trained scientific observers from the National Observer Programs of the Pacific Island Countries and Territories. Specimens were selected from 10°S to 25°S and from 157°E to 176°W, covering the Economic Exclusive Zone (EEZ) of both New Caledonia and Fiji (Figure 30). Fork length (FL) was measured to the lowest cm and ranged respectively for yellowfin, bigeye and skipjack from 60 to 160 cm (121 ± 18 cm; mean ± SD), 64-160 cm (108 ± 21 cm; mean ± SD) and 42-90 cm (72 ± 7 cm; mean ± SD). For each fish, a white muscle sample was collected from the anal area and stored frozen at -20°C prior to analyses.

Environmental variables: Seven oceanographic variables shown to influence variability of Hg concentrations in tropical tuna (Houssard et al., 2019) were used in this study to explore the physical drivers of Hg concentrations at the surface and at depth. Surface variables included monthly mean sea surface temperature (SST in °C) from the National Oceanic and Atmospheric Administration (NOAA, https://www.ncdc.noaa.gov/oisst (Reynolds et al., 2002); and monthly chlorophyll-a observations (Chl-a, mg.m_3) from a continuous dataset of merged L4 Ocean Colour products provided by GlobColour (http://globcolour.info). Monthly means of net primary production (NPP, mg $C.m^{-2}.day^{-1}$) were derived from a vertically generalized production model (VGPM, http://www.science.oregonstate.edu/ocean.productivity/custom.php; Behrenfeld and Falkowski, 1997). Variables at depth or sub-surface included the mixed layer depth (MLD) and depths of the 12°C and 20°C isotherms (D_{iso12} and D_{iso20}, m), all obtained from the monthly global ARMOR3D L4 dataset (Guinehut et al., 2012). The Oceanic Niño Index (ONI), used to monitor the El Niño-Southern Oscillation (ENSO), was also collected over the study period. Except for this last variable, all monthly data were extracted on a 1° x 1° grid from 2001 to 2018. Assuming the relative oceanic homogeneity of the New Caledonia- Fiji region (Houssard et al., 2017; Le Borgne et al., 2011), physical variables were averaged over the entire study area to examine only temporal relationships between tuna Hg concentrations and the environment. Furthermore, given the long process of MeHg bioaccumulation in tuna muscle (Kwon et al., 2016), we assumed that Hg values of a given individual captured at a single date and place is not exclusively explained by the environmental conditions at this date, but also by the conditions prevailing during the previous

months or years. As ^{15}N turnover (~ six months) in tuna white muscle is known to be shorter than MeHg turnover (Madigan et al., 2012), all oceanographic variables were averaged over a six-month period preceding individual capture date to explain both Hg and nitrogen isotope data.

Estimates of baseline phytoplankton δ ^{15}N values: To explore the potential relationship between the nitrogen cycle and change in tuna Hg concentrations at the top of the food web, baseline phytoplankton $\delta^{15}N$ values were estimated from a model of ocean biogeochemistry and isotopes (MOBI, Somes et al., 2017) at each tuna sample location and year from a hindcast simulation. The biogeochemical component is a 2N2PZD (2 Nutrients, 2 Phytoplankton, 1 Zooplankton, and 1 Detritus) ecosystem model (Somes and Oschlies, 2015). The processes in the model that fractionate the nitrogen isotopes (i.e., preferentially incorporate ^{14}N into the product) are phytoplankton NO_3^- assimilation (6 ‰), zooplankton excretion (4 ‰), N_2 fixation (1‰), water column denitrification (20 ‰) and benthic denitrification (6 ‰), in which the respective fractionation factor yields the $\delta^{15}N$ difference between substrate and product (Somes et al., 2010). The baseline $\delta^{15}N$ values reproduce the major features in a global seafloor $\delta^{15}N$ database (Tesdal et al., 2013).

Analytical methods

Total mercury concentration analysis: Total Hg concentrations were analysed on 590 samples: 326 yellowfin, 116 bigeye and 148 skipjack. The majority (*n* = 458) of total Hg concentrations were performed on homogenized freeze-dried samples by thermal decomposition, gold amalgamation and atomic adsorption detection (DMA-80, Milestone, Italy) at GET (Toulouse, France). Blanks and two biological standard reference materials, TORT-3 (lobster hepatopancreas; Hg = 292 ± 22 ng.g^{-1} dw) and IAEA-436 (tuna fish flesh homogenate; Hg = 4190 ± 360 ng.g^{-1} dw), covering a wide range of Hg concentrations, were routinely used in each analytical batch to check Hg measurement accuracy. Complementary Hg data (*n* = 132, only skipjack tuna) were analysed at the IRD laboratory in Noumea (New Caledonia) by hot plate acidic digestion (HNO_3-H_2O_2) followed by Cold Vapor Atomic Fluorescence Spectroscopy. Blanks and one biological standard reference materials, DOMR-4 (fish protein; Hg = 412 ± 36 ng.g^{-1} dw) were routinely used in each analytical batch to check Hg measurement accuracy and traceability. Hg contents are expressed on a dry weight basis (dw).

Bulk muscle and compound-specific stable isotope analysis: Muscle stable isotope ratios were measured on the 590 samples analysed in Hg but also on complementary samples available from our study area (*n* = 85) but in too limited quantities to perform both Hg and stable isotope analyses. In total, 675 samples were therefore analysed for stable isotopes: 360 yellowfin, 150 bigeye and 165 skipjack. $\delta^{15}N$ and $\delta^{13}C$ values were obtained from ~1 mg homogenized freeze-dried samples packed in tin cups and were analysed using a Costech elemental analyser coupled to an isotope ratio mass spectrometer (Thermo Scientific Delta Advantage with a Conflo IV interface) at Union College (New York, USA). Reference standards (EA Consumables sorghum flour ($\delta^{13}C$ = -13.78 ± 0.17, $\delta^{15}N$ = 1.58 ± 0.15), in house acetanilide ($\delta^{13}C$ = -34.07, $\delta^{15}N$ = -0.96), IAEA-N-2 ammonium sulfate ($\delta^{15}N$ = 20.3 ± 0.2), and IAEA-600 caffeine ($\delta^{13}C$ = -27.771 ± 0.043, $\delta^{15}N$ = 1.0 ± 0.2)) were used for isotopic corrections, and to assign the data to the appropriate isotopic scale with analytical precision better than 0.1 ‰. Percent C and N were calculated using additional acetanilide standards of varying mass. Corrections were done using a regression method. Results were

reported in the d unit notation and expressed as parts per thousand (‰) relative to international standards (atmospheric N_2 for nitrogen and Vienna Pee Dee belemnite (VPDB) for carbon). Reproducibility of several samples measured in triplicate was < 0.2 ‰. For samples with elevated lipid content (C:N > 3.5), $\delta^{13}C$ values were corrected using a mass balance equation with parameters derived from Atlantic bluefin tuna muscle (Logan et al., 2008).

For AA-CSIA, we used both published (Houssard et al., 2017) and newly-analysed amino acid compound-specific $\delta^{15}N$ data on yellowfin tuna (*n* = 10) which had the most robust time series among the three tuna species on individuals collected in 2003, 2007, 2010, 2013, 2016 and 2018 (*n* = 16). To do so, the freeze-dried samples were prepared by acid hydrolysis followed by esterification and trifluoroacetylation as per Dale et al. (2011). The $\delta^{15}N$ isotope values of individual amino acids were determined with a Trace GC gas chromatograph interfaced with a Delta V Plus isotope ratio mass spectrometer (IRMS) through a GC-C combustion furnace (980°C), reduction furnace (650°C) and liquid N_2 cold trap. The samples (0.5 mL) were injected splitless onto a forte BPX5 capillary column (30 m x 0.32 mm x 1.0 mm film thickness) at an injector temperature of 180°C with a constant helium flow rate of 1.5 $mL.min^{-1}$. The column was initially held at 50°C for 2 min and then increased to 120°C at a rate of $10°C.min^{-1}$. Once at 120°C, the temperature was increased at a rate of $4°C.min^{-1}$ to 195°C and then at $5°C.min^{-1}$ to 235°C where it was held for 5 min. The temperature was then further increased to 300°C at $15°C.min^{-1}$ and held for 8 min. All samples were analysed at least in triplicate. The $\delta^{15}N$ values were normalised as follows: each sample analysis consisted of three separate IRMS analyses bracketed by a suite of amino acids with known $\delta^{15}N$ values. The slope and intercept of known versus measured values were then used to correct the measured values for the sample set. Reproducibility associated with isotopic analysis of glutamic acid and phenylalanine averaged ± 0.44 ‰ (1 SD) and ranged from ± 0.06 ‰ to ± 0.85 ‰ respectively.

Tuna trophic position was estimated using the difference of $\delta^{15}N$ values in trophic (Tr-AA) and source (Sr-AA) amino acids, obtained by the following equation:

$$TP_{Tr-Sr} = \frac{\delta^{15}N_{Tr-AA} - \delta^{15}N_{Sr-AA} + \beta_{Tr-Sr}}{TEF_{Tr-Sr}} + 1$$

where $\delta^{15}N_{Sr-AA}$ is the weighted average of glycine and phenylalanine $\delta^{15}N_{AA}$ values, and $\delta^{15}N_{Tr-AA}$ the weighted average of alanine, glutamic acid, leucine and proline $\delta^{15}N_{AA}$ values. β_{Tr-Sr} is the difference between Tr-AA and Sr-AA in primary producers and TEF_{Tr-Sr} is the ^{15}N enrichment between Tr-AA and Sr-AA per TP. β_{Tr-Sr} and TEF_{Tr-Sr} were set respectively at 3.6 and 5.7 (Bradley et al., 2015). Using the weighted average of Sr-AA and Tr-AA reduced uncertainty due to the possible large variations of $\delta^{15}N_{AA}$ values (Hayes et al., 1990). Uncertainty in TP estimates was calculated by propagation of errors according to Bradley et al. (2015) with a mean error of 0.4.

Statistical analysis

Distribution differences of Hg concentrations, muscle $\delta^{15}N$ and $\delta^{13}C$ values between species were first tested with a Kruskal-Wallis test followed by Dunn's post hoc test as hypothesis of normality was not met.

Transformation of mercury concentrations: Tuna Hg concentrations were log-transformed to guarantee the homogeneity of variance (Zuur et al., 2010). Further, as Hg is known to bioaccumulate with length (and age), a power-law relationship ($\log(Hg) = a \times (FL - b)^C - d$) was fit between log(Hg) and fish length

(fork length, FL) to characterize the bioaccumulative processes in each tuna species and remove this length effect in further analysis. This allowed the influence of other potential factors governing Hg concentrations in tuna to be investigated. Residuals from the length-based Hg model (i.e., observed values e predicted values) were extracted and used to calculate length-standardized Hg concentrations (at mean species lengths, i.e., FL = 100 cm for yellowfin and bigeye and at FL = 70 cm for skipjack), thereafter defined as "standardized Hg concentrations".

Temporal trend and structure analysis: Temporal patterns of Hg concentrations in tuna were examined with Moran's eigenvectors maps (MEM) which are derived from a spectral decomposition of the temporal relationships among the sampling dates (Dray et al., 2006). This decomposition generates orthogonal eigenfunctions that can then be used in statistical models as explanatory variables representing the temporal pattern observed. Species-specific temporal eigenfunction analyses were conducted on log(Hg) and standardized Hg concentrations separately following the method of Legendre and Gauthier (2014). To account for the seasonality in our study region, each variable was aggregated by year and season, resulting in 36 season/year couples (i.e., austral winter and austral summer per year from 2001 to 2018). Briefly, long-term trends of Hg concentrations were first tested on seasonal means of Hg concentrations with a redundancy analysis (RDA) followed by an ANOVA like permutation test. Secondly, to investigate the temporal structure of log(Hg) and standardized Hg concentrations, we built distance-based matrices among the sampling periods and distance-based MEMs (dbMEM) eigenfunctions. As sampling design was not regular for the three tuna species, dbMEMs were built over the 36 seasons, then the seasons with no sample for a species were removed as recommended with irregularly designed sampling surveys (Brind'Amour et al., 2018). dbMEMs modelling positive (i.e., observations that are closer in time tend to display values that are more similar than observations paired at random) or negative temporal correlation between seasons were selected and tested with redundancy analysis (RDA) followed by ANOVA like permutation tests to reveal any temporal structure in the response variables. Temporal structure of Hg concentrations was investigated only for yellowfin and skipjack as there was not enough data per season for bigeye.

For potential ecological and environmental drivers of Hg concentrations, only long-term trends were investigated as no particular seasonal structure was revealed for both log(Hg) and standardized Hg concentrations. RDA followed by ANOVA like permutation tests were then fitted separately on tuna muscle $\delta^{15}N$ and $\delta^{13}C$ values, and on each environmental variable (SST, MLD, Chl-a, NPP, D_{iso12} and D_{iso20}). For TP estimates and Sr-AA $\delta^{15}N$ values, as few data were available, long-term trends were investigated using a linear regression fitted along years.

Effects of physical and ecological drivers on the temporal variability of Hg content: Generalized additive models (GAM) were used to test the effects of potential predictors on temporal variations of Hg concentrations following the formulae:

$$Y = \alpha + s_1(X_1) + s_2(X_2) + \ldots + s_n(X_n) + \varepsilon$$

where Y is the expected value of the response variable (i.e., log(Hg) or standardized Hg concentrations), a is the model intercept, $s_i(X_i)$ is a thin-plate-spline smooth function of the explanatory variable i, and ε is the error term. Standardized Hg concentrations were assumed to follow a Gamma distribution while log(Hg) a Gaussian one. Explanatory variables tested included surface (SST, Chl-a, NPP and ONI) and deep

(D_{iso12}, D_{iso20} and MLD) oceanographic variables as well as ecological ($\delta^{15}N$ and $\delta^{13}C$ values) factors. Fish length was also added in the models testing log(Hg). Before performing model computation, variance inflation factors (VIF) were calculated between all explanatory variables to detect collinearity. Covariates with the highest VIF were subsequently removed until the highest VIF value was < 5 (Zuur et al., 2010). With this method, MLD and Chl-a were found to be collinear to other variables and were then removed from the explanatory variables. D_{iso12} and D_{iso20} were highly correlated, so only separate models using either D_{iso12} or D_{iso20} were tested. Explanatory variables were fitted in the GAM with a low spline complexity (k = 3) to reduce over-fitting. A backward selection approach was used and we chose the model with the lowest Akaike's Information Criterion corrected for small samples sizes (AICc, Burnham and Anderson, 2004). Finally, for each best-fit GAM, assumptions of residuals temporal trend and auto-correlation were examined graphically with diagnostic plots. The deviance explained (% DE) for each model was compared to assess predictive capacity. To determine the amount of variation explained by each explanatory variable, we fitted a separate model for individual variable. GAM were fitted in R using the mgcv package (Wood and Wood, 2015).

Effects of baseline processes on tuna Hg concentrations and tuna $\delta^{15}N$ values: To investigate the potential influence of baseline processes, in particular the effect of different nitrogen sources (NO_3^- , NO_2) fuelling primary productivity in this region (Bonnet et al., 2017; Garcia et al., 2007; Shiozaki et al., 2014), we fitted linear regressions between MOBI estimates of phytoplankton $\delta^{15}N$ values and both standardized Hg concentrations and muscle $\delta^{15}N$ values in the three tuna species. Complementary linear regressions were fitted on yellowfin samples analysed in $\delta^{15}N$ AA-CSIA to compare standardized Hg concentrations, tuna muscle $\delta^{15}N$ values and phytoplankton $\delta^{15}N$ estimates regarding Sr-AA $\delta^{15}N$ values, used as proxies of baseline nitrogen isotope values. All statistical analyses were performed with R 3.6.1 (R Core Team, 2018).

Results

Patterns and temporal variability of mercury concentrations

Mercury concentrations (mean ± SD, min-max, dw) differed according to species (Kruskal-Wallis, $p < 0.001$) with significantly higher levels in bigeye (2.7 ± 1.7 $mg.g^{-1}$, 0.3-8.6 $mg.g^{-1}$; Dunn's test, $p < 0.001$) than in yellowfin (0.7 ± 0.5 $mg.g^{-1}$, 0.1-5.1 $mg.g^{-1}$) and in skipjack (0.7 ± 0.3 $mg.g^{-1}$, 0.2-1.7 $mg.g^{-1}$) (Figure 31 a; SI Appendix D, Figure S1). Fish length and log(Hg) were positively correlated and fish length explained respectively 45 %, 39 % and 18 % of the muscle Hg variations in bigeye, yellowfin and skipjack. Coefficients (a, b, c and d) of the power-law relationships are specified per species in Figure 31 2c. Inter-annual variability from 2001 to 2018 was detected in both log-transformed and standardized Hg concentrations for each tuna species, yet no significant long-term temporal trends were detected (Figure 31a & d; Table 1). Furthermore, models based upon the MEM were not significant for any variable and any tuna species (Table 1). This illustrates the lack of any significant seasonal structure of log(Hg) and standardized Hg concentrations between 2001 and 2018 in the southwestern Pacific Ocean.

Table 2. Summary of the temporal analysis. ANOVA like permutation results to test temporal trend and structure of log(Hg), standardized Hg concentrations, muscle $\delta^{15}N$ values and $\delta^{13}C$ values of tropical tunas. FL = fork length; n = number of individuals; F and p-value = statistics of the test. * indicates significant temporal trends.

Species	Response variable	FL (cm) min-max	*n*	Temporal trend		MEM modelling positive correlation		MEM modelling negative correlation	
				F	***p*-value**	***F***	***p*-value**	***F***	***p*-value**
bigeye	log(Hg)	64-160	116	0.088	0.800	Not enough data			
	standardized Hg		116	0.055	0.799	Not enough data			
	$\delta^{15}N$		163	0.132	0.254	Not tested			
	$\delta^{13}C$		163	4.043	0.044 *	Not tested			
yellowfin	log(Hg)	60-160	326	4.340	0.056	0.678	0.760	2.495	0.131
	standardized Hg		326	0.026	0.888	0.4903	0.887	2.15	0.202
	$\delta^{15}N$		386	0.019	0.580	Not tested			
	$\delta^{13}C$		386	10.651	0.005 *	Not tested			
skipjack	log(Hg)	42-90	148	1.470	0.247	666.170	0.053	Not enough data	
	standardized Hg		148	2.248	0.169	54.523	0.127	Not enough data	
	$\delta^{15}N$		165	1.186	0.308	Not tested			
	$\delta^{13}C$		165	4.321	0.041 *	Not tested			

Temporal variability of tuna isotopic ratios and trophic position

Muscle $\delta^{15}N$ values varied between the three tuna species (Kruskal-Wallis, $p < 0.001$; Dunn's test, $p < 0.001$ between all pairs of species). Highest $\delta^{15}N$ values were found in bigeye (12.6 ± 1.6‰), intermediate values in yellowfin (10.8 ± 1.8 ‰) and lowest values in skipjack (9.9 ± 1.4‰) (Figure 31 e; SI Appendix D, Figure S1). For the three species, inter-annual variability between 2001 and 2018 was detected on muscle $\delta^{15}N$ values but no increasing or decreasing long-term trends were found (Figure 31 e; Table 2). Similarly, $\delta^{13}C$ values differed between species (Kruskal-Wallis, $p < 0.001$; Dunn's test, $p < 0.01$ between all pairs of species) with highest values in bigeye (-16.2 ± 1.0 ‰), intermediate values in yellowfin (-16.4 ± 1.0 ‰) and lowest values in skipjack (-16.8 ± 1.1 ‰) (Figure 31 f; SI Appendix D, Figure S1). Contrary to muscle $\delta^{15}N$ values, $\delta^{13}C$ values were found to decrease significantly between 2001 and 2018 by a mean annual rate of 0.08‰ for bigeye and skipjack and of 0.07 ‰ for yellowfin (Figure 31 f; Table 2). TP estimates and Sr-AA $\delta^{15}N$ values in yellowfin varied respectively from 3.4 to 5.5 (4.5 ± 0.5) and -5.1 to 11.7 ‰ (0.4 ±

3.9) (Figure 32). Like muscle $\delta^{15}N$ values, they varied inter-annually between 2003 and 2018, however they showed no significant long-term trend ($p > 0.05$).

Seasonal variability and trend of the environmental variables

Over the six environmental variables considered, only the depth of the isotherm 20°C (D_{iso20}) was found to increase significantly over the two last decades (Figure 33; SI Appendix D, Table S2, $p < 0.05$). The five other variables (SST, Chl-a, MLD, NPP and D_{iso12}) remained stable between 2001 and 2018 (all $p > 0.05$). All physical variables showed strong seasonality over our study period (Figure 34).

Drivers of the inter-annual variability of tuna Hg content

For bigeye, yellowfin and skipjack respectively, the best models explained 74.4, 49.4 and 27.5 % of deviance for log(Hg) and 29.3, 16 and 14.2 % of deviance for standardized Hg concentrations (Table 3; Figure 34; SI Appendix D, Figure S2). For the three species, fish length appeared as the best stand-alone predictor of log(Hg), explaining 61.8, 49.4 and 21.3% of the deviance for bigeye, yellowfin and skipjack respectively. Considering standardized Hg concentrations (i.e., residuals from the length-based Hg models), muscle $\delta^{15}N$ values were found to be the best stand-alone predictor of Hg distribution for bigeye and yellowfin; but they were not selected in skipjack's best model. Generally, Hg concentrations were found to increase with decreasing $\delta^{15}N$ values. $\delta^{13}C$ values were significant in the best models of both bigeye and skipjack with lower Hg concentrations related to decreasing $\delta^{13}C$ values. SST was selected in the best model of yellowfin only, with response curve predicting lower Hg concentrations when SST increased. No other oceanographic variables were selected in the optimal models.

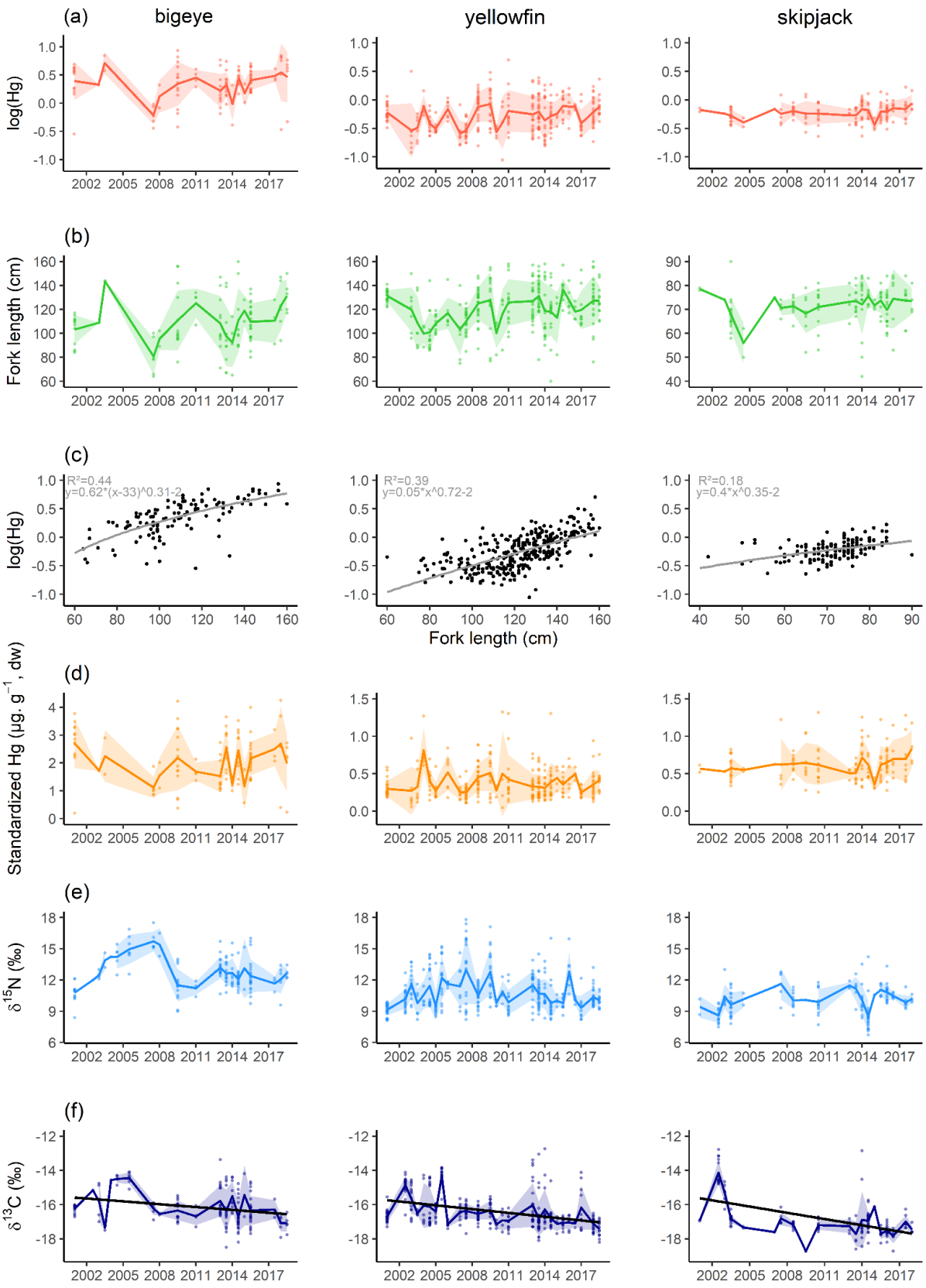

Figure 32. Time series of **a)** log(Hg), **b)** tuna fork length (cm), **d)** standardized Hg concentrations (µg.g^{-1}, dw), e) tuna muscle $\delta^{15}N$ values (‰), and f) tuna muscle $\delta^{13}C$ values (‰) (the black lines represent the significant temporal trends). **c)** power-law relationship between log(Hg) and fork length. The coloured lines and shadows give respectively the seasonal means and standard deviations. The dots are the observation values.

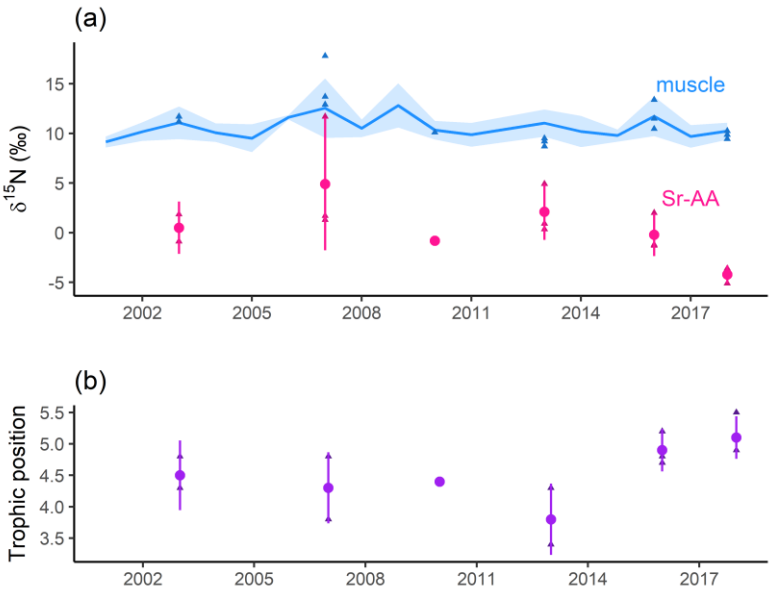

Figure 33. a) Time series of muscle $\delta^{15}N$ values (blue), source amino acid (Sr-AA) $\delta^{15}N$ values (pink) (‰) and **b)** trophic position (TP) estimates (purple) in yellowfin. The blue line and the blue shadow give respectively the annual means and standard deviation of muscle $\delta^{15}N$ values. The dots and lines represent respectively the mean values and the standard deviations of Sr-AA $\delta^{15}N$ values and TP estimates. The triangles are the observations for the selected yellowfin samples analysed for AA-CSIA.

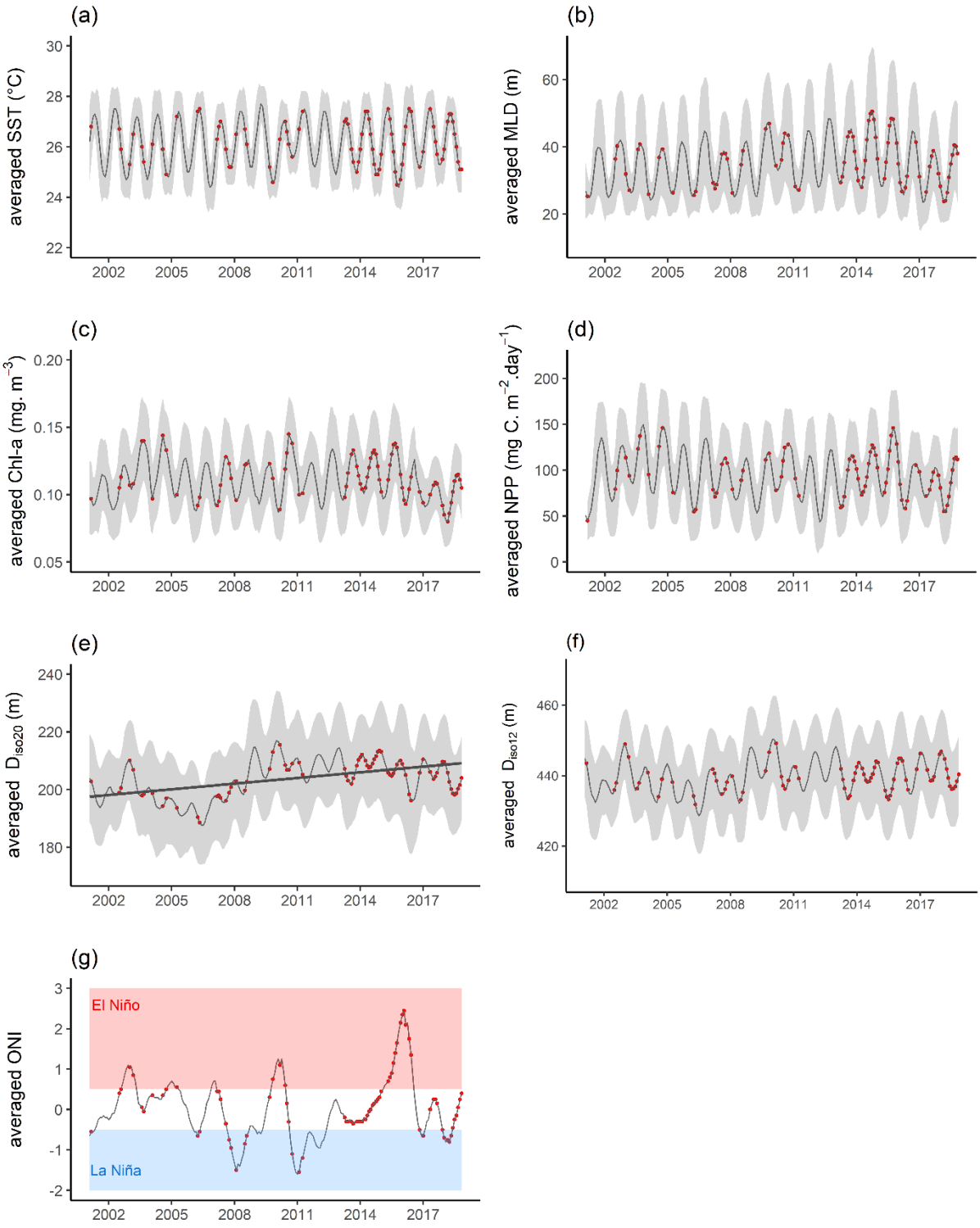

Figure 34. Seasonal variations of 6-month averages of oceanic variables in the New Caledonian-Fiji region, **a)** sea surface temperature (°C), **b)** mixed layer depth (m), **c)** Chl-a ($mg.m^{-3}$), **d)** net primary production ($mg\ C.m^{-2}.day^{-1}$), **e)** depth of isotherm 20°C (m), **f)** depth of isotherm 12°C (m), and **g)** oceanic Niño index (ONI, in red: El Niño event; in blue: La Niña event). The dots represent the months with tuna samples. The grey lines and shadows give respectively the monthly means and standard deviations over the 6-month period. The black regression line represents the significant temporal trend.

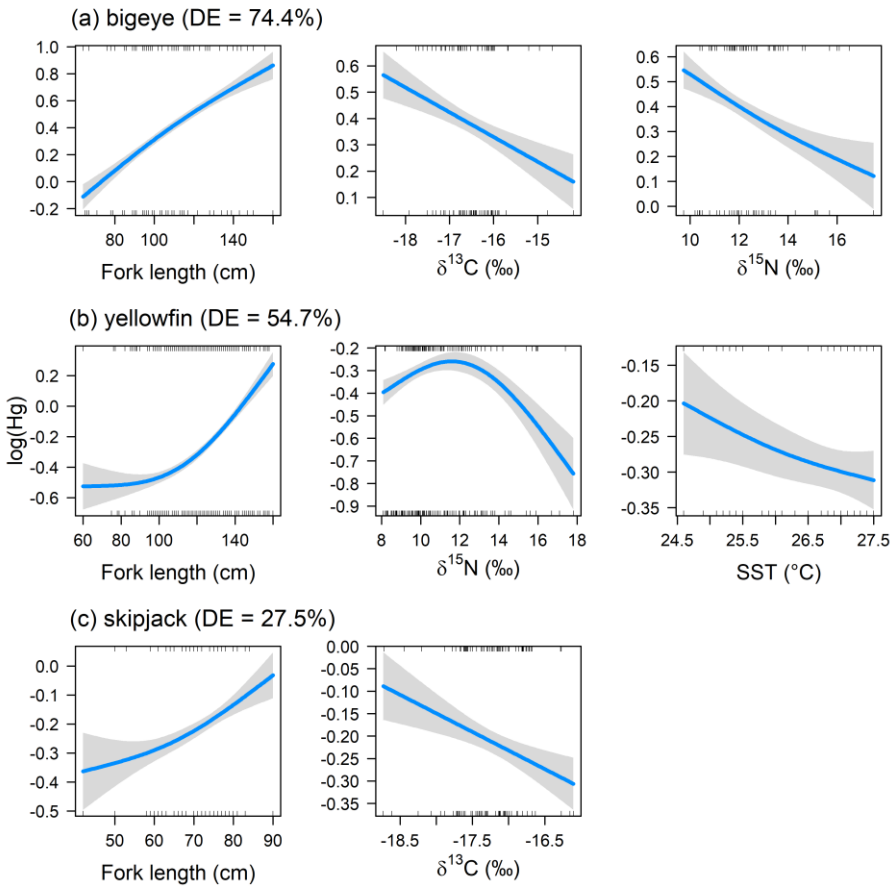

Figure 35. Results of the optimal generalized additive models (GAM) predicting log(Hg) in **a)** bigeye, **b)** yellowfin, and **c)** skipjack. The blue lines give the expected values while the grey bands show the confidence interval for the expected values. The ticks at the top and the bottom are the observed values' position associated to positive and negative model residuals. DE = deviance explained.

Table 3. Results of the optimal generalized additive models (GAM) predicting log(Hg) and standardized Hg concentrations in bigeye, yellowfin, and skipjack. DE = deviance explained; p-value = statistics of the model.

Species	Response variable	Explanatory variables	DE (%)	*p*-value
		Length	61.8	<0.001
		$\delta^{13}C$	11.4	<0.001
bigeye	log(Hg)	$\delta^{15}N$	10.5	<0.001
		Length + $\delta^{13}C$ + $\delta^{15}N$	74.4	
		$\delta^{15}N$	17	<0.001
	standardized Hg	$\delta^{13}C$	8.6	<0.001
		$\delta^{15}N$ + $\delta^{13}C$	29.3	
		Length	49.4	<0.001
		$\delta^{15}N$	13.2	<0.001
yellowfin	log(Hg)	SST	0.34	0.027
		Length + $\delta^{15}N$ + SST	54.7	

		$\delta^{15}N$	12.4	<0.001
	standardized Hg	SST	2.31	<0.001
		$\delta^{15}N$ + SST	16.0	
		Length	21.3	<0.001
skipjack	log(Hg)	$\delta^{13}C$	9.3	<0.001
		Length + $\delta^{13}C$	27.5	
	standardized Hg	$\delta^{13}C$	14.2	<0.001

Mercury concentrations and tuna $\delta^{15}N$ values in relation to baseline processes

Standardized Hg concentrations and estimated phytoplankton $\delta^{15}N$ values were negatively correlated for bigeye and yellowfin ($p < 0.05$) while no significant linear relationship was found for skipjack (Figure 35 a). Conversely, tuna muscle $\delta^{15}N$ values were positively correlated to phytoplankton $\delta^{15}N$ estimates for the three species (Figure 35 b, $p < 0.05$). For yellowfin samples analysed in AACSIA, standardized Hg was found to be negatively correlated to source amino acids (Sr-AA) $\delta^{15}N$ values, while both tuna muscle and estimated baseline $\delta^{15}N$ values were positively correlated to Sr-AA $\delta^{15}N$ values (Figures 35 c, d & e, all $p < 0.05$).

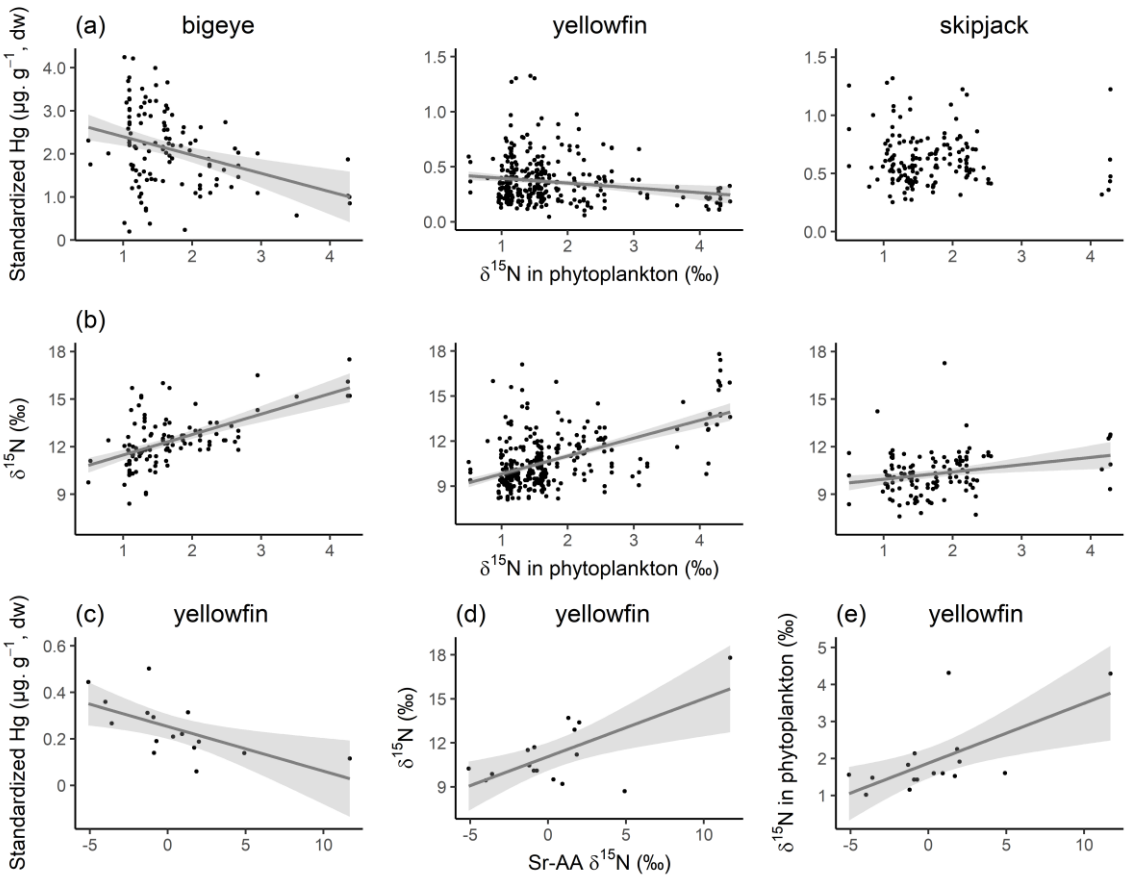

Figure 36. Effects of baseline processes on tuna mercury (Hg) concentrations and muscle $\delta^{15}N$ values. Relationships between **a)** standardized Hg concentrations (µg.g^{-1}, dw) and estimated baseline phytoplankton $\delta^{15}N$ values (‰);

and **b)** tuna muscle $\delta^{15}N$ values (‰) and estimated baseline phytoplankton $\delta^{15}N$ values (‰). In selected yellowfin samples analysed for AA-CSIA, relationships between **c)** standardized Hg concentrations ($\mu g.g^{-1}$, dw) and Sr-AA $\delta^{15}N$ values (‰); **d)** muscle $\delta^{15}N$ values (‰) and Sr-AA $\delta^{15}N$ values (‰); and **e)** estimated baseline phytoplankton $\delta^{15}N$ values (‰) and Sr-AA $\delta^{15}N$ values (‰). The lines represent the significant linear relationships between the two variables and the grey bands show the confidence intervals.

Discussion

We report the first long-term temporal study of Hg concentrations in tropical commercial tuna from the southwestern Pacific Ocean. Contrary to existing temporal studies of tuna Hg content in the north Pacific Ocean (Hawaii, Drevnick et al., 2015) and in the north western Atlantic Ocean (Lee et al., 2016), our study revealed the absence of a significant long-term trend of Hg concentrations in tuna from the New Caledonia-Fiji region during the last two decades. Strong inter-annual variability of Hg concentrations was however found in all three tuna species and was mainly related to the variability in tuna sampled lengths among years and to biogeochemical processes occurring at the primary producer level.

Mercury concentrations in tropical tuna

Among the three species, only bigeye tuna exhibited Hg concentrations exceeding the food safety guideline of 1 $mg.g^{-1}$ (wet weight) (WHO and UNEP Chemicals, 2008), representing 32 % of the sampled specimens. Overall, most of these individuals (86 %) were bigger than 110 cm. A few yellowfin were also above the food safety guideline but represented only 0.6 % of the dataset. This illustrates the need to consider both tuna species and fish size when addressing recommendations in terms of food security regarding Hg content.

Relative differences of Hg concentration between the three studied tuna species in the southwestern Pacific Ocean were similar to those reported in the northeastern and north western Pacific Ocean (Blum et al., 2013; Choy et al., 2009; García-Hernández et al., 2007; Yamashita et al., 2005). The highest Hg content in bigeye compared to the two other species is presumably the result of three confounding factors: a higher TP for this species, a deeper vertical habitat facilitating its access to mesopelagic prey with enhanced Hg concentrations, and a longer lifespan (Choy et al., 2009; Houssard et al., 2019). The significant differences between species muscle $\delta^{15}N$ values could indeed suggest a slightly higher TP for bigeye compared to yellowfin and skipjack, as reported in the eastern Atlantic and the western Indian oceans (Sardenne et al., 2016, 2019). On the other hand, these differences of $\delta^{15}N$ values could also reflect distinct foraging habitat with bigeye occupying deeper habitats where prey are characterized by higher $\delta^{15}N$ values due to baseline effects (Hannides et al., 2013).

Decadal stability of tuna mercury concentrations

Our study revealed no significant long-term trend of Hg concentrations between 2001 and 2018 in the New Caledonia-Fiji region despite significant inter-annual variability (discussed separately below). As samples were collected opportunistically onboard fishing boats, it was not possible to perform our temporal analysis on the same number of samples for each species. The most complete and continuous yellowfin dataset illustrates the absence of a time trend over the 18 years, and similar finding applies to both skipjack and bigeye tuna.

Our observed stable long-term trends contrast with the estimated Hg increases of 3.8 % annually reported in yellowfin tuna caught near Hawaii from 1971 to 2008 (Drevnick et al., 2015) and the mean annual decreasing rate of 19 % from the 1990s to the early 2000s found in the Atlantic bluefin tuna from the north western Atlantic Ocean (Lee et al., 2016). In this later study, the authors suggested that lower Hg concentrations could be related to the reduction of anthropogenic Hg emission in North America, implying a direct link between Hg anthropogenic fluctuations and tuna Hg concentrations.

Our findings seem to confirm the fact that Hg bioaccumulation in fish do not necessarily follow the global suspected increase of anthropogenic Hg emissions to the atmosphere and instead suggest regional differences in oceanic Hg loads. The lack of long-term trend could be explained in part by the remoteness of our region, similar to most of the southwestern Pacific Ocean, which has low anthropogenic emissions and negligible loadings from anthropogenic sources on a total global emissions scale (AMAP and UN Environment, 2019; Horowitz et al., 2017). The absence of detectable decadal trend in tuna Hg concentrations in this region mirrors the absence of consistent temporal trend in atmospheric Hg concentrations in the southern hemisphere (Slemr et al., 2020). Our contrasted results with the two other temporal studies of Hg concentrations in tuna, located in the northern hemisphere, could be also related to distinct methodological approaches used to investigate the temporal trend over time. Drevnick et al. (2015) performed their temporal analysis on distinct, and highly heterogeneous datasets covering only three years (1971, 1998 and 2008) over a long study period (37 years), and with a limited number of individuals for the most recent period (n = 14 in 2008). Conversely, we used a quasi-continuous long-term dataset analysed in the same laboratory from 2001 to 2018 with a larger sample size and more powerful statistical tools. Finally, unlike our study, no ecological proxies were available in these two other temporal studies of Hg content; therefore, it was not possible to investigate the potential confounding ecological contribution to the decreasing or increasing long-term trends of tuna Hg concentrations.

Drivers of temporal variability of tuna Hg concentrations

For the three tuna species, body length of sampled fish appeared to be the most important driver of inter-annual variability of Hg concentrations with highest and lowest Hg concentrations in the time series related to larger and smaller fish respectively (Figure 31 a, b & c). This reflects the well-known bioaccumulative properties of MeHg in organisms (Adams, 2004; Cai et al., 2007; Houssard et al., 2019) and is mainly related to the variability in tuna sampled sizes among years. Therefore, length-standardized Hg concentrations are important to use when investigating factors governing Hg bioaccumulation in tuna. This strong relationship between length and Hg content (61.8 %, 49.4 % and 21.3 % for bigeye, yellowfin and skipjack respectively) explains the relatively low scores of our modelling approach for length-standardized Hg concentration as most of the variation is already explained by fish length. Furthermore, for yellowfin and skipjack, where the variance of bulk Hg concentrations is lower compared to bigeye, by extracting the residuals from the length-based Hg models to calculate standardized Hg concentrations, we consequently reduced these variances even more and therefore, the variability to be explained in our GAMs.

Considering the ontogenetic dietary shift in bigeye and yellowfin (Sardenne et al., 2016), fitting GAMs on distinct fish length classes (e.g., small < 100 cm vs large tuna > 100 cm) would have been interesting to investigate differences among the main processes governing Hg methylation and MeHg bioaccumulation. Unfortunately, not enough data were available to do so. Considering standardized Hg concentrations (i.e., residuals from length-based Hg models), inter-annual variability of Hg concentrations

in bigeye and yellowfin best correlated with muscle $\delta^{15}N$ values, and our predictions showed generally higher Hg concentrations associated with lower muscle $\delta^{15}N$ values. In the literature, most studies found that Hg is strongly correlated to organism $\delta^{15}N$ values, yet through a positive relationship, reflecting Hg biomagnification along the pelagic food web (Cai et al., 2007; Teffer et al., 2014). Nevertheless, when exploring muscle $\delta^{15}N$ values at the species level, it is important to keep in mind that they result from trophic dynamics along the food web, but also from biogeochemical processes at the base of the ecosystem (baseline effects). Here, muscle $\delta^{15}N$ values were positively correlated to estimated baseline phytoplankton $\delta^{15}N$ values and Sr-AA $\delta^{15}N$ values, used to track baseline changes in nutrient sources and uptake. Therefore, temporal variations of muscle d15N values would predominantly reflect changes at the base of the food web. This could be related to the high levels of diazotrophy well documented in our study region (Bonnet et al., 2017; Garcia et al., 2007; Shiozaki et al., 2014) and characterized by low POM $\delta^{15}N$ values (~ 1 ‰). Atmospheric nitrogen deposition from pollution (which typically has $\delta^{15}N$ values ranging from -7 to 0 ‰) could also explain the low basal $\delta^{15}N$ values; yet as nitrogen emissions are supposed to be low in our study area compared to the north Pacific Ocean, this phenomenon is likely of less importance compared to diazotrophy (Gobel et al., 2013; Reay et al., 2008). Thereby, the response curves associated with muscle d15N values (i.e., higher Hg concentrations associated with lower $\delta^{15}N$ values and thus with higher diazotrophy) in our models may suggest that the nitrogen cycle and/or diazotrophy (i.e., baseline effects) are likely to drive Hg concentrations in the upper part of the oceanic pelagic food web, probably triggering Hg net methylation and bioavailability at the base of the food web during diazotroph blooms and/or their resulting remineralization. This finding is in line with the recent study by Wu et al. (2019) who revealed in a meta-analysis that bioconcentration (i.e., MeHg transfer from water into the base of the food web) was a better descriptor of fish MeHg concentrations than biomagnification in pelagic food web. The influence of the nitrogen cycle and/or diazotrophy on Hg concentrations seems to be also confirmed by the negative correlations found in this study between standardized Hg concentrations and both Sr-AA $\delta^{15}N$ values and estimated baseline $\delta^{15}N$ values.

The community structure and growth of primary producers, as inferred by tuna d13C values, also seems to influence the observed inter-annual variability of Hg concentrations, particularly for both bigeye and skipjack tuna, with Hg concentrations predicted to decrease with increasing d13C values. Here, d13C values were the only ecological parameter showing a significant decline between 2001 and 2018. The same trends were found at the global scale and were attributed to a potential global shift of the phytoplankton community structure and/or physiology (Lorrain et al., 2020). The lack of a corresponding long-term Hg trend in our study may suggest that the carbon cycle is likely to impact Hg fate in oceans and tuna but to a lesser extent than the nitrogen cycle, and in particular diazotroph blooms.

As dinitrogen fixers typically thrive in warm and stratified waters, those conditions, more than the nitrogen cycle itself, could be linked to the Hg cycle. Recent model predictions made on Atlantic bluefin tuna show that increasing tissue Hg concentrations were related to rising seawater temperatures (Schartup et al., 2019). Furthermore, experimental studies on estuarine and freshwater fish have found that warmer temperatures enhanced MeHg bioaccumulation (Dijkstra et al., 2013; Maulvault et al., 2016). However, in this study SST was selected in the optimal model for yellowfin only, showing an opposing response curve to the above hypothesis, i.e., lower Hg concentrations in tuna related to higher SST. Our response curve for yellowfin is in agreement with Houssard et al. (2019) where Hg content was found to decrease spatially with increasing SST. Considering the potential impact of stratification, the depth of isotherm 12°C (D_{iso12}, which can be used as a proxy of the thermocline and thus stratification) was not selected in any of our optimal models. In Houssard et al. (2019), D_{iso12} was found as the second main driver (after fish length) of the spatial variability of tuna Hg content with Hg concentrations enhanced in regions

characterized by deeper thermoclines. These distinct results may suggest that the stand-alone temporal variability of the thermocline depth is not responsible for the inter-annual variations of Hg concentrations in tuna muscle. While discussing the impact of these environmental variables, it is worthwhile mentioning that we worked at a sub-regional scale where temporal variability is low compared to large spatial variability investigated in these other studies. For example, the ranges of our physical variables, especially for D_{iso12} (428-451 m), were reduced compared to the ones investigated in Houssard et al. (2019) (D_{iso12}: 200-460 m), which can explain their limited impact in our models.

Including complementary Hg data from the environment (i.e., Hg concentrations in seawater and total gaseous Hg) in our modelling approach could have improved our model scores and helped characterize how Hg levels in tuna reflect Hg levels in water or in the atmosphere. Unfortunately, such data are scarce and no time series over the two last decades were available in our study area.

Implications for global-scale monitoring of mercury

With the adoption of the Minamata Convention in 2013, governments are asked to control and reduce anthropogenic Hg emissions which will require integrating biological tools into monitoring efforts so that the efficiency of political decisions can be tracked. Considering that tuna fisheries are among the world's most important fisheries, with a commercial value estimated at 41 billion $US/y in 2012 (Macfadyen, 2016), quantifying nutritional risks along with benefits are becoming important when addressing food and nutritional security. Furthermore, knowing that oceans have undergone large physical and biogeochemical modifications in the last decades (e.g., surface warming, acidification, deoxygenation or changes in primary productivity) (Bopp et al., 2013; Kwiatkowski et al., 2017), it has become necessary to assess the predictive capacity of environmental variables on Hg methylation and bioaccumulation to understand potential climate-driven ecological changes.

With a continuous and long-term dataset, we revealed for the first time the absence of significant decadal trend of Hg concentrations in tropical tuna from the New Caledonia-Fiji region. This contrasts with the two other available temporal studies from distinct areas (Drevnick et al., 2015; Lee et al., 2016) and thus illustrates the complexity of the Hg cycle and the fact that Hg in tuna does not necessarily follow the suspected recent increasing Hg trends in global oceans, especially in the southern hemisphere. Our results however seem consistent with the remoteness of our study region in terms of low anthropogenic emissions, and thus seem to confirm the hypothesis of distinct hemispherical ocean patterns of Hg anthropogenic deposition.

Strong inter-annual variability was found in the three tuna species and was mainly due to fish length variability among samples. This suggests the importance of using a fish length-based approach to address the question of Hg spatial and temporal trends in tuna even at small (e.g., sub-regional) scales. This includes accounting for different types of fishing gear (e.g., purse seine and longline) employed since fishing gears are known to preferentially select certain tuna fish sizes.

Finally, our novel complementary investigation of baseline and trophic ecological tracers highlights i) no significant decadal change in tuna TP during this 18 year period, and ii) the influence of baseline processes for bigeye and yellowfin, related to the nitrogen cycle and/or diazotrophy, possibly enhancing Hg methylation and/ or MeHg bioavailability at the base of the food web. Knowing that the largest bioaccumulation step of MeHg is likely to occur between the water compartment and unicellular planktonic organisms - relative to trophic amplification processes - more attention needs to be paid to

ecological and physiological processes occurring at the base of marine ecosystems to better capture Hg spatio-temporal trends at the top of the ocean food webs. Lastly, our study emphasizes the need for more systematic collection of Hg and stable isotope data in different marine reservoirs, including iHg in the water column, from both hemispheres to compare MeHg production, degradation and bioaccumulation in oceans at a global scale.

Acknowledgments

We thank the large team of observers and supervisors from the National Observer Programs of the Pacific Island Countries and Territories and FSM Arrangement Observer Program who collected the tuna samples. We are grateful to the WCPFC (Western and Central Pacific Fisheries Commission) Tuna Tissue Bank and the SPC (Pacific Community) Pacific Marine Specimen Bank which gave us access to the tuna tissue samples. We thank the LAMA laboratory, especially Jean-Louis Duprey and Stéphanie Berne for Hg analyses, as well as the Union College Stable Isotope Laboratory team Anouk Verheyden, Sarah Katz, and Madelyn Miller. We also thank Pablo Brosset for his helpful discussions. Finally we thank the four anonymous referees for their remarks and suggestions that substantially improved the manuscript. Funding was provided by the Pacific Fund VACOPA project and ANR-17-CE34-0010 MERTOX from the French Agence Nationale de la Recherche. The U.S. National Science Foundation funded Union College's isotope ratio mass spectrometer and peripherals (NSF-MRI #1229258).

Authors' contribution

Anaïs Médieu: Conceptualization, Methodology, Formal analysis, Writing - original draft, Writing e review& editing, David Point: Conceptualization, Resources, Writing - review & editing, Supervision, Funding acquisition, Aurore Receveur: Conceptualization, Methodology, Writing - review & editing, Olivier Gauthier: Methodology, Supervision, Valérie Allain: Resources, Writing – review & editing, Heidi Pethybridge: Writing - review & editing. Christophe E. Menkes: Resources, Writing - review & editing. David P. Gillikin: Formal analysis, Writing - review & editing. Andrew T. Revill: Formal analysis, Writing - review & editing. Christopher Somes: Resources, Writing - review & editing. Jeremy Collin: Resources. Anne Lorrain: Conceptualization, Resources, Writing - review & editing, Supervision, Funding acquisition.

Chapter 2. Long-term trends of tuna mercury concentrations for the global ocean

In prep

Anaïs Médieu[1], David Point[2], Jeroen E. Sonke[2], Pearse B. Buchanan[3], Nathalie Bodin[4], Douglas H. Adams[5], Anders Bignert[6], David G. Streets[7], Frédéric Ménard[8], C. Anela Choy[9], Valérie Allain[10], Takaaki Itai[11], Bridget E. Ferriss[12], Bernard Bourlès[13], Laure Laffont[2], Olivier Gauthier[1], Anne Lorrain[1]

[1] Univ Brest, CNRS, IRD, Ifremer, LEMAR, F-29280 Plouzané, France
[2] Observatoire Midi-Pyrénées, GET, UMR CNRS 5563/IRD 234, Université Paul Sabatier Toulouse 3, Toulouse, France
[3] University of Liverpool, Department of Earth, Ocean and Ecological Sciences, Liverpool, UK
[4] Sustainable Ocean Seychelles (SOS), BeauBelle, Mahé, Seychelles
[5] Florida Fish and Wildlife Conservation Commission, Fish and Wildlife Research Institute, Melbourne FL, 32901, USA
[6] Department of Environmental Research and Monitoring, Swedish Museum of Natural History, Frescativägen 40, 114 18 Stockholm, Sweden
[7] Department of Environmental Health, Harvard T.H. Chan School of Public Health, Boston, MA 02115, United States of America
[8] Aix Marseille Univ., Univ. de Toulon, CNRS, IRD, MIO, Marseille, France
[9] Scripps Institution of Oceanography, University of California San Diego, La Jolla, California 92037, USA
[10] Pacific Community, Oceanic Fisheries Programme, Nouméa, New-Caledonia
[11] Department of Earth and Planetary Sciences, Graduate School of Science, The University of Tokyo, Bunkyo-Ku, Tokyo, 113-0033, Japan
[12] National Research Council, under contract to Northwest Fisheries Science Center, National Marine Fisheries Service (NMFS), National Oceanic and Atmospheric Administration (NOAA), Seattle, WA 98112, USA
[13] IRD, IMAGO, Plouzané, France

Abstract

Centuries of anthropogenic mercury emissions have considerably modified the global mercury cycle. While reducing future mercury emissions aims to protect human health, it is unclear how a remobilization of legacy mercury, climate change effects, and regional emission trajectories will affect methylmercury concentrations in seawater and marine food webs. Here, we compiled existing and newly acquired mercury concentrations in tropical tunas (yellowfin, bigeye, and skipjack) in six distinct regions of the global ocean to explore the multidecadal temporal variability of mercury content in pelagic top predators between 1970 and 2020. We show strong inter-annual variability of tuna mercury concentrations at the global scale, once accounting for bioaccumulation with tuna size. We find increasing mercury concentrations in skipjack in the late 1990s in the northwestern Pacific, likely resulting from concomitant increasing anthropogenic mercury emissions in Asia. Elsewhere in the Pacific, Indian and Atlantic Oceans, we reveal stable long-term trends of tuna mercury concentrations, which contrast with an overall decline in mercury emissions, atmospheric mercury concentrations and deposition since the 1970s, and with specific regional trends. We suggest that the slow or absent response in tuna mercury to global mercury release most likely reflects the inertia of the surface ocean reservoir, which is supplied by legacy mercury accumulated in the subsurface ocean over centuries. Alternatively, a decline in mercury loading to the surface ocean could have been compensated by increased methylmercury bioavailability or bioaccumulation due to global change effects on marine mercury biogeochemistry and ecology, yet no evidence was found to support this. Our global temporal study highlights that the actions implemented by the Minamata Convention are currently insufficient to assure a reduction in mercury concentrations in highly consumed pelagic fish. Finally, it calls for long and continuous time series of mercury concentrations in marine biota to i) document the responses of marine biotic mercury to changes in anthropogenic mercury emissions, ii) investigate the climate-induced changes in biotic mercury, and iii) ultimately assess mercury exposure to humans.

Keywords: methylmercury, tropical tunas, global temporal heterogeneity, anthropogenic emissions, Minamata Convention.

Introduction

Mercury (Hg) is a widespread heavy metal of particular concern to wildlife and human health. It is emitted to the atmosphere by natural sources (e.g., volcanism) and anthropogenic activities mainly as gaseous elemental Hg^0 (Outridge et al., 2018). In the global ocean, the major source of Hg is atmospheric deposition of inorganic Hg and ocean Hg^0 uptake (Jiskra et al., 2021). Rivers also deliver significant amounts of Hg to estuarine and coastal oceans, but only a small fraction of this Hg is transported to open ocean regions (Liu et al., 2021). In the ocean, a fraction of these Hg inputs is naturally converted into methylmercury (MeHg), a neurotoxin that bioaccumulates and biomagnifies in aquatic food webs, leading to elevated MeHg concentrations in top predators like tunas (Hintelmann, 2010). Consumption of seafood, tunas in particular, is considered to be one of the main routes of human exposure to MeHg (Sunderland, 2007), with MeHg representing the major chemical form (> 91 %) of total Hg in tuna muscle tissue (Houssard et al., 2019). The United Nations Environmental Program Minamata Convention (www.mercuryconvention.org) sets out a range of measures to protect human health and the environment from anthropogenic Hg releases, and therefore requires monitoring studies to assess the efficiency of its political measures.

Although humans started using Hg about 4,000 years ago, approximately 95 % of anthropogenic Hg releases are estimated to have occurred during the five last centuries, mainly related to the use of Hg in gold and silver mining, technologic applications of Hg, chemical manufacturing, coal burning and metallurgy (Streets et al., 2019a). Cumulative releases have been largest in North America and Europe, yet anthropogenic emissions from these two regions have declined since the 1970s, following emission reduction measures. Conversely, anthropogenic Hg releases in Asia have sharply increased since the 1980s, making this region the leading contributor to Hg emissions worldwide (Streets et al., 2019b). These cumulative anthropogenic Hg uses and emissions have considerably modified the natural global Hg cycle (Selin et al., 2008). In the atmosphere, higher Hg^0 levels are measured in the northern hemisphere compared to the southern hemisphere, following the spatial distribution of Hg emissions (Sprovieri et al., 2016). Sediment and peat records of anthropogenic Hg deposition also suggest a larger anthropogenic Hg enrichment (by a factor of 4) in the northern hemisphere (C. Li et al., 2020). In the open ocean, total Hg concentrations in thermocline waters (100 to 1,000 m) are suspected to have tripled in response to anthropogenic Hg releases (Lamborg et al., 2014), but it is still unclear how the fraction of anthropogenic Hg is converted into MeHg in seawater, and ultimately biomagnified in marine biota. Being able to capture and predict spatial and temporal Hg trends in marine food webs is crucial to anticipate changes in human exposure and evaluate the effectiveness of reducing Hg emissions in the context of the implementation of the Minamata Convention.

Tunas display relatively high Hg concentrations and are widely exploited worldwide, with skipjack (*Katsuwonus pelamis*) and yellowfin (*Thunnus albacares*) being the third and the eighth most consumed marine species worldwide, respectively (FAO, 2018). Tunas are therefore often considered as potential bio-indicators for Hg monitoring in relation to human health, and for the detection of spatial and temporal Hg trends in marine ecosystems. This implies that tunas are able to integrate local and global Hg sources over different spatial and temporal scales. Tunas have been broadly studied regarding their Hg content, mainly at relatively limited spatial scales (Bodin et al., 2017; Chouvelon et al., 2017; Houssard et al., 2019; Kojadinovic et al., 2006; Nicklisch et al., 2017), highlighting highly variable Hg concentrations among species and ocean regions. This variability likely results from a complex interplay of processes that include physiology (organism's age and length), trophic ecology (e.g., foraging habitat), marine biogeochemistry (in situ MeHg bioavailability), ocean physics (e.g., mixing, light intensity), and Hg emissions and deposition (Choy et al., 2009; Houssard et al., 2019; F. Wang et al., 2019). A recent study conducted across the Pacific

Ocean highlighted the role of natural biogeochemical processes alongside regional anthropogenic emissions for driving spatial patterns in skipjack Hg concentrations (Médieu et al., 2022, see chapter 9). Meanwhile, temporal trends in tuna Hg content show contrasting results between oceanic basins (Drevnick et al., 2015; Drevnick and Brooks, 2017; Kraepiel et al., 2003; Lee et al., 2016; Médieu et al., 2021a). In the southwestern Pacific, stable Hg concentrations were observed between 2001 and 2018 in tropical tunas (i.e., bigeye, *Thunnus obesus*, yellowfin, and skipjack) (Médieu et al., 2021a). In the central north Pacific (Hawaii), stable Hg concentrations were found in yellowfin between 1970 and the 1990s (Kraepiel et al., 2003). A re-evaluation of these stable trends in the light of new data showed increasing Hg concentrations in yellowfin, as well as in bigeye (Drevnick et al., 2015; Drevnick and Brooks, 2017). In the northern Atlantic Ocean, Lee et al., (2016) revealed decreasing Hg levels in Atlantic bluefin tuna (*T. thynnus*) from 2004 to 2012. These latter temporal studies suggested a potential role for anthropogenic Hg emissions, citing recent increases in Asian emissions and the concomitant reduction in North America. Given the significant changes in anthropogenic Hg releases during the last four decades (i.e., decrease in North America and Europe, and increase in Asia), more temporal studies on tuna Hg concentrations since the 1970s from different ocean regions are needed to investigate if top predators of the global ocean reflect variable anthropogenic Hg releases to the environment.

Here, we compiled data from the existing literature for the global ocean alongside newly acquired tuna Hg concentrations to explore temporal tuna Hg variability in the global ocean through the lens of six contrasted regions of the Pacific, Atlantic and Indian Oceans. Our study focused on tropical tunas (i.e., yellowfin, bigeye, and skipjack), three circumtropical species that are characterized by different lifespans, growth rates and vertical habitats (Olson et al., 2016). Often classified as highly migratory, tropical tunas have been shown to display relatively restrictive movements and site fidelity (Anderson et al., 2019; Fonteneau and Hallier, 2015; Richardson et al., 2018; Schaefer et al., 2015; Sibert and Hampton, 2003), compared to other species (e.g. Atlantic bluefin) that undergo large trans-Atlantic migrations (Block et al., 2005), and should therefore be able to reflect temporal and spatial MeHg patterns of their ecosystems. In the different ocean regions, we first standardized Hg concentrations by tuna length to account for Hg bioaccumulation through time, and we then explored and discussed the extent of residual temporal variability in terms of inter-annual differences and decadal trends. Our study reveals high inter-annual variability of standardized Hg levels in tropical tunas at the global scale, and highlights different temporal responses of tuna Hg content to changes in anthropogenic Hg emissions, depending on the ocean region.

Materials and methods

Sample and data compilation

We compiled 1,834 published and 672 unpublished muscle tuna samples with total Hg concentrations in six distinct regions of the Pacific, Atlantic and Indian Oceans (Figure 36; SI Appendix E Table S1), allowing temporal analysis covering several decades from 1970 to 2020. In the Pacific, this corresponds to 509 yellowfin (1970-2008, range of sampling years) and 494 bigeye (1971-2007) in the central north Pacific (Hawaii), and 105 skipjack in the northwestern Pacific (along the Asian coasts, 1997-2007). This also includes 582 Hg data results for tropical tunas (*n* = 326 yellowfin, 114 bigeye and 142 skipjack) from the southwestern Pacific from 2001 to 2018 (Médieu et al., 2021a) to allow global comparison of Hg temporal variability in tunas with the same statistical approach. In the Atlantic Ocean, it includes 76 yellowfin in the tropical northwestern Atlantic (1999-2012), and 245 yellowfin in the eastern central Atlantic (Gulf of Guinea, 1971-2020). In the western Indian Ocean, it corresponds to 193 yellowfin (2001-2020), 169 bigeye (2001-2020), and 133 skipjack (2001-2018). Published data were obtained directly from tables in Drevnick & Brooks (2017) (Boush and Thieleke, 1983; Brooks, 2004; Kaneko and Ralston, 2007; Kraepiel et al., 2003; Rivers et al., 1972) and Peterson et al. (1973) (Ivory Coast Fisheries Service, 1972), or from contributions by the original authors (Adams, 2004; Blum et al., 2013; Bodin et al., 2017; Choy et al., 2009; Ferriss and Essington, 2011; Kojadinovic et al., 2006).

Tuna samples were collected onboard commercial, recreational, and scientific fishing vessels by multiple research programs. For each fish, a white muscle sample was collected, and metadata, i.e., sampling year, average or precise catch location, total weight and/or fork length (FL) were also provided. When only fish weight were available (Boush and Thieleke, 1983; Brooks, 2004; Kaneko and Ralston, 2007; Kraepiel et al., 2003; Peterson et al., 1973; Rivers et al., 1972), we converted fish weight into fork length to allow comparison between samples, using species- and ocean- specific length-weight relationships (Chassot, 2015; V. Allain personal communications).

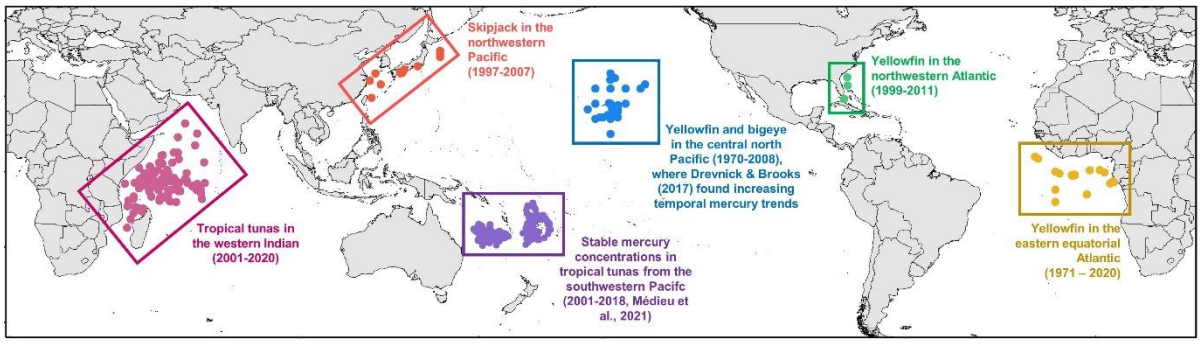

Figure 37. Ocean regions, symbolized by the six colored boxes, where the temporal variability of tuna mercury concentrations was investigated. Colored dots represent the precise sampling location of tunas when available. Data origin: central north Pacific (Blum et al., 2013; Boush and Thieleke, 1983; Brooks, 2004; Choy et al., 2009; Ferriss and Essington, 2011; Kaneko and Ralston, 2007; Kraepiel et al., 2003; Rivers et al., 1972; this study); northwestern Pacific (Médieu et al., 2022); southwestern Pacific (Médieu et al., 2021a); western Indian (Bodin et al., 2017; Kojadinovic et al., 2006; this study); northwestern Atlantic (Adams, 2004; this study); and eastern central Atlantic (Ivory Coast Fisheries Service, 1972; this study).

Total mercury analysis and standardization

Total Hg concentrations were measured on homogenized tuna muscle samples in different study-specific laboratories, with laboratory-specific reference standards. For half of the samples (~ 52 %), total Hg concentrations were measured by hot-plate acid digestion followed by cold vapor atomic fluorescence spectroscopy or cold vapor atomic absorption (Adams, 2004; Boush and Thieleke, 1983; Brooks, 2004; Ferriss and Essington, 2011; Kaneko and Ralston, 2007; Kraepiel et al., 2003; Médieu et al., 2022, 2021a; Rivers et al., 1972). For the rest of the samples (~ 48 %), total Hg concentrations were measured by thermal decomposition, gold amalgamation, and atomic absorption spectrometry (DMA-80, Milestone, Italy) (Blum et al., 2013; Choy et al., 2009; Médieu et al., 2021a). This includes 661 newly acquired Hg data in different laboratories: at GET (Toulouse, France; *n* = 172 samples from the western Indian and the eastern central Atlantic), SFA (Victoria, Seychelles; *n* = 469 samples from the western Indian and the eastern central Atlantic), and FWC-FWRI (Melbourne, Florida, USA; *n* = 20 samples from the northwestern Atlantic). Blanks and biological standard reference materials were routinely used in each analytical batch to check Hg measurement accuracy and traceability (SI Appendix E, Table S2).

While the majority of total Hg concentrations were obtained on bulk powder, some newly acquired Hg data were measured on historic lipid-free samples in the eastern central Atlantic ocean (*n* = 110, samples in 2003, 2013 and 2014). In these samples, lipids had been removed with neutral solvents to overcome bias related to lipid content when interpreting carbon stable isotope composition, as commonly done in trophic ecology studies (Bodin et al., 2009; Ménard et al., 2007). Yet, the lipid removal with neutral solvent has been shown to have no effect on total Hg concentrations in yellowfin (Médieu et al., 2021b), allowing us to compare bulk and lipid-free samples to explore the temporal variability of tuna Hg content in the eastern central Atlantic ocean.

Moreover, when total Hg concentrations were obtained on fresh samples (therefore expressed on a wet weight basis), we converted Hg concentrations assuming an average moisture value of 70 % in white muscle of tropical tunas (Bodin et al., 2017; Houssard et al., 2019; Kojadinovic et al., 2006), so that all total Hg concentrations are expressed on a dry weight (dw) basis (SI Appendix E, Table S1). Total Hg content are considered to reflect MeHg concentrations, as most of the total Hg (> 91 %) is in its methylated form in tuna white muscle (Houssard et al., 2019).

As Hg is known to bioaccumulate with fish length (and age), we fitted a power-law relationship ($\log(\mathrm{Hg}) = \mathrm{a} \times (\mathrm{FL} - \mathrm{c})^{b} - \mathrm{d}$) between log-transformed Hg concentrations and fish length (FL) to remove the length effect when exploring temporal variability, following Houssard et al. (2019) and Médieu et al. (2022, 2021a). Individual power-law relationships were fitted per species and ocean region, all years combined (Figure 37). Residuals from the length-based Hg models (i.e., observed values – predicted values) were extracted and used to calculate length-standardized Hg concentrations, thereafter defined as "standardized Hg concentrations". Mercury standardization was performed at 100 cm FL for bigeye and yellowfin, and 70 cm FL for skipjack.

Estimates of mercury emissions into the atmosphere

Mean anthropogenic Hg release estimates to the atmosphere per decade for the period 1970-2010, and annually for the six years in the period 2010- 2015 were taken from Streets et al. (2019b, 2019a, 2017, 2011). These emission estimates discern seven world regions (i.e., North America, South America, Europe, former USSR, Africa and Middle East, Asia, and Oceania), and include 17 source categories.

Statistical analyses

We first determined the "adequacy" parameter of each time series with the PIA software (developed for statistical analysis of time-series data in the framework of the Arctic Monitoring and Assessment Programme) to investigate their ability to detect trends. Adequacy is defined as the number of actual monitoring years in a time series divided by the number of sampling years required to detect a 5 % annual change in Hg concentrations with a significance level of $p < 0.05$ and 80 % statistical power (Bignert et al., 2004). A ratio ≥ 1 implies that the time series are adequate. Among the 11 time series in our global dataset, only three had an adequacy ≥ 1 (yellowfin and skipjack in the southwestern Pacific, and bigeye in the western Indian) (SI Appendix E, Figure S1).

To allow comparison among all time series, we investigated inter-annual trends of standardized Hg concentrations in tunas per species and ocean region, using Kruskal-Wallis tests, followed by a post-hoc Dunn tests with a Bonferroni correction of *p*-values. This approach avoids finding significant linear trends between samples that are sometimes more than 20 years apart, but allows highlighting patterns of Hg concentrations between old and recent data, while also accounting for the natural bioaccumulative properties of Hg. In other temporal studies (Drevnick et al., 2015; Drevnick and Brooks, 2017; Lee et al., 2016), the authors investigated temporal Hg patterns in tunas with an analysis of covariance (ANCOVA), considering fish weight as the covariance to cope with Hg bioaccumulation in tunas. In the case study of Hawaii, the use of ANCOVA required the removal of small (< 22 kg, corresponding approximately to yellowfin and bigeye smaller than 100 cm FL) and large individuals (> 76 kg, approximately tunas bigger than 155 cm FL) to meet the assumptions of the test (Drevnick and Brooks, 2017). Here, we preferred to keep all available samples by using an alternative statistical approach and to cope with bioaccumulation by length-standardizing Hg levels. Apart for the adequacy calculation, all statistical analyses were performed with the statistical open source R software 3.6.1 (R Core Team, 2018).

Mean estimates of anthropogenic Hg emissions were not available annually for the whole 1970-2020 period covered by our different time series, and we therefore could not compare statistically compare tuna Hg concentrations and anthropogenic Hg emissions. Yet, anthropogenic emissions were included when plotting tuna Hg time series to illustrate the general global and regional long-term trends of Hg releases into the atmosphere.

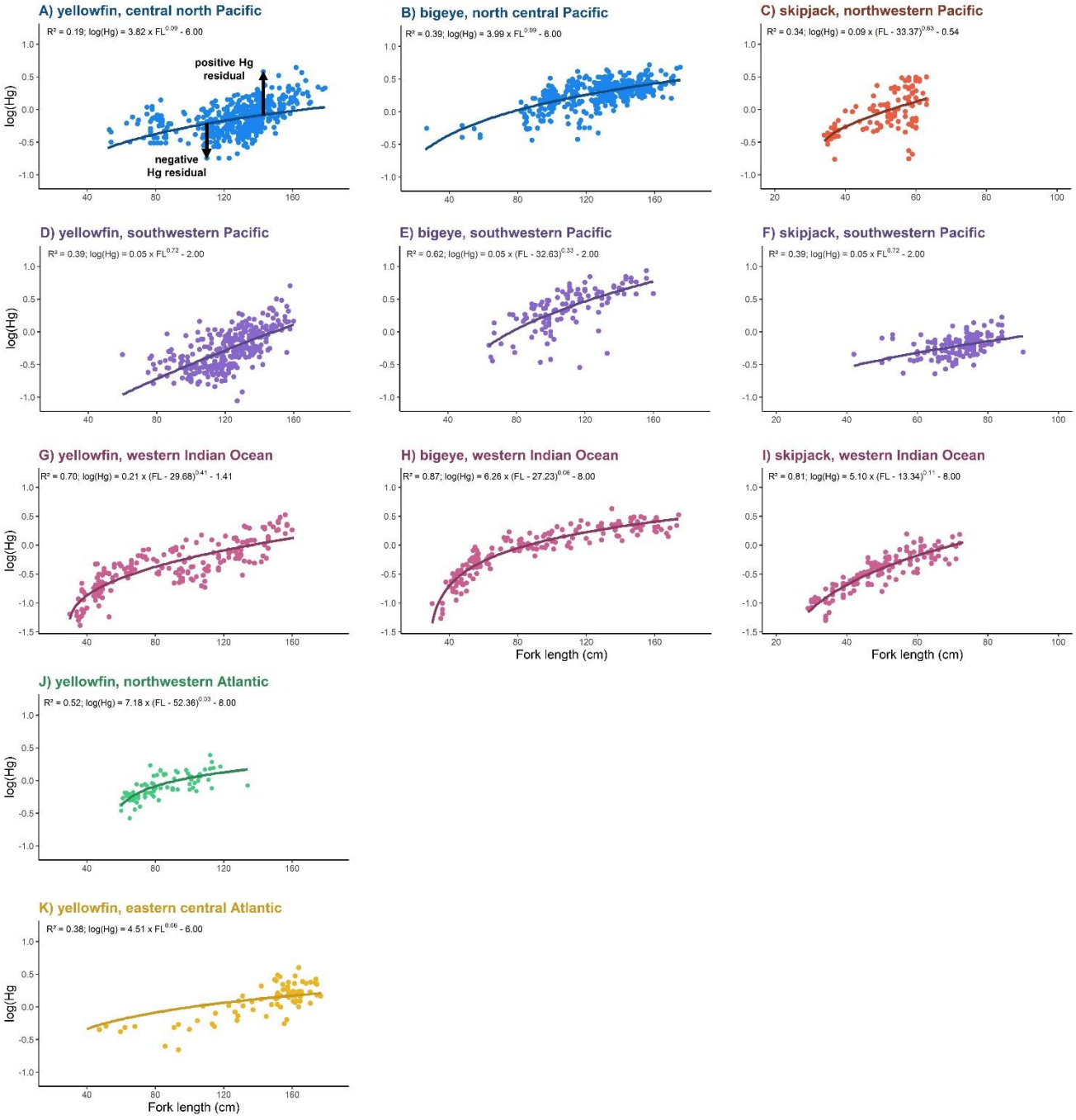

Figure 38. Power-law relationships between log-transformed observed mercury concentrations (log(Hg)) and fork length (FL), all years combined, for **A)** yellowfin, and **B)** bigeye from the central north Pacific, **C)** skipjack from the northwestern Pacific, **D)** yellowfin, **E)** bigeye, and **F)** skipjack from the southwestern Pacific, **G)**, yellowfin, **H)** bigeye, and **I)** skipjack from the western Indian, **J)** yellowfin from the northwestern Atlantic, and **K)** yellowfin from the eastern central Atlantic. The black arrows in A) symbolize the calculation of positive and negative mercury residuals.

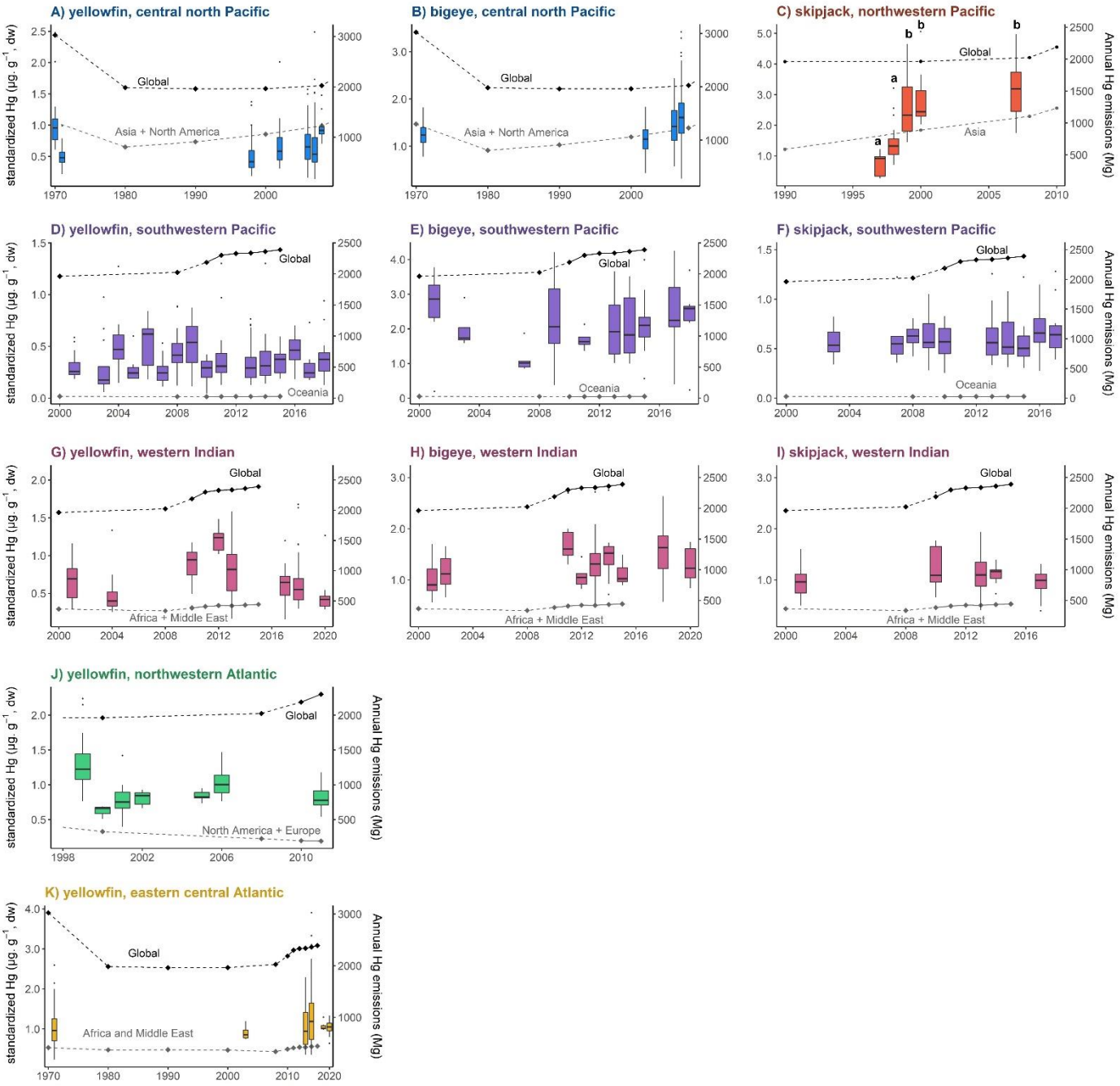

Figure 39. Temporal variability of tuna mercury (Hg) concentrations and anthropogenic emissions. Boxplots of standardized Hg concentrations (µg.g^{-1}, dw) in **A)** yellowfin, and **B)** bigeye from the central north Pacific (1970-2008), **C)** skipjack from the northwestern Pacific (1997-2007), **D)** yellowfin, **E)** bigeye, and **F)** skipjack from the yellowfin in the southwestern Pacific (2001-2018), **G)** yellowfin, **H)** bigeye, and **I)** skipjack from the western Indian (2001-2020), **J)** yellowfin from the northwestern Atlantic (1999-2011), and **K)** yellowfin in the eastern central Atlantic (1971-2020). A significant increase was found in skipjack standardized Hg levels from the northwestern Pacific only, as symbolised by the letters in C). Elsewhere, the year-to-year comparison indicates stable long-term trends of tuna standardized Hg levels. The coloured boxplots indicate the median value (thick bar), the outliers (dots) and 50 % of the data (the box itself). Diamonds represent the mean annual anthropogenic Hg emissions (Mg) at global and regional scales. The solid lines show the annual trends of emissions for the period 2010-2015, while the dashed lines show the decadal trends of emissions for the period 1970-2010.

Results and discussion

Our study documents the temporal variability of Hg concentrations in three tuna species in different regions of the global ocean. We show strong inter-annual variability of Hg concentrations in tropical tunas at the global scale, once accounting for MeHg bioaccumulation. Based on our multiple comparison approach, no long-term temporal trends were observed for all ocean regions, except for skipjack from the northwestern Pacific Ocean which exhibited significant increasing Hg concentrations since the 1990s.

Stable long-term mercury concentrations in tunas from the global ocean, except in the northwestern Pacific

In the central north Pacific Ocean (Hawaii), standardized Hg ranged from 0.14 to 2.49 $\mu g.g^{-1}$ dw (0.61 ± 0.31, mean ± sd per region) and from 0.31 to 3.42 $\mu g.g^{-1}$ dw (1.50 ± 0.48) in yellowfin and bigeye, respectively. In both species, standardized Hg concentrations varied significantly among years (Kruskal-Wallis test, $p < 0.05$), but no significant temporal pattern between the early 1970s or 1998, and more recent years (i.e., 2002, 2006, 2007 and 2008) was found (Figure 38 A & B; SI Appendix E, Table S3 A and B). Similarly, in the western Indian Ocean, standardized Hg concentrations varied from 0.16 to 1.68 $\mu g.g^{-1}$ dw (0.68 ± 0.33), from 0.54 to 2.75 $\mu g.g^{-1}$ dw (1.34 ± 0.44), and 0.40 to 2.71 $\mu g.g^{-1}$ dw (1.05 ± 0.35) in yellowfin, bigeye, and skipjack, respectively. These levels were highly variable among years (Kruskal-Wallis test, $p < 0.05$), but overall stable over the 2001-2020 period (Figure 38 G, H & I; SI Appendix E, Table S3 F, G & H). In the tropical northwestern Atlantic, standardized Hg concentrations ranged from 0.40 to 2.24 $\mu g.g^{-1}$ dw (1.03 ± 0.36) between 1999 and 2011. While concentrations were highly variable among years (Kruskal-Wallis test, $p < 0.05$), they did not show any significant temporal shift between older and recent years (Figure 38 J; SI Appendix E, Table S3 I). Standardized Hg concentrations in the eastern central Atlantic ranged from 0.23 to 3.90 $\mu g.g^{-1}$ dw (1.09 ± 0.52) between 1971 and 2020, and did not differ significantly among years (Kruskal-Wallis test, $p > 0.05$) (Figure 38 K), revealing a stable multi-decadal signal in tunas as well.

The apparent stability of Hg concentrations in tunas from the central north Pacific, the western Indian, and the northwestern and eastern central Atlantic Oceans over multiple decades is consistent with stable Hg concentrations within tropical tunas from the southwestern Pacific (Médieu et al., 2021a), again evidenced here (Figure 38 D, E & F; SI Appendix E, Table S3 D & E). Moreover, the range of standardized values found in yellowfin, bigeye and skipjack at a same length are similar across these five regions (Figure 38). In the central north Pacific, our results are in accordance with stable yellowfin Hg concentrations found between 1970 and the 1990s when first investigated (Kraepiel et al., 2003). But the apparent stability seen in our data contrasts with more recent reports of increasing trends in yellowfin (+5.5 ± 1.6 %/yr during 1998-2008) and bigeye (+3.9 ± 2.1 %/yr during 2002-2008), which were suggested to result from an increasing transport and deposition of anthropogenic Hg, as well as the lateral flow of water masses from the north west Pacific (Drevnick et al., 2015; Drevnick and Brooks, 2017). Our stable long-term trends of tuna Hg concentrations also contrast with reported annual decrease of 0.018 ± 0.003 % between 2004 and 2012 in bluefin tuna from the northwestern Atlantic, which was proposed to reflect a reduction in North American Hg emissions (Lee et al., 2016).

In the temporal studies from the North Atlantic and North Pacific where significant trends were reported, the authors suggest a direct link between anthropogenic Hg emissions and deposition and

Hg concentrations in tunas (Drevnick and Brooks, 2017; Lee et al., 2016). At the regional scale, our stable decadal Hg concentrations in the central north Pacific and the northwestern Atlantic do not mirror regional changes in emissions, namely the decline in from North America and Europe, and the increase in Asia. More broadly, they also do not follow the decreasing Hg^0 concentrations measured in the northern hemisphere since 1990 (Zhang et al., 2016), or since 1970 (EMEP, www.emep.int, Figure 38). On the other hand, stable tuna Hg concentrations from the southwestern Pacific, the western Indian, and the eastern central Atlantic follow the low and stable anthropogenic Hg emissions into the atmosphere from Oceania, Africa and Middle East, respectively. Yet they contrast with the increasing trend of Hg emissions reported for the southern hemisphere since the 1980s (Streets et al., 2017). This disconnect between estimated regional variations in emissions and stable Hg concentrations in biota has been documented in other marine and freshwater ecosystems (F. Wang et al., 2019) and likely results from i) different response times between the surface ocean, the subsurface ocean, and the atmosphere, and ii) the large amount of legacy Hg (i.e., historically emitted Hg that continues to cycle through biogeochemical compartments) in the subsurface ocean. Surface ocean (0 – 100 m) is a small reservoir that has been pointed out to be particularly sensitive to changes in anthropogenic Hg emissions and deposition (Amos et al., 2013). However, the surface ocean is also supplied with Hg from the underlying subsurface ocean (100 – 1500 m), which has received large amounts of legacy Hg over decades to centuries of Hg export from the surface ocean by particle scavenging and mixing. A global box model study illustrated how both the surface and subsurface oceans may take decades before showing a decrease in Hg, in response to decreasing anthropogenic Hg emissions and deposition (Amos et al., 2013). Inhabiting the surface (mainly skipjack and yellowfin) and mesopelagic (mainly bigeye, foraging below the thermocline) waters, tropical tunas are likely to reflect this time lag of responses between the atmosphere and the ocean. This would explain why we cannot detect significant temporal trend in tuna Hg from the central north and southwestern Pacific, the western Indian, and the northwestern and eastern central Atlantic, but only natural variations among years, which instead may reflect individual differences in foraging behavior, and variability in biogeochemical properties of seawater which play an important role in the rate of microbial *in situ* MeHg production (Malcolm et al., 2010; Monperrus et al., 2007). Moreover, in the central north Pacific Ocean, our contrasted results with the increasing tuna Hg concentrations revealed by Drevnick & Brooks (2017) with almost same datasets may result from our distinct statistical methodological approaches (see methods section).

Increasing tuna mercury concentrations in close vicinity of the eastern Asian region, the leading contributor of recent mercury emissions worldwide

Standardized Hg concentrations in skipjack along the Asian coasts ranged from 0.27 to 5.06 $\mu g.g^{-1}$ dw (2.14 ± 1.10) over the whole period 1997-2007 (Figure 38 C). They were overall higher than standardized values of skipjack's individuals at the same length in the southwestern Pacific (from 0.25 to 1.32 $\mu g.g^{-1}$ dw, Figure 38 F), especially in the recent years (> 2000) with values 3-4 times higher. Standardized Hg concentrations in skipjack also varied significantly among years (Kruskal-Wallis test, $p < 0.05$), with values in 1997 and 1998 significantly lower than values in 1999, 2000, and 2007 (Dunn test, $p < 0.05$) (Figure 38 C; SI Appendix E, Table S3 C). This suggests that standardized Hg concentrations in skipjack significantly increased at the end of the 1990s in the northwestern Pacific, and remained high throughout the 2000s. This incline contrasts with apparently stable Hg

concentrations found elsewhere in the Pacific, Indian and Atlantic Oceans (this study and Médieu et al., 2021a).

A significant increase in skipjack Hg from the northwestern Pacific likely results from a concomitant increase of anthropogenic Hg inputs from Asia, especially eastern Asia, where anthropogenic Hg emissions sharply increased between the 1980s and 2010, and thereafter stabilized, making this region the leading Hg contributor worldwide (Streets et al., 2019a, 2019b). The Eastern China and Yellow Seas are also known to receive significant anthropogenic Hg inputs from rivers (Liu et al., 2021). Resulting from these atmospheric and riverine releases, enriched Hg levels were measured in both seawater and sediments along the Asian Coasts (Fu et al., 2010; Kim et al., 2019; Laurier et al., 2004). In the Pacific Ocean, the hotspot of tuna Hg concentrations along the Asian coasts was mainly explained by elevated atmospheric Hg^0, suggesting a regional contribution of anthropogenic Hg in this particular region. In the rest of the Pacific, the spatial variability of Hg concentrations was related to natural ocean biogeochemical processes (Médieu et al., 2022). Here, the significant temporal increase of skipjack Hg concentrations concomitant with the massive increase of anthropogenic Hg inputs from Asia is an additional argument to suggest that pelagic biota do respond to recent anthropogenic Hg release, but with a significant effect only detectable in the immediate geographic vicinity of the Asian coasts.

Improvements and recommendations

We investigated Hg variability in tropical tunas, three species that display different vertical habitats (i.e., skipjack and yellowfin are epipelagic species while bigeye frequently occupy waters below the thermocline), which could have led to different responses of tuna Hg to temporal and spatial changes of anthropogenic Hg emissions. Yet, given our contrasted results in skipjack Hg from the northwestern Pacific and the western Indian Oceans, we assume datasets are suitable to compare responses of tuna Hg to fluctuations of anthropogenic emissions. Nevertheless, in the northwestern Pacific, given the different timescale responses of the surface and the subsurface oceans as explained previously, it would be valuable to explore Hg temporal variability over the same period in a mesopelagic tuna species (e.g., bigeye) to investigate if similar equilibrium between atmospheric Hg and marine biota Hg occurs in mesopelagic ecosystems.

While discussing our results, it is also worthwhile mentioning that the impact of anthropogenic Hg emissions on tuna Hg concentrations may be complicated by changes in tuna foraging ecology and/or ocean physical and biogeochemical processes, both occurring at local or regional scales, and known to control the speciation, bioavailability, and bioaccumulation of current and legacy emitted Hg (Houssard et al., 2019; Malcolm et al., 2010; Sunderland et al., 2009; Villar et al., 2020). Contrary to a temporal study in the southwestern Pacific (Médieu et al., 2021a), we could not investigate the possible confounding ecological contribution to the temporal variability of tuna Hg concentrations, as trophic data (i.e., stable nitrogen isotopes) were missing for a large number of samples in the respective time series. Nevertheless, trophic aspects have been recently identified to have little impact on Hg concentrations in tropical tunas, compared to ocean biogeochemistry and tuna habitat at both spatial and temporal scales (Houssard et al., 2019; Médieu et al., 2022, 2021a), suggesting that temporal variability of foraging ecology may weakly impact the responses to global changes of anthropogenic Hg releases.

Conversely, biogeochemical and physical properties have been identified as key drivers of Hg concentrations in tunas (Houssard et al., 2019; Médieu et al., 2022). Over the decades encompassed by our data, the oceanic environment has experienced anthropogenically-forced warming and deoxygenation of the upper ocean (Bindoff et al., 2019). The combination of these multiple stressors acts multiplicatively on ocean ecosystems (Gruber et al., 2021), in particular having severe negative effects on the fitness of aerobic species (Cheung et al., 2013; Deutsch et al., 2015; Sampaio et al., 2021). However, the apparent stability of tuna Hg concentrations over multiple decades suggests that the underlying warming and deoxygenation of the ocean has yet to appreciably affect MeHg production and accumulation in marine food webs, in so much as it has not been a primary driver of MeHg bioaccumulation. Although warmer seawater temperatures have been suggested to enhance MeHg levels in Atlantic bluefin tuna (Schartup et al., 2019), and estuarine and freshwater fishes (Dijkstra et al., 2013; Maulvault et al., 2016), there is no evidence herein that the recent acceleration of heat uptake by the ocean (Cheng et al., 2019) has significantly elevated tuna Hg concentrations. Similarly, the effect of widespread deoxygenation in the open ocean and in coastal areas since the 1970s (Bindoff et al., 2019; Breitburg et al., 2018; Schmidtko et al., 2017), which all else being equal should favour microbial MeHg formation, does not appear in our data. The lack of strong temporal trends in tuna due to ocean warming and deoxygenation is however not so surprising given that spatial gradients in these properties are far greater than long-term temporal trends. Moreover, the signal of secular changes may be engulfed by the noise of inter-annual variability in these properties, which may in part explain the strong variability in our data. Finally, changes in ocean productivity and nutrient enrichment of coastal ecosystems may also have confounding effects on decadal trends of tuna Hg concentrations, as primary production and carbon export are key drivers of MeHg at depth. Nonetheless, continuous long-term temporal series of tuna Hg concentrations with corresponding environmental parameters would be useful to investigate the relative importance of biogeochemical properties on MeHg formation and bioavailability in seawater in the context of changing anthropogenic Hg releases.

Implications for mercury monitoring in the global ocean and marine biota

With the adoption of the Minamata Convention, marine bio-indicator species are required to monitor Hg in relation to human health, and to investigate spatial and temporal Hg trends in marine ecosystems. This assumes that some marine species are able to integrate local and global Hg sources over different spatial and temporal scales, which requires long-term temporal series as well as large and high-resolution spatial studies to verify these assumptions. Here, we provide an assessment of temporal patterns of tuna Hg concentrations in different regions of the global ocean, and highlight two types of responses of Hg concentrations in tunas to decadal shifts of global anthropogenic Hg emissions. In the global ocean, with the exception of the northwestern Pacific, our study suggests stable long-term Hg concentrations in tropical tunas, although concentrations were highly variable among years, likely reflecting natural ecological and biogeochemical processes that overrule the potential influence of anthropogenic Hg emissions on the global ocean. Conversely, we show that Hg concentrations in skipjack caught along the Asian coasts increased significantly in the late 1990s before stabilising in recent years, while more recent samples would be necessary to validate the results. These contrasting responses suggest that at the local scale of the Asian coasts, in the immediate vicinity of emission sources, Hg concentrations in surface tuna may reflect the massive increase of anthropogenic

Hg emissions through time. Yet, on a global scale, the divergence between stable Hg concentration in tropical tunas and clear regional variations in emissions highlight the large inventory of legacy Hg that continues cycling in oceans. Taken together, our results highlight that tropical tunas are able to reflect concomitant increasing anthropogenic Hg emissions to the atmosphere, but may take several decades to decline as a result of emission reduction measures.

Our study therefore suggests that tropical tunas can be used as sentinels of marine Hg pollution to provide insights for the future design and implementation of large-scale Hg biomonitoring efforts to evaluate the effectiveness of the Minamata Convention. Overall, this highlights the need for more systematic and continuous collection of tuna Hg concentrations with corresponding biological (i.e., fish length or age), ecological (i.e., carbon and nitrogen stable isotopes), and biogeochemical (e.g., depth at which heterotrophy exceeds autotrophy, oxygen in subsurface waters, net primary production) data to strengthen our understanding of the global changes associated to shifts of anthropogenic Hg releases. Combined with complementary direct measurements of atmospheric deposition and seawater Hg concentrations in different regions of the global ocean, the use of tunas as biomonitoring agents of Hg could also aid in the exploration of legacy and recent anthropogenic Hg releases, and the potential time lags between changing emissions in the atmosphere and Hg accumulation in marine food webs. Moreover, these continuous and long-term Hg series would be valuable to investigate the impacts of climate-induced changes on tuna Hg content and MeHg bioaccumulation in general, given the importance of biogeochemical processes on MeHg bioavailability. Finally, they would also contribute to the monitoring of human Hg exposure through ocean food consumption.

Acknowledgments

This study was conducted in the framework of ANR-17-CE34-0010 MERTOX (unravelling the origin of methylMERcury TOXin in marine ecosystems, 2017 – 2021, PI David Point) from the French Agence Nationale de la Recherche. It benefited from financial support of the Région Bretagne and Université de Bretagne Occidentale (UBO). We are grateful to our sampling providers, including the Environmental Specimen Bank in Ehime University (Japan), the CRO-IRD-IEO team in charge of tropical tunas purse-seine fisheries monitoring in Abidjan (Ivory Coast), the Western and Central Pacific Fisheries Commission Tuna Tissue Bank, the Pacific Marine Specimen Bank managed by the Pacific Community (SPC), and the NOAA Pacific Islands Region Observer Program. We also thank the US IMAGO of IRD and the volunteers who collected tuna samples during the PIRATA cruises (https://doi.org/10.18142/14). We are grateful to Emmanuel Chassot from IRD and IOTC (Seychelles) for providing species-specific length-weight relationships in the Atlantic Ocean.

Chapter 3. Evidence that Pacific tuna mercury levels are driven by marine methylmercury production and anthropogenic inputs

Anaïs Médieu[1,*], David Point[2], Takaaki Itai[3], Hélène Angot[4], Pearse J. Buchanan[5], Valérie Allain[6], Leanne Fuller[7], Shane Griffiths[7], David P. Gillikin[8], Jeroen E. Sonke[2], Lars-Eric Heimbürger-Boavida[9], Marie-Maëlle Desgranges[9], Christophe E. Menkes[10], Daniel J. Madigan[11], Pablo Brosset[1,12,13], Olivier Gauthier[1], Alessandro Tagliabue[5], Laurent Bopp[14], Anouk Verheyden[8], Anne Lorrain[1]

[1]Univ Brest, CNRS, IRD, Ifremer, LEMAR, F-29280 Plouzané, France
[2]Observatoire Midi-Pyrénées, GET, UMR CNRS 5563/IRD 234, Université Paul Sabatier Toulouse 3, Toulouse, France
[3]Department of Earth and Planetary Sciences, Graduate School of Science, The University of Tokyo, Bunkyo-Ku, Tokyo, 113-0033, Japan
[4]Extreme Environments Research Laboratory, École Polytechnique Fédérale de Lausanne (EPFL) Valais Wallis, Sion, Switzerland
[5]University of Liverpool, Department of Earth, Ocean and Ecological Sciences, Liverpool, UK
[6]Pacific Community, Oceanic Fisheries Programme, Nouméa, New-Caledonia
[7]Inter-American Tropical Tuna Commission, 8901 La Jolla Shores Drive, La Jolla, CA, USA
[8]Department of Geosciences, Union College, 807 Union St., Schenectady, NY, 12308, USA
[9]Aix Marseille Université, CNRS/INSU, Universite de Toulon, IRD, Mediterranean Institute of Oceanography (MIO) UM 110, 13288, Marseille, France
[10]ENTROPIE (UMR 9220), IRD, Univ. de la Réunion, CNRS, Nouméa, Nouvelle-Calédonie
[11]Department of Integrative Biology, University of Windsor, Windsor, ON, Canada
[12]Ifremer, Laboratoire de Biologie Halieutique, ZI Pointe du Diable - CS 10070, 29 280 Plouzané, France
[13]ESE, Ecology and Ecosystem Health, Agrocampus Ouest, INRAE, Rennes 35042, France
[14]LMD/IPSL, Ecole Normale Supérieure/PSL University, CNRS, Ecole Polytechnique, Sorbonne Université, Paris, France

Manuscript published in PNAS (https://doi.org/10.1073/pnas.2113032119)

Abstract

Pacific Ocean tuna is among the most-consumed seafood products but contains relatively high levels of the neurotoxin methylmercury. Limited observations suggest tuna mercury levels vary in space and time, yet the drivers are not well understood. Here, we map mercury concentrations in skipjack tuna across the Pacific Ocean and build generalized additive models to quantify the anthropogenic, ecological, and biogeochemical drivers. Skipjack mercury levels display a fivefold spatial gradient, with maximum concentrations in the northwest near Asia, intermediate values in the east, and the lowest levels in the west, southwest, and central Pacific. Large spatial differences can be explained by the depth of the seawater methylmercury peak near low-oxygen zones, leading to enhanced tuna mercury concentrations in regions where oxygen depletion is shallow. Despite this natural biogeochemical control, the mercury hotspot in tuna caught near Asia is explained by elevated atmospheric mercury concentrations and/or mercury river inputs to the coastal shelf. While we cannot ignore the legacy mercury contribution from other regions to the Pacific Ocean (e.g., North America and Europe), our results suggest that recent anthropogenic mercury release, which is currently largest in Asia, contributes directly to present-day human mercury exposure.

Significance

Humans are exposed to toxic methylmercury mainly by consuming marine fish. New environmental policies under the Minamata Convention rely on a yet-poorly-known understanding of how mercury emissions translate into fish methylmercury levels. Here, we provide the first detailed map of mercury concentrations from skipjack tuna across the Pacific. Our study shows that the natural functioning of the global ocean has an important influence on tuna mercury concentrations, specifically in relation to the depth at which methylmercury concentrations peak in the water column. However, mercury inputs originating from anthropogenic sources are also detectable, leading to enhanced tuna mercury levels in the northwestern Pacific Ocean that cannot be explained solely by oceanic processes.

Keywords: methylmercury, skipjack tuna, biogeochemistry, atmospheric inputs, spatial modeling

Introduction

Mercury (Hg) is a global pollutant that affects both ecosystems and human health. Mercury is emitted to the atmosphere by natural processes (e.g., volcanism) and anthropogenic activities (e.g., fossil fuel combustion and artisanal and small-scale gold mining) (Outridge et al., 2018) mainly as gaseous elemental Hg^0. Atmospheric Hg can be deposited or taken up at the ocean surface (Jiskra et al., 2021). Rivers deliver significant amounts of Hg to estuarine and coastal oceans, but only a small fraction of this Hg is transported to open ocean regions (Liu et al., 2021). In the ocean, a substantial fraction of inorganic Hg is naturally transformed to methylmercury (MeHg) in the subsurface waters (Bowman et al., 2020b; Mason and Fitzgerald, 1990). The neurotoxic MeHg naturally bioaccumulates and biomagnifies in aquatic food webs, leading to elevated concentrations in higher-trophic-level organisms such as tunas. Humans are exposed to MeHg mainly by the consumption of marine fishes, and tunas in particular, with MeHg representing the major chemical form (> 91 %) of total Hg in tuna muscle (Houssard et al., 2019; Mergler et al., 2007; Sunderland, 2007). The United Nations Environmental Program Minamata Convention (131 parties in June 2021) aims to protect human health and the environment from anthropogenic Hg. Governments and policy makers must therefore balance economic, environmental, and health interests. Understanding the factors that drive MeHg concentrations in tunas, and how climate change interferes in the process is therefore critical to policy makers and, ultimately, to limiting human exposure to MeHg.

In line with the spatial distribution of Hg emissions, observations show higher atmospheric Hg^0 levels in the northern hemisphere compared to the southern hemisphere (Sprovieri et al., 2016). Sediment and peat records of atmospheric Hg deposition also suggest a larger anthropogenic Hg enrichment in the northern hemisphere (C. Li et al., 2020). Anthropogenic Hg emissions are thought to have tripled the concentrations of total Hg in the thermocline waters (100 to 1,000 m) of the global ocean relative to deeper older waters (Lamborg et al., 2014), yet still unclear is how these anthropogenic Hg inputs are converted into methylmercury in oceans. Subsurface MeHg concentrations are higher in the eastern Pacific Ocean, with coastal and upwelling areas exhibiting the highest proportion of MeHg relative to total Hg (Bowman et al., 2016, 2020).

Methylmercury uptake and biomagnification associated with fish age (and length), feeding ecology, and habitat use are known factors influencing Hg bioaccumulation in tunas (Chouvelon et al., 2017; Choy et al., 2009; Houssard et al., 2019; Médieu et al., 2021a). A recent global-scale study documenting the distribution of tuna Hg concentrations at 11 different locations found up to an eightfold difference among sites but did not identify the drivers of this variability (Nicklisch et al., 2017). Another study conducted at high spatial resolution in the southwestern Pacific Ocean suggested that ocean physics, local ocean biogeochemistry, and tuna habitat play important roles in determining tuna Hg concentrations (Houssard et al., 2017, 2019). Meanwhile, temporal trends in tuna Hg show contrasting results between oceanic basins. Decreasing Hg concentrations were observed in Atlantic bluefin tuna (*Thunnus thynnus*) from the northern Atlantic Ocean between 1990 and 2000 (Lee et al., 2016). In the Pacific Ocean, stable Hg concentrations between 2001 and 2018 were observed in tropical tunas (i.e., yellowfin, *T. albacares*; bigeye, *T. obesus*; and skipjack, *Katsuwonus pelamis*) from the southwestern Pacific (Médieu et al., 2021a), while increasing Hg levels in yellowfin and bigeye tunas since 1970 were documented in the central north Pacific (CNPO) (Drevnick and Brooks, 2017). These contrasting trends suggest that tuna Hg may be sensitive to spatiotemporal changes in anthropogenic Hg emissions and ocean uptake and/or regional variations in biogeochemical processes or foraging

ecology that affect tuna exposure to MeHg. Studies of large spatial coverage are therefore needed to investigate the control and relative importance of atmospheric Hg sources, oceanic Hg methylation, and foraging ecology on tuna Hg concentrations.

Here, we report the highest spatially resolved dataset of Hg concentrations of skipjack tuna, with records from six distinct areas of the Pacific Ocean (n = 661, from ~45°N to 25°S, Figure 39 A). As the third most consumed marine fish species worldwide (FAO, 2018), it is a species of high commercial and human health importance. Although classified as highly migratory, this epipelagic and fast-growing tuna species shows relatively restricted movements and high site fidelity rates in the Pacific Ocean (Fonteneau and Hallier, 2015; Sibert and Hampton, 2003) and thus should be able to reflect spatial MeHg patterns in surface water food webs. We applied generalized additive models (GAM) to 1) explore geographical patterns, including hemispheric differences, of tuna Hg concentrations and 2) disentangle the driving factors of tuna Hg spatial variability. In particular, we used atmospheric Hg^0 model estimates, ecological tracers in tuna, biogeochemical estimates at the base of food webs, and oceanographic variables to explore the relative contribution of anthropogenic Hg emissions, ocean biogeochemistry, and tuna foraging ecology to observed tuna Hg concentrations.

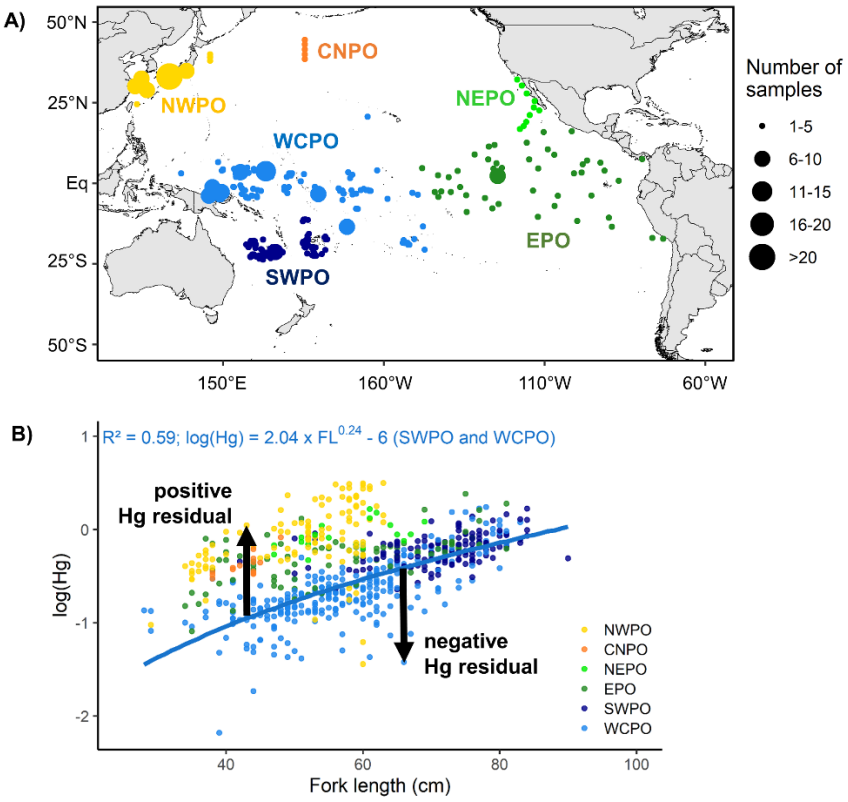

Figure 40. Skipjack tuna sample provenance and mercury concentrations. **A)** Map of skipjack sampling locations, with the size of the circles proportional to the number of individuals collected. **B)** Power-law relationship between log(observed Hg) and skipjack fork length. The relationship was fitted on samples from the SWPO and WCPO only, but Hg residuals were calculated for all samples (symbolized by the black arrows). Oceanic areas: NWPO = northwestern Pacific; CNPO = central north Pacific; NEPO = northeastern Pacific; EPO = eastern Pacific; SWPO = southwestern Pacific; WCPO = western central Pacific.

Results and Discussion

Spatial variability of tuna mercury concentrations

As Hg is known to bioaccumulate with fish size (Cai et al., 2007), we fitted a length-based model to the observed Hg concentrations to calculate length-standardized Hg concentrations (Figure 39 B, at mean length = 60 cm fork length; see Materials and Methods), hereafter defined as standardized Hg concentrations, in contrast to observed Hg concentrations. This normalizing approach allowed us to explore the spatial distribution of Hg concentration anomalies not explained by Hg bioaccumulation and fish size differences among individuals but likely due instead to other processes (e.g., anthropogenic emissions, ocean biogeochemistry, or tuna foraging ecology) (Houssard et al., 2019; Médieu et al., 2021a).

Observed Hg concentrations in skipjack ranged from 0.01 to 3.15 µg.g^{-1} dry weight (0.56 ± 0.51 µg.g^{-1} dw, mean ± SD; Figure 40 A; SI Appendix F, Figure S1), which is comparable to values reported near Hawaii and in the western Indian Ocean for the same species (Bodin et al., 2017; Kaneko and Ralston, 2007; Kojadinovic et al., 2006). The relatively low Hg levels in skipjack tuna are consistent with the ecology and biology of this species. Compared to other tropical tuna species that exhibit higher Hg concentrations, skipjack tuna are characterized by a lower trophic position, a shallower vertical habitat that allows access to epipelagic prey with lower Hg concentrations, and a shorter lifespan (Choy et al., 2009; Olson et al., 2016).

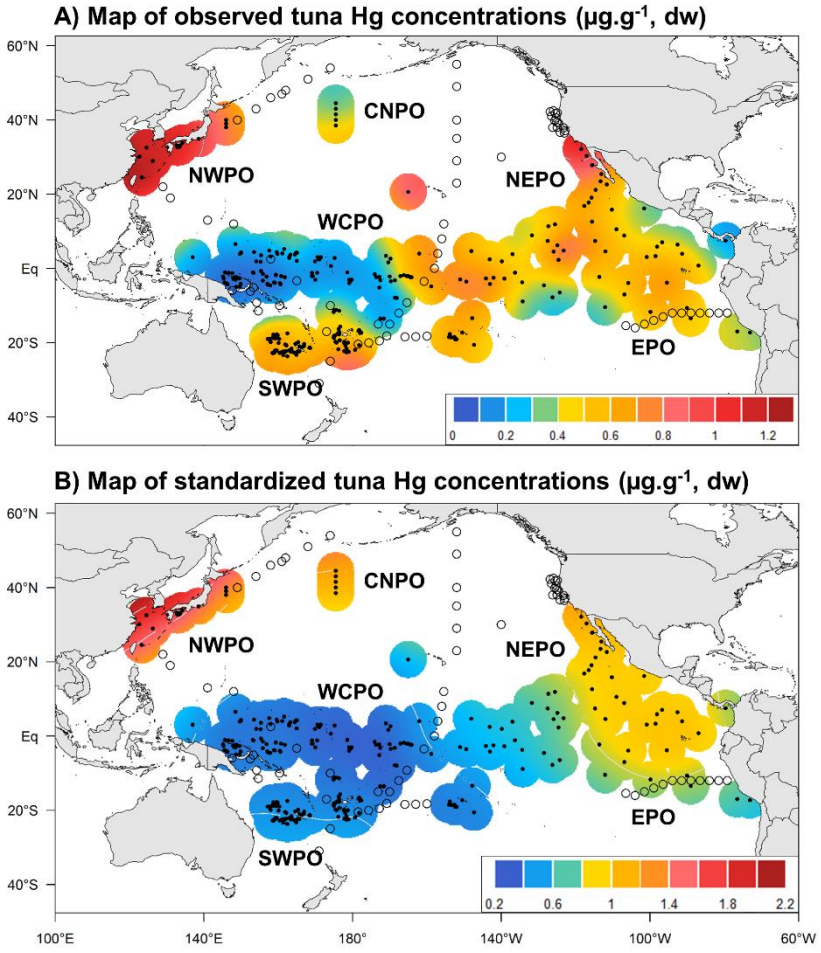

Figure 41. Spatial variability of skipjack mercury (Hg) concentrations. Smoothed spatial contour maps of **A)** observed and **B)** standardized Hg concentrations (µg.g^{-1}, dw) in skipjack white muscle samples from the Pacific Ocean. The black dots represent the location of skipjack samples. Ocean areas correspond to the samples origin: NWPO = northwestern Pacific; CNPO = central north Pacific; NEPO = northeastern Pacific; EPO = eastern Pacific; SWPO = southwestern Pacific; WCPO = western central Pacific.

Observed and standardized Hg concentrations in skipjack tuna were both highly variable in the Pacific Ocean. Standardized Hg concentrations were significantly higher in the northern than in the southern hemisphere (Figure 40 B), which is consistent with latitudinal Hg gradients observed in other Pacific Ocean reservoirs (i.e., atmosphere, seawater, and marine sediments) (Figure 41; SI Appendix F, Figure S2). Significant spatial differences of standardized Hg concentrations were also detected at smaller spatial scales within the Pacific, among the defined oceanic areas (Kruskal–Wallis test, $p < 0.001$; Figure 40 B; SI Appendix F, Figure S1). The highest standardized Hg concentrations were found in the northwestern Pacific (NWPO), where they were 1.5 to 2 times higher than in the CNPO and eastern regions (i.e., northeastern [NEPO] and eastern [EPO] Pacific) and 4 to 5 times higher than in the southwestern (SWPO) and the western central (WCPO) Pacific Ocean (Figure 40 B). The only two available spatial studies of Hg in tropical yellowfin and bigeye tunas also suggested higher Hg concentrations in the EPO compared to the central and western regions (Ferriss and Essington, 2011; Houssard et al., 2019).

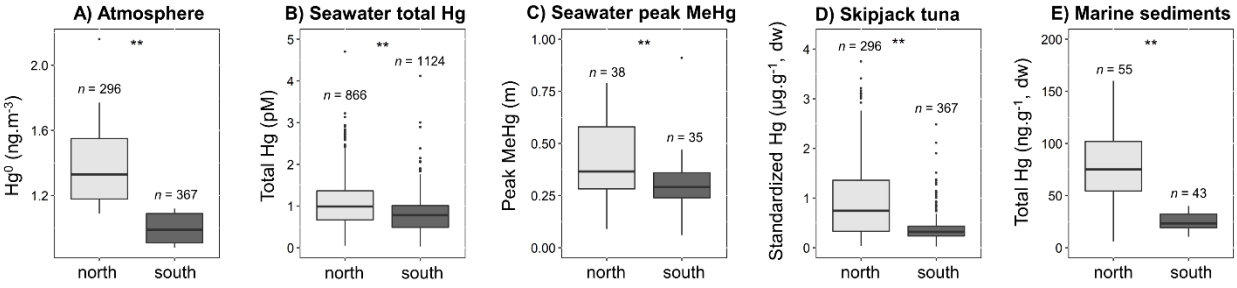

Figure 42. Hemispheric mercury gradients in different in different Pacific Ocean reservoirs. The boxplots illustrate the hemispheric gradient of **A)** atmospheric Hg^0 model estimates ($ng.m^{-3}$) extracted at tuna sampling locations (see Materials and Methods), **B)** observed total Hg concentrations (pM) in seawater (Bowman et al., 2016; Coale et al., 2018; Ganachaud et al., 2017; Kim et al., 2017; Laurier et al., 2004; Munson et al., 2015), **C)** observed MeHg concentrations at peak (pM) in seawater (Bowman et al., 2016; Coale et al., 2018; Ganachaud et al., 2017; Hammerschmidt et al., 2013; Kim et al., 2017; Munson et al., 2015; Sunderland et al., 2009), **D)** standardized total Hg concentrations ($\mu g.g^{-1}$, dw) in skipjack tuna (this study), and **E)** observed total Hg concentrations ($ng.g^{-1}$, dw) in marine sediments (Aksentov and Sattarova, 2020; Hayes et al., 2021; Jiskra et al., 2021; Kannan and Falandysz, 1998; Sun et al., 2020; Yin et al., 2015; Young et al., 1973). ** indicates significant differences between the northern and southern hemisphere (Kruskal-Wallis test; $p < 0.01$).

The main drivers of this spatial variability were identified with GAM. The optimal model explained 72 % (deviance explained [DE]) of the spatial variability of observed tuna Hg concentrations and included fish length, proxies for the depth of seawater MeHg peak production (i.e., the depth of net heterotrophy and $[O_2]$ in subsurface waters; see Materials and Methods) and atmospheric Hg^0 model estimates (Figure 42). Baseline-corrected tuna $\delta^{15}N$ values were used as a proxy for the tuna trophic position to investigate trophic processes and Hg biomagnification through the pelagic food webs. They were, however, not selected in the best model, indicating that spatial trophic effects (i.e., geographical changes in foraging ecology) have a limited influence on the spatial variability of tuna Hg concentrations, as already observed in the WCPO (Houssard et al., 2019). Furthermore, the absence of the effect of particulate organic matter $\delta^{15}N$ estimates in our optimal GAM also indicates that spatial changes of the nitrogen cycle at the base of the marine food web may be of weak importance to explain spatial changes of tuna Hg concentrations at the large Pacific Ocean scale. Conversely, given the

selected drivers in the optimal GAM, the spatial variability of skipjack Hg concentrations is more likely to result from 1) variable seawater MeHg concentrations at the base of the food web among oceanic areas and/or 2) variable amounts of surface ocean inorganic Hg loading from the atmosphere, as discussed in the two following sections.

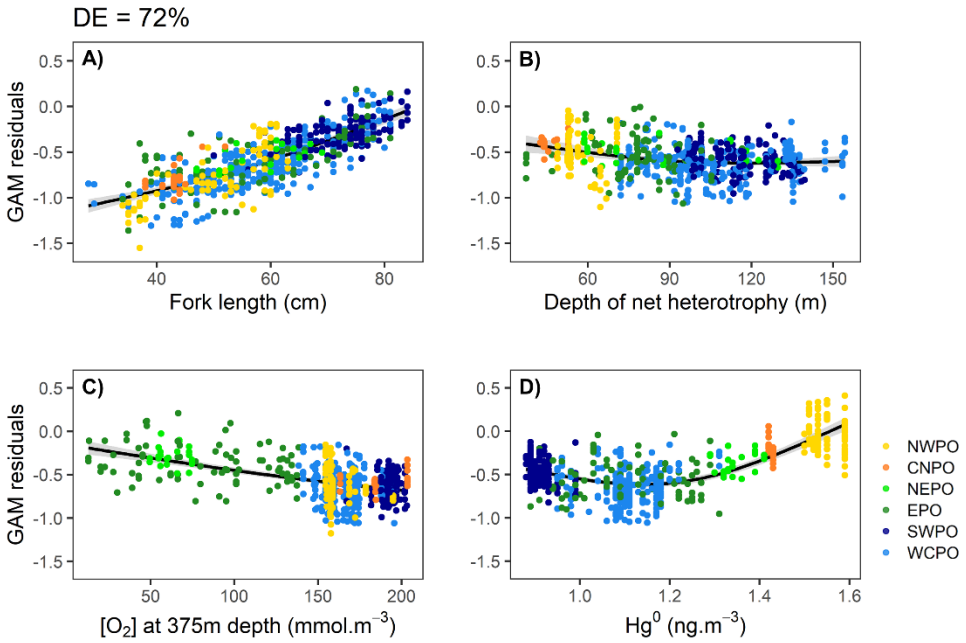

Figure 43. Optimal GAM predicting observed mercury concentrations in skipjack tuna. The main drivers of the spatial variability of log(observed Hg) were **A)** fish length, **B)** the depth of net heterotrophy, **C)** [O2] in subsurface waters, and **D)** Hg^0 model estimates. The DE percentage of the model is reported on the top of the figure. Colored dots are the partial residuals of the GAM by oceanic areas. Black lines show the expected values, and grey bands show confidence intervals for the expected value, which are twice the standard error. Oceanic areas: NWPO = northwestern Pacific; CNPO = central north Pacific; NEPO = northeastern Pacific; EPO = eastern Pacific; SWPO = southwestern Pacific; WCPO = western central Pacific.

Natural marine biogeochemical drivers of the spatial variability of skipjack mercury concentrations

A key aspect when investigating Hg variability in marine biota is its relationship with seawater MeHg concentrations, which may vary as a function of biogeochemical processes. In the Pacific Ocean, observed MeHg data in seawater are scarce and are available at limited and low spatial resolution in comparison with our skipjack Hg dataset (Figure 40). To overcome this limitation, we used a combination of biogeochemical and physical proxies of seawater peak MeHg concentrations to assess the influence of ocean biogeochemistry on skipjack Hg burden. In the optimal model, the spatial variability of skipjack Hg concentrations was largely explained by the depth of net heterotrophy (i.e., the depth at which autotrophy is overcome by heterotrophy), which is a proxy for the depth of peak seawater MeHg concentrations, and $[O_2]$ in subsurface waters (Figure 42 B and C). Response curves indicated that these two variables combined might be of particular importance to explain the west-to-east gradient of tuna Hg content. Higher tuna Hg concentrations found in the east (i.e., NEPO and EPO) were linked to low subsurface $[O_2]$ and shallow net heterotrophy, while lower standardized Hg

concentrations in the west (i.e., SWPO and WCPO) were associated with higher subsurface [O_2] and deeper net heterotrophy (SI Appendix F, Figures S3 and S4). This pattern suggests that oxygen-poor conditions and shallow bacterial loops both associated with the intense remineralization of organic matter are responsible for enhanced concentrations and/or bioavailability of MeHg at the base of marine food webs.

Marine MeHg concentrations generally peak in low-oxygen thermocline waters, and in the Pacific Ocean, slightly higher MeHg concentrations were measured in the suboxic oxygen minimum zone of the Peruvian upwelling system (Bowman et al., 2016). Although most known Hg methylators are strict anaerobic microorganisms (e.g., sulfate- and iron-reducing bacteria) (Parks et al., 2013), there is abundant evidence that Hg can be methylated in oxic marine waters (Malcolm et al., 2010; Monperrus et al., 2007; Villar et al., 2020), potentially due to anaerobic microniches in otherwise oxygenated environments that support methylation (Bianchi et al., 2018). Our results indicate that high seawater MeHg concentrations are not only induced by ambient low-oxygen conditions but also by more intense and shallower remineralization that could be responsible for generating anaerobic microniches with active methylation. Indeed, when exploring observed depths of seawater peak MeHg concentrations in relation to our combination of biogeochemical and physical model estimates with GAMs, variables selected in the optimal model were [O_2] in subsurface waters and the depth of net heterotrophy (SI Appendix F, Figure S5). Also consistent with this hypothesis is the fact that a shallower peak of MeHg concentrations was measured in the eastern part of the equatorial Pacific Ocean compared to the western part (Kim et al., 2017). Knowing that skipjack tuna remain in the upper 100 m and occupy the surface trophic niche throughout the Pacific Ocean, a shallower peak of MeHg concentrations in the EPO would contribute to higher MeHg bioavailability in surface pelagic food webs in this region, which translates here into skipjack spatial Hg distribution. Overall, these correlations between tuna Hg concentrations and subsurface [O_2] alongside the depth of net heterotrophy strongly suggest that the biogeochemical conditions of the Pacific Ocean naturally induce large spatial variability of Hg concentrations in marine fish.

Anthropogenic releases enhancing tuna mercury concentrations in the northwestern Pacific Ocean

In addition to fish length and biogeochemical and physical variables, Hg^0 model estimates were selected in the optimal GAM (Figure 42 D). Higher Hg concentrations in tuna, found in the NWPO and, to a lesser extent, in the CNPO and NEPO, were associated with higher atmospheric Hg^0 model estimates (Figure 42 D), suggesting a link between atmospheric Hg emissions and Hg in tuna in the northern Pacific. In particular, the highest standardized Hg concentrations in the NWPO occurred under the Asian atmospheric outflow, characterized by high levels of Asian anthropogenic Hg emissions (Streets et al., 2019a). Knowing the very shallow heterotrophic conditions in the NWPO, one could argue that the biogeochemical processes alone (i.e., higher seawater MeHg concentrations combined with a shallower MeHg peak), as explained previously, are responsible for higher skipjack Hg concentrations in this oceanic region. To account for these potential confounding effects, we defined a modified version of our optimal GAM deliberately excluding Hg^0 model estimates (i.e., using only fish length, depth of net heterotrophy, and subsurface [O_2]) and used it to predict skipjack Hg concentrations across the Pacific. When mapping the difference between observed and predicted Hg concentrations (Figure 43), tuna Hg concentrations appeared to be correctly predicted in the entire

Pacific except in the NWPO, which highlights that biogeochemical processes alone, combined with fish length, do not allow predicting the spatial variability of observed skipjack Hg concentrations in this region. In the NWPO, GAM output values indeed underestimate the skipjack Hg concentrations compared to what is observed. This highlights the presence of an additional contribution most likely governed by anthropogenic Hg inputs along the Asian coasts, in particular in the East China and Yellow Seas. Enhanced Hg concentrations in tuna from the NWPO are in accordance with enriched Hg levels in both seawater and sediments from the same area (Fu et al., 2010; Kim et al., 2019; Laurier et al., 2004).

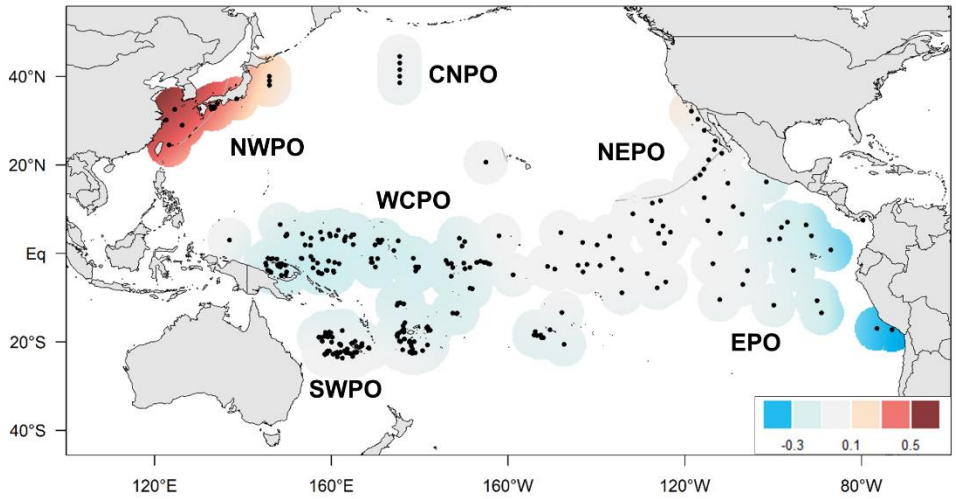

Figure 44. Relative contribution of current local anthropogenic emissions to tuna mercury concentrations. Smoothed spatial contour maps of the difference between observed and GAM predicted mercury concentration (µg.g^{-1}, dw) in skipjack white muscle samples from the Pacific Ocean. The GAM included fish length, depth of net heterotrophy, and subsurface [O_2], explaining most of tuna mercury variability, except an Asian outflow mercury contribution in the NWPO. The black dots represent the location of skipjack samples. Oceanic areas: NWPO = northwestern Pacific; CNPO = central north Pacific; NEPO = northeastern Pacific; EPO = eastern Pacific; SWPO = southwestern Pacific; WCPO = western central Pacific.

It is worthwhile to mention that we did not consider the potential influence of riverine inputs in our modeling approach. These inputs, although generally considered negligible in the open ocean (Zhang et al., 2015), deliver significant amounts of anthropogenic Hg near coastal areas, especially in the Eastern China and Yellow Seas (Kim et al., 2019; Liu et al., 2021). Nevertheless, we consider that Hg^0 model estimates are good surrogates to investigate the anthropogenic contribution of Hg in skipjack tuna, since high atmospheric Hg levels near industrialized landmasses should also translate into enhanced river inputs. Also important when discussing the burden of anthropogenic Hg in tuna is the contribution of legacy Hg to current marine predator Hg levels. Legacy Hg is the stock of historically emitted Hg that is presently stored in terrestrial soils and in the intermediate and deep ocean. The legacy of past North American and European anthropogenic emissions and deposition are estimated to account for about 30 % of global anthropogenic Hg in the surface ocean (Amos et al., 2013) and to be also responsible for high modern Hg^0 concentrations in the atmosphere (Horowitz et al., 2017). This suggests that despite the clear regional contribution of currently enhanced Hg inputs from the Asian Pacific region, skipjack tuna from the Pacific in general also display a fingerprint of legacy Hg originating from other historic contributing regions that continue to supply the atmosphere and surface ocean with legacy Hg. Yet the surface ocean is a small reservoir (2,600 Mg) of similar size to the atmosphere

(4,400 Mg) (Outridge et al., 2018) and has been pointed out to be particularly sensitive to recent anthropogenic emissions (Amos et al., 2015), suggesting that recent Asian emissions may be partly responsible for the observed Hg hotspot in tuna from the NWPO. Overall, our findings suggest that pelagic biota do respond to recent anthropogenic Hg release but with a significant effect only detectable at the regional scale in the NWPO.

Implications for mercury monitoring in the global ocean and marine biota

This study provides an assessment of broad-scale and high-resolution spatial patterns of Hg concentrations in skipjack tuna from the Pacific Ocean. Our spatial interpolation of length-standardized Hg concentrations revealed two primary areas where tuna are relatively enriched in Hg in the Pacific Ocean: the northwest near Asia, and, to a lesser extent, the upwelling regions of the NEPO and southeast Pacific off the coasts of North and South America. The complementary use of ecological tracers alongside biogeochemical and physical variables showed 1) a marine biogeochemistry control, likely via variations in the concentrations of MeHg and the depth at which peak concentrations exist within the water column, which drives the spatial variability of skipjack Hg across the Pacific Ocean, and 2) a cumulated local anthropogenic Hg release effect enhancing tuna Hg levels along the Asian coasts.

Although Hg concentrations in skipjack were low compared to other tropical tuna species and were below the upper threshold of food safety guidelines (1 $\mu g.g^{-1}$, wet weight [i.e., 3.3 $\mu g.g^{-1}$, dw]) (WHO and UNEP Chemicals, 2008), our results raise questions regarding human exposure to Hg through the consumption of tunas. Globally, skipjack is the third most consumed marine fish and the most consumed tuna species (FAO, 2018), and the Pacific Ocean remains the primary source of tunas, representing more than 65 % of global catch (ISSF, 2019). Skipjack Hg concentrations along the Asian coasts mirror atmospheric Hg0 concentrations, and therefore anthropogenic Hg emissions and releases, illustrating a link between recent Asian anthropogenic Hg emissions, marine pelagic fish Hg levels, and human MeHg exposure. In the eastern region, the observations of growing low oxygen zones (Schmidtko et al., 2017; Stramma et al., 2008) and their predicted climate-driven expansion in the coming decades (Bindoff et al., 2019; Deutsch et al., 2011) may point to more favorable conditions for MeHg formation. However, parallel changes in primary production and organic matter export, which are key components driving MeHg production at depth, could alter this trend. Although global models tend to project declines in both the production of organic matter by primary producers and its export to the ocean interior in low-latitude oceans over the present century, there are significant uncertainties associated with a range of poorly constrained processes, especially for the EPO (Laufkötter et al., 2016; Tagliabue et al., 2020). Further research is needed to better constrain the integrated impacts of climate change, ocean deoxygenation, and organic matter export on MeHg production and, by extension, MeHg concentrations in tunas.

Our results indicate that Hg levels in skipjack tuna reflect regional anthropogenic atmospheric Hg0 distribution, suggesting they can be used as sentinels of Hg pollution, complementary to direct observations of atmospheric deposition and seawater Hg concentrations, and could therefore provide insights for the future design and implementation of large-scale Hg biomonitoring efforts to evaluate the effectiveness of the Minamata Convention. Given the expected different lifetimes of Hg in the atmosphere (i.e., up to several months) versus in oceans and marine biota (i.e., decades or even

thousands of years), these complementary measurements of Hg would be particularly valuable to better evaluate the effect of legacy and recent anthropogenic Hg releases. On the other hand, the importance of natural biogeochemical processes driving MeHg production and enhanced tuna Hg concentrations brings additional information on the potential response of the marine Hg cycle to climate change (Schartup et al., 2019). Further large-spatial-scale studies, combined with Hg environmental data and biogeochemical variables, are needed for other common tuna species (e.g., yellowfin and bigeye) to investigate if a similar response is present in other highly consumed emblematic pelagic fishes. Similarly, complementary large-scale spatial patterns of Hg concentrations in tunas from the Atlantic and Indian Oceans would be valuable for understanding the control factors of Hg in marine predators at the global ocean scale.

Materials and Methods

Mercury Concentrations and Ecological Tracers in Skipjack Tuna

A total of 661 samples of skipjack tuna with Hg concentration data were compiled from published and unpublished studies (Figure 39 A; SI Appendix F, Table S1). Samples were collected onboard commercial (longline, purse seine, troll, and pole-and-line) and recreational fishing boats from 122°E to 73°W and 24°S to 45°N, and metadata (i.e., dates, position, and gear type) were provided for each sample. Fork length (FL) was measured and ranged from29 to 90 cm (58 ± 12 cm; mean ± SD). For each fish, a white muscle tissue sample was collected and stored frozen prior to analyses. Data were classified by oceanic areas: NWPO, CNPO, NEPO, EPO, SWPO, and WCPO (Figure 39). Sampling spanned from 1997 to 2018, with no temporal sampling bias between oceanic areas (SI Appendix F, Figure S6). Total Hg concentrations were measured using homogenized freeze-dried samples in different study-specific laboratories, with laboratory-specific reference standards (SI Appendix F, Table S1). For the majority of samples (n = 528, ∼80 % of the total number of samples), total Hg concentrations were obtained by hot-plate acid digestion (HNO_3-H_2O_2) followed by cold vapor atomic fluorescence spectroscopy. For the rest (n = 133, ∼20 % of the total number of samples), total Hg concentrations were measured by thermal decomposition, gold amalgamation, and atomic absorption spectrometry (DMA-80, Milestone). Blanks and biological standard reference materials were routinely used in each analytical batch to check Hg measurement accuracy and traceability. Hg contents are expressed on a dw basis and are considered to reflect MeHg concentrations, as most of the total Hg (> 91 %) is in its methylated form in tuna white muscle (Houssard et al., 2019).

To account for potential confounding ecological effects, in particular, changes in trophic position, habitat, and feeding pathway, bulk muscle carbon and nitrogen isotopic compositions were also determined when sufficient material was available (n = 475, SI Appendix F, Table S1). Measured in the tissues of consumers, carbon isotopes ($\delta^{13}C$) provide information on feeding pathways and habitat associations, while nitrogen isotopes ($\delta^{15}N$) are used to estimate trophic position, as $\delta^{15}N$ values increase predictably between prey and consumer. For each sample, $\delta^{13}C$ and $\delta^{15}N$ values were measured on homogenized freeze-dried samples packed in tin cups and analyzed with an elemental analyzer (online C-N analyzer or Costech elemental analyzer) coupled to an isotope ratio mass spectrometer. Results were reported in the δ unit notation and expressed as parts per thousand (‰) relative to international standards (atmospheric N_2 for nitrogen and Vienna Pee Dee belemnite for carbon). Depending on the laboratory, a combination of certified and/or in-house reference materials

were used to determine that uncertainty was below 0.2 ‰ (SI Appendix F, Table S1). For samples with elevated lipid content (C:N > 3.5, *n* = 51), $\delta^{13}C$ values were corrected using a mass balance equation with parameters derived from Atlantic bluefin tuna muscle (Logan et al., 2008).

Measured Seawater Methylmercury Concentrations in the Pacific Ocean

Seawater MeHg data from the Pacific Ocean were compiled from the literature from both filtered and unfiltered samples (Bowman et al., 2016; Coale et al., 2018; Ganachaud et al., 2017; Hammerschmidt and Bowman, 2012; Kim et al., 2019; Laurier et al., 2004; Munson et al., 2015; Sunderland et al., 2009). In particular, we used the maximum total Hg and MeHg concentrations observed in the water column (picomolar) and the depth of maximum MeHg concentrations (meters). When MeHg concentrations were not measured directly from the water samples, we used the sum of monomethylmercury and dimethylmercury.

Anthropogenic and Natural Environmental Model Estimates Driving Mercury Bioaccumulation

The global chemical transport model GEOS-Chem, version v11-02 was used to simulate atmospheric Hg0 concentrations. The model couples a three-dimensional atmosphere, a two-dimensional (2D) subsurface-slab ocean, and a 2D terrestrial reservoir at a 6 × 7.5° horizontal resolution. Additional details on model design are given by Angot et al. (2018) and Travnikov et al. (2017). The simulation was performed using an anthropogenic emissions inventory developed for the year 2015 in the context of the latest Global Mercury Assessment (UN Environment, 2019). The simulation was driven with assimilated meteorological data from the NASA Goddard Earth Observing System (MERRA-2). In order to account for inter-annual variability, the simulation was performed with meteorological data for the years 2013 through 2015 following a 1-y spin-up. Annually averaged Hg0 concentrations were extracted from grids for which tuna samples were collected. In order to account for the spatial migration of skipjack tuna, Hg^0 concentrations were averaged over adjacent grid boxes. Note that adjacent grid boxes with a fraction of ocean < 50 % were not taken into account in the average calculation. Model outputs were evaluated against available globally distributed observations (SI Appendix F, Figure S2).

As seawater MeHg data were not available at a large spatial scale and high resolution in the Pacific Ocean, we used a suite of physical and biogeochemical variables known to influence MeHg production in seawater (Bowman et al., 2020b; Gustin et al., 2020; Mason et al., 2012; Sunderland et al., 2009) in addition to Hg environmental data. Variables included sea surface temperature (SST, °C), depth of net heterotrophy (meters), depth of oxycline (meters), depth of the mixed layer (MLD, meters), total chlorophyll (Chl-a, milligrams.m^{-3}) averaged over the upper 100 m, and vertically integrated net primary production (NPP, milligrams C.m^{-2}.$days^{-1}$). Oxygen concentrations in subsurface waters (i.e., 375 m, mmol.m^{-3}) were also included, as Hg methylation is known to occur in the subsurface layer and as this variable has been identified as the first best environmental predictor of tuna trophic position (Pethybridge et al., 2018a). Baseline estimates included $\delta^{15}N$ of particulate organic matter ($\delta^{15}N_{POM}$, ‰) and $\delta^{13}C$ of dissolved inorganic carbon ($\delta^{13}C_{DIC}$, ‰) averaged over the upper 100 m. Selected parameters were extracted from the same hindcast simulation, guaranteeing

internal consistency among all of them. Simulations were performed using the isotope-enabled version of the Pelagic Interactions Scheme for Carbon and Ecosystem Studies version 2 biogeochemical model attached to the Nucleus for European Modeling of the Ocean version 4.0 (NEMO) general ocean circulation model (Aumont et al., 2015). The model was forced by the Japanese Reanalysis 55 from 1958 to the present (Tsujino et al., 2018). Ocean model resolution is nominally 2° but approaches 0.5° near the equator, while vertical resolution varies between 10- to 500-m thickness over 31 levels between the surface and the abyssal ocean. All outputs on the NEMO curvilinear, tripolar grid were regridded onto a regular 1° × 1° horizontal grid prior to data extraction using the remap function in Climate Data Operators (Schulzweida, 2019). Simulated physical variables were extracted from grid cells nearest to the date and location of tuna samples using the samplexyt_nrst function of the Ferret program (https://ferret.pmel.noaa.gov/Ferret/). Given the long Hg isotopic turnover during bioaccumulation in tuna white muscle (~700 days; Kwon et al., 2016), we assumed that Hg values of a given individual captured at a single date and place are not exclusively explained by the environmental conditions at this date but also by prior conditions over previous months or years. As ^{15}N turnover in tuna white muscle is approximately 6 months (Madigan et al., 2012), we extracted averages of the listed variables above over 6 months prior to the actual sampling dates, as already done in previous studies on other tropical tuna species (Houssard et al., 2019; Médieu et al., 2021a; Pethybridge et al., 2018a).

Spatial Interpolation and Main Drivers of Mercury Concentrations in Skipjack

Tuna Hg concentrations were first log-transformed to guarantee the homogeneity of variance (Zuur et al., 2010). Furthermore, as Hg is known to bioaccumulate with length (and age), a power-law relationship ($\log(\mathrm{Hg}) = \mathrm{a} \times (\mathrm{FL} - \mathrm{b})^{\mathrm{C}} - \mathrm{d}$) was fit between log(observed Hg) and fish length (FL) to characterize the bioaccumulative processes in skipjack tuna and remove this length effect for further analyses. As the SWPO and WCPO display slow anthropogenic emissions and negligible loadings from anthropogenic sources (UN Environment, 2019), the power-law relationship was fitted on samples from thes regions only (Figure 39 B). This allowed for investigation of the influence of potential factors, other than length, governing Hg concentrations in tuna and for quantifying the potential Hg enrichment due to anthropogenic emissions. Residuals from the length-based Hg model (i.e., observed values - predicted values) were extracted and used to calculate length-standardized Hg concentrations (at mean skipjack length, i.e., FL = 60 cm).

A GAM was used to generate smoothed spatial contour maps of observed and standardized Hg levels in skipjack tuna, following the equation

$$\mathrm{Y} = \alpha + \mathrm{s}_1(\mathrm{X}_1) + \mathrm{s}_2(\mathrm{X}_2) + \ldots + \mathrm{s}_\mathrm{n}(\mathrm{X}_\mathrm{n}) + \varepsilon$$

where Y is the expected value of the response variable (i.e., observed and standardized Hg concentrations), α is the model intercept, $\mathrm{s}_\mathrm{i}(\mathrm{X}_\mathrm{i})$ is a thin-plate-spline smooth function of the explanatory variable i, and ε is the error term. Here, spatially interpolated maps were generated by fitting 2D thin plate regression splines on the catch sample location, i.e., s(longitude, latitude). Observed and standardized Hg concentrations were assumed to follow a Gamma distribution, and a log link was used in both cases. Spatial interpolation was applied at a 0.25° resolution, with a buffer of 5° around each tuna sample to avoid excessive interpolation where no data were available.

GAMs were also used to test the relative importance of potential predictors on spatial variations of Hg concentrations. The response variable, log(observed Hg), was assumed to follow a Gaussian distribution. Explanatory variables tested included surface (SST, Chl-a, and NPP) and deep (MLD, depth of net heterotrophy, depth of oxycline, and $[O_2]$ in subsurface waters) oceanographic variables. Fish length, baseline outputs ($\delta^{15}N_{POM}$ and $\delta^{13}C_{DIC}$), and atmospheric Hg^0 estimates were also tested. To account for ecological processes, we also included tuna $\delta^{13}C$ values and baseline-corrected tuna $\delta^{15}N$ values (i.e., tuna bulk $\delta^{15}N$ values - $\delta^{15}N_{POM}$ values) as a proxy for tuna trophic position. Before performing model computation, variance inflation factors (VIF) were calculated between all explanatory variables to detect collinearity. Covariates with the highest VIF were subsequently removed until the highest VIF value was < 5 (Zuur et al., 2010). With this method, MLD, Chl-a, and SST were found to be collinear with other variables and were removed as explanatory variables. The remaining explanatory variables (i.e., fish length, $\delta^{13}C$ and baseline-corrected tuna $\delta^{15}N$ values, $\delta^{15}N_{POM}$ and $\delta^{13}C_{DIC}$, NPP, $[O_2]$ in subsurface waters, depth of net heterotrophy, depth of oxycline, and Hg^0 estimates) were fitted in the GAM with a low spline complexity (k = 3) to reduce overfitting. A backward selection approach was used, and we chose the model with the lowest Akaike's Information Criterion corrected for small sample sizes (Burnham and Anderson, 2004). Finally, for the best-fit GAM, assumptions of the residuals trend and autocorrelation were examined graphically with diagnostic plots. The percent DE of the model was compared to assess predictive capacity. All statistical analyses were performed with R 3.6.1 (R Core Team, 2018), and GAMs were fitted using themgcv package (Wood and Wood, 2015).

Acknowledgments

We are grateful to our sampling providers, including the many fishery observer programs and fishermen. In particular, we thank the Western and Central Pacific Fisheries Commission Tuna Tissue Bank, the Pacific Marine Specimen Bank managed by the Pacific Community (SPC), and the Environmental Specimen Bank in Ehime University, as well as Robert Olson and Felipe Galvan-Magaña. We thank Laure Laffont from Geosciences Environnement Toulouse (GET) and Jean-Louis Duprey and Stéphanie Berne from Laboratoire des Moyens Analytiques (LAMA) for Hg analyses, as well as the Union College Stable Isotope Laboratory team, Sarah Katz, and Madelyn Miller. Shelagh Zegers provided valuable analytical assistance at Stony Brook University. We thank Laura Tremblay-Boyer from Dragonfly Data Science for her contribution in designing smooth-contour maps in R. H.A. acknowledges Noelle E. Selin and the use of the Svante cluster provided by the Massachusetts Institute of Technology's Joint Program on the Science and Policy of Global Change. We are grateful to two anonymous referees for providing thoughtful comments on the manuscript. This study was funded by the Pacific Fund VACOPA Project (spatial VAriations of COntaminants levels in PAcific ocean trophic webs) and ANR-17-CE34-0010 MERTOX (unravelling the origin of methylMERcury TOXin in marine ecosystems, 2017–2021) from the French Agence Nationale de la Recherche. The US NSF funded Union College's isotope ratio mass spectrometer and peripherals (NSF-Major Research Instrumentation No. 1229258). This work was supported by the Interdisciplinary Graduate School for the Blue Planet (ANR-17-EURE-0015) and cofunded by a grant from the French government under the program "Investissements d'Avenir." P.B. was also supported by a grant from the Regional Council of Brittany (SAD program, Stratégie d'Attractivité Durable). H.A. received financial support from the Swiss National Science Foundation (Grant No. 200021_188478).

Chapter 4. Tropical tunas mirror patterns of mercury bioavailability and pollution in the global ocean

---

First draft (not reviewed by all co-authors yet)

Anaïs Médieu[1], David Point[2], Pearse B. Buchanan[3], Heidi Pethybridge[4], Valérie Allain[5], Nathalie Bodin[6,7], Hélène Angot[8], Leanne Fuller[9], Bridget E. Ferriss[10], Laia Munoz[11], Flavia Lucena[12], Douglas H. Adams[13], John M. Logan[14], David P. Gillikin[15], Jeroen E. Sonke[2], Lars-Eric Heimbürger-Boavida[16], Andrew T. Revill[4], Frédéric Ménard[16], Felipe Galván-Magaña[17], Takaaki Itai[18], B.K. Kolita Kamal Jinadasa[19], Ana Carolina Pizzochero[20], Joao Paulo Machado Torres[21], Andrea Luna-Acosta[22], Daniel J. Madigan[23], Marie-Maëlle Desgranges[16], Marina Renedo[2], Anouk Verheyden[15], Jean-Marie Munaron[1], Alessandro Tagliabue[3], Laurent Bopp[24], Laure Laffont[2], Olivier Gauthier[1], Anne Lorrain[1]

[1]Univ Brest, CNRS, IRD, Ifremer, LEMAR, F-29280 Plouzané, France
[2]Observatoire Midi-Pyrénées, GET, UMR CNRS 5563/IRD 234, Université Paul Sabatier Toulouse 3, Toulouse, France
[3]University of Liverpool, Department of Earth, Ocean and Ecological Sciences, Liverpool, UK
[4]CSIRO Oceans and Atmosphere, Hobart, Tasmania, Australia
[5]Pacific Community, Oceanic Fisheries Programme, Nouméa, New-Caledonia
[6]Research Institute for Sustainable Development (IRD), Victoria, Mahé, Seychelles
[7]Sustainable Ocean Seychelles (SOS), BeauBelle, Mahé, Seychelles
[8]Extreme Environments Research Laboratory, École Polytechnique Fédérale de Lausanne (EPFL) Valais Wallis, Sion, Switzerland
[9]Inter-American Tropical Tuna Commission, 8901 La Jolla Shores Drive, La Jolla, CA, USA
[10]National Research Council, under contract to Northwest Fisheries Science Center, National Marine Fisheries Service (NMFS), National Oceanic and Atmospheric Administration (NOAA), Seattle, WA 98112, USA
[11]Universidad San Francisco de Quito, Equador
[12]Departamento de Pesca e Aquicultura, Universidade Federal Rural de Pernambuco (UFRPE), Av. Dom Manuel s/n, Recife, Pernambuco, 52171-900, Brazil
[13]Florida Fish and Wildlife Conservation Commission, Fish and Wildlife Research Institute, Melbourne FL, 32901, USA
[14]Massachusetts Division of Marine Fisheries, New Bedford, MA, 02744, USA
[15]Department of Geosciences, Union College, 807 Union St., Schenectady, NY, 12308, USA
[16]Aix Marseille Université, CNRS/INSU, Universite de Toulon, IRD, Mediterranean Institute of Oceanography (MIO) UM 110, 13288, Marseille, France
[17]Instituto Politécnico Nacional, Centro Interdisciplinario de Ciencias Marinas, Avenida IPN, s/n Colonia Playa Palo de Santa Rita, C.P. 23096 La Paz, Baja California Sur, Mexico
[18]Department of Earth and Planetary Sciences, Graduate School of Science, The University of Tokyo, Bunkyo-Ku, Tokyo, 113-0033, Japan
[19]Analytical Chemistry Laboratory, National Aquatic Resources Research and Development Agency (NARA), Colombo-15, Sri Lanka
[20]Federal University of Rio de Janeiro, Biophysics Institute Carlos Chagas Filho, Radioisotopes Laboratory Eduardo Penna Franca, Av. Carlos Chagas Filho, 373 CCS - Bl. G, Rio de Janeiro, RJ, Brazil
[21]Federal University of Rio de Janeiro, Biophysics Institute Carlos Chagas Filho, Organic Micropollutants Laboratory Jan Japenga, Av. Carlos Chagas Filho, 373 CCS - Bl. G, Rio de Janeiro, RJ, Brazil
[22]Departamento de Ecología y Territorio, Facultad de Estudios Ambientales y Rurales, Pontificia Universidad Javeriana, Transversal 4 # 42-00, Bogotá, Colombia
[23]Department of Integrative Biology, University of Windsor, Windsor, ON, Canada
[24]LMD/IPSL, Ecole Normale Supérieure/PSL University, CNRS, Ecole Polytechnique, Sorbonne Université, Paris, France

Introduction

Mercury (Hg) is a widely distributed trace element of particular concern for both ecosystems and human health, whose toxicity relies on its chemical form. It is discharged to the environment, mainly as gaseous elemental Hg (Hg^0), by natural processes (e.g., volcanism) and anthropogenic activities (e.g., artisanal and small-scale gold mining and fossil fuel combustion) (Outridge et al., 2018). Centuries of anthropogenic Hg use and production have modified the global Hg cycle, and atmospheric Hg concentrations are estimated to have increased by about 450 % above natural levels (Outridge et al., 2018). Anthropogenic Hg emissions are also thought to have tripled the concentrations of total Hg in the thermocline waters (100 – 1,000 m) of the global ocean, relative to deeper older waters (Lamborg et al., 2014); yet still unclear is how these anthropogenic Hg inputs are converted in oceans into methylmercury (MeHg), the most toxic chemical form of Hg, and finally accumulated in marine food webs.

The major Hg sources for oceans are atmospheric deposition of inorganic Hg and direct Hg^0 uptake (Jiskra et al., 2021). Rivers also deliver significant amounts of Hg to estuarine and coastal oceans, but only a small fraction of these Hg inputs is transported to open ocean regions (Liu et al., 2021). In oceans, an unknown fraction of Hg is naturally converted into the organometallic toxin MeHg. The balance between microbial and abiotic methylation processes and demethylation reactions (dominated by photo-degradation in ocean surface waters), controls the net oceanic MeHg production and bioavailability for marine food webs (Gustin et al., 2020; Heimbürger et al., 2010; Monperrus et al., 2007; Parks et al., 2013; Villar et al., 2020). Depth profiles in the open ocean consistently show that MeHg concentrations are highest in the sub-thermocline oxygen minimum zone, but with evidence of differential MeHg net production across the global ocean, suggesting that MeHg bioavailability and accumulation in marine food webs may also vary spatially (Bowman et al., 2020b). Despite important progress in environmental Hg sciences, measurements of Hg speciation in oceans remain overall scarce, and fundamental questions on where, how, and when MeHg is formed in the global ocean remain unanswered. Also important yet poorly documented are the climate-induced changes of MeHg formation, especially the impacts of changes in ocean circulation, productivity, and growth of oxygen minimum zones (Krabbenhoft and Sunderland, 2013; Mason et al., 2012).

The United Nations Environmental Program Minamata Convention (www.mercuryconvention.org) aims at protecting human health and the environment from the adverse effects of Hg, requiring governments to control and reduce anthropogenic Hg emissions. Marine fish consumption represents the most important MeHg exposure pathways for humans, with MeHg health and socioeconomic costs estimated to several billion euros per year worldwide (Trasande et al., 2005). Given the natural biomagnification properties of MeHg in marine food webs, higher MeHg concentrations are found in marine top predators (e.g. tunas and billfishes), sometimes exceeding food safety guidelines (i.e., 1 $mg.kg^{-1}$ of fresh tissue) (WHO and UNEP Chemicals, 2008). Mercury accumulation in tunas has been broadly documented at local and regional ocean scales in different tuna species (e.g., Bodin et al., 2017; Chouvelon et al., 2017; Ferriss and Essington, 2011; Houssard et al., 2019), with up to an eightfold difference in Hg concentrations reported in yellowfin (*Thunnus albacares*) among 11 different study sites (Nicklisch et al., 2017). Yet, identifying the origin and factors behind this spatial variability has been a puzzling challenge given the complex interplay between physical (e.g., light intensity), biogeochemical (e.g., MeHg bioavailability at the base of marine food webs), physiological (e.g., organism's length and age), and ecological factors (e.g., tuna's foraging

depth or trophic position). Recent high-resolution spatial studies in the Pacific Ocean suggested in particular that local ocean biogeochemistry, and tuna vertical habitat are key drivers of tuna Hg concentrations (Houssard et al., 2019; Médieu et al., 2022). In addition to these natural controls, tuna Hg concentrations in the northwestern Pacific have been shown to be influenced locally by high anthropogenic Hg releases along the Asian coasts (Médieu et al., 2022). Finally, Hg concentrations in migrating bluefin tunas were observed to reflect dissolved Hg levels at 13 different locations in 4 ocean basins (Tseng et al., 2021). High-resolution spatial studies of large coverage remain needed to investigate further the relative importance of variable tuna biology and trophic ecology, ocean MeHg net production, and atmospheric Hg sources on tuna Hg concentrations.

Here, we report the highest spatially resolved maps of Hg concentrations in tropical tunas, i.e., bigeye (*T. obesus*), yellowfin, and skipjack (*Katsuwonus pelamis*) for the global ocean (n = 4,889, Figure 44). These three circumtropical tuna species are extensively exploited worldwide, accounting for more than 90 % of the global tuna fishery (FAO, 2018), and are therefore of high commercial and human health importance. Moreover, given their different lifespans, growth patterns and vertical habitats (Olson et al., 2016), we hypothesized that tropical tunas are good environmental archives to i) explore differential biological and ecological processes susceptible to drive Hg accumulation in tunas, and ii) investigate the vertical and horizontal spatial variability of seawater MeHg concentrations at the base of tropical pelagic marine food webs. We applied generalized additive (mixed) models on tuna Hg concentrations, combining biological and ecological tracers in tunas, alongside marine physical and biogeochemical, and atmospheric Hg^0 model estimates to explore the origin of geographical patterns of Hg concentrations in tropical tunas. Complementary amino acid nitrogen stable isotope values were also used to further explore the relative importance of trophic processes to Hg accumulation in tropical tunas. Our study reveals that the spatial variability of Hg concentrations in tropical tunas for the global ocean are mainly explained by i) variable tuna foraging depth and biogeochemically-induced MeHg profiles, and ii) recent anthropogenic Hg emissions from Asia.

Materials and methods

Mercury data compilation

A total of 4,889 tuna samples with Hg concentrations (i.e., 1,422 bigeye, 2,467 yellowfin, and 1,000 skipjack) were compiled from published and unpublished regional studies and assembled into a global database (SI Appendix G, Table S1). Samples were collected onboard commercial and recreational fishing vessels, and metadata (i.e., date, position and gear type) were provided for each sample. Fork length (FL) was measured and ranged from 29 to 185 cm (98 ± 37, mean ± sd), 30 to 180 cm (96 ± 33), and 25 to 90 cm (56 ± 13) for bigeye, yellowfin, and skipjack respectively. For each fish, a white muscle sample tissue was collected and stored frozen prior to analyses. Sampling spanned from 1997 to 2020 by multiple research programs, with no temporal sampling bias among oceanic areas, for any of the three species (SI Appendix G, Figure S1). Data were classified by oceanic areas (Figure 44): northwestern Pacific (NWPO), central north Pacific (CNPO), northeastern Pacific (NEPO), eastern central Pacific (ECPO), southeastern Pacific (SEPO), southwestern Pacific (SWPO), western central Pacific (WCPO), northwestern Atlantic (NWAO), western central Atlantic (WCAO), eastern

central Atlantic (ECAO), central north Indian (CNIO), central western Indian (CWIO), Reunion Island (REU), and Mozambique Channel (MOZ).

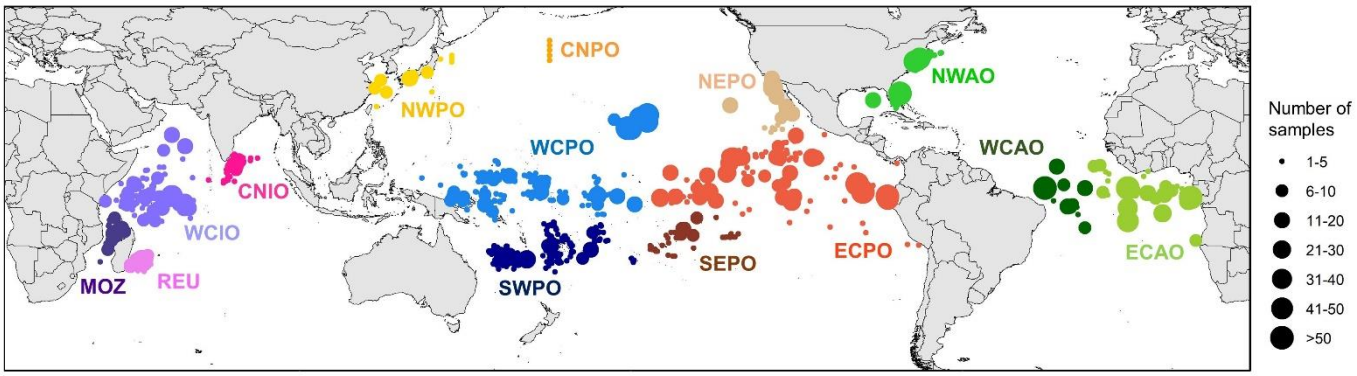

Figure 45. Tropical tunas sample provenance. Map of oceanic areas and samples' locations for bigeye, yellowfin, and skipjack tunas. The size of circles are proportional to the number of individuals collected. Oceanic areas: NWPO = northwestern Pacific; CNPO = central north Pacific; NEPO = northeastern Pacific; ECPO = eastern central Pacific; SEPO = southeastern Pacific; SWPO = southwestern Pacific; WCPO = western central Pacific; NWAO = northwestern Atlantic; WCAO = western central Atlantic; ECAO = eastern central Atlantic; CNIO = central north Indian; WCIO = western central Indian; REU = Reunion Island; MOZ = Mozambique Channel.

Mercury concentrations and ecological tracers in tropical tunas

Total Hg concentrations were measured on powdered and homogenized samples in different laboratories, with laboratory-specific reference standards (SI Appendix G, Table S1). For the majority of samples, (n = 3,028, ~ 62 % of the total number of samples), total Hg concentrations were obtained by thermal decomposition, gold amalgamation and atomic absorption spectrometry. The rest of the dataset (n = 1,861, 38 %) were measured by acid digestion followed by cold vapor atomic fluorescence spectroscopy. Blank and biological standard reference materials were routinely used in each analytical batch to check Hg measurement accuracy and traceability. Most of the samples were analysed freeze-dried; and in case of fresh frozen samples, we converted Hg concentrations considering 70% of moisture in white muscle of tropical tunas (Bodin et al., 2017; Houssard et al., 2019; Kojadinovic et al., 2006), so that all total Hg concentrations are expressed on a dry weight (dw) basis. Furthermore, some measurements of total Hg concentrations were done on lipid-free muscle samples (n < 12 %), as recommended for carbon stable isotope analyses to avoid bias related to lipid content (see next paragraph). Yet, this does not prevent us from integrating these Hg concentrations in our global dataset as it has been shown that lipid-free muscle tissues can be used equivalently to bulk muscle tissues to document Hg concentrations in tropical tunas (Médieu et al., 2021b). Total Hg concentrations are considered to reflect MeHg concentrations as most of total Hg (> 91 %) is in its methylated form in tropical tunas (Houssard et al., 2019).

To account for potential confounding ecological effects, in particular changes in trophic position, habitat, and feeding pathway, bulk muscle carbon and nitrogen isotopic compositions were also determined when sufficient material was available (n = 3,517 corresponding to 1,082 bigeye, 1,706 yellowfin, and 729 skipjack, SI Appendix G, Table S1). Measured in the tissues of consumers, nitrogen

isotopes ($\delta^{15}N$) are used to estimate their trophic position as $\delta^{15}N$ values increase predictably between prey and consumer, while carbon isotopes ($\delta^{13}C$) provide information on feeding pathways and habitat associations (Fry, 2006). For each sample, $\delta^{13}C$ and $\delta^{15}N$ values were measured on homogenized freeze-dried samples packed in tin cups and analysed with an elemental analyser (on-line C-N analyser or Costech elemental analyser) coupled to an isotope ratio mass spectrometer. Results were reported in the δ unit notation and expressed as parts per thousand (‰) relative to international standards (atmospheric N_2 for nitrogen and Vienna Pee Dee belemnite (VPDB) for carbon). Depending on the laboratory, a combination of certified and/or in-house reference materials were used to determine that uncertainty was below 0.2 ‰ (SI Appendix G, Table S1). Tuna $\delta^{13}C$ values were corrected for lipids, either with chemical extraction (*n* = 813, 17 %), or using a mass balance equation for samples with elevated lipid content (C:N > 3.5, *n* = 572, 12 %), with parameters derived from Atlantic bluefin tuna muscle (Logan et al., 2008).

Knowing the complex primary production dynamics influencing nitrogen isotopic baseline at a global scale, we also used amino acid compound-specific $\delta^{15}N$ values in a subset of samples (*n* = 118) to provide complementary estimates of tuna's trophic position (Choy et al., 2015; Lorrain et al., 2015b). We compiled data from the existing literature in the southwestern Pacific (*n* = 26 yellowfin samples, Houssard et al., 2017; Médieu et al., 2021a), and acquired new values in the global ocean (*n* = 28 yellowfin + 57 bigeye + 7 skipjack). Freeze-dried samples were prepared by acid hydrolysis followed by esterification and trifluoroacetylations as per (Dale et al., 2011). The $\delta^{15}N$ isotope values of individual amino acids were determined with a Trace GC gas chromatograph interfaced with a Delta V Plus isotope mass spectrometer (IRMS) through a GC-C combustion furnace (980 °C), reduction furnace (650 °C) and liquid N_2 cold trap. The samples (0.5 µL) were injected splitless onto a forte BPX5 capillary column (30 m w 0.32 mm x 1.0 µm film thickness) at an injector temperature of 180°C with a constant helium flow rate of 1.5 $mL.min^{-1}$. The column was initially held at 50°C for 2 min and then increased to 120°C at a rate 4°$C.min^{-1}$ to 195 °C and then at 5°$C.min^{-1}$ to 235°C where it was held for 5 min. The temperature was then further increased to 300°C at 15°$C.min^{-1}$ and held for 8 min. All samples were analysed at least in triplicate. The $\delta^{15}N$ values were normalized as follows: each sample analysis consisted of three separate IRMS analyses bracketed by a suite of amino acids with known $\delta^{15}N$ values. The slope and intercept of known versus measured were then used to correct the measured values for the sample set. Reproducibility associated with isotopic analysis of glutamic acid and phenylalanine were < 1 ‰.

Tuna trophic position was estimated using the difference of $\delta^{15}N$ values in trophic (Tr-AA) and source (Sr-AA) amino acids, obtained by the following equation:

$$TP_{Tr-Sr} = \frac{\delta^{15}N_{Tr-AA} - \delta^{15}N_{Sr-AA} + \beta_{Tr-Sr}}{TEF_{Tr-Sr}} + 1$$

where $\delta^{15}N_{Sr-AA}$ is the weighted average of glycine and phenylalanine $\delta^{15}N_{AA}$ values, and $\delta^{15}N_{Tr-AA}$ the weighted average of alanine, glutamic acid, leucine and proline $\delta^{15}N_{AA}$ values. β_{Tr-Sr} is the difference between Tr-AA and Sr-AA in primary producers and TEF_{Tr-Sr} is the ^{15}N enrichment between Tr-AA and Sr-AA per TP. β_{Tr-Sr} and TEF_{Tr-Sr} were set respectively at 3.6 and 5.7 (Bradley et al., 2015). Using the weighted average of Sr-AA and Tr-AA reduced uncertainty due to the possible large variations of $\delta^{15}N_{AA}$ values (Hayes et al., 1990). Uncertainty in TP estimates was calculated by propagation of errors according to Bradley et al. (2015) with a mean error of 0.4.

Tuna age estimation and age standardization of mercury concentrations

Given that MeHg bioaccumulates with fish age and length, and that tuna growth vary among species and ocean basins (Murua et al., 2017), we estimated fish age to explore the effect of differential growth patterns on tuna Hg bioaccumulation, as done in another global study (Tseng et al., 2021). We used growth parameters from the respective last tuna stock assessments when data were available (Dortel et al., 2015; Eveson et al., 2015; Farley et al., 2020; Hallier et al., 2005; ICCAT, 2019, 2014; Vincent et al., 2019), or from recently published studies (Griffiths et al., 2019). This corresponds to two growth curves in the Pacific (i.e., eastern and western) and one single curve in the Indian Ocean for each of the three species. In the Atlantic Ocean, while one growth curve was used for bigeye and yellowfin, two separated curves were fitted for eastern and western Atlantic skipjack.

We fitted power-law relationships ($\log(\mathrm{Hg}) = \mathrm{a} \times (\mathrm{age} - \mathrm{c})^b - \mathrm{d}$) between log-transformed observed Hg concentrations and fish age (years) to characterize the bioaccumulative processes in tropical tunas and remove the effect of differential growth patterns among species and ocean basins (Figure 45). For the three species, we fitted four bioaccumulative curves corresponding to the four major ocean basins: Atlantic, Indian, eastern and western Pacific. Residuals from the age-based Hg models (i.e., observed values – predicted values) were extracted for all samples and used to calculate age-standardized Hg concentrations (at mean age of 3 years for the three species, when all tunas have reached sexual maturity), hereafter defined as standardized Hg concentrations, in contrast to observed Hg concentrations. This allowed for investigation of the influence of potential factors, other than growth, governing Hg concentrations in tunas. The parameters used to fit the power-law relationships, and the percentages of deviance explained (R^2) are available in SI Appendix G, Table S2.

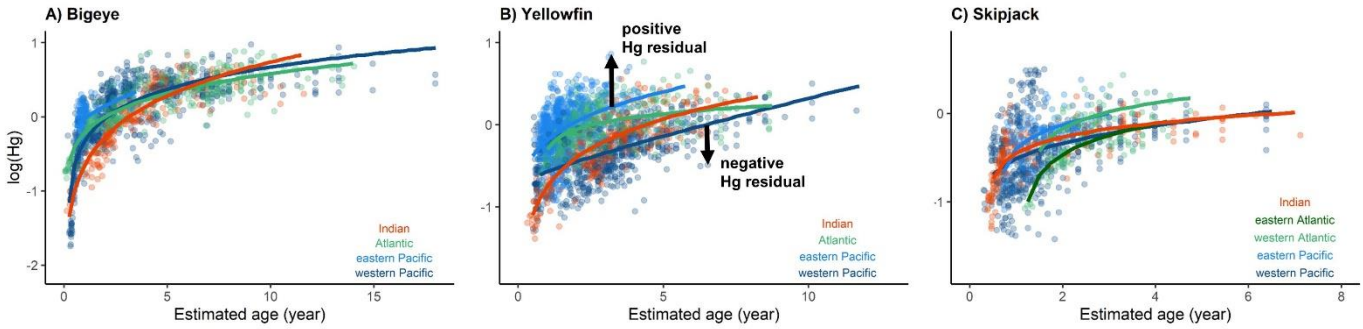

Figure 46. Age-standardization of tuna mercury (Hg) concentrations. Power-law relationships between log-transformed observed Hg (log(Hg)) and individuals' estimated age for **A)** bigeye, **B)** yellowfin, and **C)** skipjack tunas. Separated relationships were fitted per ocean basins (see methods section): four curves (i.e., Indian, Atlantic, western Pacific, and eastern Pacific Oceans) were for bigeye and yellowfin, and five curves for skipjack (i.e., Indian, western Pacific, eastern Pacific, western Atlantic and eastern Atlantic Oceans). The parameters used to fit the power-law relationship $(log(Hg) = a \times (age - c)^b - d)$, and the percentage of deviance explained (R^2) are available in SI Appendix G, Table S2. Black arrows in A) symbolise positive and negative Hg residuals calculated from the power-law relationships.

Natural and anthropogenic environmental model estimates driving spatial differences of mercury concentrations

The global chemical transport model GEOS-Chem, version v11-02, was used to simulate atmospheric Hg^0 concentrations. The model couples a 3D atmosphere, a 2D subsurface-slab ocean,

and a 2D terrestrial reservoir at a 6 x 7.5° horizontal resolution. Additional details on model design are given by Angot et al. (2018) and Travnikov et al. (2017). The simulation was performed using an anthropogenic emissions inventory developed for the year 2015 in the context of the latest Global Mercury Assessment (UN Environment, 2019). The simulation was driven with assimilated meteorologicaly data from the NASA Goddard Earth Observing System (MERRA-2). In order to account for interannual variability, the simulation was performed with meteorological data for the years 2013-2015 following a one-year spin-up. Annually-averaged Hg^0 concentrations were extracted from grids where tuna samples were collected. In order to account for the spatial migration of skipjack tuna, Hg^0 concentrations were averaged over adjacent grid boxes. Note that adjacent grid boxes with a fraction of ocean < 50 % were not taken into account in the average calculation. Model outputs were evaluated against available globally-distributed observations.

To explore the relative importance of tuna ecological and marine biogeochemical processes on Hg accumulation in tunas, we used a combination of ocean circulation and biogeochemistry model outputs as proxies of these processes. Variables used to investigate the effects of Hg biogeochemistry in the ocean included the depth of net heterotrophy (m), depth of oxycline (m), depth of the mixed layer (MLD, m), total chlorophyll (Chl-a, $mg.m^{-3}$) averaged over the upper 100 m, vertically integrated net primary production (NPP, mg $C.m^{-2}.day^{-1}$), and the rate of organic carbon exported through 100 m, and at the depth of net heterotrophy ($mol.m^{-2}.s^{-1}$) (Bowman et al., 2020b; Gustin et al., 2020; Mason et al., 2012; Sunderland et al., 2009). Model outputs that are likely to reflect tuna ecology, in particular tuna foraging depth, included sea surface temperature (SST, °C), and the depths of isotherms 12°C and 20°C (Abascal et al., 2018; Houssard et al., 2017; Pethybridge et al., 2018a). Oxygen concentrations in subsurface waters (i.e., 375 m, $mmol.m^{-3}$) were also included as Hg methylation in known to occur in the subsurface layer and as this variable has been identified as the first best environmental predictor of tuna trophic position (Pethybridge et al., 2018a). We also added baseline estimates, i.e., $\delta^{15}N$ of particulate organic matter ($\delta^{15}N_{POM}$, ‰) and $\delta^{13}C$ of dissolved inorganic carbon ($\delta^{13}C_{DIC}$, ‰) averaged over the upper 100 m

Selected parameters were extracted from the same hindcast simulation, guaranteeing internal consistency among all of them. Simulations were performed using the isotope-enabled version of the Pelagic Interactions Scheme for Carbon and Ecosystem Studies version 2 (PISCESiso-v2) biogeochemical model, attached to the Nucleus for European Modelling of the Ocean version 4.0 (NEMOv4) general ocean circulation model (Aumont et al., 2015). The model was forced by the Japanese Reanalysis 55 (JRA55) from 1958-present (Tsujino et al., 2018). Ocean model resolution is nominally 2° but approaches 0.5° near the equator, while vertical resolution varies between 10 to 500 m thickness over 31 levels between the surface and the abyssal ocean. All outputs on the NEMO curvilinear, tripolar grid were regridded onto a regular 1° x 1° horizontal grid prior to data extraction using the *remap* function in Climate Data Operators (Schulzweida, 2019). Simulated physical variables were extracted from grid cells nearest to the date and location of tuna samples using the *samplexyt_nrst* function of the Ferret program (https://ferret.pmel.noaa.gov/Ferret/). Given the long Hg isotopic turnover during bioaccumulation in tuna white muscle (~ 700 days, Kwon et al., 2016), we assumed that Hg values of a given individual captured at a single date and place is not exclusively explained by the environmental conditions at this date, but also by prior conditions over previous months or years. As ^{15}N turnover in tuna white muscle is approximately six months (Madigan et al., 2012), we extracted averages of the listed variables above over six months prior to the actual sampling

dates, as already done in previous studies on other tropical tuna species (Houssard et al., 2019; Médieu et al., 2022, 2021a; Pethybridge et al., 2018a).

Statistical comparison, spatial interpolation and main drivers of mercury concentrations in tropical tunas

All statistical analyses were performed with the statistical open source R software 3.6.1 (R Core Team, 2018).

We used analyses of variance (ANOVA) and post-hoc Tukey tests on log-transformed Hg concentrations to compare Hg levels among species and regions, with *p*-values adjusted for multiple comparisons using the Bonferroni correction method.

We fitted generalized additive models (GAM) with the mgcv package (Wood and Wood, 2015) to generate smoothed spatial contour maps of observed and standardized Hg levels for each tropical tuna species. Spatially interpolated maps were generated by fitting two dimensional thin plate regression splines on catch sample location (i.e., s(longitude, latitude)). Observed and standardized Hg concentrations were assumed to follow a Gamma distribution and a log link was used in both cases. Spatial interpolation was applied at a 0.25° resolution, with a buffer of 5° around each tuna sample to avoid excessive interpolation where no data were available.

We constructed generalized additive mixed models (GAMM) using the gamm4 package (Wood and Scheipl, 2020) to examine the relationships between tuna Hg concentrations and biological, ecological, biogeochemical and anthropogenic factors. The responses variables, log(observed Hg), were assumed to follow a Gaussian distribution. Oceans were incorporated as a random effect to account for intra-group correlations and overdispersal that frequently arises in spatial analyses. Explanatory variables tested included surface (SST, Chl-a, NPP, and the rate of organic carbon exported through 100 m) and deep (MLD, depth of net heterotrophy, depth of oxycline, depths of isotherms 12°C and 20°C, the rate of organic carbon exported at the depth of net heterotrophy, and $[O_2]$ in subsurface waters) oceanographic variables. Fish age, baseline outputs ($\delta^{15}N_{POM}$ and $\delta^{13}C_{POM}$), and atmospheric Hg^0 estimates were also tested. To account for ecological processes, we also included tuna $\delta^{13}C$ values, and baseline-corrected tuna $\delta^{15}N$ values (i.e., tuna bulk $\delta^{15}N$ values - $\delta^{15}N_{POM}$ values), as a proxy for tuna trophic position. Before performing model computation, variance inflation factors (VIF) were calculated between all explanatory variables to detect collinearity. Covariates with the highest VIF were subsequently removed until the highest VIF value was < 5 (Zuur et al., 2010). The remaining explanatory variables (i.e., fish age, $\delta^{13}C$ and baseline-corrected tuna $\delta^{15}N$ values, $\delta^{15}N_{POM}$ and $\delta^{13}C_{POM}$, NPP, $[O_2]$ in subsurface waters, depth of net heterotrophy, depth of oxycline, depth of isotherm (12°C or 20°C), and Hg^0 estimates) were fitted in the GAMM with a low spline complexity (k = 5) to reduce over-fitting. A forward selection approach was used, and we chose the model with the lowest Akaike's Information Criterion corrected for small sample sizes (AICc) (Burnham and Anderson, 2004). Finally, for the best-fit GAMM, assumptions of the residuals trend and auto-correlation were examined graphically with diagnostic plots. The coefficient of determination (R^2) of the model was used to assess predictive capacity.

Results and discussion

Spatial variability of mercury concentrations in tropical tunas in the global ocean

Observed Hg concentrations (mean ± sd, min - max, dry weight) were significantly different (ANOVA & Tukey, $p < 0.05$) and highly variable among tuna species: 1.73 ± 1.35 (0.02 - 9.45) $\mu g.g^{-1}$, 0.91 ± 0.72 (0.04 - 7.26) $\mu g.g^{-1}$, and 0.56 ± 0.47 (0.04 - 3.15) $\mu g.g^{-1}$ in bigeye, yellowfin, and skipjack respectively (Figure 46; SI Appendix G, Figure S2). Bigeye exhibited 2 times and 3 times higher global mean observed Hg concentrations than yellowfin and skipjack, respectively, while yellowfin had 1.5 higher mean observed Hg concentrations than skipjack. Among the three species, only bigeye (n = 165, 12 % of the total number of bigeye samples) from almost all regions of the three ocean (except in the northeastern and eastern central Pacific, and in the Mozambique Channel) displayed Hg concentrations exceeding the food safety guidelines of 1 $\mu g.g^{-1}$ (wet weight, i.e. ~ 3.3 $\mu g.g^{-1}$ dw) (WHO and UNEP Chemicals, 2008) (SI Appendix G, Figure S2). Most of these individuals (80 %) were bigger than 120 cm FL. A few yellowfin (n = 21), also originated from the three oceans, were also above this limit but representing less than 1 % of the total number of yellowfin samples. This illustrates further the need to consider both tuna species and fish size when addressing recommendations in terms of food security regarding Hg content in each region, as already shown by other studies (Houssard et al., 2019; Médieu et al., 2021a).

To account for MeHg bioaccumulation and variable growth rates between tuna species and ocean regions, we calculated age-standardized Hg concentrations (at 3 years, Material & Methods) to explore the spatial distribution of Hg level anomalies not explained by Hg bioaccumulation and fish age differences between individuals and species. Global means of standardized Hg concentrations showed significant differences among all species (ANOVA & Tukey, $p < 0.05$), with highest values in bigeye (1.58 ± 0.89, 0.21 - 6.56 $\mu g.g^{-1}$), followed by yellowfin (1.16 ± 0.92, 0.07 - 8.37 $\mu g.g^{-1}$), and finally skipjack (0.86 ± 0.74, 0.05 - 5.53 $\mu g.g^{-1}$) (Figure 47; SI Appendix G, Figure S3). Differences of standardized Hg concentrations were also observed at the spatial scale. Skipjack and yellowfin, the two epipelagic species, displayed overall the same global spatial patterns, with highest means of standardized Hg concentrations observed in the northwestern, the central north (for skipjack only as there is no yellowfin sample in this area), and the eastern Pacific, and lowest mean values in the western central Pacific. High mean standardized Hg values were also found in northwestern Atlantic for skipjack. For bigeye, a mesopelagic species, the highest mean was observed in the southwestern Pacific while the lowest was found in the Mozambique Channel. Variance of standardized Hg concentrations was highest in the Pacific (0.96, 1.10 and 0.75 $\mu g^2.g^{-2}$ for bigeye, yellowfin, and skipjack, respectively) and lowest in the Indian (0.20, 0.16 and 0.10 $\mu g^2.g^{-2}$) for the three species. At the region scale, variance was highest in the southwestern Pacific for bigeye (1.51 $\mu g^2.g^{-2}$), the eastern central Pacific for yellowfin (1.27 $\mu g^2.g^{-2}$), and the northwestern Pacific for skipjack (1.68 $\mu g^2.g^{-2}$) (SI Appendix G, Figure S3).

The best global models explained 64, 44, and 64 % of the variability of observed Hg concentrations in bigeye, yellowfin, and skipjack, respectively (Figure 48). The same optimal model was found for yellowfin and skipjack, including fish age, the depth of net heterotrophy, $[O_2]$ in subsurface waters, and atmospheric Hg^0 model outputs. For bigeye, the optimal model included fish age and the depth of isotherm 12°C (used as a proxy for the thermocline depth). In the three optimal models, tuna trophic position, estimated from baseline-corrected tuna $\delta^{15}N$ values (Materials and methods) were never selected, revealing that potential trophic effects (i.e., geographical changes in foraging ecology) have a limited influence on the spatial variability of tuna Hg concentrations at the

global scale, as already observed in the Pacific Ocean (Houssard et al., 2019; Médieu et al., 2022). Given the selected variables in the best models, the variability of standardized Hg concentrations among tropical tunas and ocean areas likely result from i) ii) variable seawater MeHg concentrations at the base of marine food web combined to variable tuna foraging depths, and ii) variable amounts of surface ocean inorganic Hg loading from the atmosphere, as discussed in the two following sections.

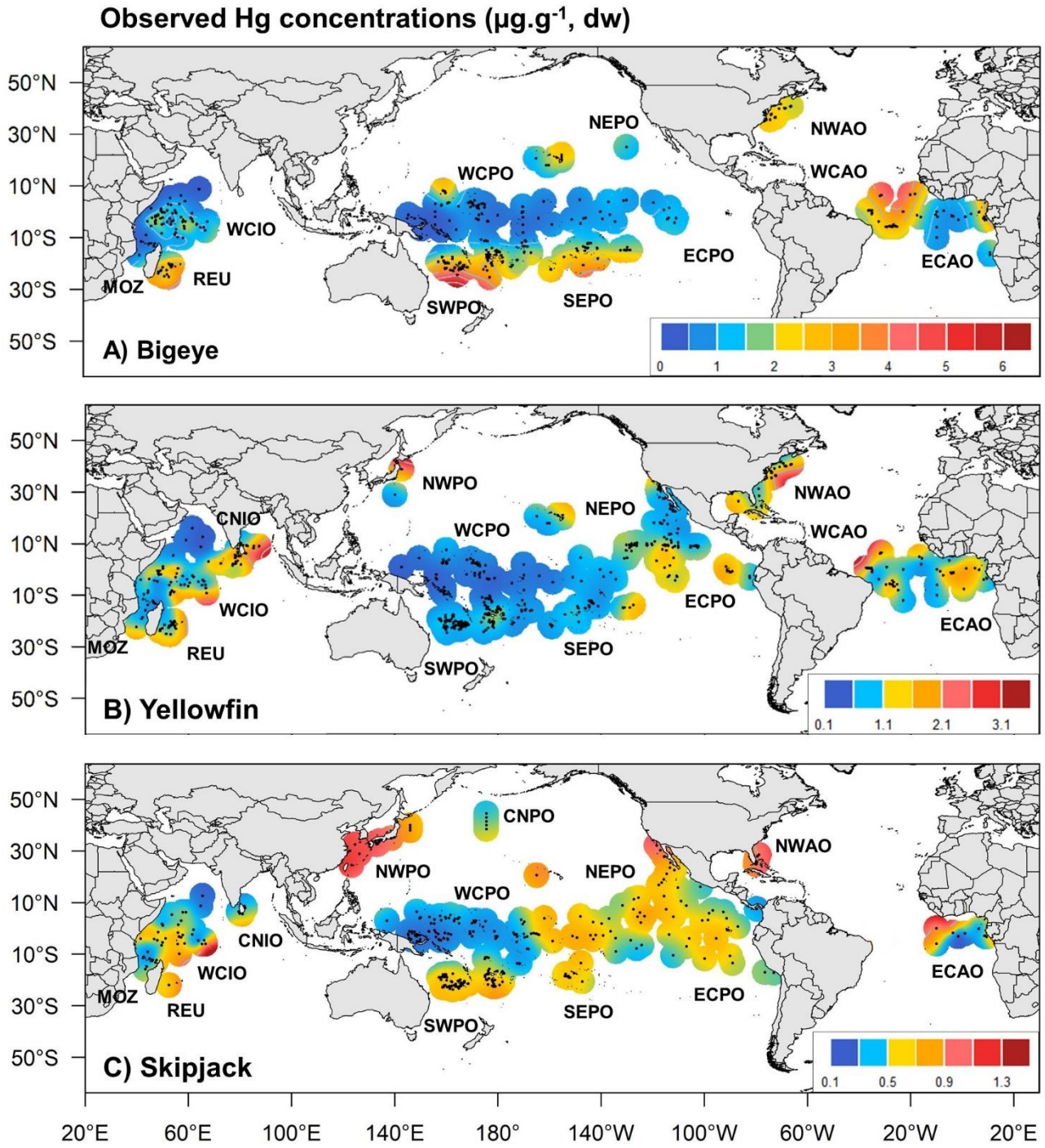

Figure 47. Spatial distribution of mercury (Hg) concentrations in tropical tunas for the global ocean. Smoothed spatial contour maps of observed Hg concentrations (µg.g^{-1}, dw) measured in white muscle samples of **A)** bigeye, **B)** yellowfin, and **C)** skipjack tunas from the Indian, Pacific, and Atlantic Oceans. The black dots represent the location of tuna samples. Oceanic areas: NWPO = northwestern Pacific; CNPO = central north Pacific; NEPO = northeastern Pacific; ECPO = eastern central Pacific; SEPO = southeastern Pacific; SWPO = southwestern Pacific; WCPO = western central Pacific; NWAO = northwestern Atlantic; WCAO = western central Atlantic; ECAO = eastern central Atlantic; CNIO = central north Indian; WCIO = western central Indian; REU = Reunion Island; MOZ = Mozambique Channel.

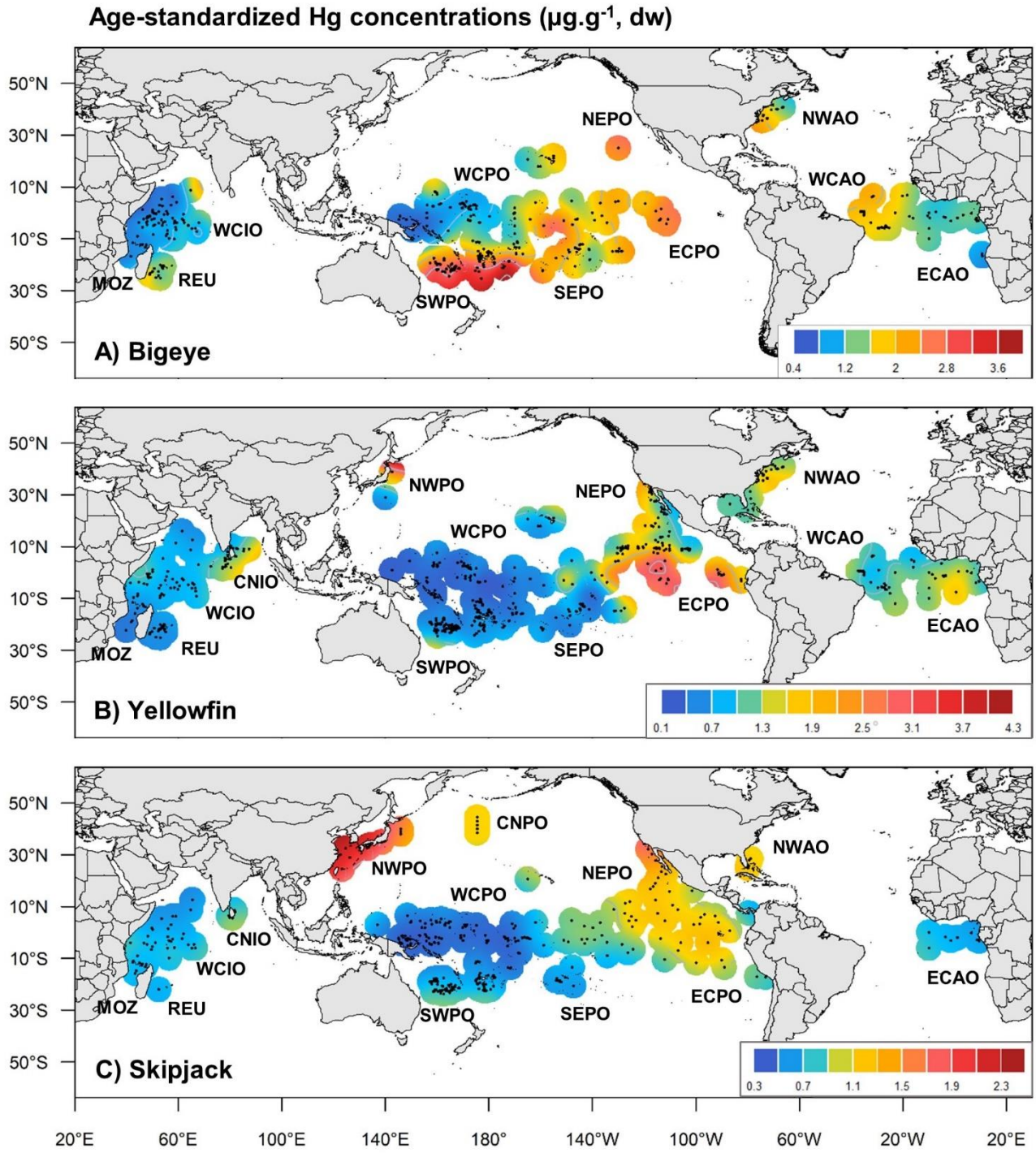

Figure 48. Spatial distribution of standardized mercury (Hg) concentration in tropical tunas at the global scale. Smoothed spatial contour maps of age-standardized Hg concentrations (at 3 years, µg.g^{-1}, dw) in white muscle samples of **A)** bigeye, **B)** yellowfin, and **C)** skipjack tunas from the Indian, Pacific, and Atlantic Oceans. The black dots represent the location of tuna samples. Oceanic areas: NWPO = northwestern Pacific; CNPO = central north Pacific; NEPO = northeastern Pacific; ECPO = eastern central Pacific; SEPO = southeastern Pacific; SWPO = southwestern Pacific; WCPO = western central Pacific; NWAO = northwestern Atlantic; WCAO = western central Atlantic; ECAO = eastern central Atlantic*; CNIO = central north Indian; WCIO = western central Indian; REU = Reunion Island; MOZ = Mozambique Channel.*

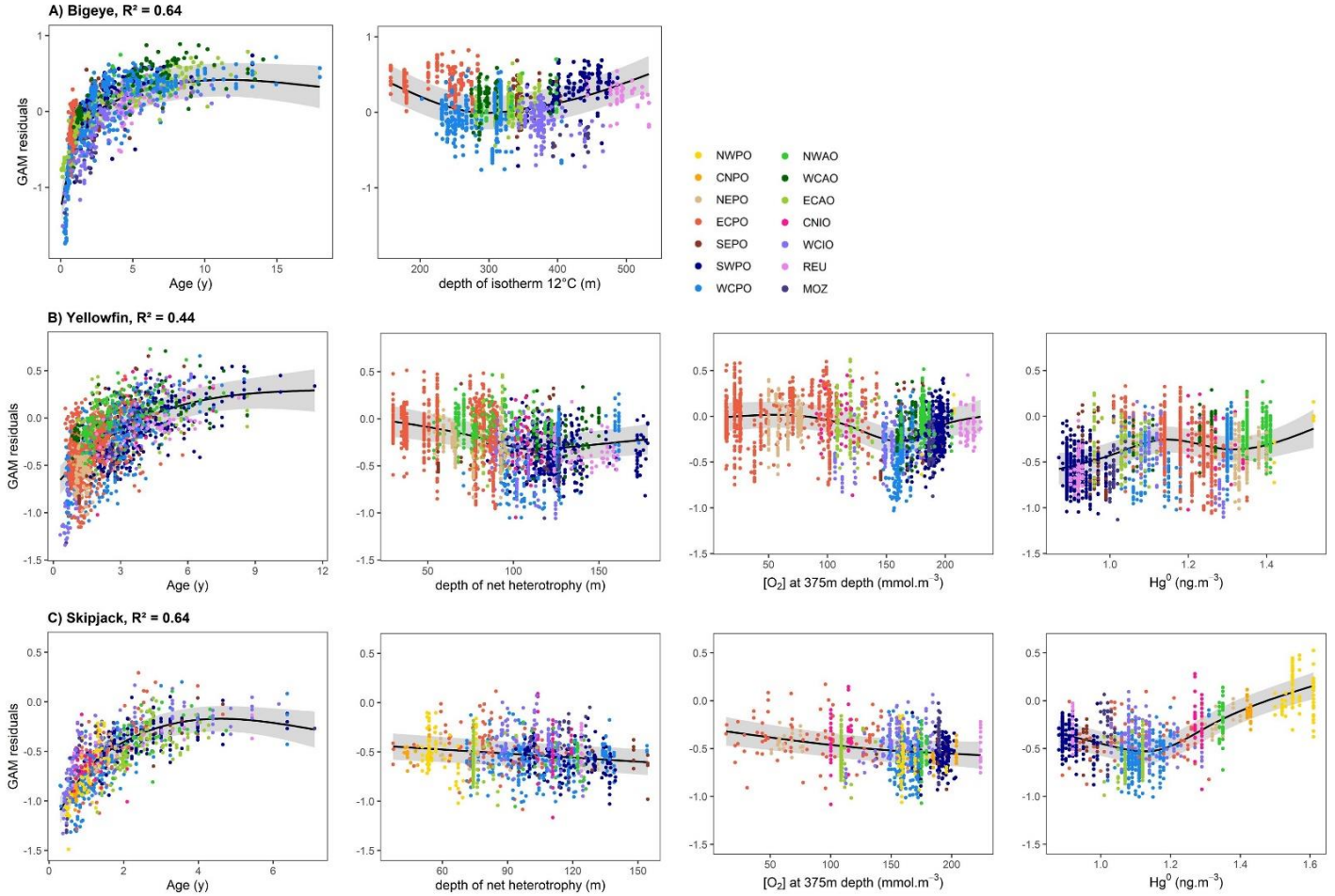

Figure 49. Optimal GAMM predicting observed mercury concentrations in tropical tunas. For **A)** bigeye, the main drivers of the spatial variability of log-transformed mercury concentrations were fish age and the depth of isotherm 12°C, while for **B)** yellowfin and **C)** skipjack, the main drivers were fish age, the depth of net heterotrophy, $[O_2]$ at subsurface and Hg^0 model estimates. The coefficients of determination (R^2) of the three models are reported on the top of the different panels. Colored dots are the partial residuals of the GAM by oceanic areas. Black lines show the expected values, and grey bands show confidence intervals, which are twice the standard error. Oceanic areas: NWPO = northwestern Pacific; CNPO = central north Pacific; NEPO = northeastern Pacific; ECPO = eastern central Pacific; SEPO = southeastern Pacific; SWPO = southwestern Pacific; WCPO = western central Pacific; NWAO = northwestern Atlantic; WCAO = western central Atlantic; ECAO = eastern central Atlantic; CNIO = central north Indian; WCIO = western central Indian; REU = Reunion Island; MOZ = Mozambique Channel.

Natural marine biogeochemical control of the spatial variability of mercury concentrations in tropical tunas

A major aspect when investigating Hg variability in marine biota is its relationship with seawater MeHg concentrations, which may vary vertically and horizontally (Bowman et al., 2020b), as a function of marine biogeochemical processes and different tuna ecology. The optimal models revealed distinct drivers of Hg concentrations depending on the tuna species.

For yellowfin and skipjack, the spatial variability of standardized Hg concentrations was largely explained by the depth of net heterotrophy (i.e. depth at which autotrophy is overcome by heterotrophy), and [O_2] in subsurface waters (Figure 48 B & C). Response curves fitted at the global scale were largely influenced by the west-east gradient of tuna Hg concentrations in the Pacific Ocean. Higher Hg concentrations found in yellowfin and skipjack in the east Pacific (i.e., NEPO and ECPO) were mainly explained by low subsurface [O_2] and shallow net heterotrophy, while lower tuna Hg concentrations in the west Pacific (i.e., SWPO and WCPO) were linked to higher [O_2] and deeper net heterotrophy. To a lesser extent, response curve also indicates that a shallower depth of heterotrophy in the northwestern and the eastern central Atlantic is responsible for higher Hg concentrations in yellowfin compared to the western central Atlantic. These results are in accordance with our previous study focused on skipjack Hg concentrations in the Pacific, where we hypothesized that ambient low-oxygen conditions combined to a more intense and shallower remineralization in the eastern Pacific were responsible for a shallower peak of MeHg concentrations (Médieu et al., 2022). While there is no seawater MeHg data in the equatorial Atlantic to confirm our hypothesis, dissolved MeHg data along a west-east transect in the equatorial Pacific does show a shallower peak of MeHg concentrations in the eastern part compared to the western part (Barbosa et al., 2022; Bowman et al., 2016). Finding the same biogeochemical drivers of skipjack Hg concentrations when working at the global scale reinforces our hypothesis that the spatial variability of Hg levels in this epipelagic species is mainly explained by the depth of bioavailable MeHg peak in the water column. Moreover, it highlights the particular conditions of the eastern Pacific compared to the other regions of the global ocean, where oxygen-poor conditions and shallow bacterial loops both associated with the intense degradation of organic matter are likely responsible for higher Hg concentrations in surface tunas (Figure 49 A).

Here, same biogeochemical drivers were found for both skipjack and yellowfin, which suggests that yellowfin, like skipjack, tend to accumulate more MeHg in areas where they are exposed to a shallower peak of MeHg concentrations. Tagging studies indeed show that both yellowfin and skipjack occupy mainly the epipelagic layer, preferentially inhabiting the surface mixed layer above the thermocline (< 200 m) (Reygondeau et al., 2012; Sabarros et al., 2015; Schaefer et al., 2009, 2007), which explains why they display overall the same spatial patterns of standardized Hg concentrations and the same biogeochemical drivers. Yet, it is worthwhile to mention that the model for yellowfin explains less spatial variability of Hg concentrations (R^2 = 0.44) than the one for skipjack (R^2 = 0.66). Although these two species share general biological characteristics, yellowfin, especially adults, are also known to display more frequent and/or deeper dives during the day thanks to physical and physiological modifications (e.g., allometric development of a swim bladder allowing them to swim deeper), likely to increase their capability to catch deeper preys (Olson et al., 2016). During these deeper dives, yellowfin forage in waters enriched in dissolved MeHg, and have therefore access to enriched MeHg mesopelagic preys, compared to skipjack. This likely explain the higher standardized Hg concentrations in yellowfin than in skipjack in all ocean basins.

For bigeye, only one physical variable was selected in the optimal GAMM in addition to fish age: the depth of isotherm 12°C, a proxy for the thermocline depth (Figure 48 A). Its U shape response curve shows that increasing depths of isotherm 12°C generally induce higher standardized Hg concentrations in bigeye at the global scale, with high standardized Hg concentrations in bigeye in the southwestern Pacific, and to a lesser extent in the REU, associated to the deepest foraging depths. But the response curve also highlights the exception of the eastern Pacific (i.e., ECPO), where high standardized Hg vales are associated to very shallow depths of isotherm 12°C (< 300 m). Contrary to other tropical tunas and thanks to physiological particularities, bigeye is known to occupy depths below the thermocline during daytime, presumably to target prey organisms of the vertically-migrating deep-scattering layer (Fuller et al., 2015; Song et al., 2009). Depth of isotherm 12°C is therefore generally used as a proxy for bigeye vertical habitat, as evidenced in the Pacific Ocean (Abascal et al., 2018), and confirmed in the Indian and Atlantic Oceans when compared with tagging data (Reygondeau et al., 2012; Sabarros et al., 2015; Yang et al., 2020). Our results therefore suggest that increasing Hg concentrations in bigeye are mainly explained by deeper foraging depths, as already found in regional studies in the central north (i.e., Hawaii) and the western central Pacific Ocean (Choy et al., 2009; Houssard et al., 2019). Yet, this general assumption leads to a paradox in the eastern Pacific Ocean, where we would expect very low standardized Hg concentrations in bigeye. In the Pacific Ocean, bigeye foraging depth has been shown to display a longitudinal pattern, becoming progressively shallower from west to east, with bigeye remaining in the upper 250 m in the eastern equatorial Pacific (versus > 450 m in the southwestern Pacific; Abascal et al., 2018; Schaefer et al., 2009). This indicates that high standardized Hg concentrations in bigeye in the eastern Pacific result from the combination of i) a reduced vertical habitat and, ii) a shallow peak of dissolved MeHg concentrations (Bowman et al., 2016), likely associated to the intense and shallow degradation of organic matter in this ocean basins, as explained previously with the optimal GAMMs of yellowfin and skipjack. Given our GAMM results at the global scale, we therefore hypothesize that it is not only the thermocline depth that drives Hg concentrations in bigeye, but rather the match between the depths of both the thermocline, and the peak of MeHg concentrations in the water column (Figure 49).

Following this assumption, it is interesting to notice that bigeye in the southwestern Pacific exhibited higher Hg concentrations than in Reunion Island, while bigeye from these two regions are supposed to forage deep below the thermocline (up to 600 m) (Abascal et al., 2018; Sabarros et al., 2015). This suggests that dissolved MeHg concentrations in deep waters are also different in these two areas (Figure 49 B & C). Unfortunately, no seawater MeHg data are available around Reunion Island and in the western Indian Ocean to investigate further this assumption. Dissolved MeHg data in the southwestern Pacific suggest high MeHg concentrations at depth (between 0.2 and 0.4 pM in the 400-600 depth layer), compared to the rest of the Pacific (Barbosa et al., 2022), likely resulting from differences in Hg sources and/or net MeHg production rates in the water column. Measurements of MeHg data in both seawater and phytoplankton remain needed and crucial in these two areas to investigate further what could lead to spatial differences of bigeye Hg concentrations in these two areas.

Overall, our results indicate that the spatial variability of Hg concentrations in tropical tunas at the global scale is mainly driven by the vertical and horizontal variability of seawater MeHg concentrations and the species-specific foraging depth. Epipelagic tuna species display higher Hg concentrations in areas where the peak of dissolved MeHg concentrations is shallow, while Hg concentrations in mesopelagic tuna species (i.e., bigeye) reflect a match between tuna foraging depth,

and the depth at which MeHg concentrations peak in the water column. The importance of dissolved MeHg concentrations to explain tuna Hg concentrations has been previously evidenced with positive correlations between tuna Hg levels and seawater MeHg profiles in tropical tunas in the southwestern Pacific (Barbosa et al., 2022), and in bluefin tuna at the global scale (Tseng et al., 2021). Such link between dissolved MeHg concentrations and Hg accumulation in marine top predators is expected but rarely observed due to scarce MeHg data in the water column.

While discussing the importance of tuna foraging depth and MeHg sources in the water column to explain the spatial variability of tuna Hg concentrations, some could argue that confounding trophic processes might be at play as well. Higher Hg concentrations in bigeye exhibiting a deeper foraging habitat could indeed result from deeper preys enriched in Hg and/or with a higher trophic position level (Ferriss and Essington, 2014b). To further explore the relative importance of trophic processes, we used tuna trophic positions estimated with amino acid $\delta^{15}N$ values measured in tuna samples from the global ocean (SI Appendix G, Figure S4 A). The absence of significant relationship between tuna Hg concentrations and trophic positions for bigeye and yellowfin agree with our GAMM results and confirm the limited importance of geographic changes of trophic ecology to explain the spatial variability of tuna Hg concentrations (SI Appendix G, Figure S4 B & C), as already documented in regional studies (Houssard et al., 2019; Médieu et al., 2022). Nevertheless, the correlation between dissolved MeHg concentrations and Hg accumulation in tunas implies that Hg concentrations in tunas' preys also vary with the vertical and horizontal spatial patterns of MeHg concentrations in seawater. Alternatively, our results are also consistent with the possible enhanced absorption of MeHg through gills, given their high ventilation rates and their physiological adaptations of their oxygen transport system (Boddington et al., 1979; Hall et al., 1997), as suggested by Barbosa et al. (2022).

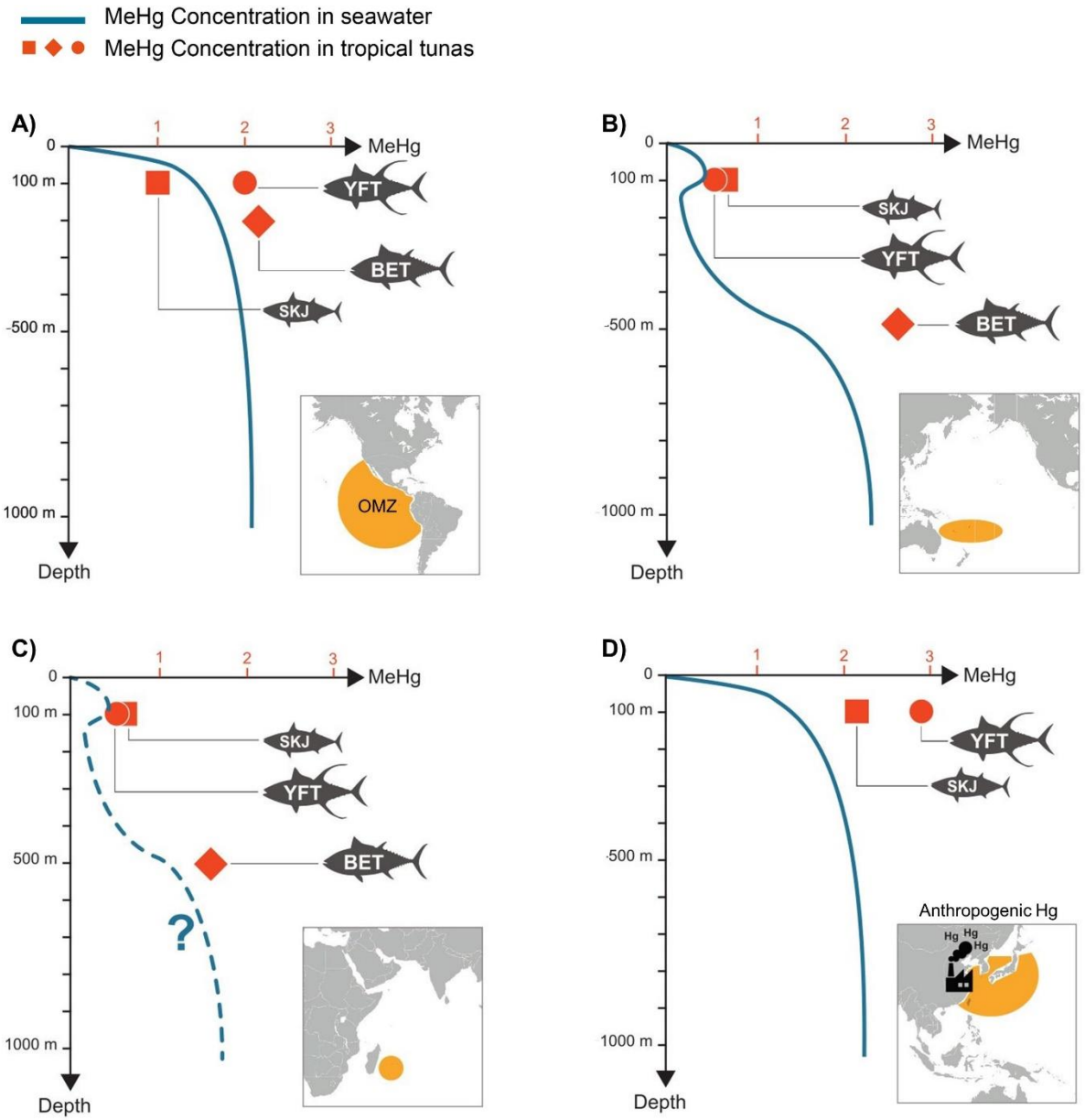

Figure 50. Schematic figure illustrating the spatial and inter-species variability of tuna mercury (Hg) concentrations (orange icons) in relation to the geographic location (inserts at the bottom right) and the vertical and horizontal spatial variability of dissolved methylmercury (MeHg) concentrations (blue lines). **A)** In the eastern central Pacific, the three tropical tunas exhibit standardized high Hg concentrations, resulting from i) a common shallow foraging habitat, and ii) a shallow and high peak of dissoved MeHg concentrations, resulting from the oxygen minimum zone (OMZ) and shallow heterotrophy conditions. **B)** In the southwestern Pacific, standardized Hg concentrations are low in skipjack and yellowfin, but at their highest level in bigeye, likely resulting from skipjack and yellowfin inhabiting shallow waters with low dissolved MeHg concentrations, and bigeye foraging in deeper waters where the peak of dissolved MeHg concentration is deep and high. **C)** Around La Reunion (i.e., southwestern Indian), standardized Hg concentrations are low in skipjack and yellowfin, and intermediate in bigeye. Although there is no dissolved MeHg profile available in this region, we hypothesize these inter-species differences result from low dissolved MeHg concentrations is surface waters where skipjack and yellowfin are found, and relatively high dissolved MeHg concentrations in deeper waters where bigeye forage. **D)** Along the Asian coasts, standardized Hg concentrations are the highest for skipjack and yellowfin (no Hg data in bigeye are available in this region). These Hg hotspots likely result from shallow heterotrophic conditions leading to higher MeHg concentrations in surface waters, and to an additional contribution of anthropogenic Hg releases from Asia.

Asian anthropogenic inputs enhancing tuna mercury concentrations in the northwestern Pacific

In addition to fish age, Hg^0 model estimates were selected in the best model of both epipelagic species: skipjack and yellowfin (Figure 48 B & C). For these two species, response curves indicate that high tuna standardized Hg concentrations in the northwestern Pacific are mainly explained by highest Hg^0 model estimates in this area, although more yellowfin samples along the Asian costs would be needed to confirm this significant trend. This highlights an additional local contribution of anthropogenic Hg releases from Asia to tuna Hg concentrations in the northwestern Pacific, as already suggested at the Pacific Ocean scale with skipjack only (Figure 49 D) (Médieu et al., 2022). Like skipjack, yellowfin is an epipelagic species that remains overall in the first 200 m in the water column. Unfortunately, no bigeye samples were available in this ocean region to investigate if anthropogenic Hg loadings from the atmosphere along the Asian coasts can also lead to higher MeHg bioavailability for mesopelagic marine food webs. Overall, our global study confirms that anthropogenic Hg releases tend to enhance Hg concentrations in tunas but only in the immediate geographic vicinity of the Asian coasts. Elsewhere in the global ocean, the spatial variability of Hg concentrations in tunas is mainly related to ecological and/or marine biogeochemical processes.

Implications for mercury monitoring in the global ocean and marine biota

This study provides the first assessment of global-scale and high-resolution spatial patterns of Hg concentrations in tropical tuna species. It suggests a strong link between MeHg concentrations in seawater and Hg accumulation in tunas, as recently evidenced in bluefin tunas at the global scale (Tseng et al., 2021). In particular, our spatial interpolation of age-standardized Hg concentrations in different tropical tunas revealed two main spatial patterns depending on species-specific foraging depth. For epipelagic species, i.e., skipjack and yellowfin, higher Hg concentrations are found in the northwestern Pacific and, to a lesser extent the eastern Pacific, while for bigeye, a mesopelagic species, highest Hg concentrations are shown in the southwestern Pacific, followed by the eastern equatorial Pacific. The complementary use of ecological tracers in these species alongside biogeochemical and physical variables in the ocean showed the importance of i) marine biogeochemical processes inducing variable vertical and horizontal MeHg concentrations at the base of pelagic food webs, coupled to ii) tuna vertical habitat, to explain the large spatial variability of tuna Hg concentrations at the global scale. Moreover, our study also confirms a cumulated local anthropogenic Hg release effect that enhances tuna Hg concentrations along the Asian coasts.

This multi-species and global-scale study therefore indicates that Hg concentrations in tropical tunas seem to mirror the horizontal and vertical distribution of oceanic MeHg concentrations, and also reflect regional anthropogenic atmospheric Hg^0 distribution. These results suggest that the three tropical tuna species can be used conjointly as sentinels of Hg pollution and MeHg bioavailability at the base of marine food webs, complementary to direct observations of atmospheric Hg deposition and seawater Hg concentrations and speciation. Given their high exploitation worldwide (i.e., they account for more than 90 % of the global tuna fishery (FAO, 2018), tropical tunas appear as good candidates to implement the future design and implementation of large-scale Hg bio-monitoring efforts in surface and sub-surface oceans to evaluate the effectiveness of the Minamata Convention. Furthermore, large spatial and temporal Hg trends in tropical tunas could provide additional insights

on the potential impact of climate-induced changes on the global marine Hg cycle (Schartup et al., 2019). Integrating tropical tunas' prey Hg analyses at large spatial scales seems to be a necessary avenue of future research to investigate further variable MeHg concentrations in seawater and Hg accumulation along oceanic food webs.

Acknowledgments

General: We are grateful to our sampling providers including the many onboard observers, fishermen, and researchers who collected the samples in each of the ocean basins. This includes the Environmental Specimen Bank in Ehime University (Japan), the CRO-IRD-IEO, and SFA teams in charge of tropical tunas purse-seine fisheries monitoring in Abidjan (Ivory Coast) and Victoria Port (Seychelles), respectively, as well as the Western and Central Pacific Fisheries Commission Tuna Tissue Bank, the Pacific Marine Specimen Bank managed by the Pacific Community (SPC), and the NOAA Pacific Islands Region Observer Program. We also thank Bernard Bourlès, US IMAGO of IRD and the volunteers who collected tuna samples during the PIRATA cruises (https://doi.org/10.18142/14). This work contributes to CLIOTOP WG3-Task team 01. We acknowledge Emmanuel Chassot and Dan Fu from IOTC (Seychelles), Daniel Gartner from IRD (France), John Walter from NOAA (USA), Shane Griffiths from IATTC (USA), and Matthew Vincent from SPC (New Caledonia) for their help to acquire species- and ocean- specific growth parameters. We are grateful to Sébastien Hervé from IUEM (France) for artwork. We thank Jean-Louis Duprey and Stéphanie Berne from the LAMA laboratory (New Caledonia) for Hg analyses, as well as the Union College Stable Isotope Laboratory team Sarah Katz, and Madelyn Miller. HA acknowledges Noelle E. Selin from MIT (USA) and the use of the Svante cluster provided by the Massachusetts Institute of Technology's Joint Program on the Science and Policy of Global Change.

Funding: This study was conducted in the framework of the ANR-17-CE34-0010 MERTOX (unravelling the origin of methylMERcury TOXin in marine ecosystems, 2017-2021, PI DP) from the French Agence Nationale de la Recherche, and was also funded by the Pacific Fund VACOPA project (spatial Variations of Contaminants levels in Pacific ocean trophic webs, PI AL). This study benefited from financial support of the Région Bretagne and Université de Bretagne Occidentale (UBO), and ISblue project, Interdisciplinary graduate school for the blue planet (ANR-17-EURE-0015). The U.S. National Science Foundation funded Union College's isotope ratio mass spectrometer and peripherals (NSF-MRI #1229258). HA received financial support from the Swiss National Science Foundation (grant no 200021_188478).

General discussion: synthesis, caveats and perspectives

The main objective of this thesis was to advance the understanding about what controls the origin and fate of MeHg in different tuna species at the global scale. Our study focussed on tropical tunas (i.e., bigeye, yellowfin, and skipjack), three species highly exploited and consumed worldwide (FAO, 2018), that display contrasted biological (growth and lifespan) and ecological (e.g., foraging diet and trophic ecology) characteristics (Olson et al., 2016), likely inducing different patterns of Hg bioaccumulation. We built the largest database of Hg concentrations in tunas at the global scale yet, integrating corresponding tuna biological and ecological data, marine physical and biogeochemical variables, and atmospheric Hg estimations. We provided the first broad-scale and high-resolution maps of Hg concentrations in tropical tunas for the global ocean, and explored the key processes driving Hg accumulation in these pelagic top predators. The exploration of tuna Hg concentrations at different temporal (Chapters 1 & 2) and spatial (Chapters 3 & 4) scales highlighted six important points:

- tuna age, and to a lesser extent tuna length, are key parameters to explain Hg variability among individuals at the global scale, confirming the importance of standardizing Hg levels when exploring and comparing Hg accumulation at temporal and spatial scales;
- variable Hg concentrations among tuna species and ocean regions mainly result from the combined effect of i) marine biogeochemical processes leading to vertical and horizontal variability of MeHg concentrations in seawater, and ii) species-specific tuna foraging depths;
- conversely, spatial changes of tuna trophic ecology are of minor importance to explain the spatial variability of Hg concentrations in tunas;
- recent anthropogenic Hg releases from Asia have leaded to enhanced Hg concentrations in epipelagic tunas in the northwestern Pacific Ocean. Elsewhere, although variable among years, global tuna Hg concentrations remained relatively stable over the past decades, highlighting that the buffering capacity of the ocean is likely higher than expected due to the i) large burden of accumulated legacy anthropogenic Hg, ii) the unknown fraction of these emissions converted into marine MeHg, and iii) the uncertain but possible long turnover of MeHg in the global ocean;
- tuna muscle samples are able to reflect Hg exposure in pelagic ecosystems, integrating local and global Hg sources over different spatial and temporal scales, and are therefore powerful monitoring tools to evaluate the effectiveness of the Minamata Convention;
- among tropical tunas, only bigeye, from the three oceans, exhibited Hg concentrations exceeding the food safety guidelines 1 $\mu g.g^{-1}$ (fresh tissue) in some regions.

The importance of considering growth rate when investigating tuna mercury concentrations at the global scale

Effects of tuna growth rates on the spatial variability of tuna mercury concentrations

Given the natural bioaccumulative properties of MeHg in organisms with age and size, we always standardized Hg concentrations before investigating temporal and spatial variability of tuna Hg burden. In Chapters 1, 2, and 3, we calculated standardized Hg levels following the method developed by Houssard et al. (2019), fitting a bioaccumulative curve between Hg concentrations and fish fork length, a morphometric data easily collected during tuna sampling. For our global and comparative spatial study (Chapter 4), because tuna growth vary among species and ocean basins (Murua et al., 2017), we decided to standardize Hg concentrations using fish age estimates, rather than fish length for a more accurate comparison at the global scale. This allowed taking into account the natural physiological process of Hg bioaccumulation over time, but also exploring the variability of Hg concentrations when considering inter- and intra- specific differences of tuna growth patterns (Figure 50), as done in other global studies (Tseng et al., 2021). Standardizing at the same age also allows comparing tuna Hg concentrations among regions considering a same time of Hg exposure. The comparison of global spatial patterns of length- and age- standardized Hg concentrations in tunas revealed that the length-standardization approach tend to induce spatial bias at the global scale, resulting in enhanced but biased Hg variability among ocean basins that are in reality related to differential growth rates among ocean basins (Figure 51). For instance, skipjack Hg concentrations standardized at 60 cm displayed significant differences among some ocean basins: eastern central Atlantic > western central Indian > western central Pacific, while we found overall similar age-standardized Hg concentrations in these three large regions. This enhanced but biased Hg variability of length-standardized Hg results from the fact that a skipjack of 60 cm is approximately 1.5 years old in the western central Pacific, 3 years old in the western Indian, and 4 years old in the eastern Atlantic (Figure 50 C), and therefore does not reflect a same time of Hg exposure.

To explore the effect of different growth patterns on tuna Hg concentrations, we estimated tuna age from tuna length using species- and ocean- specific growth models, as recommended by fisheries scientists for tuna stock assessments (Figure 50). Growth models describe the change of length as a function of age, and can take different forms from relatively simple (i.e., the von Bertalanffy growth curve), to more complex forms (e.g., the two-stanza growth curve of tropical tunas in the western Indian Ocean). For assessment and management purpose, growth of wild tropical tunas has been the subject of considerable research efforts since the 1960s through analysis of mark-recapture data, size frequency distribution of commercial fishery catches, and ageing from calcified and bony structures (Diaz, 1963; Schaefer et al., 1961). Yet, because of the inherent difficulty of using hard parts to estimate growth in tunas, of applying tagging programs to highly migratory species, and of obtaining representative samples of the whole population, some uncertainties currently remain regarding tuna growth models, especially on the mechanisms driving growth differences among ocean basins (e.g., size-specific migration, spatial variation in growth) (Murua et al., 2017).

Overall, given the differences of growth rates among species and ocean basins, and the associated spatial discrepancies revealed between length- and age- standardized Hg concentrations, we recommend using age-standardized Hg concentrations when exploring tuna Hg accumulation in

different regions and species. For each tuna species, there are several growth models available, calculated with different methods, sampling strategy, and sampling coverage, that is why we advise estimating fish age with the equations used by the regional fishery management organizations (RFMOs) in the latest tuna stock assessments, as done in this thesis. When working at the regional scale, given the potential bias associated to age estimation, we assume that length-standardization of Hg concentrations remains relevant to explore the spatial variability of tuna Hg content.

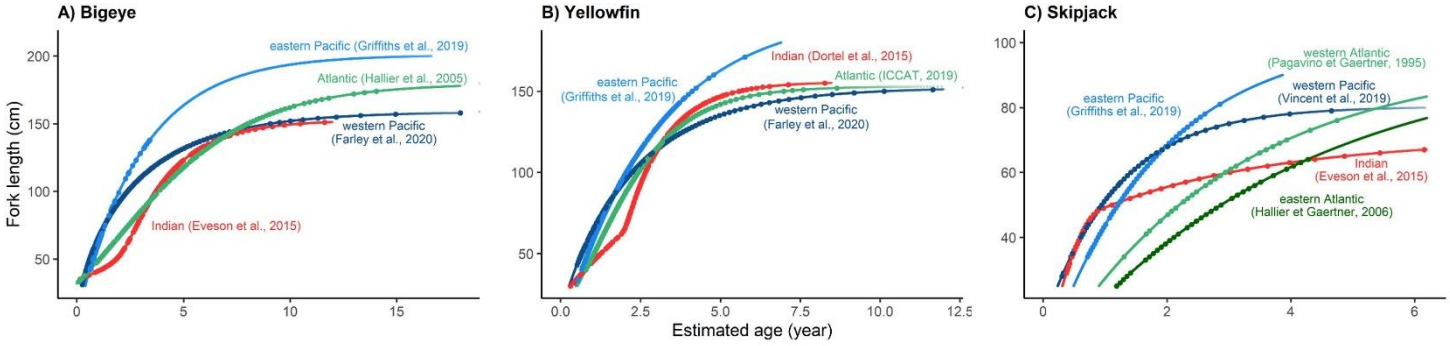

Figure 51. Inter-ocean basins comparison of tropical tunas' growth patterns. The growth parameters and curves used to estimate tuna age were obtained from the last stock assessments when data were available (Dortel et al., 2015; Eveson et al., 2015; Farley et al., 2020; Hallier et al., 2005; ICCAT, 2019, 2014; Vincent et al., 2019) or from recently published studies (Griffiths et al., 2019) (see methods section). The dots on the curves represent our tuna samples for which fish age was estimated.

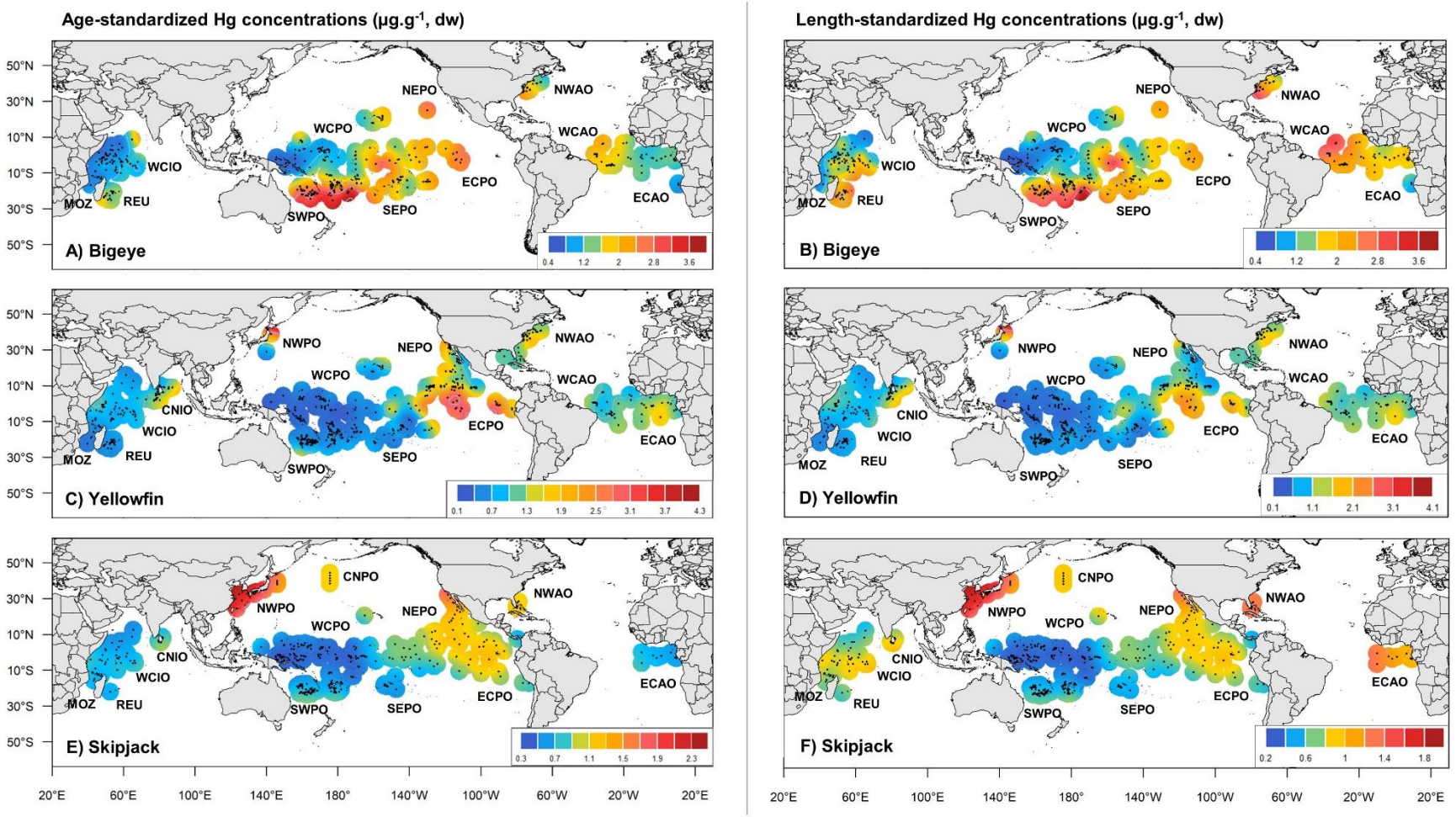

Figure 52. Comparison of mercury (Hg) standardization methods considering fish age (left) or fish length (right). Smoothed spatial contour maps of age-standardized Hg concentrations (µg.g^{-1}, dw) in **A)** bigeye, **C)** yellowfin, and **E)** skipjack, and length-standardized Hg concentrations in **B)** bigeye, **D)** yellowfin, and **F)** skipjack. The black dots represent the location of tuna samples. Oceanic areas: NWPO = northwestern Pacific; CNPO = central north Pacific; NEPO = northeastern Pacific; ECPO = eastern central Pacific; SEPO = southeastern Pacific; SWPO = southwestern Pacific; WCPO = western central Pacific; NWAO = northwestern Atlantic; WCAO = western central Atlantic; ECAO = eastern central Atlantic; CNIO = central north Indian; WCIO = western central Indian; REU = Reunion Island; MOZ = Mozambique Channel.

Effects of different tuna growth rates on inter-species differences of mercury concentrations

Regarding inter-species differences, even when considering different growth rates among species at the global scale, we show that age-standardized Hg concentrations still vary significantly among all tropical tunas, with bigeye exhibiting the highest Hg concentrations, and skipjack the lowest ones (Chapter 4). This suggests that other factors not related to bioaccumulation with age are at play. We hypothesized that such differences are mainly related to i) differences of tuna vertical habitat among species and ocean regions and, ii) the vertical and horizontal spatial gradients of marine MeHg concentrations and bioavailability at the base of marine food webs, controlled by biogeochemical processes. Yet, these significant differences among species can also result from a Hg dilution effect associated to tuna growth: at a same age, faster growing species (skipjack, followed by yellowfin) display lower Hg concentrations than the slow growing bigeye. Such Hg bio-dilution with growth has already been documented in hake (*Merluccius merluccius*) and salmon (*Salmo salar*) (Cossa et al., 2012; Ward et al., 2010), and relies on the assumption that consumption rates (i.e., how much food fish consume) and activity cost (i.e., how much of their energy fish allocate to activity) are equal among species (Trudel and Rasmussen, 2006). When investigating further the inter-species differences of age-standardized Hg concentrations in each ocean area, differences among species (BET > YFT > SKJ) are less obvious (Figure 52), which can suggest that the effect of growth is of less importance compared to regional ecological (i.e., tuna foraging depth) or biogeochemical processes, and/or that metabolic differences among species might also be at play. Future research, including for instance mass balance and/or bioenergetic (e.g., DEB) models, would be valuable to investigate the potential impact of Hg bio-dilution associated to different tuna growth rates.

Furthermore, these inter-species differences of Hg concentrations could be related to ontogenetic shifts in feeding behaviours and trophic status (i.e., prey species composition and size distribution) (Graham et al., 2007; Young et al., 2010b). Apart from changes in diet, the growth of a predator also offers the opportunity to feed on similar but larger preys, likely more concentrated in MeHg. In addition, ontogenetic shifts of vertical habitats are observed in tunas: while juvenile bigeye preferentially occupy the epipelagic layer, adults are known to occupy depths below the thermocline and to display daily vertical movement patterns presumably to exploit more effectively prey organisms (Brill et al., 2005; Fuller et al., 2015; Song et al., 2009). Similarly, adult yellowfin can also display frequent and/or deeper dives during the day thanks to physical and physiological modifications (e.g., allometric development of a swim bladder allowing them to swim deeper). Taken all together with age or length, these ecological changes could modify the exposure of tropical tunas to MeHg, leading to possible masked confounding effects when standardizing Hg concentrations. To avoid such bias when exploring the main drivers of Hg accumulation in tunas, we fitted our models (GAM or GAMM) on observed Hg concentrations, rather than on standardized Hg values. Moreover, even when accounting for the age/length effect, the vertical foraging depth (explored with the depth of isotherm 12°C) was significant in the global model of bigeye, highlighting the importance of i) Hg bioaccumulation in fish through time, and ii) other ecological and biogeochemical processes at play, as discussed below.

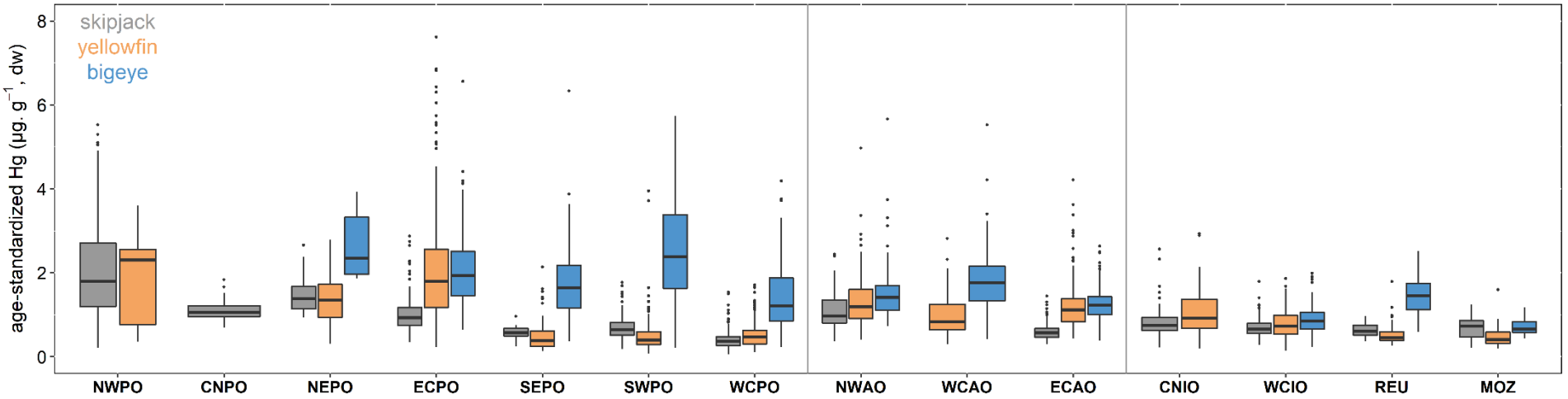

Figure 53. Boxplots of age-standardized mercury (Hg) concentrations (µg.g^{-1}, dw) at 3 years in skipjack (grey), yellowfin (orange), and bigeye (blue) at the global scale. Oceanic regions: NWPO = northwestern Pacific; CNPO = central north Pacific; NEPO = northeastern Pacific; ECPO = eastern central Pacific; SEPO = southeastern Pacific; SWPO = southwestern Pacific; WCPO = western central Pacific; NWAO = northwestern Atlantic; WCAO = western central Atlantic; ECAO = eastern central Atlantic; CNIO = central north Indian; WCIO = western central Indian; REU = Reunion Island; MOZ = Mozambique Channel.

The importance of tuna foraging depth in the context of marine methylmercury depth profiles and bioavailability to explain tuna mercury concentrations

Tropical tunas reflect global patterns of dissolved methylmercury concentrations

Our multidisciplinary and high-resolution spatial studies revealed that the spatial variability of standardized Hg concentrations in tropical tunas is mainly explained by an interplay between i) biogeochemical processes that govern the vertical and horizontal variability of MeHg concentrations in seawater, and ii) ecological processes related to interspecific differences of foraging depth (Chapters 3 & 4). Mercury concentrations in epipelagic tunas (i.e., skipjack and yellowfin) are enhanced in areas where the peak of dissolved MeHg concentrations is shallower. In mesopelagic species like bigeye, higher Hg concentrations can be explained by the fact that this species forage in deeper waters where dissolved MeHg concentrations are generally higher. Such link between MeHg concentrations and bioavailability in seawater and Hg accumulation in marine top predators is expected but rarely observed due to scarce MeHg data in the water column. This link has been detailed with significant positive trends between seawater MeHg levels and Hg concentrations in muscle and blood samples of tropical tunas and albacore from the southwestern Pacific (Figure 53) (Barbosa et al., 2022; Hg concentrations in tropical tuna muscle samples of this study are included in our global spatial study). At the global scale, same positive correlation has been found with muscle bluefin samples (Tseng et al., 2021). In our spatial studies (Chapters 3 & 4), we could not investigate similar correlations at large ocean scale given the scarce and low spatial resolution of MeHg data in seawater mismatching tuna sample location. Yet our results are in accordance with the few available MeHg profiles in the Pacific Ocean (Figures 4 B & 5) (Barbosa et al., 2022; Bowman et al., 2015; Munson et al., 2015). While our results provide new insights to understand both the distribution of Hg levels in tunas and the critical processes driving the global mercury cycle, they also call for more measurements of MeHg concentrations in both seawater and phytoplankton, in particular in the Indian and the equatorial Atlantic Oceans, to validate our hypothesis at the global scale. A global 3D model for MeHg formation and uptake at the base of marine food webs has been recently developed within the Massachussetts Institute of Technology general circulation model (Zhang et al., 2020). Comparing our global Hg observations in tunas with these model estimates of MeHg in seawater and plankton would be valuable to explore further our results, and to help constraining the model parametrization including Hg data in marine top predators.

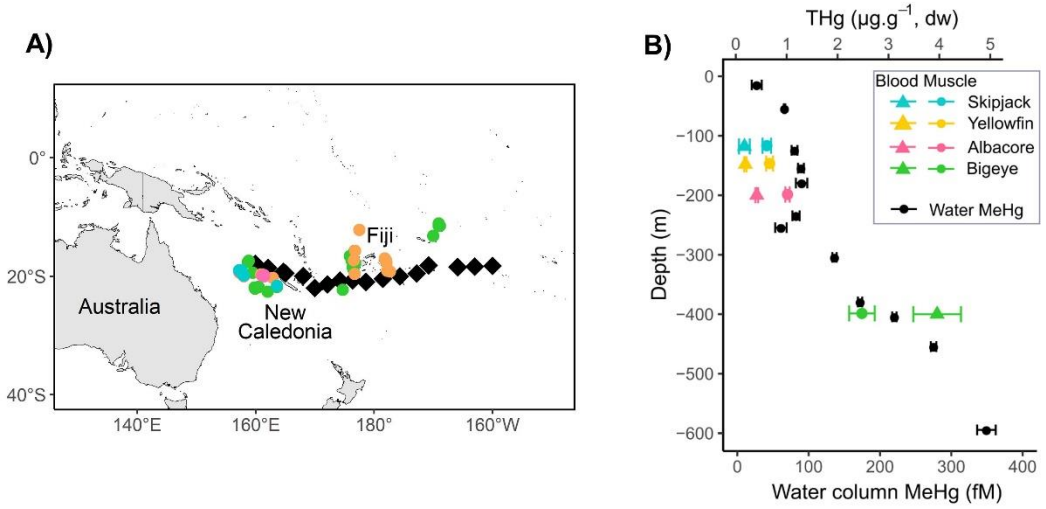

Figure 54. A) Location of seawater (black diamonds) and tuna (colored dots) blood and muscle samples used to investigate the link between tuna mercury concentrations and dissolved methylmercury levels. **B)** Relationship between total mercury concentrations (THg, µg.g^{-1}, dw) in tropical tunas and albacore, and dissolved methylmercury (MeHg) concentrations (fM, average depth profile from all locations) in the southwestern Pacific Ocean, from Barbosa et al. (2022). Mercury concentrations in tropical tuna muscle samples for this study are included in our global spatial study (Chapter 4).

Tuna mercury concentrations at the global scale may reveal baseline processes governing the marine methylmercury cycle

In the eastern central Pacific, where tropical tunas mainly remain in the surface waters (Abascal et al., 2018; Schaefer et al., 2009), high age-standardized Hg concentrations found in the three species were related to low oxygen concentrations and shallow depth of net heterotrophy in our GAM analyses. We therefore hypothesized that oxygen-poor conditions and shallow bacterial loops, associated with the intense degradation of organic matter, are likely to induce high dissolved MeHg concentrations in shallow waters. This is in accordance with a relatively high proportion of dissolved MeHg (relative to total Hg) in surface waters of the eastern central Pacific, compared to other parts of the Pacific (Bowman et al., 2016, 2020). Mercury methylation is generally considered to occur in low-oxygen deep thermocline waters during organic matter remineralisation, involving iron-reducing bacteria and methanogens (Fleming et al., 2006; Hamelin et al., 2011). Yet there are also observations suggesting *in situ* Hg methylation in the oxygenated surface waters, likely related to the remineralisation of sinking particulate organic matter (Cossa et al., 2009; Hammerschmidt and Bowman, 2012; Heimbürger et al., 2010; Monperrus et al., 2007; Sunderland et al., 2009). Methylation in oxic marine waters could be also related to anaerobic micro-environments, like sinking particles and aggregates (Bianchi et al., 2018; Ortiz et al., 2015). In the eastern Pacific, our modeling approach underlined that high tuna Hg levels were not only associated to low oxygen conditions, but also to important and shallow heterotrophy, likely favouring Hg methylation closer to the surface, in contact with surface food webs. Furthermore, given the importance of low oxygen conditions to explain high tuna Hg concentrations, our results suggest that the predicted climate-driven expansion of oxygen minimum zone (Bindoff et al., 2019; Deutsch et al., 2011) could create more favourable conditions for

shallow MeHg production, although parallel changes in primary production and organic matter export could also alter this trend (Tagliabue et al., 2020). Future research, including laboratory experiments and observations of seawater MeHg, remains needed to better understand the mechanisms at play leading to a shallow and relatively high peak of dissolved MeHg concentrations in this particular area. Additional tuna samples in other oxygen minimum zones (e.g., the Arabian Sea in the northwestern Indian Ocean, or in the Peruvian ecosystem) could be also valuable to help evaluating the relative importance of shallow and extended oxygen minimum zone for MeHg production and bioaccumulation in marine food webs.

In the southwestern Pacific, we revealed different patterns of Hg accumulation in tropical tunas, with highest age-standardized Hg concentrations found in this area for bigeye, while concentrations remained low for skipjack and yellowfin. In this area, bigeye has been shown to forage deeper than in the eastern Pacific (Figure 54), while skipjack and yellowfin remain mostly in surface waters from west to east. This contrasted pattern among species, compared to the eastern Pacific, suggest bigeye is exposed to higher deep MeHg concentrations in the southwestern Pacific, therefore pointing out to a particular enrichment of dissolved MeHg concentrations in this area, i.e., relatively low MeHg concentrations in surface waters and high concentrations in mesopelagic waters (> 400 m). This suspected enrichment in MeHg in the southwestern Pacific mesopelagic zone compared to the eastern Pacific tend to mirror direct observations made in this region (Figures 53 & 55). Moreover, standardized Hg concentrations of bigeye in the southwestern Pacific are approximately 2 times higher than in the eastern Pacific, which is in line with corresponding seawater MeHg concentrations at their respective foraging depth in these two areas (i.e., ~ 0.2 pM at 450 m in the southwestern Pacific, and 0.1 pM at 200 m at ~ 120°W on the MeHg transect) (Figure 55). This deeper enrichment in MeHg in the southwestern Pacific could be related to different hypotheses to be investigated with more attention in the future.

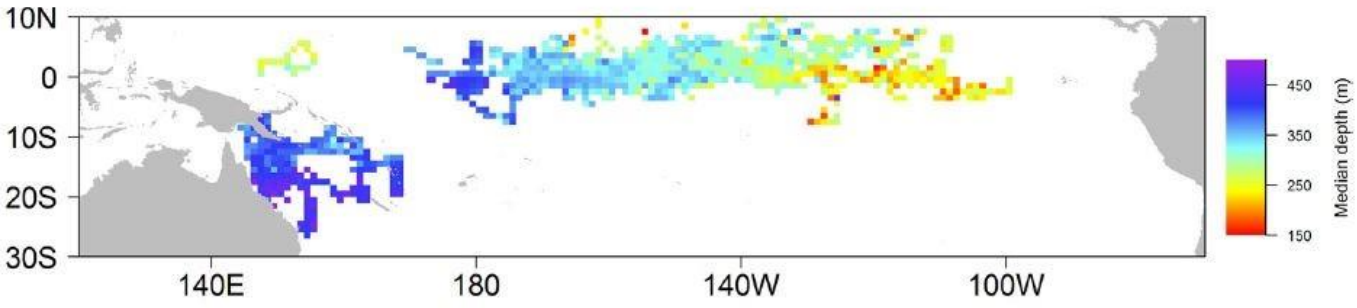

Figure 55. Median observed daytime depth of bigeye average at 1° x 1°, from Abascal et al. (2018).

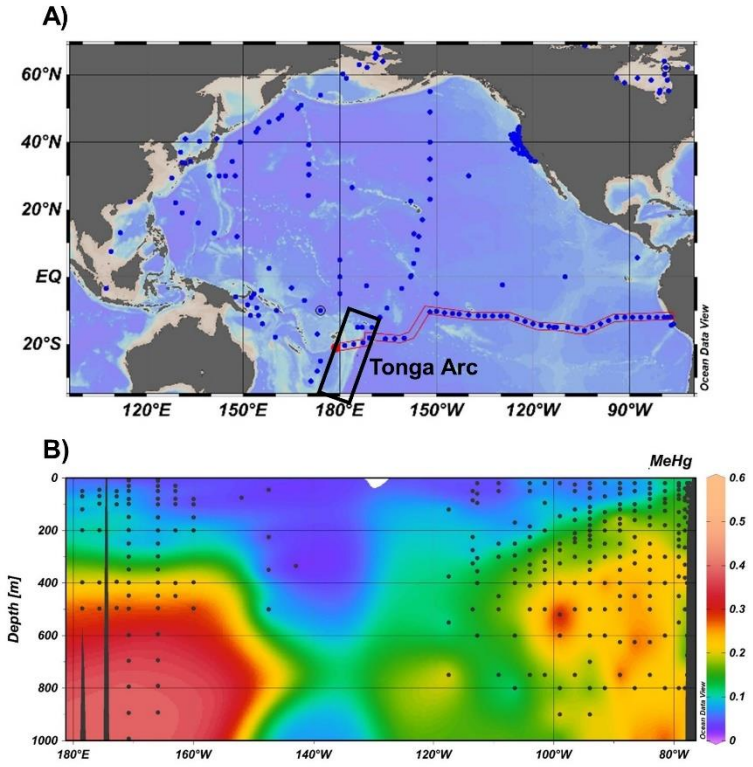

Figure 56. A) Location of the Tonga Arc (black box) and the water sampling section across the tropical South Pacific (top), and **B)** corresponding profile of dissolved methylmercury (MeHg) concentrations (pM) (bottom), from Desgranges et al. (in prep). Data used to produce this profile: eastern Pacific (Bowman et al., 2015), and western Pacific (Barbosa et al., 2022; Desgranges et al., in prep).

The first hypothesis relies on the possible influence of hydrothermal vents in the region, as the southwestern Pacific has island arc volcanism and Hg hydrothermal inputs (Figure 55 A) (Lee et al., 2015), that could lead to higher MeHg concentrations at the base of marine food webs. Hydrothermal circulation is indeed an important source of metals, including Hg, that precipitate as metal sulfides and oxides/oxyhydroxides to form metal-rich deposits near the hydrothermal vent (Bagnato et al., 2017; Tivey, 2007). To explore further the possible hydrothermal influence on deep MeHg concentrations, we tested in the global GAMM analysis of bigeye (i.e., a mesopelagic tuna that is susceptible to reflect peak of MeHg concentrations in subsurface waters) the difference of iron concentrations between NEMO-PISCES simulations with and without hydrothermal iron inputs, averaged over the upper 400 m. This proxy of hydrothermal vents was not significant in the GAMM of bigeye, suggesting i) no significant influence of hydrothermal vents on high bigeye Hg concentrations, and/or ii) an inappropriate proxy for Hg releases from hydrothermal fluids. In the Tonga Arc (Figure 55 A), hydrothermal sediments and molluscs have been showed to display high total Hg concentrations, but very low MeHg concentrations, indicating that hydrothermal fluids may increase Hg levels in the immediate vicinity of the vents by forming insoluble complexes, but with low impact on Hg methylation (Lee et al., 2015). Following these conclusions and the results of our modeling approach, we hypothesize that Hg releases from hydrothermal vents have a low impact on local MeHg net production and accumulation in pelagic marine food webs in the southwestern Pacific, although measurements of MeHg concentrations in seawater close to the hydrothermal vents remain needed to investigate further this aspect. Both Tonga (doi 10.17600/18000884) (Figure 55 A) and MERTOX ANR projects, and the thesis of Marie-Maëlle Desgranges (in progress) on marine Hg biogeochemistry should help improving our understanding on this aspect.

Another hypothesis to explain high MeHg levels in subsurface waters and high Hg concentrations in bigeye in the southwestern Pacific is the influence of dinitrogen fixers, possibly fuelling baseline Hg methylation and/or MeHg bioavailability at the base of marine food webs, as suggested in Chapter 1. Compared to other regions in the Pacific where primary production relies on NO_3^- (with particulate organic matter $\delta^{15}N$ values ~ 4 ‰), the southwestern Pacific is known to be a hotspot for N_2 fixation (particulate organic matter $\delta^{15}N$ values ~ 1 ‰), with diazotrophy showing some spatial and large seasonal variability (Bonnet et al., 2017; Garcia et al., 2007; Shiozaki et al., 2014). The predominant nitrogen-fixing cyanobacteria, *Trichodesmium*, has been recently evidenced to be a potential source of methylcobalamin (Walworth et al., 2018), the methyl derivate of vitamin B_{12}, that is suspected to act as the methyl donor in abiotic Hg methylation (Bertilsson and Neujahr, 1971; Chen et al., 2007). Subsurface peak of MeHg concentrations could therefore result from the combined effects of i) photochemical degradation of MeHg in surface waters, and ii) high MeHg net production in subsurface layers, likely enhanced by exported methylcobalamin via sinking. The role of Hg-ligand binding, in particular involving cobalt, has been suggested recently to contribute significantly to abiotic methylation mechanisms in oligotrophic waters of the southwestern Pacific Ocean (Munson et al., 2018). In our global spatial study, we explored this diazotroph influence on tuna Hg concentrations with baseline $\delta^{15}N$ values estimated by two different biogeochemical models: MOBI, the model used at the beginning of the thesis for the temporal study in the New Caledonia-Fiji region (Chapter 1), and PISCES, the one used later in the two spatial studies (Chapters 3 & 4). While including baseline $\delta^{15}N$ values estimated by MOBI slightly improved the optimal GAMM of bigeye, with high bigeye Hg concentrations in the southwestern Pacific explained by low baseline $\delta^{15}N$ values, baseline $\delta^{15}N$ values estimated by PISCES did not provide the same good statistical results. We also tested the relative influence of N_2 fixation rates estimated by PISCES, yet it did not allow revealing either a significant influence of diazotrophy on high bigeye Hg concentrations in the southwestern Pacific. These contrasted GAMM results for bigeye likely rely on the parametrization discrepancies between MOBI and PISCES, in particular, on the differential consideration and estimation of anthropogenic nitrogen deposition (characterized by an approximate isotopic signature of -4 ‰) in the two models that may lead to large differences of estimated baseline $\delta^{15}N$ values (e.g., in the southwestern Pacific, baseline $\delta^{15}N$ is estimated at ~ 4 ‰ by PISCES, and at ~ 2 ‰ by MOBI) (Figure 56). To date, a multi-model $\delta^{15}N$ inter-comparison study remains needed to better understand and quantify the global changes of the nitrogen cycle and their impact on primary production and MeHg production in the ocean. Moreover, laboratory experiments are necessary to investigate further the possible link between cobalamin production by diazotrophs in surface waters and abiotic Hg methylation through methylcobalamin.

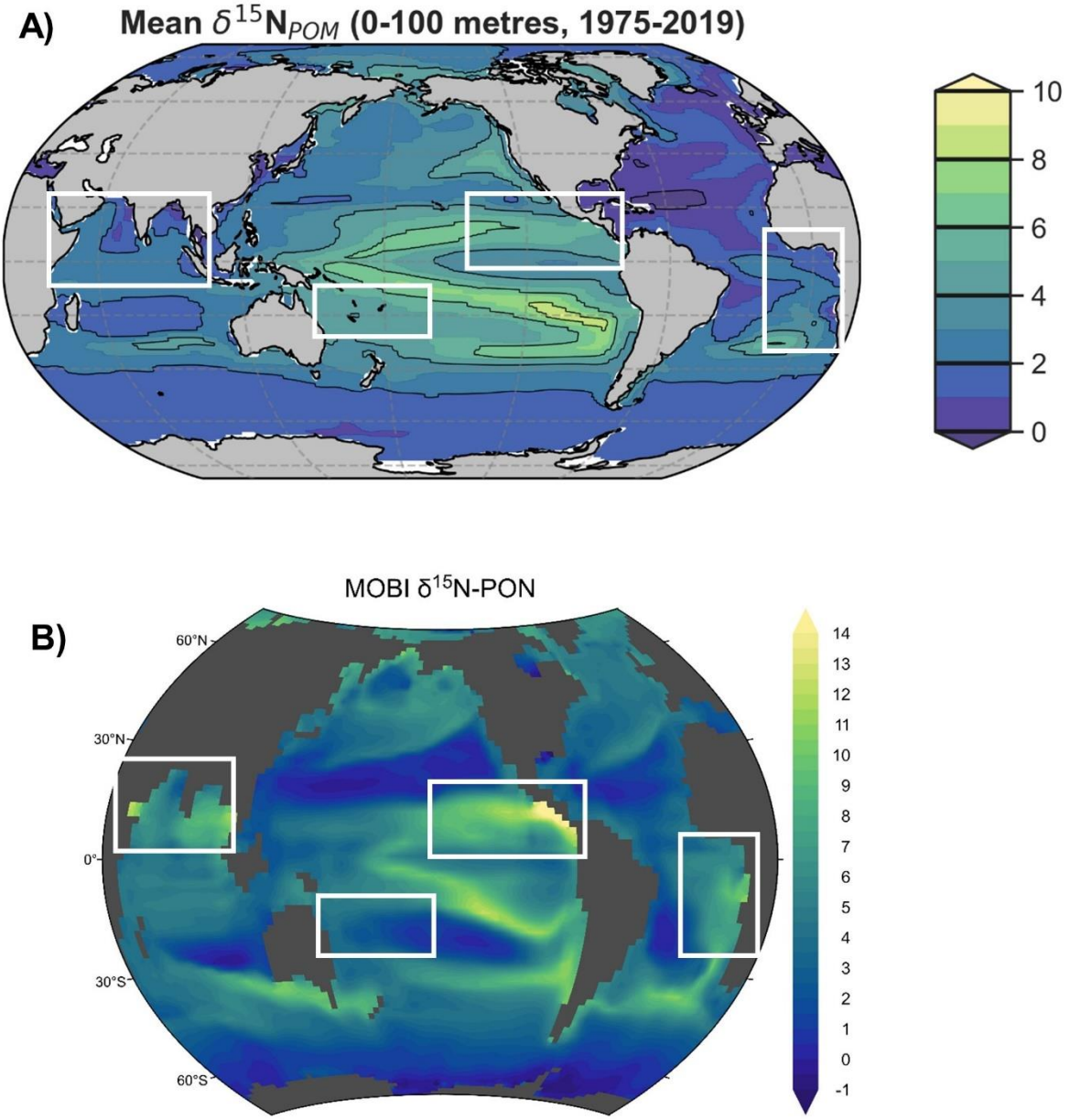

Figure 57. Isoscapes of nitrogen stable isotopes ($\delta^{15}N$, ‰) estimated in particulate organic matter by **A)** PISCES, and **B)** MOBI models. In both model, particulate organic matter include large and small sinking particulates (detritus), but exclude live phytoplankton and zooplankton. White boxes indicate the ocean areas where PISCES and MOBI predict major different baseline $\delta^{15}N$ estimates in the tropical ocean.

The limited importance of trophic processes to explain the spatial variability of tuna mercury concentrations

In this thesis, we showed that tuna foraging depth was a key driver to explain the variability of Hg concentrations among species and oceans. The importance of this ecological factor has already been documented in pelagic top predators in different ocean regions (Blum et al., 2013; Choy et al., 2009; Houssard et al., 2019), yet still unclear was the relative importance of confounding trophic versus baseline biogeochemical processes. High Hg concentrations in tunas exhibiting a deeper vertical habitat could indeed result from deeper preys enriched in Hg and/or with a higher trophic level, than preys in surface. Ferris and Essington (2014) attempted to determine whether the length of the food chain or differential MeHg sources in the water column could explain the difference in Hg concentrations in tunas from the equatorial Pacific regions, and finally concluded on the difficulty of interpreting these results without a reliable estimate of trophic position values. In this thesis, the use of tuna ecological data in our GAM(M) analysis alongside the exploration of global compound-specific amino acid $\delta^{15}N$ data in tunas indicated that the spatial variability of tuna Hg levels was mainly explained by the vertical and horizontal spatial variability of MeHg bioavailabilty in the water column, and was poorly related to trophic effects (Chapters 1, 3 and 4). These results are in accordance with the fact that Hg incorporation in phytoplankton (i.e., MeHg bioconcentration) represents the largest Hg increase in marine food webs, with Hg concentrations in phytoplankton up to 100 000 times higher than in ambient waters (Schartup et al., 2018). Conversely, MeHg levels at the top of pelagic top predators are approximately 600 times higher than at the base of the food web, if we consider a mean MeHg concentration of 1 $ng.g^{-1}$ weight wet (ww) in phytoplankton (Gosnell and Mason, 2015; Schartup et al., 2018; Zhang et al., 2020), and a mean Hg concentration of 0.6 $\mu g.g^{-1}$ ww (i.e., ~ 2 $\mu g.g^{-1}$ dry weight) in tropical tunas (Chapter 4). The sharp increase in phytoplankton compared to the rest of the food web confirms that changes of MeHg at the base of marine food webs are likely to induce larger spatial variability in top predators than the length of the food webs, as already documented in a meta-analysis of Hg levels in pelagic food webs (Wu et al., 2019).

Estimations of trophic processes

In our modeling approach, the exploration of the relative importance of trophic effects on tuna Hg concentrations relied on the combined use of bulk tuna $\delta^{15}N$ values corrected by baseline $\delta^{15}N$ model estimates (by MOBI or PISCES). This allowed taking into account the known spatial variability of the baseline isotopic signature that often limits the use of bulk $\delta^{15}N$ values in a consumer when estimating its trophic position in ecological studies. Yet, such consideration of the nitrogen baseline effects to explore trophic processes remains controversial for different reasons. First, to overcome the difficulty of obtaining precise tissue to diet trophic discrimination factors, we considered relative tuna trophic levels (i.e., tuna $\delta^{15}N$ values - estimated baseline $\delta^{15}N$ values), as done in other large-scale trophic ecology studies in tunas (Pethybridge et al., 2018a). Secondly, different isotopic turnover rates of ^{15}N between particulate organic matter (~ weeks, Dore et al., 2002) and tunas (~ 6 months, Madigan et al., 2012) could influence our results, although we used 6-month averages of baseline $\delta^{15}N$ model outputs to overcome this possible issue. Moreover, we used baseline $\delta^{15}N$ model estimates averaged over the upper surface layer (100 m for PISCES, and 130 m for MOBI), which may not reflect the higher baseline $\delta^{15}N$ values in deeper waters (Hannides et al., 2013), where bigeye, and to a lesser extent yellowfin, are known to forage. Finally and as explained previously, baseline $\delta^{15}N$ values estimated by

PISCES and MOBI are quite variable in some regions (as symbolized by the box boxes in Figure 56), which may raise questions about the reliability of our baseline-corrected tuna $\delta^{15}N$ values. To overcome the potential issues associated to the use of baseline-corrected tuna $\delta^{15}N$ values when exploring trophic effects, we also used amino acid $\delta^{15}N$ values measured in a hundred of tuna samples in the global ocean. Compound-specific amino acid $\delta^{15}N$ techniques represent advantages for trophic ecology studies as they allow deriving more accurate estimates of trophic positions (Choy et al., 2015; Lorrain et al., 2015b). Yet, these techniques are costly and cannot be applied to thousands of tuna samples, thus we could not include trophic position estimates in our modelling approach. Moreover, they remain uneasy to interpret given the variability and difficulties to measure them, and there is still no consensus on which source and trophic amino acids to consider when estimating trophic position (e.g., Houssard et al., 2017; Le-Alvarado et al., 2021; Troina et al., 2021 that use different combinations of amino acids to estimate trophic positions, either only phenylalanine or lysine, either an average of 3 or more amino acids). Nevertheless, the parallel exploration of amino acid $\delta^{15}N$ values measured in yellowfin and bigeye at the global scale confirmed our hypothesis of low trophic influence on tuna Hg concentrations (SI Appendix G, Figure S4), therefore validating our estimation methods of trophic and baseline processes at large spatial scales in our modeling approach.

Implications for mercury concentrations in pelagic food webs

Although trophic processes are likely of low importance to explain the spatial variability of Hg concentrations in tunas, the link between tuna Hg concentrations and bioavailable dissolved MeHg concentrations implies that Hg concentrations in tuna preys vary similarly with MeHg concentrations in seawater, given that Hg accumulates in organisms mainly through dietary intake. Tunas, in particular bigeye, are thought to display vertical movement patterns to exploit more efficiently prey organisms (Brill et al., 2005; Fuller et al., 2015), but as opportunistic feeders, they likely also feed at different depths in the water column. Tunas are also suspected to feed on a variety of mid-trophic micronekton preys, including shallow (those residing above 200 m), vertically-migrating (those that move between shallow and 500 – 600 m), and deep (inhabiting waters > 200 m permanently) preys, although yellowfin and bigeye have been shown to preferentially feed on epipelagic scombrid and mesopelagic paralepidid fishes, respectively, at the global scale (Duffy et al., 2017). To date, only few studies have documented Hg levels in micronekton species (Annasawmy et al., 2022; Brewer et al., 2012), calling for more investigation to better understand Hg transfer along marine pelagic food webs.

In addition to documenting Hg accumulation processes along marine food webs, the combined use of Hg data in tunas and low trophic level organisms offers research perspectives for modeling Hg fluxes in pelagic ecosystems through end-to-end models. Combining upper trophic level models (e.g., Apex Predators ECOSystem Model, APECOSM, Maury, 2010) to ocean general circulation and biogeochemistry models (e.g., NEMO-PISCES), these end-to-end models would indeed provide valuable information to document the impact on upper trophic levels of global biogeochemical changes in ocean (e.g., changes in phytoplankton iron uptake, Tagliabue et al., 2020). In the coming years, Hg concentrations in tuna and micronekton species are planned be integrated in upper trophic level models, which could represent a first step in modeling Hg fluxes from seawater to marine top predators.

The overlooked waterborne uptake of methylmercury?

Finally, given the importance of the vertical and horizontal variability of MeHg in seawater versus the more limited influence of trophic processes governing spatial variability of tuna Hg, one could argue that our results may support the alternative possibility of a complementary contribution of waterborne MeHg uptake through gills, adding up to a dietary uptake, as already suggested in different studies. Recently, Barbosa et al. (2022) revealed i) a steep relationship between dissolved MeHg levels and Hg concentrations in muscle and blood of tunas, and ii) higher Hg levels in blood than in muscle in tuna species exhibiting a deeper vertical habitat (Figures 53 B & 57). Furthermore, Cossa et al. (1994) hypothesized that diffusion of dissolved gaseous dimethyl-Hg (which accounts for about half of total MeHg at depth) through the gills could be a significant pathway for MeHg accumulation, in addition to dietary intake. Experimental studies (mostly involving freshwater fishes) on waterborne MeHg uptake showed that MeHg concentrations in muscle responded linearly to dissolved MeHg concentrations, also highlighting a significant contribution, though not dominant, of waterborne MeHg uptake (Boddington et al., 1979; Hall et al., 1997). Finally, Wang et al. (2011) found that fish MeHg direct uptake through the gills was controlled by swimming speed and respiration rates. To support their high metabolic performance, tunas display physiological adaptations of their oxygen transport system (i.e., large gill surface area, thin blood-water barrier, and small water to branchial capillarity diffusion distance), which support ventilation volumes 5 to 10 times higher than those of other teleost and enable over 50 % O_2 extraction efficiencies (compared to 25 – 33 % in other fishes) (Brill and Bushnell, 2001; Bushnell and Jones, 1994). These physiological modifications could possibly enhance the direct uptake of MeHg through gills compared to other marine species. Further experimental and field studies, e.g., including measurement of Hg concentrations in gills, could help elucidate the species-specific traits related to diffusion of dissolved water compounds in Hg accumulation in fish and its relative contribution relative to dietary MeHg uptake.

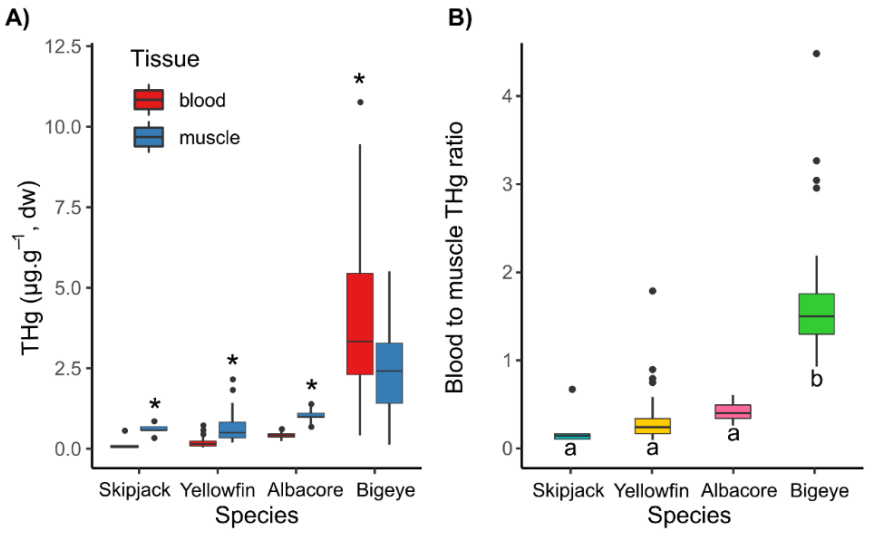

Figure 58. Boxplots of **A)** total mercury concentrations (THg, µg.g^{-1}, dw) in muscle and blood tissue, and **B)** blood to muscle THg ratio in bigeye, yellowfin, albacore and skipjack in the southwestern Pacific, from Barbosa et al. (2022). * indicates significant differences between tissues and 'a' and 'b' letters indicate significant different groups.

Capturing the anthropogenic influence on tuna mercury levels at different spatial and temporal scales

The influence of past, current and future anthropogenic mercury releases on tuna mercury concentrations

In this thesis, we revealed for the first time a link between increasing anthropogenic Hg emissions into the atmosphere from Asia in the late 1990 and the beginning of 2000s, and concomitant increasing Hg concentrations in epipelagic tunas in the northwestern Pacific (Chapters 2, 3 and 4). In other areas of the global ocean, our temporal investigation revealed long-term stable Hg concentrations in tunas over the last decades (Chapters 2 & 4), contrasting with both increasing Hg trends reported in yellowfin and bigeye in the central north Pacific (Drevnick et al., 2015; Drevnick and Brooks, 2017), and decreasing Hg concentrations found in bluefin in the North Atlantic Ocean (Lee et al., 2016). The apparent stability of Hg concentrations in tropical tunas at the global scale also contrasts with specific regional atmospheric trends of Hg emissions, concentrations and deposition (i.e., decrease in North America and Europe, and increase in Asia). At the global scale, there is still no consensus on atmospheric trends, but long-term tuna Hg concentrations differ with both the overall decline in atmospheric Hg in the northern hemisphere since the 1970s reported by Zhang et al. (2016) (Figure 58 A), and with global increasing Hg emissions since 1990s estimated by Streets et al. (2019b). We assumed that these discrepancies between temporal Hg data in tunas and the atmosphere likely result from i) different response times between the surface ocean (years), the subsurface ocean (years to decades), and the atmosphere, and ii) the accumulated burden of legacy anthropogenic Hg in the subsurface ocean. A global box model study indeed showed that a complete elimination of anthropogenic Hg emissions (from 2016 on) should lead to an immediate 10 % decline in the surface ocean, followed by a subsequent gradual decline, with 65 % of the initial loading remaining in 2100, as a result of a continuous legacy Hg supply from the subsurface ocean (Figure 58 B) (Amos et al., 2013). Combined all together, our results suggest that i) the cumulated massive anthropogenic Hg releases from Asia in the recent decades have led to higher Hg concentrations in surface tunas at the local scale of the northwestern Pacific, but that ii) the reduction of anthropogenic Hg inputs to the environment from North America and Europe will take years to decades before tuna Hg levels start measurable dropping in the global ocean. These findings shed light on the impact of anthropogenic Hg releases on human exposure to Hg through the consumption of tunas. In the context of the Minamata Convention, the time lag between stable tuna Hg concentrations and decreasing atmospheric Hg emissions and deposition makes it all the more pressing to control and reduce Hg emissions as early as possible.

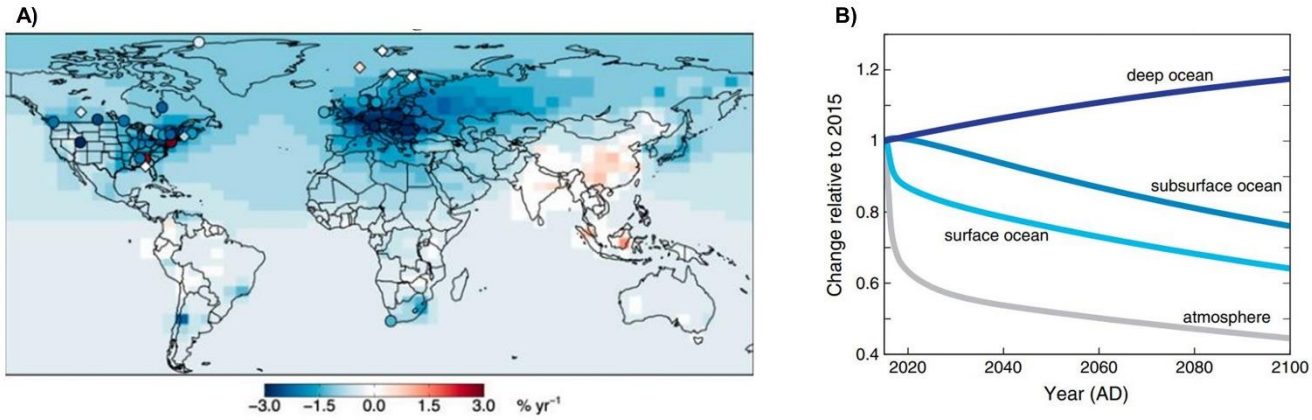

Figure 59. A) Trends in atmospheric mercury elemental concentrations from 1990 to present, from Zhang et al. (2016). Circles and diamonds are observations, and the background shows the trends computed in the GEOS-Chem model driven by the revised 1990 and 2010 anthropogenic emissions inventories. **B)** Change in reservoir masses relative to 2015 under a scenario of zero primary anthropogenic emissions after 2015, from Amos et al. (2013).

Given the expected different lifetimes of Hg in the different reservoirs, a global, continuous and complementary monitoring of Hg in the atmosphere, seawater, and marine biota is requested and crucial to assess the effects of legacy and recent anthropogenic Hg releases, and correctly evaluate the effectiveness of the reduction emissions policies. Attention should be paid in particular to the northwestern Pacific, given the massive cumulated Hg emissions from Asia in the last decades (Streets et al., 2019a), and the contrasted recent trends of atmospheric Hg monitoring in both remote and urban sites of East Asia (Fu et al., 2015; Nguyen et al., 2019; Tang et al., 2018). In this region, our time series of skipjack Hg ends in 2007, more recent samples are therefore needed to investigate the effects of the recent air pollution control policies on tuna Hg levels. Moreover, high-resolution Hg data in epipelagic and mesopelagic tuna species along the Asian coasts and in the open ocean would be valuable to investigate at fine scale the influence of changing anthropogenic Hg emissions on the vertical and horizontal variability of dissolved MeHg concentrations in coastal and offshore waters of this area.

The limits of evaluating the influence of anthropogenic mercury releases with atmospheric mercury model estimates

In this thesis, we used atmospheric Hg^0 concentrations estimated by the GEOS-Chem to investigate the link between anthropogenic Hg emissions into the atmosphere and tuna Hg concentrations. It is arguable that Hg net deposition (i.e., dry deposition + wet deposition – reemission to the atmosphere) is a more relevant proxy as deposition is commonly recognized to be the primary pathway of Hg inputs to oceans (Horowitz et al., 2017; Selin et al., 2007). Nevertheless, Zhang et al. (2019) showed that Hg gas exchange over the ocean is poorly constrained due to the lack of direct flux measurements. We therefore choose not to rely on net deposition results but rather on atmospheric Hg^0 concentrations, whose spatial distribution is well constrained (Travnikov et al., 2017). Moreover, a recent study using the stable isotope composition of total Hg in seawater and marine biota reveals

that global atmospheric Hg^0 uptake by the oceans is equally important as Hg wet and dry deposition (Jiskra et al., 2021). This justifies the use of Hg^0 estimates in our spatial studies to evaluate the influence of anthropogenic emissions on tuna Hg concentrations.

Also arguable is the fact that the GEOS-Chem simulation was performed using an anthropogenic emissions inventory developed for the year 2015 in the context of the latest Global Mercury Assessment (UN Environment, 2019). At the global scale, anthropogenic Hg emissions to the atmosphere showed variability in the two last decades, but the world sub-regions exhibited overall continuous temporal trends (e.g., general decrease of Hg emissions in North America and Europe versus an increase in Asia) (Streets et al., 2019b). Although our tuna samples range from 1997 to 2020, we therefore assume that the GEOS-Chem parametrization on recent years remains suitable for our spatial studies, as long as we used Hg^0 model estimates to investigate large spatial patterns, not temporal trends, of tuna Hg levels.

When discussing the impacts of anthropogenic Hg releases to tuna Hg concentrations, it is worthwhile to mention that we did not consider the potential influence of riverine inputs in our modeling approach. Riverine inputs are generally considered negligible for the global open ocean (Zhang et al., 2015), but are susceptible to deliver significant amounts of Hg in coastal areas, including anthropogenically-emitted Hg (Liu et al., 2021). While this may have low impact in areas where high atmospheric Hg releases correlate with enhanced riverine Hg inputs (e.g., along the Asian coasts), this may lead to an underestimation of the anthropogenic influence on tuna Hg concentrations in areas where Hg releases in rivers dominate atmospheric emissions. The tropical western Atlantic in particular is supposed to receive significant amounts of Hg from the Amazon River (Liu et al., 2021). In this area, although bigeye exhibit higher standardized Hg concentrations than in the eastern central Atlantic, we doubt there is a significant contribution from riverine discharges as no such spatial pattern is found in yellowfin Hg concentrations. We rather hypothesize that variable Hg concentrations in bigeye and yellowfin in the equatorial Atlantic result from differences of foraging depths and/or variable profiles of dissolved MeHg. Yet, tuna tagging data, as well as measurements of MeHg concentrations and speciation in this ocean basin remain needed to explore further this hypothesis. The eastern Indian Ocean is also supposed to receive large amounts of anthropogenic Hg from both Asian and Indonesian rivers basins (Liu et al., 2021). The higher standardized Hg concentrations observed in skipjack and yellowfin in the central north Indian Ocean could suggest a local contribution of these riverine inputs to tuna Hg concentrations, although more samples remain needed in this area and in the eastern Indian to verify this aspect. Overall, more complementary MeHg data in seawater and tuna samples from coastal regions are needed to investigate further if riverine Hg inputs significantly contribute to the marine MeHg cycle, i.e., if they are efficiently transformed into MeHg in seawater and ultimately biomagnified along marine food webs. In the context of climate change, increased precipitation intensity and incidence of extreme storm events may lead to enhanced riverine Hg export to coastal oceans, making it essential to precisely quantify the impact of rivers on the global Hg cycle.

Tunas, ocean sentinels to investigate the global mercury cycle

Tropical tunas, tools to monitor the effectiveness of the Minamata Convention

This thesis revealed that tropical tunas, combined all together, are able to reflect Hg exposure in surface and subsurface waters, integrating both local (e.g., anthropogenic Hg releases along the Asian costs), and global Hg sources over different spatial and temporal scales. Moreover, we recently revealed similar spatial patterns of tropical tunas Hg concentrations in both white muscle and blood tissues, the latest being supposed to reflect a short exposure time (Bearhop et al., 2000), which highlights the pertinence of tuna muscle tissue as biological archive to investigate the spatial variability of Hg levels in oceans (Barbosa et al., 2022). These different outcomes indicate that tropical tunas can be used as marine sentinels of Hg pollution in tropical and subtropical pelagic ecosystems, and can therefore provide valuable information for the implementation of large-scale Hg bio-monitoring efforts when assessing the effectiveness of reduction emission measures, as requested by the Minamata Convention.

The vast majority of the tuna samples used in this thesis were collected onboard or during the landing of commercial fishing vessels. This technique provides a considerable gain of time, effort, and cost for scientists in charge of sample collection. Yet, this implies that the spatial and temporal coverage, as well as the fishing gear and technique, depend solely on the fishermen and fishing companies, and therefore explains why some ocean regions are poorly covered in our spatial studies. In the Indian Ocean in particular, while industrial fisheries (dominated by purse seine) intensively exploit tuna stocks in the western region around the Seychelles archipelago, artisanal and/or semi-artisanal fisheries (i.e., gillnet, handline, trolling, and coastal longline) dominate along the coasts of Yemen, Oman, Pakistan, India, Sri Lanka, and Indonesia (IOTC, 2020). This, coupled to the fact that there is no collaboration yet with these coastal countries make it more difficult to access samples in these areas. Furthermore, our sampling strategy can induce variability in tuna length resulting for different fishing gears selecting preferentially certain tuna fish sizes. In the eastern Pacific Ocean for instance, fishing companies target principally surface tunas with purse seine, i.e., mainly skipjack, but also yellowfin and juvenile bigeye (IATTC, 2021), explaining why we have mainly small bigeye individuals in this area. In other areas (e.g., Reunion island, the southwestern Pacific), fishermen preferentially target adult yellowfin and bigeye in deeper waters with longlines. Although our length- (or age-) standardization approach allows taking into account this spatial variability of fishing gears and tuna length among samples, it is important to keep in mind the biological and ecological consequences of this sampling bias when exploring Hg accumulation in tunas.

During this thesis, it was initially planned to also investigate Hg concentrations in albacore, a commercially harvested pelagic species distributed throughout most tropical and temperate oceans. Yet, given the low spatial coverage of albacore samples (n = 900 but at a low spatial resolution, Figure 59 A), we could not explore high-resolution spatial patterns of Hg concentrations in the global ocean, nor the underlying bioaccumulation processes, as we did for tropical tunas. A rapid investigation of age-standardized Hg concentrations (at 3 years) in albacore suggests intermediate Hg concentrations between epipelagic species (i.e., skipjack and yellowfin) and the mesopelagic bigeye (ANOVA & Tukey, $p < 0.05$) (Figure 59 B). At tropical latitude, albacore likely exhibit a distinct diel vertical pattern similar to bigeye, occupying shallower warmer waters at night, and deeper cooler waters below the mixed

layer depth during the day; while in temperate latitudes, albacore are suspected to remain in shallower waters almost all of the time (Williams et al., 2015). Further investigation on albacore Hg concentrations would be valuable for understanding processes governing Hg accumulation in this species, and for assessing the potentiality of albacore as a fourth sentinel of the vertical and horizontal variability of MeHg concentrations in oceans.

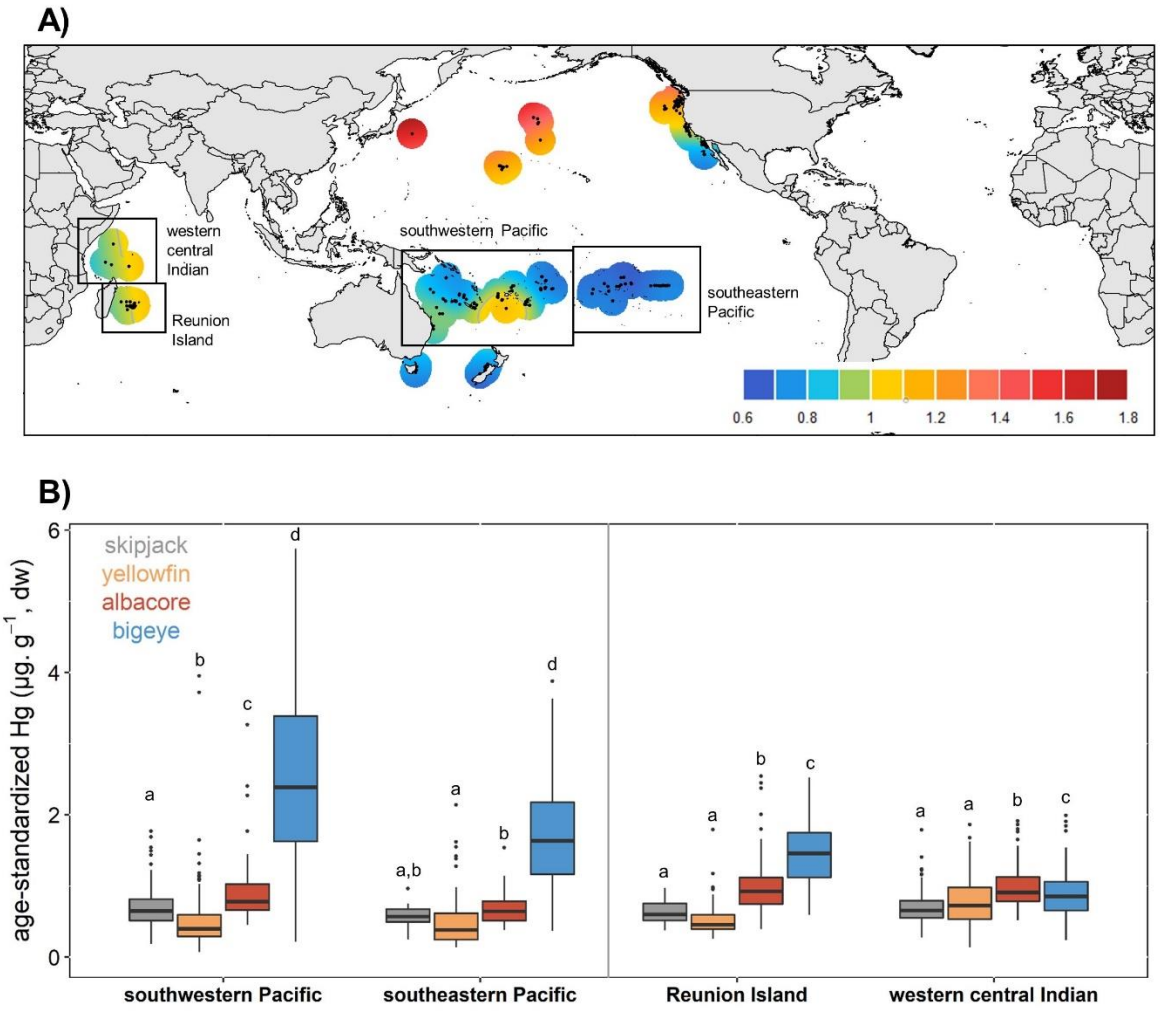

Figure 60. **A)** Smoothed spatial contour maps of age-standardized mercury (Hg) concentrations (µg.g^{-1}, dw) in albacore. Caution should be used when interpreting the spatial pattern of these concentrations in the Indian Ocean as the spatial GAM in this ocean basin has a low score and creates an artificial longitudinal gradient. A larger spatial coverage in West Indian and North Pacific Oceans remain needed to properly document the spatial variability of albacore Hg concentrations in these two ocean basins. **B)** Boxplot comparing age-standardized Hg concentrations (µg.g^{-1}, dw) in skipjack (grey), yellowfin (orange), albacore (red), and bigeye (blue) in different regions of the Pacific and Indian Oceans where samples for the four species are available. The letters show significant differences among tuna species within each ocean region. No albacore Hg concentrations from the Atlantic Ocean are available in our global database.

Tunas, possible biological archives to get new insight on the marine mercury cycle in the global ocean in the context of climate change

Disentangling the main factors governing total Hg concentrations in tunas, this thesis contributes to a better understanding of the global Hg cycle in the ocean, and raises major questions about the mechanisms of marine MeHg production, the resilience of ocean ecosystems to anthropogenic Hg releases, and the climate-related changes of the global Hg cycle in oceans. Until recently, current Hg analytical tools offered limited molecular resolution and throughput to capture, characterize, and quantify complex *in situ* biogeochemical processes operating at ultra-trace levels. Yet the recent development of CSIA of organometallic compounds now opens a new source of knowledge about tracing their environmental behavior (Masbou et al., 2015a), allowing the isotopic measurement of both the carbon ($\delta^{13}C$) and Hg ($\delta^{202}Hg$, $\Delta^{199}Hg$) atoms embedded in the MeHg molecule. Part of the MERTOX project is the measurement of these CSIA signatures to investigate further the links between organic matter and MeHg formation. Mercury stable isotope values were measured on more than 500 tuna muscle samples from the global ocean and should provide new insights to address the question of MeHg formation and degradation pathways (Renedo et al., in prep). Selecting tuna samples to be analysed, and producing the first smoothed contour maps of tuna Hg stable isotopes were also part of this thesis research. Furthermore, the comparison of tuna MeHg $\delta^{13}C$ values with baseline $\delta^{13}C$ isoscapes of marine organic matter (e.g., PISCES) should help improving our understanding of i) possible preferential sites for Hg methylation in oceans and/or continuous/discontinuous MeHg production, and ii) possible spatial variability of the biogeochemical mechanisms involved in MeHg production (Point et al., in prep).

These innovative tools could also offer new perspectives to investigate how climate change can affect MeHg concentrations in marine food webs. In the Northern Humboldt current system off Peru for instance, where El Niño Southern Oscillation induces climate forcing, the combined analysis of Hg stable isotopes, total Hg concentrations, and $\delta^{15}N$ values in marine avian top predators, alongside biogeochemical model estimates, revealed concomitant reduced MeHg formation (due to the deepening of the oxycline) and degradation (due to reduced productivity, carbon export, and remineralization) processes during El Niño events, leading to stable seabird MeHg concentrations over time (Figure 60) (Renedo et al., 2021). In the Arctic, $\Delta^{199}Hg$ values in marine biological samples showed the influence of sea ice on Hg photodegradation (Point et al., 2011), and documented the effect of climate change on the Hg cycle (Masbou et al., 2015b). Similar studies using our global tuna tissue bank should allow investigating the climate-induced changes of MeHg formation and degradation in pelagic marine food webs of tropical ecosystems. Bulk muscle $\delta^{13}C$ signature in tunas has been evidenced to record major changes of the global carbon cycle from 2000 to 2015, capturing not only the Suess effect (i.e., fossil fuel-derived and isotopically light carbon being incorporating into marine ecosystems), but also profound changes at the base of marine food webs, whether on a global scale or in the southwestern Pacific (Lorrain et al., 2020). In parallel, we showed stable Hg concentrations in tropical tunas in the New Caledonia-Fiji region between 2001 and 2018 (Chapter 1). Measuring the $\delta^{13}C$ signature in tuna MeHg using the same continuous and long-term temporal series in the southwestern would be therefore valuable to explore further how the MeHg cycle is locally impacted by climate-induced changes of the carbon cycle.

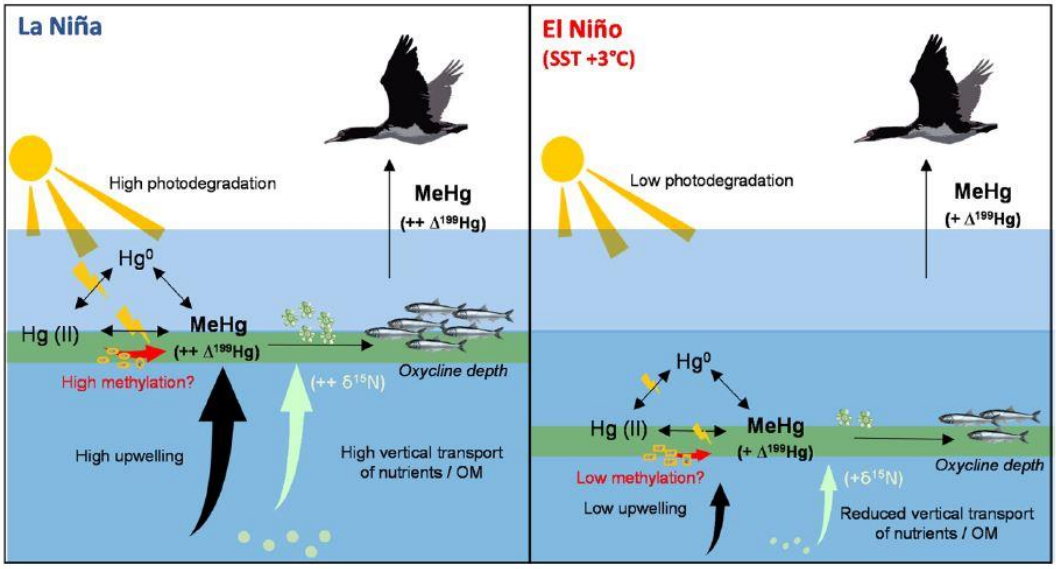

Figure 61. Schematic figure illustrating the value of mercury (Hg) stable isotope (Δ^{199}Hg) to explore the dominant Hg processes during contrasted El Niño Southern Oscillation events, from Renedo et al. (2021). During La Niña (left panel), the conditions of higher supply of nutrient may favor productivity, potentially enhancing in situ microbial methylation/demethylation of Hg in the oxygen minimum zone off Peru. However, because the oxycline is shallower, the extent of methylmercury (MeHg) photodemethylation would be high (leading to higher Δ199Hg values). Conversely, during El Niño, lower nutrient supply and remineralization may reduce microbial Hg methylation rates, and, as the oxycline is much deeper, MeHg photodegradation processes would be inhibited. Both processes (MeHg formation and MeHg degradation) seem to be compensated, leading to stable MeHg concentrations in the Peruvian food web during extreme El Niño Southern Oscillation events.

Overall, the relevance of tuna muscle samples as monitoring tools of the effectiveness of the Minamata Convention, and the research perspectives resulting from the development of new analytical methods (e.g., δ^{13}C, δ^{202}Hg, Δ^{199}Hg in MeHg) illustrate the research potential extent of our global tuna Hg dataset. This global compilation benefited from the IMBER CLIOTOP program (Climate Impact on Top Predators) and the associated gold mine of already collected and preserved tuna samples with corresponding metadata, which had already allowed addressing major ecological questions in tunas (Logan et al., 2020; Lorrain et al., 2020; Pethybridge et al., 2018a). In the framework of this thesis, new international collaborations were made to increase the spatial and temporal coverage of tuna Hg data in the global ocean. In the equatorial Atlantic, an annual tuna sampling has been set up during the PIRATA research cruises (https://doi.org/10.18142/14), which should help documenting both annual variability and long-term temporal trends of tuna Hg in this area.

Are tunas safe to eat?

In this thesis, we provided the first assessment of global-scale and high-resolution spatial patterns of observed Hg concentrations in tropical tuna species, showing highly variable Hg concentrations among species and regions. In addition to contributing to a better understanding of the global marine Hg cycle, this work also addresses important social issues in terms of food safety. We indeed provided maps revealing the potential risks associated with tuna consumption according to the geographical origin, and highlighted that among tropical tunas, only bigeye, from the three oceans, exhibited Hg concentrations exceeding the food safety guidelines of 1 $\mu g.g^{-1}$ (wet weight) (WHO and UNEP Chemicals, 2008). Yet, we deliberately chose not to make any recommendation of tuna consumption, given the complexity of the processes driving Hg toxicity (e.g., dose and frequency of Hg consumed, and age or developmental stage of the person exposed), the physiological responses associated to human Hg exposure, and the nutritional benefits of tunas that may counterbalance Hg toxicity. This was also not the scope of the thesis.

Tropical tunas are of high commercial importance as they account for more than 90 % of the global tuna fisheries, supporting a globalised international industry, but also the livelihoods and employment of local communities and fishermen who depend on them (FAO, 2018). In terms of food and nutrition security, they provide a major source of proteins, essential fatty acids, vitamins and minerals, especially for coastal and island populations (Di Bella et al., 2015; Sirot et al., 2012). Discouraging the consumption of tunas in such regions could have significant nutritional and economic consequences for local populations, and it is therefore necessary to assess the potential risk of Hg exposure associated with tuna consumption, alongside the nutritional value of tunas, and the social and economic context of a given region. In Pacific Island countries and territories for instance, tunas have been identified as key food resources for good nutrition to complement declining coastal resources in a context of high levels of diabetes and obesity, while taking into account their Hg content (Bell et al., 2015). In New Caledonia, the public health department of the government provided to the local population weekly recommendations regarding the consumption of different fish species inhabiting the New Caledonian waters, including tunas, taking into account the different Hg burden in each species, and the age or the developmental stage of the person exposed (Table 4). Benefit-risk assessments, taking into account Hg, omega-3 and mineral elements contents, of tuna species should be done for different people categories to improve our knowledge on tunas' nutritional value, as already done for other marine species (Sardenne et al., 2020; P. Wang et al., 2019).

Another avenue of research in terms of food safety is the antagonism between Hg and selenium, that has been widely documented experimentally (Gailer et al., 2000; Ohi et al., 1976) and in wildlife (M. Li et al., 2020; Yang et al., 2008). Selenium is a metalloid included in the composition of proteins that prevent certain cardiovascular diseases and may counteract the effects of MeHg. Recent studies in seabirds, marine mammals, and billfishes suggest that MeHg detoxification pathway implies the *in vivo* transformation of MeHg-cysteine complexes into selenocysteinate $[Hg(Sec)_4]$ complexes, which are in turn biomineralized into inert inorganic Hg selenide (HgSe) (Manceau et al., 2021a, 2021b, 2021c). To date, no such MeHg detoxification mechanism has been demonstrated in tunas, and the general Hg-selenium antagonism remains poorly understood in these pelagic species. Different studies reported selenium in excess molar of Hg in tuna muscle, suggesting general healthy profile of tunas,

with selenium sequestering Hg, thereby reducing Hg toxicity (Kaneko and Ralston, 2007; Kojadinovic et al., 2007). During this thesis and in the framework of a M.Sc internship (Antoine Le Gohalen), we started exploring the Hg-selenium antagonism in tropical tunas, compiling data from the existing literature alongside newly acquired selenium concentrations in tuna samples of our global database that were already analysed in total Hg concentrations. In the southwestern Pacific Ocean (New Caledonia), we also compiled Hg and selenium concentrations in other pelagic (e.g., billfishes), and coastal (e.g., snappers) species to explore further the nutritional value of different fish species of the region.

Table 4. Weekly dietary guidelines of fish species inhabiting the waters off New Caledonia, including tunas (orange), to reduce risks of mercury exposure, adapted in English from the Government of New Caledonia (2019).

	Marlins, swordfish	Bigeye tuna	Spanish mackerel, snapper	Yellowfin and albacore tunas	Lagoon fishes
Children 10 – 40 kg	avoid	avoid	once a week	once a week	without restriction
Pregnant women 50 – 80 kg	avoid	avoid	once a week	once a week	without restriction
Other adults 50 – 80 kg	less than once a week	once a week	twice a week	three times a week	without restriction

Children: one portion = 75 g
Adults (including pregnant women): 1 portion = 150 g.

Conclusion

This thesis provides the first global and high-resolution assessment of spatial and temporal patterns of Hg concentrations in tropical tunas. Through a global and multidisciplinary approach, we highlighted the combined importance of i) marine biogeochemical processes leading to variable MeHg levels in seawater, ii) tuna foraging depth, and iii) anthropogenic Hg releases, which further advances our understanding of both the distribution of Hg levels in tuna and the critical processes driving global Hg cycling. This work raises important questions about the mechanisms of marine MeHg production, the resilience of ocean ecosystems to anthropogenic Hg releases, and the climate-related changes of the global Hg cycle in oceans. Furthermore, this thesis revealed that tropical tunas reflect Hg exposure in pelagic ecosystems, which confirms they are good bio-indicators for Hg monitoring in oceans, and thus represent relevant management tools to address the main challenges of the Minamata Convention. We therefore further demonstrated the power of long-term biological monitoring in pelagic top predators to reveal complex mechanisms at the base of marine food webs, and the importance of ecological and biological knowledge of the considered species to properly interpret Hg concentrations in tunas. We believe similar multidisciplinary and global modeling approach on other marine emblematic species could benefit to the general understanding of the global marine Hg cycle. Most importantly, this thesis offers several avenues of research that we believe deserve further investigation. Figure 61 presents some of these research perspectives that i) have to be continued in the coming years, ii) are currently under investigation by our team, and iii) will be further explored after this thesis.

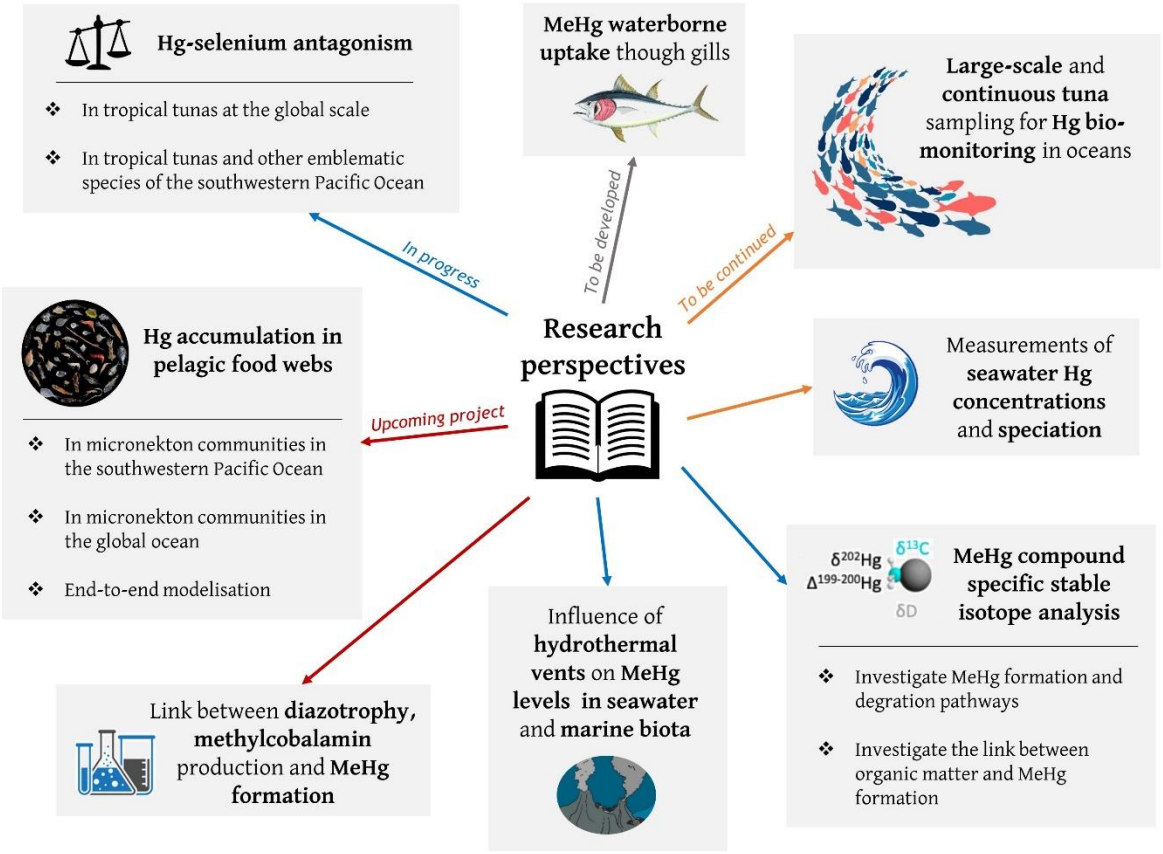

Figure 62. Schematic figure of the thesis perspectives regarding the global mercury (Hg) cycle and methylmercury (MeHg) formation and accumulation along marine food webs. Arrows show the work that are actually in progress (blue), that need to be continued (orange), that are planned in the coming years (red), and that should be further developed (grey).

Supplementary information

Appendix A

Supplementary Information for General Introduction

Table S1. Literature review of the studies investigating total mercury concentrations (THg) in muscle tissues of four tuna species. *n*: number of tuna individuals; dw: dry weight; wet: wet weight. When available, the type of fish length is specified: FL: fork length; CFL: curved fork length; TL: total length; SL: standard length.

Ocean (site)	*n*	Sampling year(s)	Fish length (cm) mean ± sd (range)	Fish weight (kg) mean ± sd (range)	THg (µg.g^{-1}, dw) mean ± sd (range)	THg (µg.g^{-1}, ww) mean ± sd (range)	MeHg/THg (%) mean ± sd (range)	Water (%) mean ± sd (range)	Reference
Bigeye									
Atlantic	121	2005 – 2007	141 ± 32 FL (70 – 200)	55.5 ± 33.2 (6.0 – 137.0)	not available	0.898 ± 0.466 (0.324 – 3.133)	not available	not available	Chen et al., 2011
Atlantic	7	not available	not available	38.9 (35.0 – 43.0)	not available	0.27 ± 0.01	71.0 ± 4.0	not available	Yamashita et al., 2005
Atlantic	30	2001	121 ± 27 (60 – 167)	not available	not available	0.750 ± 0.198 (0.344 – 1.290)	not available	not available	Besada, 2006
Atlantic (Ivory Coast)	90	not available	not available	not available	not available	0.226 ± 0.065	not available	not available	Mathias et al., 2014
Atlantic (Azores)	15	2011	not available	10.6 ± 0.8	not available	0.139 ± 0.021	not available	not available	Torres et al., 2016
Atlantic (Brazil)	30	2015	83 ± 18 FL (54 – 139)	13.0 ± 9.0 (2.9 – 51.0)	not available	0.545 ± 0.339 (0.095 – 1.748)	not available	not available	Lacerda et al., 2017
Atlantic (Morocco/Mauritania)	3	2019	not available	not available	not available	0.904	not available	not available	Garcia-Vazquez et al., 2021
Indian (east)	110	2005 – 2007	130 ± 31 FL (53 – 198)	41.1 ± 26.6 (1.0 – 110.0)	not available	0.679 ± 0.231 (0.217 – 1.880)	not available	not available	Chen et al., 2011
Indian (western central)	27	2014 – 2015	87 ± 46 FL	not available	not available	0.339 ± 0.291	not available	72.8 ± 2.6	Bodin et al., 2017
Indian (southern)	126	2012 – 2017	not available	58.5 ± 39.6 (10.6 – 120.0)[a]	not available	0.222 ± 0.128 (0.045 – 0.529)[a]	not available	not available	Handayani et al., 2019
Andaman Sea	8	1975	102 ± 29 TL (56 – 148)	20.9 ± 16.7 (3.0 – 55.0)	not available	0.114 ± 0.066 (0.027 – 0.223)	not available	not available	Menasveta and Siriyong, 1977
Indian (Bay of Bengal)	1	2007	52 TL	2.0	not available	0.201	not available	not available	Sompongchaiyakul et al., 2008
Pacific	30	not available	not available	59.4 (41.0 – 99.0)	not available	0.980 ± 0.340	71.0 ± 5.0	not available	Yamashita et al., 2005

Ocean (site)	*n*	Sampling year(s)	Fish length (cm) mean ± sd (range)	Fish weight (kg) mean ± sd (range)	THg (µg.g^{-1}, dw) mean ± sd (range)	THg (µg.g^{-1}, ww) mean ± sd (range)	MeHg/THg (%) mean ± sd (range)	Water (%) mean ± sd (range)	Reference
Pacific (Hawaii)	104	1971	not available	57.2 ± 18.1 (21.3 – 101.6)	not available	0.580 ± 0.130 (0.300 – 0.870)	not available	not available	Boush and Thieleke, 1983
Pacific (Hawaii)	19	2004	not available	41.6 ± 14.5 (18.1 – 71.3)	not available	0.477 ± 0.162 (0.250 – 0.831)	not available	not available	Brooks, 2004
Pacific (Hawaii)	50	2006	not available	41.2 ± 20.4 (11.3 – 89.8)	not available	0.579 ± 0.216 (0.165 – 1.030)	not available	not available	Kaneko and Ralston, 2007
Pacific (Hawaii)	3	2007	127 ± 42 FL (82 – 164)	not available	not available	0.613 ± 0.175 (0.421 – 0.763)	not available	not available	Blum et al., 2013
Pacific (Hawaii)	50	2007	not available	(12 - 20)	not available	0.420[b]	not available	not available	Ferriss and Essington, 2011
Pacific (Hawaii)	24	2008	not available	43.4 ± 10.2 (16.2 – 75.0)	not available	0.626 ± 0.221 (0.259 – 1.211)	not available	not available	Choy et al., 2009
Pacific (east)	150	2002 – 2003	not available	(2 – 12)	not available	0.250[b]	not available	not available	Ferriss and Essington, 2011
Pacific (northern and central)	75	2005 – 2006	141 ± 27 FL (81 – 200)	53.4 ± 28.1 (9.0 – 140.0)	not available	0.929 ± 0.668 (0.158 – 3.324)	70.0 ± 14.0 (39 – 100)	not available	Chen et al., 2014
Pacific (Fiji)	3	not available	103 ± 17 (86 – 120)	28.3 ± 13.9 (13 – 40)	not available	0.533 ± 0.260 (0.280 – 0.800)	not available	not available	Kumar et al., 2004
Pacific (ARCHm)[c]	116	2001 – 2015	103 ± 25 SFL (49 – 160)	not available	not available	0.719 ± 0.478 (0.038 – 2.607)	91.0 ± 10.0[d]	70[d]	Houssard et al., 2019
Pacific (SPSGm)[c]	58	2001 – 2015	111 ± 20 SFL (68 – 175)	not available	not available	0.535 ± 0.306 (0.103 – 1.308)	91.0 ± 10.0[d]	70[d]	Houssard et al., 2019
Pacific (NPTG)[c]	14	2001 – 2015	137 ± 7 SFL (123 – 147)	not available	not available	0.912 ± 0.485 (0.212 – 2.015)	91.0 ± 10.0[d]	70[d]	Houssard et al., 2019
Pacific (PEQD)[c]	50	2001 – 2015	67 ± 19 SFL (42 – 105)	not available	not available	0.137 ± 0.081 (0.021 – 0.372)	91.0 ± 10.0[d]	70[d]	Houssard et al., 2019
Pacific (WARMm)[c]	126	2001 – 2015	77 ± 31 SFL (31 – 150)	not available	not available	0.168 ± 0.272 (0.005 – 2.815)	91.0 ± 10.0[d]	70[d]	Houssard et al., 2019
Yellowfin									
Atlantic	13	2001	120 ± 18 (96 – 145)	not available	not available	0.297 ± 0.079 (0.166 – 0.531)	not available	not available	Besada, 2006

Ocean (site)	*n*	Sampling year(s)	Fish length (cm) mean ± sd (range)	Fish weight (kg) mean ± sd (range)	THg (µg.g^{-1}, dw) mean ± sd (range)	THg (µg.g^{-1}, ww) mean ± sd (range)	MeHg/THg (%) mean ± sd (range)	Water (%) mean ± sd (range)	Reference
Atlantic (northwest)	10	not available	93 ± 3 SL	not available	not available	0.430 ± 0.085	not available	not available	Nicklisch et al., 2017
Atlantic (northwest)	47	2008 – 2011	102 ± 15 CFL	20.4 ± 1.6	not available	0.304 ± 0.087 (0.044 – 0.503)	not available	72.0 ± 2.0	Teffer et al., 2014
Atlantic (northwest)	45	2003 - 2008	102 ± 3 TL[e] (79 – 120)	not available	not available	0.200 ± 0.170	not available	not available	Burger, 2011
Atlantic (Florida)	56	1999 – 2002	84 FL (60 – 134)	not available	not available	0.250 ± 0.120 (0.068 – 0.650)	not available	not available	Adams, 2004
Atlantic (Gulf of Mexico)	9	not available	104 ± 13 SL	not available	not available	0.230 ± 0.171	not available	not available	Nicklisch et al., 2017
Atlantic (Gulf of Mexico)	18	2005 - 2006	not available	not available	not available	0.190 ± 0.150	97.0 ± 0.5[f]	not available	Senn et al., 2010
Atlantic (Gulf of Mexico)	103	2002 - 2003	112 ± 17 TL (54 – 159)	not available	not available	0.180 ± 0.150 (0.070 – 0.870)	not available	not available	Cai et al., 2007
Atlantic (northeast)	10	not available	80 ± 7 SL	not available	not available	0.206 ± 0.035	not available	not available	Nicklisch et al., 2017
Atlantic (Morocco/Mauritania)	13	2019	not available	not available	not available	0.504	not available	not available	Garcia-Vazquez et al., 2021
Atlantic (Ivory Coast)	264	not available	not available	not available	not available	0.181 ± 0.046	not available	not available	Mathias et al., 2014
Atlantic (Gulf of Guinea)	11	2004	45 ± 5 FL (38 – 55)	1.2 ± 0.3 (0.8 – 1.8)	not available	0.060 ± 0.021 (0.036 – 0.090)	98.4	not available	Voegborlo et al., 2006
Atlantic (southeast)	8	not available	85 ± 23 SL	not available	not available	0.348 ± 0.101	not available	not available	Nicklisch et al., 2017
Atlantic (Brazil)	20	2009 – 2010	72 ± 28 TL (45 – 176)	6.6 ± 10.2 (1.3 – 47.6)	not available	0.120 ± 0.070 (0.030 – 0.280)	not available	not available	Moura Reis Manhães et al., 2020
Atlantic (Brazil)	52	2015	92 ± 28 FL (42 – 150)	16.8 ± 13.3 (1.3 – 60.0)	not available	0.159 ± 0.079 (0.048 – 0.500)	not available	not available	Lacerda et al., 2017
Atlantic (Brazil)	8	2004 - 2005	57 ± 21 (43 – 107)	5.7 ± 3.2 (2.5 – 12.0)	not available	0.080 ± 0.050 (0.033 – 0.172)	not available	not available	Medeiros et al., 2008
Atlantic (South Africa)	14	not available	not available	(29.0 – 50.8)	not available	0.726 ± 0.216	not available	not available	Bosch et al., 2016

Ocean (site)	*n*	Sampling year(s)	Fish length (cm) mean ± sd (range)	Fish weight (kg) mean ± sd (range)	THg (µg.g^{-1}, dw) mean ± sd (range)	THg (µg.g^{-1}, ww) mean ± sd (range)	MeHg/THg (%) mean ± sd (range)	Water (%) mean ± sd (range)	Reference
Indian	10	not available	97 ± 2 FL	not available	not available	0.245 ± 0.055	not available	not available	Nicklisch et al., 2017
Indian (Oman)	346	2007 - 2009	not available	not available	not available	0.033 ± 0.087 (0.010 – 0.570)	not available	not available	Al-Busaidi et al., 2011
Indian (western central)	5	2014 – 2015	133 ± 3 FL	not available	not available	0.375 ± 0.166	not available	72.6 ± 3.3	Bodin et al., 2017
Indian (Mozambique Channel)	20	2004	109 FL (82 – 156)	not available	0.510 ± 0.320	0.128 ± 0.080[g]	not available	75.0 ± 2.0	Kojadinovic et al., 2006
Indian (Reunion Island)	19	2004	104 FL (49 – 170)	not available	0.700 ± 0.490	0.182 ± 127[g]	not available	74.0 ± 2.0	Kojadinovic et al., 2006
Indian (Sri Lanka)	65	2017	124 ± 33 (64 – 180)	45.9 ± 13.9 (25.5 – 91.6)	not available	0.480 ± 0.350	not available	not available	Jinadasa et al., 2019
Indian (southern)	23	2012 - 2017	not available	62.4 ± 45.1 (10.6 – 120.2)[a]	not available	0.229 ± 0.151 (0.081 – 0.676)[a]	not available	not available	Handayani et al., 2019
Andaman Sea	16	1975	142 ± 22 TL (78 – 170)	41.6 ± 14.3 (7.0 – 70.0)	not available	0.144 ± 0.051 (0.026 – 0.234)	not available	not available	Menasveta and Siriyong, 1977
Indian (Bay of Bengal)	2	2007	139 TL (137 – 140)	36.5 (35 - 38)	not available	0.092 (0.061 – 0.124)	not available	not available	Sompongchaiyakul et al., 2008
Pacific (Japan)	53	2003 - 2007	not available	not available	not available	0.330 ± 0.210	81.0 ± 12.0	not available	Hisamichi et al., 2010
Pacific (north China Sea)	10	not available	97 ± 4 SL	not available	not available	0.269 ± 0.027	not available	not available	Nicklisch et al., 2017
Pacific (south China Sea)	10	not available	109 ± 9 SL	not available	not available	0.181 ± 0.042	not available	not available	Nicklisch et al., 2017
Pacific (northwest)	10	not available	100 ± 1 SL	not available	not available	0.064 ± 0.016	not available	not available	Nicklisch et al., 2017
Pacific (Hawaii)	22	1970	not available	67.6 ± 8.7 (38.8 – 97.5)	not available	0.535 ± 0.253 (0.240 – 1.320)	91.5 ± 7.0	not available	Rivers et al., 1972
Pacific (Hawaii)	100	1971	not available	45.8 ± 10.4 (10.0 – 84.4)	not available	0.220 ± 0.060 (0.090 – 0.390)	not available	not available	Boush and Thieleke, 1983

Ocean (site)	*n*	Sampling year(s)	Fish length (cm) mean ± sd (range)	Fish weight (kg) mean ± sd (range)	THg (µg.g^{-1}, dw) mean ± sd (range)	THg (µg.g^{-1}, ww) mean ± sd (range)	MeHg/THg (%) mean ± sd (range)	Water (%) mean ± sd (range)	Reference
Pacific (Hawaii)	104	1998	not available	44.9 ± 8.1 (27.2 – 70.8)	not available	0.210 ± 0.112 (0.012 – 0.679)	not available	not available	Kraepiel et al., 2003
Pacific (Hawaii)	17	2002	not available	45.3 ± 11.6 (24.8 – 66.7)	not available	0.307 ± 0.124 (0.149 – 0.570)	not available	not available	Brooks, 2004
Pacific (Hawaii)	50	2006	not available	41.1 ± 16.7 (13.2 – 76.2)	not available	0.300 ± 0.180	not available	not available	Kaneko and Ralston, 2007
Pacific (Hawaii)	50	2007	not available	(6 – 25)	not available	0.160[b]	not available	not available	Ferriss and Essington, 2011
Pacific (Hawaii)	14	2007	not available	35.7 ± 12.6 (22.5 – 70.8)	not available	0.259 ± 0.143 (0.115 – 0.642)	not available	not available	Choy et al., 2009
Pacific (Hawaii)	3	2007 – 2008	108 ± 31 FL (79 – 141)	not available	not available	0.286 ± 0.101 (0.225 – 0.402)	not available	not available	Blum et al., 2013
Pacific (Hawaii)	10	not available	117 ± 19 SL	not available	not available	0.602 ± 0.181	not available	not available	Nicklisch et al., 2017
Pacific (east)	194	2002 - 2003	not available	(1 – 44)	not available	0.190[b]	not available	not available	Ferriss and Essington, 2011
Pacific (Baja California Sur)	68	2006	74 ± 11 FL (55 – 94)	not available	0.510 ± 0.320	0.153[h]	not available	not available	Ordiano-Flores et al., 2011
Pacific (northeast)	10	not available	56 ± 2 SL	not available	not available	0.154 ± 0.026	not available	not available	Nicklisch et al., 2017
Pacific (east)	200	2006	92 ± 20 FL (61 – 146)	not available	0.980 ± 0.680	0.294[h]	not available	not available	Ordiano-Flores et al., 2011
Pacific (east)	10	not available	71 ± 4 SL	not available	not available	0.297 ± 0.176	not available	not available	Nicklisch et al., 2017
Pacific (Equator)	44	2013 - 2014	(74 – 163) TL	not available	not available	1.400 ± 1.300 (0.005 – 6.000)	not available	not available	Araújo and Cedeño-Macias, 2016
Pacific (ARCHm)[c]	282	2001 – 2015	117 ± 22 SFL (54 – 158)	not available	not available	0.196 ± 0.176 (0.016 – 1.531)	93.0 ± 7.0[d]	70[d]	Houssard et al., 2019
Pacific (SPSGm)[c]	32	2001 – 2015	120 ± 21 SFL (73 – 160)	not available	not available	0.229 ± 0.169 (0.040 – 0.678)	93.0 ± 7.0[d]	70[d]	Houssard et al., 2019
Pacific (NPTG)[c]	2	2001 – 2015	131 SFL (129 – 132)	not available	not available	0.238 (0.177 – 0.300)	93.0[d]	70[d]	Houssard et al., 2019

Ocean (site)	*n*	Sampling year(s)	Fish length (cm) mean ± sd (range)	Fish weight (kg) mean ± sd (range)	THg (µg.g^{-1}, dw) mean ± sd (range)	THg (µg.g^{-1}, ww) mean ± sd (range)	MeHg/THg (%) mean ± sd (range)	Water (%) mean ± sd (range)	Reference
Pacific (PEQD)[c]	5	2001 – 2015	81 ± 39 SFL (49 – 126)	not available	not available	0.085 ± 0.044 (0.028 – 0.134)	93.0 ± 7.0[d]	70[d]	Houssard et al., 2019
Pacific (WARMm)[c]	96	2001 – 2015	90 ± 27 SFL (43 -154)	not available	not available	0.082 ± 0.077 (0.016 – 0.578)	93.0 ± 7.0[d]	70[d]	Houssard et al., 2019
Pacific (Fiji)	22	not available	69 ± 30 (27 – 141)	15.0 ± 9.1 (2.8 – 53.0)	not available	0.113 ± 0.120 (<0.020 – 0.400)	not available	not available	Kumar et al., 2004
Pacific (Vanuatu)	2	not available	96.5 (95 – 98)	17.5 (15 – 20)	not available	< 0.020	not available	not available	Kumar et al., 2004
Pacific (Australia)	17	2006 and 2009	not available	not available	not available	0.432 ± 0.204	not available	not available	Endo et al., 2016
Pacific (New Zealand)	11	2006 and 2011	not available	not available	not available	0.330 ± 0.178	not available	not available	Endo et al., 2016
Pacific (Cook Islands)	19	2019	not available	not available	not available	0.350	not available	not available	Garcia-Vazquez et al., 2021
Pacific (southwest)	10	not available	108 ± 26 SL	not available	not available	0.239 ± 0.151	not available	not available	Nicklisch et al., 2017
Skipjack									
Mediterranean Sea (Balearic islands)	26	2017	63 ± 4 SFL (54 – 74)	5.3 ± 1.1	not available	0.137 ± 0.034	not available	not available	Chanto-García et al., 2021
Atlantic (Ivory Coast)	96	not available	not available	not available	not available	0.199 ± 0.038	not available	not available	Mathias et al., 2014
Atlantic (Azores)	53	1993 – 1994	50 FL (28 – 84)	not available	not available	0.192 (0.089 – 0.336)	94.1 (82.0 – 100.0)	not available	Andersen and Depledge, 1997
Atlantic (Azores)	15	2011	not available	3.3 ± 0.2	not available	0.040 ± 0.012	not available	not available	Torres et al., 2016
Atlantic (Brazil)	29	2009 – 2010	51 ± 11 TL 32 – 82	2.9 ± 2.8 0.6 – 16	not available	0.200 ± 0.080 (0.040 – 0.390)	not available	not available	Moura Reis Manhães et al., 2020
Red Sea	12	2015	not available	not available	0.318 ± 0.026	0.089[j]	not available	not available	Al-Najjar et al., 2019

Ocean (site)	*n*	Sampling year(s)	Fish length (cm) mean ± sd (range)	Fish weight (kg) mean ± sd (range)	THg (µg.g^{-1}, dw) mean ± sd (range)	THg (µg.g^{-1}, ww) mean ± sd (range)	MeHg/THg (%) mean ± sd (range)	Water (%) mean ± sd (range)	Reference
Indian (Oman)	102	2007- 2009	not available	not available	not available	0.063 ± 0.104 (0.010 – 0.386)	not available	not available	Al-Busaidi et al., 2011
Indian (western central)	13	2014 – 2015	57 ± 10 FL	not available	not available	0.205 ± 0.112	not available	71.9 ± 2.2	Bodin et al., 2017
Indian (Reunion Island)	39	2004	68 FL (41 – 85)	not available	0.670 ± 0.260	0.149 ± 0.075[g]	not available	71.0 ± 3.0	Kojadinovic et al., 2006
Indian (Bay of Bengal)	29	2007	46 ± 10 TL (37 – 77)	1.7 ± 1.5 (0.8 – 6.4)	not available	0.110 ± 0.153 (0.005 – 0.625)	not available	not available	Sompongchaiyakul et al., 2008
Pacific (Hawaii)	20	not available	not available	not available	not available	0.380 (0.270 – 0.520)	not available	not available	Rivers et al., 1972
Pacific (Hawaii)	10	2006	not available	8.6 ± 1.3 (6.4 – 10.4)	not available	0.340 ± 0.100	not available	not available	Kaneko and Ralston, 2007
Pacific (Hawaii)	3	2008	75 ± 5 FL (70 – 80)	not available	not available	0.329 ± 0.068 (0.258 – 0.394)	not available	not available	Blum et al., 2013
Pacific (Fiji)	12	not available	45 ± 1 (45 – 47)	2.6 ± 0.4 (1.8 – 2.8)	not available	0.059 ± 0.044 (<0.020 – 0.160)	not available	not available	Kumar et al., 2004
Albacore									
Mediterranean Sea	127	1999	not available	6.3 ± 1.5 (4.0 – 8.7)	not available	1.170 ± 0.230 (0.840 – 1.450)	91.3 ± 9.1 (77.1 – 100.0)	not available	Storelli et al., 2002
Mediterranean Sea (Balearic islands)	26	2017	75 ± 9 SFL (62 – 91)	7.5 ± 2.4	not available	0,200 ± 0,060	not available	not available	Chanto-García et al., 2021
Mediterranean Sea (Adriatic Sea)	137	2003	not available	(4.4 – 7.7)	not available	1.56 (0.88 – 2.34)	not available	not available	Storelli and Marcotrigiano, 2004
Atlantic	24	2001	69 ± 11 (51 – 95)	not available	not available	0.216 ± 0.096 (0.118 – 0.564)	not available	not available	Besada, 2006
Atlantic (northwest)	15	2008 – 2011	98 ± 6 CFL	18.1 ± 0.9	not available	0.455 ± 0.144 (0.294 – 0.683)	not available	72.0 ± 2.0	Teffer et al., 2014
Atlantic (Azores)	46	1993 – 1994	96 FL (87 – 117)	not available	not available	0.370 (0.218 – 1.132)	92.1 (85.8 – 97.2)	not available	Andersen and Depledge, 1997
Atlantic (Azores)	14	2019	not available	not available	not available	0.168	not available	not available	Garcia-Vazquez et al., 2021
Atlantic (Gulf of Guinea)	3	2019	not available	not available	not available	0.362	not available	not available	Garcia-Vazquez et al., 2021

Ocean (site)	*n*	Sampling year(s)	Fish length (cm) mean ± sd (range)	Fish weight (kg) mean ± sd (range)	THg (µg.g^{-1}, dw) mean ± sd (range)	THg (µg.g^{-1}, ww) mean ± sd (range)	MeHg/THg (%) mean ± sd (range)	Water (%) mean ± sd (range)	Reference
Atlantic (South Africa)	197	2013 – 2014	87 ± 8 FL	not available	0.958 ± 0.443	0.288 ± 0.133[j]	not available	not available	Chouvelon et al., 2017
Indian (Reunion Island)	128	2013 – 2014	102 ± 5 FL	not available	1.708 ± 0.629	0.512 ± 0.189[j]	not available	not available	Chouvelon et al., 2017
Indian (Seychelles)	118	2013 – 2014	96 ± 5 FL	not available	1.403 ± 0.406	0.421 ± 0.122[j]	not available	not available	Chouvelon et al., 2017
Indian (western central)	30	2014 – 2015	97 ± 5 FL	not available	not available	0.478 ± 0.140	not available	69.8 ± 2.7	Bodin et al., 2017
Pacific (Japan)	61	2003 – 2007	not available	not available	not available	0.420 ± 0.120	82.0 ± 10.0	not available	Hisamichi et al., 2010
Pacific (northeast)	91	2003	69 ± 9 FL (51 – 86)	6.5 ± 2.2 (3.1 – 11.6)	not available	0.137 ± 0.048 (0.027 – 0.260)	not available	63.5 ± 3.5 (56.9 – 72.4)	Morrissey et al., 2005
Pacific (Hawaii)	20	2006	not available	22.6 ± 3.9 (16.3 – 29.9)	not available	0.500 ± 0.240	not available	not available	Kaneko and Ralston, 2007
Pacific (ARCHm)[c]	132	2001 – 2015	93 ± 7 SFL (65 – 108)	not available	not available	0.334 ± 0.162 (0.053 – 1.389)	not available	70[d]	Houssard et al., 2019
Pacific (SPSGm)[c]	39	2001 – 2015	97 ± 6 SFL (86 – 106)	not available	not available	0.279 ± 0.116 (0.143 – 0.579)	not available	70[d]	Houssard et al., 2019
Pacific (WARMm)[c]	2	2001 – 2015	88 SFL (87 – 89)	not available	not available	0.262 (0.245 – 0.279)	not available	70[d]	Houssard et al., 2019
Pacific (South Australia)	20	2001 – 2015	60 ± 12 SFL (48 – 92)	not available	not available	0.183 ± 0.080 (0.098 – 0.326)[c]	not available	70[d]	Houssard et al., 2019
Pacific (New Zealand)	26	2001 – 2015	65 ± 12 SFL (43 – 90)	not available	not available	0.180 ± 0.058 (0.110 – 0.302)[c]	not available	70[d]	Houssard et al., 2019
Pacific (New Zealand)	6	1990	95 – 97[k]	not available	not available	0.49	not available	71.0 ± 4.0 (63.5 – 74.8)	Vlieg et al., 1993
Pacific (New Zealand)	10	1988	64 (63 – 65)	4.5 (4.0 – 4.7)	not available	0.170 (0.140 – 0.210)	not available	not available	Love et al., 2003
Pacific (Fiji)	31	not available	73 ± 15 (41 – 100)	21.3 ± 11.1 (10 – 42)	not available	0.336 ± 0.227 (0.030 – 1.010)	not available	not available	Kumar et al., 2004
Pacific (western and central north)	115	2001 – 2006	90 ± 10 FL (67 – 118)	16.5 ± 5.6 (5.9 – 32.2)	not available	0.444 ± 0.148 (0.239 – 1.180)	67.0 ± 19.0 (32 – 100)	not available	Chen et al., 2014

[a] Data extracted from Fig. 1 of Handayani et al. (2019).

[b] Mean values estimated visually on Fig. 2 and 3 for yellowfin and bigeye respectively, in Ferriss and Essington (2011).

[c] The regions correspond to biogeochemical Longhurst provinces, modified as in Houssard et al. (2017).

[d] The proportion of MeHg relative to THg was calculated on a subset of 21 bigeye and 39 yellowfin individuals. The percent of moisture was estimated on a subset of 811 samples, combining bigeye, yellowfin and albacore samples (Houssard et al., 2019).

[e] Only 14 of the 45 yellowfin samples had length determinations (Burger, 2011).

[f] The proportion of MeHg relative to THg was determined on 3 individuals only (Senn et al., 2010).

[g] Hg concentrations in wet weight were estimated considering species- and region-specific percentage of moisture in Kojadinovic et al. (2006).

[h] Hg concentrations in wet weight were estimated considering 70% of moisture in Pacific tuna white muscle, as in Houssard et al. (2019).

[i] Hg concentrations in wet weight were estimated considering 72% of moisture, as measured in white muscle tissue of skipjack from the western Indian Ocean in Bodin et al. (2017).

[j] Hg concentrations in wet weight were estimated considering 70% of moisture, as measured in white muscle tissue of albacore in Chouvelon et al. (2017).

[k] Only 2 of the albacore samples had length determinations (Vlieg et al., 1993).

Appendix B

Supplementary Information for Material and Methods

Table S1. Summary of species- and ocean- specific growth models and parameters used to estimate fish age with fish fork length. L_∞ is the asymptotic fork length, L_1 and L_A are the mean lengths of the first age class, and the oldest age class, respectively. k is the von Bertalanffy growth coefficient, while k_1 and k_2 are growth rate coefficients of first and second stanza, respectively. α is the age relative to t_0 at which the change in growth occurs, and β is the transition rate between k_1 and k_2. b and m are parameters of the Richards growth model.

Species	**Ocean basin**	**Growth model**	L_∞ (cm)	k (yr^{-1})	k_1 (yr^{-1})	k_2 (yr^{-1})	t_0 (yr)	t_{max} (yr)	b	α (yr)	β (yr^{-1})	m	L_1 (cm)	L_A (cm)	References
Bigeye	Atlantic	Richards	179.9	0.281			-0.32		-7.185			2280.4			ICCAT, 2018
	Indian	two stanza	152.5		0.06	0.45	-4.2			6.4	3.2				Eveson et al., 2015
	Eastern Pacific	von Bertalanffy	200.8	0.33			-0.1	16							Griffiths et al., 2019
	Western Pacific	Richards	158.8	0.267			-1.836		0.617						Farley et al., 2020
Yellowfin	Atlantic	von Bertalanffy													ICCAT, 2019
	Indian	two stanza	155.7		0.184	0.78	-0.85			2.865	19.821				Dortel et al., 2015
	Eastern Pacific	von Bertalanffy	198.9	0.341			0.002	5							Griffiths et al., 2019
	Western Pacific	Richards	152.2	0.397			-0.548		0.847						Farley et al., 2020
Skipjack	Eastern Atlantic	von Bertalanffy	97.26	0.251											Hallier and Gaertner, 2006
	Western Atlantic	von Bertalanffy	94.9	0.34											Pagavino and Gaertner, 1995
	Indian	two stanza	70.5		1.41	0.35	0			0.8	18.9				Eveson et al., 2015
	Eastern Pacific	von Bertalanffy	102	0.55			-0.02	12							Griffiths et al., 2019
	Western Pacific	von Bertalanffy[a]		0.212				16[a]					25.7051	78.0308	Vincent et al., 2019
Albacore	Indian (females)	von Bertalanffy	103.8	0.38			-0.86								Farley et al., 2019
	Indian (males)	von Bertalanffy	110.6	0.34			-0.87								Farley et al., 2019

	Eastern Pacific	von Bertalanffy	112.9	0.253			-2.239	15							Griffiths et al., 2019
	Western Pacific	Logistic	102.1	0.61			1.12								Williams et al., 2012

[a] For this growth model, t_{max} is in quarter, not in year.

Table S2. Summary of tuna samples collected in the Indian, Pacific, and Atlantic Oceans, and analysed for total mercury (THg) concentrations, as well as carbon and nitrogen stable isotopes ($\delta^{13}C$ and $\delta^{15}N$). *n* = sample size; FL = fork length.

Ocean basins	*n*	FL (cm) min – max	Sampling period	Methods for THg concentrations analysis	Methods for $\delta^{13}C$ and $\delta^{15}N$ analysis
Bigeye					
Indian	227	30 – 174	2001 – 2020	a, b	p, q, r
Pacific	851	31 – 175	2001 – 2018	a, c, d	p, and not detailed
Atlantic	314	29 – 185	2002 – 2020	a, b	p, q, r, s, t
Yellowfin					
Indian	324	30 – 180	2001 – 2020	a, b, e, f	p, q, r, u
Pacific	1,614	34 – 171	2001 – 2018	a, c, d, g, h, i, j	p, v, w, and not detailed
Atlantic	494	40 – 174	1999 – 2020	a, b, k, l	p, q, r, s
Skipjack					
Indian	213	29 – 85	2001 – 2018	a, b	p, q, r, u
Pacific	661	28 – 90	1997 – 2018	a, d, h, j, m	p, w, and not detailed
Atlantic	129	25 – 76	2001 – 2020	a, k, l	p, r, s, u
Albacore					
Indian	433	74 – 118	2013 – 2014	b, n	q
Pacific	467	20 – 120	1998 – 2018	a, h, j, o	p, w

Methods and reference material for total Hg concentrations analysis

[a] Thermal decomposition, gold amalgamation and atomic adsorption detection (DMA-80, Milestone, Italy) in GET (Toulouse, France). Reference standards: TORT-3, ERM-CE464, IAEA-436, and BCR-464.

[b] Thermal decomposition, gold amalgamation and atomic adsorption detection (DMA-80, Milestone, Italy) in SFA (Victoria, Seychelles). Reference standards: large homogenized wet samples of bigeye tuna white muscle BET-M (Hg = 141 ± 4 $ng.g^{-1}$ ww) and liver BET-L (Hg = 986 ± 36 $ng.g^{-1}$ ww), as well as the certified reference material IAEA-436.

[c] Microwave acid digestion followed by inductively coupled plasma mass spectrometry using a collision cell at the University of Washington's Environmental Health Lab (Seattle, USA). Reference standards: SMR. (Ferriss and Essington, 2011)

[d] Thermal decomposition, gold amalgamation and atomic adsorption detection (DMA-80, Milestone, Italy). Reference standards: DOMR-4 and ERM-CE464. (Blum et al., 2013)

[e] Microwave acid digestion followed by cold vapor atomic absorption spectrometry (Varian 240 FS, Mulgrave, Australia). Reference standards: canned fish offal (T/07243, total Hg = 707 (469 - 946) $ng.g^{-1}$ ww), and canned crab meat (T/07279, total Hg = 106 (59 – 152) $ng.g^{-1}$ ww). (Jinadasa et al., 2019)

[f] Thermal decomposition, gold amalgamation and atomic adsorption detection (AMA 254, Altec, Czech Republic). Reference standards: TORT-2. (Kojadinovic et al., 2006)

[g] Thermal decomposition, gold amalgamation and atomic adsorption detection (DMA-80, Milestone, Italy) at the University of North Carolina Wilmington (Wilmington, USA). Reference standards: DORM-4 and DOLT-5.

[h] Thermal decomposition, gold amalgamation and atomic adsorption detection (DMA-80, Milestone, Italy) in Stony Brook University (NY, USA). Reference standards: DORM-4.

[i] Microwave acid digestion followed by atomic absorption spectrophotometer (AAS, PerkinElmer Analyst 100) coupled to a hybride generator in cold vapor (PerkinElmer MHS-10). Reference standards: IAEA-407. (Ordiano-Flores et al., 2011)

[j] Hot plate acid digestion (HNO_3-H_2O_2) followed by cold vapor atomic fluorescence spectroscopy (HG-450, Hiranuma, Japan) in Center for Marine Environmental Studies (CMES), Ehime University, Japan. Reference standards: ERM-CE464, DOLT-4, and NIST-SRM1566b.

[k] Acid digestion followed by cold vapor atomic absorption spectrometry in FWC-DEP laboratory (Tallahassee, FL, USA). Reference standards: DOLT-2 and DOLT-3. (Adams, 2004)

[l] Thermal decomposition, gold amalgamation and atomic adsorption detection (DMA-80, Milestone, Italy) in FWC-FWRI (Melbourne, FL, USA). Reference standards: DOLT-3, DOLT-4, DORM-2, and TORT-2.

[m] Hot plate acidic digestion (HNO_3-H_2O_2) followed by cold vapor atomic fluorescence spectroscopy in IRD Noumea (New Caledonia). Reference standards: DOMR-4.

[n] Thermal decomposition, gold amalgamation and atomic adsorption detection (AMA 254, Altec, Czech Republic). Reference standards: IAEA-142. (Chouvelon et al., 2017)

[o] Hot plate acidic digestion followed by cold vapor atomic fluorescence spectroscopy. (Morrissey et al., 2005)

Methods and reference materials for $\delta^{15}N$ and $\delta^{13}C$ analysis

[p] Costech elemental analyser coupled to an isotope ratio mass spectrometer (Thermo Scientific Delta Advantage with a Conflo IV interface) at Union College (New York, USA). Reference standards: EA Consumables sorghum flour, in house acetanilide ($\delta^{13}C$ = -34.07 ‰, $\delta^{15}N$ = -0.96 ‰), IAEA-N_2 ammonium sulfate, and IAEA-600 caffeine.

[q] Elemental analyser (Flash EA 1112, Thermo Scientific, Milan, Italy) coupled to an isotope ratio mass spectrometer (Delta V Advantage with a Conflo IV Interface, Thermo Scientific, Bremen, Germany) at the LIENSs stable isotope facility (La Rochelle, France). Reference standards: USGS-24, IAEA-CHE, IAEA-600, IAEA-N_2, and IAEA-NO_3^-. (Sardenne et al., 2016)

[r] Europea Scientific ANCANT 20-20 Stable Isotope Analyzer with ANCA-NT Solid/Liquid Preparation Module (PDZ Europa LTd., Crewz, UK). (Ménard et al., 2007)

[s] Continuous flow mass spectrometer (Delta V+ with a conflo IV interface, Thermo Scientific, Bremen, Germany) coupled to an elemental analyzer (Flash EA 2000, Thermo Scientific, Milan, Italy) at the Pôle Spectrométrie Océan (Plouzané, France). Reference standards: USGS-61, USGS-62, USGS-63 for carbon and nitrogen.

[t] PDZ Europa ANCA-GSL elemental analyzer interfaced to a PDZ Europa 20-20 isotope ratio mass spectrometer (Sercon Ltd., Cheshire, UK) at the UC Davis Stable Isotope Facility. Reference materials: IAEA-600, USGS-40, USGS-41, USGS-42, USGS-43, USGS-61, USGS-64, and USGS-65.

[u] Continuous-flow isotope-ratio mass spectrometry (CF-IRMS) using a Europa Scientific ANCA-NT 20-20 Stable Isotope Analyzer with ANCA-NT Solid/Liquid Preparation Module (Europa Scientific). Reference standards: two laboratory standards (leucine) calibrated against 'Europa flour' and IAEA standards N1 and N2. (Kojadinovic et al., 2008).

[v] Thermo Delta mass spectrometer (IRMS) at the Center for Marine Science at the University of North Carolina Wilmington (Wilmington, USA). Reference standards: depleted glutamic acid USGS-40, and enriched glutamic acid USGS-41.

[w] On-line C-N analyser coupled with a Delta XP isotope ratio mass spectrometer at the University of Hawaii (USA). Reference standards: replicate of atmospheric nitrogen and V-PDB.

Appendix C

Lipid-free tuna muscle samples are suitable for total mercury analysis

Anaïs Médieu[1], Fany Sardenne[1], Anne Lorrain[1], Nathalie Bodin[2,3], Chloé Pazart[1], Hervé Le Delliou[1], David Point[4]

[1]Univ Brest, CNRS, IRD, Ifremer, LEMAR, F-29280 Plouzané, France
[2]Research Institute for Sustainable Development (IRD), Victoria, Mahé, Seychelles
[3]Sustainable Ocean Seychelles (SOS), BeauBelle, Mahé, Seychelles
[4]Observatoire Midi-Pyrénées, GET, UMR CNRS 5563/IRD 234, Université Paul Sabatier Toulouse 3, Toulouse, France

Published as short note in Marine Environmental Research
(https://doi.org/10.1016/j.marenvres.2021.105385)

Abstract

Tropical tunas are largely consumed worldwide, providing major nutritional benefits to humans, but also representing the main exposure to methylmercury, a potent neurotoxin that biomagnifies along food webs. The combination of ecological tracers (nitrogen and carbon stable isotopes, $\delta^{15}N$ and $\delta^{13}C$) to mercury concentrations in tunas is scarce yet crucial to better characterize the influence of tuna foraging ecology on mercury exposure and bioaccumulation. Given the difficulties to get modern and historical tuna samples, analyses have to be done on available and unique samples. However, $\delta^{13}C$ values are often analysed on lipid-free samples to avoid bias related to lipid content. While lipid extraction with non-polar solvents is known to have no effect on $\delta^{15}N$ values, its impact on mercury concentrations is still unclear. We used white muscle tissues of three tropical tuna species to evaluate the efficiency and repeatability of different lipid extraction protocols commonly used in $\delta^{13}C$ and $\delta^{15}N$ analysis. Dichloromethane was more efficient than cyclohexane in extracting lipids in tuna muscle, while the automated method appeared more efficient but as repeatable as the manual method. Lipid extraction with dichloromethane had no effect on mercury concentrations. This may result from i) the affinity of methylmercury to proteins in tuna flesh, ii) the low lipid content in tropical tuna muscle samples, and iii) the non-polar nature of dichloromethane. Our study suggests that lipid-free samples, usually prepared for tropical tuna foraging ecology research, can be used equivalently to bulk samples to document in parallel mercury concentrations at a global scale.

Keywords: methylmercury, fat content, delipidation, yellowfin, bigeye, skipjack

Graphical abstract

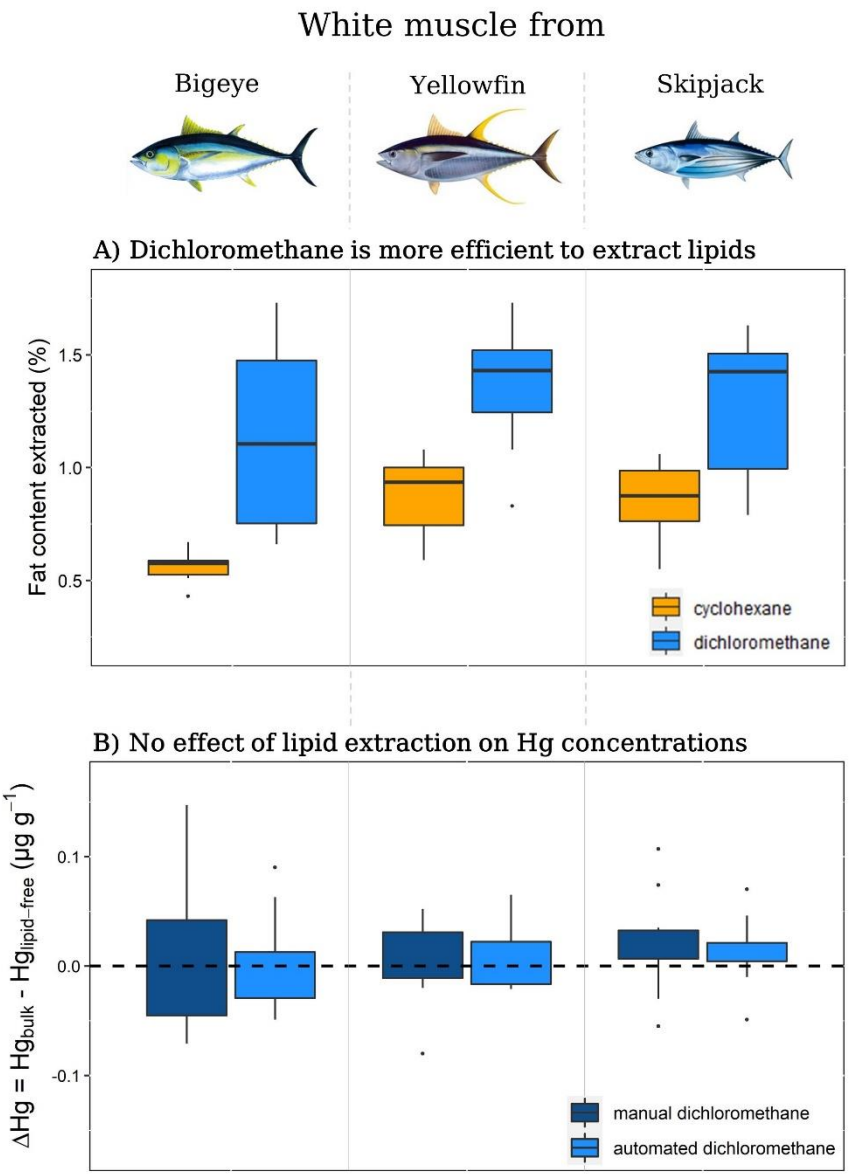

Introduction

Mercury (Hg) is a widespread heavy metal of particular concern to wildlife and human health. In oceans, it is naturally converted into methylmercury (MeHg), its organic and highest neurotoxic form, well known for its persistence and unique bioaccumulation properties in food webs (Hintelmann, 2010). Consumption of contaminated seafood is considered as the main route of human exposure to MeHg. Top predators like tunas are known to display relatively high MeHg concentrations, sometimes exceeding food safety guidelines (1 $\mu g.g^{-1}$ fresh tissue) (WHO and UNEP Chemicals, 2008) depending on the oceanic basin and the tuna species. Yet, tunas are also among the most popular marine species consumed worldwide, particularly tropical species that account for more than 90% of the global tuna fishery (FAO, 2018). In terms of food and nutrition security, they provide a major source of proteins, essential fatty acids, vitamins and minerals (Di Bella et al., 2015; Sirot et al., 2012).

Knowing their economic importance, nutritional benefits and potential impact on human health, tropical tunas have been studied broadly but at relatively small spatial scale to document their Hg exposure and characterize the processes driving Hg biomagnification along food webs (Bodin et al., 2017; Chouvelon et al., 2017; Houssard et al., 2019; Kojadinovic et al., 2006; Nicklisch et al., 2017). Complex regional interplay between physical (e.g., light intensity), geochemical (e.g., redox status), physiological (e.g., organism's length and age), and ecological factors (e.g., tuna's foraging depth) have been identified to govern Hg concentrations in these top predators (Choy et al., 2009; Houssard et al., 2019; Kojadinovic et al., 2006; Médieu et al., 2021a; F. Wang et al., 2019). Nevertheless, key global aspects remain poorly understood, in particular biogeochemical methylation/demethylation mechanisms controlling MeHg bioavailability at the base of the food web, as well as factors driving both fate and accumulation through the food web. Global studies combining Hg concentrations and ecological tracers are therefore needed to clarify these points, especially in the context of the UNEP Minamata Convention since monitoring studies in marine biota have become essential the better characterize Hg cycle and fate in oceans.

Pelagic food web structuration and functioning have been broadly investigated, mainly through the use of carbon and nitrogen stable isotopes data ($\delta^{13}C$ and $\delta^{15}N$ values) (Fry, 2006). Recently, collaborative and global studies relying upon $\delta^{13}C$ and $\delta^{15}N$ values enabled identifying broad-scale patterns of trophic structure, movements and trophodynamics of tunas in relation to environmental conditions (Logan et al., 2020; Lorrain et al., 2020; Pethybridge et al., 2018a). Based on individual records with associated metadata (i.e., fish length, fishing date and position) (Bodin et al., 2020), these collaborative and global studies also represent a gold mine of already collected and preserved samples to characterize spatial and/or temporal Hg trends in tunas.

An issue with global modern and historical datasets is that samples from different laboratories are not always processed the same way. To account for the influence of lipids on $\delta^{13}C$ values (DeNiro and Epstein, 1977) while making a single analysis for both $\delta^{13}C$ and $\delta^{15}N$ values, $\delta^{13}C$ values are either produced from i) bulk tissue and a mathematical correction (Sardenne et al., 2015), or from ii) lipid-free tissue, with lipids removed through various methods and solvents selected not to alter δ15N values. In the latter case, manual or automated (high temperature and pressure) methods are generally applied with solvents of low polarity such as dichloromethane and cyclohexane (Bodin et al., 2009; Ménard et al., 2007). While these methods do not affect $\delta^{15}N$ values and provide valuable data on lipid content, nothing is known regarding their effect on Hg content, restricting the development of

global studies on tuna Hg concentration with preserved samples prepared for tuna foraging ecology research.

Here, we investigated i) the efficiency and repeatability of two common lipid extraction methods (manual and automated) and two neutral solvents (dichloromethane and cyclohexane) on lipid content determination (experiment A), and ii) the influence of the most efficient solvent for lipid extraction on total Hg concentrations (experiment B). Experiments were carried out in three tropical tuna species, i.e., bigeye (*Thunnus obesus*), yellowfin (*T. albacares*) and skipjack (*Katsuwonus pelamis*), and on white muscle tissues, the commonly used tissue in studies investigating both trophic ecology and Hg bioaccumulation and the final storage for MeHg in fish.

Material & methods

Sample collection

All bigeye, yellowfin, and skipjack tuna samples (n_{total} = 33) were collected in the western Indian Ocean during the unloading of commercial vessels (purse seine) at Victoria port (Seychelles). To test for efficiency and repeatability of different lipid extraction protocols (experiment A), we used three individuals, one per tuna species ($n_{exp\ A}$ = 3). To test for the effect of lipid extraction on Hg concentrations (experiment B), we used 10 other individuals per tuna species ($n_{exp\ B}$ = 30), all collected from the same fishing set. For these 30 individuals, fork length (FL) was measured to the lowest cm and ranged respectively for bigeye, yellowfin and skipjack from 44 to 91 cm (62 ± 17 cm), 35 to 129 cm (70 ± 35 cm), and 34 to 64 cm (45 ± 10 cm). For both experiments, white muscle samples of around 20 g (wet weight) were collected in the front dorsal position, stored frozen at -20 ◦C, freeze-dried for 48 h with an Alpha 1–4 LD freeze-dryer (Christ, Coueron, France) and finally ground to a fine homogeneous powder using a MM400 grinder (Retsch, Eragny sur Oise, France) prior to lipid extraction and total Hg analyses.

Lipid extraction protocols

Two lipid extraction methods (manual and automated) and neutral solvents (dichloromethane and cyclohexane) were first tested on five replicates of three individuals, one per tropical tuna species, to identify the most efficient and repeatable method and solvent in extracting lipids (experiment A, $n_{exp\ A}$ = 3, Figure S1 A). The use of one single individual per tuna species allowed overcoming the potential bias related to inter-individual variability when estimating both efficiency and repeatability of the lipid extraction methods, as recommended and done in other studies testing for different lipid extraction methods (AOCS, 2017; JCGM, 2012; Sardenne et al., 2019a). All lipid extractions were done at LEMAR (Plouzan´e, France).

Manual extraction: Following the method of Ménard et al., (2007), 100 ± 4 mg of each powdered and dried aliquot were mixed with 10 mL of solvent for 1 h using a rotary shaker. The mixture of the powder and the solvent was then separated by centrifugation at 2500 rpm for 10 min at 10°C. The lipid-free powders were stored in a dry-room until total Hg analysis, while the lipid extracts were collected in a pre-weighted vial and evaporated to dryness under N_2 flow with a N-evap 111 nitrogen evaporator (OA-SYS, Berlin, USA).

Automated extraction :150 ± 10 mg of homogenized dried aliquot were extracted with 20 mL of solvent at 100°C under 1400 psi for 10 min using a ASE 350 Accelerated Solvent Extractor (Dionex, Voisins de Bretonneux, France), following the method of (Bodin et al., 2009). The lipid-free powders were stored in a dry-room until total Hg analysis, while the lipid extracts were collected in a pre-weighted vial and evaporated to dryness under N_2 flow with a N-evap 111 nitrogen evaporator (OA-SYS, Berlin, USA).

Total lipid content

For both extraction methods, lipid residuals were weighted on a Mettler Toledo MX5 analytical micro-balance (Mettler Toledo, Colombus, Ohio) to the nearest 0.001 mg to determine the total lipid content (TLC, %) of the samples, expressed on a dry weight basis (dw).

Total mercury analysis

The potential impact of lipid extraction methods on Hg concentrations was assessed on 10 individuals per tuna species, with Hg concentrations determined on both bulk and lipid-free powders (Experiment B, $n_{exp\ B}$ = 30, Figure S1 B). Total Hg concentrations were measured on powdered, dried and homogenized tissue by thermal decomposition, gold amalgamation and atomic adsorption (AMA 254, Altec, Czech Republic, Száková et al., 2004) at GET (Toulouse, France). Blanks and two biological materials, TORT-3 (lobster hepatopancreas; Hg = 292 ± 22 $ng.g^{-1}$ dw) and BCR-464 (tuna fish; Hg = 5240 ± 100 $ng.g^{-1}$ dw), covering a wide range of Hg concentrations, were routinely used every 5 – 10 samples in each analytical batch to check Hg measurement accuracy. Recovery rates (defined as the ratios of observed value by certified value) were calculated for the two certified reference materials (TORT-3: 100 ± 3 %; and BCR-464: 100 ± 2 %) and variability was below 4%. Total Hg concentrations are expressed in $\mu g.g^{-1}$ (equivalent to part per million, ppm), on a dw basis.

Statistical analysis

All statistical analyses were performed with the statistical open source R software 3.6.1 (R Core Team, 2018). We first evaluated the efficiency of both solvents (i.e., dichloromethane and cyclohexane) and methods (i.e., manual and automated) in extracting lipids with an analysis of variance (ANOVA) on TLC values (experiment A). The higher the TLC values, the higher the efficiency. Repeatability of each 3 extraction experiment was assessed per tropical tuna species using the coefficient of variation (CV, defined as the ratio of standard deviation by mean) of TLC values measured on the five replicate samples. The lower the CV, the higher the repeatability. Then, we assessed the influence of manual and automated extraction methods on total Hg concentrations with two separated paired *t*-test on ΔHg values (with ΔHg = Hgbulk – Hglipid-free) (experiment B). For these two tests, we considered all individuals ($n_{exp\ B}$ = 30 pairs of observations), no matter the species, as ΔHg values do not significantly differ between species (ANOVA, $p > 0.05$ for both methods). TLC, ΔHg values, and residuals of ANOVA were tested for normality with a Shapiro test. Observations were considered as outliers according to the "1.5 rule", i.e., if they were less that Q1 – 1.5*IQR, or greater than Q3 +

1.5*IQR, where Q1, Q3 and IQR are the lower quantile, upper quantile and inter-quantile range (defined as Q3-Q1), respectively.

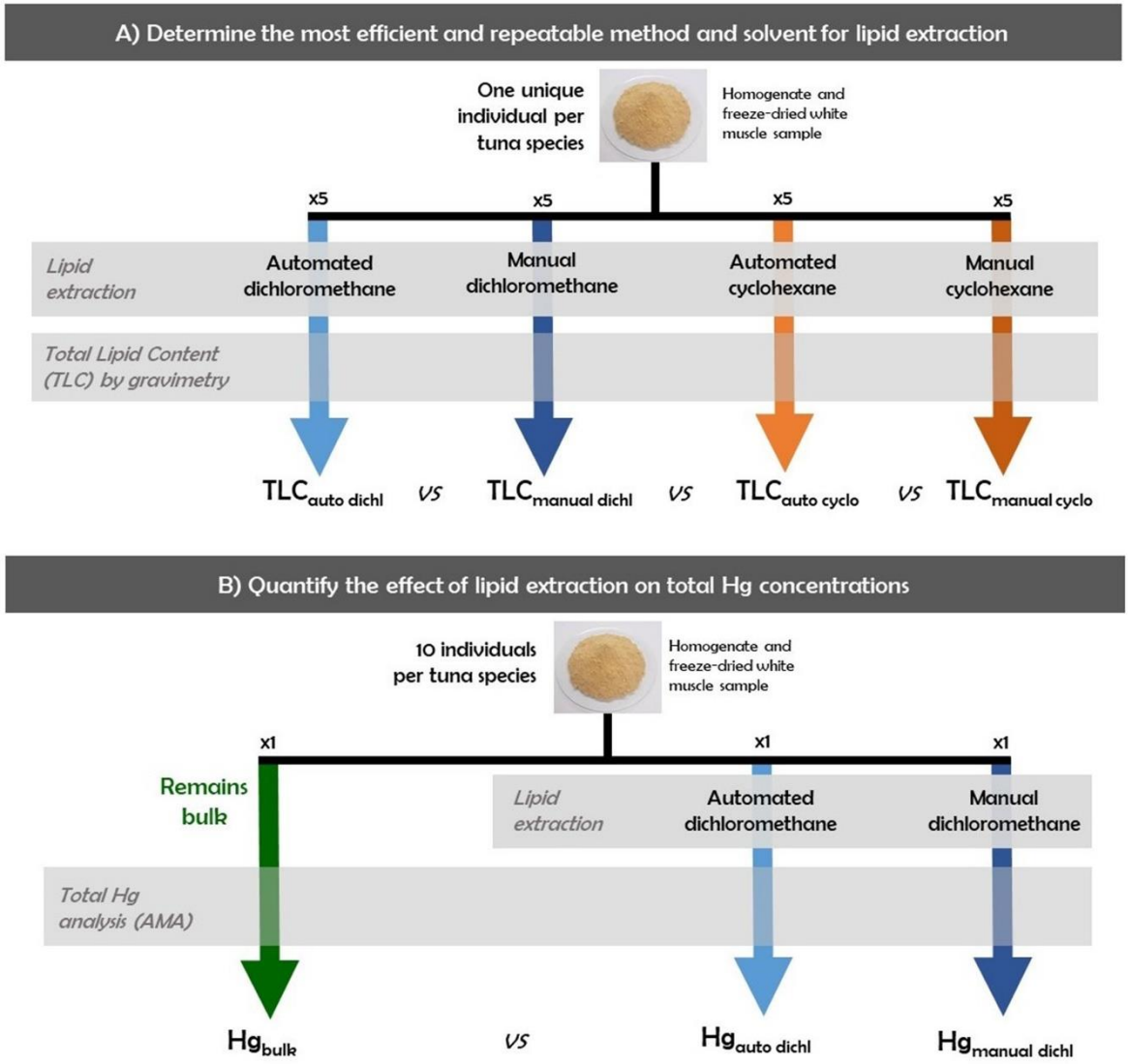

Figure S1. Outline of the two experiments testing for **A)** the efficiency and repeatability of each lipid extraction protocol (manual and automated method, and dichloromethane and cyclohexane solvent) using five replicates of the same individual per tropical tuna species; and for **B)** the influence of manual and automated method with dichloromethane on total mercury (Hg) concentrations ($n_{exp\ B}$ = 30 individuals). TLC = Total Lipid Content. See Material and methods for details.

Results & discussion

Efficiency and repeatability of lipid extraction methods and solvents

TLC values measured in white muscle varied between 0.4 and 1.7 % dw. These values are similar to levels reported in same tropical tuna species from the Indian (~ 3 %, Sardenne et al., 2016),

Atlantic (~ 6 %, Sardenne et al., 2019b) and Pacific (~ 2 %, Peng et al., 2013) Oceans, which confirms tropical tunas are lean species.

For the three tropical tuna species, TLC values were significantly higher when lipids were extracted with dichloromethane than with cyclohexane (Figure S2; ANOVA, $p < 0.01$). Dichloromethane and cyclohexane are both non-polar solvents recommended for routine analysis of lipids/fatty acids and/or prior $\delta^{13}C$ and $\delta^{15}N$ analysis cyclohexane (Bodin et al., 2009; Ménard et al., 2007). Here, the higher efficiency of dichloromethane may result from its slightly higher Snyder polarity index (3.1) compared to cyclohexane (0.2) and therefore to the fact that dichloromethane, although a neutral solvent is likely to extract some membrane polar lipids (e.g., phospholipids and sphingolipids) too, increasing TLC values. Nevertheless, this might be of minor importance regarding the protein fraction as this solvent has been shown to have negligible effects on the $\delta^{15}N$ values across tissues and tuna species (Sardenne et al., 2015).

Regarding differences between manual and automated methods, TLC values were significantly higher for bigeye and skipjack replicates for the automated extraction (Figure S2; ANOVA, $p < 0.05$). For bigeye replicates, interaction between solvent and method was also significant, showing that the efficiency of the extraction method depends on the solvent used, with automated extraction with dichloromethane being the most efficient protocol to extract lipids (Figure S2, ANOVA $p < 0.05$). Conversely, TLC values did not differ significantly between the two extraction methods for yellowfin replicates (Figure S2; ANOVA, $p > 0.05$). The higher efficiency of the automated method may be explained by its combined conditions of elevated temperature and pressure that maintain solvents near their supercritical region where they have high extraction properties (Ramos et al., 2002). This suggests that lipid extraction with automated method would be preferred over manual method. On the other hand, this automated method is twice more costly in polluting solvent, and its cleaning steps are longer compared to the manual method. Considering the low difference in extraction efficiency and the fact that is was significant only for skipjack and bigeye replicates, both manual and automated methods are relevant to extract lipids from lean tropical tuna muscle tissues.

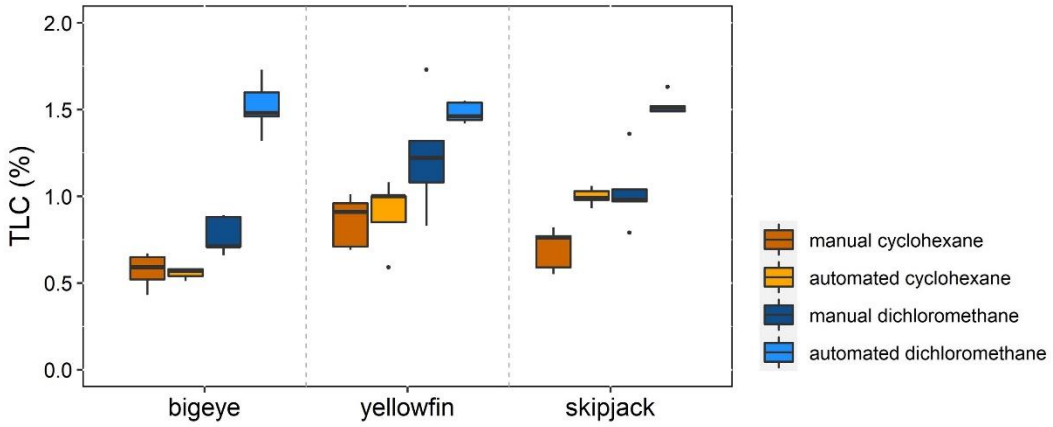

Figure S2. Boxplots of total lipid content (TLC, % dry weight) associated to the four lipid extraction protocols and measured in five replicates of each single individual per tuna species. Thick bar is the median value, points are outliers of five replicates, and the box contains 50 % of the data.

The repeatability of the different experiments varied between the protocols between 4 and 27 %, but remained overall lower than 18 % (Table S1). Acceptable repeatability often ranges between 5 and 10 %, but for lean tissues like white muscle of tropical tunas, repeatability down 20–30 % is considered acceptable too, as found in other studies (Bodin et al., 2009; Dodds et al., 2004). As expected, automated method showed generally lower CV values, as ASE 350 has been developed to reduce handling steps and to ensure increased reproducibility. This would be another argument to prefer the automated method; yet given the pros and cons arguments listed above, both manual and automated methods remain acceptable for the lipid extraction from white muscle tissue of tropical tunas.

3.2. Influence of lipid extraction on total Hg concentrations

Bulk total Hg concentrations (mean ± sd, min-max, dw) varied between tuna species (Kruskal-Wallis, $p < 0.05$), with significantly higher levels in bigeye (0.81 ± 0.47 $\mu g.g^{-1}$, 0.20–1.37 $\mu g.g^{-1}$; Dunn's test, $p < 0.05$) than yellowfin (0.38 ± 0.27 $\mu g.g^{-1}$, 0.12–1.03 $\mu g.g^{-1}$) and skipjack (0.30 ± 0.17 $\mu g.g^{-1}$, 0.12–0.61 $\mu g.g^{-1}$). Those levels and differences are similar to those reported previously in the western Indian Ocean or in both north and south Pacific Oceans for similar fish size ranges (Bodin et al., 2017; Choy et al., 2009; Médieu et al., 2021a). The highest Hg concentrations in bigeye are likely to result from confounding effects: a higher trophic position, a deeper vertical habitat giving access to mesopelagic species with higher Hg concentrations, and a longer lifespan compared to the two other tropical tunas (Choy et al., 2009; Olson et al., 2016).

Manual and automated lipid extractions with dichloromethane did not significantly affect Hg concentrations in white muscle samples of the three tuna species (Figure S3; paired *t*-test, $p > 0.05$). This agrees with Cipro et al., (2017) where no difference of Hg levels was found between bulk and lipid-free muscle samples of two marine fish (i.e., *Notothenia coriiceps* and *N. rossii*). This may be related to the particular chemical properties of MeHg in fish flesh and the polarity of the solvent used for lipid extraction. In tuna white muscle, most of total Hg (> 91 %) is in its methylated form (Bloom, 1992; Houssard et al., 2019), which is known to bioaccumulate in the protein fraction of the muscle, mostly by forming complexes with the amino acid cysteine (Amlund et al., 2007; Leaner and Mason, 2004; Manceau et al., 2021c). On the other hand, we used dichloromethane, a neutral solvent that does not affect the protein fraction by limiting the removal of proteins bound to membrane lipids (Bodin et al., 2009). Thus, by preserving the Hg-protein fraction in muscle tissues during lipid extraction, we assumed to have preserved MeHg concentrations of the samples. The absence of a significant effect of lipid extraction on Hg concentrations may be due also to the low lipid content of tropical tuna species (< 6 %), as measured in our experiment and showed in other studies (Peng et al., 2013; Sardenne et al., 2016, 2019b), and therefore to an unchanged mass balance in the samples. Finally, when discussing the effects of the different protocols tested, it is worthwhile mentioning that high temperature and pressure conditions of the automated extraction did not significantly affect total Hg concentrations neither, suggesting no thermal and pressure degradation of the total Hg pool in the samples. This confirms that MeHg is bound up tightly to the protein fraction in fish muscle tissues, where it is known to remain for a long time (Leaner and Mason, 2004).

Conclusion

This study reveals the higher efficiency of dichloromethane compared to cyclohexane to extract lipids in tropical tuna white muscle tissue, which may be attributed to its slightly higher polarity index. Automated method appeared more efficient than manual method to extract lipids, especially when used with dichloromethane, which may be attributed to the combined conditions of elevated temperature and pressure. Repeatability of all experiments were in acceptable ranges considering that we were working on lean samples.

We show no significant effect of lipid extraction with dichloromethane on total Hg concentrations in tropical tuna white muscle tissue. This may be related to i) the affinity of MeHg (i.e., the most abundant Hg chemical form in tuna muscles) to proteins, ii) the relative low lipid content in white muscle tissue of tropical tuna species, and iii) the non-polar characteristics of dichloromethane, known to efficiently extract storage lipids without affecting the protein fraction. This suggests that white muscle samples that have undergone lipid extraction with dichloromethane can be used equivalently to bulk samples to investigate Hg bioaccumulation in these pelagic top predators from the western Indian Ocean. Knowing that tropical tunas in the Atlantic, Indian and Pacific Oceans all have relatively low lipid content in white muscle tissue (< 6 %, Peng et al., 2013; Sardenne et al., 2016, 2019b), this suggests that our results might be valid at a global scale, but further studies are needed to confirm this statement. As lipid content can vary between tissues, species and oceanic basins because of differences in diet and/or in energy allocation strategies (i.e., how energy is distributed among metabolic functions), we recommend using bulk samples to infer precisely Hg concentrations in marine fish other than tropical tunas. Further studies would be particularly needed for tissues and species with high lipid content (e.g., swordfish white muscle tissue, between 20 and 40% dw, Young et al., 2010).

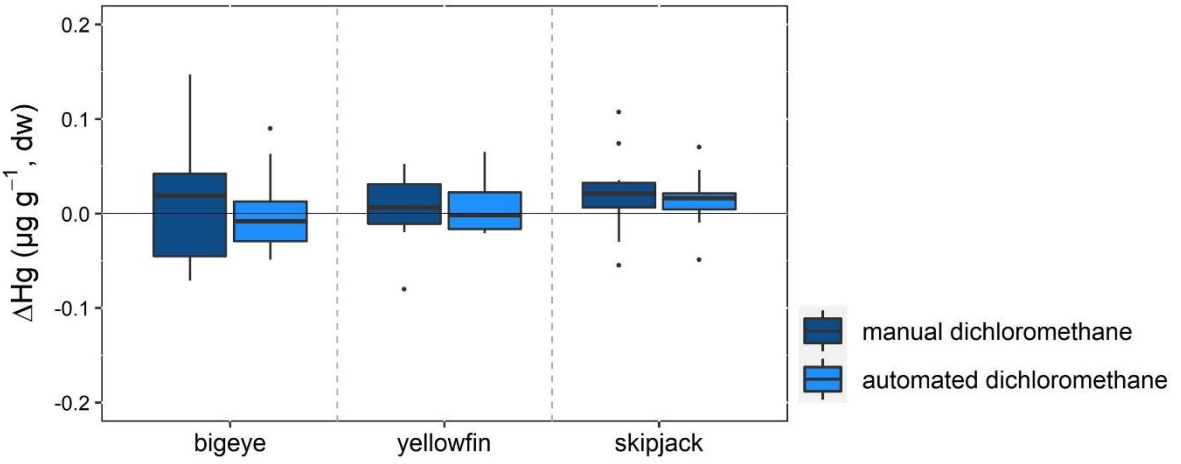

Figure S3. Boxplots of the differences of mercury (Hg) concentrations (µg.g^{-1}, dry weight) between bulk and lipid-free samples. Box colours display lipid extraction methods (manual and automated). Thick bar is the median value, points are outliers, and the box contains 50 % of the data.

Acknowledgments

We thank the fishermen and crews of the SAPMER fishing company who gave the tuna samples. We are grateful to Jean-Marie Munaron from LEMAR (Plouzané, France) for his help with lipid extractions and the access to his lab. We thank Laure Laffont from GET (Toulouse, France) for mercury analyses.

Funding: Funding was provided by ANR-17-CE34-0010, MERTOX from the French Agence Nationale de la Recherche.

Author contribution

Anaïs Médieu: Conceptualization, Methodology, Investigation, Writing – original draft. Fany Sardenne: Conceptualization, Methodology, Supervision, Writing – review & editing. Anne Lorrain: Conceptualization, Supervision, Writing – review & editing. Nathalie Bodin: Conceptualization, Methodology, Resources, Writing – review & editing. Chloé Pazart: Investigation. Hervé Le Delliou: Investigation, Resources. David Point: Conceptualization, Supervision, Resources, Writing – review & editing.

Supplementary information

Table S1. Results of experiment A, mean ± sd; CV of total lipid content (TLC, % dry weight) extracted.

	Manual extraction		Automated extraction	
	cyclohexane	dichloromethane	cyclohexane	dichloromethane
bigeye	0.6 ± 0.1; 17	0.8 ± 0.1; 14	0.6 ± 0; 5	1.5 ± 0.2; 10
yellowfin	0.9 ± 0.1; 17	1.2 ± 0.3; 27	0.9 ± 0.2; 21	1.5 ± 0.1; 4
skipjack	0.7 ± 0.1; 17	1.0 ± 0.2; 20	1.0 ± 0; 5	1.5 ± 0.1; 4

Appendix D

Supplementary Information for

Stable mercury concentrations of tropical tunas in the south western Pacific Ocean: An 18-year monitoring study

Anaïs Médieu, David Point, Aurore Receveur, Olivier Gauthier, Valérie Allain, Heidi Pethybridge, Christophe E. Menkes, David P. Gillikin, Andrew T. Revill, Christopher Somes, Jeremy Collin, Anne Lorrain

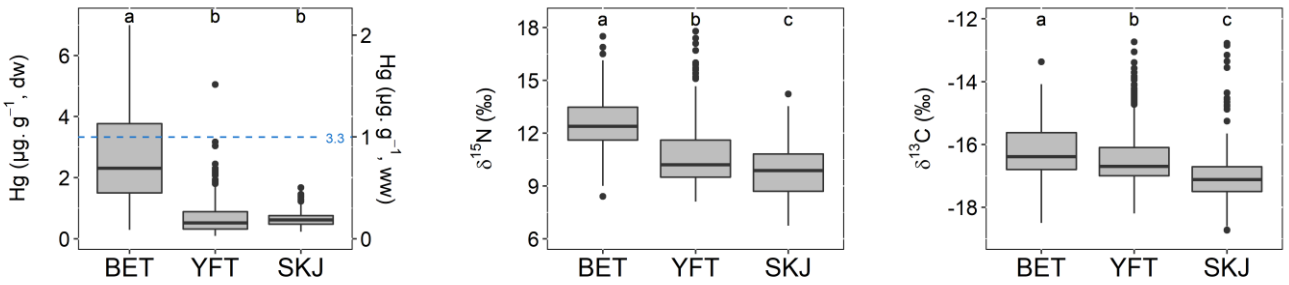

Figure S1. Boxplot of Hg concentrations (µg.g^{-1}), δ^{15}N and δ^{13}C values (‰) in white muscle tissues of bigeye (BET), yellowfin (YFT), and skipjack (SKJ) caught in the New Caledonia-Fiji region. The blue dashed line corresponds to the safety limit guideline of 1 µg.g^{-1} of wet weight, i.e. 3.3 µg.g^{-1} of dry weight. Letters indicate significant differences between species according to Dunn's post hoc test.

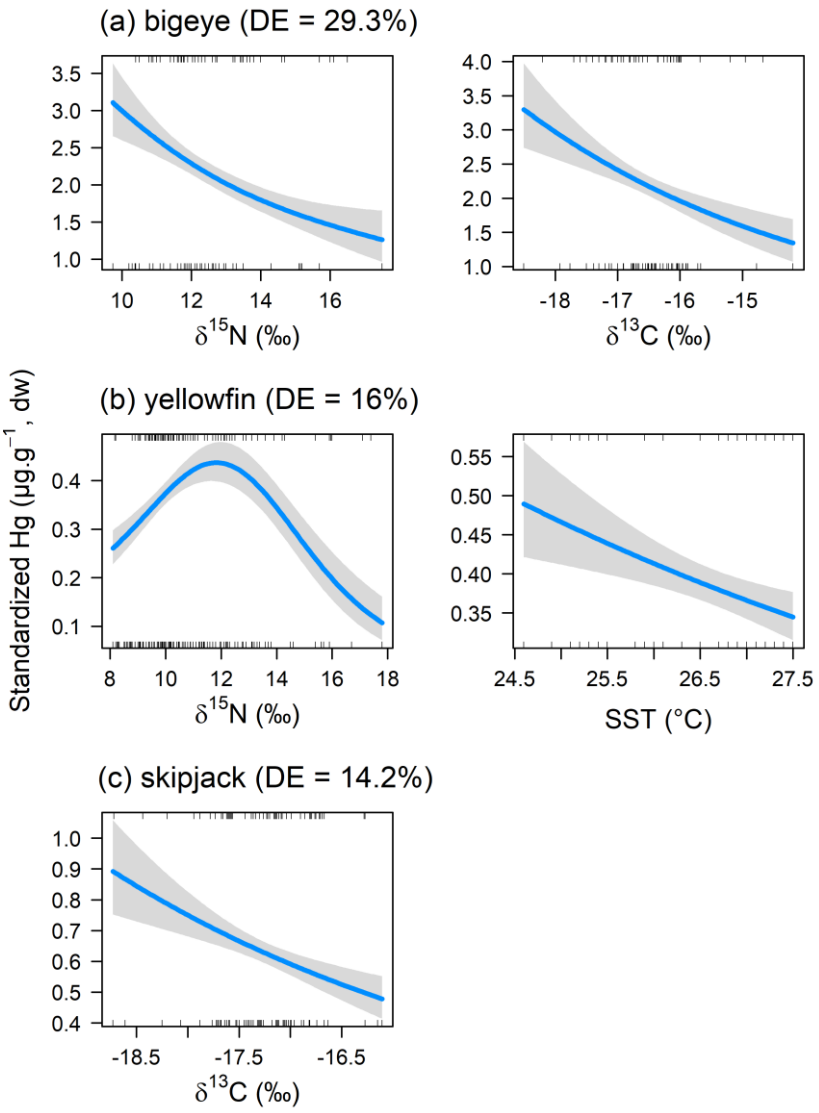

Figure S2. Results of the optimal generalized additive models (GAM) predicting standardized Hg concentrations in **a)** bigeye, **b)** yellowfin, and **c)** skipjack. The blue line gives the expected values while the grey band shows the confidence interval for the expected value. The ticks at the top and the bottom are the observed values position associated respectively to positive and negative model residuals. DE: deviance explained.

Table S1. Number of samples per year, season and species. Summer (from December to May) and winter (from May to December) refer to the two main austral seasons of the study area.

Sampling year	Season	Bigeye	Yellowfin	Skipjack
2001	summer	13	25	2
	winter			
2003	summer	2	7	1
	winter	2	6	18
2004	summer		4	
	winter		13	2
2005	summer		11	
	winter			
2006	summer		7	
	winter			
2007	summer		8	1
	winter	6	21	5
2008	summer	2		
	winter		29	11
2009	summer			
	winter	14	16	8
2010	summer		4	
	winter		4	13
2011	summer	4	14	
	winter			
2013	summer	11	22	4
	winter	11	30	11
2014	summer	4	17	15
	winter	9	19	8
2015	summer	2	4	3
	winter	22	11	9
2016	summer		6	18
	winter		4	6
2017	summer		10	
	winter	3		9
2018	summer	6	22	4
	winter	5	12	
Total		116	326	148

Table S2. ANOVA like permutation results to test temporal trends of environmental variables between 2001 and 2018. *F* and *p*-value: statistics of the tests. * indicates significant temporal trend

Environmental variable	Range of variation	Temporal trend	
		F	***p*-value**
Sea surface temperature (SST)	24 – 28 °C	0.065	0.792
Mixed Layer Depth (MLD)	23 – 51 m	1.762	0.207
Chlorophyll-a (Chl-a)	0.08 – 0.15 $mg.m^{-3}$	0.114	0.739
Net Primary Production (NPP)	43 – 150 mg $C.m^{-2}.day^{-1}$	4.016	0.053
Depth of 20°C isotherm (D_{iso20})	187 – 217 m	13.864	0.003 *
Depth of 12°C isotherm (D_{iso12})	428 – 451 m	2.600	0.115

Appendix E

Supplementary Information for

Long-term trends of tuna mercury concentrations for the global ocean

Anaïs Médieu, David Point, Jeroen E. Sonke, Pearse B. Buchanan, Nathalie Bodin, Douglas H. Adams, Anders Bignert, David G. Streets, Frédéric Ménard, C. Anela Choy, Valérie Allain, Takaaki Itai, Bridget E. Ferriss, Bernard Bourlès, Olivier Gauthier, Anne Lorrain

Figure S1. Statistical power of temporal trend data for mercury concentrations in yellowfin (dots), bigeye (triangles), and skipjack (diamonds) in six different regions of the global ocean. Adequacy was calculated following the methods of Bignert et al. (2004), considering a significance level of $p < 0.05$ and 80 % statistical power. Datasets falling within the lower right portion of the graph are more than adequate in terms of statistical power, while those in the upper left portion are inadequate.

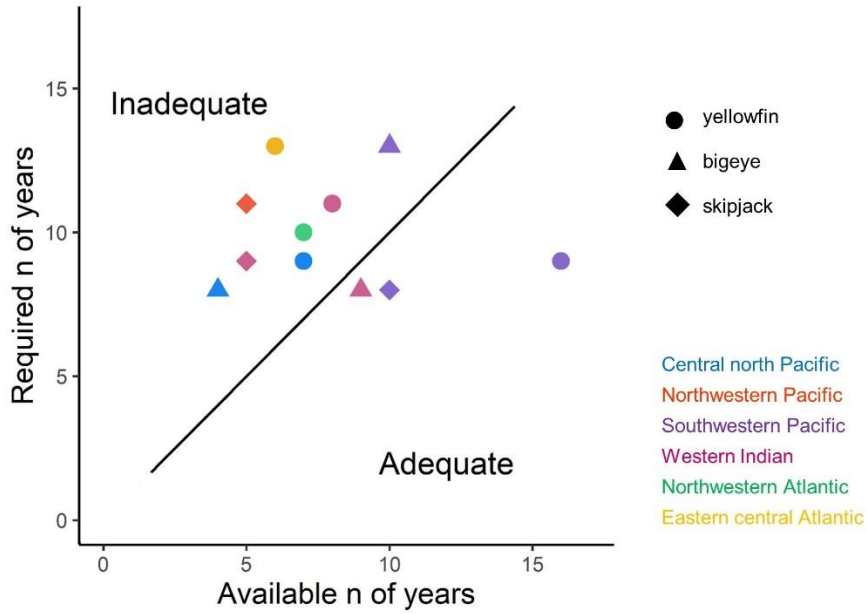

Table S1. Summary of tuna samples collected in the Pacific, Atlantic, and Indian Oceans and analysed for total mercury (THg) concentrations. *n* = sample size; sd = standard deviation.

Ocean area	Species	Sampling year	*n*	Fish length (cm) mean ± sd	THg (µg.g^{-1}, dw) mean ± sd	References
North central Pacific (Hawaii)	yellowfin	1970	22	157 ± 15	1.782 ± 0.845	Rivers et al., 1972
		1971	100	138 ± 12	0.727 ± 0.218	Boush and Thieleke, 1983
		1998	104	138 ± 8	0.707 ± 0.369	Kraepiel et al., 2003
		2002	20	134 ± 16	1.023 ± 0.686	Brooks, 2004
		2006	50	134 ± 19	1.012 ± 0.588	Kaneko and Ralston, 2007
		2007	199	113 ± 19	0.730 ± 0.443	Blum et al., 2013; Choy et al., 2009; Ferriss and Essington, 2011, this study
		2008	14	95 ± 24	0.910 ± 0.404	Blum et al., 2013; Choy et al., 2009
	bigeye	1971	104	138 ± 15	1.942 ± 0.425	Boush and Thieleke, 1983
		2002	20	122 ± 16	1.572 ± 0.618	Brooks, 2004
		2006	50	126 ± 21	2.005 ± 0.820	Kaneko and Ralston, 2007
		2007	320	123 ± 24	2.141 ± 0.853	Blum et al., 2013; Choy et al., 2009; Ferriss and Essington, 2011; this study
Northwestern Pacific (Asian coasts)	skipjack	1997	8	59 ± 1	0.507 ± 0.256	Médieu et al., 2022
		1998	34	52 ± 6	0.741 ± 0.301	Médieu et al., 2022
		1999	46	49 ± 11	1.328 ± 0.917	Médieu et al., 2022
		2000	7	48 ± 1	1.309 ± 0.504	Médieu et al., 2022
		2007	10	58 ± 2	2.138 ± 0.702	Médieu et al., 2022
Southwestern Pacific (New Caledonia and Fiji)	yellowfin	2001	25	131 ± 5	0.631 ± 0.201	Médieu et al., 2021
		2003	13	115 ± 20	0.504 ± 0.812	Médieu et al., 2021
		2004	17	101 ± 15	0.508 ± 0.295	Médieu et al., 2021
		2005	11	108 ± 7	0.323 ± 0.095	Médieu et al., 2021
		2006	7	117 ± 13	0.729 ± 0.252	Médieu et al., 2021
		2007	29	108 ± 14	0.304 ± 0.141	Médieu et al., 2021
		2008	29	125 ± 13	0.870 ± 0.417	Médieu et al., 2021
		2009	16	128 ± 23	1.075 ± 0.764	Médieu et al., 2021
		2010	8	108 ± 18	0.411 ± 0.286	Médieu et al., 2021
		2011	14	126 ± 19	0.974 ± 1.260	Médieu et al., 2021
		2013	52	129 ± 15	0.752 ± 0.565	Médieu et al., 2021
		2014	40	118 ± 21	0.619 ± 0.450	Médieu et al., 2021

Southwestern Pacific (New Caledonia and Fiji)	yellowfin	2015	11	137 ± 9	0.871 ± 0.379	Médieu et al., 2021
		2016	10	124 ± 10	0.830 ± 0.356	Médieu et al., 2021
		2017	14	119 ± 21	0.513 ± 0.385	Médieu et al., 2021
		2018	30	129 ± 15	0.779 ± 0.448	Médieu et al., 2021
	bigeye	2001	13	103 ± 12	2.989 ± 1.409	Médieu et al., 2021
		2003	4	126 ± 20	3.758 ± 2.293	Médieu et al., 2021
		2007	6	81 ± 15	0.644 ± 0.226	Médieu et al., 2021
		2009	14	111 ± 25	3.069 ± 2.412	Médieu et al., 2021
		2011	4	125 ± 12	2.947 ± 0.895	Médieu et al., 2021
		2013	22	103 ± 24	2.251 ± 1.477	Médieu et al., 2021
		2014	14	106 ± 25	2.384 ± 1.176	Médieu et al., 2021
		2015	23	111 ± 15	2.683 ± 1.156	Médieu et al., 2021
		2017	5	110 ± 17	3.342 ± 2.440	Médieu et al., 2021
		2018	9	131 ± 15	4.558 ± 1.935	Médieu et al., 2021
	skipjack	2003	19	68 ± 7	0.544 ± 0.131	Médieu et al., 2021
		2007	6	71 ± 3	0.641 ± 0.316	Médieu et al., 2021
		2008	11	71 ± 3	0.652 ± 0.124	Médieu et al., 2021
		2009	8	68 ± 8	0.645 ± 0.351	Médieu et al., 2021
		2010	13	71 ± 8	0.621 ± 0.225	Médieu et al., 2021
		2013	25	73 ± 10	0.644 ± 0.213	Médieu et al., 2021
		2014	13	74 ± 6	0.692 ± 0.311	Médieu et al., 2021
		2015	14	73 ± 4	0.601 ± 0.283	Médieu et al., 2021
		2016	22	71 ± 9	0.682 ± 0.223	Médieu et al., 2021
		2017	11	73 ± 7	0.746 ± 0.348	Médieu et al., 2021
Western Indian (Seychelles and Mozambique Channel)	yellowfin	2001	15	96 ± 38	0.615 ± 0.445	this study
		2004	23	108 ± 17	0.543 ± 0.368	Kojadinovic et al., 2006; this study
		2010	9	92 ± 52	0.954 ± 0.819	this study
		2012	5	153 ± 4	2.493 ± 0.340	this study
		2013	67	92 ± 33	0.731 ± 0.638	this study
		2017	14	114 ± 29	0.846 ± 0.522	this study
		2018	50	52 ± 24	0.229 ± 0.196	this study
		2020	10	131 ± 17	0.708 ± 0.249	this study

Western Indian (Seychelles and Mozambique Channel)	bigeye	2001	19	67 ± 31	0.552 ± 0.476	this study
		2002	11	131 ± 26	1.650 ± 0.515	this study
		2011	10	105 ± 26	1.851 ± 0.611	this study
		2012	6	142 ± 10	1.780 ± 0.266	this study
		2013	64	84 ± 38	1.022 ± 0.863	this study
		2014	8	109 ± 63	1.876 ± 1.496	this study
		2015	8	162 ± 8	2.238 ± 0.367	this study
		2018	33	59 ± 14	0.685 ± 0.412	this study
		2020	10	99 ± 4	1.278 ± 0.349	this study
	skipjack	2001	30	54 ± 11	0.489 ± 0.263	this study
		2010	8	46 ± 9	0.564 ± 0.555	this study
		2013	67	53 ± 11	0.553 ± 0.331	this study
		2014	8	34 ± 4	0.135 ± 0.070	this study
		2018	20	46 ± 11	0.312 ± 0.236	this study
Northwestern Atlantic (tropical US coasts)	yellowfin	1999	33	88 ±15	1.149 ±0.417	Adams, 2004
		2000	3	105 ± 34	0.654 ± 0.257	Adams, 2004
		2001	14	76 ± 19	0.633 ± 0.337	Adams, 2004
		2002	6	80 ± 14	0.663 ± 0.125	Adams, 2004
		2005	5	66 ± 2	0.581 ± 0.059	this study
		2006	8	99 ±5	1.033 ± 0.232	this study
		2011	7	86 ±13	0.734 ± 0.269	this study
Eastern central Atlantic (Gulf of Guinea)	yellowfin	1971	77	142 ± 31	1.431 ± 0.761	Ivory Coast Fisheries Service, 1972
		2003	6	68 ± 13	0.648 ± 0.132	this study
		2013	46	122 ± 21	1.226 ± 0.663	this study
		2014	58	130 ± 31	1.545 ± 0.787	this study
		2019	6	56 ± 4	0.659 ± 0.079	this study
		2020	52	59 ± 10	0.670 ± 0.116	this study

Table S2. Summary (mean ± standard deviation) of certified total mercury concentrations and recovery rates for the respective reference materials used in the different laboratories for newly acquired total mercury concentrations.

Laboratory	**Reference materials**	**Certified value** ($ng.g^{-1}$)	**Recovery rate** (%)
GET (Toulouse, France)	TORT-3 (lobster hepatopancreas)	292 ± 22	97 ± 4
	IAEA-436 (tuna fish flesh homogenate)	4190 ± 360	93 ± 3
	BCR-464 (tuna fish flesh homogenate)	5240 ± 100	102 ± 2
SFA (Victoria, Seychelles)	in-house homogenized sample of bigeye white muscle	141 ± 4	
	in-house homogenized sample of bigeye liver	986 ± 36	
	IAEA-436 (tuna fish)	4190 ± 360	
FWC-FWRI (Melbourne, FL USA)	DOLT-3 (dogfish liver)	3370 ± 140	114 ± 6
	DOLT-4 (dogfish liver)	2580 ± 220	99 ± 1
	DORM-2 (dogfish muscle)	4640 ± 260	107 ± 8
	TORT-2 (lobster hepatopancreas)	270 ± 60	106 ± 11

Table S3. Year-to-year comparisons of tuna mercury concentrations. Results of the post-hoc Dunn's tests for **A)** yellowfin and **B)** bigeye from the central north Pacific, **C)** skipjack in the northwestern Pacific, **D)** yellowfin, and **E)** bigeye from the southwestern Pacific, **F)** yellowfin, **G)** bigeye, and **H)** skipjack from the western Indian, and **I)** yellowfin from the tropical northwestern Atlantic. No Dunn tests were performed for standardized Hg concentrations in yellowfin from the eastern central Atlantic, and skipjack from the southwestern Pacific, as no significant differences were found among years in these two cases (Kruskal-Wallis test, $p > 0.05$).

A) Yellowfin in central north Pacific

	1971	*1998*	*2002*	*2006*	*2007*	*2008*
1970	**< 0.05**	**< 0.05**	0.07	**< 0.05**	**< 0.05**	1.00
1971		1.00	0.80	**< 0.05**	0.06	**< 0.05**
1998			0.06	**< 0.05**	**< 0.05**	**< 0.05**
2002				1.00	1.00	0.14
2006					1.00	**< 0.05**
2007						**< 0.05**

B) Bigeye in central north Pacific

	2002	*2006*	*2007*
1971	1.00	0.07	**< 0.05**
2002		0.25	**< 0.05**
2006			0.24

C) Skipjack in the northwestern Pacific

	1998	*1999*	*2000*	*2007*
1997	0.84	**< 0.05**	**< 0.05**	**< 0.05**
1998		**< 0.05**	**< 0.05**	**< 0.05**
1999			1.00	1.00
2000				1.00

D) Yellowfin in the southwestern Pacific

	2003	*2004*	*2005*	*2006*	*2007*	*2008*	*2009*	*2010*	*2011*	*2013*	*2014*	*2015*	*2016*	*2017*	*2018*
2001	1.00	0.43	1.00	1.00	1.00	0.41	0.79	1.00	1.00	1.00	1.00	1.00	1.00	1.00	1.00
2003		**< 0.05**	1.00	0.59	1.00	**< 0.05**	0.07	1.00	1.00	1.00	1.00	1.00	0.23	1.00	1.00
2004			0.31	1.00	**< 0.05**	1.00	1.00	1.00	1.00	0.26	1.00	1.00	1.00	0.37	1.00
2005				1.00	1.00	0.37	0.51	1.00	1.00	1.00	1.00	1.00	1.00	1.00	1.00
2006					0.27	1.00	1.00	1.00	1.00	1.00	1.00	1.00	0.06	1.00	1.00
2007						**< 0.05**	**< 0.05**	1.00	1.00	1.00	1.00	1.00	1.00	1.00	0.22
2008							1.00	1.00	1.00	0.17	1.00	1.00	1.00	0.43	1.00
2009								1.00	1.00	0.56	1.00	1.00	1.00	0.64	1.00
2010									1.00	1.00	1.00	1.00	1.00	1.00	1.00
2011										1.00	1.00	1.00	1.00	1.00	1.00
2013											1.00	1.00	1.00	1.00	1.00
2014												1.00	1.00	1.00	1.00
2015													1.00	1.00	1.00
2016														1.00	1.00
2017															1.00

E) Bigeye in the southwestern Pacific

	2003	*2007*	*2009*	*2011*	*2013*	*2014*	*2015*	*2017*	*2018*
2001	1.00	**< 0.05**	1.00	0.94	0.61	1.00	1.00	1.00	1.00
2003		1.00	1.00	1.00	1.00	1.00	1.00	1.00	1.00
2007			0.38	1.00	0.68	0.95	0.40	0.49	0.09
2009				1.00	1.00	1.00	1.00	1.00	1.00
2011					1.00	1.00	1.00	1.00	1.00
2013						1.00	1.00	1.00	1.00
2014							1.00	1.00	1.00
2015								1.00	1.00
2017									1.00

F) Yellowfin in the western Indian

	2004	*2010*	*2012*	*2013*	*2017*	*2018*	*2020*
2001	0.35	1.00	0.20	1.00	1.00	1.00	1.00
2004		**< 0.05**	**< 0.05**	**< 0.05**	1.00	0.56	1.00
2010			1.00	1.00	0.95	0.16	**< 0.05**
2012				0.38	0.09	**< 0.05**	**< 0.05**
2013					1.00	0.27	0.10
2017						1.00	1.00
2018							1.00

G) Bigeye in the western Indian

	2002	*2011*	*2012*	*2013*	*2014*	*2015*	*2018*	*2020*
2001	1.00	**< 0.05**	1.00	0.19	0.29	1.00	**< 0.05**	1.00
2002		0.09	1.00	1.00	1.00	1.00	0.15	1.00
2011			0.08	0.20	1.00	0.09	1.00	1.00
2012				1.00	1.00	1.00	0.17	1.00
2013					1.00	1.00	0.15	1.00
2014						1.00	1.00	1.00
2015							0.19	1.00
2018								1.00

H) Skipjack in the western Indian

	2010	*2013*	*2014*	*2018*
2001	0.95	0.54	1.00	1.00
2010		1.00	1.00	1.00
2013			1.00	1.00
2014				1.00

I) Yellowfin in the northwestern Atlantic

	2000	*2001*	*2002*	*2005*	*2006*	*2011*
1999	**< 0.05**	**< 0.05**	**< 0.05**	0.32	0.09	**< 0.05**
2000		0.62	0.83	0.45	0.42	0.93
2001			1.00	0.99	1.00	0.99
2002				0.98	0.99	1.00
2005					1.00	0.90
2006						0.89

Appendix F

Supplementary Information for

Pacific tuna mercury levels driven by marine methylmercury production and anthropogenic emissions

Anaïs Médieu[1,*], David Point[2], Takaaki Itai[3], Hélène Angot[4], Pearse J. Buchanan[5], Valérie Allain[6], Leanne Fuller[7], Shane Griffiths[7], David P. Gillikin[8], Jeroen E. Sonke[2], Lars-Eric Heimbürger-Boavida[9], Marie-Maëlle Desgranges[9], Christophe E. Menkes[10], Daniel J. Madigan[11], Pablo Brosset[1,12], Olivier Gauthier[1], Alessandro Tagliabue[5], Laurent Bopp[13], Anouk Verheyden[8], Anne Lorrain[1]

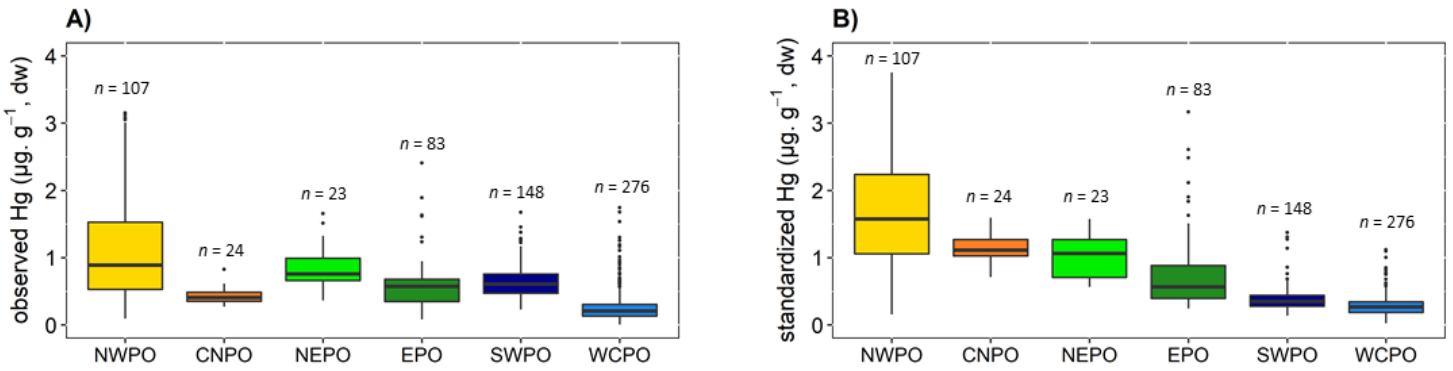

Figure S1. Inter-regional variability of mercury concentrations in skipjack tunas. Boxplot of (A) observed and (B) standardized Hg concentrations (µg.g^{-1}, dw). Box colors correspond to oceanic regions: NWPO = northwestern Pacific Ocean; CNPO = central north Pacific Ocean; NEPO = northeastern Pacific Ocean; EPO = eastern Pacific Ocean; SWPO = southwestern Pacific Ocean; WCPO = western and central Pacific Ocean.

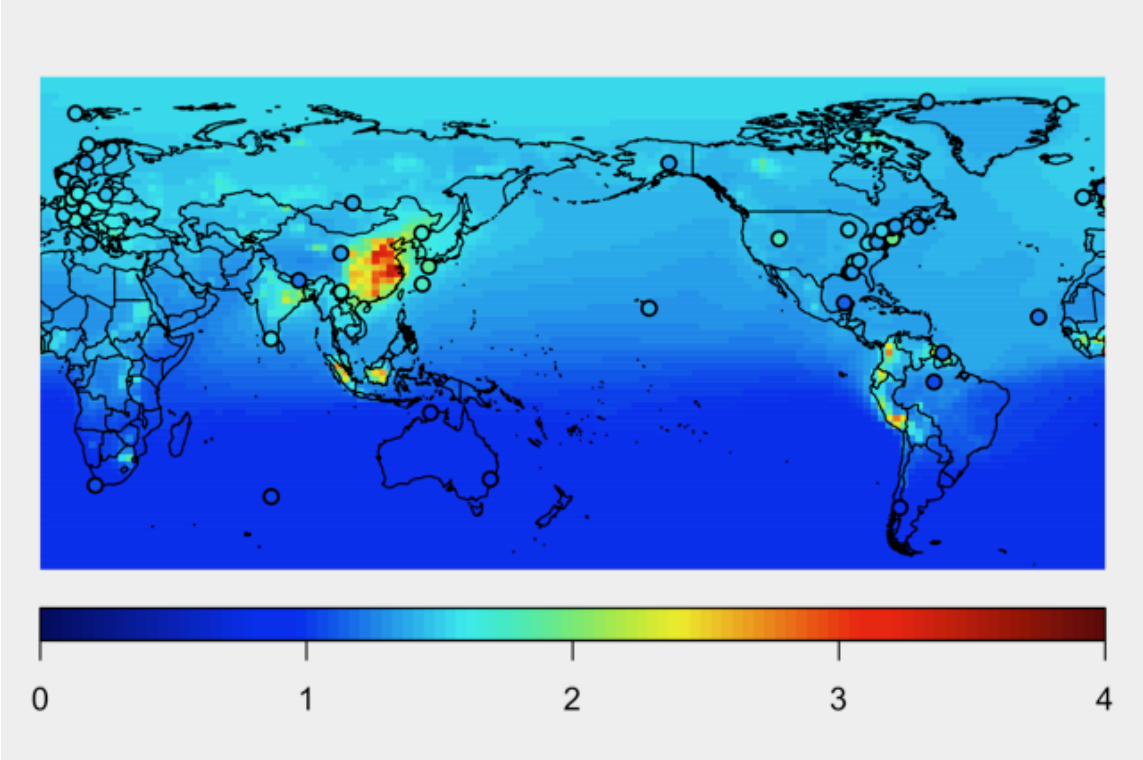

Figure S2. Hemispheric distribution of atmospheric mercury levels. The map illustrates the global distribution of Hg^0 concentrations in surface air in $ng.m^{-3}$. Model values (background) are annual means for 2013-2015, and observations (symbols) are for 2013-2015 as previously compiled by UN Environment (2019). We used modelled Hg^0 concentrations as a proxy of anthropogenic Hg inputs to the oceanic environment to evaluate the link between anthropogenic Hg emissions and Hg levels in tunas. It is arguable that Hg net deposition (i.e., dry deposition + wet deposition – reemission to the atmosphere) is a more relevant proxy as deposition is commonly recognised to be the primary pathway of Hg inputs to oceans. Nevertheless, Zhang et al. (2019) showed that Hg gas exchange over the ocean is poorly constrained due to the lack of direct flux measurements. We therefore chose not to rely on net deposition results but rather on atmospheric Hg^0 concentrations, whose spatial distribution is well constrained (Travnikov et al., 2017). Furthermore, a recent study using the stable isotope composition of total Hg in seawater and marine biota indicates that global atmospheric Hg^0 uptake by the oceans is equally important as Hg wet and dry deposition (Jiskra et al., 2021). This justifies the use of Hg^0 estimates in our study to evaluate the influence of anthropogenic emissions on Hg levels in skipjack.

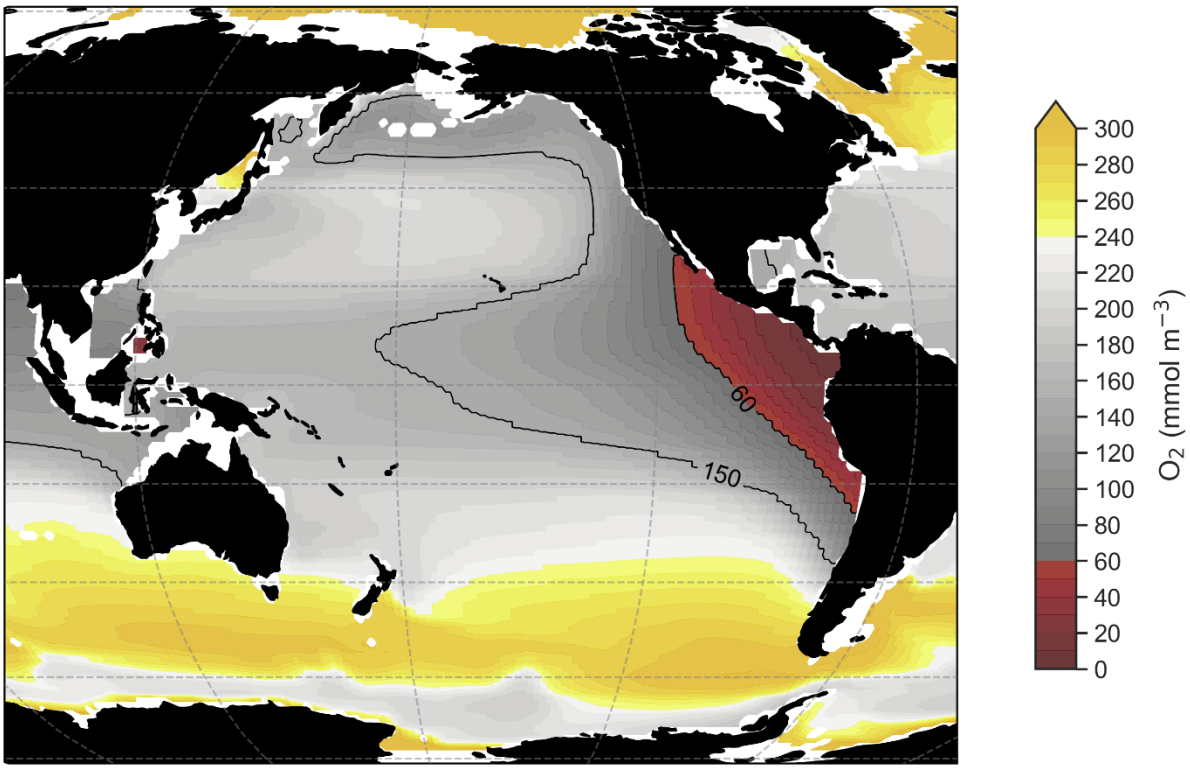

Figure S3. Spatial distribution of oxygen concentrations in subsurface waters (at 375m, mmol.m^{-3}) from Hindcast simulation (1975-2019).

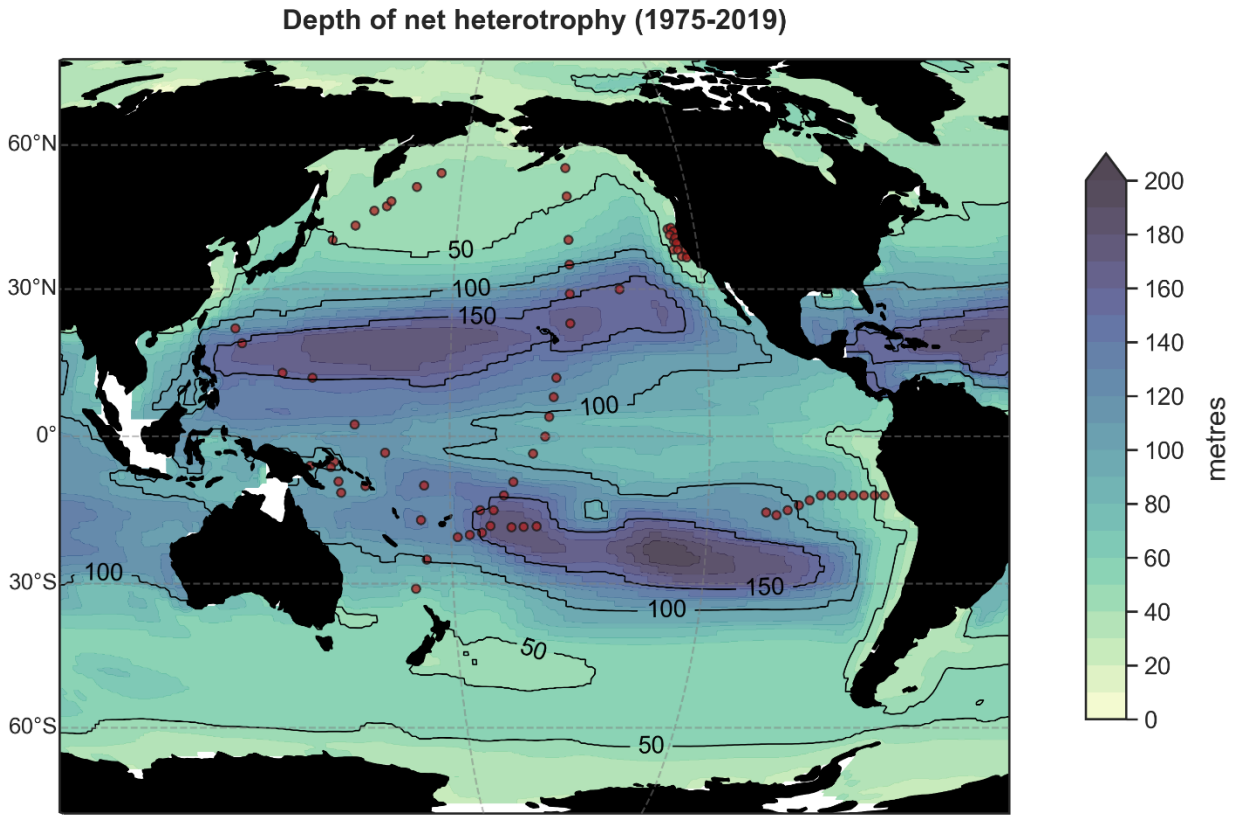

Figure S4. Spatial distribution of the depth of net heterotrophy (m) from Hindcast simulation (1975-2019). Red dots are locations of published MeHg samples (see methods section).

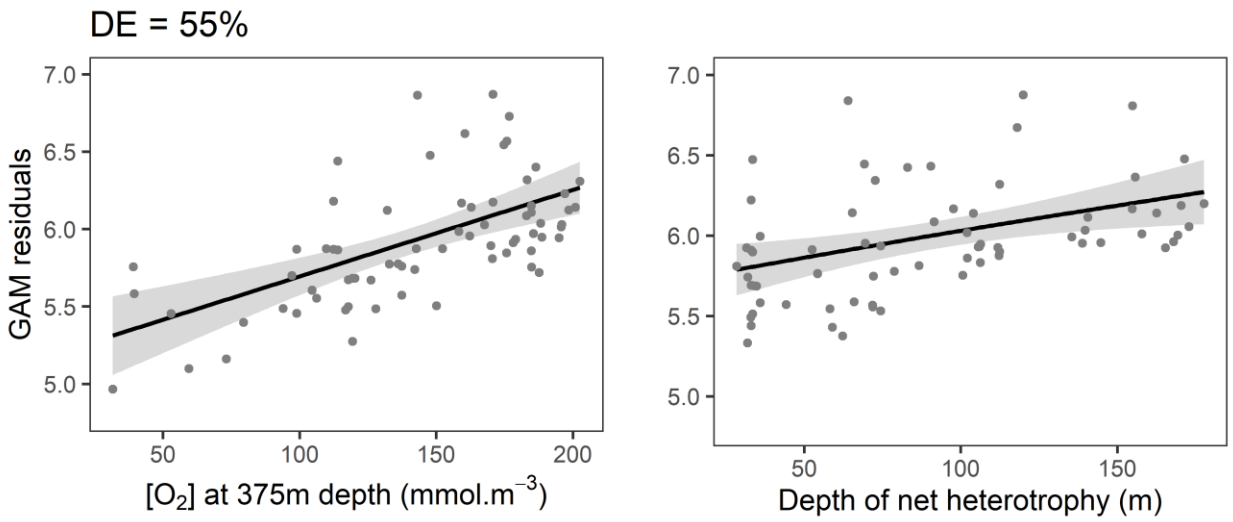

Figure S5. Optimal generalized additive model (GAM) predicting the depth of peak seawater methylmercury concentrations. The main drivers are $[O_2]$ in subsurface waters, and the depth of net heterotrophy. The deviance explained (DE, %) of the model is reported on the top of the figure.

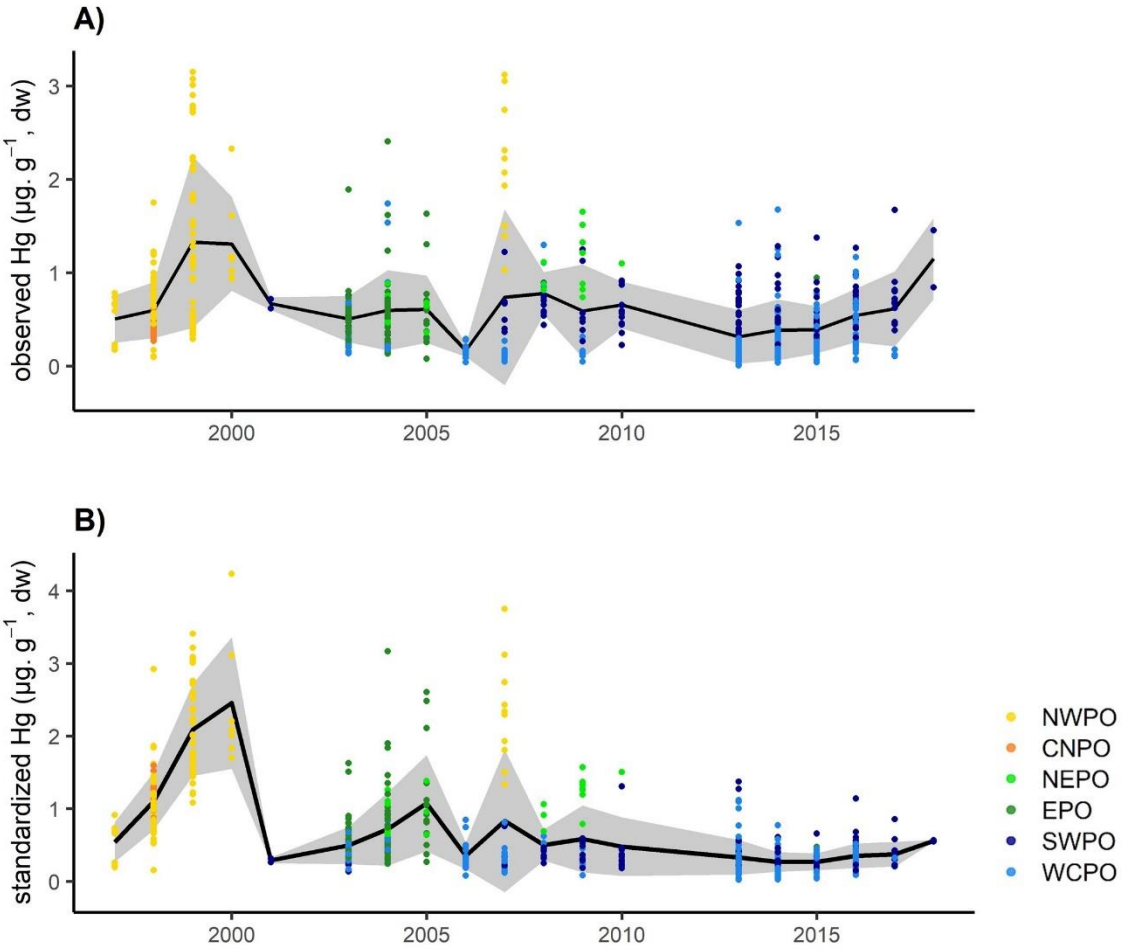

Figure S6. Time series of (A) observed, and (B) standardized mercury concentrations in skipjack tuna samples analysed in this study. The black line and shadow give respectively the annual mean and standard deviation. Coloured dots refer to oceanic region of the samples. Oceanic regions: NWPO = northwestern Pacific Ocean; CNPO = central north Pacific Ocean; NEPO = northeastern Pacific Ocean; EPO = eastern Pacific Ocean; SWPO = southwestern Pacific Ocean; WCPO = western and central Pacific Ocean.

Table. S1. Summary of skipjack samples collected in the Pacific Ocean and analysed for mercury (Hg) concentrations and stable isotope analyses ($\delta^{13}C$ and $\delta^{15}N$). FL= fork length.

Oceanic regions	*n*	FL (cm) min -max	Sampling period	Fishing gear	Method for total Hg concentration analysis	Method for $\delta^{13}C$ and $\delta^{15}N$ analysis	References
NWPO northwestern Pacific	107	29 – 63	1997 – 2007	Purse seine and pole-and-line	a	f	this study
CNPO central north Pacific	24	38 – 52	1998	Purse seine and pole-and-line	a	f	this study
NEPO northeastern Pacific	23	43 – 69	2004 – 2010	Hook-and-line and purse seine	b, c	f, g	this study
EPO eastern Pacific	83	34 – 81	2003 – 2015	Purse seine and longline	c, d	f	this study
SWPO southwestern Pacific	148	42 – 90	2001 – 2018	Longline	d	f	Médieu et al., 2021a
WCPO western and central Pacific	276	28 – 83	2003 – 2017	Pole-and-line, purse seine, longline, troll, and unknown	a, c, d, e	f, and not detailed	this study and Blum et al., 2013

Methods and reference material for total Hg analysis:

[a] Hot plate acidic digestion (HNO_3-H_2O_2) followed by cold vapor atomic fluorescence spectroscopy (HG-450, Hiranuma, Japan) in Center for Marine Environmental Studies (CMES), Ehime University, Japan. Reference standards: ERM-CE464 (tuna fish, total Hg = 2580 ± 220 $ng.g^{-1}$ dw), DOLT-4 (dogfish liver, total Hg = 5240 ± 100 $ng.g^{-1}$ dw), and NIST-SRM1566b (oyster tissue, total Hg = 371 ± 13 $ng.g^{-1}$ dw).

[b] Thermal decomposition, gold amalgamation and atomic adsorption detection (DMA-80, Milestone, Italy) in Stony Brook University (NY, USA). Reference standards: DORM-4 (fish protein, total Hg = 412 ± 36 $ng.g^{-1}$ dw).

[c] Thermal decomposition, gold amalgamation and atomic adsorption detection (DMA-80, Milestone, Italy) in IRD GET (Toulouse, France). Standards: TORT-3 (lobster hepatopancreas, total Hg = 292 ± 22 $ng.g^{-1}$ dw) and ERM-CE464 (tuna fish, total Hg = 2580 ± 220 $ng.g^{-1}$ dw).

[d] Hot plate acidic digestion (HNO_3-H_2O_2) followed by cold vapor atomic fluorescence spectroscopy in IRD Noumea (New Caledonia). Reference standards: DOMR-4 (fish protein, total Hg = 412 ± 36 ng.g^{-1} dw).

[e] Thermal decomposition, gold amalgamation and atomic adsorption detection (DMA-80, Milestone, Italy). Reference standards: DOMR-4 (fish protein, total Hg = 412 ± 36 ng.g^{-1} dw) and ERM-CE464 (tuna fish, total Hg = 2580 ± 220 ng.g^{-1} dw).

Methods and reference materials for $\delta^{15}N$ and $\delta^{13}C$ analysis:

[f] Union College (New York, USA): Costech elemental analyser coupled to an isotope ratio mass spectrometer (Thermo Scientific Delta Advantage with a Conflo IV interface). Reference standards: EA Consumables sorghum flour ($\delta^{13}C$ = -13.78 ± 0.17, $\delta^{15}N$ = 1.58 ± 0.15), in house acetanilide ($\delta^{13}C$ = -34.07, $\delta^{15}N$ = -0.96), IAEA-N-2 ammonium sulfate ($\delta^{15}N$ = 20.3 ± 0.2), and IAEA-600 caffeine ($\delta^{13}C$ = -27.771 ± 0.043, $\delta^{15}N$ = 1.0 ± 0.2).

[g] University of Hawaii (USA): On-line C-N analyser coupled with a Delta XP isotope ratio mass spectrometer. Reference standards: replicate of atmospheric nitrogen and V-PDB.

Appendix G

Supplementary Information for

Tropical tunas mirror patterns of mercury bioavailability and pollution in the global ocean

Anaïs Médieu, David Point, Pearse B. Buchanan, Heidi Pethybridge, Valérie Allain, Nathalie Bodin, Hélène Angot, Leanne Fuller, Bridget E. Ferriss, Laia Munoz, Flavia Lucena, Douglas H. Adams, John M. Logan, David P. Gillikin, Jeroen E. Sonke, Lars-Eric Heimbürger-Boavida, Andrew T. Revill, Frédéric Ménard, Felipe Galván-Magaña, Takaaki Itai, B.K. Kolita Kamal Jinadasa, Ana Carolina Pizzochero, Joao Paulo Machado Torres, Andrea Luna-Acosta, Daniel J. Madigan, Marie-Maëlle Desgranges, Marina Renedo, Anouk Verheyden, Jean-Marie Munaron, Alessandro Tagliabue, Laurent Bopp, Olivier Gauthier, Anne Lorrain

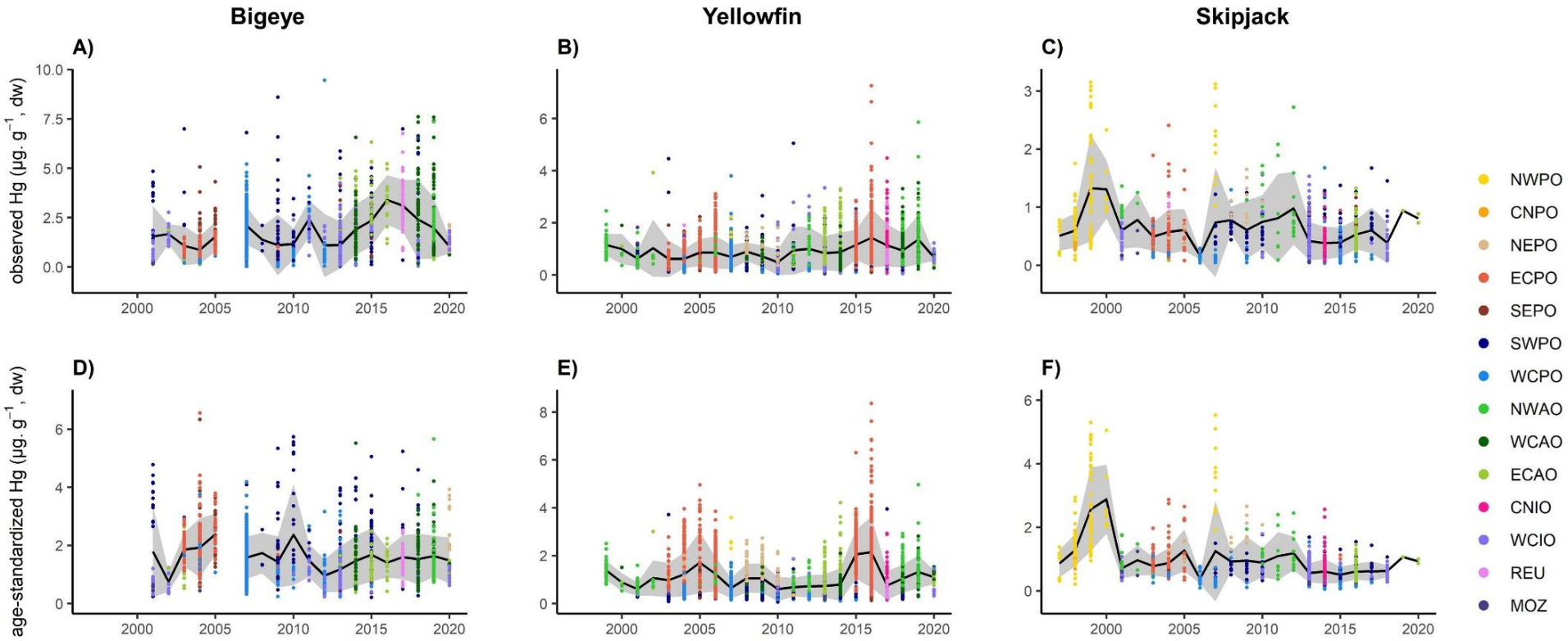

Figure S1. Time series of observed and age-standardized mercury (Hg) concentrations in tropical tuna samples analyzed in this study. **A)**, **B)** and **C)** show temporal trends of observed Hg concentrations (µg.g^{-1}, dw), while **D)**, **E)** and **F)** represent temporal trends of age-standardized Hg concentrations (µg.g^{-1}, dw) in bigeye, yellowfin, and skipjack respectively. The black line and shadow give respectively the annual means and standard deviation. Colored dots refer to oceanic regions of the samples. Oceanic areas: NWPO = northwestern Pacific; CNPO = central north Pacific; NEPO = northeastern Pacific; ECPO = eastern central Pacific; SEPO = southeastern Pacific; SWPO = southwestern Pacific; WCPO = western central Pacific; NWAO = northwestern Atlantic; CAO = central Atlantic; CNIO = central north Indian; WCIO = western central Indian; REU = Reunion Island; MOZ = Mozambique Channel.

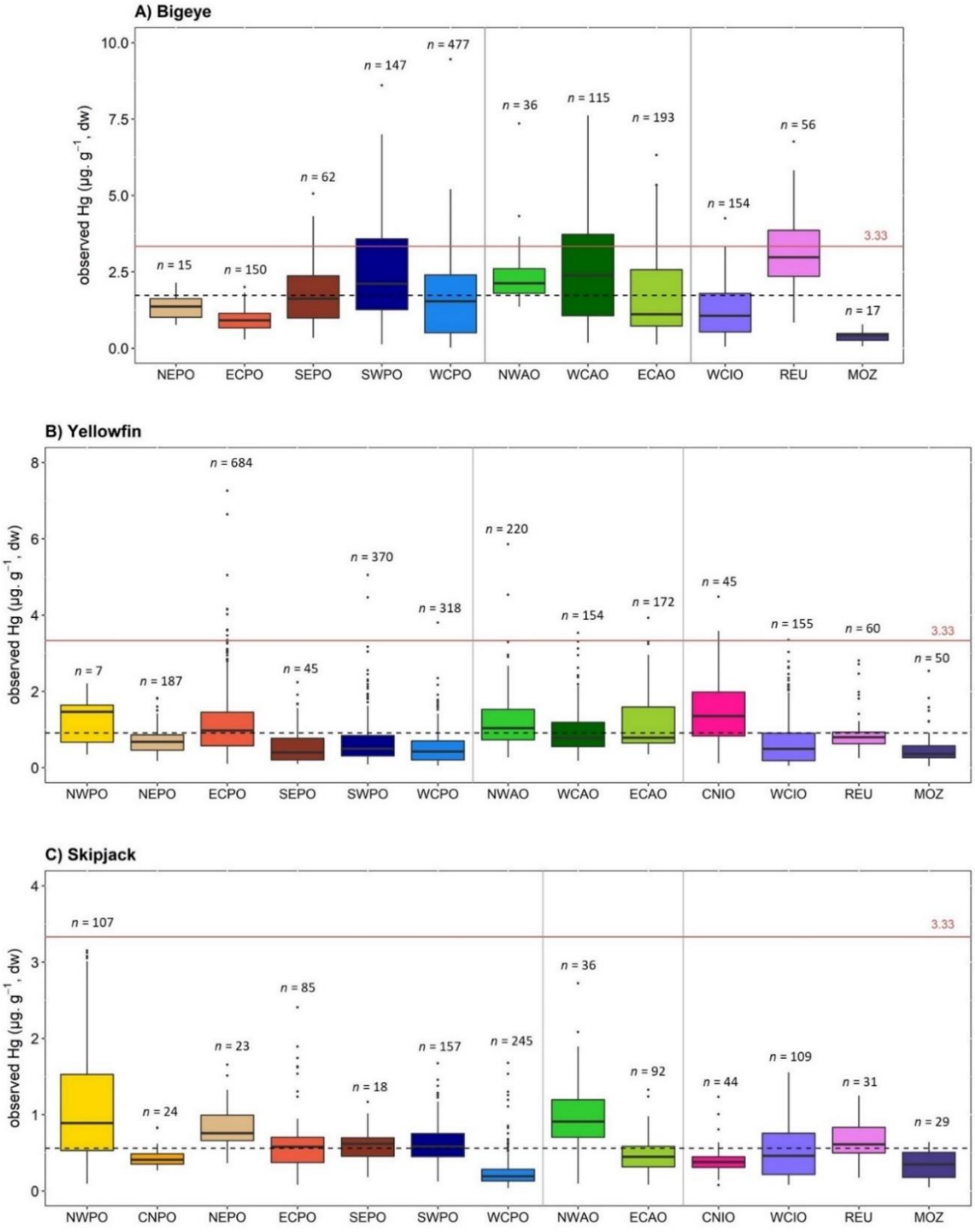

Figure S2. Inter-regional variability of observed mercury (Hg) concentrations in tropical tunas at the global scale. Boxplots of observed Hg concentrations (µg.g^{-1}, dw) in (A) bigeye, (B) yellowfin, and (C) skipjack tunas. The horizontal dashed lines represent the global means for the species. The solid red lines correspond to the food safety guideline of 1 µg.g^{-1} wet weight (i.e., 3.33 µg.g^{-1} dw). Box colors correspond to oceanic regions: NWPO = northwestern Pacific; CNPO = central north Pacific; NEPO = northeastern Pacific; ECPO = eastern central Pacific; SEPO = southeastern Pacific; SWPO = southwestern Pacific; WCPO = western central Pacific; NWAO = northwestern Atlantic; WCAO = western central Atlantic; ECAO = eastern central Atlantic; CNIO = central north Indian; WCIO = western central Indian; REU = Reunion Island; MOZ = Mozambique Channel.

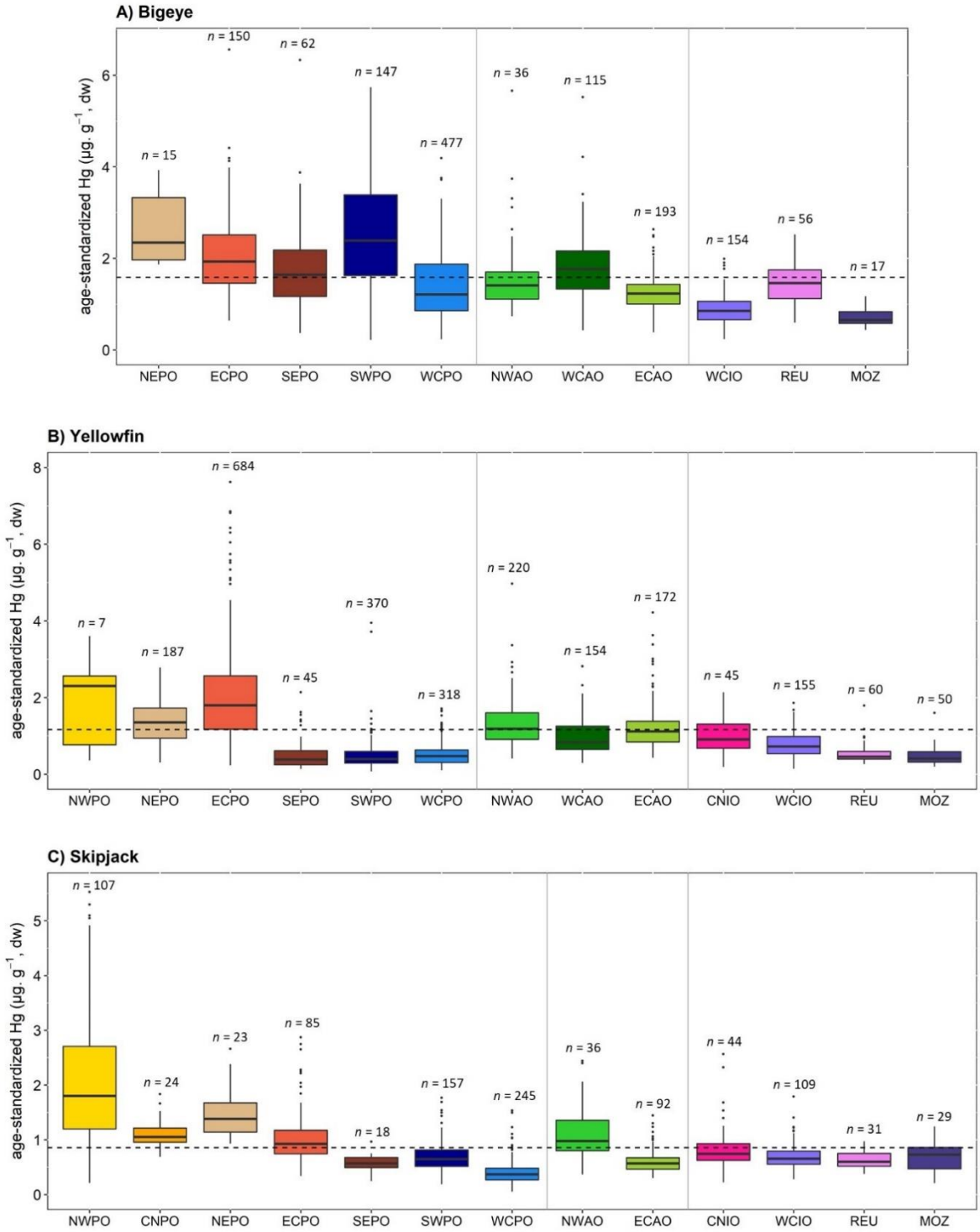

Figure S3. Inter-regional variability of standardized mercury (Hg) concentrations in tropical tunas at the global scale. Boxplots of age-standardized Hg concentrations (µg.g^{-1}, dw) at 3 years old in **A)** bigeye, **B)** yellowfin, and **C)** skipjack tunas. The horizontal dashed lines represent the global means for the species. Box colors correspond to oceanic regions: NWPO = northwestern Pacific; CNPO = central north Pacific; NEPO = northeastern Pacific; ECPO = eastern central Pacific; SEPO = southeastern Pacific; SWPO = southwestern Pacific; WCPO = western central Pacific; NWAO = northwestern Atlantic; WCAO = western central Atlantic; ECAO = eastern central Atlantic; CNIO = central north Indian; WCIO = western central Indian; REU = Reunion Island; MOZ = Mozambique Channel.

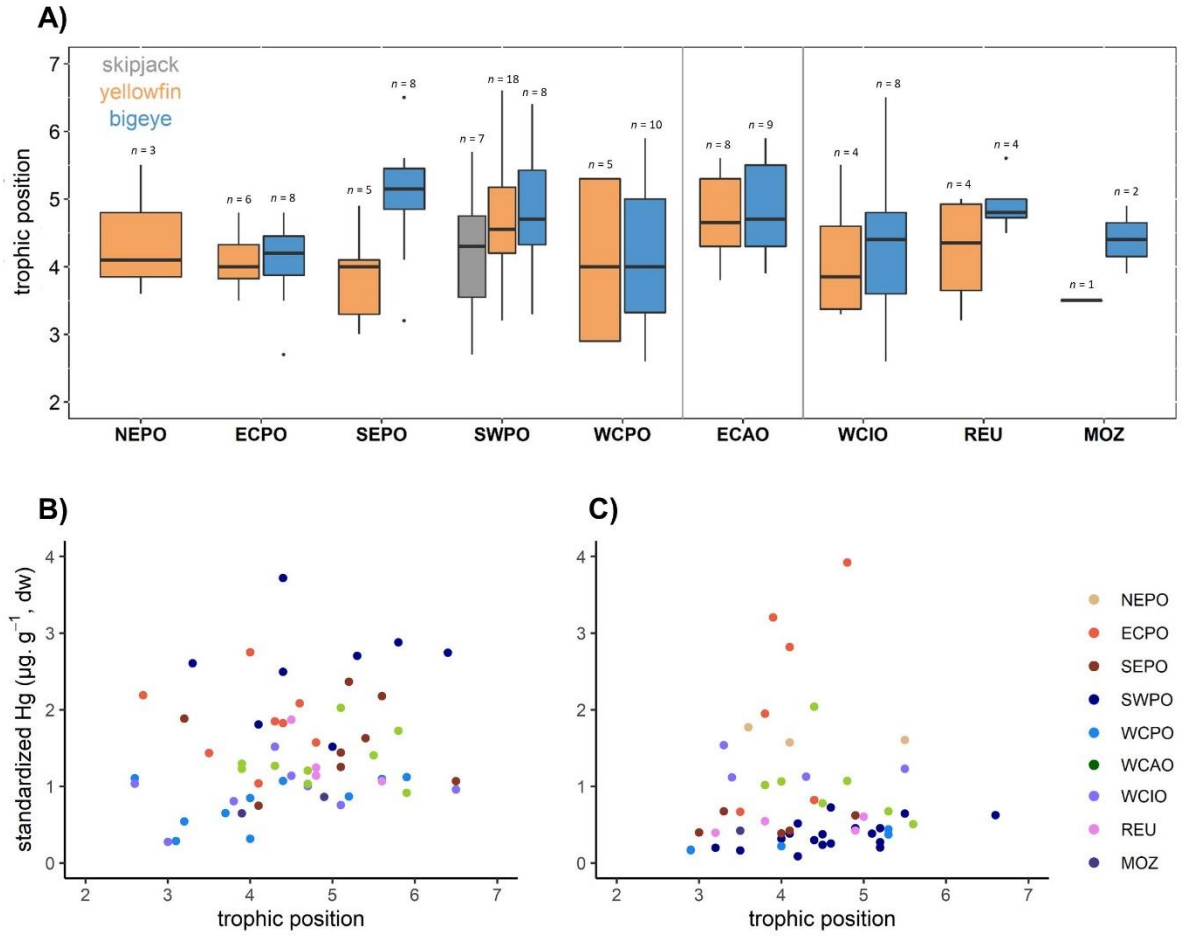

Figure S4. Relationship between standardized Hg concentrations and trophic position in tunas**. A)** Boxplots of trophic position estimated for skipjack (grey), yellowfin (orange), and bigeye (blue) with amino acid $\delta^{15}N$ values (see methods section). **B)** and **C)** show the absence of significant relationship between tuna standardized Hg concentrations and trophic positions, in bigeye and yellowfin, respectively. Oceanic areas: NEPO = northeastern Pacific; ECPO = eastern central Pacific; SEPO = southeastern Pacific; SWPO = southwestern Pacific; WCPO = western central Pacific; ECAO = eastern central Atlantic; WCIO = western central Indian; REU = Reunion Island; MOZ = Mozambique Channel.

Table S1. Summary of tropical tuna samples collected in the Pacific, Atlantic and Indian Oceans, and analysed for total mercury (Hg) concentrations and stable isotope analyses ($\delta^{13}C$ and $\delta^{15}N$). *n* = sample size; FL= fork length.

Ocean basins	Oceanic regions	*n*	FL (cm) min - max	Sampling period	Methods for total Hg concentrations analysis	Methods for $\delta^{13}C$ and $\delta^{15}N$ analysis	References for Hg data
Bigeye							
Pacific	NEPO northeastern Pacific	15	42 – 114	unknown	a	o	this study
	ECPO eastern central Pacific	150	43 – 99	2003 – 2009	a, b	o	Ferriss and Essington, 2011; Houssard et al., 2019
	SEPO southeastern Pacific	62	68 – 175	2004 – 2015	a	o	Houssard et al., 2019
	SWPO sout western Pacific	147	49 – 170	2001 – 2018	a	o	Houssard et al., 2019; Médieu et al., 2021
	WCPO western central Pacific	477	31 – 175	2003 – 2015	a, b, c	o, and not detailed	this study and Blum et al., 2013; Ferriss and Essington, 2011; Houssard et al., 2019
Atlantic	NWAO northwestern Atlantic	36	75 – 148	2018 – 2019	a	p	this study
	WCAO western central Atlantic	115	47 – 185	2014 – 2020	a		this study
	ECAO central Atlantic	193	29 – 173	2002 – 2020	a	o, q, r, s	this study
Indian	CWIO central western Indian	154	30 – 174	2001 – 2020	a, d	o, r, s	this study and Bodin et al., 2017
	REU Reunion Island	56	91 – 152	2017	a	o	this study
	MOZ Mozambique Channel	17	36 – 115	2001 – 2013	a	o, r, s	this study
Yellowfin							
Pacific	NWPO northwestern Pacific	7	71 – 111	2007 – 2011	e	o	this study
	NEPO northeastern Pacific	187	50 – 113	2003 – 2010	b, f, g	o, t	Ferriss and Essington, 2011; Madigan et al., 2018; Ordiano-Flores et al., 2011

Ocean basins	Oceanic regions	*n*	FL (cm) min - max	Sampling period	Methods for total Hg concentrations analysis	Methods for $\delta^{13}C$ and $\delta^{15}N$ analysis	References for Hg data
Pacific	ECPO eastern central Pacific	684	34 – 171	2003 – 2016	a, b, g, h	o, u	this study and Ferriss and Essington, 2011; Houssard et al., 2019; Ordiano-Flores et al., 2011
	SEPO southeastern Pacific	45	63 – 160	2003 – 2016	a	o	Houssard et al., 2019
	SWPO southwestern Pacific	370	54 – 160	2001 – 2018	a	o	Houssard et al., 2019; Médieu et al., 2021
	WCPO western central Pacific	318	43 – 154	2004 – 2015	a, b, c	o, and not detailed	this study and Blum et al., 2013; Ferriss and Essington, 2011; Houssard et al., 2019
Atlantic	NWAO northwestern Atlantic	220	60 – 166	1999 – 2019	a, i, j, k	o	this study and Adams, 2004
	WCAO western central Atlantic	154	40 – 169	2000 – 2020	a		this study
	ECAO central Atlantic	172	44 – 174	2000 – 2020	a	o, q, r, s	this study
Indian	CNIO central north Indian	45	64 – 180	2017	l		Jinadasa et al., 2019
	CWIO central western Indian	155	30 – 165	2001 – 2020	a, d, l	o, v	this study and Bodin et al., 2017; Jinadasa et al., 2019
	REU Reunion Island	60	63 – 171	2004 – 2017	a, m	o, v	this study and Kojadinovic et al., 2006
	MOZ Mozambique Channel	50	36 – 165	2001 – 2015	a, m	o, r, s, v	this study and Kojadinovic et al., 2006
Skipjack							
Pacific	NWPO northwestern Pacific	107	29 – 63	1997 – 2007	e	o	Médieu et al., 2022
	CNPO central north Pacific	24	38 – 52	1998	e	o	Médieu et al., 2022
	NEPO northeastern Pacific	23	43 – 69	2004 – 2010	a, f	o, t	Médieu et al., 2022
	ECPO eastern central Pacific	85	34 – 81	2003 – 2015	a, n	o	Médieu et al., 2022

Ocean basins	Oceanic regions	*n*	FL (cm) min - max	Sampling period	Methods for total Hg concentrations analysis	Methods for $\delta^{13}C$ and $\delta^{15}N$ analysis	References for Hg data
Pacific	SEPO southeastern Pacific	18	48 – 81	2004 – 2016	a, n	o	Médieu et al., 2022
	SWPO southwestern Pacific	157	42 – 90	2001 – 2018	a	o	Médieu et al., 2021, 2022
	WCPO western central Pacific	245	28 – 83	2003 – 2017	a, c	o and not detailed	Blum et al., 2013; Médieu et al., 2022
Atlantic	NWAO northwestern Atlantic	36	34 – 76	2001 – 2012	a, j, k		this study
	CAO central Atlantic	93	25 – 64	2003 – 2020	a	o, q, s	this study
Indian	CNIO central north Indian	44	36 – 56	2014	a		this study
	CWIO central western Indian	109	29 – 72	2001 – 2018	a, d	o, r, s	this study and Bodin et al., 2017
	REU Reunion Island	31	41 – 85	2004	m	v	Kojadinovic et al., 2006
	MOZ Mozambique Channel	29	34 – 71	2001 – 2013	a	o, r, s	this study

Methods and reference material for total Hg concentrations analysis

[a] Thermal decomposition, gold amalgamation and atomic adsorption detection (DMA-80, Milestone, Italy) in GET (Toulouse, France). Reference standards: TORT-3 (lobster hepatopancreas, total Hg = 292 ± 22 ng.g^{-1} dw), ERM-CE464 (tuna fish, total Hg = 2580 ± 220 ng.g^{-1} dw), IAEA-436 (tuna fish, total Hg = 4190 ± 360 ng.g^{-1} dw), and BCR-464 (tuna fish, total Hg = 5240 ± 100 ng.g^{-1} dw).

[b] Microwave acid digestion followed by inductively coupled plasma mass spectrometry using a collision cell at the University of Washington's Environmental Health Lab (Seattle, USA). Reference standards: SMR 1946 (Lake Superior fish tissue, total Hg = 433 ± 9 ng.g^{-1} dw).

[c] Thermal decomposition, gold amalgamation and atomic adsorption detection (DMA-80, Milestone, Italy). Reference standards: DOMR-4 (fish protein, total Hg = 412 ± 36 ng.g^{-1} dw) and ERM-CE464 (tuna fish, total Hg = 2580 ± 220 ng.g^{-1} dw).

[d] Thermal decomposition, gold amalgamation and atomic adsorption detection (DMA-80, Milestone, Italy) in SFA (Victoria, Seychelles). Reference standards: large homogenized wet samples of bigeye tuna white muscle BET-M (Hg = 141 ± 4 ng.g^{-1} ww) and liver BET-L (Hg = 986 ± 36 ng.g^{-1} ww), as well as the certified reference material IAEA-436 (tuna fish flesh homogenate, Hg = 4190 ± 360 ng.g^{-1} dw).

[e] Hot plate acid digestion (HNO_3-H_2O_2) followed by cold vapor atomic fluorescence spectroscopy (HG-450, Hiranuma, Japan) in Center for Marine Environmental Studies (CMES), Ehime University, Japan. Reference standards: ERM-CE464 (tuna fish, total Hg = 2580 ± 220 ng.g^{-1} dw), DOLT-4 (dogfish liver, total Hg = 5240 ± 100 ng.g^{-1} dw), and NIST-SRM1566b (oyster tissue, total Hg = 371 ± 13 ng.g^{-1} dw).

[f] Thermal decomposition, gold amalgamation and atomic adsorption detection (DMA-80, Milestone, Italy) in Stony Brook University (NY, USA). Reference standards: DORM-4 (fish protein, total Hg = 412 ± 36 ng.g^{-1} dw).

[g] Microwave acid digestion followed by atomic absorption spectrophotometer (AAS, PerkinElmer Analyst 100) coupled to a hybride generator in cold vapor (PerkinElmer MHS-10). Reference standards: IAEA-407 (fish homogenate, total Hg = 222 ± 24 ng.g^{-1} dw).

[h] Thermal decomposition, gold amalgamation and atomic adsorption detection (DMA-80, Milestone, Italy) at the University of North Carolina Wilmington (Wilmington, USA). Reference standards: DORM-4 (fish protein, total Hg = 412 ± 36 ng.g^{-1} dw) and DOLT-5 (dogfish liver, total Hg = 440 ± 180 ng.g^{-1} dw).

[i] Acid digestion followed by cold vapor atomic absorption spectrometry in DEP laboratory (Florida, USA). Reference standards: DOLT-2 (dogfish liver, total Hg = 1990 ± 100 ng.g^{-1} dw).

[j] Acid digestion followed by cold vapor atomic absorption spectrometry in FWC-DEP laboratory (Tallahassee, FL, USA). Reference standards: DOLT-2 and DOLT-3. (Adams, 2004)

[k] Thermal decomposition, gold amalgamation and atomic adsorption detection (DMA-80, Milestone, Italy) in FWC-FWRI (Melbourne, FL, USA). Reference standards: DOLT-3, DOLT-4, DORM-2, and TORT-2.

[l] Microwave acid digestion followed by cold vapor atomic absorption spectrometry (Varian 240 FS, Mulgrave, Australia). Reference standards: canned fish offal (T/07243, total Hg = 707 (469 - 946) ng.g^{-1} ww), and canned crab meat (T/07279, total Hg = 106 (59 – 152) ng.g^{-1} ww)

[m] Thermal decomposition, gold amalgamation and atomic adsorption detection (AMA 254, Altec, Czech Republic) at LIENSs (La Rochelle, France). Reference standards: TORT-2 (lobster hepatopancreas, total Hg = 270 ± 60 ng.g^{-1} dw)

[n] Hot plate acidic digestion (HNO_3-H_2O_2) followed by cold vapor atomic fluorescence spectroscopy in IRD Noumea (New Caledonia). Reference standards: DOMR-4 (fish protein, total Hg = 412 ± 36 ng.g^{-1} dw).

Methods and reference materials for $\delta^{15}N$ and $\delta^{13}C$ analysis

[o] Costech elemental analyser coupled to an isotope ratio mass spectrometer (Thermo Scientific Delta Advantage with a Conflo IV interface) at Union College (New York, USA). Reference standards: EA Consumables sorghum flour ($\delta^{13}C$ = -13.78 ± 0.17 ‰, $\delta^{15}N$ = 1.58 ± 0.15 ‰), in house acetanilide ($\delta^{13}C$ = -34.07 ‰, $\delta^{15}N$ = -0.96 ‰), IAEA-N_2 ammonium sulfate ($\delta^{15}N$ = 20.3 ± 0.2 ‰), and IAEA-600 caffeine ($\delta^{13}C$ = -27.771 ± 0.043 ‰, $\delta^{15}N$ = 1.0 ± 0.2 ‰).

[p] PDZ Europa ANCA-GSL elemental analyzer interfaced to a PDZ Europa 20-20 isotope ratio mass spectrometer (Sercon Ltd., Cheshire, UK) at the UC Davis Stable Isotope Facility. Reference materials: IAEA-600, USGS-40, USGS-41, USGS-42, USGS-43, USGS-61, USGS-64, and USGS-65.

[q] Continuous flow mass spectrometer (Delta V+ with a conflo IV interface, Thermo Scientific, Bremen, Germany) coupled to an elemental analyzer (Flash EA 2000, Thermo Scientific, Milan, Italy) at the Pôle Spectrométrie Océan (Plouzané, France). Reference standards: USGS-61, USGS-62, USGS-63 for carbon and nitrogen.

[r] Elemental analyser (Flash EA 1112, Thermo Scientific, Milan, Italy) coupled to an isotope ratio mass spectrometer (Delta V Advantage with a Conflo IV Interface, Thermo Scientific, Bremen, Germany) at the LIENSs stable isotope facility (La Rochelle, France). Reference standards: USGS-24 ($\delta^{13}C$ = -16.05 ± 0.04 ‰), IAEA-CHE ($\delta^{13}C$ = -24.72 ± 0.04 ‰), IAEA-600 ($\delta^{13}C$ = -27.77 ± 0.04 ‰; $\delta^{15}N$ = 1.0 ± 0.2 ‰), IAEA-N2 ($\delta^{15}N$ = 20.3 ± 0.2 ‰), and IAEA-NO_3^- ($\delta^{15}N$ = 4.7 ± 0.2 ‰).

[s] Europea Scientific ANCA-NT 20-20 Stable Isotope Analyzer with an ANCA-NT Solid/Liquid Preparation Module (PDZ Europa Ltd., Crewz, UK) at the Scottish Crop Institute (Dundee, Scotland).

[t] University of Hawaii (USA): On-line C-N analyser coupled with a Delta XP isotope ratio mass spectrometer. Reference standards: replicate of atmospheric nitrogen and V-PDB.

[u] Costech elemental analyser coupled to an isotope ratio mass spectrometer at the Center for Marine Science at the University of North Carolina Wilmington (Wilmington, USA). Reference standards: depleted glutamic acid USGS-40 (), and enriched glutamic acid USGS-41 ($\delta^{13}C$ = -34.07 ‰, $\delta^{15}N$ = -0.96 ‰).

[v] Europa Scientific ANCA-NT 20-20 Stable Isotope Analyzer with ANCA-NT Solid/Liquid Preparation Module (Europa Scientific Ltd., Dundee, UK) at the LIENSs stable isotope facility (La Rochelle, France). Reference standards: “Europa flour” ($\delta^{13}C$ = -27.21 ± 0.13 ‰, $\delta^{15}N$ = 2.73 ± 0.17 ‰), and IAEA N1 ($\delta^{15}N$ = 0.4 ± 0.2 ‰) and N2 ($\delta^{15}N$ = 20.3 ± 0.2 ‰).

Table S2. Summary of age-standardization of mercury concentrations in tropical tunas at the global scale. Parameters used to fit power-law relationships $(\log(\mathrm{Hg}) = \mathrm{a} \times (\mathrm{age} - \mathrm{c})^{b} - \mathrm{d})$ between log(observed Hg) and estimated fish age, and the associated percentage of deviance explained (R^2). *n* = sample size.

Species	Ocean basins	*n*	a	b	c	d	R^2
Bigeye	western Pacific	682	7.74	0.05	0.17	8.00	0.68
	eastern Pacific	169	0.26	0.64	0.54	0.18	0.29
	Atlantic	344	2.39	0.13	0.00	2.60	0.77
	Indian	227	5.15	0.10	0.00	5.81	0.79
Yellowfin	western Pacific	743	0.14	0.86	0.51	0.65	0.34
	eastern Pacific	868	1.30	0.23	0.00	1.49	0.21
	Atlantic	546	7.91	0.02	0.77	8.00	0.34
	Indian	310	7.28	0.06	0.07	8.00	0.70
Skipjack	western Pacific	552	5.23	0.05	0.00	5.73	0.18
	eastern Pacific	107	0.64	0.32	0.72	0.81	0.34
	western Atlantic	36	7.90	0.03	1.30	8.00	0.57
	eastern Atlantic	92	7.58	0.04	1.12	8.00	0.64
	Indian	213	7.64	0.03	0.37	8.00	0.66

Appendix H

Article in the Pacific Fisheries Community Newsletter

English version on line: https://coastfish.spc.int/en/publications/bulletins/fisheries-newsletter/530

Quand les thons permettent de cartographier la contamination au mercure dans l'océan

Anaïs Médieu[1], David Point[2], Valérie Allain[3] et Anne Lorrain[4]

En sushi, en boîte ou en steak, le thon est l'un des poissons marins les plus consommés au monde. Pourtant, il est également connu pour contenir du méthylmercure, la forme chimique la plus toxique du mercure, notamment pour le système nerveux, avec des risques élevés pour la santé chez le fœtus et le jeune enfant (Encadré 1). Les nouvelles politiques environnementales de la Convention de Minamata[5] qui visent à réduire les émissions de mercure et ainsi les impacts sanitaires pour l'homme, reposent sur une faible connaissance de la manière dont ces émissions se répercutent dans les poissons. Ici, nous fournissons la première carte détaillée des concentrations de mercure de la bonite à ventre rayée dans l'Océan Pacifique et mettons pour la première fois en évidence un lien entre les émissions anthropiques de mercure et les concentrations dans cette espèce dans le nord-ouest Pacifique (Médieu et al., 2022). Notre étude montre également que le fonctionnement naturel de l'océan a une influence importante sur les concentrations de mercure dans le thon, notamment en fonction de la profondeur à laquelle les concentrations de méthylmercure sont maximales dans la colonne d'eau.

Dans une précédente étude sur trois espèces de thons (thon jaune, thon obèse et thon blanc) dans le Pacifique ouest et central, nous avions révélé que les concentrations en mercure étaient plus élevées pour les poissons les plus grands et plongeant plus profondément, mais dépendaient aussi de l'espèce et de l'origine géographique (Houssard et al., 2019) (cf Lettre d'information sur les pêches de la CPS n° 158, *Taille, espèce, zone de pêche : qu'est-ce qui fait montre le mercure dans les thons*). Dans cette nouvelle étude pluridisciplinaire, financée par le projet MERTOX de l'Agence Nationale de la Recherche[6], l'Institut de Recherche pour le Développement (IRD) et la Communauté Pacifique (CPS) avec l'aide de nombreux partenaires et l'accès à plusieurs banques d'échantillons[7], se sont intéressés à l'origine du mercure retrouvé dans les thons à l'échelle du pacifique (Figure 1A) en se focalisant sur la bonite à ventre rayé (*Katsuwonus pelamis*), espèce la plus consommée à l'échelle mondiale.

L'intérêt de la bonite pour étudier la biodisponibilité du mercure dans les océans ?

Sur l'ensemble des 650 échantillons de bonites analysés, aucune concentration de mercure ne dépasse les seuils sanitaires préconisés (1 mg/kg de tissu frais, WHO and UNEP Chemicals, 2008) (Figure 1B). La bonite fait partie des espèces de thon les moins concentrées en mercure, pourtant elle reste intéressante pour comprendre et cartographier la contamination au mercure dans les océans. D'un point de vue sanitaire d'abord, c'est l'espèce de thon la plus pêchée (essentiellement dans l'océan

[1] Doctorante, Université Bretagne Occidentale - LEMAR
[2] Chercheur, IRD - GET
[3] Chargée de recherche halieutique principale, CPS
[4] Chercheuse, IRD - LEMAR
[5] www.mercuryconvention.org
[6] ANR MERTOX https://www.get.omp.eu/recherche/projets-scientifiques/mertox/
[7] La Western and Central Pacific Fisheries Commission Tuna Tissue Bank, la Pacific Marine Specimen Bank gérée par la CPS, l'Environmental Specimen Bank de l'université de Tokyo (Japon), ainsi que la banque d'échantillons de la commission interaméricaine du thon tropical (IATTC), et celle de Daniel Madigan (Université de Windsor, Etats-Unis).

Pacifique) et consommée, celle que l'on retrouve en grande partie dans les conserves de thon, constituant une source de protéines animales importante à l'échelle mondiale. D'un point de vue biologique et écologique, cette espèce se distingue par une croissance rapide et une distribution verticale très en surface (dans les 100 premiers mètres de la colonne d'eau), quand d'autres espèces de thon, comme le thon blanc ou le thon obèse plongent quotidiennement à plus de 500 mètres de profondeur pour s'alimenter. En choisissant de travailler sur cette espèce de surface, nous avons fait l'hypothèse qu'elle serait en mesure de refléter les niveaux de mercure dans les eaux de surface. Il est estimé que ces niveaux ont triplé en réponse aux émissions anthropiques dans l'atmosphère (Encadré 1). Par ailleurs, cette espèce fait aussi l'objet de divers programmes de recherche et alimente des banques d'échantillons grâce au travail des observateurs à bord des bateaux de pêche dans tout le Pacifique. Ainsi nous avons pu analyser le mercure de la bonite dans des régions très contrastées du Pacifique (Figure 1A), et explorer différents mécanismes pouvant influencer la bioaccumulation du mercure dans les réseaux trophiques. En particulier, nous disposions d'échantillons de bonites au large de l'Asie, zone caractérisée par des fortes émissions anthropiques de mercure dans l'atmosphère (Encadré 1).

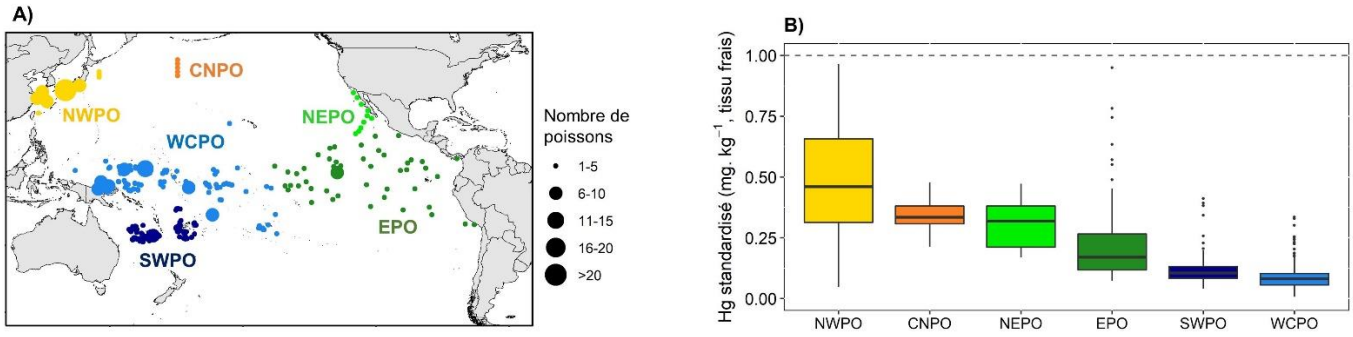

Figure 1. A) Distribution spatiale des bonites analysées en mercure dans six régions de l'océan Pacifique (NWPO, NCPO, NEPO, EPO, SWPO et WCPO). B) Concentrations standardisées de mercure (mg/kg, tissu frais) dans la bonite en fonction des six régions du Pacifique, pour une taille standard de 60 cm. La ligne horizontale pointillée indique la concentration maximale de mercure autorisée (1 mg/kg, tissu frais) pour les grands prédateurs tels que les thons.

Des concentrations variables entre régions du Pacifique

Comme le mercure se bioaccumule naturellement durant la vie des organismes (les poissons plus âgés/grands ont des concentrations en mercure plus élevées), nous avons d'abord standardisé les concentrations de mercure à une taille donnée (60 cm, soit la taille moyenne de l'ensemble des bonites analysées). De forts gradients de concentrations standardisées ont ainsi pu être mis en évidence entre les régions du Pacifique (Figures 1B & 2) : elles sont 1,5 à 2 fois plus élevées dans le nord-ouest Pacifique que dans les régions du centre-nord et de l'est, et 4 à 5 fois plus élevées que dans les régions intertropicales du centre-ouest et sud-ouest Pacifique.

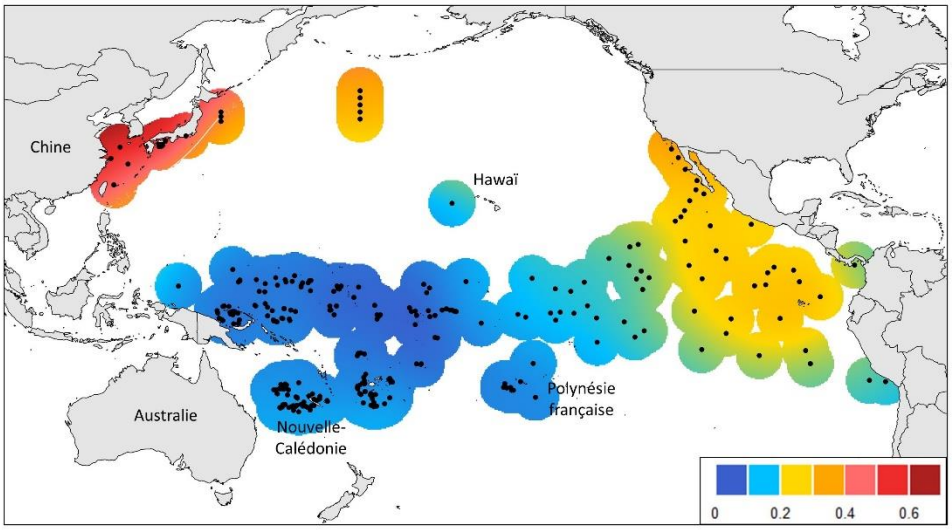

Figure 2. Distribution spatiale des concentrations de mercure (mg.kg^{-1}, tissu frais) dans la bonite pour une taille standard de 60 cm. Les points noirs représentent la position de capture des poissons analysés.

Des gradients de mercure dans les thons induits par le fonctionnement biogéochimique naturel de l'océan

Pour tenter d'expliquer cette forte variabilité spatiale, nous avons utilisé un ensemble de traceurs afin d'identifier si les mécanismes sous-jacents d'accumulation étaient liés à des différences d'alimentation des thons, de biodisponibilité du méthylmercure à la base des réseaux trophiques, ou d'émissions anthropiques de mercure. Avec cette approche, nous avons ainsi pu montrer que des processus biogéochimiques en lien avec le fonctionnement de l'océan Pacifique induisent naturellement de forts gradients spatiaux de mercure dans les thons. En particulier, les concentrations en mercure relativement plus élevées à l'est et dans le nord-ouest Pacifique (Figure 2) semblent être dues à un océan pauvre en oxygène, surtout à l'est, en raison de la dégradation de la matière organique en surface par des bactéries. Nous faisons l'hypothèse que ces conditions particulières sont responsables dans ces zones d'un pic de méthylmercure dans l'eau plus proche de la surface (< 100 mètres), comparé à la partie ouest, où le pic de méthylmercure est plus profond, entre 400 et 800 mètres. La proximité du pic de méthylmercure vers la surface au contact plus direct de la chaîne alimentaire laisse penser que sa biodisponibilité est plus importante. Dans les régions où se produit ce phénomène, les organismes des réseaux trophiques de surface, dont la bonite, peuvent ingérer et accumuler plus de méthylmercure dans ces zones par rapport au reste du Pacifique.

L'importance des émissions anthropiques de mercure dans le nord-ouest Pacifique

Mais les concentrations très élevées dans le Pacifique nord-ouest (Figure 2), peuvent aussi s'expliquer par la proximité géographique avec d'importantes sources d'émissions anthropiques (Encadré 1). Elles pourraient en effet résulter des apports récents en mercure dans l'atmosphère associés à l'usage intensif des combustibles fossiles dans les centrales asiatiques pour la production d'électricité. Ces apports anthropiques (Figure 3) viendraient s'ajouter aux processus biogéochimiques naturels favorables à la biodisponibilité en surface du méthylmercure dans les réseaux trophiques.

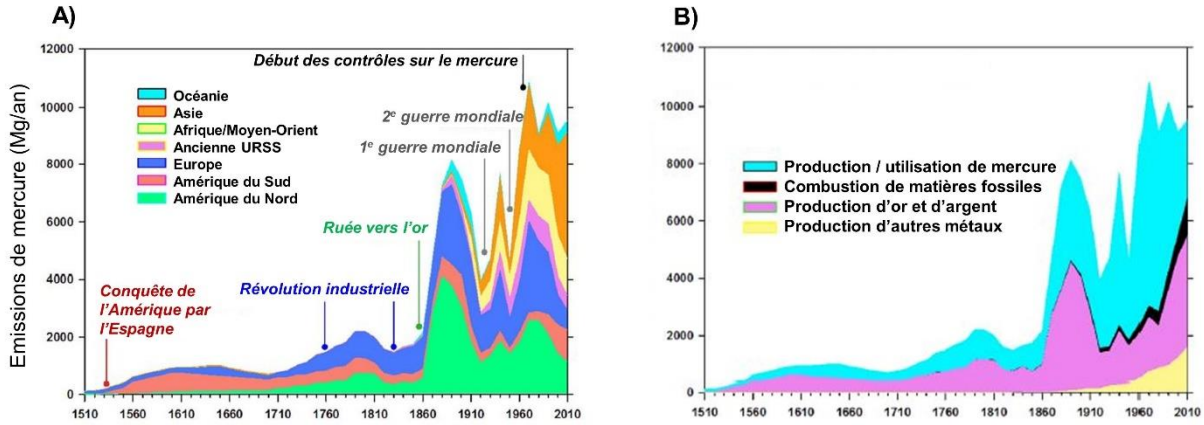

Figure 3. Evolution temporelle des émissions anthropiques de mercure entre 1510 et 2010, en fonction des régions du monde (gauche), et des types de source d'émissions (droite), adapté de Streets et al. (2019). La catégorie « production / utilisation de mercure » inclue la production de mercure utilisé dans l'extraction d'or et d'argent (techniques d'amalgamation), ainsi que dans diverses applications commerciales, comme la production de chlore et de soude caustique, ou le traitement des déchets.

Quelles implications pour la compréhension du cycle du mercure et la Convention de Minamata ?

Dans cette étude, nous avons mis en évidence pour la première fois un lien entre les émissions anthropiques de mercure et les concentrations de mercure dans les thons, dans le Pacifique nord-ouest. De façon générale, même si les concentrations en mercure dans les bonites restent toujours en deçà des concentrations maximales autorisées, il apparaît primordial de contrôler et réduire les rejets anthropiques de mercure dans l'environnement pour préserver la santé des humains et des écosystèmes, comme exigé par la Convention de Minamata, entrée en vigueur en 2017.

Par ailleurs, en révélant l'importance de processus biogéochimiques naturels dans l'accumulation du mercure, notre étude renforce l'hypothèse d'un potentiel impact du changement climatique sur les concentrations de méthylmercure au sein des réseaux trophiques marins. L'expansion de la zone minimum d'oxygène à l'est du Pacifique déjà observée et prévue pour les prochaines décennies, pourrait ainsi favoriser la formation et la biodisponibilité du méthylmercure à la base des réseaux trophiques. En parallèle, des changements de productivité primaire et d'export de la matière organique, pourraient aussi venir contrecarrer cette tendance. Aujourd'hui, les modèles de circulation océanique ne permettent pas de prédire précisément ces changements biogéochimiques, notamment dans les zones tropicales comme à l'est du Pacifique, et l'impact du changement climatique sur le cycle du mercure reste donc à élucider.

Enfin, notre étude suggère que la bonite constitue une bonne espèce bio-indicatrice de la contamination au mercure dans les océans, puisqu'elle semble capable de refléter l'exposition au mercure d'un écosystème donné (ici les eaux de surface du Pacifique) tout en intégrant plusieurs sources de mercure à diverses échelles spatiales. Combiné à des mesures de mercure dans l'air et l'océan, la bonite pourrait ainsi fournir des informations essentielles à la conception et à la mise en œuvre future de bio-surveillance du mercure à grande échelle, comme exigé pour évaluer l'efficacité de la Convention de Minamata. Une étude comparable, mais à l'échelle globale (incluant les océans Indien et Atlantique) et combinant d'autres espèces emblématiques de thons (thon jaune et thon obèse) est en cours pour confirmer ou non les résultats de notre étude.

Encadré 1. Le cycle du (méthyl)mercure dans les océans : les grandes incertitudes face aux activités anthropiques et au changement climatique

Le mercure est émis dans l'atmosphère sous forme gazeuse par des sources naturelles (comme les éruptions volcaniques) mais principalement par des activités humaines (émissions anthropiques), telles que la combustion de charbon ou l'orpaillage (Figure A). Ce mercure inorganique se dépose dans les océans où il est en partie transformé en méthylmercure, une neurotoxine. Celle-ci s'accumule naturellement dans les tissus des organismes au cours de leur vie (bioaccumulation) ainsi que le long des réseaux trophiques (bioamplification). Pour cette raison, les prédateurs marins comme les thons, présentent des concentrations en méthylmercure élevées, le méthylmercure étant la forme majoritaire (> 91 %) du pool total de mercure. L'humain est ensuite exposé au méthylmercure via sa consommation de poissons marins.

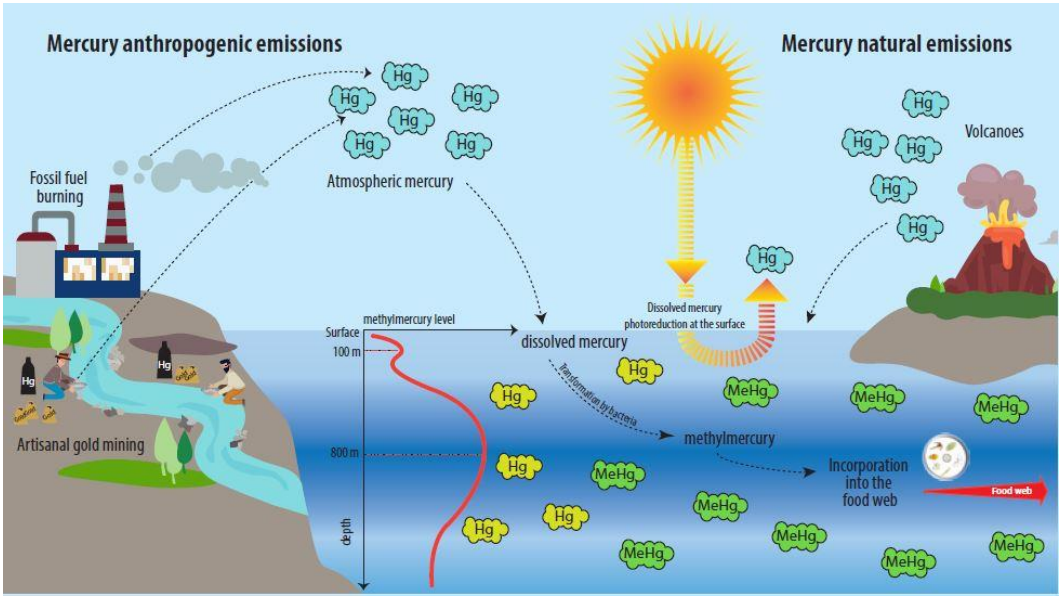

Figure A. d'où vient le méthylmercure (MeHg) présent dans l'océan ? (Source : Anne Lorrain et al. 2019 ; Illustration Constance Odiardo)

Initiées il y a cinq siècles par l'Europe et l'Amérique du Nord, les émissions anthropiques proviennent aujourd'hui en grande partie de l'Asie, notamment de la Chine, où elles ont particulièrement augmenté au cours des deux dernières décennies en lien avec l'usage de combustibles fossiles pour la production d'énergie (UN Environment, 2019) (voir Figure 3 en page…). L'ensemble des émissions anthropiques a profondément modifié le cycle du mercure. On estime qu'elles ont augmenté de 450 % les concentrations de mercure dans l'atmosphère (Outridge et al., 2018), cet enrichissement étant plus important dans l'hémisphère nord que dans l'hémisphère sud (C. Li et al., 2020) (Figure B). Dans l'océan, les émissions anthropiques auraient multiplié par trois le pool total de mercure (mercure inorganique + méthylmercure) (Lamborg et al., 2014) ; cependant, l'impact sur les concentrations de méthylmercure dans l'eau et les organismes marins, en particulier les grands prédateurs, reste non documenté.

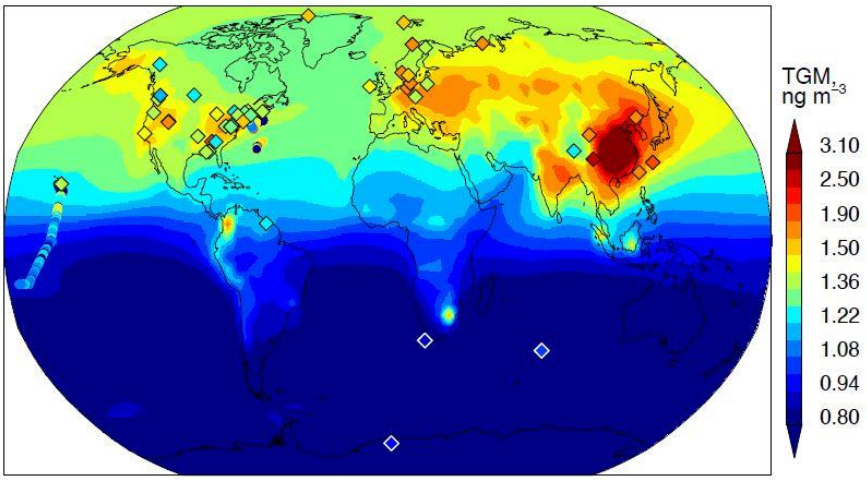

Figure B. Distribution globale des concentrations modélisées de mercure gazeux dans l'atmosphère, d'après Horowitz et al. (2017). Les losanges représentent des mesures de concentrations de mercure gazeux dans l'atmosphère et servent à valider la modélisation de ces mêmes concentrations.

Autre grande incertitude concernant le cycle du mercure : l'impact du changement climatique, en particulier sur la formation du méthylmercure et sa biodisponibilité à la base des réseaux trophiques marins. Il est communément admis que le mercure gazeux dissous dans l'eau est transformé en méthylmercure (méthylation), notamment sous l'action de bactéries, dans les zones profondes de l'océan moins oxygénées (entre 400 et 800 mètres de profondeur). Ce méthylmercure peut être retransformé en mercure gazeux (déméthylation) dans les couches de surface, où il sera potentiellement réémis vers l'atmosphère. Les processus de méthylation/déméthylation sont encore mal connus, pourtant c'est bien l'équilibre entre les deux qui conditionne ensuite la quantité de méthylmercure biodisponible à la base des réseaux trophiques marins. Le changement climatique, parce qu'il est susceptible de modifier la circulation et la productivité des océans, et d'étendre les zones de minimum d'oxygène, pourrait aussi profondément modifier le cycle du mercure.

References

Abascal, F.J., Peatman, T., Leroy, B., Nicol, S., Schaefer, K., Fuller, D.W., Hampton, J., 2018. Spatiotemporal variability in bigeye vertical distribution in the Pacific Ocean. Fisheries Research 204, 371–379. https://doi.org/10.1016/j.fishres.2018.03.013

Abeysinghe, K.S., Qiu, G., Goodale, E., Anderson, C.W.N., Bishop, K., Evers, D.C., Goodale, M.W., Hintelmann, H., Liu, S., Mammides, C., Quan, R.-C., Wang, J., Wu, P., Xu, X.-H., Yang, X.-D., Feng, X., 2017. Mercury flow through an Asian rice-based food web. Environmental Pollution 229, 219–228. https://doi.org/10.1016/j.envpol.2017.05.067

Adams, D.H., 2004. Total mercury levels in tunas from offshore waters of the Florida Atlantic coast. Marine Pollution Bulletin 49, 659–663. https://doi.org/10.1016/j.marpolbul.2004.06.005

Agather, A.M., Bowman, K.L., Lamborg, C.H., Hammerschmidt, C.R., 2019. Distribution of mercury species in the Western Arctic Ocean (U.S. GEOTRACES GN01). Marine Chemistry 216, 103686. https://doi.org/10.1016/j.marchem.2019.103686

Aksentov, K.I., Sattarova, V.V., 2020. Mercury geochemistry of deep-sea sediment cores from the Kuril area, northwest Pacific. Progress in Oceanography 180, 102235. https://doi.org/10.1016/j.pocean.2019.102235

Al-Busaidi, M., Yesudhason, P., Al-Mughairi, S., Al-Rahbi, W.A.K., Al-Harthy, K.S., Al-Mazrooei, N.A., Al-Habsi, S.H., 2011. Toxic metals in commercial marine fish in Oman with reference to national and international standards. Chemosphere 85, 67–73. https://doi.org/10.1016/j.chemosphere.2011.05.057

Al-Najjar, T., Dahiyat, N., Sharari, N., Wahsha, M., Khalaf, M., 2019. Levels of mercury in three species of tuna (Katsuwonus pelamis, Auxis thazard and Euthynnus affinis) collected from the Jordanian coast of the Gulf of the Aqaba, Red Sea. Fresenius Environmental Bulletin 28, 8.

AMAP, UN Environment, 2019. Technical Background Report for the Global Mercury Assessment 2018. Arctic Monitoring and Assessment Programme, Oslo, Norway/UN Environment Programme, Chemicals and Health Branch. Geneva, Switzerland.

Amlund, H., Lundebye, A.-K., Berntssen, M.H.G., 2007. Accumulation and elimination of methylmercury in Atlantic cod (Gadus morhua L.) following dietary exposure. Aquatic Toxicology 83, 323–330. https://doi.org/10.1016/j.aquatox.2007.05.008

Amos, H.M., Jacob, D.J., Kocman, D., Horowitz, H.M., Zhang, Y., Dutkiewicz, S., Horvat, M., Corbitt, E.S., Krabbenhoft, D.P., Sunderland, E.M., 2014. Global Biogeochemical Implications of Mercury Discharges from Rivers and Sediment Burial. Environ. Sci. Technol. 48, 9514–9522. https://doi.org/10.1021/es502134t

Amos, H.M., Jacob, D.J., Streets, D.G., Sunderland, E.M., 2013. Legacy impacts of all-time anthropogenic emissions on the global mercury cycle. Global Biogeochemical Cycles 27, 410–421. https://doi.org/10.1002/gbc.20040

Amos, H.M., Sonke, J.E., Obrist, D., Robins, N., Hagan, N., Horowitz, H.M., Mason, R.P., Witt, M., Hedgecock, I.M., Corbitt, E.S., Sunderland, E.M., 2015. Observational and Modeling Constraints on Global Anthropogenic Enrichment of Mercury. Environ. Sci. Technol. 49, 4036–4047. https://doi.org/10.1021/es5058665

Andersen, J.L., Depledge, M.H., 1997. A survey of total mercury and methylmercury in edible fish and invertebrates from Azorean waters. Marine Environmental Research 44, 331–350. https://doi.org/10.1016/S0141-1136(97)00011-1

Anderson, G., Lal, M., Hampton, J., Smith, N., Rico, C., 2019. Close Kin Proximity in Yellowfin Tuna (Thunnus albacares) as a Driver of Population Genetic Structure in the Tropical Western and Central Pacific Ocean. Front. Mar. Sci. 0. https://doi.org/10.3389/fmars.2019.00341

Angot, H., Hoffman, N., Giang, A., Thackray, C.P., Hendricks, A.N., Urban, N.R., Selin, N.E., 2018. Global and Local Impacts of Delayed Mercury Mitigation Efforts. Environ. Sci. Technol. 52, 12968–12977. https://doi.org/10.1021/acs.est.8b04542

Annasawmy, P., Point, D., Romanov, E.V., Bodin, N., 2022. Mercury concentrations and stable isotope ratios (δ13C and δ15N) in pelagic nekton assemblages of the south-western Indian Ocean. Marine Pollution Bulletin 174, 113151. https://doi.org/10.1016/j.marpolbul.2021.113151

AOCS, 2017. Determination of Precision of Analytical Methods. Evaluation and design of test methods.

Araújo, C.V.M., Cedeño-Macias, L.A., 2016. Heavy metals in yellowfin tuna (Thunnus albacares) and common dolphinfish (Coryphaena hippurus) landed on the Ecuadorian coast. Science of The Total Environment 541, 149–154. https://doi.org/10.1016/j.scitotenv.2015.09.090

Archer, D.E., Blum, J.D., 2018. A model of mercury cycling and isotopic fractionation in the ocean. Biogeosciences 15, 6297–6313. https://doi.org/10.5194/bg-15-6297-2018

Arrizabalaga, H., Costas, E., Juste, J., González-Garcés, A., Nieto, B., López-Rodas, V., 2004. Population structure of albacore Thunnus alalunga inferred from blood groups and tag-recapture analyses. Mar. Ecol. Prog. Ser. 282, 245–252. https://doi.org/10.3354/meps282245

Arrizabalaga, H., Dufour, F., Kell, L., Merino, G., Ibaibarriaga, L., Chust, G., Irigoien, X., Santiago, J., Murua, H., Fraile, I., Chifflet, M., Goikoetxea, N., Sagarminaga, Y., Aumont, O., Bopp, L., Herrera, M., Marc Fromentin, J., Bonhomeau, S., 2015. Global habitat preferences of commercially valuable tuna. Deep Sea Research Part II: Topical Studies in Oceanography, Impacts of climate on marine top predators 113, 102–112. https://doi.org/10.1016/j.dsr2.2014.07.001

Atwell, L., Hobson, K.A., Welch, H.E., 1998. Biomagnification and bioaccumulation of mercury in an arctic marine food web: insights from stable nitrogen isotope analysis 55, 8.

Aumont, O., Ethé, C., Tagliabue, A., Bopp, L., Gehlen, M., 2015. PISCES-v2: an ocean biogeochemical model for carbon and ecosystem studies. Geosci. Model Dev. 8, 2465–2513. https://doi.org/10.5194/gmd-8-2465-2015

Bagnato, E., Oliveri, E., Acquavita, A., Covelli, S., Petranich, E., Barra, M., Italiano, F., Parello, F., Sprovieri, M., 2017. Hydrochemical mercury distribution and air-sea exchange over the submarine hydrothermal vents off-shore Panarea Island (Aeolian arc, Tyrrhenian Sea). Marine Chemistry 194, 63–78. https://doi.org/10.1016/j.marchem.2017.04.003

Barbosa, R.V., Point, D., Médieu, A., Allain, V., Gillikin, D.P., Couturier, L.I.E., Munaron, J.-M., Roupsard, F., Lorrain, A., 2022. Mercury concentrations in tuna blood and muscle mirror seawater methylmercury in the Western and Central Pacific Ocean. Marine Pollution Bulletin 180, 113801. https://doi.org/10.1016/j.marpolbul.2022.113801

Barkay, T., Miller, S.M., Summers, A.O., 2003. Bacterial mercury resistance from atoms to ecosystems. FEMS Microbiol Rev 27, 355–384. https://doi.org/10.1016/S0168-6445(03)00046-9

Barkley, R.A., Neill, W.H., Gooding, R.M., 1978. Skipjack tuna, Katsuwonus pelamis, habitat based on temperature and oxygen requirements, Fishery Bulletin. National Marine Fisheries Service.

Bashmakov, V.F., Fao, C., Colombo, W. on S.A. of Y.T. in the I.O. eng 7-12 O. 1991, Zamorov, V.V., Romanov, E.V., 1991. Diet composition of tunas caught with long lines and purse seines in the Western Indian Ocean. FAO, Colombo (Sri Lanka).

Bearhop, S., Ruxton, G.D., Furness, R.W., 2000. Dynamics of mercury in blood and feathers of great skuas. Environmental Toxicology and Chemistry 19, 1638–1643. https://doi.org/10.1002/etc.5620190622

Behrenfeld, M.J., Falkowski, P.G., 1997. Photosynthetic rates derived from satellite-based chlorophyll concentration. Limnology and Oceanography 42, 1–20. https://doi.org/10.4319/lo.1997.42.1.0001

Bell, J.D., Allain, V., Allison, E.H., Andréfouët, S., Andrew, N.L., Batty, M.J., Blanc, M., Dambacher, J.M., Hampton, J., Hanich, Q., Harley, S., Lorrain, A., McCoy, M., McTurk, N., Nicol, S., Pilling, G., Point, D., Sharp, M.K., Vivili, P., Williams, P., 2015. Diversifying the use of tuna to improve food security and public health in Pacific Island countries and territories. Marine Policy 51, 584–591. https://doi.org/10.1016/j.marpol.2014.10.005

Bell, J.D., Reid, C., Batty, M.J., Allison, E.H., Lehodey, P., Rodwell, L., Pickering, T.D., Gillett, R., Johnson, J.E., Hobday, A.J., Demmke, A., 2011. Implications of climate change for contributions by fisheries and aquaculture to Pacific Island economies and communities, in: Vulnerability of Tropical Pacific Fisheries and Aquaculture to Climate Change: Summary for

Pacific Island Countries and Territories. Secretariat of the Pacific Community, Noumea, New Caledonia, p. 71.

Bernhoft, R.A., 2012. Mercury Toxicity and Treatment: A Review of the Literature. Journal of Environmental and Public Health 2012, 1–10. https://doi.org/10.1155/2012/460508

Bertilsson, L., Neujahr, H.Y., 1971. Methylation of mercury compounds by methylcobalamin. Biochemistry 10, 2805–2808. https://doi.org/10.1021/bi00790a024

Besada, V., 2006. Mercury, cadmium, lead, arsenic, copper and zinc concentrations in albacore, yellowfin tuna and bigeye tuna from the Atlantic Ocean. Ciencias Marinas 32, 439–445. https://doi.org/10.7773/cm.v32i22.1083

Bianchi, D., Weber, T.S., Kiko, R., Deutsch, C., 2018. Global niche of marine anaerobic metabolisms expanded by particle microenvironments. Nature Geosci 11, 263–268. https://doi.org/10.1038/s41561-018-0081-0

Bielsa, N.P., Ollé, J., Macías, D., Saber, S., Viñas, J., 2021. Genetic validation of the unexpected presence of a tropical tuna, bigeye tuna (Thunnus obesus), in the Mediterranean. Journal of Fish Biology 99, 1761–1764. https://doi.org/10.1111/jfb.14866

Bignert, A., Riget, F., Braune, B., Outridge, P., Wilson, S., 2004. Recent temporal trend monitoring of mercury in Arctic biota – how powerful are the existing data sets? J. Environ. Monit. 6, 351–355. https://doi.org/10.1039/B312118F

Bindoff, N.L., Cheung, W.W.L., Kairo, J.G., Arístegui, J., Guinder, V.A., Hallberg, R., Hilmi, N.J.M., Jiao, N., Karim, M.S., Levin, L., O'Donoghue, S., Purca Cuicapusa, S.R., Rinkevich, B., Suga, T., Tagliabue, A., Williamson, P., 2019. Changing Ocean, Marine Ecosystems, and Dependent Communities, in: Pörtner, H.-O., Roberts, D.C., Masson-Delmotte, V., Zhai, P., Tignor, M., Poloczanska, E., Mintenbeck, K., Alegría, A., Nicolai, M., Okem, A., Petzold, J., Rama, B., Weyer, N.M. (Eds.), IPCC Special Report on the Ocean and Cryosphere in a Changing Climate. Intergovernmental Panel on Climate Change, Switzerland, pp. 477–587.

Bjørklund, G., Dadar, M., Mutter, J., Aaseth, J., 2017. The toxicology of mercury: Current research and emerging trends. Environmental Research 159, 545–554. https://doi.org/10.1016/j.envres.2017.08.051

Block, B.A., Teo, S.L.H., Walli, A., Boustany, A., Stokesbury, M.J.W., Farwell, C.J., Weng, K.C., Dewar, H., Williams, T.D., 2005. Electronic tagging and population structure of Atlantic bluefin tuna. Nature 434, 1121–1127. https://doi.org/10.1038/nature03463

Bloom, N.S., 1992. On the Chemical Form of Mercury in Edible Fish and Marine Invertebrate Tissue. Can. J. Fish. Aquat. Sci. 49, 1010–1017. https://doi.org/10.1139/f92-113

Blum, J.D., Popp, B.N., Drazen, J.C., Anela Choy, C., Johnson, M.W., 2013. Methylmercury production below the mixed layer in the North Pacific Ocean. Nature Geoscience 6, 879–884. https://doi.org/10.1038/ngeo1918

Boddington, M.J., Mackenzie, B.A., deFreitas, A.S.W., 1979. A respirometer to measure the uptake efficiency of waterborne contaminants in fish. Ecotoxicology and Environmental Safety 3, 383–393. https://doi.org/10.1016/0147-6513(79)90028-9

Bodin, N., Budzinski, H., Le Ménach, K., Tapie, N., 2009. ASE extraction method for simultaneous carbon and nitrogen stable isotope analysis in soft tissues of aquatic organisms. Analytica Chimica Acta 643, 54–60. https://doi.org/10.1016/j.aca.2009.03.048

Bodin, N., Lesperance, D., Albert, R., Hollanda, S., Michaud, P., Degroote, M., Churlaud, C., Bustamante, P., 2017. Trace elements in oceanic pelagic communities in the western Indian Ocean. Chemosphere 174, 354–362. https://doi.org/10.1016/j.chemosphere.2017.01.099

Bodin, N., Pethybridge, H., Duffy, L.M., Lorrain, A., Allain, V., Logan, J.M., Ménard, F., Graham, B., Choy, C.A., Somes, C.J., Olson, R.J., Young, J.W., 2020. Global data set for nitrogen and carbon stable isotopes of tunas. Ecology. https://doi.org/10.1002/ecy.3265

Bonnet, S., Caffin, M., Berthelot, H., Moutin, T., 2017. Hot spot of N2 fixation in the western tropical South Pacific pleads for a spatial decoupling between N2 fixation and denitrification. Proc Natl Acad Sci USA 114, E2800–E2801. https://doi.org/10.1073/pnas.1619514114

Bopp, L., Resplandy, L., Orr, J.C., Doney, S.C., Dunne, J.P., Gehlen, M., Halloran, P., Heinze, C., Ilyina, T., Séférian, R., Tjiputra, J., Vichi, M., 2013. Multiple stressors of ocean ecosystems in the 21st century: projections with CMIP5 models. Biogeosciences 10, 6225–6245. https://doi.org/10.5194/bg-10-6225-2013

Bosch, A.C., O'Neill, B., Sigge, G.O., Kerwath, S.E., Hoffman, L.C., 2016. Mercury accumulation in Yellowfin tuna (Thunnus albacares) with regards to muscle type, muscle position and fish size. Food Chemistry 190, 351–356. https://doi.org/10.1016/j.foodchem.2015.05.109

Boush, G.M., Thieleke, J.R., 1983. Total mercury content in yellowfin and bigeye tuna. Bull. Environ. Contam. Toxicol. 30, 291–297. https://doi.org/10.1007/BF01610135

Bowman, K.L., Collins, R.E., Agather, A.M., Lamborg, C.H., Hammerschmidt, C.R., Kaul, D., Dupont, C.L., Christensen, G.A., Elias, D.A., 2020a. Distribution of mercury-cycling genes in the Arctic and equatorial Pacific Oceans and their relationship to mercury speciation. Limnology and Oceanography 65, S310–S320. https://doi.org/10.1002/lno.11310

Bowman, K.L., Hammerschmidt, C.R., Lamborg, C.H., Swarr, G., 2015. Mercury in the North Atlantic Ocean: The U.S. GEOTRACES zonal and meridional sections. Deep Sea Research Part II: Topical Studies in Oceanography, GEOTRACES GA-03 - The U.S. GEOTRACES North Atlantic Transect 116, 251–261. https://doi.org/10.1016/j.dsr2.2014.07.004

Bowman, K.L., Hammerschmidt, C.R., Lamborg, C.H., Swarr, G.J., Agather, A.M., 2016. Distribution of mercury species across a zonal section of the eastern tropical South Pacific Ocean (U.S. GEOTRACES GP16). Marine Chemistry 186, 156–166. https://doi.org/10.1016/j.marchem.2016.09.005

Bowman, K.L., Lamborg, C.H., Agather, A.M., 2020b. A global perspective on mercury cycling in the ocean. Science of The Total Environment 710, 136166. https://doi.org/10.1016/j.scitotenv.2019.136166

Boyd, E., Barkay, T., 2012. The Mercury Resistance Operon: From an Origin in a Geothermal Environment to an Efficient Detoxification Machine. Frontiers in Microbiology 3, 349. https://doi.org/10.3389/fmicb.2012.00349

Bradley, C.J., Wallsgrove, N.J., Choy, C.A., Drazen, J.C., Hetherington, E.D., Hoen, D.K., Popp, B.N., 2015. Trophic position estimates of marine teleosts using amino acid compound specific isotopic analysis. Limnology and Oceanography: Methods 13, 476–493. https://doi.org/10.1002/lom3.10041

Bratkič, A., Vahčič, M., Kotnik, J., Obu Vazner, K., Begu, E., Woodward, E.M.S., Horvat, M., 2016. Mercury presence and speciation in the South Atlantic Ocean along the 40°S transect. Global Biogeochemical Cycles 30, 105–119. https://doi.org/10.1002/2015GB005275

Breitburg, D., Levin, L.A., Oschlies, A., Grégoire, M., Chavez, F.P., Conley, D.J., Garçon, V., Gilbert, D., Gutiérrez, D., Isensee, K., Jacinto, G.S., Limburg, K.E., Montes, I., Naqvi, S.W.A., Pitcher, G.C., Rabalais, N.N., Roman, M.R., Rose, K.A., Seibel, B.A., Telszewski, M., Yasuhara, M., Zhang, J., 2018. Declining oxygen in the global ocean and coastal waters. Science 359, eaam7240. https://doi.org/10.1126/science.aam7240

Brewer, D.T., Morello, E.B., Griffiths, S., Fry, G., Heales, D., Apte, S.C., Venables, W.N., Rothlisberg, P.C., Moeseneder, C., Lansdell, M., Pendrey, R., Coman, F., Strzelecki, J., Jarolimek, C.V., Jung, R.F., Richardson, A.J., 2012. Impacts of gold mine waste disposal on a tropical pelagic ecosystem. Marine Pollution Bulletin 64, 2790–2806. https://doi.org/10.1016/j.marpolbul.2012.09.009

Brill, R.W., Bigelow, K.A., Musyl, M.K., Fritsches, K.A., Warrant, E.J., 2005. Bigeye tuna (Thunnus obesus) behavior and physiology and their relevance to stock assessments and fishery biology (No. 57 (2)), Col. Vol. Sci. Pap. ICCAT.

Brill, R.W., Bushnell, P.G., 2001. The cardiovascular system of tunas, in: Fish Physiology, Tuna: Physiology, Ecology, and Evolution. Academic Press, pp. 79–120. https://doi.org/10.1016/S1546-5098(01)19004-7

Brind'Amour, A., Mahévas, S., Legendre, P., Bellanger, L., 2018. Application of Moran Eigenvector Maps (MEM) to irregular sampling designs. Spatial Statistics 26, 56–68. https://doi.org/10.1016/j.spasta.2018.05.004

Brooks, B., 2004. Mercury levels in tuna and other major commercial fish species in Hawaii. Presented at the Proceedings of the 2004 National Forum on Contalinants in Fish, San Diego, CA, USA, p. 24.

Buchheister, A., Latour, R.J., 2010. Turnover and fractionation of carbon and nitrogen stable isotopes in tissues of a migratory coastal predator, summer flounder (Paralichthys dentatus). Can. J. Fish. Aquat. Sci. 67, 445–461. https://doi.org/10.1139/F09-196

Burger, J., 2011. Mercury and selenium levels in 19 species of saltwater fish from New Jersey as a function of species, size, and season. Science of the Total Environment 12.

Burnham, K.P., Anderson, D.R., 2004. Multimodel Inference: Understanding AIC and BIC in Model Selection. Sociological Methods & Research 33, 261–304. https://doi.org/10.1177/0049124104268644

Bushnell, P.G., Jones, D.R., 1994. Cardiovascular and respiratory physiology of tuna: adaptations for support of exceptionally high metabolic rates. Environ Biol Fish 40, 303–318. https://doi.org/10.1007/BF00002519

Cai, Y., Rooker, J.R., Gill, G.A., Turner, J.P., 2007. Bioaccumulation of mercury in pelagic fishes from the northern Gulf of Mexico. Canadian Journal of Fisheries and Aquatic Sciences 64, 458–469. https://doi.org/10.1139/f07-017

Carey, F.G., Kanwisher, J.W., Stevens, E.D., 1984. Bluefin tuna warm their viscera during digestion 22.

Carey, F.G., Teal, J.M., Kanwisher, J.W., Lawson, K.D., 1971. Warm-bodied fish. American Zoologist 11, 137–143.

Celo, V., Lean, D.R.S., Scott, S.L., 2006. Abiotic methylation of mercury in the aquatic environment. Science of The Total Environment, Selected papers from the 7th International Conference on Mercury as a Global Pollutant, Ljubljana, Slovenia June 27 - July 2, 2004 368, 126–137. https://doi.org/10.1016/j.scitotenv.2005.09.043

Chanto-García, D.A., Saber, S., Macías, D., Sureda, A., Hernández-Urcera, J., Cabanellas-Reboredo, M., 2021. Species-specific heavy metal concentrations of tuna species: the case of Thunnus alalunga and Katsuwonus pelamis in the Western Mediterranean. Environ Sci Pollut Res. https://doi.org/10.1007/s11356-021-15700-w

Chassot, E., 2015. A review of morphometric data available for tropical tunas: updating relationships for purse seine fisheries data processing (working document). IRD, Ob7.

Chen, B., Wang, T., Yin, Y., He, B., Jiang, G., 2007. Methylation of inorganic mercury by methylcobalamin in aquatic systems. Applied Organometallic Chemistry 21, 462–467. https://doi.org/10.1002/aoc.1221

Chen, C., Amirbahman, A., Fisher, N., Harding, G., Lamborg, C., Nacci, D., Taylor, D., 2008. Methylmercury in Marine Ecosystems: Spatial Patterns and Processes of Production, Bioaccumulation, and Biomagnification. EcoHealth 5, 399–408. https://doi.org/10.1007/s10393-008-0201-1

Chen, C.-Y., Lai, C.-C., Chen, K.-S., Hsu, C.-C., Hung, C.-C., Chen, M.-H., 2014. Total and organic mercury concentrations in the muscles of Pacific albacore (Thunnus alalunga) and bigeye tuna (Thunnus obesus). Marine Pollution Bulletin 85, 606–612. https://doi.org/10.1016/j.marpolbul.2014.01.039

Chen, M.H., Teng, P.Y., Chen, C.Y., Hsu, C.C., 2011. Organic and total mercury levels in bigeye tuna, Thunnus obesus, harvested by Taiwanese fishing vessels in the Atlantic and Indian Oceans. Food Additives and Contaminants: Part B 4, 15–21. https://doi.org/10.1080/19393210.2010.535908

Cheng, L., Abraham, J., Hausfather, Z., Trenberth, K.E., 2019. How fast are the oceans warming? Science 363, 128–129. https://doi.org/10.1126/science.aav7619

Cheung, W.W.L., Sarmiento, J.L., Dunne, J., Frölicher, T.L., Lam, V.W.Y., Deng Palomares, M.L., Watson, R., Pauly, D., 2013. Shrinking of fishes exacerbates impacts of global ocean changes

on marine ecosystems. Nature Clim Change 3, 254–258. https://doi.org/10.1038/nclimate1691

Chikaraishi, Y., Ogawa, N., Ohkouchi, N., 2010. Further evaluation of the trophic level estimation based on nitrogen isotopic composition of amino acids. Earth, Life, and Isotopes 37–51.

Chikaraishi, Y., Ogawa, N.O., Kashiyama, Y., Takano, Y., Suga, H., Tomitani, A., Miyashita, H., Kitazato, H., Ohkouchi, N., 2009. Determination of aquatic food-web structure based on compound-specific nitrogen isotopic composition of amino acids. Limnology and Oceanography: Methods 7, 740–750. https://doi.org/10.4319/lom.2009.7.740

Chouvelon, T., Brach-Papa, C., Auger, D., Bodin, N., Bruzac, S., Crochet, S., Degroote, M., Hollanda, S.J., Hubert, C., Knoery, J., Munschy, C., Puech, A., Rozuel, E., Thomas, B., West, W., Bourjea, J., Nikolic, N., 2017. Chemical contaminants (trace metals, persistent organic pollutants) in albacore tuna from western Indian and south-eastern Atlantic Oceans: Trophic influence and potential as tracers of populations. Science of The Total Environment 596–597, 481–495. https://doi.org/10.1016/j.scitotenv.2017.04.048

Choy, C.A., Popp, B.N., Hannides, C.C.S., Drazen, J.C., 2015. Trophic structure and food resources of epipelagic and mesopelagic fishes in the North Pacific Subtropical Gyre ecosystem inferred from nitrogen isotopic compositions: Trophic structure of pelagic fishes. Limnology and Oceanography 60, 1156–1171. https://doi.org/10.1002/lno.10085

Choy, C.A., Popp, B.N., Kaneko, J.J., Drazen, J.C., 2009. The influence of depth on mercury levels in pelagic fishes and their prey. Proceedings of the National Academy of Sciences 106, 13865–13869. https://doi.org/10.1073/pnas.0900711106

Cipro, C.V.Z., Bustamante, P., Montone, R.C., 2017. Influence of Delipidation on Hg Analyses in Biological Tissues: A Case Study for an Antarctic Ecosystem. Water Air Soil Pollut 228, 188. https://doi.org/10.1007/s11270-017-3367-8

Clarkson, T.W., Magos, L., Myers, G.J., 2003. The Toxicology of Mercury — Current Exposures and Clinical Manifestations. New England Journal of Medicine 349, 1731–1737. https://doi.org/10.1056/NEJMra022471

Coale, K.H., Heim, W.A., Negrey, J., Weiss-Penzias, P., Fernandez, D., Olson, A., Chiswell, H., Byington, A., Bonnema, A., Martenuk, S., Newman, A., Beebe, C., Till, C., 2018. The distribution and speciation of mercury in the California current: Implications for mercury transport via fog to land. Deep Sea Research Part II: Topical Studies in Oceanography 151, 77–88. https://doi.org/10.1016/j.dsr2.2018.05.012

Codex Alimentarius, 1991. Guideline Levels for Methylmercury in Fish CAC/GL 7-1991.

Collette, B.B., Reeb, C., Block, B.A., 2001. Systematics of the tunas and mackerels (Scombridae), in: Fish Physiology, Tuna: Physiology, Ecology, and Evolution. Academic Press, pp. 1–33. https://doi.org/10.1016/S1546-5098(01)19002-3

Compeau, G.C., Bartha, R., 1985. Sulfate-Reducing Bacteria: Principal Methylators of Mercury in Anoxic Estuarine Sediment. Applied and Environmental Microbiology 50, 498–502. https://doi.org/10.1128/aem.50.2.498-502.1985

Cossa, D., Averty, B., Pirrone, N., 2009. The origin of methylmercury in open Mediterranean waters. Limnol. Oceanogr. 54, 837–844. https://doi.org/10.4319/lo.2009.54.3.0837

Cossa, D., Harmelin-Vivien, M., Mellon-Duval, C., Loizeau, V., Averty, B., Crochet, S., Chou, L., Cadiou, J.-F., 2012. Influences of Bioavailability, Trophic Position, and Growth on Methylmercury in Hakes (Merluccius merluccius) from Northwestern Mediterranean and Northeastern Atlantic. Environ. Sci. Technol. 46, 4885–4893. https://doi.org/10.1021/es204269w

Cossa, D., Heimbürger, L.-E., Lannuzel, D., Rintoul, S.R., Butler, E.C.V., Bowie, A.R., Averty, B., Watson, R.J., Remenyi, T., 2011. Mercury in the Southern Ocean. Geochimica et Cosmochimica Acta 75, 4037–4052. https://doi.org/10.1016/j.gca.2011.05.001

Cossa, D., Martin, J.-M., Sanjuan, J., 1994. Dimethylmercury formation in the Alboran Sea. Marine Pollution Bulletin 28, 381–384. https://doi.org/10.1016/0025-326X(94)90276-3

Cravatte, S., Kestenare, E., Eldin, G., Ganachaud, A., Lefèvre, J., Marin, F., Menkes, C., Aucan, J., 2015. Regional circulation around New Caledonia from two decades of observations. Journal of Marine Systems 148, 249–271. https://doi.org/10.1016/j.jmarsys.2015.03.004

Dagorn, L., Holland, K.N., Hallier, J.-P., Taquet, M., Moreno, G., Sancho, G., Itano, D.G., Aumeeruddy, R., Girard, C., Million, J., Fonteneau, A., 2006. Deep diving behavior observed in yellowfin tuna (Thunnus albacares). Aquatic Living Resources 19, 85–88. https://doi.org/10.1051/alr:2006008

Dale, J., Wallsgrove, N., Popp, B., Holland, K., 2011. Nursery habitat use and foraging ecology of the brown stingray Dasyatis lata determined from stomach contents, bulk and amino acid stable isotopes. Mar. Ecol. Prog. Ser. 433, 221–236. https://doi.org/10.3354/meps09171

Davidson, P.W., Leste, A., Benstrong, E., Burns, C.M., Valentin, J., Sloane-Reeves, J., Huang, L.-S., Miller, W.A., Gunzler, D., van Wijngaarden, E., Watson, G.E., Zareba, G., Shamlaye, C.F., Myers, G.J., 2010. Fish consumption, mercury exposure, and their associations with scholastic achievement in the Seychelles Child Development Study. NeuroToxicology, Gene-Environment Interactions in Neurotoxicology: The 12th Biennial Meeting of the International Neurotoxicology Association 31, 439–447. https://doi.org/10.1016/j.neuro.2010.05.010

de la Higuera, M., Akharbach, H., Hidalgo, M.C., Peragón, J., Lupiáñez, J.A., García-Gallego, M., 1999. Liver and white muscle protein turnover rates in the European eel (Anguilla anguilla): effects of dietary protein quality. Aquaculture 179, 203–216. https://doi.org/10.1016/S0044-8486(99)00163-5

Debes, F., Weihe, P., Grandjean, P., 2016. Cognitive deficits at age 22 years associated with prenatal exposure to methylmercury. Cortex, What's your poison? Neurobehavioural consequences of exposure to industrial, agricultural and environmental chemicals 74, 358–369. https://doi.org/10.1016/j.cortex.2015.05.017

DeNiro, M.J., Epstein, S., 1977. Mechanism of carbon isotope fractionation associated with lipid synthesis. Science 197, 261–263. https://doi.org/10.1126/science.327543

Deutsch, C., Brix, H., Ito, T., Frenzel, H., Thompson, L., 2011. Climate-Forced Variability of Ocean Hypoxia. Science 333, 336–339. https://doi.org/10.1126/science.1202422

Deutsch, C., Ferrel, A., Seibel, B., Pörtner, H.-O., Huey, R.B., 2015. Climate change tightens a metabolic constraint on marine habitats. Science 348, 1132–1135. https://doi.org/10.1126/science.aaa1605

Di Bella, G., Potortì, A.G., Lo Turco, V., Bua, D., Licata, P., Cicero, N., Dugo, G., 2015. Trace elements in Thunnus Thynnus from Mediterranean Sea: benefit-risk assessment for consumer. Food Additives & Contaminants: Part B 8, 175–181. https://doi.org/10.1080/19393210.2015.1030347

Diaz, E.L., 1963. An increment technique for estimating growth parameters of tropical tunas, as applied to yellowfin tuna (Thunnus albacares) (No. Inter-Am. Tropic. Tuna Commission Bull. 8 (7)).

Dickson, K.A., 1996. Locomotor muscle of high-performance fishes: What do comparisons of tunas with ectothermic sister taxa reveal? Comparative Biochemistry and Physiology Part A: Physiology 113, 39–49. https://doi.org/10.1016/0300-9629(95)02056-X

Dijkstra, J.A., Buckman, K.L., Ward, D., Evans, D.W., Dionne, M., Chen, C.Y., 2013. Experimental and Natural Warming Elevates Mercury Concentrations in Estuarine Fish. PLoS ONE 8, e58401. https://doi.org/10.1371/journal.pone.0058401

Dodds, E.D., McCoy, M.R., Geldenhuys, A., Rea, L.D., Kennish, J.M., 2004. Microscale recovery of total lipids from fish tissue by accelerated solvent extraction. J Amer Oil Chem Soc 81, 835–840. https://doi.org/10.1007/s11746-004-0988-2

Dore, J.E., Brum, J.R., Tupas, L.M., Karl, D.M., 2002. Seasonal and interannual variability in sources of nitrogen supporting export in the oligotrophic subtropical North Pacific Ocean. Limnology and Oceanography 47, 1595–1607. https://doi.org/10.4319/lo.2002.47.6.1595

Dortel, E., Sardenne, F., Bousquet, N., Rivot, E., Million, J., Le Croizier, G., Chassot, E., 2015. An integrated Bayesian modeling approach for the growth of Indian Ocean yellowfin tuna.

Fisheries Research, IO Tuna tagging 163, 69–84. https://doi.org/10.1016/j.fishres.2014.07.006

Dray, S., Legendre, P., Peres-Neto, P.R., 2006. Spatial modelling: a comprehensive framework for principal coordinate analysis of neighbour matrices (PCNM). Ecological Modelling 196, 483–493. https://doi.org/10.1016/j.ecolmodel.2006.02.015

Drevnick, P.E., Brooks, B.A., 2017. Mercury in tunas and blue marlin in the North Pacific Ocean. Environmental Toxicology and Chemistry 36, 1365–1374. https://doi.org/10.1002/etc.3757

Drevnick, P.E., Lamborg, C.H., Horgan, M.J., 2015. Increase in mercury in Pacific yellowfin tuna: Mercury in yellowfin tuna. Environ Toxicol Chem 34, 931–934. https://doi.org/10.1002/etc.2883

Driscoll, C.T., Chen, C.Y., Hammerschmidt, C.R., Mason, R.P., Gilmour, C.C., Sunderland, E.M., Greenfield, B.K., Buckman, K.L., Lamborg, C.H., 2012. Nutrient supply and mercury dynamics in marine ecosystems: A conceptual model. Environmental Research, Mercury in Marine Ecosystems: Sources to Seafood Consumers 119, 118–131. https://doi.org/10.1016/j.envres.2012.05.002

Druon, J.-N., Chassot, E., Murua, H., Lopez, J., 2017. Skipjack Tuna Availability for Purse Seine Fisheries Is Driven by Suitable Feeding Habitat Dynamics in the Atlantic and Indian Oceans. Frontiers in Marine Science 4, 315. https://doi.org/10.3389/fmars.2017.00315

Duffy, L.M., Kuhnert, P.M., Pethybridge, H.R., Young, J.W., Olson, R.J., Logan, J.M., Goñi, N., Romanov, E., Allain, V., Staudinger, M.D., Abecassis, M., Choy, C.A., Hobday, A.J., Simier, M., Galván-Magaña, F., Potier, M., Ménard, F., 2017. Global trophic ecology of yellowfin, bigeye, and albacore tunas: Understanding predation on micronekton communities at ocean-basin scales. Deep Sea Research Part II: Topical Studies in Oceanography, Future of oceanic animals in a changing ocean 140, 55–73. https://doi.org/10.1016/j.dsr2.2017.03.003

Endo, T., Kimura, O., Fujii, Y., Haraguchi, K., 2016. Relationship between mercury, organochlorine compounds and stable isotope ratios of carbon and nitrogen in yellowfin tuna (Thunnus albacares) taken from different regions of the Pacific and Indian Oceans. Ecological Indicators 69, 340–347. https://doi.org/10.1016/j.ecolind.2016.04.021

Engstrom, D.R., Fitzgerald, W.F., Cooke, C.A., Lamborg, C.H., Drevnick, P.E., Swain, E.B., Balogh, S.J., Balcom, P.H., 2014. Atmospheric Hg Emissions from Preindustrial Gold and Silver Extraction in the Americas: A Reevaluation from Lake-Sediment Archives. Environ. Sci. Technol. 48, 6533–6543. https://doi.org/10.1021/es405558e

Eveson, J.P., Million, J., Sardenne, F., Le Croizier, G., 2015. Estimating growth of tropical tunas in the Indian Ocean using tag-recapture data and otolith-based age estimates. Fisheries Research, IO Tuna tagging 163, 58–68. https://doi.org/10.1016/j.fishres.2014.05.016

FAO (Ed.), 2018. The state of world fisheries and aquaculture 2018 - Meeting the sustainable development goals. Rome.

Farley, J., Eveson, P., Bonhommeau, S., Dhurmeea, Z., West, W., Bodin, N., 2019. Growth of albacore tuna (Thunnus alalunga) n the western Indian Ocean ising direct age estimates (No. IOTC-2019-WPTmT07(DP)-21_Rev1). Indian Ocean Tuna Commission (IOTC).

Farley, J., Krusic-Golub, K., Eveson, P., Roupsard, F., Sanchez, C., Nicol, S., Hampton, J., 2020. Age and growth of yellowfin and bigeye tuna in the western and central Pacific Ocean from otoliths (WCPFC-SC16-2020/SA-WP-02).

Farley, J.H., Williams, A.J., Hoyle, S.D., Davies, C.R., Nicol, S.J., 2013. Reproductive Dynamics and Potential Annual Fecundity of South Pacific Albacore Tuna (Thunnus alalunga). PLOS ONE 8, e60577. https://doi.org/10.1371/journal.pone.0060577

Ferriss, B.E., Essington, T.E., 2014a. Can fish consumption rate estimates be improved by linking bioenergetics and mercury mass balance models? Application to tunas. Ecological Modelling 272, 232–241. https://doi.org/10.1016/j.ecolmodel.2013.10.010

Ferriss, B.E., Essington, T.E., 2014b. Does trophic structure dictate mercury concentrations in top predators? A comparative analysis of pelagic food webs in the Pacific Ocean. Ecological Modelling 278, 18–28. https://doi.org/10.1016/j.ecolmodel.2014.01.029

Ferriss, B.E., Essington, T.E., 2011. Regional patterns in mercury and selenium concentrations of yellowfin tuna (Thunnus albacares) and bigeye tuna (Thunnus obesus) in the Pacific Ocean. Can. J. Fish. Aquat. Sci. 68, 2046–2056. https://doi.org/10.1139/f2011-120

Fitzgerald, W.F., Engstrom, D.R., Mason, R.P., Nater, E.A., 1998. The Case for Atmospheric Mercury Contamination in Remote Areas. Environ. Sci. Technol. 32, 1–7. https://doi.org/10.1021/es970284w

Fitzgerald, W.F., Lamborg, C.H., Hammerschmidt, C.R., 2007. Marine Biogeochemical Cycling of Mercury. Chemical reviews 107, 22.

Fitzgerald, William.F., Lamborg, C., 2014. Geochemistry of mercury in the environment. Elsevier.

Fleming, E.J., Mack, E.E., Green, P.G., Nelson, D.C., 2006. Mercury Methylation from Unexpected Sources: Molybdate-Inhibited Freshwater Sediments and an Iron-Reducing Bacterium. Applied and Environmental Microbiology 72, 457–464. https://doi.org/10.1128/AEM.72.1.457-464.2006

Fonteneau, A., Hallier, J.-P., 2015. Fifty years of dart tag recoveries for tropical tuna: A global comparison of results for the western Pacific, eastern Pacific, Atlantic, and Indian Oceans. Fisheries Research 163, 7–22. https://doi.org/10.1016/j.fishres.2014.03.022

Fry, B., 2006. Stable isotope ecology. Springer, New York, NY.

Fu, X., Feng, X., Zhang, G., Xu, W., Li, X., Yao, H., Liang, P., Li, J., Sommar, J., Yin, R., Liu, N., 2010. Mercury in the marine boundary layer and seawater of the South China Sea: Concentrations, sea/air flux, and implication for land outflow. J. Geophys. Res. 115, D06303. https://doi.org/10.1029/2009JD012958

Fu, X.W., Zhang, H., Yu, B., Wang, X., Lin, C.-J., Feng, X.B., 2015. Observations of atmospheric mercury in China: a critical review. Atmos. Chem. Phys. 15, 9455–9476. https://doi.org/10.5194/acp-15-9455-2015

Fuller, D.W., Schaefer, K.M., Hampton, J., Caillot, S., Leroy, B., 2015. Vertical movements, behavior, and habitat of bigeye tuna (Thunnus obesus) in the equatorial central Pacific Ocean. Fisheries Research 172, 57–70. https://doi.org/10.1016/j.fishres.2015.06.024

Gailer, J., George, G.N., Pickering, I.J., Madden, S., Prince, R.C., Yu, E.Y., Denton, M.B., Younis, H.S., Aposhian, H.V., 2000. Structural Basis of the Antagonism between Inorganic Mercury and Selenium in Mammals. Chem. Res. Toxicol. 13, 1135–1142. https://doi.org/10.1021/tx000050h

Gajdosechova, Z., Lawan, M.M., Urgast, D.S., Raab, A., Scheckel, K.G., Lombi, E., Kopittke, P.M., Loeschner, K., Larsen, E.H., Woods, G., Brownlow, A., Read, F.L., Feldmann, J., Krupp, E.M., 2016. In vivo formation of natural HgSe nanoparticles in the liver and brain of pilot whales. Sci Rep 6, 34361. https://doi.org/10.1038/srep34361

Ganachaud, A., Cravatte, S., Sprintall, J., Germineaud, C., Alberty, M., Jeandel, C., Eldin, G., Metzl, N., Bonnet, S., Benavides, M., Heimburger, L.-E., Lefèvre, J., Michael, S., Resing, J., Quéroué, F., Sarthou, G., Rodier, M., Berthelot, H., Baurand, F., Grelet, J., Hasegawa, T., Kessler, W., Kilepak, M., Lacan, F., Privat, E., Send, U., Van Beek, P., Souhaut, M., Sonke, J.E., 2017. The Solomon Sea: its circulation, chemistry, geochemistry and biology explored during two oceanographic cruises. Elementa: Science of the Anthropocene 5. https://doi.org/10.1525/elementa.221

Garcia, N., Raimbault, P., Sandroni, V., 2007. Seasonal nitrogen fixation and primary production in the Southwest Pacific: nanoplankton diazotrophy and transfer of nitrogen to picoplankton organisms. Mar. Ecol. Prog. Ser. 343, 25–33. https://doi.org/10.3354/meps06882

García-Hernández, J., Cadena-Cárdenas, L., Betancourt-Lozano, M., García-De-La-Parra, L.M., García-Rico, L., Márquez-Farías, F., 2007. Total mercury content found in edible tissues of top predator fish from the Gulf of California, Mexico. Toxicological & Environmental Chemistry 89, 507–522. https://doi.org/10.1080/02772240601165594

Garcia-Vazquez, E., Geslin, V., Turrero, P., Rodriguez, N., Machado-Schiaffino, G., Ardura, A., 2021. Oceanic karma? Eco-ethical gaps in African EEE metal cycle may hit back through seafood

contamination. Science of The Total Environment 762, 143098. https://doi.org/10.1016/j.scitotenv.2020.143098
Genchi, G., Sinicropi, M., Carocci, A., Lauria, G., Catalano, A., 2017. Mercury Exposure and Heart Diseases. IJERPH 14, 74. https://doi.org/10.3390/ijerph14010074
Gillett, R., 2009. Fisheries in the Economies of the Pacific Island Countries and Territories. Asian Development Bank.
Gilmour, C.C., Podar, M., Bullock, A.L., Graham, A.M., Brown, S.D., Somenahally, A.C., Johs, A., Hurt, R.A., Bailey, K.L., Elias, D.A., 2013. Mercury Methylation by Novel Microorganisms from New Environments. Environ. Sci. Technol. 47, 11810–11820. https://doi.org/10.1021/es403075t
Gobel, A.R., Altieri, K.E., Peters, A.J., Hastings, M.G., Sigman, D.M., 2013. Insights into anthropogenic nitrogen deposition to the North Atlantic investigated using the isotopic composition of aerosol and rainwater nitrate: NITRATE ISOTOPES IN MARINE AEROSOLS. Geophys. Res. Lett. 40, 5977–5982. https://doi.org/10.1002/2013GL058167
Gosnell, K.J., Dam, H.G., Mason, R.P., 2021. Mercury and Methylmercury Uptake and Trophic Transfer from Marine Diatoms to Copepods and Field Collected Zooplankton. Marine Environmental Research 105446. https://doi.org/10.1016/j.marenvres.2021.105446
Gosnell, K.J., Mason, R.P., 2015. Mercury and methylmercury incidence and bioaccumulation in plankton from the central Pacific Ocean. Marine Chemistry 177, 772–780. https://doi.org/10.1016/j.marchem.2015.07.005
Government of New Caledonia, 2019. Recommendations consommation de poissons et mercure.
Graham, B.S., Grubbs, D., Holland, K., Popp, B.N., 2007. A rapid ontogenetic shift in the diet of juvenile yellowfin tuna from Hawaii. Mar Biol 150, 647–658. https://doi.org/10.1007/s00227-006-0360-y
Graham, B.S., Koch, P.L., Newsome, S.D., McMahon, K.W., Aurioles, D., 2010. Using Isoscapes to Trace the Movements and Foraging Behavior of Top Predators in Oceanic Ecosystems, in: West, J.B., Bowen, G.J., Dawson, T.E., Tu, K.P. (Eds.), Isoscapes. Springer Netherlands, Dordrecht, pp. 299–318. https://doi.org/10.1007/978-90-481-3354-3_14
Graham, J.B., 1975. Heat exchange in the yellowfin tuna, Thunnus albacares, and skipjack tuna, Katsuwonus pelamis, and the adaptive significance of elevated body temperatures in scombrid fishes. Fish. Bull. 73, 219–229.
Graham, J.B., Dickson, K.A., 2004. Tuna comparative physiology. Journal of Experimental Biology 207, 4015–4024. https://doi.org/10.1242/jeb.01267
Grandjean, P., Weihe, P., White, R.F., Debes, F., Araki, S., Yokoyama, K., Murata, K., Sørensen, N., Dahl, R., Jørgensen, P.J., 1997. Cognitive Deficit in 7-Year-Old Children with Prenatal Exposure to Methylmercury. Neurotoxicology and Teratology 19, 417–428. https://doi.org/10.1016/S0892-0362(97)00097-4
Griffiths, S., Kesner-Reyes, K., Garilao, C., Duffy, L., Román, M., 2019. Ecological Assessment of the Sustainable Impacts of Fisheries (EASI-Fish): a flexible vulnerability assessment approach to quantify the cumulative impacts of fishing in data-limited settings. Mar. Ecol. Prog. Ser. 625, 89–113. https://doi.org/10.3354/meps13032
Gruber, N., Boyd, P.W., Frölicher, T.L., Vogt, M., 2021. Biogeochemical extremes and compound events in the ocean. Nature 600, 395–407. https://doi.org/10.1038/s41586-021-03981-7
Guinehut, S., Dhomps, A.-L., Larnicol, G., Traon, P.-Y.L., 2012. High resolution 3-D temperature and salinity fields derived from in situ and satellite observations. Ocean Science 8, 845–857. https://doi.org/10.5194/os-8-845-2012
Gurvan, M., Bourdallé-Badie, R., Chanut, J., Clementi, E., Coward, A., Ethé, C., Iovino, D., Lea, D., Lévy, C., Lovato, T., Martin, N., Masson, S., Mocavero, S., Rousset, C., Storkey, D., Vancoppenolle, M., Müeller, S., Nurser, G., Bell, M., Samson, G., 2019. NEMO ocean engine. https://doi.org/10.5281/zenodo.3878122
Gustin, M.S., Bank, M.S., Bishop, K., Bowman, K., Branfireun, B., Chételat, J., Eckley, C.S., Hammerschmidt, C.R., Lamborg, C., Lyman, S., Martínez-Cortizas, A., Sommar, J., Tsui, M.T.-K., Zhang, T., 2020. Mercury biogeochemical cycling: A synthesis of recent scientific

advances. Science of The Total Environment 737, 139619. https://doi.org/10.1016/j.scitotenv.2020.139619

Hall, B.D., Bodaly, R.A., Fudge, R.J.P., Rudd, J.W.M., Rosenberg, D.M., 1997. Food as the Dominant Pathway of Methylmercury Uptake by Fish. Water, Air, & Soil Pollution 100, 13–24. https://doi.org/10.1023/A:1018071406537

Hallier, J.-P., Gaertner, D., 2006. Estimated growth rate of the skipjack tuna (Katsuwonus pelamis) from tagging surveys conducted in the senegalese area (1996-1999) within a meta-analysis framework 11.

Hallier, J.-P., Stequert, B., Maury, O., Bard, F.-X., 2005. Growth of bigeye tuna (Thunnus obesus) in the eastern Atlantic Ocean from tagging-recapture data and otolith readings 14.

Hamelin, S., Amyot, M., Barkay, T., Wang, Y., Planas, D., 2011. Methanogens: Principal Methylators of Mercury in Lake Periphyton. Environ. Sci. Technol. 45, 7693–7700. https://doi.org/10.1021/es2010072

Hammerschmidt, C.R., Bowman, K.L., 2012. Vertical methylmercury distribution in the subtropical North Pacific Ocean. Marine Chemistry 132–133, 77–82. https://doi.org/10.1016/j.marchem.2012.02.005

Hammerschmidt, C.R., Finiguerra, M.B., Weller, R.L., Fitzgerald, W.F., 2013. Methylmercury Accumulation in Plankton on the Continental Margin of the Northwest Atlantic Ocean. Environ. Sci. Technol. 47, 3671–3677. https://doi.org/10.1021/es3048619

Handayani, T., Maarif, M.S., Riani, E., Djazuli, N., 2019. Mercury levels and tolerable weekly intakes (TWI) of tuna and tuna-like species from the Southern Indian Ocean (Indonesia): Public health perspective. Biodiversitas 20, 504–509. https://doi.org/10.13057/biodiv/d200229

Hannides, C.C.S., Popp, B.N., Choy, C.A., Drazen, J.C., 2013. Midwater zooplankton and suspended particle dynamics in the North Pacific Subtropical Gyre: A stable isotope perspective. Limnology and Oceanography 58, 1931–1946. https://doi.org/10.4319/lo.2013.58.6.1931

Harris, H.H., 2003. The Chemical Form of Mercury in Fish. Science 301, 1203–1203. https://doi.org/10.1126/science.1085941

Havelková, M., Dušek, L., Némethová, D., Poleszczuk, G., Svobodová, Z., 2008. Comparison of Mercury Distribution Between Liver and Muscle – A Biomonitoring of Fish from Lightly and Heavily Contaminated Localities. Sensors 8, 4095–4109. https://doi.org/10.3390/s8074095

Hayes, C.T., Costa, K.M., Anderson, R.F., Calvo, E., Chase, Z., Demina, L.L., Dutay, J.-C., German, C.R., Heimbürger-Boavida, L.-E., Jaccard, S.L., Jacobel, A., Kohfeld, K.E., Kravchishina, M.D., Lippold, J., Mekik, F., Missiaen, L., Pavia, F.J., Paytan, A., Pedrosa-Pamies, R., Petrova, M.V., Rahman, S., Robinson, L.F., Roy-Barman, M., Sanchez-Vidal, A., Shiller, A., Tagliabue, A., Tessin, A.C., Hulten, M. van, Zhang, J., 2021. Global Ocean Sediment Composition and Burial Flux in the Deep Sea. Global Biogeochemical Cycles 35, e2020GB006769. https://doi.org/10.1029/2020GB006769

Hayes, J.M., Freeman, K.H., Popp, B.N., Hoham, C.H., 1990. Compound-specific isotopic analyses: A novel tool for reconstruction of ancient biogeochemical processes. Organic Geochemistry, Proceedings of the 14th International Meeting on Organic Geochemistry 16, 1115–1128. https://doi.org/10.1016/0146-6380(90)90147-R

Heimbürger, L.-E., Cossa, D., Marty, J.-C., Migon, C., Averty, B., Dufour, A., Ras, J., 2010. Methyl mercury distributions in relation to the presence of nano- and picophytoplankton in an oceanic water column (Ligurian Sea, North-western Mediterranean). Geochimica et Cosmochimica Acta 74, 5549–5559. https://doi.org/10.1016/j.gca.2010.06.036

Hein, M., Pedersen, M., Sand-Jensen, K., 1995. Size-dependent nitrogen uptake in micro- and macroalgae. Mar. Ecol. Prog. Ser. 118, 247–253. https://doi.org/10.3354/meps118247

Hintelmann, H., 2010. Organomercurials. Their Formation and Pathways in the Environment, in: Organometallics in Environment and Toxicology: Metal Ions in Life Sciences. pp. 365–401. https://doi.org/10.1039/9781849730822-00365

Hisamichi, Y., Haraguchi, K., Endo, T., 2010. Levels of Mercury and Organochlorine Compounds and Stable Isotope Ratios in Three Tuna Species Taken from Different Regions of Japan. Environ. Sci. Technol. 44, 5971–5978. https://doi.org/10.1021/es1008856

Holmes, C.D., Jacob, D.J., Corbitt, E.S., Mao, J., Yang, X., Talbot, R., Slemr, F., 2010. Global atmospheric model for mercury including oxidation by bromine atoms. Atmospheric Chemistry and Physics 10, 12037–12057. https://doi.org/10.5194/acp-10-12037-2010

Horowitz, H.M., Jacob, D.J., Zhang, Y., Dibble, T.S., Slemr, F., Amos, H.M., Schmidt, J.A., Corbitt, E.S., Marais, E.A., Sunderland, E.M., 2017. A new mechanism for atmospheric mercury redox chemistry: implications for the global mercury budget. Atmospheric Chemistry and Physics 17. https://doi.org/10.5194/acp-17-6353-2017

Houssard, P., Lorrain, A., Tremblay-Boyer, L., Allain, V., Graham, B.S., Menkes, C.E., Pethybridge, H., Couturier, L.I.E., Point, D., Leroy, B., Receveur, A., Hunt, B.P.V., Vourey, E., Bonnet, S., Rodier, M., Raimbault, P., Feunteun, E., Kuhnert, P.M., Munaron, J.-M., Lebreton, B., Otake, T., Letourneur, Y., 2017. Trophic position increases with thermocline depth in yellowfin and bigeye tuna across the Western and Central Pacific Ocean. Progress in Oceanography 154, 49–63. https://doi.org/10.1016/j.pocean.2017.04.008

Houssard, P., Point, D., Tremblay-Boyer, L., Allain, V., Pethybridge, H., Masbou, J., Ferriss, B.E., Baya, P.A., Lagane, C., Menkes, C.E., Letourneur, Y., Lorrain, A., 2019. A Model of Mercury Distribution in Tuna from the Western and Central Pacific Ocean: Influence of Physiology, Ecology and Environmental Factors. Environmental Science & Technology 53, 1422–1431. https://doi.org/10.1021/acs.est.8b06058

Hynes, H.B.N., 1950. The Food of Fresh-Water Sticklebacks (Gasterosteus aculeatus and Pygosteus pungitius), with a Review of Methods Used in Studies of the Food of Fishes. Journal of Animal Ecology 19, 36–58. https://doi.org/10.2307/1570

Ichinokawa, M., Coan, A.L., Takeuchi, Y., 2008. Transoceanic migration rates of young North Pacific albacore, Thunnus alalunga, from conventional tagging data. Can. J. Fish. Aquat. Sci. 65, 1681–1691. https://doi.org/10.1139/F08-095

Ikemoto, T., Kunito, T., Tanaka, H., Baba, N., Miyazaki, N., Tanabe, S., 2004. Detoxification Mechanism of Heavy Metals in Marine Mammals and Seabirds: Interaction of Selenium with Mercury, Silver, Copper, Zinc, and Cadmium in Liver. Arch Environ Contam Toxicol 47, 402–413. https://doi.org/10.1007/s00244-004-3188-9

Indian Ocean Tuna Commission, 2020. Review of the statistical data and fishery trends for tropical tunas.

Inter-Americaln Tropical Tuna Commission, 2021. Report on the tuna fishery, stocks, and ecosystem in the eastern Pacific Ocean in 2020 (No. IATTC-98-01).

International Commission for the Conservation of Atlantic Tunas (ICCAT), 2019. Report of the 2019 ICCAT yellowfin tuna stock assessment meeting. Grand-Bassam, Côte d'Ivoire.

International Commission for the Conservation of Atlantic Tunas (ICCAT), 2018. Report of the 2018 ICCAT bigeye tuna stock assessment meeting. Pasaia, Spain.

International Commission for the Conservation of Atlantic Tunas (ICCAT), 2014. Report of the 2014 ICCAT east and west Atlantic skipjack stock assessment meeting. Dakar.

ISSF, 2021. Status of the World Fisheries for Tuna: March 2021 (ISSF Technical Report 2021-10). International Seafood Sustainability Foundation, Washington, D.C., USA.

ISSF, 2019. Status of the world fisheries for tuna. Mar. 2019. ISSF Technical Report 2019-07. International Seafood Sustainability Foundation, Washington, D.C., USA.

IUCN, 2017. The IUCN Red List of Threatened Species [WWW Document]. IUCN Red List of Threatened Species. URL https://www.iucnredlist.org/en (accessed 10.25.21).

Ivory Coast Fisheries Service, 1972. La contamination mercurielle des thons. Mercury contamination in tuna fish. Abidjan.

JCGM, 2012. International vocabulary of metrology - Basic and general concepts and associated terms (VIM).

Jinadasa, B.K.K.K., Chathurika, G.S., Jayasinghe, G.D.T.M., Jayaweera, C.D., 2019. Mercury and cadmium distribution in yellowfin tuna (Thunnus albacares) from two fishing grounds in the Indian Ocean near Sri Lanka. Heliyon 5, e01875. https://doi.org/10.1016/j.heliyon.2019.e01875

Jiskra, M., Heimbürger-Boavida, L.-E., Desgranges, M.-M., Petrova, M.V., Dufour, A., Ferreira-Araujo, B., Masbou, J., Chmeleff, J., Thyssen, M., Point, D., Sonke, J.E., 2021. Mercury stable isotopes constrain atmospheric sources to the ocean. Nature 597, 678–682. https://doi.org/10.1038/s41586-021-03859-8

Juan-Jordá, M.J., Mosqueira, I., Freire, J., Ferrer-Jorda, E., Dulvy, N.K., 2016. Global scombrid life history data set. Ecology 97, 809.

Kaneko, J.J., Ralston, N.V.C., 2007. Selenium and Mercury in Pelagic Fish in the Central North Pacific Near Hawaii. Biol Trace Elem Res 119, 242–254. https://doi.org/10.1007/s12011-007-8004-8

Kannan, K., Falandysz, J., 1998. Speciation and Concentrations of Mercury in Certain Coastal Marine Sediments. Water, Air, & Soil Pollution 103, 129–136. https://doi.org/10.1023/A:1004967112178

Kim, H., Lee, K., Lim, D.-I., Nam, S.-I., Han, S. hee, Kim, J., Lee, E., Han, I.-S., Jin, Y.K., Zhang, Y., 2019. Increase in anthropogenic mercury in marginal sea sediments of the Northwest Pacific Ocean. Science of The Total Environment 654, 801–810. https://doi.org/10.1016/j.scitotenv.2018.11.076

Kim, H., Soerensen, A.L., Hur, J., Heimburger, L.-E., Hahm, D., Rhee, T.S., Noh, S., Han, S., 2017. Methylmercury mass budgets and distribution characteristics in the Western Pacific Ocean. Environmental Science and Technology 51, 1186–1194. https://doi.org/10.1021/acs.est.6b04238

Kim, H., Van Duong, H., Kim, E., Lee, B.-G., Han, S., 2014. Effects of phytoplankton cell size and chloride concentration on the bioaccumulation of methylmercury in marine phytoplankton. Environmental Toxicology 29, 936–941. https://doi.org/10.1002/tox.21821

Kojadinovic, J., Ménard, F., Bustamante, P., Cosson, R., Le Corre, M., 2008. Trophic ecology of marine birds and pelagic fishes from Reunion Island as determined by stable isotope analysis. Marine Ecology Progress Series 361, 239–251. https://doi.org/10.3354/meps07355

Kojadinovic, J., Potier, M., Le Corre, M., Cosson, R.P., Bustamante, P., 2007. Bioaccumulation of trace elements in pelagic fish from the Western Indian Ocean. Environmental Pollution, Lichens in a Changing Pollution Environment 146, 548–566. https://doi.org/10.1016/j.envpol.2006.07.015

Kojadinovic, J., Potier, M., Le Corre, M., Cosson, R.P., Bustamante, P., 2006. Mercury content in commercial pelagic fish and its risk assessment in the Western Indian Ocean. Science of The Total Environment 366, 688–700. https://doi.org/10.1016/j.scitotenv.2006.02.006

Krabbenhoft, D.P., Sunderland, E.M., 2013. Global change and mercury. Science 341, 1457–1458. https://doi.org/10.1126/science.1242838

Kraepiel, A.M.L., Keller, K., Chin, H.B., Malcolm, E.G., Morel, F.M.M., 2003. Sources and Variations of Mercury in Tuna. Environmental Science & Technology 37, 5551–5558. https://doi.org/10.1021/es0340679

Kumar, M., Aalbersberg, B., Mosley, L., 2004. Mercury Levels in Fijian Seafoods and Potential Health Implications (IAS technical report).

Kwiatkowski, L., Bopp, L., Aumont, O., Ciais, P., Cox, P.M., Laufkötter, C., Li, Y., Séférian, R., 2017. Emergent constraints on projections of declining primary production in the tropical oceans. Nature Clim Change 7, 355–358. https://doi.org/10.1038/nclimate3265

Kwon, S.Y., Blum, J.D., Madigan, D.J., Block, B.A., Popp, B.N., 2016. Quantifying mercury isotope dynamics in captive Pacific bluefin tuna (Thunnus orientalis). Elem Sci Anth 4, 000088. https://doi.org/10.12952/journal.elementa.000088

Lacerda, L.D., Goyanna, F., Bezerra, M.F., Silva, G.B., 2017. Mercury Concentrations in Tuna (Thunnus albacares and Thunnus obesus) from the Brazilian Equatorial Atlantic Ocean. Bull Environ Contam Toxicol 98, 149–155. https://doi.org/10.1007/s00128-016-2007-0

Lamborg, C.H., Damm, K.L.V., Fitzgerald, W.F., Hammerschmidt, C.R., Zierenberg, R., 2006. Mercury and monomethylmercury in fluids from Sea Cliff submarine hydrothermal field, Gorda Ridge. Geophysical Research Letters 33. https://doi.org/10.1029/2006GL026321

Lamborg, C.H., Hammerschmidt, C.R., Bowman, K.L., 2016. An examination of the role of particles in oceanic mercury cycling. Phil. Trans. R. Soc. A. 374, 20150297. https://doi.org/10.1098/rsta.2015.0297

Lamborg, C.H., Hammerschmidt, C.R., Bowman, K.L., Swarr, G.J., Munson, K.M., Ohnemus, D.C., Lam, P.J., Heimbürger, L.-E., Rijkenberg, M.J.A., Saito, M.A., 2014. A global ocean inventory of anthropogenic mercury based on water column measurements. Nature 512, 65–68. https://doi.org/10.1038/nature13563

Landrigan, P.J., Stegeman, J.J., Fleming, L.E., Allemand, D., Anderson, D.M., Backer, L.C., Brucker-Davis, F., Chevalier, N., Corra, L., CZERUCKA, D., Bottein, M.-Y.D., Demeneix, B., Depledge, M., Deheyn, D.D., Dorman, C.J., Fénichel, P., Fisher, S., Gaill, F., Galgani, F., Gaze, W.H., Giuliano, L., Grandjean, P., Hahn, M.E., Hamdoun, A., Hess, P., Judson, B., Laborde, A., Mcglade, J., Mu, J., Mustapha, A., Neira, M., Noble, R.T., Pedrotti, M.L., Reddy, C., Rocklöv, J., Scharler, U.M., Shanmugam, H., Taghian, G., Van De Water, J.A.J.M., Vezzulli, L., Weihe, P., Zeka, A., Raps, H., Rampal, P., 2020. Human Health and Ocean Pollution. Annals of Global Health 86, 151. https://doi.org/10.5334/aogh.2831

Langford, N., Ferner, R., 1999. Toxicity of mercury. Journal of Human Hypertension 651–656.

Laufkötter, C., Vogt, M., Gruber, N., Aumont, O., Bopp, L., Doney, S.C., Dunne, J.P., Hauck, J., John, J.G., Lima, I.D., Seferian, R., Völker, C., 2016. Projected decreases in future marine export production: the role of the carbon flux through the upper ocean ecosystem. Biogeosciences 13, 4023–4047. https://doi.org/10.5194/bg-13-4023-2016

Laurier, F.J.G., Mason, R.P., Gill, G.A., Whalin, L., 2004. Mercury distributions in the North Pacific Ocean—20 years of observations. Marine Chemistry, Special Issue in honor of Dr. William F. Fitzgerald 90, 3–19. https://doi.org/10.1016/j.marchem.2004.02.025

Lavoie, R.A., Bouffard, A., Maranger, R., Amyot, M., 2018. Mercury transport and human exposure from global marine fisheries. Sci Rep 8, 6705. https://doi.org/10.1038/s41598-018-24938-3

Le Borgne, R., Allain, V., Griffiths, S.P., Matear, R.J., McKinnon, A.D., Richardson, A.J., Young, J.W., 2011. Vulnerability of open ocean food webs in the tropical Pacific to climate change, in: Vulnerability of Tropical Pacific Fisheries and Aquaculture to Climate Change. Secretariat of the Pacific Community, New Caledonia, pp. 189–249.

Le Faucheur, S., Campbell, P.G.C., Fortin, C., Slaveykova, V.I., 2014. Interactions between mercury and phytoplankton: Speciation, bioavailability, and internal handling. Environmental Toxicology and Chemistry 33, 1211–1224. https://doi.org/10.1002/etc.2424

Le-Alvarado, M., Romo-Curiel, A.E., Sosa-Nishizaki, O., Hernández-Sánchez, O., Barbero, L., Herzka, S.Z., 2021. Yellowfin tuna (Thunnus albacares) foraging habitat and trophic position in the Gulf of Mexico based on intrinsic isotope tracers. PLOS ONE 16, e0246082. https://doi.org/10.1371/journal.pone.0246082

Leaner, J.J., Mason, R.P., 2004. Methylmercury uptake and distribution kinetics in Sheepshead Minnows, Cyprinodon Variegatus, after exposure to Ch3Hg-spiked food. Environ Toxicol Chem 23, 2138. https://doi.org/10.1897/03-258

Lee, C.-S., Fisher, N.S., 2019. Microbial generation of elemental mercury from dissolved methylmercury in seawater. Limnology and Oceanography 64, 679–693. https://doi.org/10.1002/lno.11068

Lee, C.-S., Fisher, N.S., 2017. Bioaccumulation of methylmercury in a marine copepod. Environmental Toxicology and Chemistry 36, 1287–1293. https://doi.org/10.1002/etc.3660

Lee, C.-S., Fisher, N.S., 2016. Methylmercury uptake by diverse marine phytoplankton. Limnology and Oceanography 61, 1626–1639. https://doi.org/10.1002/lno.10318

Lee, C.-S., Lutcavage, M.E., Chandler, E., Madigan, D.J., Cerrato, R.M., Fisher, N.S., 2016. Declining Mercury Concentrations in Bluefin Tuna Reflect Reduced Emissions to the North Atlantic

Ocean. Environmental Science & Technology 50, 12825–12830. https://doi.org/10.1021/acs.est.6b04328

Lee, S., Kim, S.-J., Ju, S.-J., Pak, S.-J., Son, S.-K., Yang, J., Han, S., 2015. Mercury accumulation in hydrothermal vent mollusks from the southern Tonga Arc, southwestern Pacific Ocean. Chemosphere 127, 246–253. https://doi.org/10.1016/j.chemosphere.2015.01.006

Legendre, P., Gauthier, O., 2014. Statistical methods for temporal and space-time analysis of community composition data. Proceedings of the Royal Society B: Biological Sciences 281, 20132728–20132728. https://doi.org/10.1098/rspb.2013.2728

Lehnherr, I., St. Louis, V.L., Hintelmann, H., Kirk, J.L., 2011. Methylation of inorganic mercury in polar marine waters. Nature Geosci 4, 298–302. https://doi.org/10.1038/ngeo1134

Leroy, B., Phillips, J.S., Nicol, S., Pilling, G.M., Harley, S., Bromhead, D., Hoyle, S., Caillot, S., Allain, V., Hampton, J., 2013. A critique of the ecosystem impacts of drifting and anchored FADs use by purse-seine tuna fisheries in the Western and Central Pacific Ocean. Aquatic Living Resources 26, 49–61. https://doi.org/10.1051/alr/2012033

Lewis, A.D., 1990. South Pacific albacore stock structure : a review of available information, Third South Pacific Albacore Research Workshop Working Paper No. 5. South Pacific Commissio, Noumea, New Caledonia.

Li, C., Shen, J., Zhang, Jin, Lei, P., Kong, Y., Zhang, Jichao, Tang, W., Chen, T., Xiang, X., Wang, S., Zhang, W., Zhong, H., 2021. The silver linings of mercury: Reconsideration of its impacts on living organisms from a multi-timescale perspective. Environment International 155, 106670. https://doi.org/10.1016/j.envint.2021.106670

Li, C., Sonke, J.E., Le Roux, G., Piotrowska, N., Van der Putten, N., Roberts, S.J., Daley, T., Rice, E., Gehrels, R., Enrico, M., Mauquoy, D., Roland, T.P., De Vleeschouwer, F., 2020. Unequal Anthropogenic Enrichment of Mercury in Earth's Northern and Southern Hemispheres. ACS Earth Space Chem. 4, 2073–2081. https://doi.org/10.1021/acsearthspacechem.0c00220

Li, H., Lin, X., Zhao, J., Cui, L., Wang, L., Gao, Y., Li, B., Chen, C., Li, Y.-F., 2019. Intestinal Methylation and Demethylation of Mercury. Bull Environ Contam Toxicol 102, 597–604. https://doi.org/10.1007/s00128-018-2512-4

Li, M., Juang, C.A., Ewald, J.D., Yin, R., Mikkelsen, B., Krabbenhoft, D.P., Balcom, P.H., Dassuncao, C., Sunderland, E.M., 2020. Selenium and stable mercury isotopes provide new insights into mercury toxicokinetics in pilot whales. Science of The Total Environment 710, 136325. https://doi.org/10.1016/j.scitotenv.2019.136325

Licata, P., Trombetta, D., Cristani, M., Naccari, C., Martino, D., Caló, M., Naccari, F., 2005. Heavy Metals in Liver and Muscle of Bluefin Tuna (Thunnus thynnus) Caught in the Straits of Messina (Sicily, Italy). Environ Monit Assess 107, 239–248. https://doi.org/10.1007/s10661-005-2382-1

Liu, M., Zhang, Q., Cheng, M., He, Y., Chen, L., Zhang, H., Cao, H., Shen, H., Zhang, W., Tao, S., Wang, X., 2019. Rice life cycle-based global mercury biotransport and human methylmercury exposure. Nat Commun 10, 5164. https://doi.org/10.1038/s41467-019-13221-2

Liu, M., Zhang, Q., Maavara, T., Liu, S., Wang, X., Raymond, P.A., 2021. Rivers as the largest source of mercury to coastal oceans worldwide. Nat. Geosci. 1–6. https://doi.org/10.1038/s41561-021-00793-2

Logan, J.M., Jardine, T.D., Miller, T.J., Bunn, S.E., Cunjak, R.A., Lutcavage, M.E., 2008. Lipid corrections in carbon and nitrogen stable isotope analyses: comparison of chemical extraction and modelling methods. Journal of Animal Ecology 77, 838–846. https://doi.org/10.1111/j.1365-2656.2008.01394.x

Logan, J.M., Pethybridge, H., Lorrain, A., Somes, C.J., Allain, V., Bodin, N., Choy, C.A., Duffy, L., Goñi, N., Graham, B., Langlais, C., Ménard, F., Olson, R., Young, J., 2020. Global patterns and inferences of tuna movements and trophodynamics from stable isotope analysis. Deep Sea Research Part II: Topical Studies in Oceanography 175, 104775. https://doi.org/10.1016/j.dsr2.2020.104775

Lorrain, A., Clavier, J., Thébault, J., Tremblay-Boyer, L., Houlbrèque, F., Amice, E., Le Goff, M., Chauvaud, L., 2015a. Variability in diel and seasonal in situ metabolism of the tropical gastropod Tectus niloticus. Aquat. Biol. 23, 167–182. https://doi.org/10.3354/ab00618

Lorrain, A., Graham, B.S., Popp, B.N., Allain, V., Olson, R.J., Hunt, B.P.V., Potier, M., Fry, B., Galván-Magaña, F., Menkes, C.E.R., Kaehler, S., Ménard, F., 2015b. Nitrogen isotopic baselines and implications for estimating foraging habitat and trophic position of yellowfin tuna in the Indian and Pacific Oceans. Deep Sea Research Part II: Topical Studies in Oceanography 113, 188–198. https://doi.org/10.1016/j.dsr2.2014.02.003

Lorrain, A., Pethybridge, H., Cassar, N., Receveur, A., Allain, V., Bodin, N., Bopp, L., Choy, C.A., Duffy, L., Fry, B., Goñi, N., Graham, B.S., Hobday, A.J., Logan, J.M., Ménard, F., Menkes, C.E., Olson, R.J., Pagendam, D.E., Point, D., Revill, A.T., Somes, C.J., Young, J.W., 2020. Trends in tuna carbon isotopes suggest global changes in pelagic phytoplankton communities. Glob Change Biol 26, 458–470. https://doi.org/10.1111/gcb.14858

Love, J.L., Rush, G.M., McGrath, H., 2003. Total mercury and methylmercury levels in some New Zealand commercial marine fish species. Food Additives and Contaminants 20, 37–43. https://doi.org/10.1080/0265203021000019676

Lowe, T.E., Brill, R.W., Cousins, K.L., 2000. Blood oxygen-binding characteristics of bigeye tuna (Thunnus obesus), a high-energy-demand teleost that is tolerant of low ambient oxygen. Marine Biology 136, 1087–1098. https://doi.org/10.1007/s002270000255

Luengen, A.C., Fisher, N.S., Bergamaschi, B.A., 2012. Dissolved organic matter reduces algal accumulation of methylmercury. Environmental Toxicology and Chemistry 31, 1712–1719. https://doi.org/10.1002/etc.1885

Macfadyen, G., 2016. Study of the global estimate of the value of tuna fisheries - Phase 3 Report. Poseidon Aquatic Resource Management Ltd.

Madigan, D., Snodgrass, O., Fisher, N., 2018. From migrants to mossbacks: tracer- and taginferred habitat shifts in the California yellowtail Seriola dorsalis. Mar. Ecol. Prog. Ser. 597, 221–230. https://doi.org/10.3354/meps12593

Madigan, D.J., Litvin, S.Y., Popp, B.N., Carlisle, A.B., Farwell, C.J., Block, B.A., 2012. Tissue Turnover Rates and Isotopic Trophic Discrimination Factors in the Endothermic Teleost, Pacific Bluefin Tuna (Thunnus orientalis). PLOS ONE 7, e49220. https://doi.org/10.1371/journal.pone.0049220

Malcolm, E.G., Schaefer, J.K., Ekstrom, E.B., Tuit, C.B., Jayakumar, A., Park, H., Ward, B.B., Morel, F.M.M., 2010. Mercury methylation in oxygen deficient zones of the oceans: No evidence for the predominance of anaerobes. Marine Chemistry 122, 11–19. https://doi.org/10.1016/j.marchem.2010.08.004

Manceau, A., Bourdineaud, J.-P., Oliveira, R.B., Sarrazin, S.L.F., Krabbenhoft, D.P., Eagles-Smith, C.A., Ackerman, J.T., Stewart, A.R., Ward-Deitrich, C., del Castillo Busto, M.E., Goenaga-Infante, H., Wack, A., Retegan, M., Detlefs, B., Glatzel, P., Bustamante, P., Nagy, K.L., Poulin, B.A., 2021a. Demethylation of Methylmercury in Bird, Fish, and Earthworm. Environ. Sci. Technol. 55, 1527–1534. https://doi.org/10.1021/acs.est.0c04948

Manceau, A., Brossier, R., Poulin, B.A., 2021b. Chemical Forms of Mercury in Pilot Whales Determined from Species-Averaged Mercury Isotope Signatures. ACS Earth and Space Chemistry. https://doi.org/10.1021/acsearthspacechem.1c00082

Manceau, A., Gaillot, A.-C., Glatzel, P., Cherel, Y., Bustamante, P., 2021c. In Vivo Formation of HgSe Nanoparticles and Hg–Tetraselenolate Complex from Methylmercury in Seabirds—Implications for the Hg–Se Antagonism. Environ. Sci. Technol. 55, 1515–1526. https://doi.org/10.1021/acs.est.0c06269

Martinez del Rio, C., Wolf, N., Carleton, S.A., Gannes, L.Z., 2009. Isotopic ecology ten years after a call for more laboratory experiments. Biological Reviews 84, 91–111. https://doi.org/10.1111/j.1469-185X.2008.00064.x

Martínez-Cortizas, A., Pontevedra-Pombal, X., García-Rodeja, E., Nóvoa-Muñoz, J.C., Shotyk, W., 1999. Mercury in a Spanish Peat Bog: Archive of Climate Change and Atmospheric Metal Deposition. Science 284, 939–942. https://doi.org/10.1126/science.284.5416.939

Masbou, J., Point, D., Guillou, G., Sonke, J.E., Lebreton, B., Richard, P., 2015a. Carbon Stable Isotope Analysis of Methylmercury Toxin in Biological Materials by Gas Chromatography Isotope Ratio Mass Spectrometry. Analytical Chemistry 87, 11732–11738. https://doi.org/10.1021/acs.analchem.5b02918

Masbou, J., Point, D., Sonke, J.E., Frappart, F., Perrot, V., Amouroux, D., Richard, P., Becker, P.R., 2015b. Hg Stable Isotope Time Trend in Ringed Seals Registers Decreasing Sea Ice Cover in the Alaskan Arctic. Environ. Sci. Technol. 49, 8977–8985. https://doi.org/10.1021/es5048446

Mason, R., Pirrone, N., 2009. Mercury fate and transport in the global atmosphere: Emissions, measurements and models. Springer-Verlag New York.

Mason, R.P., Choi, A.L., Fitzgerald, W.F., Hammerschmidt, C.R., Lamborg, C.H., Soerensen, A.L., Sunderland, E.M., 2012. Mercury biogeochemical cycling in the ocean and policy implications. Environmental Research 119, 101–117. https://doi.org/10.1016/j.envres.2012.03.013

Mason, R.P., Fitzgerald, W.F., 1990. Alkylmercury species in the equatorial Pacific. Nature 347, 457–459. https://doi.org/10.1038/347457a0

Mason, R.P., Reinfelder, J.R., Morel, F.M.M., 1996. Uptake, Toxicity, and Trophic Transfer of Mercury in a Coastal Diatom. Environ. Sci. Technol. 30, 1835–1845. https://doi.org/10.1021/es950373d

Mason, R.P., Rolfhus, K.R., Fitzgerald, W.F., 1998. Mercury in the North Atlantic. Marine Chemistry 61, 37–53. https://doi.org/10.1016/S0304-4203(98)00006-1

Mason, R.P., Sheu, G.-R., 2002. Role of the ocean in the global mercury cycle. Global Biogeochem. Cycles 16, 40-1-40–14. https://doi.org/10.1029/2001GB001440

Mathias, K.K., Justin, S.S., Irène, K.A., Célestin, A.B., Maius, B.G.H., 2014. Accumulation of Cadmium, Lead, and Mercury in Different Organs of Three Tuna Fish Species from Coastal Zone of Cote d'Ivoire 3, 5.

Maulvault, A.L., Custódio, A., Anacleto, P., Repolho, T., Pousão, P., Nunes, M.L., Diniz, M., Rosa, R., Marques, A., 2016. Bioaccumulation and elimination of mercury in juvenile seabass (Dicentrarchus labrax) in a warmer environment. Environmental Research 149, 77–85. https://doi.org/10.1016/j.envres.2016.04.035

Maury, O., 2010. An overview of APECOSM, a spatialized mass balanced "Apex Predators ECOSystem Model" to study physiologically structured tuna population dynamics in their ecosystem. Progress in Oceanography, Special Issue: Parameterisation of Trophic Interactions in Ecosystem Modelling 84, 113–117. https://doi.org/10.1016/j.pocean.2009.09.013

McMahon, K.W., Hamady, L.L., Thorrold, S.R., 2013a. A review of ecogeochemistry approaches to estimating movements of marine animals. Limnology and Oceanography 58, 697–714. https://doi.org/10.4319/lo.2013.58.2.0697

McMahon, K.W., Hamady, L.L., Thorrold, S.R., 2013b. Ocean ecogeochemistry: a review. Oceanography and Marine Biology: An Annual Review 327–374.

McMahon, K.W., McCarthy, M.D., 2016. Embracing variability in amino acid δ15N fractionation: mechanisms, implications, and applications for trophic ecology. Ecosphere 7, e01511. https://doi.org/10.1002/ecs2.1511

McMahon, K.W., Polito, M.J., Abel, S., McCarthy, M.D., Thorrold, S.R., 2015. Carbon and nitrogen isotope fractionation of amino acids in an avian marine predator, the gentoo penguin (Pygoscelis papua). Ecol Evol 5, 1278–1290. https://doi.org/10.1002/ece3.1437

Medeiros, R.J., Márprevico, E.T., São Clemente, S.C., Ferreira, M.S., 2008. Distribuição do metal mercúrio em atum (Thunnus albacares) e pescada bicuda (Cynoscion microlepidotus) capturados no litoral do Rio de Janeiro, Brasil. Arq. Bras. Med. Vet. Zootec. 60, 656–662. https://doi.org/10.1590/S0102-09352008000300020

Médieu, A., Point, D., Itai, T., Angot, H., Buchanan, P.J., Allain, V., Fuller, L., Griffiths, S., Gillikin, D.P., Sonke, J.E., Heimbürger-Boavida, L.-E., Desgranges, M.-M., Menkes, C.E., Madigan, D.J., Brosset, P., Gauthier, O., Tagliabue, A., Bopp, L., Verheyden, A., Lorrain, A., 2022. Evidence that Pacific tuna mercury levels are driven by marine methylmercury production and anthropogenic inputs. PNAS 119, 8. https://doi.org/10.1073/pnas.2113032119

Médieu, A., Point, D., Receveur, A., Gauthier, O., Allain, V., Pethybridge, H., Menkes, C.E., Gillikin, D.P., Revill, A.T., Somes, C.J., Collin, J., Lorrain, A., 2021a. Stable mercury concentrations of tropical tuna in the south western Pacific ocean: An 18-year monitoring study. Chemosphere 263, 128024. https://doi.org/10.1016/j.chemosphere.2020.128024

Médieu, A., Sardenne, F., Lorrain, A., Bodin, N., Pazart, C., Le Delliou, H., Point, D., 2021b. Lipid-free tuna muscle samples are suitable for total mercury analysis. Marine Environmental Research 169, 105385. https://doi.org/10.1016/j.marenvres.2021.105385

Ménard, F., Lorrain, A., Potier, M., Marsac, F., 2007. Isotopic evidence of distinct feeding ecologies and movement patterns in two migratory predators (yellowfin tuna and swordfish) of the western Indian Ocean. Marine Biology 153, 141–152. https://doi.org/10.1007/s00227-007-0789-7

Menasveta, P., Siriyong, R., 1977. Mercury content in several predacious fish in the Andaman Sea. Marine Pollution Bulletin 8, 200–204.

Mergler, D., Anderson, H.A., Chan, L.H.M., Mahaffey, K.R., Murray, M., Sakamoto, M., Stern, A.H., 2007. Methylmercury Exposure and Health Effects in Humans: A Worldwide Concern. AMBIO: A Journal of the Human Environment 36, 3–11. https://doi.org/10.1579/0044-7447(2007)36[3:MEAHEI]2.0.CO;2

Monperrus, M., Tessier, E., Amouroux, D., Leynaert, A., Huonnic, P., Donard, O.F.X., 2007. Mercury methylation, demethylation and reduction rates in coastal and marine surface waters of the Mediterranean Sea. Marine Chemistry, Mercury Cycling in Surface and Deep Waters of the Mediterranean Sea 107, 49–63. https://doi.org/10.1016/j.marchem.2007.01.018

Morel, F.M.M., Kraepiel, A.M.L., Amyot, M., 1998. The Chemical Cycle and Bioaccumulation of Mercury. Annual Review of Ecology and Systematics 29, 543–566. https://doi.org/10.1146/annurev.ecolsys.29.1.543

Morrissey, M.T., Rasmussen, R., Okada, T., 2005. Mercury Content in Pacific Troll-Caught Albacore Tuna (Thunnus alalunga). Journal of Aquatic Food Product Technology 13, 41–52. https://doi.org/10.1300/J030v13n04_04

Moura Reis Manhães, B., de Souza Picaluga, A., Bisi, T.L., de Freitas Azevedo, A., Torres, J.P.M., Malm, O., Lailson-Brito, J., 2020. Tracking mercury in the southwestern Atlantic Ocean: the use of tuna and tuna-like species as indicators of bioavailability. Environ Sci Pollut Res 27, 6813–6823. https://doi.org/10.1007/s11356-019-07275-4

Munson, K.M., Lamborg, C.H., Boiteau, R.M., Saito, M.A., 2018. Dynamic mercury methylation and demethylation in oligotrophic marine water. Biogeosciences 15, 6451–6460. https://doi.org/10.5194/bg-15-6451-2018

Munson, K.M., Lamborg, C.H., Swarr, G.J., Saito, M.A., 2015. Mercury species concentrations and fluxes in the Central Tropical Pacific Ocean. Global Biogeochemical Cycles 29, 656–676. https://doi.org/10.1002/2015GB005120

Murua, H., Rodriguez-Marin, E., Neilson, J.D., Farley, J.H., Juan-Jordá, M.J., 2017. Fast versus slow growing tuna species: age, growth, and implications for population dynamics and fisheries management. Rev Fish Biol Fisheries 27, 733–773. https://doi.org/10.1007/s11160-017-9474-1

Nguyen, L.S.P., Sheu, G.-R., Lin, D.-W., Lin, N.-H., 2019. Temporal changes in atmospheric mercury concentrations at a background mountain site downwind of the East Asia continent in 2006–2016. Science of The Total Environment 686, 1049–1056. https://doi.org/10.1016/j.scitotenv.2019.05.425

Nicklisch, S.C.T., Bonito, L.T., Sandin, S., Hamdoun, A., 2017. Mercury levels of yellowfin tuna (Thunnus albacares) are associated with capture location. Environmental Pollution 229, 87–93. https://doi.org/10.1016/j.envpol.2017.05.070

Nikolic, N., Montes, I., Lalire, M., Puech, A., Bodin, N., Arnaud-Haond, S., Kerwath, S., Corse, E., Gaspar, P., Hollanda, S., Bourjea, J., West, W., Bonhommeau, S., 2020. Connectivity and population structure of albacore tuna across southeast Atlantic and southwest Indian Oceans inferred from multidisciplinary methodology. Sci Rep 10, 15657. https://doi.org/10.1038/s41598-020-72369-w

Nikolic, N., Morandeau, G., Hoarau, L., West, W., Arrizabalaga, H., Hoyle, S., Nicol, S.J., Bourjea, J., Puech, A., Farley, J.H., Williams, A.J., Fonteneau, A., 2017. Review of albacore tuna, Thunnus alalunga, biology, fisheries and management. Rev Fish Biol Fisheries 27, 775–810. https://doi.org/10.1007/s11160-016-9453-y

Ohi, G., Nishigaki, S., Seki, H., Tamura, Y., Maki, T., Konno, H., Ochiai, S., Yamada, H., Shimamura, Y., Mizoguchi, I., Yagyu, H., 1976. Efficacy of selenium in tuna and selenite in modifying methylmercury intoxication. Environmental Research 12, 49–58. https://doi.org/10.1016/0013-9351(76)90008-6

Oliveira Ribeiro, C.A., Rouleau, C., Pelletier, É., Audet, C., Tjälve, H., 1999. Distribution Kinetics of Dietary Methylmercury in the Arctic Charr (Salvelinus alpinus). Environ. Sci. Technol. 33, 902–907. https://doi.org/10.1021/es980242n

Olson, R.J., Duffy, L.M., Kuhnert, P.M., Galván-Magaña, F., Bocanegra-Castillo, N., Alatorre-Ramírez, V., 2014. Decadal diet shift in yellowfin tuna Thunnus albacares suggests broad-scale food web changes in the eastern tropical Pacific Ocean. Marine Ecology Progress Series 497, 157–178. https://doi.org/10.3354/meps10609

Olson, R.J., Popp, B.N., Graham, B.S., López-Ibarra, G.A., Galván-Magaña, F., Lennert-Cody, C.E., Bocanegra-Castillo, N., Wallsgrove, N.J., Gier, E., Alatorre-Ramírez, V., Ballance, L.T., Fry, B., 2010. Food-web inferences of stable isotope spatial patterns in copepods and yellowfin tuna in the pelagic eastern Pacific Ocean. Progress in Oceanography, CLimate Impacts on Oceanic TOp Predators (CLIOTOP) 86, 124–138. https://doi.org/10.1016/j.pocean.2010.04.026

Olson, R.J., Young, J.W., Ménard, F., Potier, M., Allain, V., Goñi, N., Logan, J.M., Galván-Magaña, F., 2016. Chapter Four: Bioenergetics, Trophic Ecology, and Niche Separation of Tunas, in: Advances in Marine Biology. Elsevier, pp. 199–344. https://doi.org/10.1016/bs.amb.2016.06.002

Ordiano-Flores, A., Galván-Magaña, F., Rosiles-Martínez, R., 2011. Bioaccumulation of Mercury in Muscle Tissue of Yellowfin Tuna, Thunnus albacares, of the Eastern Pacific Ocean. Biological Trace Element Research 144, 606–620. https://doi.org/10.1007/s12011-011-9136-4

Ordiano-Flores, A., Rosíles-Martínez, R., Galván-Magaña, F., 2012. Biomagnification of mercury and its antagonistic interaction with selenium in yellowfin tuna Thunnus albacares in the trophic web of Baja California Sur, Mexico. Ecotoxicology and Environmental Safety 86, 182–187. https://doi.org/10.1016/j.ecoenv.2012.09.014

Ortiz, V.L., Mason, R.P., Evan Ward, J., 2015. An examination of the factors influencing mercury and methylmercury particulate distributions, methylation and demethylation rates in laboratory-generated marine snow. Marine Chemistry 177, 753–762. https://doi.org/10.1016/j.marchem.2015.07.006

Outridge, P.M., Mason, R.P., Wang, F., Guerrero, S., Heimbürger-Boavida, L.E., 2018. Updated Global and Oceanic Mercury Budgets for the United Nations Global Mercury Assessment 2018. Environ. Sci. Technol. 52, 11466–11477. https://doi.org/10.1021/acs.est.8b01246

Pagavino, M., Gaertner, D., 1995. Ajuste de una curva de crecimiento a frecuencias de tallas de atun listado (Katsuwonus pelamis) pescado en el mar Caribe suroriental.

Pan-Hou, H.S.K., Imura, N., 1981. Biotransformation of mercurials by intestinal microorganisms isolated from yellowfin tuna. Bull. Environ. Contam. Toxicol. 26, 359–363. https://doi.org/10.1007/BF01622102

Parks, J.M., Johs, A., Podar, M., Bridou, R., Hurt, R.A., Smith, S.D., Tomanicek, S.J., Qian, Y., Brown, S.D., Brandt, C.C., Palumbo, A.V., Smith, J.C., Wall, J.D., Elias, D.A., Liang, L., 2013. The Genetic Basis for Bacterial Mercury Methylation. Science 339, 1332–1335. https://doi.org/10.1126/science.1230667

Pecoraro, C., Zudaire, I., Bodin, N., Murua, H., Taconet, P., Díaz-Jaimes, P., Cariani, A., Tinti, F., Chassot, E., 2017. Putting all the pieces together: integrating current knowledge of the biology, ecology, fisheries status, stock structure and management of yellowfin tuna (Thunnus albacares). Rev Fish Biol Fisheries 27, 811–841. https://doi.org/10.1007/s11160-016-9460-z

Peng, S., Chen, C., Shi, Z., Wang, L., 2013. Amino Acid and Fatty Acid Composition of the Muscle Tissue of Yellowfin Tuna (Thunnus Albacares) and Bigeye Tuna (Thunnus Obesus). Journal of Food and Nutrition Research 4.

Peterson, C.L., Klawe, W.L., Sharp, G.D., 1973. Mercury in tunas: a review. Fishery Bulletin 71, 11.

Pethybridge, H., Choy, C.A., Logan, J.M., Allain, V., Lorrain, A., Bodin, N., Somes, C.J., Young, J., Ménard, F., Langlais, C., Duffy, L., Hobday, A.J., Kuhnert, P., Fry, B., Menkes, C., Olson, R.J., 2018a. A global meta-analysis of marine predator nitrogen stable isotopes: Relationships between trophic structure and environmental conditions. Global Ecology and Biogeography 27, 1043–1055. https://doi.org/10.1111/geb.12763

Pethybridge, H., Choy, C.A., Polovina, J.J., Fulton, E.A., 2018b. Improving Marine Ecosystem Models with Biochemical Tracers. Annual Review of Marine Science 10, 199–228. https://doi.org/10.1146/annurev-marine-121916-063256

Phillips, D.L., Eldridge, P.M., 2006. Estimating the timing of diet shifts using stable isotopes. Oecologia 147, 195–203. https://doi.org/10.1007/s00442-005-0292-0

Pickhardt, P.C., Fisher, N.S., 2007. Accumulation of Inorganic and Methylmercury by Freshwater Phytoplankton in Two Contrasting Water Bodies. Environ. Sci. Technol. 41, 125–131. https://doi.org/10.1021/es060966w

Pirrone, N., Cinnirella, S., Feng, X., Finkelman, R.B., Friedli, H.R., Leaner, J., Mason, R., Mukherjee, A.B., Stracher, G.B., Streets, D.G., Telmer, K., 2010. Global mercury emissions to the atmosphere from anthropogenic and natural sources. Atmos. Chem. Phys. 10, 5951–5964. https://doi.org/10.5194/acp-10-5951-2010

Podar, M., Gilmour, C.C., Brandt, C.C., Soren, A., Brown, S.D., Crable, B.R., Palumbo, A.V., Somenahally, A.C., Elias, D.A., 2015. Global prevalence and distribution of genes and microorganisms involved in mercury methylation. Science Advances 1, e1500675. https://doi.org/10.1126/sciadv.1500675

Point, D., Sonke, J.E., Day, R.D., Roseneau, D.G., Hobson, K.A., Vander Pol, S.S., Moors, A.J., Pugh, R.S., Donard, O.F.X., Becker, P.R., 2011. Methylmercury photodegradation influenced by sea-ice cover in Arctic marine ecosystems. Nature Geosci 4, 188–194. https://doi.org/10.1038/ngeo1049

Popp, B.N., Graham, B.S., Olson, R.J., Hannides, C.C.S., Lott, M.J., López-Ibarra, G.A., Galván-Magaña, F., Fry, B., 2007. Insight into the Trophic Ecology of Yellowfin Tuna, Thunnus albacares, from Compound-Specific Nitrogen Isotope Analysis of Proteinaceous Amino Acids. Terrestrial Ecology 1, 173–190.

Post, J.R., Vandenbos, R., McQueen, D.J., 1996. Uptake rates of food-chain and waterborne mercury by fish: field measurements, a mechanistic model, and an assessment of uncertainties 53, 13.

Potier, M., Lucas, V., Marsac, F., Sabatié, R., Ménard, F., 2002. On-going research activities on trophic ecology of tuna in equatorial ecosystems of the Indian Ocean. Presented at the 4th session of the IOTC working party on tropical tunas, Shangai, China, pp. 3–11.

R Core Team, 2018. R: A language and environment for statistical computing; 2015. Vienna, Austria.

Ramirez, M.D., Besser, A.C., Newsome, S.D., McMahon, K.W., 2021. Meta-analysis of primary producer amino acid δ15N values and their influence on trophic position estimation. Methods in Ecology and Evolution 12, 1750–1767. https://doi.org/10.1111/2041-210X.13678

Ramos, L., Kristenson, E.M., Brinkman, U.A.T., 2002. Current use of pressurised liquid extraction and subcritical water extraction in environmental analysis. Journal of Chromatography A, Sample Handling 975, 3–29. https://doi.org/10.1016/S0021-9673(02)01336-5

Reay, D.S., Dentener, F., Smith, P., Grace, J., Feely, R.A., 2008. Global nitrogen deposition and carbon sinks. Nature Geosci 1, 430–437. https://doi.org/10.1038/ngeo230

Renedo, M., 2018. Identification of sources and bioaccumulation pathways of MeHg in subantarctic penguins: a stable isotopic investigation. Scientific Reports 10.

Renedo, M., Point, D., Sonke, J.E., Lorrain, A., Demarcq, H., Graco, M., Grados, D., Gutiérrez, D., Médieu, A., Munaron, J.M., Pietri, A., Colas, F., Tremblay, Y., Roy, A., Bertrand, A., Bertrand, S.L., 2021. ENSO Climate Forcing of the Marine Mercury Cycle in the Peruvian Upwelling Zone Does Not Affect Methylmercury Levels of Marine Avian Top Predators. Environ. Sci. Technol. 55, 15754–15765. https://doi.org/10.1021/acs.est.1c03861

Reygondeau, G., Maury, O., Beaugrand, G., Fromentin, J.M., Fonteneau, A., Cury, P., 2012. Biogeography of tuna and billfish communities. Journal of Biogeography 39, 114–129. https://doi.org/10.1111/j.1365-2699.2011.02582.x

Reynolds, R.W., Rayner, N.A., Smith, T.M., Stokes, D.C., Wang, W., 2002. An Improved In Situ and Satellite SST Analysis for Climate. J. Climate 15, 1609–1625. https://doi.org/10.1175/1520-0442(2002)015<1609:AIISAS>2.0.CO;2

Richardson, A.J., Downes, K.J., Nolan, E.T., Brickle, P., Brown, J., Weber, N., Weber, S.B., 2018. Residency and reproductive status of yellowfin tuna in a proposed large-scale pelagic marine protected area. Aquatic Conservation: Marine and Freshwater Ecosystems 28, 1308–1316. https://doi.org/10.1002/aqc.2936

Rivers, J.B., Pearson, J.E., Shultz, C.D., 1972. Total and organic mercury in marine fish. Bull. Environ. Contam. Toxicol. 8, 257–266. https://doi.org/10.1007/BF01684554

Roger, C., Fao, C., Mahe, E.C. on I.O.T. eng 4-8 O. 1993 S. 5, Ardill, J.D., 1994. On feeding conditions for surface tunas (yellowfin, Thunnus albacares and skipjack, Katsuwonus pelamis) in the Western Indian Ocean. FAO, Colombo (Sri Lanka).

Sabarros, P.S., Romanov, E.V., Bach, P., 2015. Vertical behavior and habitat preferences of yellowfin and bigeye tuna in the South West Indian Ocean inferred from PSAT tagging data. IOTC–2015–WPTT17–42 Rev_1. Presented at the Seventeenth Session of the IOTC Working Party on Tropical Tuna, Montpellier, France, p. 16.

Saber, S., Macías, D., Gómez-Vives, M.J., García-Barcelona, S., de Urbina, J.O., 2020. Standardized catch rates of skipjack from the Mediterranean Spanish recreational fishery (2006-2018), in: Collect. Vol. Sci. Pap. ICCAT. pp. 867–873.

Sampaio, E., Santos, C., Rosa, I.C., Ferreira, V., Pörtner, H.-O., Duarte, C.M., Levin, L.A., Rosa, R., 2021. Impacts of hypoxic events surpass those of future ocean warming and acidification. Nat Ecol Evol 5, 311–321. https://doi.org/10.1038/s41559-020-01370-3

Sardenne, F., Bodin, N., Chassot, E., Amiel, A., Fouché, E., Degroote, M., Hollanda, S., Pethybridge, H., Lebreton, B., Guillou, G., Ménard, F., 2016. Trophic niches of sympatric tropical tuna in the Western Indian Ocean inferred by stable isotopes and neutral fatty acids. Progress in Oceanography 146, 75–88. https://doi.org/10.1016/j.pocean.2016.06.001

Sardenne, F., Bodin, N., Médieu, A., Antha, M., Arrisol, R., Le Grand, F., Bideau, A., Munaron, J.-M., Le Loc'h, F., Chassot, E., 2020. Benefit-risk associated with the consumption of fish bycatch from tropical tuna fisheries. Environmental Pollution 267, 115614. https://doi.org/10.1016/j.envpol.2020.115614

Sardenne, F., Bodin, N., Metral, L., Crottier, A., Le Grand, F., Bideau, A., Brisset, B., Bourjea, J., Saraux, C., Bonhommeau, S., Kerzérho, V., Bernard, S., Rouyer, T., 2019a. Effects of extraction method and storage of dry tissue on marine lipids and fatty acids. Analytica Chimica Acta 1051, 82–93. https://doi.org/10.1016/j.aca.2018.11.012

Sardenne, F., Diaha, N.C., Amandé, M.J., Zudaire, I., Couturier, L.I.E., Metral, L., Le Grand, F., Bodin, N., 2019b. Seasonal habitat and length influence on the trophic niche of co-occurring tropical

tunas in the eastern Atlantic Ocean. Can. J. Fish. Aquat. Sci. 76, 69–80. https://doi.org/10.1139/cjfas-2017-0368

Sardenne, F., Ménard, F., Degroote, M., Fouché, E., Guillou, G., Lebreton, B., Hollanda, S.J., Bodin, N., 2015. Methods of lipid-normalization for multi-tissue stable isotope analyses in tropical tuna: Lipid-normalization for multi-tissue SIA in tuna. Rapid Commun. Mass Spectrom. 29, 1253–1267. https://doi.org/10.1002/rcm.7215

Schaefer, J.K., Fuller, D.W., 2007. Vertical movement patterns of skipjack tuna (Katsuwonus pelamis) in the eastern equatorial Pacific Ocean, as revealed with archival tags. Fishery Bulletin 105, 379–389.

Schaefer, J.K., Rocks, S.S., Zheng, W., Liang, L., Gu, B., Morel, F.M.M., 2011. Active transport, substrate specificity, and methylation of Hg(II) in anaerobic bacteria. PNAS 108, 8714–8719. https://doi.org/10.1073/pnas.1105781108

Schaefer, J.K., Szczuka, A., Morel, F.M.M., 2014. Effect of Divalent Metals on Hg(II) Uptake and Methylation by Bacteria. Environ. Sci. Technol. 48, 3007–3013. https://doi.org/10.1021/es405215v

Schaefer, K., Fuller, D., Hampton, J., Caillot, S., Leroy, B., Itano, D., 2015. Movements, dispersion, and mixing of bigeye tuna (Thunnus obesus) tagged and released in the equatorial Central Pacific Ocean, with conventional and archival tags. Fisheries Research 161, 336–355. https://doi.org/10.1016/j.fishres.2014.08.018

Schaefer, K.M., Fuller, D.W., 2010. Vertical movements, behavior, and habitat of bigeye tuna (Thunnus obesus) in the equatorial eastern Pacific Ocean, ascertained from archival tag data. Mar Biol 157, 2625–2642. https://doi.org/10.1007/s00227-010-1524-3

Schaefer, K.M., Fuller, D.W., Block, B.A., 2009. Vertical Movements and Habitat Utilization of Skipjack (Katsuwonus pelamis), Yellowfin (Thunnus albacares), and Bigeye (Thunnus obesus) Tunas in the Equatorial Eastern Pacific Ocean, Ascertained Through Archival Tag Data, in: Nielsen, J.L., Arrizabalaga, H., Fragoso, N., Hobday, A., Lutcavage, M., Sibert, J. (Eds.), Tagging and Tracking of Marine Animals with Electronic Devices, Reviews: Methods and Technologies in Fish Biology and Fisheries. Springer Netherlands, Dordrecht, pp. 121–144. https://doi.org/10.1007/978-1-4020-9640-2_8

Schaefer, K.M., Fuller, D.W., Block, B.A., 2007. Movements, behavior, and habitat utilization of yellowfin tuna (Thunnus albacares) in the northeastern Pacific Ocean, ascertained through archival tag data. Mar Biol 152, 503–525. https://doi.org/10.1007/s00227-007-0689-x

Schaefer, M., Chatwin, B., Broadhead, G., 1961. Tagging and recovery of tropical tunas. Technical report IATTC, La Jolla, California (USA).

Schartup, A.T., Ndu, U., Balcom, P.H., Mason, R.P., Sunderland, E.M., 2015. Contrasting Effects of Marine and Terrestrially Derived Dissolved Organic Matter on Mercury Speciation and Bioavailability in Seawater. Environ. Sci. Technol. 49, 5965–5972. https://doi.org/10.1021/es506274x

Schartup, A.T., Qureshi, A., Dassuncao, C., Thackray, C.P., Harding, G., Sunderland, E.M., 2018. A Model for Methylmercury Uptake and Trophic Transfer by Marine Plankton. Environ. Sci. Technol. 52, 654–662. https://doi.org/10.1021/acs.est.7b03821

Schartup, A.T., Thackray, C.P., Qureshi, A., Dassuncao, C., Gillespie, K., Hanke, A., Sunderland, E.M., 2019. Climate change and overfishing increase neurotoxicant in marine predators. Nature 1–3. https://doi.org/10.1038/s41586-019-1468-9

Schmidtko, S., Stramma, L., Visbeck, M., 2017. Decline in global oceanic oxygen content during the past five decades. Nature 542, 335–339. https://doi.org/10.1038/nature21399

Schulzweida, U., 2019. CDO User guide. 1–206. https://doi.org/doi:10.5281/zenodo.3539275

Schuster, P.F., Krabbenhoft, D.P., Naftz, D.L., Cecil, L.D., Olson, M.L., Dewild, J.F., Susong, D.D., Green, J.R., Abbott, M.L., 2002. Atmospheric Mercury Deposition during the Last 270 Years: A Glacial Ice Core Record of Natural and Anthropogenic Sources. Environ. Sci. Technol. 36, 2303–2310. https://doi.org/10.1021/es0157503

Schwarcz, H.P., 1991. Some theoretical aspects of isotope paleodiet studies. Journal of Archaeological Science 18, 261–275. https://doi.org/10.1016/0305-4403(91)90065-W

Scutt Phillips, J., Pilling, G.M., Leroy, B., Evans, K., Usu, T., Lam, C.H., Schaefer, K.M., Nicol, S., 2017. Revisiting the vulnerability of juvenile bigeye (Thunnus obesus) and yellowfin (T. albacares) tuna caught by purse-seine fisheries while associating with surface waters and floating objects. PLoS ONE 12, e0179045. https://doi.org/10.1371/journal.pone.0179045

Selin, N.E., Jacob, D.J., Park, R.J., Yantosca, R.M., Strode, S., Jaeglé, L., Jaffe, D., 2007. Chemical cycling and deposition of atmospheric mercury: Global constraints from observations. Journal of Geophysical Research 112. https://doi.org/10.1029/2006JD007450

Selin, N.E., Jacob, D.J., Yantosca, R.M., Strode, S., Jaeglé, L., Sunderland, E.M., 2008. Global 3-D land-ocean-atmosphere model for mercury: Present-day versus preindustrial cycles and anthropogenic enrichment factors for deposition. Global Biogeochemical Cycles 22, 13. https://doi.org/10.1029/2007GB003040

Semeniuk, K., Dastoor, A., 2017. Development of a global ocean mercury model with a methylation cycle: Outstanding issues. Global Biogeochemical Cycles 31, 400–433. https://doi.org/10.1002/2016GB005452

Senn, D.B., Chesney, E.J., Blum, J.D., Bank, M.S., Maage, A., Shine, J.P., 2010. Stable Isotope (N, C, Hg) Study of Methylmercury Sources and Trophic Transfer in the Northern Gulf of Mexico. Environ. Sci. Technol. 44, 1630–1637. https://doi.org/10.1021/es902361j

Shiozaki, T., Kodama, T., Furuya, K., 2014. Large-scale impact of the island mass effect through nitrogen fixation in the western South Pacific Ocean. Geophysical Research Letters 41, 2907–2913. https://doi.org/10.1002/2014GL059835

Sibert, J., Hampton, J., 2003. Mobility of tropical tunas and the implications for fisheries management. Marine Policy 27, 87–95. https://doi.org/10.1016/S0308-597X(02)00057-X

Sirot, V., Leblanc, J.-C., Margaritis, I., 2012. A risk–benefit analysis approach to seafood intake to determine optimal consumption. Br J Nutr 107, 1812–1822. https://doi.org/10.1017/S0007114511005010

Slemr, F., Angot, H., Dommergue, A., Magand, O., Barret, M., Weigelt, A., Ebinghaus, R., Brunke, E.-G., Pfaffhuber, K.A., Edwards, G., Howard, D., Powell, J., Keywood, M., Wang, F., 2015. Comparison of mercury concentrations measured at several sites in the Southern Hemisphere. Atmospheric Chemistry and Physics 15, 3125–3133. https://doi.org/10.5194/acp-15-3125-2015

Slemr, F., Martin, L., Labuschagne, C., Mkololo, T., Angot, H., Magand, O., Dommergue, A., Garat, P., Ramonet, M., Bieser, J., 2020. Atmospheric mercury in the Southern Hemisphere – Part 1: Trend and inter-annual variations in atmospheric mercury at Cape Point, South Africa, in 2007–2017, and on Amsterdam Island in 2012–2017. Atmos. Chem. Phys. 20, 7683–7692. https://doi.org/10.5194/acp-20-7683-2020

Soerensen, A.L., Sunderland, E.M., Holmes, C.D., Jacob, D.J., Yantosca, R.M., Skov, H., Christensen, J.H., Strode, S.A., Mason, R.P., 2010. An Improved Global Model for Air-Sea Exchange of Mercury: High Concentrations over the North Atlantic. Environmental Science & Technology 44, 8574–8580. https://doi.org/10.1021/es102032g

Somes, C.J., Oschlies, A., 2015. On the influence of “non-Redfield” dissolved organic nutrient dynamics on the spatial distribution of N2 fixation and the size of the marine fixed nitrogen inventory. Global Biogeochemical Cycles 29, 973–993. https://doi.org/10.1002/2014GB005050

Somes, C.J., Schmittner, A., Galbraith, E.D., Lehmann, M.F., Altabet, M.A., Montoya, J.P., Letelier, R.M., Mix, A.C., Bourbonnais, A., Eby, M., 2010. Simulating the global distribution of nitrogen isotopes in the ocean. Global Biogeochem. Cycles 24, n/a-n/a. https://doi.org/10.1029/2009GB003767

Somes, C.J., Schmittner, A., Muglia, J., Oschlies, A., 2017. A Three-Dimensional Model of the Marine Nitrogen Cycle during the Last Glacial Maximum Constrained by Sedimentary Isotopes. Frontiers in Marine Science 4. https://doi.org/10.3389/fmars.2017.00108

Sompongchaiyakul, P., Hantow, J., Sornkrut, S., Sumontha, M., 2008. An Assessment of Mercury Concentration in Fish Tissues Caught from Three Compartments of the Bay of Bengal, The Ecosystem-Based Fishery Management in the Bay of Bengal. Thailand.

Song, L., Zhou, J., Zhou, Y., Nishida, T., Jiang, W., Wang, J., 2009. Environmental preferences of bigeye tuna, Thunnus obesus, in the Indian Ocean: an application to a longline fishery. Environ Biol Fish 85, 153–171. https://doi.org/10.1007/s10641-009-9474-7

Song, S., Selin, N.E., Soerensen, A.L., Angot, H., Artz, R., Brooks, S., Brunke, E.-G., Conley, G., Dommergue, A., Ebinghaus, R., Holsen, T.M., Jaffe, D.A., Kang, S., Kelley, P., Luke, W.T., Magand, O., Marumoto, K., Pfaffhuber, K.A., Ren, X., Sheu, G.-R., Slemr, F., Warneke, T., Weigelt, A., Weiss-Penzias, P., Wip, D.C., Zhang, Q., 2015. Top-down constraints on atmospheric mercury emissions and implications for global biogeochemical cycling. Atmospheric Chemistry and Physics 15, 7103–7125. https://doi.org/10.5194/acp-15-7103-2015

Sprovieri, F., Pirrone, N., Bencardino, M., D'Amore, F., Carbone, F., Cinnirella, S., Mannarino, V., Landis, M., Ebinghaus, R., Weigelt, A., Brunke, E.-G., Labuschagne, C., Martin, L., Munthe, J., Wängberg, I., Artaxo, P., Morais, F., Barbosa, H. de M.J., Brito, J., Cairns, W., Barbante, C., Diéguez, M. del C., Garcia, P.E., Dommergue, A., Angot, H., Magand, O., Skov, H., Horvat, M., Kotnik, J., Read, K.A., Neves, L.M., Gawlik, B.M., Sena, F., Mashyanov, N., Obolkin, V., Wip, D., Feng, X.B., Zhang, H., Fu, X., Ramachandran, R., Cossa, D., Knoery, J., Marusczak, N., Nerentorp, M., Norstrom, C., 2016. Atmospheric mercury concentrations observed at ground-based monitoring sites globally distributed in the framework of the GMOS network. Atmospheric Chemistry and Physics 16, 11915–11935. https://doi.org/10.5194/acp-16-11915-2016

Storelli, M.M., Giacominelli-Stuffler, R., Storelli, A., Marcotrigiano, G.O., 2005. Accumulation of mercury, cadmium, lead and arsenic in swordfish and bluefin tuna from the Mediterranean Sea: A comparative study. Marine Pollution Bulletin 50, 1004–1007. https://doi.org/10.1016/j.marpolbul.2005.06.041

Storelli, M.M., Marcotrigiano, G.O., 2004. Content of mercury and cadmium in fish (Thunnus alalunga) and cephalopods (Eledone moschata) from the south-eastern Mediterranean Sea. Food Additives and Contaminants 21, 1051–1056. https://doi.org/10.1080/02652030400023127

Storelli, M.M., Stuffler, R.G., Marcotrigiano, G.O., 2002. Total and methylmercury residues in tuna-fish from the Mediterranean sea. Food Additives & Contaminants 19, 7.

Stramma, L., Johnson, G.C., Sprintall, J., Mohrholz, V., 2008. Expanding Oxygen-Minimum Zones in the Tropical Oceans. Science 320, 655–658. https://doi.org/10.1126/science.1153847

Streets, D.G., Devane, M.K., Lu, Z., Bond, T.C., Sunderland, E.M., Jacob, D.J., 2011. All-Time Releases of Mercury to the Atmosphere from Human Activities. Environmental Science & Technology 45, 10485–10491. https://doi.org/10.1021/es202765m

Streets, D.G., Horowitz, H.M., Jacob, D.J., Lu, Z., Levin, L., ter Schure, A.F.H., Sunderland, E.M., 2017. Total Mercury Released to the Environment by Human Activities. Environ. Sci. Technol. 51, 5969–5977. https://doi.org/10.1021/acs.est.7b00451

Streets, D.G., Horowitz, H.M., Lu, Z., Levin, L., Thackray, C.P., Sunderland, E.M., 2019a. Five hundred years of anthropogenic mercury: spatial and temporal release profiles. Environ. Res. Lett. 14, 084004. https://doi.org/10.1088/1748-9326/ab281f

Streets, D.G., Horowitz, H.M., Lu, Z., Levin, L., Thackray, C.P., Sunderland, E.M., 2019b. Global and regional trends in mercury emissions and concentrations, 2010–2015. Atmospheric Environment 201, 417–427. https://doi.org/10.1016/j.atmosenv.2018.12.031

Sun, X., Yin, R., Hu, L., Guo, Z., Hurley, J.P., Lepak, R.F., Li, X., 2020. Isotopic tracing of mercury sources in estuarine-inner shelf sediments of the East China Sea. Environmental Pollution 262, 114356. https://doi.org/10.1016/j.envpol.2020.114356

Sunderland, E.M., 2007. Mercury Exposure from Domestic and Imported Estuarine and Marine Fish in the U.S. Seafood Market. Environmental Health Perspectives 115, 235–242. https://doi.org/10.1289/ehp.9377

Sunderland, E.M., Krabbenhoft, D.P., Moreau, J.W., Strode, S.A., Landing, W.M., 2009. Mercury sources, distribution, and bioavailability in the North Pacific Ocean: Insights from data and models. Global Biogeochemical Cycles 23, 14. https://doi.org/10.1029/2008GB003425

Sunderland, E.M., Mason, R.P., 2007. Human impacts on open ocean mercury concentrations. Global Biogeochemical Cycles 21, 15. https://doi.org/10.1029/2006GB002876

Száková, J., Kolihová, D., Miholová, D., Mader, P., 2004. Single-Purpose Atomic Absorption Spectrometer AMA-254 for Mercury Determination and its Performance in Analysis of Agricultural and Environmental Materials. Chem. Pap. 5.

Tagliabue, A., Barrier, N., Du Pontavice, H., Kwiatkowski, L., Aumont, O., Bopp, L., Cheung, W.W.L., Gascuel, D., Maury, O., 2020. An iron cycle cascade governs the response of equatorial Pacific ecosystems to climate change. Global Change Biology 26, 6168–6179. https://doi.org/10.1111/gcb.15316

Tang, Y., Wang, S., Wu, Q., Liu, K., Wang, L., Li, S., Gao, W., Zhang, L., Zheng, H., Li, Z., Hao, J., 2018. Recent decrease trend of atmospheric mercury concentrations in East China: the influence of anthropogenic emissions. Atmospheric Chemistry and Physics 18, 8279–8291. https://doi.org/10.5194/acp-18-8279-2018

Teffer, A.K., Staudinger, M.D., Taylor, D.L., Juanes, F., 2014. Trophic influences on mercury accumulation in top pelagic predators from offshore New England waters of the northwest Atlantic Ocean. Marine Environmental Research 101, 124–134. https://doi.org/10.1016/j.marenvres.2014.09.008

Tesdal, J.-E., Galbraith, E.D., Kienast, M., 2013. Nitrogen isotopes in bulk marine sediment: linking seafloor observations with subseafloor records. Biogeosciences 10, 101–118. https://doi.org/10.5194/bg-10-101-2013

Tivey, M.K., 2007. Generation of seafloor hydrothermal vent fluids and associated mineral deposits. Oceanography 20, 50–65.

Torres, P., Rodrigues, A., Soares, L., Garcia, P., 2016. Metal Concentrations in Two Commercial Tuna Species from an Active Volcanic Region in the Mid-Atlantic Ocean. Arch Environ Contam Toxicol 70, 341–347. https://doi.org/10.1007/s00244-015-0249-1

Trasande, L., Landrigan Philip J., Schechter Clyde, 2005. Public Health and Economic Consequences of Methyl Mercury Toxicity to the Developing Brain. Environmental Health Perspectives 113, 590–596. https://doi.org/10.1289/ehp.7743

Travnikov, O., Angot, H., Artaxo, P., Bencardino, M., Bieser, J., D'Amore, F., Dastoor, A., De Simone, F., Diéguez, M. del C., Dommergue, A., Ebinghaus, R., Feng, X.B., Gencarelli, C.N., Hedgecock, I.M., Magand, O., Martin, L., Matthias, V., Mashyanov, N., Pirrone, N., Ramachandran, R., Read, K.A., Ryjkov, A., Selin, N.E., Sena, F., Song, S., Sprovieri, F., Wip, D., Wängberg, I., Yang, X., 2017. Multi-model study of mercury dispersion in the atmosphere: atmospheric processes and model evaluation. Atmospheric Chemistry and Physics 17, 5271–5295. https://doi.org/10.5194/acp-17-5271-2017

Troina, G.C., Riekenberg, P., van der Meer, M.T.J., Botta, S., Dehairs, F., Secchi, E.R., 2021. Combining isotopic analysis of bulk-skin and individual amino acids to investigate the trophic position and foraging areas of multiple cetacean species in the western South Atlantic. Environmental Research 201, 111610. https://doi.org/10.1016/j.envres.2021.111610

Trudel, M., Rasmussen, J.B., 2006. Bioenergetics and mercury dynamics in fish: a modelling perspective. Can. J. Fish. Aquat. Sci. 63, 1890–1902. https://doi.org/10.1139/f06-081

Tsagarakis, K., Darmanin, S.A., Al Mabruk, S.A.A., Auriemma, R., Azzurro, E., Badouvas, N., Bakiu, R., Bariche, M., Battaglia, P., Betti, F., Borme, D., Cacciamani, R., Cali, F., Corsini-Foka, M., Crocetta, F., Dalyan, C., Deidun, A., Digenis, M., Domenichetti, F., Dragičević, B., Dulčić, J., Durucan, F., Guy-Haim, T., Kesici, N.B., Lardi, P., Manitaras, Y., Michailidis, N., Piraino, S., Rizgalla, J., Siapatis, A., Soldo, A., Stipa, M.G., Terbiyik Kurt, T., Tiralongo, F., Tsiamis, K., Vella,

A., Vella, N., Zava, B., Gerovasileiou, V., 2021. “New records of rare species in the Mediterranean Sea” (October 2021). Medit. Mar. Sci. 22, 627. https://doi.org/10.12681/mms.26669

Tseng, C.-M., Ang, S.-J., Chen, Y.-S., Shiao, J.-C., Lamborg, C.H., He, X., Reinfelder, J.R., 2021. Bluefin tuna reveal global patterns of mercury pollution and bioavailability in the world’s oceans. Proceedings of the National Academy of Sciences 6.

Tsujino, H., Urakawa, S., Nakano, H., Small, R.J., Kim, W.M., Yeager, S.G., Danabasoglu, G., Suzuki, T., Bamber, J.L., Bentsen, M., Böning, C.W., Bozec, A., Chassignet, E.P., Curchitser, E., Boeira Dias, F., Durack, P.J., Griffies, S.M., Harada, Y., Ilicak, M., Josey, S.A., Kobayashi, C., Kobayashi, S., Komuro, Y., Large, W.G., Le Sommer, J., Marsland, S.J., Masina, S., Scheinert, M., Tomita, H., Valdivieso, M., Yamazaki, D., 2018. JRA-55 based surface dataset for driving ocean–sea-ice models (JRA55-do). Ocean Modelling 130, 79–139. https://doi.org/10.1016/j.ocemod.2018.07.002

Tzadik, O.E., Curtis, J.S., Granneman, J.E., Kurth, B.N., Pusack, T.J., Wallace, A.A., Hollander, D.J., Peebles, E.B., Stallings, C.D., 2017. Chemical archives in fishes beyond otoliths: A review on the use of other body parts as chronological recorders of microchemical constituents for expanding interpretations of environmental, ecological, and life-history changes. Limnology and Oceanography: Methods 15, 238–263. https://doi.org/10.1002/lom3.10153

UN Environment, 2019. Global mercury assessment 2018.

Vanderklift, M.A., Ponsard, S., 2003. Sources of variation in consumer-diet 15N enrichment: a meta-analysis. Oecologia 136, 169–182. https://doi.org/10.1007/s00442-003-1270-z

Villar, E., Cabrol, L., Heimbürger-Boavida, L.-E., 2020. Widespread microbial mercury methylation genes in the global ocean. Environmental Microbiology Reports 12, 277–287. https://doi.org/10.1111/1758-2229.12829

Vincent, M.T., Pilling, G.M., Hampton, J., 2019. Stock assessment of skipjack tuna in the western and central Pacific Ocean (WCPFC-SC15-2019/SA-WP-05-Rev2).

Vlieg, P., Murray, T., Body, D.R., 1993. Nutritional data on six oceanic pelagic fish species from New Zealand waters. Journal of Food Composition and Analysis 6, 45–54. https://doi.org/10.1006/jfca.1993.1006

Voegborlo, R.B., Matsuyama, A., Akagi, H., Adimado, A.A., Ephraim, J.H., 2006. Total Mercury and Methylmercury Accumulation in the Muscle Tissue of Frigate (Auxis thazard thazard) and Yellow Fin (Thunnus albacares) Tuna from the Gulf of Guinea, Ghana. Bull Environ Contam Toxicol 76, 840–847. https://doi.org/10.1007/s00128-006-0995-x

Wada, E., Hattori, A., 1990. Nitrogen in the Sea: Forms, Abundance, and Rate Processes. CRC Press.

Walworth, N.G., Lee, M.D., Suffridge, C., Qu, P., Fu, F.-X., Saito, M.A., Webb, E.A., Sañudo-Wilhelmy, S.A., Hutchins, D.A., 2018. Functional Genomics and Phylogenetic Evidence Suggest Genus-Wide Cobalamin Production by the Globally Distributed Marine Nitrogen Fixer Trichodesmium. Frontiers in Microbiology 9.

Wang, F., Outridge, P.M., Feng, X., Meng, B., Heimbürger-Boavida, L.-E., Mason, R.P., 2019. How closely do mercury trends in fish and other aquatic wildlife track those in the atmosphere? - Implications for evaluating the effectiveness of the Minamata Convention. Science of the Total Environment 674, 58–70. https://doi.org/10.1016/j.scitotenv.2019.04.101

Wang, P., Chen, S., Chen, Z., Huo, W., Huang, R., Huang, W., Peng, J., Yang, X., 2019. Benefit–risk assessment of commonly consumed fish species from South China Sea based on methyl mercury and DHA. Environ Geochem Health 41, 2055–2066. https://doi.org/10.1007/s10653-019-00254-1

Wang, R., Wong, M.-H., Wang, W.-X., 2011. Coupling of methylmercury uptake with respiration and water pumping in freshwater tilapia Oreochromis niloticus. Environmental Toxicology and Chemistry 30, 2142–2147. https://doi.org/10.1002/etc.604

Wang, X., Wu, F., Wang, W.-X., 2017. In Vivo Mercury Demethylation in a Marine Fish (Acanthopagrus schlegeli). Environ. Sci. Technol. 51, 6441–6451. https://doi.org/10.1021/acs.est.7b00923

Ward, D.M., Nislow, K.H., Chen, C.Y., Folt, C.L., 2010. Reduced Trace Element Concentrations in Fast-Growing Juvenile Atlantic Salmon in Natural Streams. Environ. Sci. Technol. 44, 3245–3251. https://doi.org/10.1021/es902639a

Weaver, A.J., Eby, M., Wiebe, E.C., Bitz, C.M., Duffy, P.B., Ewen, T.L., Fanning, A.F., Holland, M.M., MacFadyen, A., Matthews, H.D., Meissner, K.J., Saenko, O., Schmittner, A., Wang, H., Yoshimori, M., 2001. The UVic earth system climate model: Model description, climatology, and applications to past, present and future climates. Atmosphere-Ocean 39, 361–428. https://doi.org/10.1080/07055900.2001.9649686

Weihe, P., Grandjean, P., Debes, F., White, R., 1996. Health implications for Faroe Islanders of heavy metals and PCBs from pilot whales. Science of The Total Environment, Marine Mammals And The Marine Environment 186, 141–148. https://doi.org/10.1016/0048-9697(96)05094-2

Williams, A.J., Allain, V., Nicol, S.J., Evans, K.J., Hoyle, S.D., Dupoux, C., Vourey, E., Dubosc, J., 2015. Vertical behavior and diet of albacore tuna (Thunnus alalunga) vary with latitude in the South Pacific Ocean. Deep Sea Research Part II: Topical Studies in Oceanography 113, 154–169. https://doi.org/10.1016/j.dsr2.2014.03.010

Williams, A.J., Farley, J.H., Hoyle, S.D., Davies, C.R., Nicol, S.J., 2012. Spatial and Sex-Specific Variation in Growth of Albacore Tuna (Thunnus alalunga) across the South Pacific Ocean. PLoS ONE 7, e39318. https://doi.org/10.1371/journal.pone.0039318

Williams, P., Reid, C., 2018. Overview of tuna fisheries in the WCPO including economic conditions - 2017. Presented at the WCPFC - TCC14 - 2018, Majuro, Republic of Marshall Islands, p. 68.

Won, E.-J., Choi, B., Hong, S., Khim, J.S., Shin, K.-H., 2018. Importance of accurate trophic level determination by nitrogen isotope of amino acids for trophic magnification studies: A review. Environmental Pollution 238, 677–690. https://doi.org/10.1016/j.envpol.2018.03.045

Wood, S., Scheipl, F., 2020. Package “gamm4”. R package version 0.2-6.

Wood, S., Wood, M.S., 2015. Package “mgcv”. R package version (No. 1.8-28).

World Health Organization, UNEP Chemicals, 2008. Guidance for identifying populations at risk from mercury exposure. Geneva, Switzerland.

Wu, P., Kainz, M.J., Bravo, A.G., Åkerblom, S., Sonesten, L., Bishop, K., 2019. The importance of bioconcentration into the pelagic food web base for methylmercury biomagnification: A meta-analysis. Science of The Total Environment 646, 357–367. https://doi.org/10.1016/j.scitotenv.2018.07.328

Xu, L.-Q., Liu, X.-D., Sun, L., Chen, Q.-Q., Yan, H., Liu, Y., Luo, Y.-H., Huang, J., 2011. A 700-year record of mercury in avian eggshells of Guangjin Island, South China Sea. Environmental Pollution 159, 889–896. https://doi.org/10.1016/j.envpol.2010.12.021

Yamashita, Y., Omura, Y., Okazaki, E., 2005. Total mercury and methylmercury levels in commercially important fishes in Japan. Fisheries Sci 71, 1029–1035. https://doi.org/10.1111/j.1444-2906.2005.01060.x

Yang, D.-Y., Chen, Y.-W., Gunn, J.M., Belzile, N., 2008. Selenium and mercury in organisms: Interactions and mechanisms. Environ. Rev. 16, 71–92. https://doi.org/10.1139/A08-001

Yang, S., Song, L., Zhang, Y., Fan, W., Zhang, B., Dai, Y., Zhang, H., Zhang, S., Wu, Y., 2020. The Potential Vertical Distribution of Bigeye Tuna (Thunnus obesus) and Its Influence on the Spatial Distribution of CPUEs in the Tropical Atlantic Ocean. Journal of Ocean University of China 19, 669–680. https://doi.org/10.1007/s11802-020-4264-0

Yin, R., Feng, X., Chen, B., Zhang, J., Wang, W., Li, X., 2015. Identifying the Sources and Processes of Mercury in Subtropical Estuarine and Ocean Sediments Using Hg Isotopic Composition. Environ. Sci. Technol. 49, 1347–1355. https://doi.org/10.1021/es504070y

Young, D.R., Johnson, J.N., Soutar, A., Isaacs, J.D., 1973. Mercury Concentrations in Dated Varved Marine Sediments collected off Southern California. Nature 244, 273–275. https://doi.org/10.1038/244273a0

Young, J.W., Guest, M.A., Lansdell, M., Phleger, C.F., Nichols, P.D., 2010a. Discrimination of prey species of juvenile swordfish Xiphias gladius (Linnaeus, 1758) using signature fatty acid

analyses. Progress in Oceanography, CLimate Impacts on Oceanic TOp Predators (CLIOTOP) 86, 139–151. https://doi.org/10.1016/j.pocean.2010.04.028

Young, J.W., Lansdell, M.J., Campbell, R.A., Cooper, S.P., Juanes, F., Guest, M.A., 2010b. Feeding ecology and niche segregation in oceanic top predators off eastern Australia. Mar Biol 157, 2347–2368. https://doi.org/10.1007/s00227-010-1500-y

Zhang, T., Hsu-Kim, H., 2010. Photolytic degradation of methylmercury enhanced by binding to natural organic ligands. Nature Geosci 3, 473–476. https://doi.org/10.1038/ngeo892

Zhang, Y., Horowitz, H., Wang, J., Xie, Z., Kuss, J., Soerensen, A.L., 2019. A Coupled Global Atmosphere-Ocean Model for Air-Sea Exchange of Mercury: Insights into Wet Deposition and Atmospheric Redox Chemistry. Environ. Sci. Technol. 53, 5052–5061. https://doi.org/10.1021/acs.est.8b06205

Zhang, Y., Jacob, D.J., Dutkiewicz, S., Amos, H.M., Long, M.S., Sunderland, E.M., 2015. Biogeochemical drivers of the fate of riverine mercury discharged to the global and Arctic oceans. Global Biogeochemical Cycles 29, 854–864. https://doi.org/10.1002/2015GB005124

Zhang, Y., Jacob, D.J., Horowitz, H.M., Chen, L., Amos, H.M., Krabbenhoft, D.P., Slemr, F., St. Louis, V.L., Sunderland, E.M., 2016. Observed decrease in atmospheric mercury explained by global decline in anthropogenic emissions. Proc Natl Acad Sci USA 113, 526–531. https://doi.org/10.1073/pnas.1516312113

Zhang, Y., Jaeglé, L., Thompson, L., Streets, D.G., 2014. Six centuries of changing oceanic mercury. Global Biogeochemical Cycles 28, 1251–1261. https://doi.org/10.1002/2014GB004939

Zhang, Y., Soerensen, A.L., Schartup, A.T., Sunderland, E.M., 2020. A Global Model for Methylmercury Formation and Uptake at the Base of Marine Food Webs. Global Biogeochem. Cycles 34. https://doi.org/10.1029/2019GB006348

Zuur, A.F., Ieno, E.N., Elphick, C.S., 2010. A protocol for data exploration to avoid common statistical problems: Data exploration. Methods in Ecology and Evolution 1, 3–14. https://doi.org/10.1111/j.2041-210X.2009.00001.x

DOCTORAT SCIENCES BRETAGNE DE LA MER LOIRE ET DU LITTORAL

UBO Université de Bretagne Occidentale

Titre : Origine, déterminants et modélisation statistique des concentrations en méthylmercure dans les thons à l'échelle globale

Mots clés : mercure, variabilité spatio-temporelle, écologie trophique, biogéochimie marine, émissions anthropiques

Résumé : Le thon est l'un des poissons marins les plus consommés au monde malgré ses concentrations relativement élevées en méthylmercure (MeHg), la forme toxique du mercure (Hg). De fortes variations de ces concentrations entre espèces et régions sont observées mais encore peu comprises. Pour étudier l'origine et le devenir du MeHg dans les thons à l'échelle globale, nous avons constitué la plus grande base de données de concentrations de Hg dans les thons tropicaux (thon obèse, albacore et bonite à ventre rayé, n > 5700), intégrant des données biologiques et écologiques des thons, des variables physiques et biogéochimiques de l'océan, et des estimations de Hg atmosphérique. Une hausse des niveaux de Hg dans les thons a été constatée à la fin des années 1990 dans le Pacifique Nord-Ouest, en lien avec l'augmentation des émissions anthropiques de Hg depuis l'Asie. Ailleurs, les concentrations de Hg dans les thons sont restés stables au cours du temps, suggérant une inertie de l'océan de surface due au Hg anthropique accumulé au cours des siècles dans l'océan de subsurface. La cartographie des concentrations de Hg dans les thons a montré de fortes variations spatiales, dues à la variabilité de profondeur de plongée des thons et des niveaux de MeHg dissous dans l'eau, induites par des processus biogéochimiques. Nos études spatiales ont enfin confirmé un effet local des émissions anthropiques de Hg augmentant les concentrations de Hg dans les thons au large de l'Asie. Cette thèse démontre que les thons sont des outils de bio-surveillance pertinents pour documenter les changements du cyle marin du Hg, dans un contexte de réduction des émissions anthropiques et de changement climatique.

Title: Origin, controlling factors, and statistical modelling of methylmercury concentrations in tunas at a global scale

Keywords : mercury, spatio-temporal variability, trophic ecology, marine biogeochemistry, anthropogenic emissions

Abstract: Tunas are among the most consumed seafood products but contain relatively high levels of methylmercury (MeHg), the most toxic form of mercury (Hg). Limited observations suggest tuna Hg levels vary in space and time, yet the drivers are not well understood. This thesis aimed to explore the origin and fate of MeHg in tunas at the global scale. We built the largest Hg database in tropical tunas (bigeye, yellowfin, and skipjack, n > 5,700), alongside tuna biological and ecological data, marine physical and biogeochemical variables, and atmospheric Hg estimates. Increasing tuna Hg concentrations were found in the late 1990s in the northwestern Pacific, concomitant with increasing anthropogenic Hg emissions from Asia. Elsewhere, we revealed stable long-term tuna Hg levels, which contrasts with an overall decline in Hg emissions and deposition, and suggests an inertia of the surface ocean resulting from legacy Hg accumulated in subsurface ocean over centuries. Moreover, global maps of tuna Hg levels highlighted strong spatial patterns among tunas, once accounting for MeHg bioaccumulation with tuna age/length. Our multidisciplinary approach showed the combined importance of marine biogeochemistry governing MeHg profiles in seawater, and tuna foraging depth, to explain these spatial patterns. Our spatial studies also confirmed a local anthropogenic Hg release effect enhancing tuna Hg levels along the Asia coasts. Complementary to observations of atmospheric Hg deposition and seawater MeHg levels, this thesis elevates tunas as releveant bio-monitoring tools to document changes of the marine Hg cycle in a context of reduction emission measures and climate change.